National Library
of Canada

Bibliothèque nationale
du Canada

Canadian Theses Service

Service des thèses canadiennes

Ottawa, Canada
K1A 0N4

NOTICE

The quality of this microform is heavily dependent upon the quality of the original thesis submitted for microfilming. Every effort has been made to ensure the highest quality of reproduction possible.

If pages are missing, contact the university which granted the degree.

Some pages may have indistinct print especially if the original pages were typed with a poor typewriter ribbon or if the university sent us an inferior photocopy.

Reproduction in full or in part of this microform is governed by the Canadian Copyright Act, R.S.C. 1970, c. C-30, and subsequent amendments.

AVIS

La qualité de cette microforme dépend grandement de la qualité de la thèse soumise au microfilmage. Nous avons tout fait pour assurer une qualité supérieure de reproduction.

S'il manque des pages, veuillez communiquer avec l'université qui a conféré le grade.

La qualité d'impression de certaines pages peut laisser à désirer, surtout si les pages originales ont été dactylographiées à l'aide d'un ruban usé ou si l'université nous a fait parvenir une photocopie de qualité inférieure.

La reproduction, même partielle, de cette microforme est soumise à la Loi canadienne sur le droit d'auteur, SRC 1970, c. C-30, et ses amendements subséquents.

NL-339 (r. 88/04) c

Canada

THE UNIVERSITY OF ALBERTA

A STUDY OF FLOW IN CURVED OPEN CHANNELS

BY

YEE-CHUNG JIN ©

A THESIS
SUBMITTED TO THE FACULTY OF GRADUATE STUDIES AND RESEARCH IN PARTIAL
FULFILMENT OF THE REQUIREMENTS FOR THE DEGREE
OF DOCTOR OF PHILOSOPHY

DEPARTMENT OF CIVIL ENGINEERING

EDMONTON, ALBERTA
SPRING, 1990

National Library
of Canada

Bibliothèque nationale
du Canada

Canadian Theses Service

Service des thèses canadiennes

Ottawa, Canada
K1A 0N4

NOTICE

The quality of this microform is heavily dependent upon the quality of the original thesis submitted for microfilming. Every effort has been made to ensure the highest quality of reproduction possible.

If pages are missing, contact the university which granted the degree.

Some pages may have indistinct print especially if the original pages were typed with a poor typewriter ribbon or if the university sent us an inferior photocopy.

Reproduction in full or in part of this microform is governed by the Canadian Copyright Act, R.S.C. 1970, c. C-30, and subsequent amendments.

AVIS

La qualité de cette microforme dépend grandement de la qualité de la thèse soumise au microfilmage. Nous avons tout fait pour assurer une qualité supérieure de reproduction.

S'il manque des pages, veuillez communiquer avec l'université qui a conféré le grade.

La qualité d'impression de certaines pages peut laisser à désirer, surtout si les pages originales ont été dactylographiées à l'aide d'un ruban usé ou si l'université nous a fait parvenir une photocopie de qualité inférieure.

La reproduction, même partielle, de cette microforme est soumise à la Loi canadienne sur le droit d'auteur, SRC 1970, c. C-30, et ses amendements subséquents.

ISBN 0-315-60173-6

NL-339 (r. 88/04) c

Canada

THE UNIVERSITY OF ALBERTA

RELEASE FORM

NAME OF AUTHOR:	YEE-CHUNG JIN
TITLE OF THESIS:	A STUDY OF FLOW IN CURVED OPEN CHANNELS
DEGREE:	DOCTOR OF PHILOSOPHY
YEAR THIS DEGREE GRANTED:	SPRING 1990

Permission is hereby granted to THE UNIVERSITY OF ALBERTA LIBRARY to reproduce single copies of this thesis and to lend or sell such copies for private, scholarly or scientific research purposes only.

The author reserves other publication rights, and neither the thesis or extensive extracts from it may be printed nor otherwise reproduced without the author's written permission.

Permanent Address:

23 McGregor Crescent
P.O.Box 687
Pinawa, Manitoba
Canada, T6H 4M5

Date: April 26, 1990

THE UNIVERSITY OF ALBERTA

FACULTY OF GRADUATE STUDIES AND RESEARCH

The undersigned certify that they have read, and recommend to the Faculty of Graduate Studies and Research for acceptance, a thesis entitled A STUDY OF FLOW IN CURVED OPEN CHANNELS submitted by YEE-CHUNG JIN in partial fulfilment of the requirements for the degree of DOCTOR OF PHILOSOPHY.

Dr. P.M. Steffler

Dr. N. Rajaratnam

Dr. R. Gerard

T. Hrudey
Dr. T. Hrudey

K.C.Cheng
Dr. K.C. Cheng

Ben C Yen
Dr. B.C. Yen

DATE: Apr. 23, 90

ABSTRACT

A depth-averaged model formulated in the Cartesian coordinate system has been introduced for simulating the velocity distribution in curved open channels. The finite element method is used to simplify the geometry problems in practical cases such as irregular cross sections and channels of varying plan curvature. The mathematical model consists of the depth-averaged continuity equation, the momentum equations, and two moment of momentum equations for closure purposes. The numerical analysis predicts satisfactory depth-averaged longitudinal and transverse velocities as well as reasonable secondary flows.

The experimental part of this study is not only to provide the data for calibrating the numerical model but also to investigate the flow in a 270° open channel of half trapezoidal cross-section concentrating on flow effects on the outside bank. The purpose of this part of investigation was to provide some understanding of flow mechanics which may be useful in the design of riprap protection. Three runs with varying depth were conducted for a completely smooth boundary. Two additional runs with varying outside slope roughness were also performed. Velocities and shear stresses were measured using a Laser Doppler Anaemometer. Velocity and shear velocity distributions for all sections and runs are presented and compared. In the smooth channel runs, it was found that the shear stress or attack velocity did not significantly vary up the outside bank slope. Longitudinal variation was significant, indicating a possibility for longitudinal zoning of riprap protection. For the roughened boundaries, a significant variation of shear up the slope and a much higher stress at the toe of the slope was found.

The comparison of the numerical prediction and the experimental results is included. The mathematical model discussed here can be applied to other channel flow problems where secondary flow and its effects are important.

ACKNOWLEDGEMENTS

Numerous people made this research possible, and it is impossible to give each one credit. To those persons not mentioned below, I thank you for your time and effort.

First of all, I would like to thank my major supervisor Dr. P. M. Steffler for his patience and guidance which were invaluable during my graduate studies and in the preparation of this thesis. Appreciation is also expressed to the other members of my supervisory committee, Dr. N. Rajaratnam and Professor A. W. Peterson for their advice and counsel. I also like to thank Dr. R. Gerard for the helpful comments upon a draft of this thesis.

I like to thank the Research Management Division of Alberta Environment and Natural Sciences and Engineering Research Council for their financial support during most of the research, and T. Blench Hydraulics Lab which provided all the experimental facilities and the computer resources.

I also like to express my gratitude to Mr. S. Lovell for his assistance in designing and maintaining the experimental facility, and Mr. R. Gitzel and Mr. D. Lathe for maintaining the electronic equipments and computer used in this research.

Special thanks to Mr. S. Solanki, Mrs. F. Hicks and Dr. D. Ophori for the review of this thesis. Deepest gratitude to my wife, Weigen, whose constant encouragement and understanding helped make this work possible.

Table of Contents

page

1 INTRODUCTION 1

2 THEORETICAL ANALYSIS 7

- 2.1 Mathematical Model 7
  - 2.1.1 Kinematic Surface and Bed Condition 7
  - 2.1.2 Continuity and Momentum Equations 8
  - 2.1.3 The Depth-averaged Vertical Velocity 16
  - 2.1.4 The Moment of Momentum Equations 17
  - 2.1.5 Reduction of the Governing Equations 21
  - 2.1.6 Velocity Functions 24
  - 2.1.7 Shear Stress Model 25
  - 2.1.8 Boundary Conditions 29
  - 2.1.9 Summary 30
- 2.2 Simple Model 31
  - 2.2.1 Simple model 31
  - 2.2.2 Comparison and Discussion 34
    - 2.2.2.1 Steffler's Experiments 34
    - 2.2.2.2 De Vriend's Experiments 36
    - 2.2.2.3 Yen's Experiments 37
  - 2.2.3 Conclusion 37

3 NUMERICAL ANALYSIS 46

3.1 Numerical Formulation 46

3.1.1 Galerkin's Method 47

3.1.2 Finite Element Formulation 49

3.1.3 Boundary Conditions and Artificial Diffusion 55

3.1.4 Computer Coding 56

3.2 Numerical Tests 58

3.2.1 Test for Uniform Flow Problem 58

3.2.2 Test for Non-uniform Flow Problem 59

3.2.3 Test for the Rectangular Free Overfall 60

3.2.4 Test for Flow in a 60 Degree Bend 64

4 EXPERIMENTAL STUDY 73

4.1 Introduction 73

4.2 Experimental Facilities and Procedure 73

4.3 Data Analysis 76

4.3.1 Limits for Logarithmic Velocity Equation 76

4.3.2 Rough Boundary Datum 79

4.3.3 Boundary Shear Stress 79

4.3.4 Equivalent Roughness 80

4.4 Experimental Results 81

4.4.1 Smooth Boundary 81

4.4.2 Rough Boundary on the Sloped Bank 82

5 DISCUSSION OF THE EXPERIMENTAL RESULTS 222

5.1 Introduction 222

5.2 Discussion 222

5.2.1 Longitudinal Velocity 222

5.2.2 Longitudinal Shear Velocity 224

5.2.3 Correlation of Depth Averaged Velocity and Shear Stress 226

5.2.4 Momentum Transport 228

5.2.5 Transverse Velocity 231

6 COMPARISON AND DISCUSSION 265

6.1 Steffler's Experiments 265

6.2 LFM Experiments 269

6.3 De Vriend's Experiments 269

6.4 Comparison of the Experimental Data 271

7 CONCLUSIONS 296

BIBLIOGRAPHY 300

APPENDIX COMPUTER PROGRAM 305

List of Tables

page

Table 3.1 Uniform Flow Test 59

Table 4.1 Significant Details of the Experiments 76

Table of Figures

page

Figure 2.1 Coordinate definition 38

Figure 2.2 Variation of I_m.............................. 39

Figure 2.3 Variation of k_*.............................. 39

Figure 2.4 The layout of Steffler's experiment 40

Figure 2.5 Variation of bed shear stress angle ϕ (experimental data) 41

Figure 2.6 Variation of k_* (experimental data)......... 41

Figure 2.7 The comparison of transverse surface velocity for Steffler's experimental data 42

Figure 2.8 Plan view of De Vriend's 90° bend (De Vriend, 1976) 43

Figure 2.9 Channel geometry of De Vriend's 90° bend (De Vriend, 1976) 44

Figure 2.10 The comparison of transverse surface velocity for De Vriend's (1976) experimental data 44

Figure 2.11 The comparison of transverse surface velocity for De Vriend's (1978) experimental data 45

Figure 2.12 The comparison of transverse bed stress for Yen's (1965) experimental data 45

Figure 3.1 Flow chart of the solving procedure 66

Figure 3.2 Program structure 67

Figure 3.3 Finite element mesh for the non-uniform flow problem 68

Figure 3.4 Comparison of the longitudinal velocity profiles for the non-uniform flow problem 68

Figure 3.5 Rectangular free overfall 69

Figure 3.6 Comparison of the numerical and experimental longitudinal velocity profiles for the free overfall problem 69
Figure 3.7 Pressure distribution for the free overfall problem 70
Figure 3.8 Vertical velocity distribution for the free overfall problem 70
Figure 3.9 Comparison of the longitudinal velocity profiles for the free overfall problem (with the extra pressure deviation terms) ... 71
Figure 3.10 The hypothetical 60 degree bended channel 71
Figure 3.11 The numerical result for 60 degree bend 72
Figure 4.1 Dimensions of the channel section 84
Figure 4.2 Flume and locations of the measurement stations 84
Figure 4.3 Details of Roughness #2 85
Figure 4.4 Details of Roughness #1 86
Figure 4.5 Determination of roughness datum 87
Figure 4.6 Velocity profile normal to the boundary 88
Figure 4.7 Dimensionless velocity profile 89
Figure 4.8 u velocity distribution (run 1, section 1) 90
Figure 4.9 u velocity distribution (run 1, section 2) 91
Figure 4.10 u velocity distribution (run 1, section 3) 92
Figure 4.11 u velocity distribution (run 1, section 4) 93
Figure 4.12 u velocity distribution (run 1, section 5) 94
Figure 4.13 u velocity distribution (run 1, section 6) 95
Figure 4.14 u velocity distribution (run 1, section 7) 96

Figure 4.15 u velocity distribution (run 1, section 8) 97

Figure 4.16 u velocity distribution (run 1, section 9) 98

Figure 4.17 u velocity distribution (run 1, section 10) 99

Figure 4.18 u velocity distribution (run 1, section 11) 100

Figure 4.19 v velocity distribution (run 1, section 1) 101

Figure 4.20 v velocity distribution (run 1, section 2) 102

Figure 4.21 v velocity distribution (run 1, section 3) 103

Figure 4.22 v velocity distribution (run 1, section 4) 104

Figure 4.23 v velocity distribution (run 1, section 5) 105

Figure 4.24 v velocity distribution (run 1, section 6) 106

Figure 4.25 v velocity distribution (run 1, section 7) 107

Figure 4.26 v velocity distribution (run 1, section 8) 108

Figure 4.27 v velocity distribution (run 1, section 9) 109

Figure 4.28 v velocity distribution (run 1, section 10) 110

Figure 4.29 v velocity distribution (run 1, section 11) 111

Figure 4.30 $\overline{u'u'}$ turbulence intensity distribution (run 1, section 1) 112

Figure 4.31 $\overline{u'u'}$ turbulence intensity distribution (run 1, section 2) 113

Figure 4.32 $\overline{u'u'}$ turbulence intensity distribution (run 1, section 3) 114

Figure 4.33 $\overline{u'u'}$ turbulence intensity distribution (run 1, section 4) 115

Figure 4.34 $\overline{u'u'}$ turbulence intensity distribution (run 1, section 5) 116

Figure 4.35 $\overline{u'u'}$ turbulence intensity distribution (run 1, section 6) 117

Figure 4.36 $\overline{u'u'}$ turbulence intensity distribution (run 1, section 7) 118

Figure 4.37 $\overline{u'u'}$ turbulence intensity distribution (run 1, section 8) 119

Figure 4.38 $\overline{u'u'}$ turbulence intensity distribution (run 1, section 9) 120

Figure 4.39 $\overline{u'u'}$ turbulence intensity distribution (run 1, section 10) 121

Figure 4.40 $\overline{u'u'}$ turbulence intensity distribution (run 1, section 11) 122

Figure 4.41 $\overline{v'v'}$ turbulence intensity distribution (run 1, section 1) 123

Figure 4.42 $\overline{v'v'}$ turbulence intensity distribution (run 1, section 2) 124

Figure 4.43 $\overline{v'v'}$ turbulence intensity distribution (run 1, section 3) 125

Figure 4.44 $\overline{v'v'}$ turbulence intensity distribution (run 1, section 4) 126

Figure 4.45 $\overline{v'v'}$ turbulence intensity distribution (run 1, section 5) 127

Figure 4.46 $\overline{v'v'}$ turbulence intensity distribution (run 1, section 6) 128

Figure 4.47 $\overline{v'v'}$ turbulence intensity distribution (run 1, section 7) 129

Figure 4.48 $\overline{v'v'}$ turbulence intensity distribution (run 1, section 8) 130

Figure 4.49 $\overline{v'v'}$ turbulence intensity distribution (run 1, section 9) 131

Figure 4.50 $\overline{v'v'}$ turbulence intensity distribution (run 1, section 10) 132

Figure 4.51 $\overline{v'v'}$ turbulence intensity distribution (run 1, section 11) 133
Figure 4.52 u velocity distribution (run 4, section 1) 134
Figure 4.53 u velocity distribution (run 4, section 2) 135
Figure 4.54 u velocity distribution (run 4, section 3) 136
Figure 4.55 u velocity distribution (run 4, section 4) 137
Figure 4.56 u velocity distribution (run 4, section 5) 138
Figure 4.57 u velocity distribution (run 4, section 6) 139
Figure 4.58 u velocity distribution (run 4, section 7) 140
Figure 4.59 u velocity distribution (run 4, section 8) 141
Figure A.60 u velocity distribution (run 4, section 9) 142
Figure 4.61 u velocity distribution (run 4, section 10) 143
Figure 4.62 u velocity distribution (run 4, section 11) 144
Figure 4.63 v velocity distribution (run 4, section 1) 145
Figure 4.64 v velocity distribution (run 4, section 2) 146
Figure 4.65 v velocity distribution (run 4, section 3) 147
Figure 4.66 v velocity distribution (run 4, section 4) 148
Figure 4.67 v velocity distribution (run 4, section 5) 149
Figure 4.68 v velocity distribution (run 4, section 6) 150

Figure 4.69 v velocity distribution (run 4, section 7) 151
Figure 4.70 v velocity distribution (run 4, section 8) 152
Figure 4.71 v velocity distribution (run 4, section 9) 153
Figure 4.72 v velocity distribution (run 4, section 10) 154
Figure 4.73 v velocity distribution (run 4, section 11) 155
Figure 4.74 $\overline{u'u'}$ turbulence intensity distribution (run 4, section 1) 156
Figure 4.75 $\overline{u'u'}$ turbulence intensity distribution (run 4, section 2) 157
Figure 4.76 $\overline{u'u'}$ turbulence intensity distribution (run 4, section 3) 158
Figure 4.77 $\overline{u'u'}$ turbulence intensity distribution (run 4, section 4) 159
Figure 4.78 $\overline{u'u'}$ turbulence intensity distribution (run 4, section 5) 160
Figure 4.79 $\overline{u'u'}$ turbulence intensity distribution (run 4, section 6) 161
Figure 4.80 $\overline{u'u'}$ turbulence intensity distribution (run 4, section 7) 162
Figure 4.81 $\overline{u'u'}$ turbulence intensity distribution (run 4, section 8) 163
Figure 4.82 $\overline{u'u'}$ turbulence intensity distribution (run 4, section 9) 164
Figure 4.83 $\overline{u'u'}$ turbulence intensity distribution (run 4, section 10) 165
Figure 4.84 $\overline{u'u'}$ turbulence intensity distribution (run 4, section 11) 166
Figure 4.85 $\overline{v'v'}$ turbulence intensity distribution (run 4, section 1) 167
Figure 4.86 $\overline{v'v'}$ turbulence intensity distribution (run 4, section 2) 168

Figure 4.87 $\overline{v'v'}$ turbulence intensity distribution (run 4, section 3) 169

Figure 4.88 $\overline{v'v'}$ turbulence intensity distribution (run 4, section 4) 170

Figure 4.89 $\overline{v'v'}$ turbulence intensity distribution (run 4, section 5) 171

Figure 4.90 $\overline{v'v'}$ turbulence intensity distribution (run 4, section 6) 172

Figure 4.91 $\overline{v'v'}$ turbulence intensity distribution (run 4, section 7) 173

Figure 4.92 $\overline{v'v'}$ turbulence intensity distribution (run 4, section 8) 174

Figure 4.93 $\overline{v'v'}$ turbulence intensity distribution (run 4, section 9) 175

Figure 4.94 $\overline{v'v'}$ turbulence intensity distribution (run 4, section 10) 176

Figure 4.95 $\overline{v'v'}$ turbulence intensity distribution (run 4, section 11) 177

Figure 4.96 u velocity distribution (run 5, section 1) 178

Figure 4.97 u velocity distribution (run 5, section 2) 179

Figure 4.98 u velocity distribution (run 5, section 3) 180

Figure 4.99 u velocity distribution (run 5, section 4) 181

Figure 4.100 u velocity distribution (run 5, section 5) 182

Figure 4.101 u velocity distribution (run 5, section 6) 183

Figure 4.102 u velocity distribution (run 5, section 7) 184

Figure 4.103 u velocity distribution (run 5, section 8) 185

Figure 4.104 u velocity distribution (run 5, section 9) 186

Figure 4.105 u velocity distribution (run 5, section 10) 187
Figure 4.106 u velocity distribution (run 5, section 11) 188
Figure 4.107 v velocity distribution (run 5, section 1) 189
Figure 4.108 v velocity distribution (run 5, section 2) 190
Figure 4.109 v velocity distribution (run 5, section 3) 191
Figure 4.110 v velocity distribution (run 5, section 4) 192
Figure 4.111 v velocity distribution (run 5, section 5) 193
Figure 4.112 v velocity distribution (run 5, section 6) 194
Figure 4.113 v velocity distribution (run 5, section 7) 195
Figure 4.114 v velocity distribution (run 5, section 8) 196
Figure 4.115 v velocity distribution (run 5, section 9) 197
Figure 4.116 v velocity distribution (run 5, section 10) 198
Figure 4.117 v velocity distribution (run 5, section 11) 199
Figure 4.118 $\overline{u'u'}$ turbulence intensity distribution (run 5, section 1) 200
Figure 4.119 $\overline{u'u'}$ turbulence intensity distribution (run 5, section 2) 201
Figure 4.120 $\overline{u'u'}$ turbulence intensity distribution (run 5, section 3) 202
Figure 4.121 $\overline{u'u'}$ turbulence intensity distribution (run 5, section 4) 203
Figure 4.122 $\overline{u'u'}$ turbulence intensity distribution (run 5, section 5) 204

Figure 4.123 $\overline{u'u'}$ turbulence intensity distribution (run 5, section 6) 205

Figure 4.124 $\overline{u'u'}$ turbulence intensity distribution (run 5, section 7) 206

Figure 4.125 $\overline{u'u'}$ turbulence intensity distribution (run 5, section 8) 207

Figure 4.126 $\overline{u'u'}$ turbulence intensity distribution (run 5, section 9) 208

Figure 4.127 $\overline{u'u'}$ turbulence intensity distribution (run 5, section 10) 209

Figure 4.128 $\overline{u'u'}$ turbulence intensity distribution (run 5, section 11) 210

Figure 4.129 $\overline{v'v'}$ turbulence intensity distribution (run 5, section 1) 211

Figure 4.130 $\overline{v'v'}$ turbulence intensity distribution (run 5, section 2) 212

Figure 4.131 $\overline{v'v'}$ turbulence intensity distribution (run 5, section 3) 213

Figure 4.132 $\overline{v'v'}$ turbulence intensity distribution (run 5, section 4) 214

Figure 4.133 $\overline{v'v'}$ turbulence intensity distribution (run 5, section 5) 215

Figure 4.134 $\overline{v'v'}$ turbulence intensity distribution (run 5, section 6) 216

Figure 4.135 $\overline{v'v'}$ turbulence intensity distribution (run 5, section 7) 217

Figure 4.136 $\overline{v'v'}$ turbulence intensity distribution (run 5, section 8) 218

Figure 4.137 $\overline{v'v'}$ turbulence intensity distribution (run 5, section 9) 219

Figure 4.138 $\overline{v'v'}$ turbulence intensity distribution (run 5, section 10) 220

Figure 4.139 $\overline{v'v'}$ turbulence intensity distribution (run 5, section 11) 221

Figure 5.1 Profiles of depth-averaged longitudinal velocity(run 1) 233

Figure 5.2 Longitudinal variation of longitudinal depth averaged velocity (run 1) 234
Figure 5.3 Profiles of depth-averaged longitudinal velocity (run 2) 235
Figure 5.4 Longitudinal variation of longitudinal depth averaged velocity (run 2) 236
Figure 5.5 Profiles of depth-averaged longitudinal velocity (run 3) 237
Figure 5.6 Longitudinal variation of longitudinal depth averaged velocity (run 3) 238
Figure 5.7 Profiles of depth-averaged longitudinal velocity (run 4) 239
Figure 5.8 Longitudinal variation of longitudinal depth averaged velocity (run 4) 240
Figure 5.9 Profiles of depth-averaged longitudinal velocity (run 5) 241
Figure 5.10 Longitudinal variation of longitudinal depth averaged velocity (run 5) 242
Figure 5.11 Profiles of longitudinal shear velocity (run 1) 243
Figure 5.12 Longitudinal variation of shear velocity (run 1) 244
Figure 5.13 Profiles of longitudinal shear velocity (run 2) 245
Figure 5.14 Longitudinal variation of shear velocity (run 2) 246
Figure 5.15 Profiles of longitudinal shear velocity (run 3) 247
Figure 5.16 Longitudinal variation of shear velocity (run 3) 248
Figure 5.17 Profiles of longitudinal shear velocity (run 4) 249
Figure 5.18 Longitudinal variation of shear velocity (run 4) 250
Figure 5.19 Profiles of longitudinal shear velocity (run 5) 251

Figure 5.20 Longitudinal variation of shear velocity (run 5) 252

Figure 5.21 Distribution of longitudinal C_* (run 1) 253

Figure 5.22 Distribution of longitudinal C_* (run 2) 254

Figure 5.23 Distribution of longitudinal C_* (run 3) 255

Figure 5.24 Distribution of longitudinal C_* (run 4) 256

Figure 5.25 Distribution of longitudinal C_* (run 5) 257

Figure 5.26 Longitudinal variation of $\overline{UV}$ and $\overline{txy}$ for run 1 258

Figure 5.27 Longitudinal variation of $\overline{UV}$ and $\overline{\tau_{xy}}$ for run 5 258

Figure 5.28 Transverse variation of $\overline{UV}$ and $\overline{\tau_{xy}}$ for runs 1 and 5 259

Figure 5.29 Longitudinal variation of depth averaged tranverse velocity (run 1) 260

Figure 5.30 Longitudinal variation of depth averaged tranverse velocity (run 2) 261

Figure 5.31 Longitudinal variation of depth averaged tranverse velocity (run 3) 262

Figure 5.32 Longitudinal variation of depth averaged tranverse velocity (run 4) 263

Figure 5.33 Longitudinal variation of depth averaged tranverse velocity (run 5) 264

Figure 6.1 Finite element mesh for Steffler's experiment 273

Figure 6.2 Numerical prediction of Steffler's run 1 (solved with continuity and momentum equations) 274

Figure 6.3 Numerical prediction of Steffler's run 1 (solved with continuity, momentum and momemt of momentum equations) 275

Figure 6.4 The comparison of depth-averaged longitudinal velocity distribution for Steffler's run 1 276

Figure 6.5 The comparison of transverse surface velocity distribution for Steffler's run 1 277
Figure 6.6 The comparison of surface elevation for Steffler's run 1 278
Figure 6.7 The comparison of longitudinal velocity profiles for Steffler's run 1 279
Figure 6.8 The comparison of transverse velocity profiles for Steffler's run 1 280
Figure 6.9 The comparison of depth-averaged longitudinal velocity distribution for Steffler's run 2 281
Figure 6.10 The comparison of transverse surface velocity distribution for Steffler's run 2 282
Figure 6.11 The comparison of longitudinal velocity profiles for Steffler's run 2 283
Figure 6.12 The comparison of transverse velocity profiles for Steffler's run 2 284
Figure 6.13 The comparison of depth-averaged longitudinal velocity distribution for LFM experiment 285
Figure 6.14 Comparison of the depth averaged longitudinal velocity for De Vriend's experiment 286
Figure 6.15 Comparison of transverse surface velocity for De Vriend's experiment 287
Figure 6.16 Numerical prediction of run 1 288
Figure 6.17(a) The comparison of depth averaged longitudinal velocity profile between the prediction and experimental data for run 1 289
Figure 6.17(b) The comparison of depth averaged longitudinal velocity profile between the prediction and experimental data for run 1 290

Figure 6.17(c) The comparison of depth averaged longitudinal velocity profile between the prediction and experimental data for run 1 291

Figure 6.18(a) The comparison of secondary flow surface velocity between the prediction and experimental data for run 1 292

Figure 6.18(b) The comparison of secondary flow surface velocity between the prediction and experimental data for run 1 293

Figure 6.18(c) The comparison of secondary flow surface velocity between the prediction and experimental data for run 1 294

Figure 6.19 The comparison of the numerical calculation and experimental data of $\overline{UV}$ for run 1 295

LIST OF SYMBOLS

B	Channel width;
b	Channel half width;
C_*	Non-dimensional Chezy coefficient;
$F(\eta)$	Longitudinal velocity profile function;
g	Acceleration due to gravity;
$G(\eta)$	Secondary velocity profile function;
h	Depth of flow;
I_1	Integral function (Eq. 2.53);
I_2	Integral function (Eq. 2.54);
I_3	Integral function (Eq. 2.55);
I_4	Integral function (Eq. 2.60);
I_5	Integral function (Eq. 2.61);
I_m	Integral function (Eq. 2.78);
k	Actual roughness height;
k_e	Effective roughness (Eq. 5.3);
k_o	Relative roughness (Eq. 4.5);
k_s	Nikuradse's equivalent sand grain roughness;
k_*	Coefficient (Eq. 2.68);
m	The exponent of the velocity profile (Eq. 2.64);
n	Manning's coefficient;
p_o	piezometric pressure;
R	Radius of curvature of channel centreline;
r	Local radius of curvature;
U_o	Main flow velocity;

U, V	Deviation of velocity from mean depth-averaged velocity;
u, v, w	Instantaneous velocity in x, y and z directions;
$\overline{u}, \overline{v}, \overline{w}$	Depth-averaged velocity components in x, y and z directions;
u_*	Shear velocity;
u_s, v_s	Surface velocity of the secondary flow in x and y directions;
x, y, z	Cartesian coordinate system;
z_b	Channel bed elevation;
ϕ	Friction angle (Eq. 2.70);
γ	Specific weight;
η	Non-dimensional vertical coordinate (Eq. 2.52);
κ	von Karman's constant;
ν_t	Eddy viscosity;
θ	Bend angle;
ρ	Fluid density; and
τ_{bx}, τ_{by}	Fluid bed shear stress in x and y directions.

1 INTRODUCTION

Curvature affects the flow of water in an open channel in several ways. These effects include superelevation, secondary flow, redistribution of longitudinal velocities and bed scour in mobile boundaries. It is important to understand and be able to estimate these effects in a natural channel for the design of river engineering works.

Experimental and mathematical studies of flow in river bends have been performed since the nineteenth century. Boussinesq (1868) was the first to suggest a simple mathematical description of the velocity components in the case of a curved laminar flow. By the use of an order of magnitude analysis and assumptions about the velocity distribution and eddy viscosity, Rozovskii (1957) found a similar solution for transverse velocity for turbulent flow. Yen (1971) derived an approximate solution for the development and the decay of the transverse circulation.

For the flow in a bend of large width-depth ratio, the vertical velocity component is much smaller than the main flow and transverse flow except very close to the side wall. This assumption was used by Yen and Rozovskii which limited their mathematical models to two dimensional (longitudinal and lateral) motion.

It was found that the pressure distribution is hydrostatic when the depth-radius ratio is small (Kalkwijk and De Vriend, 1980). In their study, the depth-averaged method was used to simplify this three dimensional curved channel problem into two dimensions. De Vriend (1977) and Kalkwijk and De Vriend (1980) developed mathematical models based on curvilinear coordinate systems for steady flow in a shallow river of moderate curvature with gradual depth changes. They used local functions for the velocity deviation terms for transverse momentum change due to secondary flow in the depth-averaged equations. To model the effect of velocity perturbation terms, which will be discussed later, they used a term consisting of a coefficient times the centrifugal acceleration and the local depth. The coefficient depended on Chezy's C and the von Karman constant κ. The results from their model tended to underestimate the effect of secondary flow. Having assumed that the curvature of a streamline is the same as the curvature of the river bend, they concluded that, in general, steady flow in shallow water river bends can be adequately described by their model.

Leschziner and Rodi (1979) developed a three dimensional computational model in a strongly non-axisymmetric curved open channel flow. The numerical simulation was based on a finite difference solution of the full three-dimensional equations of continuity and momentum coupled with a κ-ϵ turbulence model. This model reproduced all the important features observed in river bends. However, a three-dimensional model requires a tremendous amount of computational effort.

Other attempts have been made to use two dimensional models with extra expressions to estimate the transverse motion. Among these studies, Falcon Ascanio (1979) employed the moment of momentum equation; Odgaard (1986) substituted predefined velocity profiles into the momentum equations. The axisymmetric assumption (i.e. flow is the same in every plane containing z axis) was used in both cases.

The curvilinear or cylindrical coordinate system has customarily been used in the mathematical modelling of curved channel flow. However, constant curvature and prismatic channels are rarely found in the field. The use of a Cartesian coordinate system will overcome the difficulty of finding the radius of a river bend but will increase the complexity and computational effort. In particular, simplifications based on the relative importance of radial and longitudinal terms are not possible. Harrington et al.(1978) used the depth-averaged model in a Cartesian coordinate system to simulate the flow in 180° bend. Since the transverse terms were omitted, the computed velocity at the outside bank is underestimated while the velocity at the inside bank is overestimated because of the lack of the secondary flow effect.

The present study proposes a depth-averaged model in the Cartesian coordinate system with two extra equations to simulate the flow conditions in a curved open channel. The extra two equations allow the calculation of secondary flow intensity and the effect of the secondary flow on the depth-averaged velocity field.

The finite difference method has been used to solve the shallow water equations in curved channels (De Vriend 1978, 1979, 1983) successfully. These models usually use a cylindrical coordinate system and regular mesh points. These requirements introduced two difficulties:

1) The channel geometry in the field situation is irregular and the radius of the channel curve is not a constant. Imposition of a uniform radius coordinate system will result in an inherent loss of accuracy.

2) To model locations where more details are required a smaller mesh has to be used and this mesh system also must be used throughout. Numerical calculation is wasted in areas where larger mesh spacing would suffice.

In the present study, the finite element method was chosen for the solution of the resulting equations. This method was selected because it allows the specification of the governing equations in a simple Cartesian coordinate system while actually solving them on a curvilinear grid which conforms to the channel plan.

Field data or experimental results are needed to test accuracy and reliability of the numerical formulation for simulating flow in curved open channels. There is a large amount of experimental data on curved open channel flow. However, detailed and reliable data are scarce and hard to obtain. Therefore, some experiments are carried out to provide the result for comparison with the numerical calculation.

The experimental part of this study not only provides the data for calibrating the numerical model but also investigates the flow in a 270° open channel of half trapezoidal cross-section concentrating on flow effects on the outside bank. The experimental study is also a part of a series study carried out at the University of Alberta. These studies will be directed toward the development of useable criteria for bank protection works on curved channels.

The velocity and turbulent shear stress in a curved open channel with both a smooth sloping bank and a rough bank simulating riprap protection along the river bank were measured. Rational bank protection design requires significantly more detailed information on the complex flow field in the vicinity of the bank and especially the outside bank where rapid variations occur. Present design criteria gives no recognition to the variation of the shear stress in both lateral and longitudinal directions, despite the potential importance to the total cost of the bank protection.

Rozovskii (1957), Ippen and Drinker (1962), Yen (1965) measured flow and shear stress in trapezoidal channels. Others have made measurements in natural (Odgaard, 1986) or simulated natural channel shapes (De Vriend 1978). The transverse variation of the shear stress along the sloped bank (Ghosh and Roy 1970) or the side wall of partially roughened (Ghosh 1972, Naot 1983) straight channels has been reported.

Hicks et al.(1990) investigated the flow in a smooth half trapezoidal channel bend with particular emphasis on the outside bank details. The half trapezoidal section was chosen to minimize inside bank effects on the (sloping) outside bank for a restricted flume width. Lateral and longitudinal velocity distributions were measured around a 270° bend. It was found that boundary stresses on the outside bank were significantly higher than in a straight channel and did not diminish until very close to the top of the bank. In addition, flow effects were not found to be qualitatively different between the 2 to 1 and 3 to 1 side slopes studied.

The purpose of the experimental part is not only to fill in some of the missing details of the flow mechanics in the previous research but also to investigate the velocity and shear stress near an outside bank which has larger roughness (simulating rock rip-rap) than the rest of the channel The experimental data will be useful in the development of empirical design relationships, and also to calibrate the numerical models introduced.

2 THEORETICAL ANALYSIS

2.1 **Mathematical Model**

The use of two-dimensional depth-averaged equations for solving flow problems reduces the complexity and cost with little loss in accuracy in certain cases as will be shown hereafter. A brief derivation of the continuity and momentum equations in the depth-averaged model will be given. The depth-averaged moment of momentum equations will also be introduced in this chapter in detail. These equations are derived by integrating the vertical moment of momentum equations over the depth of the flow in a Cartesian coordinate system.

2.1.1 Kinematic Surface and Bed Condition

Consider an arbitrary channel section and define Cartesian coordinates such that x is positive eastward, y positive northward and z positive vertically upward. Figure 2.1 illustrates the notation used.

Boundary conditions are needed when we integrate the three dimensional flow equations. If the equation of boundary F(x,y,z,t)=0 is used to describe every point on the boundary we have

$$\frac{DF}{Dt} = \frac{\partial F}{\partial t} + u\frac{\partial F}{\partial x} + v\frac{\partial F}{\partial y} + w\frac{\partial F}{\partial z} = 0 \qquad (2.1)$$

in which u, v and w are time-averaged velocity components in the x, y and z directions respectively. At the water surface

$$F_h(x,y,z,t) = z - (z_b(x,y) + h(x,y)) \tag{2.2}$$

where h(x,y) is the total depth of flow and $z_b(x,y)$ is the channel bed elevation. Therefore equation (2.1) becomes

$$w_h - \frac{\partial(z_b + h)}{\partial t} - u_h\frac{\partial(z_b + h)}{\partial x} - v_h\frac{\partial(z_b + h)}{\partial y} = 0 \tag{2.3}$$

where the subscript h denotes the surface velocity component. At the channel bottom, the boundary condition is independent of time for a rigid bed channel

$$F_b(x,y,z) = z - z_b(x,y) \tag{2.4}$$

Substituting into (2.1) yields

$$w_b - u_b\frac{\partial z_b}{\partial x} - v_b\frac{\partial z_b}{\partial y} = 0 \tag{2.5}$$

where subscript b refers to the velocity at the channel bed.

Equations (2.3) and (2.5) are the kinematic boundary conditions which will be used in the integration of the continuity and momentum equations.

2.1.2 Continuity and Momentum Equations

The equation for the conservation of mass for incompressible fluid is

$$\frac{\partial u}{\partial x} + \frac{\partial v}{\partial y} + \frac{\partial w}{\partial z} = 0 \qquad (2.6)$$

Integration over the depth gives

$$\int_{z_b}^{z_b+h} \frac{\partial u}{\partial x}\, dz + \int_{z_b}^{z_b+h} \frac{\partial v}{\partial y}\, dz + \int_{z_b}^{z_b+h} \frac{\partial w}{\partial z}\, dz = 0 \qquad (2.7)$$

Interchanging the order of differentiation and integration by Leibnitz' rule for the first two terms in equation (2.7) and evaluating the third term directly yields

$$\frac{\partial}{\partial x}\int_{z_b}^{z_b+h} u\, dz + \frac{\partial}{\partial y}\int_{z_b}^{z_b+h} v\, dz - \left[u_h \frac{\partial (z_b+h)}{\partial x} + v_h \frac{\partial (z_b+h)}{\partial y}\right] + w_h +$$

$$\left[u_b \frac{\partial z_b}{\partial x} + v_b \frac{\partial z_b}{\partial y}\right] - w_b = 0 \qquad (2.8)$$

Applying the kinematic surface condition, equation (2.8) reduces to the form

$$\frac{\partial}{\partial x}\int_{z_b}^{z_b+h} u\, dz + \frac{\partial}{\partial y}\int_{z_b}^{z_b+h} v\, dz = 0 \qquad (2.9)$$

By definition, the depth-averaged velocities, denoted by $\overline{u}$ and $\overline{v}$ are:

$$\overline{u} = \frac{1}{h}\int_{z_b}^{z_b+h} u\,dz \qquad (2.10)$$

and $$\overline{v} = \frac{1}{h}\int_{z_b}^{z_b+h} v\,dz \qquad (2.11)$$

Then equation (2.9) can be rewritten as

$$\frac{\partial(h\overline{u})}{\partial x} + \frac{\partial(h\overline{v})}{\partial y} = 0 \qquad (2.12)$$

This is the depth-averaged continuity equation.

For a turbulent flow of constant density fluid, the Reynold's equations of motion in x, y and z directions are

$$\frac{\partial u^2}{\partial x} + \frac{\partial uv}{\partial y} + \frac{\partial uw}{\partial z} + \frac{1}{\rho}\frac{\partial p_\star}{\partial x} - \frac{1}{\rho}\left[\frac{\partial \tau_{xx}}{\partial x} + \frac{\partial \tau_{xy}}{\partial y} + \frac{\partial \tau_{xz}}{\partial z}\right] = 0 \qquad (2.13)$$

$$\frac{\partial vu}{\partial x} + \frac{\partial v^2}{\partial y} + \frac{\partial vw}{\partial z} + \frac{1}{\rho}\frac{\partial p_\star}{\partial y} - \frac{1}{\rho}\left[\frac{\partial \tau_{yx}}{\partial x} + \frac{\partial \tau_{yy}}{\partial y} + \frac{\partial \tau_{yz}}{\partial z}\right] = 0 \qquad (2.14)$$

$$\frac{\partial wu}{\partial x} + \frac{\partial wv}{\partial y} + \frac{\partial w^2}{\partial z} + \frac{1}{\rho}\frac{\partial p_\star}{\partial z} - \frac{1}{\rho}\left[\frac{\partial \tau_{zx}}{\partial x} + \frac{\partial \tau_{zy}}{\partial y} + \frac{\partial \tau_{zz}}{\partial z}\right] = 0 \qquad (2.15)$$

where τ_{xx}, τ_{xy}, τ_{xz}, τ_{yy}, τ_{yz} and τ_{zz} are the turbulent stresses and p_* is the piezometric pressure defined as the combination of the pressure gradient and gravitational body force,

$$p_* = p_o + \gamma z \tag{2.16}$$

where p_o is the pressure and γ is the specific weight. Equations (2.13) to (2.15) are valid for incompressible flow where the Coriolis force is negligible.

By an order of magnitude analysis, assuming that u, v and w are of the same order, the turbulent shear stresses are negligible, and that the flow depth is small compared with channel width and length, equation (2.15) can be simplified to

$$\frac{\partial w^2}{\partial z} + \frac{1}{\rho}\frac{\partial p_*}{\partial z} = 0 \tag{2.17}$$

In a wide open channel, the vertical velocity w at the sections away from the side wall can be neglected. Equation (2.12) then indicates that the pressure in z direction is hydrostatic:

$$\frac{\partial p_*}{\partial z} = 0 \tag{2.18}$$

Evaluating the piezometric pressure at the water surface, equations (2.13) and (2.14) yield

$$\frac{\partial u^2}{\partial x} + \frac{\partial uv}{\partial y} + \frac{\partial uw}{\partial z} + g\,\frac{\partial (h+z_b)}{\partial x} - \frac{1}{\rho}\left[\frac{\partial \tau_{xx}}{\partial x} + \frac{\partial \tau_{xy}}{\partial y} + \frac{\partial \tau_{xz}}{\partial z}\right] = 0 \tag{2.19}$$

$$\frac{\partial vu}{\partial x} + \frac{\partial v^2}{\partial y} + \frac{\partial vw}{\partial z} + g\,\frac{\partial (h+z_b)}{\partial y} - \frac{1}{\rho}\left[\frac{\partial \tau_{yx}}{\partial x} + \frac{\partial \tau_{yy}}{\partial y} + \frac{\partial \tau_{yz}}{\partial z}\right] = 0 \tag{2.20}$$

Depth averaging equation (2.19) and applying Leibnitz' rule yields

$$\begin{aligned}
&\frac{\partial}{\partial x}\int_{z_b}^{z_b+h} u^2 dz - \frac{\partial (z_b+h)}{\partial x}u^2\Big|_{z_b+h} + \frac{\partial z_b}{\partial x}u^2\Big|_{z_b} + \frac{\partial}{\partial y}\int_{z_b}^{z_b+h} uv dz \\
&- \frac{\partial (z_b+h)}{\partial y}uv\Big|_{z_b+h} + \frac{\partial z_b}{\partial y}uv\Big|_{z_b} + uw\Big|_{z_b+h} - uw\Big|_{z_b} + \\
&gh\,\frac{\partial (h+z_b)}{\partial x} - \frac{\tau_{xz}}{\rho}\Big|_{z_b+h} + \frac{\tau_{xz}}{\rho}\Big|_{z_b} - \frac{\partial}{\partial x}\int_{z_b}^{z_b+h}\frac{\tau_{xx}}{\rho}dz - \\
&\frac{\partial}{\partial y}\int_{z_b}^{z_b+h}\frac{\tau_{xy}}{\rho}dz + \frac{\partial (z_b+h)}{\partial x}\,\frac{\tau_{xx}}{\rho}\Big|_{z_b+h} - \frac{\partial z_b}{\partial x}\,\frac{\tau_{xx}}{\rho}\Big|_{z_b} \\
&+ \frac{\partial (z_b+h)}{\partial y}\,\frac{\tau_{xy}}{\rho}\Big|_{z_b+h} - \frac{\partial z_b}{\partial y}\,\frac{\tau_{xy}}{\rho}\Big|_{z_b} = 0
\end{aligned} \tag{2.21}$$

The last four shear stress terms are negligible since they deal with the horizontal momentum transport across the sloping surface and channel bed. Applying the kinematic surface condition equation (2.21) yields

$$\frac{\partial(h\overline{u^2})}{\partial x} + \frac{\partial(h\overline{uv})}{\partial y} + gh\frac{\partial(h+z_b)}{\partial x} + \frac{\tau_{bx}}{\rho} - \frac{1}{\rho}\frac{\partial(h\overline{\tau_{xx}})}{\partial x} - \frac{1}{\rho}\frac{\partial(h\overline{\tau_{xy}})}{\partial y} = 0 \tag{2.22}$$

where τ_{bx} is the bed shear stress in the xz plane. Depth-averaged quantities are denoted by the overbar and are generally defined as

$$\overline{()} = \frac{1}{h}\int_{z_b}^{z_b+h} ()\,dz \quad . \tag{2.23}$$

The velocities may be expressed by the relations

$$u = \overline{u} + U$$

$$\text{and} \quad v = \overline{v} + V \tag{2.24}$$

where U and V are the velocity deviations defined as the difference between the total velocity component (u,v) at any position and the depth-averaged velocity $(\overline{u},\overline{v})$. By equations (2.10), (2.11), (2.23) and (2.24) we find that

$$\overline{u^2} = \bar{u}\,\bar{u} + \overline{UU} \qquad (2.25)$$

$$\overline{uv} = \bar{u}\,\bar{v} + \overline{UV} \qquad (2.26)$$

and $$\overline{v^2} = \bar{v}\,\bar{v} + \overline{VV} \qquad (2.27)$$

According to expressions (2.25) to (2.27) the x component momentum equation can be expressed as (Rodi 1982)

$$\frac{\partial(h\overline{u^2})}{\partial x} + \frac{\partial(h\bar{u}\,\bar{v})}{\partial y} + gh\frac{\partial(h+z_b)}{\partial x} - \frac{1}{\rho}\frac{\partial(h\overline{\tau_{xx}})}{\partial x} - \frac{1}{\rho}\frac{\partial(h\overline{\tau_{xy}})}{\partial y} + \frac{\tau_{bx}}{\rho}$$

$$+ \frac{\partial(\overline{UU}\,h)}{\partial x} + \frac{\partial(\overline{UV}\,h)}{\partial y} = 0 \qquad (2.28)$$

The depth-averaged turbulent stress terms in the equation above (terms four and five) can be correlated as (Pinder and Gray, 1977)

$$\overline{\tau_{xx}} = \frac{1}{h}\int_{z_b}^{z_b+h} \tau_{xx}\,dz = \rho\nu_t\frac{\partial\bar{u}}{\partial x} \qquad (2.29)$$

$$\overline{\tau_{xy}} = \frac{1}{h}\int_{z_b}^{z_b+h} \tau_{xy}\,dz = \rho\nu_t\frac{\partial\bar{u}}{\partial y} \qquad (2.30)$$

where ν_t is a coefficient of depth-averaged eddy viscosity. In practice, the influence of these turbulent stress terms

$(\tau_{xx}, \tau_{xy}, \tau_{yy})$ is usually very small. However, when the horizontal momentum transported by the turbulent motion is important, as in the case of the flow in curved channel, these terms should be included (ASCE Task Committee on Turbulence Models in Hydraulic Computations, 1988). The inclusion of these terms also has the advantage of improving computational stability. Substitution of (2.29) and (2.30) into (2.28) yields

$$\frac{\partial(h\bar{u}^2)}{\partial x} + \frac{\partial(h\bar{u}\ \bar{v})}{\partial y} + gh\frac{\partial(h+z_b)}{\partial x} - \frac{\partial}{\partial x}(h\nu_t\frac{\partial\bar{u}}{\partial x}) - \frac{\partial}{\partial y}(h\nu_t\frac{\partial\bar{u}}{\partial y})$$

$$+ \frac{\tau_{xb}}{\rho} + \frac{\partial(\overline{UU}h)}{\partial x} + \frac{\partial(\overline{UV}h)}{\partial y} = 0 \qquad (2.31)$$

Similarly, the momentum equation in the y direction is

$$\frac{\partial(h\bar{u}\ \bar{v})}{\partial x} + \frac{\partial(h\bar{v}^2)}{\partial y} + gh\frac{\partial(h+z_b)}{\partial y} - \frac{\partial}{\partial x}(h\nu_t\frac{\partial\bar{v}}{\partial x}) - \frac{\partial}{\partial y}(h\nu_t\frac{\partial\bar{v}}{\partial y})$$

$$+ \frac{\tau_{by}}{\rho} + \frac{\partial(\overline{UV}h)}{\partial x} + \frac{\partial(\overline{VV}h)}{\partial y} = 0 \qquad (2.32)$$

In deriving equations (2.31) and (2.32), two seemingly small, yet very important quantities, U and V, have been introduced. They can be neglected in most computations concerning channels with little curvature. However, in a curved channel, the terms containing U and V may be of the same order of magnitude as the other terms (Flokstra, 1977).

2.1.3 The Depth-averaged Vertical Velocity

To solve for the five unknowns $\overline{u}, \overline{v}$ and h and scales for U and V in the depth-averaged continuity and momentum equations, two extra equations are needed. Before proceeding to derive these two extra equations, multiplying the continuity equation by z and integrating over the depth yields

$$\int_{z_b}^{z_b+h} \frac{\partial uz}{\partial x}\,dz + \int_{z_b}^{z_b+h} \frac{\partial vz}{\partial y}\,dz + \int_{z_b}^{z_b+h} \frac{\partial w}{\partial z}\,dz - \int_{z_b}^{z_b+h} w\,dz = 0 \qquad (2.33)$$

Applying the Leibnitz' rule gives

$$\frac{\partial(h\overline{zu})}{\partial x} + \frac{\partial(h\overline{zv})}{\partial y} - h\overline{w} = 0 \qquad (2.34)$$

According to (2.10), (2.11), (2.23) and (2.24) the following relationships hold

$$\overline{zu} = \overline{z}\;\overline{u} + \overline{zU} \qquad (2.35)$$

and $$\overline{zv} = \overline{z}\;\overline{v} + \overline{zV} \qquad (2.36)$$

Substitution of (2.35), (2.36) in (2.34) gives

$$h\bar{w} = \frac{\partial(h\overline{zU})}{\partial x} + \frac{\partial(h\overline{zV})}{\partial y} + \bar{u}\,h\frac{\partial\bar{z}}{\partial x} + \bar{v}\,h\frac{\partial\bar{z}}{\partial y} \qquad (2.37)$$

Equation (2.37) gives the relation for $\bar{w}$ in terms of U,V which will be used later in the deriving the moment of momentum equations.

2.1.4 The Moment of Momentum Equations

The $\overline{UU}$ type of terms in the depth-averaged momentum equations (2.31) and (2.32) are very important especially for flow in curved channels. These terms transfer energy out of the circulating flow while the turbulent stresses are transferring energy to the circulating flow as stated by Flokstra. The order of magnitude of these terms has been estimated roughly equal to $0.02U_o^2$, U_o being the main flow velocity. The choice of the closure model for these terms has been investigated (Flokstra, 1977; Kalkwijk and De Vriend, 1980).

Flokstra suggests that $\overline{UV}$ can be modeled by a factor α times $\bar{u}$ and $\bar{v}$, where α depends on the velocity profile, flow depth and the curvature. The use of the Cartesian coordinate system in the momentum equations, (2.31) and (2.32), is to set up a general formulation for solving the secondary flow problem because Flokstra's formula requires that the curvature be known, which the present model tries to avoid.

Kalwkijk and De Vriend (1980) use a constant k_{sn} times the centrifugal acceleration and local flow depth to present $\overline{UU}$ type terms in the momentum equations. The curvilinear coordinate system was used. Their model tends to underestimate the secondary flow in the outer bend and overestimate the flow depth at the entrance of the bend. The bend curvature is also required as the curvilinear coordinate systems is used.

Falcon Ascanio (1979) derived the moment of momentum equation from a control volume method in a cylindrical coordinate system. The equation is based on the equilibrium between the torque of the surface and body force acting on a control volume and the moment of momentum flux acting on the control volume surface. Another approach is to integrate the vertical moment (multiplied by z) of the momentum equations over the depth of flow. The moment of momentum equation in x direction is

$$z\frac{\partial u^2}{\partial x} + z\frac{\partial uv}{\partial y} + z\frac{\partial uw}{\partial z} + \frac{z}{r}\frac{\partial p_*}{\partial x} - \frac{z}{\rho}\left[\frac{\partial \tau_{xx}}{\partial x} + \frac{\partial \tau_{xy}}{\partial y} + \frac{\partial \tau_{xz}}{\partial z}\right] = 0 \quad (2.38)$$

or

$$\frac{\partial u^2 z}{\partial x} + \frac{\partial uvz}{\partial y} + \frac{\partial uwz}{\partial z} - w + \frac{1}{\rho}\frac{\partial p_* z}{\partial x}$$

$$-\frac{1}{\rho}\left[\frac{\partial\tau_{xx}z}{\partial x} + \frac{\partial\tau_{xy}z}{\partial y} + \frac{\partial\tau_{xz}z}{\partial z}\right] + \frac{\tau_{xz}}{\rho} = 0 \qquad (2.39)$$

Depth averaging and applying Leibnitz' rule together with the surface condition and hydrostatic assumption, leads to

$$\frac{\partial h\overline{zu^2}}{\partial x} + \frac{\partial h\overline{zuv}}{\partial y} - h\overline{uw} + \bar{z}gh\frac{\partial(h+z_b)}{\partial x} - \frac{1}{\rho}\frac{\partial(h\overline{\tau_{xx}z})}{\partial x} + \frac{1}{\rho}\frac{\partial(h\overline{\tau_{xy}z})}{\partial y}$$

$$+ \frac{1}{\rho}\tau_{bx}z_b + \frac{1}{\rho}\overline{\tau_{xz}}\,h = 0 \qquad (2.40)$$

Integration of the non-linear equation introduces additional unknowns. Since the objective is to use these equations to estimate corrections to the depth-averaged equations, an approximate solution is adequate. The depth-averaged terms can be evaluated by the following assumptions.

$$\overline{zuu} = \bar{z}\,\bar{u}\,\bar{u} + 2\bar{u}\,\overline{zU} + \overline{zUU} \cong \bar{z}\,\bar{u}\,\bar{u} + 2\bar{u}\,\overline{zU} \qquad (2.41)$$

$$\overline{zuv} = \bar{z}\,\bar{u}\,\bar{v} + \bar{u}\,\overline{zV} + \bar{v}\,\overline{zU} + \overline{zUV}$$

$$\cong \bar{z}\,\bar{u}\,\bar{v} + \bar{u}\,\overline{zV} + \bar{v}\,\overline{zU} \qquad (2.42)$$

$$\frac{1}{\rho}\frac{\partial(h\overline{\tau_{xx}z})}{\partial x} \cong \frac{1}{\rho}\frac{\partial}{\partial x}(h\overline{\tau_{xx}}\,\bar{z}) = \frac{\bar{z}}{\rho}\frac{\partial(h\overline{\tau_{xx}})}{\partial x} + \frac{1}{\rho}h\overline{\tau_{xx}}\frac{\partial\bar{z}}{\partial x} \qquad (2.43)$$

$$\frac{1}{\rho}\frac{\partial(h\overline{\tau_{xy}z})}{\partial y} \cong \frac{1}{\rho}\frac{\partial}{\partial y}(h\overline{\tau_{xy}}\ \bar{z}) = \frac{\bar{z}}{\rho}\frac{\partial(h\overline{\tau_{xy}})}{\partial y} + \frac{1}{\rho}h\overline{\tau_{xy}}\frac{\partial\bar{z}}{\partial y} \qquad (2.44)$$

$$\overline{uw} = \bar{u}\ \bar{w} + \overline{UW} \cong \bar{u}\ \bar{w} \qquad (2.45)$$

and

$$\bar{z} = z_b + \frac{h}{2} \qquad (2.46)$$

In the above expressions, the quantities $\overline{zUU}$, $\overline{zUV}$ and $\overline{zVV}$ are assumed to be small compared with the other terms and will be discarded from the equations. A similar assumption can be applied to the $\overline{UW}$ term in (2.46). Since $\overline{\tau_{xx}}$ and $\overline{\tau_{xy}}$ are small, the assumptions used in (2.43) and (2.44) are adequate.

Substituting (2.41) to (2.46) into (2.40) and subtracting the momentum equation (2.31) multiplied by $\bar{z}$, the depth-averaged moment of momentum equations can be written as

$$\frac{\partial(\bar{u}\ \overline{zU}\ h)}{\partial x} + \frac{\partial(\bar{v}\ \overline{zU}\ h)}{\partial y} + \overline{zU}\ h\frac{\partial\bar{u}}{\partial x} + \overline{zV}\ h\frac{\partial\bar{u}}{\partial y} - \frac{\tau_{bx}h}{2\rho} + \frac{h\overline{\tau_{xz}}}{\rho}$$

$$- \frac{1}{\rho}h\overline{\tau_{xx}}\frac{\partial\bar{z}}{\partial x} - \frac{1}{\rho}h\overline{\tau_{xy}}\frac{\partial\bar{z}}{\partial y} = 0 \qquad (2.47)$$

Similarly, y-component moment of momentum equation can be derived as

$$\frac{\partial(\bar{u}\ \overline{zV}\ h)}{\partial x} + \frac{\partial(\bar{v}\ \overline{zV}\ h)}{\partial y} + \overline{zU}\ h\frac{\partial\bar{v}}{\partial x} + \overline{zV}\ h\frac{\partial\bar{v}}{\partial y} - \frac{\tau_{by}h}{2\rho} + \frac{h\overline{\tau_{yz}}}{\rho}$$

$$- \frac{1}{\rho} \overline{h\tau_{xy}} \frac{\partial \bar{z}}{\partial x} - \frac{1}{\rho} \overline{h\tau_{yy}} \frac{\partial \bar{z}}{\partial y} = 0 \qquad (2.48)$$

The moment of momentum equations derived differ significantly from the approach used by Falcon Ascanio. His derivation was based on the cylindrical coordinate system. The $\overline{vw}$, $\overline{\tau_{yz}}$ and $\overline{zvv}$ terms are neglected since they are small compared to the centrifugal force. However, these simplifications cannot be made for the equations in Cartesian coordinate system.

In equations (2.47) and (2.48), $\overline{zU}$ and $\overline{zV}$ are considered as dependent variables and the equations can be solved for them given $\bar{u}$, $\bar{v}$ and h. However, U and V are still needed in order to evaluate the $\overline{UU}$ type terms in equations (2.31) and (2.32). Therefore a relationship between the velocity moments and the velocity deviation correlations is required.

2.1.5 Reduction of the Governing Equations

In order to evaluate U and V in momentum equations, define the following similarity expressions for u and v as

$$u = \bar{u} F + u_s G \qquad (2.49)$$

$$v = \bar{v} F + v_s G \qquad (2.50)$$

where F and G are velocity profile functions of longitudinal and secondary flow respectively, and u_s and v_s are the surface velocities of the secondary flow. Note that secondary flows in both directions are allowed. Therefore $\overline{UV}$ can be computed from

$$\overline{UV} = \frac{1}{h}\int_{z_b}^{z_b+h} (u - \overline{u})(v - \overline{v})dz = \overline{u}\ \overline{v}\int_0^1 (F - 1)^2 d\eta$$

$$+ u_s\ v_s\int_0^1 G^2 d\eta + (u_s\overline{v} + v_s\overline{u})\int_0^1 (F - 1)G d\eta$$

$$= \overline{u}\ \overline{v}\ I_1 + u_s\ v_s\ I_2 + (u_s\overline{v} + v_s\overline{u})\ I_3 \qquad (2.51)$$

where η is the non-dimensional vertical coordinate

$$\eta = \frac{z - z_b}{h} \qquad (2.52)$$

and

$$I_1 = \int_0^1 (F - 1)^2\, d\eta \qquad (2.53)$$

$$I_2 = \int_0^1 G^2\, d\eta \qquad (2.54)$$

$$I_3 = \int_0^1 (F - 1)G\, d\eta \tag{2.55}$$

Substituting equations (2.49) and (2.50) into $\overline{VV}$, $\overline{UV}$, $\overline{zU}$ and $\overline{zV}$ and integrating over the depth result in

$$\overline{UU} = \bar{u}^2 I_1 + u_s^2 I_2 + 2u_s\bar{u}\, I_3 \tag{2.56}$$

$$\overline{VV} = \bar{v}^2 I_1 + v_s^2 I_2 + 2v_s\bar{v}\, I_3 \tag{2.57}$$

$$\overline{zU} = h\,\bar{u}\, I_4 + h\, u_s I_5 \tag{2.58}$$

$$\overline{zV} = h\,\bar{v}\, I_4 + h\, v_s I_5 \tag{2.59}$$

in which

$$I_4 = \int_0^1 (F - 1)\eta\, d\eta \tag{2.60}$$

$$I_5 = \int_0^1 G\eta\, d\eta \tag{2.61}$$

Substituting equations (2.51), (2.56) and (2.57) into momentum equations, we obtain

$$\frac{\partial(h\bar{u}^2)}{\partial x} + \frac{\partial(h\bar{u}\,\bar{v})}{\partial y} + gh\frac{\partial(h+z_b)}{\partial x} - \frac{\partial}{\partial x}\left(h\nu_t\frac{\partial\bar{u}}{\partial x}\right) - \frac{\partial}{\partial y}\left(h\nu_t\frac{\partial\bar{u}}{\partial y}\right) +$$
$$\frac{\tau_{bx}}{\rho} + \frac{\partial}{\partial x}(\bar{u}^2 I_1 + u_s^2 I_2 + 2u_s\bar{u} I_3)h + \frac{\partial}{\partial y}(\bar{u}\,\bar{v} I_1 +$$
$$u_s v_s I_2 + (u_s\bar{v} + v_s\bar{u}) I_3)h = 0 \tag{2.62}$$

$$\frac{\partial(h\bar{u}\ \bar{v})}{\partial x} + \frac{\partial(h\bar{v}^2)}{\partial y} + gh\frac{\partial(h+z_b)}{\partial y} - \frac{\partial}{\partial x}(h\nu_t\frac{\partial\bar{v}}{\partial x}) - \frac{\partial}{\partial y}(h\nu_t\frac{\partial\bar{v}}{\partial y}) +$$

$$\frac{\tau_{by}}{\rho} + \frac{\partial}{\partial x}(\bar{u}\ \bar{v}\,I_1 + u_s v_s I_2 + (u_s\bar{v} + v_s\bar{u})\,I_3)h +$$

$$\frac{\partial}{\partial y}(\bar{v}^2 I_1 + v_s^2 I_2 + 2v_s\bar{v}I_3)h = 0 \qquad (2.63)$$

Thus the system of equations (2.12), (2.62), (2.63), (2.47) and (2.48) can be solved when functions F and G and relationships for bed shear stress τ_{bx} ,τ_{by} are provided. Functions F and G can be estimated from the experimental data.

2.1.6 Velocity Functions

According to equations (2.49) and (2.50), the velocity distribution should be described in both longitudinal and lateral directions. The traditional power law can be written as (Zimmermann and Kennedy, 1978)

$$F(\eta) = \frac{m+1}{m}\left(\frac{z - z_b}{h}\right)^{\frac{1}{m}} = \frac{m+1}{m}\,\eta^{\frac{1}{m}} \qquad (2.64)$$

in which $m = \kappa C_*$, κ = von Karman's constant (≅0.4) and C_* is the dimensionless Chezy coefficient. The simple linear secondary flow profile in the curved channel may be used as the G function (Odgaard, 1986),

$$G(\eta) = \frac{2(z - z_b)}{h} - 1 = 2\eta - 1 \tag{2.65}$$

Other assumptions for these profiles are possible but these are selected for simplicity and ease of implementation. According to equations (2.64) and (2.65), equation (2.49) will give a longitudinal velocity profile in the straight channel when $u_s = 0$, and in a curved channel the equation will give a transverse velocity profile when the depth-averaged transverse velocity is nearly zero.

2.1.7 Shear Stress Model

The bottom stresses τ_{bx} and τ_{by} are generally expressed as (Pinder and Gray, 1977)

$$\tau_{bx} = \frac{\rho(\bar{u}^2 + \bar{v}^2)^{1/2}\,\bar{u}}{C_*^{\,2}} \tag{2.66}$$

$$\tau_{by} = \frac{\rho(\bar{u}^2 + \bar{v}^2)^{1/2}\,\bar{v}}{C_*^{\,2}} \tag{2.67}$$

These forms of the equations are usually used for flow calculation in estuaries and coastal regions where the secondary flow is negligible. For the computation of curved channel problems, the secondary flow effect on the bed shear stress should be included. Therefore equations (2.66) and (2.67) can be modified as follows,

$$\tau_{bx} = \frac{\rho(\bar{u}^2 + \bar{v}^2)^{1/2}\ (\bar{u} + k_* u_s)}{C_*^{\,2}} \tag{2.68}$$

$$\tau_{by} = \frac{\rho(\bar{u}^2 + \bar{v}^2)^{1/2}\ (\bar{v} + k_* v_s)}{C_*^{\,2}} \tag{2.69}$$

where $k_* u_s$ and $k_* v_s$ represent the effective secondary flow velocity near the bed. Since u_s and v_s are surface velocities, k_* should be a negative number of order unity.

k_* can be estimated from fully developed flow in a constant radius of curvature channel considerations. The flow direction close to the curved channel bed can be determined from the longitudinal and transverse velocities. If the angle of the bed shear stress coincides with the angle of the velocity vector near the bed, the following relationship holds (Engelund, 1974)

$$\tan \phi = \frac{\tau_{br}}{\tau_{b\theta}} \tag{2.70}$$

where $\tau_{b\theta}$ and τ_{br} are the bed shear stress in the tangential and radial directions respectively, and ϕ is the angle between these velocity vectors. The radial shear stress can be expressed as (Zimmermann, 1977)

$$\tau_{br} = \frac{\rho}{3}\,\frac{m+1}{m(m+2)}\,\frac{h}{r}\,\overline{u_\theta}^{2} \tag{2.71}$$

in which $\overline{u}_\theta$ is the depth-averaged velocity in the tangential direction and r is the radius of curvature. The tangential shear stress may be expressed as

$$\tau_{b\theta} = \frac{\rho\overline{u_\theta}^{2}}{C_*^{2}} \tag{2.72}$$

Substituting (2.71) and (2.72) into (2.70) yields

$$\tan\phi = \frac{m(m+1)}{3\kappa^{2}(m+2)}\,\frac{h}{r} \tag{2.73}$$

Also from the analysis of the developed secondary flow in a curved open channel in a cylindrical coordinate system, the transverse surface velocity can be expressed as (Steffler, 1984)

$$v_r = \frac{\overline{u}_\theta h}{r}\int\frac{1}{f_2}\left\{\int\left[-2f_1 - \frac{1}{C_*}\left(f_1^{2} - \overline{f_1^{2}} - \frac{r}{h}\tan\phi\right)\right]d\eta + C_1\right\}d\eta + C_2 \tag{2.74}$$

$$f_1 = \frac{u_\theta - \overline{u}_\theta}{u_*} \tag{2.75}$$

$$f_2 = \frac{\nu_t}{u_* h} \tag{2.76}$$

In these equations, u_* is the longitudinal shear velocity and C_1 and C_2 are constants of integration. The boundary conditions for the above set of equations for fully developed flow are zero shear stress at the water surface and zero net lateral discharge. When the power law is chosen as the longitudinal velocity distribution and a parabolic eddy viscosity distribution is assumed, v_r is given by the expression

$$v_r = \frac{\bar{u}_\theta h}{r} \frac{(m+1)^2}{\kappa^2 (m+2)} I_m(\eta) \tag{2.77}$$

where

$$I_m(\eta) = \int \frac{1 - \eta^{2/m}}{1 - \eta} d\eta - \iint_0^1 \frac{1 - \eta^{2/m}}{1 - \eta} d\eta \tag{2.78}$$

The numerical values of I_m for different values of m are plotted in figure 2.2. Replacing τ_{bx} and τ_{by} in equations (2.68) and (2.69) with $\tau_{b\theta}$ and τ_{br} respectively, the following relation holds :

$$\tan \phi = \frac{\tau_{br}}{\tau_{b\theta}} = \frac{k_* v_{rs}}{\bar{u}_\theta} \tag{2.79}$$

where v_{rs} is the surface velocity in the transverse direction. Combining (2.73), (2.77) and (2.79) yields

$$k_* = \frac{m}{3(m+1)} \frac{1}{I_{m_{\text{at } \eta=1}}} \tag{2.80}$$

Figure 2.3 shows the variation of the k_* value. Thus the problem can be solved when all the coefficients and functions are provided.

To recover the secondary flow components from the vertical moments, u_s and v_s can be expressed in terms of $\overline{zU}h$ and $\overline{zV}h$. Rearranging equations (2.58) and (2.59), u_s and v_s become:

$$u_s = \frac{\overline{zU}\,h - h^2 \bar{u}\, I_4}{h^2 I_5} \tag{2.81}$$

$$v_s = \frac{\overline{zV}\,h - h^2 \bar{v}\, I_4}{h^2 I_5} \tag{2.82}$$

Substituting (2.81) and (2.82) into equations (2.62) and (2.63), the moment of momentum equations can be solved for $\overline{zU}h$ and $\overline{zV}h$.

2.1.8 Boundary Conditions

The equations discussed above can be solved with the appropriate boundary conditions (Pinder and Gray, 1977). Two different types of boundaries are possible: wall boundaries where velocities, including the secondary flows, are set to zero; and boundaries where inflow and outflow conditions are set. On the inflow and outflow boundaries, either velocity or flow depth, or a relation between them such as a discharge curve or rating curve, should be specified. Similarly the surface velocities, u_s and v_s, should be specified at the inflow and outflow boundaries. Since $\overline{zU}h$ and $\overline{zV}h$ are the variables to be solved for in the moment of momentum equations, boundary conditions for $\overline{zU}h$ and $\overline{zV}h$ are calculated from given $\bar{u}$, $\bar{v}$, h, u_s and v_s at the boundaries.

2.1.9 Summary

Finally, the equations to be solved are:

$$\frac{\partial(h\bar{u})}{\partial x} + \frac{\partial(h\bar{v})}{\partial y} = 0 \qquad (2.83)$$

$$\frac{\partial(h\bar{u}^2)}{\partial x} + \frac{\partial(h\bar{u}\,\bar{v})}{\partial y} + gh\frac{\partial(h+z_b)}{\partial x} - \frac{\partial}{\partial x}(h\nu_t\,\frac{\partial\bar{u}}{\partial x}) - \frac{\partial}{\partial y}(h\nu_t\,\frac{\partial\bar{u}}{\partial y}) +$$

$$\frac{(\bar{u}^2 + \bar{v}^2)^{1/2}(\bar{u} + k_\star u_s)}{C_\star^{\,2}} + \frac{\partial}{\partial x}(\bar{u}^2 I_1 + u_s^2 I_2 + 2u_s\bar{u} I_3)h +$$

$$\frac{\partial}{\partial y}(\bar{u}\,\bar{v} I_1 + u_s v_s I_2 + (u_s\bar{v} + v_s\bar{u}) I_3)h = 0 \qquad (2.84)$$

$$\frac{\partial(h\bar{u}\,\bar{v})}{\partial x} + \frac{\partial(h\bar{v}^2)}{\partial y} + gh\frac{\partial(h+z_b)}{\partial y} - \frac{\partial}{\partial x}(h\nu_t\frac{\partial\bar{v}}{\partial x}) - \frac{\partial}{\partial y}(h\nu_t\frac{\partial\bar{v}}{\partial y}) +$$

$$\frac{(\bar{u}^2 + \bar{v}^2)^{1/2} \ (\bar{v} + k_\star v_s)}{C_\star^{\,2}} + \frac{\partial}{\partial x}(\bar{u}\,\bar{v}\,I_1 + u_s v_s I_2 +$$

$$(u_s\bar{v} + v_s\bar{u})\,I_3)h + \frac{\partial}{\partial y}(\bar{v}^2 I_1 + v_s^2 I_2 + 2v_s\bar{v}\,I_3)h = 0 \quad (2.85)$$

$$\frac{\partial(\bar{u}\,\overline{zU}h)}{\partial x} + \frac{\partial(\bar{v}\,\overline{zU}h)}{\partial y} + \overline{zU}h\frac{\partial\bar{u}}{\partial x} + \overline{zV}h\frac{\partial\bar{u}}{\partial y} - h\nu_t\frac{\partial\bar{u}}{\partial x}\frac{\partial\bar{z}}{\partial x} - h\nu_t\frac{\partial\bar{u}}{\partial y}\frac{\partial\bar{z}}{\partial y} +$$

$$2\nu_t\frac{\overline{zU}h - \bar{u}h^2 I_4}{h^2 I_5} - \frac{(\bar{u}^2 + \bar{v}^2)^{1/2}}{2C_\star^{\,2}}(\bar{u}h + k_\star\frac{\overline{zU}h - \bar{u}h^2 I_4}{h^2 I_5}) = 0 \quad (2.86)$$

$$\frac{\partial(\bar{u}\,\overline{zV}h)}{\partial x} + \frac{\partial(\bar{v}\,\overline{zV}h)}{\partial y} + \overline{zU}h\frac{\partial\bar{v}}{\partial x} + \overline{zV}h\frac{\partial\bar{v}}{\partial y} - h\nu_t\frac{\partial\bar{v}}{\partial x}\frac{\partial\bar{z}}{\partial x} - h\nu_t\frac{\partial\bar{v}}{\partial y}\frac{\partial\bar{z}}{\partial y} +$$

$$2\nu_t\frac{\overline{zV}h - \bar{v}h^2 I_4}{h^2 I_5} - \frac{(\bar{u}^2 + \bar{v}^2)^{1/2}}{2C_\star^{\,2}}(\bar{v}h + k_\star\frac{\overline{zV}h - \bar{v}h^2 I_4}{h^2 I_5}) = 0 \quad (2.87)$$

2.2 Simple Model

Before transforming the mathematical model into numerical form, a simple analysis in a cylindrical coordinate system is valuable to prove that the use of the moment of momentum equation and that the effective constant $k_\star$ is adequate.

2.2.1 Simple model

Considering a wide rectangular open channel, the momentum equation in the radial direction for flow in a bend can be reduced to (Yen, 1965)

$$-\frac{u^2}{r} + \frac{1}{\rho}\frac{\partial p_*}{\partial y} - \frac{1}{\rho}\frac{\partial \tau_{yz}}{\partial z} = 0 \qquad (2.88)$$

The cylindrical coordinate system was used, x and y are coordinates in tangential and radial directions and u, v are velocities in each directions.

Integrating equation (2.88) over the total depth and assuming a hydrostatic pressure distribution yields

$$-\frac{h\overline{u^2}}{r} + gh\frac{\partial (h+z_b)}{\partial y} + \frac{\tau_{by}}{\rho} = 0 \qquad (2.89)$$

where τ_{by} is the bed shear stress in the radial direction, z_b is the distance from reference datum and h is local flow depth as defined before. Substituting (2.25) into (2.89), the depth-averaged momentum equation in the radial direction becomes

$$-\frac{1}{r}(h\overline{u^2} + \overline{hUU}) + gh\frac{\partial (h+z_b)}{\partial y} + \frac{\tau_{by}}{\rho} = 0 \qquad (2.90)$$

The moment of momentum equation can be obtained by depth averaging equation (2.88), the momentum equation multiplied by z. The depth-averaged moment of momentum equation in the radial direction then is

$$- \frac{h\overline{zu^2}}{r} + \bar{z}\, gh \frac{\partial (h+z_b)}{\partial y} + \frac{1}{\rho} \tau_{by} z_b + \frac{1}{\rho} \overline{\tau_{yz}}\, h = 0 \qquad (2.91)$$

Substituting (2.41) and (2.90) into (2.91) yields

$$\overline{zU} = \frac{r}{2\rho\bar{u}} \left(\overline{\tau_{yz}} - \frac{\tau_{by}}{2} \right) \qquad (2.92)$$

Using the velocity profiles introduced in section 2.1.6, equations (2.49), (2.50), (2.64) and (2.65), and assuming u_s and $\bar{v}$ are small in curved channels

$$u = \bar{u} \frac{m+1}{m} \eta^{\frac{1}{m}} \qquad (2.93)$$

$$v = v_s (2\eta - 1) \qquad (2.94)$$

Therefore $\overline{zU}$ can be computed from

$$\overline{zU} = \frac{1}{h} \int_{z_b}^{z_b+h} (u - \bar{u}) z dz = \frac{\bar{u}h}{2(2m+1)} \qquad (2.95)$$

The shear stress and k_* value can be obtained through the procedure illustrated in section 2.1.7. A simple turbulent model and constant eddy viscosity (Engelund 1974) may be used

$$\overline{\tau_{yz}} = \frac{1}{h}\int_{z_b}^{z_b+h} \rho\nu_t \frac{\partial v}{\partial z}dz = \frac{2\rho\nu_t\ v_s}{h} \qquad (2.96)$$

$$\nu_t = 0.077u_*h \qquad (2.97)$$

Substituting (2.96), (2.97) and (2.68) into (2.92), the secondary surface velocity may be calculated by

$$v_s = \frac{h\bar{u}C_*}{(2m+1)r}\ \frac{1}{(0.154 - \frac{k_*}{2C_*})} \qquad (2.98)$$

2.2.2 Comparison and Discussion

The experimental results obtained by Steffler (1984), De Vriend (1976,78) and Yen (1965) were used here to compare with the simple model introduced above.

2.2.2.1 Steffler's Experiments

The experimental study was conducted using the Laser Doppler Anemometer (LDA) system available in the T. Blench Hydraulic Laboratory of the University of Alberta. Detailed velocity and turbulence measurements were made in a 270 degree smooth boundary channel bend. The flume was rectangular in shape, 1.07m wide, 0.20m deep and the radius of curvature to the centreline of the section was 3.66m. The experiment was done using two different flow depths: 0.061m in run 1 and 0.085m in run 2. The centreline bed slope was set at 0.00083. Figure 2.4 shows the flume and locations of measurement stations used in this experiment.

The flow direction close to the curved channel bed can be determined from the longitudinal and transverse velocities. If the angle of the bed shear stress coincides with the angle of the velocity vector near the bed, the k_* value can be calculated from the measured velocities and bed shear stress angle ϕ as

$$k_* = \frac{\tan\phi\bar{u}}{v_s} \qquad (2.99)$$

Figure 2.5 illustrates the variation of bed shear stress angle ϕ for run 1. Through the bend the angle ϕ is not a constant at the same radius since the flow is not fully developed. Figure 2.6 shows the variation of k_* for run 1. The cross channel distance y has been non-dimensionalized by the channel half width b. The k_* values shown were not constant, as the equation (2.80) illustrated that the $\tan\phi$ varied along the channel. Therefore the plot shows that k_* value is in the range of -1.5 to -2.5.

Figure 2.7 compares results for the surface velocity in the transverse direction. The agreement between the measured and theoretical velocities is fair in general. The model predicts particularly well for the profiles away from the side walls. Since the depth-averaged model is limited to wide open channels, the discrepancies near the wall are to be expected. This can also be explained as a consequence of the linear function used in modelling the secondary flow motion (equation 2.65). Despite the above discrepancy, the equation still predicts satisfactorily the surface velocity at the inside bank and the velocity close to the bed at the outside bank.

2.2.2.2 De Vriend's Experiments

De Vriend (1976) performed an experiment for the flow of water in a curved open channel with a fixed uneven bed. Figure 2.8 shows the plan view of the 90° curved flume. The flume consists of a 39m straight reach and a curve with a radius of 50m (to the centreline). The channel is 6m wide and had variable shape, cross-sections A_0 to B_0 are parabolic shape with zero longitudinal bed slope and cross-sections C_1 to E_0 are triangular shape with an average slope of 0.0003. The sections between B_0 to C_1 are a smooth transition zone. The geometry of these sections are plotted in figure 2.9. Two runs were conducted in the experiment, with discharges of $0.61m^3/s$ and $0.305m^3/s$. Due to the limited data available in the report, the transverse surface velocity was compared only at the section where $\theta=55^o$. Figure 2.10 shows this comparison: the agreement is fairly reasonable.

De Vriend (1978) performed a similar experiment using a similar channel of rectangular cross-section. The prediction compares reasonably well with the experimental result as shown in figure 2.11.

2.2.2.3 Yen's Experiments

Yen (1965) conducted a series of experiments to study the velocity and shear stress in curved open channels. The flume consisted of two 90° bends of 28 feet centreline radius connected in reverse direction. The run with u_o=2.27 ft/s was selected to make the comparison of the radial shear stress. Figure 2.12 shows a good match for bed shear stress in centreline of the channel between the experimental result and calculation by equation (2.71) using experimental $\overline{u}$ and v_s. This comparison also shows the use of k_* for calculating radial shear stress is reasonable.

2.2.3 Conclusion

The effect of the secondary flow on the bed shear stress was evaluated well by the variable k_*, channel roughness, depth-averaged velocity components and surface velocity of the secondary flow. The variable k_* can be estimated by the channel roughness and secondary velocity.

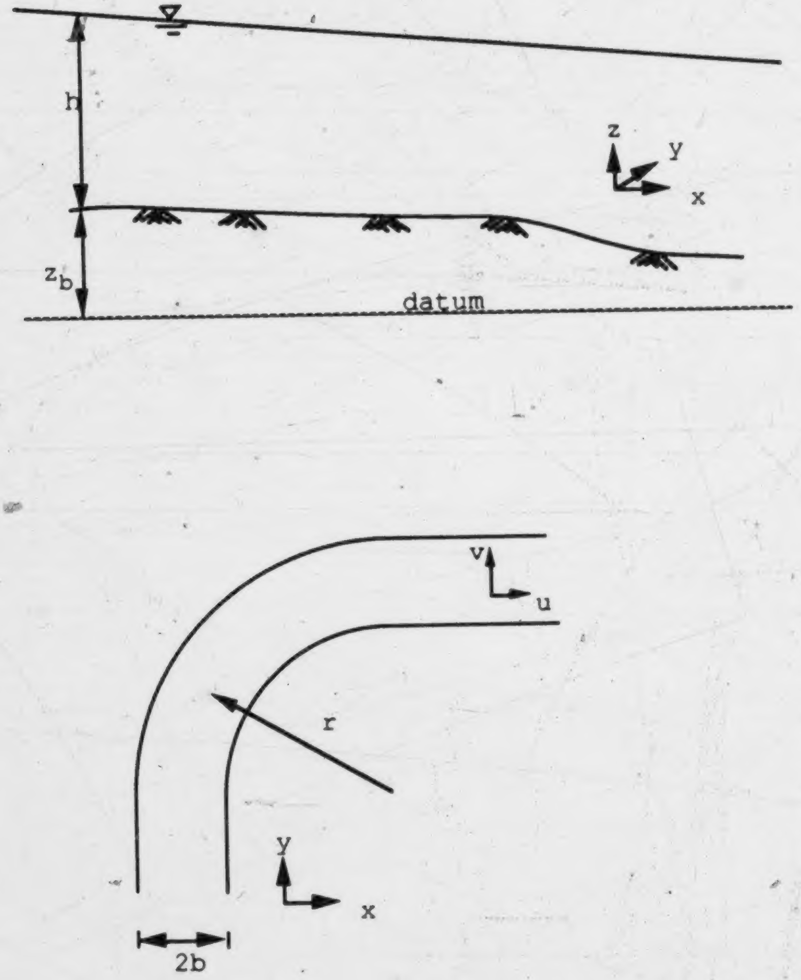
h
z
y
x
z_b
datum
v
u
r
y
x
2b

Figure 2.1 Coordinate definition

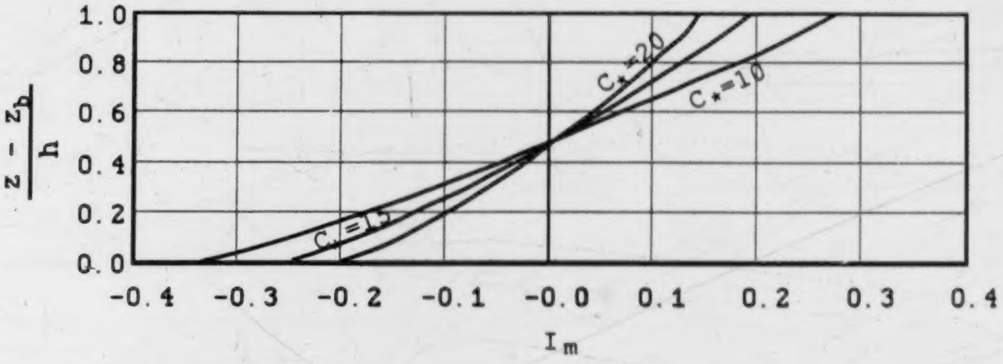

Figure 2.2 Variation of I_m

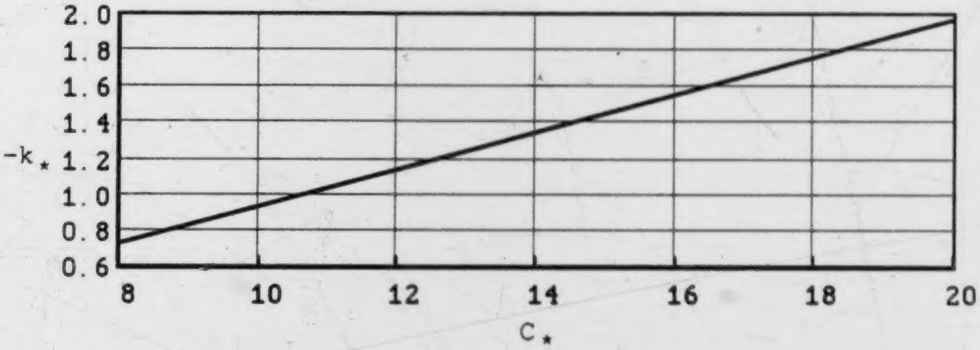

Figure 2.3 Variation of k_*

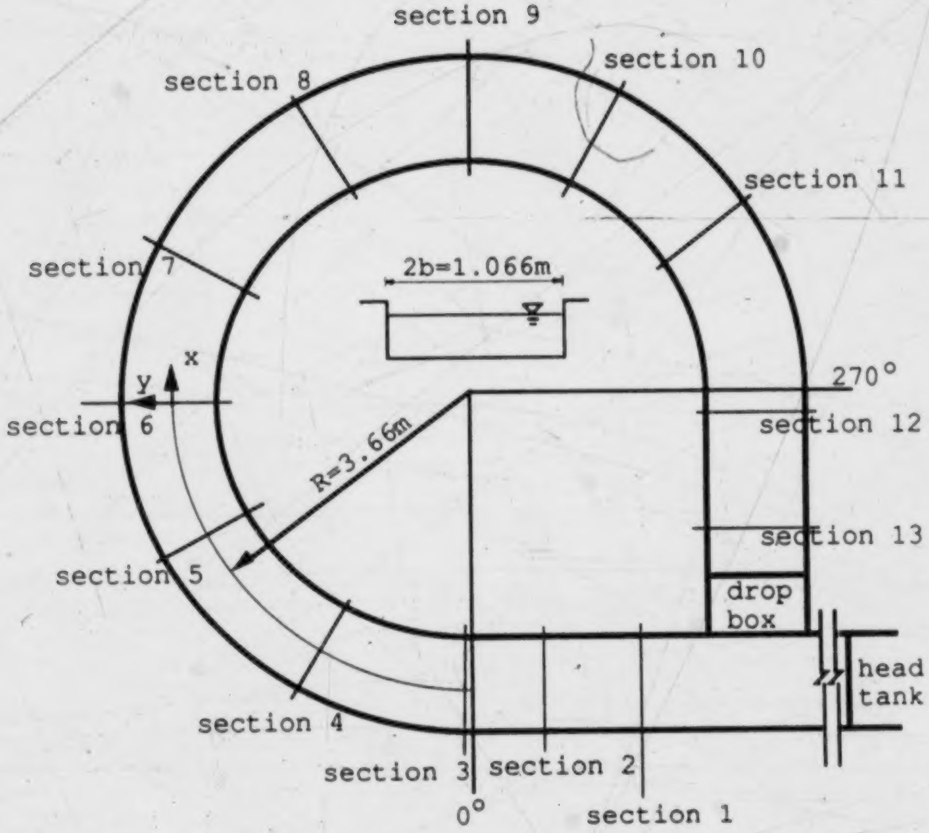
section 9
section 10
section 8
section 11
section 7
2b=1.066m
x
y
270°
section 6
section 12
R=3.66m
section 13
section 5
drop box
head tank
section 4
section 3
section 2
0°
section 1

Figure 2.4 The layout of Steffler's experiment (Steffler, 1984)

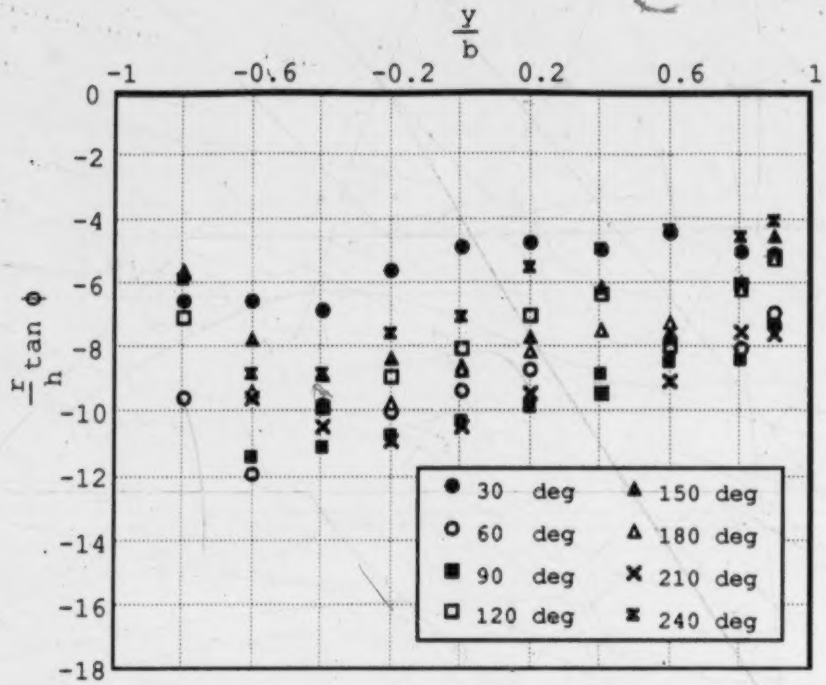

Figure 2.5 Variation of bed shear stress angle φ (experimental data)

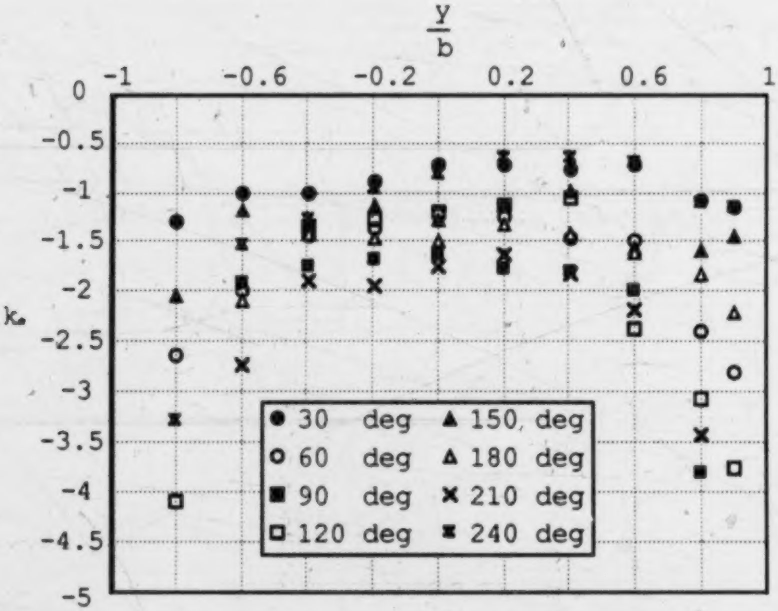

Figure 2.6 Variation of k_* (experimental data)

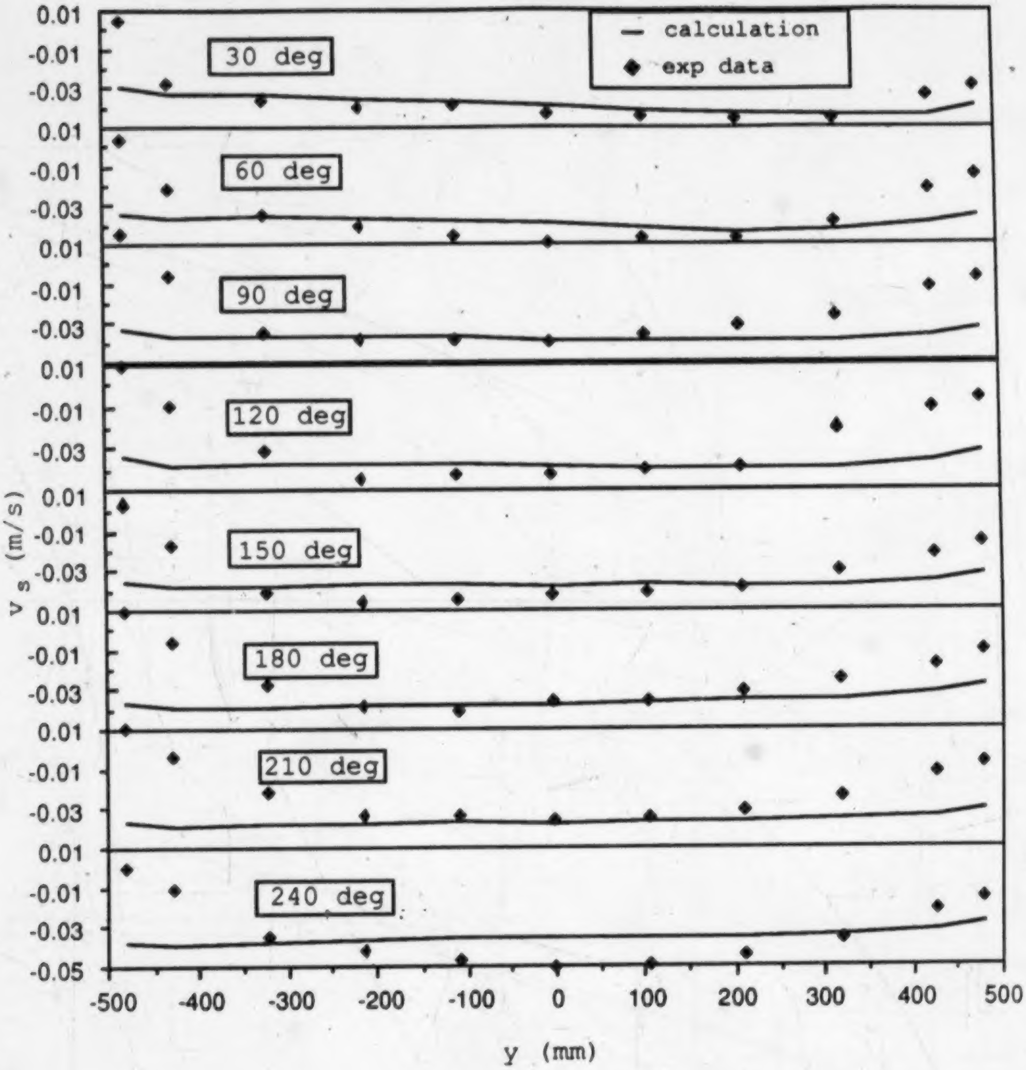

Figure 2.7 The comparison of transverse surface velocity for Steffler's experimental data

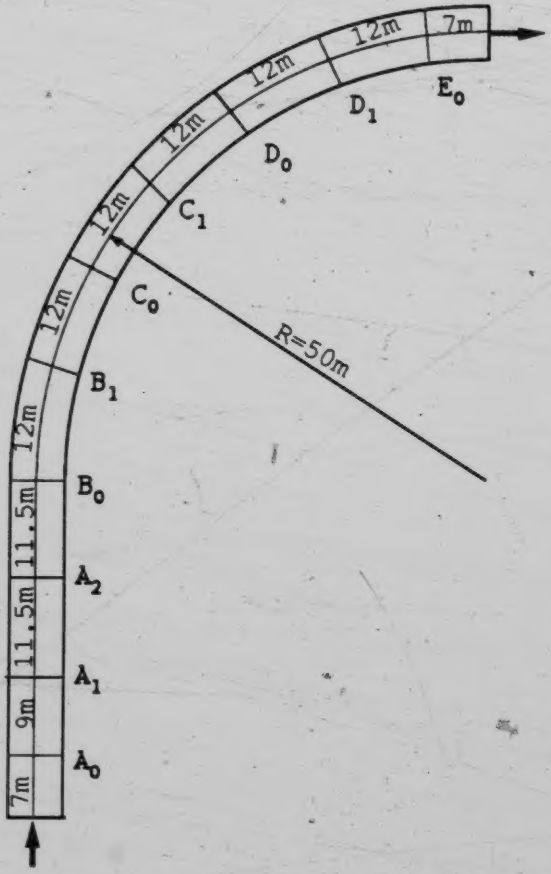
7m
9m
11.5m
11.5m
12m
12m
12m
12m
12m
12m
7m
A0
A1
A2
B0
B1
C0
C1
D0
D1
E0
R=50m

Figure 2.8 Plan view of De Vriend's 90° bend(De Vriend, 1976)

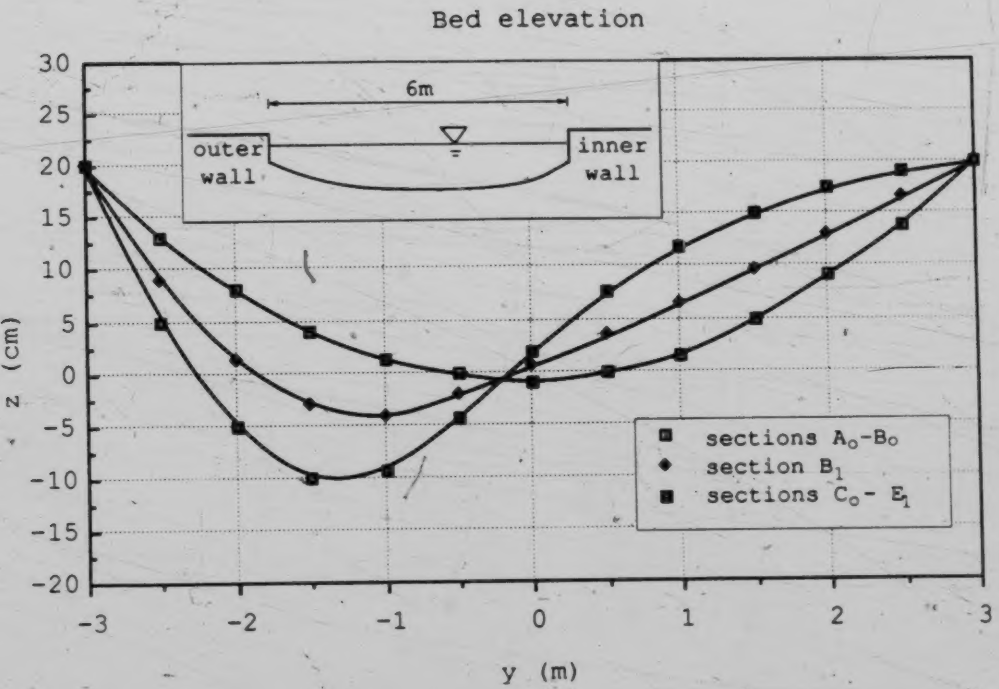

Figure 2.9 Channel geometry of De Vriend's 90° bend(De Vriend, 1976)

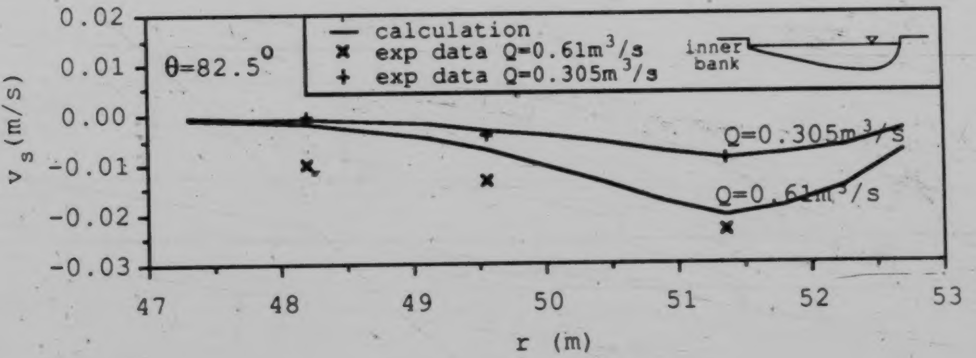

Figure 2.10 The comparison of transverse surface velocity for De Vriend's (1976) experimental data

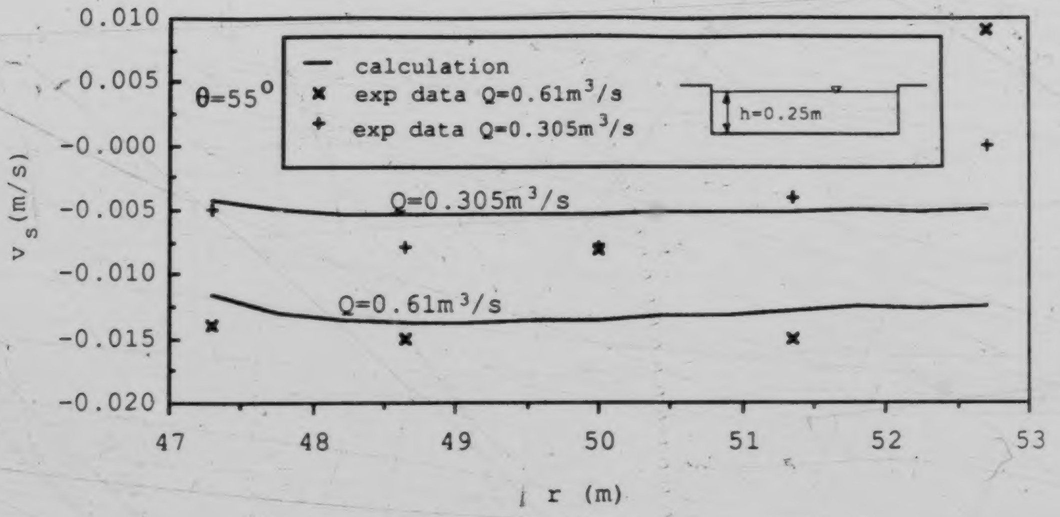

Figure 2.11 The comparison of transverse surface velocity for De Vriend's(1978) experimental data

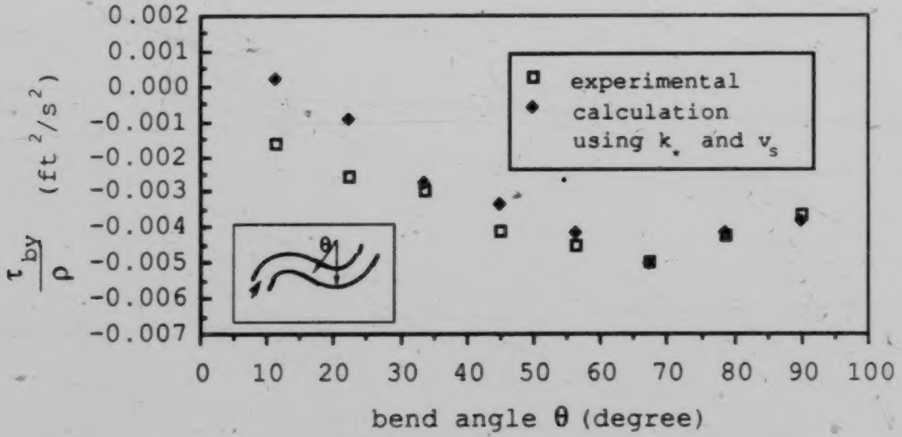

Figure 2.12 The comparison of transverse bed stress for Yen's (1965) experimental data

3 NUMERICAL ANALYSIS

3.1 Numerical Formulation

The depth averaged continuity, momentum and moment of momentum equations, (2.83) to (2.87), along with the associated boundary conditions are solved by a numerical method. The finite element method was selected because the method allows specification of the governing equations in a simple Cartesian coordinate system while actually solving them on a curvilinear grid which conforms to the channel plan.

The Galerkin finite element formulation with artificial diffusion was used in the present study. A four node bilinear isoparametric element was used for the finite element discretization. The same interpolation was used for all dependent variables. Two point Gaussian numerical intergration is adopted in the finite element model.

The flow diagram for the iterative solution procedure is shown in figure 3.1. First, equations (2.83) to (2.85) are solved for $\overline{u}$, $\overline{v}$, and h iteratively with the initial values of u_s and v_s. Then the moment of momentum equations are solved for $\overline{zU}h$ and $\overline{zV}h$. Hence u_s and v_s can be determined using equations (2.81) and (2.82). The first three equations are then resolved based upon the new values of u_s and v_s. The procedure is repeated until a convergence criteria is satisfied.

3.1.1 Galerkin's Method

The finite element method is a technique for solving partial differential equations by discretising them in the spatial dimensions. The whole space is discretised into triangular or quadrilateral elements, then all equations are summed up at each nodal point and solved.

Consider a time-independent equation

$$\mathcal{L}(\underline{\underline{u}}) = f \qquad \text{in domain } \Omega \tag{3.1}$$

where $\mathcal{L}$ is a differential operator that acts on the unknown function $\underline{\underline{u}}$ to generate the known function f. Approximating $\underline{\underline{u}}$ with a function $\underline{u}$ which is a linear combination of basis functions such as

$$\underline{u} = \sum_{i=1}^{n} f_i u_i \tag{3.2}$$

in which u_i are undetermined variables and f_i are basis functions chosen to satisfy the essential (Dirichlet) and natural (Neumann) boundary conditions

$$\underline{u} = u_o \quad \text{on essential boundary } \Gamma_{u_0}$$

$$\text{and} \quad \underline{u} = q \quad \text{on natural boundary } \Gamma_q \tag{3.3}$$

As $\underline{u}$ is an approximate solution of equation (3.1), it will yield the residual ε defined as

$$\varepsilon = \mathcal{L}(\underline{u}) - f \tag{3.4}$$

If the trial solution $\underline{u}$ is the exact solution, then $\underline{\underline{u}} = \underline{u}$, i.e. the residual is zero. To minimize the residual over the whole domain Ω, a set of weighting functions, N_i, are employed such that

$$\int_{\Omega} N_i \varepsilon \, d\Omega = 0 \qquad i=1,2,\ldots\ldots n \tag{3.5}$$

There are several weighted residual methods to transform the partial differential equations into a form where finite element method can be adopted. However, Galerkin's method was selected here due to its simplicity.

Galerkin's method is formulated by selecting the basis function f_i as the weighting function N_i. Thus the generalized equation is

$$\int_{\Omega} f_i (\mathcal{L}(\underline{u}) - f)\, d\Omega + \int_{\Gamma_{u_0}} f_i E(\underline{u}))\, d\Gamma + \int_{\Gamma_q} f_i N(\underline{u})\, d\Gamma = 0 \tag{3.6}$$

where $E(\underline{u})$ and $N(\underline{u})$ are differential operator for generating functions of $\underline{u}$ on the boundary Γ_{u_0} and Γ_q repectively.

The second integral term in (3.6) is zero for the essential portion of the boundary ($f_i=0$) and the last term is retained only on boundaries where a flux type boundary is imposed. Due to the no flux boundary condition applied in the current study, the boundary terms will be ignored in all numerical formulations introduced later.

3.1.2 Finite Element Formulation

The finite element formulation for the mathematical model introduced previously can be started by defining

$$\bar{u} = \sum_{i=1}^{n} f_i u_i \qquad (3.7)$$

$$\bar{v} = \sum_{i=1}^{n} f_i v_i \qquad (3.8)$$

$$h = \sum_{i=1}^{n} f_i h_i \qquad (3.9)$$

$$u_s = \sum_{i=1}^{n} f_i p_i \qquad (3.10)$$

$$v_s = \sum_{i=1}^{n} f_i q_i \qquad (3.11)$$

where f_i is the basis function (Taylor and Hughes 1981), which serves to connect the variation in the variable across an element with the discrete nodal values, and n is the number of nodes in each element. Due to the non-linearities in the first three equations, especially the convection terms, a suitable iterative procedure was used in which a simple convergence sequence with an updating variable was employed. For example, the Galerkin formulation for the expanded depth-averaged continuity equation reads as:

$$\sum_{i=1}^{n_e}\int_{A_e} N_i \left(\sum_{j=1}^{n} f_j h_j \sum_{k=1}^{n} u_k \frac{\partial f_k}{\partial x} + \sum_{j=1}^{n} f_j h_j \sum_{k=1}^{n} v_k \frac{\partial f_k}{\partial y}\right.$$

$$\left. + \sum_{j=1}^{n} f_j u_j \sum_{k=1}^{n} h_k \frac{\partial f_k}{\partial x} + \sum_{j=1}^{n} f_j v_j \sum_{k=1}^{n} h_k \frac{\partial f_k}{\partial y}\right) dA_e = 0 \qquad (3.12)$$

where n_e is the total number of elements and A_e is the area of the element. The outer summation refers to each element in the system and the inner summation is over the number of nodes in each of the elements. It should be noted that in order to make the finite element approximation as general as possible, basis function f_i and weighting function N_i are still used through this chapter. All terms in the governing equations (as listed in 2.1.9) are made up of a multiplication of variables or variable and a derivative of the same or of another variable. When dealing with the non-linear terms, for instance $h\partial\bar{v}/\partial y$, the variable associated with the differential is assumed to be the unknown. Therefor quation (3.12) can be rewritten in matrix form as

$$\left[N_i f_j h_j \frac{\partial f_k}{\partial x}\right] \{u\} + \left[N_i f_j h_j \frac{\partial f_k}{\partial y}\right] \{v\} +$$

$$\left[N_i f_j u_j \frac{\partial f_k}{\partial x} + N_i f_j v_j \frac{\partial f_k}{\partial y}\right] \{h\} = \{0\} \qquad (3.13)$$

Expanding the momentum equation in the x direction and employing the weighted residual approach the resulting equation can be expressed in matrix form as:

$$
\begin{aligned}
&\Big[N_i f_j h_j f_l u_l \frac{\partial f_k}{\partial x} + N_i f_j h_j f_l v_l \frac{\partial f_k}{\partial y} + v_t f_j h_j \frac{\partial N_i}{\partial x}\frac{\partial f_k}{\partial x} + \\
&v_t f_j h_j \frac{\partial N_i}{\partial y}\frac{\partial f_k}{\partial y} + (2 f_j u_j I_1 + 2 f_j p_j I_3) f_l h_l N_i \frac{\partial f_k}{\partial x} + \\
&(2 f_j v_j I_1 + 2 f_j q_j I_3) h_l f_l N_i \frac{\partial f_k}{\partial y}\Big] \{u\} + \\
&\Big[(f_j u_j I_1 + f_j p_j I_3) f_l h_l N_i \frac{\partial f_k}{\partial y}\Big] \{v\} + \\
&\Big[- v_t u_j \frac{\partial f_k}{\partial x}\frac{\partial N_i}{\partial x} - v_t u_j \frac{\partial f_k}{\partial y}\frac{\partial N_i}{\partial y} + g f_j h_j N_i \frac{\partial f_k}{\partial x} + \\
&(f_j u_j f_l u_l I_1 + 2 f_j p_j f_l u_l I_3 + 2 f_j p_j f_l p_l I_2) N_i \frac{\partial f_k}{\partial x} + (f_j u_j f_l v_l I_1 + \\
&2 f_j p_j f_l v_l I_3 + f_j q_j f_l u_l I_3 + 2 f_j p_j f_l q_l I_2) N_i \frac{\partial f_k}{\partial y}\Big] \{h\} = \\
&- \Big[N_i \frac{u_{*l}(f_j u_j + k_* f_j p_j)}{C_*} + N_i g f_l h_l z_j \frac{\partial f_j}{\partial y} + N_i (2 f_j u_j I_3 + \\
&\qquad 2 f_j p_j I_2) f_l h_l q_m \frac{\partial f_m}{\partial x} + N_i (f_j v_j I_3 + f_j q_j I_2) f_l h_l p_m \frac{\partial f_m}{\partial y} + \\
&\qquad N_i (f_j u_j I_3 + f_j p_j I_2) f_l h_l q_j \frac{\partial f_j}{\partial y}\Big] \qquad (3.14)
\end{aligned}
$$

where

$$u_{\star j} = \frac{(u_j f_j u_l f_l + v_j f_j v_l f_l)^{1/2}}{C_\star} \tag{3.15}$$

The corresponding momentum equation in the y-direction can be obtained by simply interchanging the x, y, u, v, p and q in equation (3.14). The resulting equation has the form

$$\left[(f_j v_j I_1 + f_j q_j I_3) f_j h_j N_i \frac{\partial f_k}{\partial x}\right] \{u\} +$$

$$\left[N_i f_j h_l f_l v_j \frac{\partial f_k}{\partial y} + N_i f_j h_l f_l u_j \frac{\partial f_k}{\partial x} + v_t f_j h_j \frac{\partial N_i}{\partial y} \frac{\partial f_k}{\partial y} + \right.$$

$$v_t f_j h_j \frac{\partial N_i}{\partial x} \frac{\partial f_k}{\partial x} + (2 f_j v_j I_1 + 2 f_j q_j I_3) f_l h_l N_i \frac{\partial f_k}{\partial y} +$$

$$\left.(2 f_j u_j I_1 + 2 f_j p_j I_3) h_l f_l N_i \frac{\partial f_k}{\partial x}\right] \{v\} +$$

$$\left[- v_t v_j \frac{\partial f_k}{\partial y} \frac{\partial N_i}{\partial y} - v_t v_j \frac{\partial f_k}{\partial x} \frac{\partial N_i}{\partial x} + g f_j h_j N_i \frac{\partial f_k}{\partial y} + \right.$$

$$(f_j v_j f_l v_l I_1 + 2 f_j q_j f_l v_l I_3 + 2 f_j q_j f_l q_l I_2) N_i \frac{\partial f_k}{\partial y} + (f_j v_j f_l u_l I_1 +$$

$$\left. 2 f_j q_j f_l u_l I_3 + f_j p_j f_l v_l I_3 + 2 f_j q_j f_l p_l I_2) N_i \frac{\partial f_k}{\partial x}\right] \{h\} =$$

$$- \left[N_i \frac{u_{\star j}(f_j v_j + k_\star f_j q_j)}{C_\star} + N_i g f_l h_l z_j \frac{\partial f_j}{\partial x} + N_i (2 f_j v_j I_3 + \right.$$

$$2f_j q_j I_2) f_1 h_1 q_m \frac{\partial f_m}{\partial y} + N_i (f_j u_j I_3 + f_j p_j I_2) f_1 h_1 q_m \frac{\partial f_m}{\partial x} +$$

$$N_i (f_j v_j I_3 + f_j q_j I_2) f_1 h_1 p_m \frac{\partial f_m}{\partial x}\Bigg] \qquad (3.16)$$

The solution procedure is to start with initial estimates for the primitive variables and boundary values for u, v, h, p and q, and to solve equations (3.13) to (3.16) for the values of u, v and h. A check is then made to determine if the difference between the new values and the old values is within the required tolerance at all node points,

$$\text{relative change} = \frac{\text{new value} - \text{old value}}{\text{new value}} < \text{tolerance}$$

in which the tolerance is set to be 0.005 for all runs conducted later. If the tolerence criteria was not met, a simple arithmetic mean is used to update the primitive variable,

$$\text{updated value} = \frac{\text{new value} + \text{old value}}{2}$$

and the process is repeated until the tolerence condition is satisfied.

The depth-averaged moment of momentum equations in matrix form can be expressed as

$$\Bigg[f_j u_j N_i \frac{\partial f_k}{\partial x} + 2u_j \frac{\partial f_j}{\partial x} N_i f_k - \left(\frac{-k_*}{2C_*} + \frac{2\nu_t}{f_1 u_1 f_m h_m}\right) \frac{C_* u_{*j}}{I_5 \; f_j h_j} N_i f_k$$

$$+ f_j v_j N_i \frac{\partial f_k}{\partial y} + v_j \frac{\partial f_j}{\partial y} N_i f_k \Big] \{P\} + \Big[u_j \frac{\partial f_j}{\partial y} N_i f_k \Big] \{Q\} =$$

$$\Big[v_t f_l h_l u_j \frac{\partial f_j}{\partial x} \Big(z_m \frac{\partial f_m}{\partial x} + \frac{h_m}{2} \frac{\partial f_m}{\partial x} \Big) + v_t f_l h_l u_j \frac{\partial f_j}{\partial y} \Big(z_m \frac{\partial f_m}{\partial y} + \frac{h_m}{2} \frac{\partial f_m}{\partial y} \Big) +$$

$$\Big(\frac{-k_*}{2C_*^{\,2}} + \frac{2\nu_t}{f_l u_l f_m h_m} \Big) \frac{C_* u_{*j} f_j h_j f_n u_n I_4}{I_5} \Big] N_i \tag{3.17}$$

$$\Big[v_j \frac{\partial f_j}{\partial x} N_i f_k \Big] \{P\} + \Big[f_j v_j N_i \frac{\partial f_k}{\partial y} + 2 v_j \frac{\partial f_j}{\partial y} N_i f_k - \Big(\frac{-k_*}{2C_*} +$$

$$\frac{2\nu_t}{f_l v_l f_m h_m} \Big) \frac{C_* u_{*j}}{I_5 \; f_j h_j} N_i f_k + f_j u_j N_i \frac{\partial f_k}{\partial x} + u_j \frac{\partial f_j}{\partial x} N_i f_k \Big] \{Q\} =$$

$$\Big[v_t f_l h_l v_j \frac{\partial f_j}{\partial y} \Big(z_m \frac{\partial f_m}{\partial y} + \frac{h_m}{2} \frac{\partial f_m}{\partial y} \Big) + v_t f_l h_l v_j \frac{\partial f_j}{\partial x} \Big(z_m \frac{\partial f_m}{\partial x} + \frac{h_m}{2} \frac{\partial f_m}{\partial x} \Big) +$$

$$\Big(\frac{-k_*}{2C_*^{\,2}} + \frac{2\nu_t}{f_l v_l f_m h_m} \Big) \frac{C_* u_{*j} f_j h_j f_n v_n I_4}{I_5} \Big] N_i \tag{3.18}$$

where P and Q are defined by

$$\overline{zU}\, h = \sum_{i=1}^{n} f_i P_i \tag{3.19}$$

$$\overline{zV}\, h = \sum_{i=1}^{n} f_i Q_i \tag{3.20}$$

Substituting $\overline{zU}h$ and $\overline{zV}h$ into equations (2.81) and (2.82) to calculate u_s and v_s, then the first three equations (3.13, 3.14 and 3.16) are resolved based on these new surface velocities. The procedure is repeated if the relative change between old value and the new value larger than the tolerance limit. While the tolerence condition for all variables ($\bar{u}$, $\bar{v}$, h, u_s and v_s) at all points is satisfied, then assume that the calculation is completed.

3.1.3 Boundary Conditions and Artificial Diffusion

We start with the inflow boundary condition. Here the most obvious boundary conditions are specified normal and tangential depth-averaged velocities as well as the secondary surface velocities. There is interest in inflow boundary conditions that did not require specified velocities. These can be satisfied by the following procedure: 1.selecting a straight channel at the upstream of the reach of interest and calculating the depth-averaged velocity according to Manning or Chezy equation or from the discharge curve, and letting $u_s=v_s=0$; 2. at the end of the straight channel the fully developed flow velocities, both depth-averaged and secondary surface velocity, should be computed by the model. Similarly, a long straight channel is added to the end of the reach of interest. The flow depths at the downstream end are given, and u_s and v_s are set to zero.

Oscillations are discovered in the solution of Galerkin finite element method when a downstream boundary condition forces a rapid change in the solution. The oscillations usually happen in the convection dominated case. Refining the mesh or using upwind finite element may eliminate the oscillations.

It is known that Galerkin finite element discretization leads to a central difference approximation (Brooks and Hughes, 1982). The use of upwind differencing on the convective term in the finite difference approximation to kill the oscillation is well known. The upwind convective term can be constructed simply by adding artificial diffusion (or artificial viscosity) to the central difference treatment.

For the finite element formulation introduced in the previous section, artificial diffusion is needed especially in (3.17) and (3.18). $\Delta x(u\partial^2 P/\partial x_j^2)$ is added to the diagonal terms of the moment of momentum equations to stabilize the solutions.

With the proper initial values and sufficient artificial diffusion this finite element formulation gives a stable and converging solution.

3.1.4 Computer Coding

The complete listing of the Fortran program, adapted from Taylor and Hughes(1981), is included in appendix. Figure

3.2 shows the general structure of the program. A brief description of the subroutines is given below.

DINPUT - This subroutine reads all the required data which includes the nodal point coordinates, the element connectivity table, the boundary points and the boundary values, the initial estimates and the physical properties of the flow.

SHAPE4, DJACOB and DRIVES - These subroutines prepare the information needed for the coordinate transformation and Gaussian integration in the finite element analysis. SHAPE4 consists of the shape functions and derivatives. DJACOB calculates the Jacobian matrix and its determinant. DRIVES uses the information obtained from SHAPE4 and DJACOB to calculate the global derivatives, shape functions and the element area at each Gauss point. All this information is then stored in a temporary file which will be retrieved for later use.

MATRIX - The depth-averaged continuity and momentum equations are coded in this subroutine. The elements of the force vector (the right-hand side matrix) and the stiffness matrix(the left-hand side matrix) are evaluated.

SURFAC - Forms the moment of momentum equations to calculate $\overline{zUh}$ and $\overline{zVh}$.

FRONT1 - The matrices created by MATRIX and SURFAC are assembled and solved by the frontal technique. This subroutine applies the boundary values to the matrix, assembles the matrix and performs the elimination and the substitution as a matrix solver.

ITERUV - This subroutine calls FRONT1 to set up matrix and solve for current iteration variable values. Solutions obtained at each iteration are also checked for convergence to a specified tolerance in routine TOLER.

3.2 Numerical Tests

The depth-averaged equations have been widely used in river and coastal engineering. However, the forms of the moment of momentum equations introduced earlier have not yet been shown elsewhere. This finite element model, especially the moment of momentum equation part, needs to be tested to understand its behavior before applying it to sophisticated curved channel problems. Simple cases of uniform and non-uniform flow in straight channel with rectangular cross sections were tested. The last test case was the flow around a 60 degree bend which tested all aspects of the model.

3.2.1 Test for Uniform Flow Problem

A hypothetical straight channel with rectangular cross section was used as the first numerical test. The channel was 40m long and 8m wide with bed slope of 0.006. The flow was uniform with a depth averaged velocity $\overline{u}$ = 1.0m/s, depth h = 1.0m and calculated Chezy C of 52.9m$^{1/2}$/s. The finite element mesh used in this study contained 25 nodes and 16 elements. Uniform flow was given as the initial estimates. The boundary conditions were $\overline{u}$ = 1.0m/s at the upstream; h =1.0m at the downstream end and side wall; and a no-slip condition on the side wall. The value of u_s was set to be zero at the upstream section (x=0) and at all side walls. The numerical results are shown in table 3.1. It shows that a uniform flow was predicted due to the small calculated u_s at all sections.

Table 3.1 Uniform Flow Test

x (m)	0.0	10.0	20.0	30.0	40.0
u_s (m/s)	0.000	0.0002	-.0002	.0002	.0002

3.2.2 Test for Non-uniform Flow Problem

A set of experimental data (Jasek, 1989) on the boundary layer growth in a straight channel was used here. The experiment was conducted in a rectangular channel 1.22m wide, 18m long and 0.67m deep with metal bed and plexiglass sides. Water was provided from a constant head tank supplied by a pump. The velocity distribution was measured by means of a Pitot tube with pressure transducer and water depth was recorded at 0.43m and 1m downstream of the entrance and every metre after until the flow was fully developed.

The experimental set up and the finite element mesh are shown in figure 3.3. The experimental data $\overline{u}$ and h were used as initial estimates in the numerical calculation. Chezy C was calculated to be $72.8m^{1/2}/s$ with $\overline{u}$ =0.35m/s, h=0.103m and bed slope 0.00027. The measured velocity profile at 0.43m (first measuring station in the experiment) was used to calibrate the u_s needed to generate a similar velocity profile by the equation

$$u = \overline{u} F + u_s G \tag{3.21}$$

u_s=-0.03m/s was found and set as a boundary condition at the upstream section. The surface velocity u_s at each section was calculated by the moment of momentum equations and the experimental values $\overline{u}$ and h, and then equation (3.21) was used to calculate the velocity profile at each section. The comparison of the experimental results and the numerical prediction of the velocity profile is presented in figure 3.4 which shows a satisfactory match.

3.2.3 Test for the Rectangular Free Overfall

The rectangular overfall refers to the downstream portion of a bed terminating abruptly at its lower end. Rajaratnam and Muralidhar (1968) have carried out experiments in a hydraulic model to study free overfall. The channel used was 0.46m wide, 0.38m deep and 6.1m in length with plexiglass sides and bed. Experiments were conducted for a range of negative, zero and positive bed slopes. Only a few of these runs included measurements of the velocity profiles, flow depths and pressure distributions. The run with zero bed slope was chosen for this comparison.

The finite element mesh used was the same as that for the last test. Five sections were used: at $x=0.025m$, $x=0.05m$, $x=0.1m$, $x=0.18m$ and $x=0.34m$, as shown in figure 3.5. The x was taken as zero at the brink. The depth averaged velocity $\overline{u}$ and the flow depth h at all five sections were given; u_s was set to be zero at the upstream section ($x=0.34m$).

Figure 3.6 shows the comparison of the experimental data (from Rajaratnam and Muralidhar) and the numerical prediction. It can be seen that the model predicted well for velocity profiles at sections $x=0.18m$ and $x=0.1m$. However sections $x=0.05m$ and $x=0.025m$ are close to the brink and the hydrostatic pressure distribution assumption cannot be applied due to large vertical velocities. Figures 3.7 and 3.8 show the measured pressure and vertical velocity at these sections. This confirms that the present model is limited to the following assumptions (1) vertical velocities are relatively small compared to the main velocity; (2) a hydrostatic pressure distribution condition exists. To overcome the discrepancy shown in the velocity profiles in figure 3.6, a non-hydrostatic pressure distribution is required.

The z-direction momentum equation was used to obtain the non-hydrostatic pressure distribution,

$$\frac{\partial wu}{\partial x} + \frac{\partial wv}{\partial y} + \frac{\partial w^2}{\partial z} + \frac{1}{\rho}\frac{\partial (p_o+p_e)}{\partial z} = 0 \qquad (3.22)$$

in which p_o is the hydrostatic pressure and p_e is the deviation of the pressure distribution from the hydrostatic condition(French 1985). Depth averaging (3.22) and applying the kinematic surface condition yields

$$\frac{\partial (h\overline{uw})}{\partial x} + \frac{\partial (h\overline{vw})}{\partial y} = p_b \qquad (3.23)$$

where p_b is the pressure deviation from the hydrostatic condition at the channel bed. If p_b is assumed to decrease linearly to the water surface then

$$p_e = p_b\left(1 - \frac{z-z_b}{h}\right) \qquad (3.24)$$

Integrating the pressure deviation $\partial p_e/\partial x$ in the x direction momentum equation over the depth gives

$$\frac{1}{\rho}\int_{z_b}^{z_b+h} \frac{\partial p_e}{\partial x}\, dz = \frac{p_b}{\rho}\frac{\partial \bar{z}}{\partial x} + \frac{h}{2\rho}\frac{\partial p_b}{\partial x} \qquad (3.25)$$

Similarly, the depth-averaged pressure deviation term in the moment of momentum equation can be shown to be

$$\frac{1}{\rho}\int_{z_b}^{z_b+h}\frac{\partial p_e z}{\partial x}\,dz = \bar{z}\left[\frac{p_b}{\rho}\frac{\partial \bar{z}}{\partial x}+\frac{h}{2\rho}\frac{\partial p_b}{\partial x}\right]+\frac{h}{12}\left[\frac{p_b}{\rho}\frac{\partial h}{\partial x}-\frac{h}{\rho}\frac{\partial p_b}{\partial x}\right] \qquad (3.26)$$

Replacing the pressure term, $gh\frac{\partial(h+z_b)}{\partial x}$, in the momentum equation (2.31) by (3.25), the depth-averaged momentum equation is

$$\frac{\partial(h\bar{u}^2)}{\partial x}+\frac{\partial(h\bar{u}\;\bar{v})}{\partial y}+\frac{p_b}{\rho}\frac{\partial \bar{z}}{\partial x}+\frac{h}{2\rho}\frac{\partial p_b}{\partial x}-\frac{\partial}{\partial x}\left(h\nu_t\frac{\partial \bar{u}}{\partial x}\right)-$$

$$\frac{\partial}{\partial y}\left(h\nu_t\frac{\partial \bar{u}}{\partial y}\right)+\frac{\tau_{xb}}{\rho}+\frac{\partial(\overline{UU}h)}{\partial x}+\frac{\partial(\overline{UV}h)}{\partial y}=0 \qquad (3.27)$$

Substituting the pressure term in the moment of momentum equation (2.47) yields

$$\frac{\partial(\bar{u}\;\overline{zU}\,h)}{\partial x}+\frac{\partial(\bar{v}\;\overline{zU}\,h)}{\partial y}+\overline{zU}\,h\frac{\partial \bar{u}}{\partial x}+\overline{zV}\,h\frac{\partial \bar{u}}{\partial y}-\frac{\tau_{bx}h}{2\rho}+\frac{h\overline{\tau_{xz}}}{\rho}$$

$$-\frac{1}{\rho}h\overline{\tau_{xx}}\frac{\partial \bar{z}}{\partial x}-\frac{1}{\rho}h\overline{\tau_{xy}}\frac{\partial \bar{z}}{\partial y}-\frac{h}{12}\left[\frac{p_b}{\rho}\frac{\partial h}{\partial x}-\frac{h}{\rho}\frac{\partial p_b}{\partial x}\right]=0 \qquad (3.28)$$

It may be noted that equation (3.28) is (2.47) plus

$\frac{h}{12}\left[\frac{p_b}{\rho}\frac{\partial h}{\partial x}-\frac{h}{\rho}\frac{\partial p_b}{\partial x}\right]$ for the x- direction equation;

Therefore, the following terms should be equivalent added to the left hand side of the moment of momentum equation in the y direction

$$\frac{h}{12}\left[\frac{p_b}{\rho}\frac{\partial h}{\partial y} - \frac{h}{\rho}\frac{\partial p_b}{\partial y}\right]$$

Recalculating u_s with these new terms and the experimental data for p_b, the velocity profiles for sections x=0.1m, x=0.18m and x=0.34m are plotted in figure 3.9. It can be seen that the prediction is much improved. However, since the hydrostatic pressure assumption can be applied to most open channel problems, the extra pressure terms are excluded in the present model in the following sections.

3.2.4 Test for Flow in a 60 Degree Bend

The previous tests showed that the concept of u_s used in the predefined velocity function and the moment of momentum equations introduced earlier was adequate. The simple model test in the previous chapter also showed that the use of k_* was proper for the prediction of bed shear stress. A simple hypothetical 60 degree bend was set up to examine the numerical model in the two dimensional case.

The channel consisted of a straight approach reach 20m long, a 60° curved channel with centreline radius of 15m and a 10m long straight channel to the exit. The channel cross section was trapezoidal in shape with a 4m base width and 1 to 2 side slope. The bed slope was set to 0.0012. Uniform flow was assumed at both the upstream and downstream end. The velocity and depth used were $\overline{u}$=1 m/s and h=1m. The finite element mesh used contained 40 elements and 55 nodes. The channel geometry and the finite element mesh are shown in figure 3.10. The computed depth averaged velocity vectors are shown in figure 3.11.

The results show that the flow stay constant in the straight channel before entering the bend. As the flow enter the bends, the velocity increases inside and decreases outside of the bend. At the exit of the bend, the velocity at the outside is increasing. This shows that the phenomena of the velocity redistribution are well predicted and the model is well behaved in general.

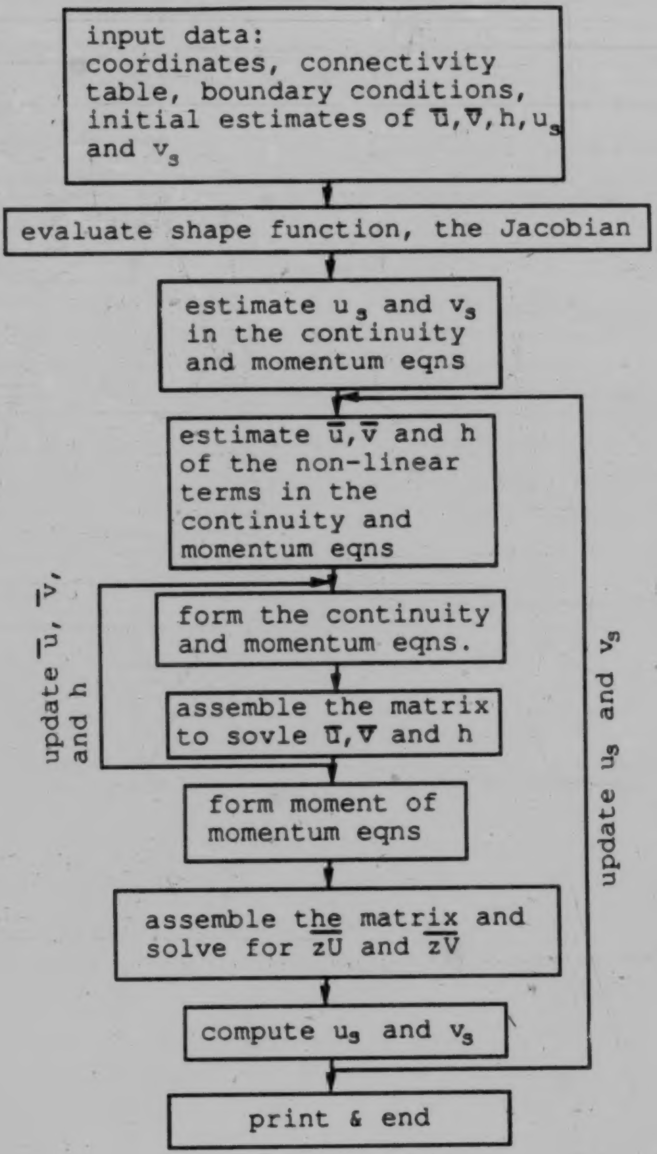
input data:
coordinates, connectivity table, boundary conditions, initial estimates of Ū,V̄,h,u_s and v_s
evaluate shape function, the Jacobian
estimate u_s and v_s in the continuity and momentum eqns
estimate ū,v̄ and h of the non-linear terms in the continuity and momentum eqns
form the continuity and momentum eqns.
assemble the matrix to sovle Ū,V̄ and h
update ū, v̄, and h
form moment of momentum eqns
assemble the matrix and solve for zU and zV
compute u_s and v_s
update u_s and v_s
print & end

Figure 3.1 Flow chart of the solving procedure

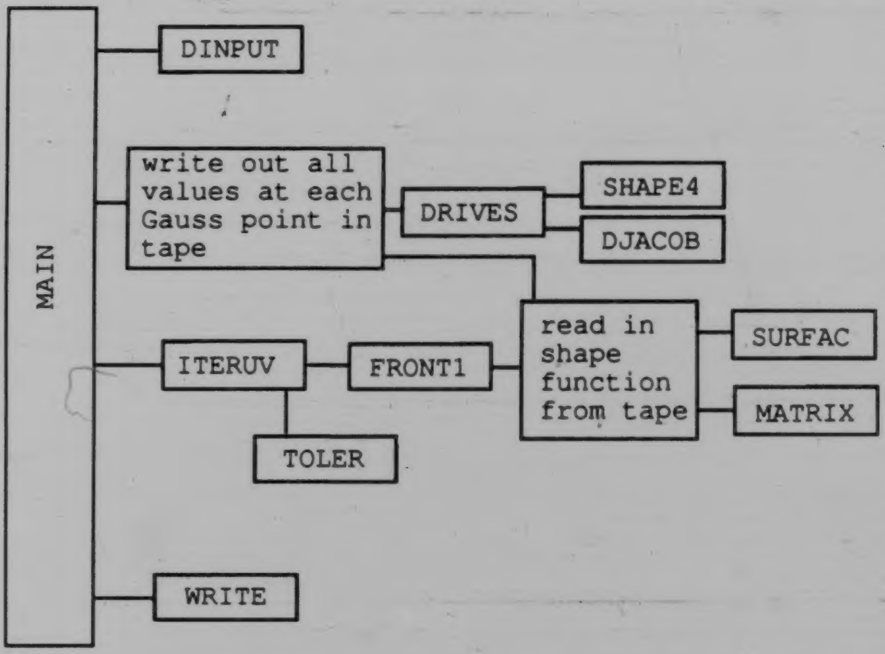
MAIN
DINPUT
write out all values at each Gauss point in tape
DRIVES
SHAPE4
DJACOB
read in shape function from tape
SURFAC
MATRIX
ITERUV
FRONT1
TOLER
WRITE

Figure 3.2 Program structure

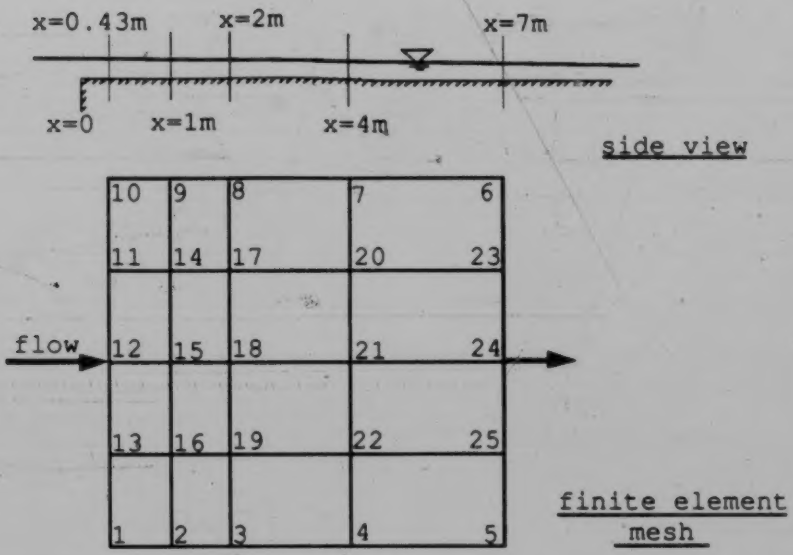
x=0.43m
x=2m
x=7m
x=0
x=1m
x=4m
side view
10
9
8
7
6
11
14
17
20
23
flow
12
15
18
21
24
13
16
19
22
25
1
2
3
4
5
finite element mesh

Figure 3.3 Finite element mesh for the non-uniform flow problem

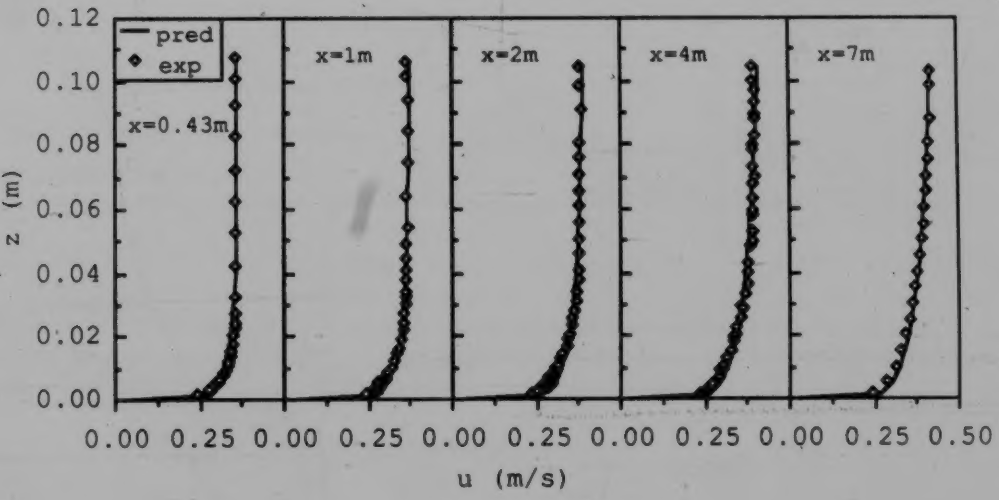

Figure 3.4 Comparison of the longitudinal velocity profiles for the non-uniform flow problem

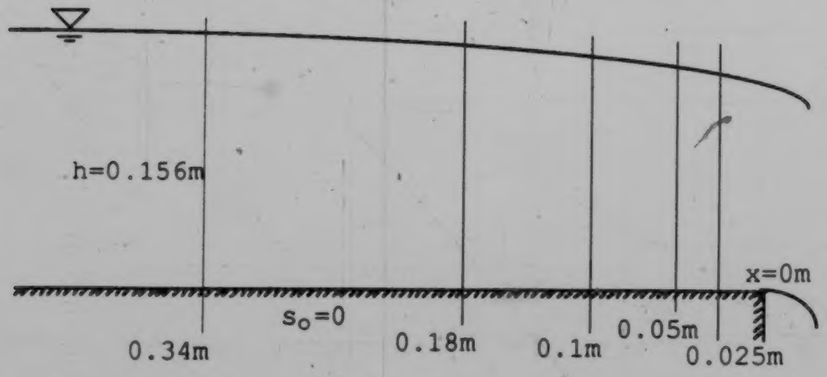
h=0.156m
x=0m
s_o=0
0.34m
0.18m
0.1m
0.05m
0.025m

Figure 3.5 Rectangular free overfall(Rajaratnam and Muralidhar, 1968)

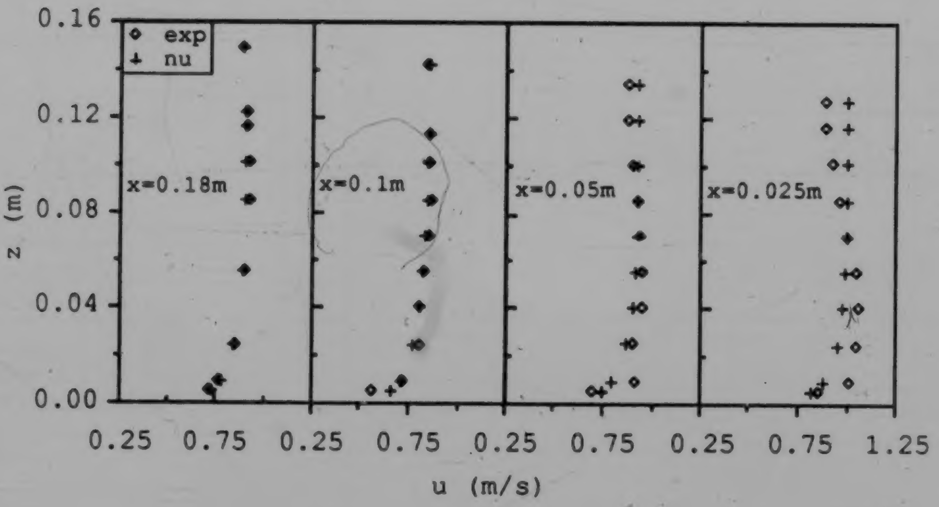

Figure 3.6 Comparison of the numerical and experimental longitudinal velocity profiles for the free overfall problem

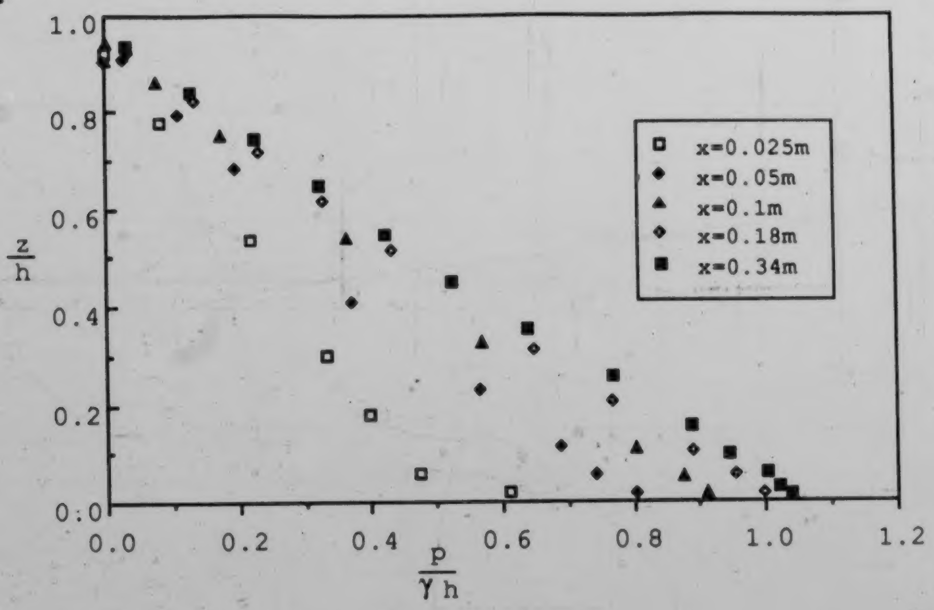

Figure 3.7 Pressure distribution for the free overfall problem (Rajaratnam and Muralidhar, 1968)

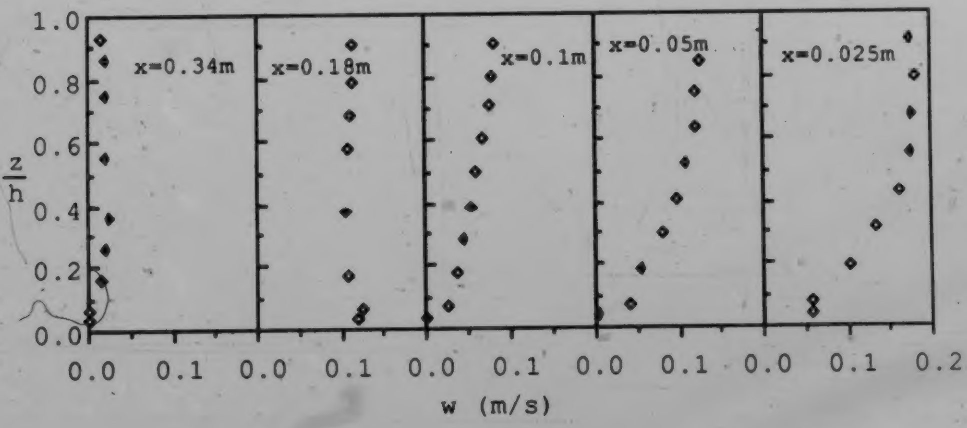

Figure 3.8 Vertical velocity distribution for the free overfall problem(Rajaratnam and Muralidhar, 1968)

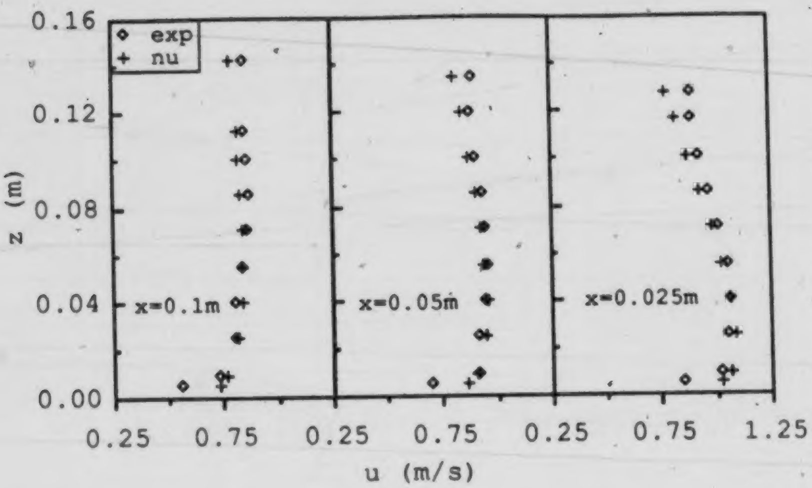

Figure 3.9 Comparison of the longitudinal velocity profiles for the free overfall problem(with the extra pressure deviation terms)

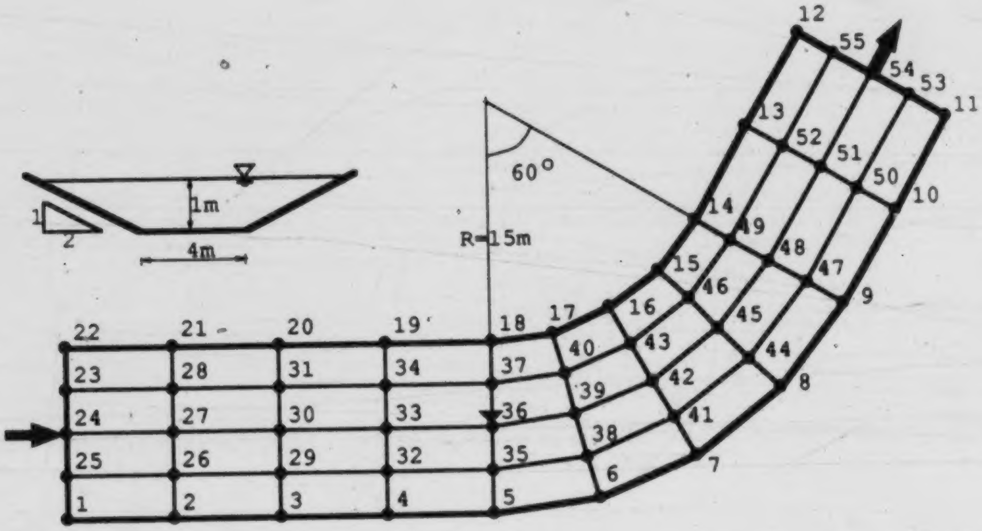
1m
4m
1
2
60°
R=15m
1
2
3
4
5
6
7
8
9
10
11
12
13
14
15
16
17
18
19
20
21
22
23
24
25
26
27
28
29
30
31
32
33
34
35
36
37
38
39
40
41
42
43
44
45
46
47
48
49
50
51
52
53
54
55

Figure 3.10 The hypothetical 60 degree bended channel

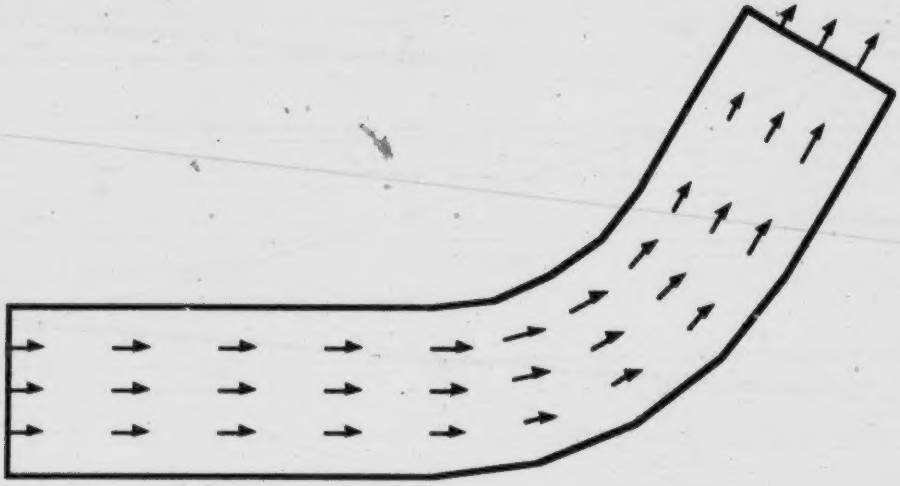

Figure 3.11 The numerical result for 60 degree bend

4 EXPERIMENTAL STUDY

4.1 Introduction

The experimental facilities used are similar to those used in the previous research (Steffler, 1984 and Hicks, 1985) at the T. Blench Hydraulics Lab in the University of Alberta. The Laser Doppler Anaemometer (LDA) was used to measure the velocities and the turbulent intensities of the channel flow. The purpose of this experimental work is to provide detailed data to calibrate the numerical model and also to investigate the flow in curved channel with smooth or rough outside banks.

4.2 Experimental Facilities and Procedure

The flume used in this experiment is shown in figures 4.1 and 4.2. It was constructed of galvanized sheet metal. Plexiglass inserts were installed at measurement locations to allow the laser beams to enter from below. The cross section was half trapezoidal in shape with 1.07m top width and 0.86m bottom width, the radius of curvature of the centreline (at half the top width) was 3.66m, and the side slope used was 2 to 1. Figure 4.2 illustrates the plan form and the locations of the measurement stations. The flume consisted of a straight section 13.4m long and a single 270° bend follow by a 2.4m straight exit section.

Water was circulated by a pump from a level-regulated sump to the bottom of a head box equipped with an overflow gate. The bed slope was set at 0.00083.

Five runs were conducted. Three were for different depths with a smooth channel, and two were for the same depth but with different roughnesses on the side slope. The roughness was expanded metal mesh and was intended to model riprap on a river bank. Sandpaper roughness was also used to investigate the transition between the fully smooth channel and the channel with rougher bank.

The laser was a 4W Argon-Ion Laser, although the actual power used was about 1W. A single light beam was generated from the Laser which was then split into three beams: blue, green and mixed. The intersection of these beams defined the measuring volume. The optics were rotated such that the blue and the mixed beam were parallel to the longitudinal direction and the green and the mixed beam were perpendicular to the longitudinal direction. Two focal lengths for the front lens, 80mm for runs 1, 4 and 5 and 160mm for runs 2 and 3, were used for this study.

The laser beams entered the flow from below in the first three runs. For runs 4 and 5, the roughness placed on the slope would have blocked the laser beams so for these runs the laser beams were directed down from the top through the water surface. To avoid variable refractions due to water surface fluctuations, a small piece of plexiglass (1" square) was placed on the top of water surface. Though the plexiglass was too small to affect the overall flow condition, the velocity close to the plexiglass may have been affected due to the existence of a boundary layer. Hence, the flow velocity very close (within about 5mm) to the surface was not measured.

Thirteen to fifteen vertical profiles were taken at each of the eleven test locations. Nine of these profiles were located on the flat part of the channel and the rest were on the slope. All profiles were taken perpendicular to the channel bed or bank. Each profile consisted of ten to twenty measurements starting as close as possible to the boundary.

At each point, the velocity and mean square turbulence intensity in the longitudinal and transverse directions, and the covariance of the velocity fluctuations were measured and averaged. A minimum sample of 10,000 readings was collected and averaged at each measuring point.

The flume and LDA are essentially the same as those used by Steffler (1984) and Hicks (1985) and further details may be found in these reports.

Table 4.1 summarize the significant details of the experimental work performed in this study.

The commonly used riprap gradation ranges from 300mm to 800mm. The length scale in the flume study was of the order of 1/40 implying that a suitable size for the model roughness should be in the range of 7.5mm to 20mm. Therefore, a 1-10H expanded metal sheet with a k_s value determined to be 8.6mm was used as roughness #2 in run 5. The dimensions of the expanded metal sheet are shown in figure 4.3. An intermediate roughness was also used in run 4 to investigate the transition between the high roughness bank (run 5) and smooth bank (runs 1 to 3). No. 36 aluminum oxide wet-or-dry cloth with a k_s value of 0.56mm was used. This sandpaper type of roughness, shown in figure 4.4, was used by Hollingshead (1972).

Table 4.1 Significant Details of the Experiments

Run no.	Boundary type (on the slope)	Width (W) (m)	Depth (h) (cm)	Average velocity (m/s)	Froude No.
1	smooth	0.931	6.0	0.42	0.174
2	smooth	0.948	7.4	0.42	0.243
3	smooth	0.963	8.7	0.46	0.248
4	roughness #1 k_s=0.56mm	0.932	6.0	0.38	0.246
5	roughness #2 k_s=8.6mm	0.934	6.2	0.36	0.213

4.3 Data Analysis

4.3.1 Limits for Logarithmic Velocity Equation

The Prandtl-von Karman logarithmic velocity equation is used to describe the distribution of velocity in a wide open channel. The equation for a smooth boundary is

$$\frac{u}{u_*} = A \log \left(\frac{zu_*}{\nu}\right) + B \qquad (4.1)$$

where A = 5.75 and B = 5.5, and u_* is the shear velocity defined as

$$u_* \equiv \sqrt{\frac{\tau_o}{\rho}} \qquad (4.2)$$

in which τ_o is the bed shear stress and ρ is the water density. It has been found that equation (4.1) is valid for $u_*z/\nu \geq 30$. The upper limit is the subject of some controversy with suggested limits ranging from 10% of the depth to the full depth itself. Nezu and Rodi (1986), based on LDA measurements, suggest that with the use of the constants given above, good shear stresses may be obtained using an upper limit of about 60% of the total depth. In the case of the curved channel velocity profiles this upper limit was used as a guideline but each profile was visually evaluated.

Considering rough turbulent flow in a wide rectangular channel, the following equation can be used (Hollingshead 1972)

$$\frac{u}{u_*} = A' \log \left(\frac{z}{k_s}\right) + B' \qquad (4.3)$$

where k_s is Nikuradse's equivalent sand grain roughness and A' and B' are numerical coefficients. A' also can be rewritten as

$$A' = \frac{2.3}{\kappa} \tag{4.4}$$

in which κ is von Karmann's constant. For κ=0.4, then A'=5.75 and B'=8.5. The relative roughness k_o can be defined as

$$k_o \equiv \frac{k}{h} \tag{4.5}$$

in which h is the channel depth and k is the actual roughness height. The small scale roughness equation (4.3) may be used for $k_o<0.3$. For $k_o>1.0$ the large scale roughness equation (Dandekar and Rodi,1982) and the velocity equation in the transition zone $0.3<k_o<1.0$ (Pe,1975) can be expressed as

$$\frac{u}{u_*} = A'' \log\left(\frac{z}{k}\right) + B'' \tag{4.6}$$

where A" and B" are numerical coefficients which depend on the roughness. These equations indicate that the velocity distribution retains a semi-logarithmic character.

For runs 4 and 5, the roughness was only applied on the sloped bank. The relative roughness increases as the depth changes along the slope. For the velocity profiles measured at h=5.32cm, 5.07cm, 3.52cm and 2.62cm, k_o was less than 0.02 for run 4. With the roughness height equal to 0.92cm in run 5, the k_o values were 0.17, 0.18, 0.26 and 0.35 respectively.

Since k_o>0.3 for only the profile measured at h=2.62cm (k_o=0.35), equation (5.3) was used throughout the analysis.

4.3.2 Rough Boundary Datum

It is necessary to determine the datum from which z is measured in order to use equation (4.6) to plot z vs u. Since the velocities measured by the laser are very close to the channel bed (<0.5mm above the boundary), only minor adjustments are required for the flow in smooth channels or in rough channels with small roughness height. For large roughness, the datum can be determined by plotting z vs u using trial and error for different datums to find the most linear semi-logarithmic plot. Figure 4.5 shows an example of the procedure used to determined the roughness datum at each profile.

4.3.3 Boundary Shear Stress

Boundary shear stress is obtained through the velocity profile and equation (4.2). Ghosh and Roy (1970) presented data on the shear stress distribution in rough trapezoidal channels. Stresses were measured by a direct shear meter, a Preston's tube and the velocity distribution. They concluded that the stress distribution calculated from the velocity profile agreed well with that obtained from direct measurement.

The shear velocity, u_*, in equations (4.1), (4.3) and (4.6) can be evaluated using the linear relationship between u and z in the semi-logarithmic plot. Figure 4.6, for example, shows a semi-logarithmic plot of u vs z, from which the shear velocity u_* can be estimated using

$$u_* = \frac{1}{5.75} \frac{u_2 - u_1}{\log \frac{z_2}{z_1}} . \tag{4.7}$$

where u_1 and u_2 are time averaged velocities interpolated from the plot at z_1 and z_2 respectively.

4.3.4 Equivalent Roughness

The equivalent roughness for the sand cloths (roughness #1) is 0.56mm (Hollingshead 1972). The equivalent roughness for roughness #2 was determined by the velocity profile method. Four velocity profiles were measured at the centre part of a straight channel covered with the expanded metal mesh. The shear velocity u_* for these test runs was determined by the procedure in section 4.3.3. By trial and error u/u_* vs. z/k_s was plotted on the semi-logarithmic graph until all the velocity points fell on the equation (4.3) line. Figure 4.7 shows the procedure and it was found that k_s=8.6mm. This value is slightly less than the actual roughness height of 9.2mm which may be explained by the open and uniform nature of the roughness elements.

4.4 Experimental Results

The experimental results of longitudinal and radial velocities and turbulence intensities obtained for runs 1, 4 and 5 are shown in figures 4.8 to 4.139. These runs have similar flow depth but different roughness on the outside bank, therefore the significant changes of the velocity and turbulent intensity distribution due to the existence of the roughness on the side slope can be clearly seen. The rest of the data can be found in the report by Jin et al. (1988). All profiles shown are referred to a common datum so that profiles on the sloping bank start at successively higher points on the vertical axis. These experimental results are briefly summarized below.

4.4.1 Smooth Boundary

The results of run 1 are shown in figures 4.8 to 4.51. Figures 4.8 to 4.18 show the variation of the longitudinal velocity profile at sections 1 to 11. Figures 4.19 to 4.29 show the variation of the transverse velocity profile at each section. The variation of the turbulence intensities in both the longitudinal and transverse directions are shown in figures 4.30 to 4.40 and figures 4.41 to 4.51, respectively. Figures 4.51 to 4.62 illustrate the results of turbulence intensities in the vertical plane extending longitudinally along the bend.

These velocity profiles show that at section 1 (0.75m before the entrance), the vertical distribution of longitudinal velocity were of classical logarithmic shape except close to the inner bank and on the slope. By a bend angle θ of 30°, the velocity had increased on the inside bank and decreased on the outside. The velocity at next section tended to be more uniform across the channel. At θ equal to 90°, the velocities close to the inside bank were lower than the average while the rest of the velocities were virtually uniform. For θ greater than 90°, the maximum velocity of the section shifted to near the outside bank. At the exit of the bend (θ = 270°) the peak velocity reached a maximum value. The last section in the straight exit reach showed the velocity distribution returning to its original state. The exit, however, was not long enough to observe the complete recovery.

The lateral velocity measurements show that the secondary flow profile almost remained the same from sections to sections for θ greater 60°. The distribution of the secondary flow across the channel was uniform and decreased near the inside wall and the outside bank.

4.4.2 Rough Boundary on the Sloped Bank

Comparison of the velocity distributions for the eleven sections of runs 1 (figures 4.8 to 4.18) and 5 (figures 4.63 to 4.73) shows that the velocity profiles are similar in the smooth, flat part of the channel but, as expected, there are significant differences on the side slope.

Figures 4.52 to 4.62 illustrate the development of secondary flow. At section 1 (the straight channel), the secondary velocity was basically very small compared with the main flow. The secondary flow started to develop when the flow entered the curve. Comparing figures 4.107 to 4.117 with figures 4.19 to 4.29 (run 1, smooth channel), the secondary flow on the flat part as expected did not change. The magnitude of the secondary flow on the sloped bank was larger than that for the smooth channel.

Figures 4.118 to 4.128 show the turbulent intensity distributions in the longitudinal direction for run 5. The turbulent intensities in the transverse direction are shown in figures 4.129 to 4.139. The comparison of these turbulent intensities for the smooth boundary and the rough boundary shows that the shape of these profiles are similar.

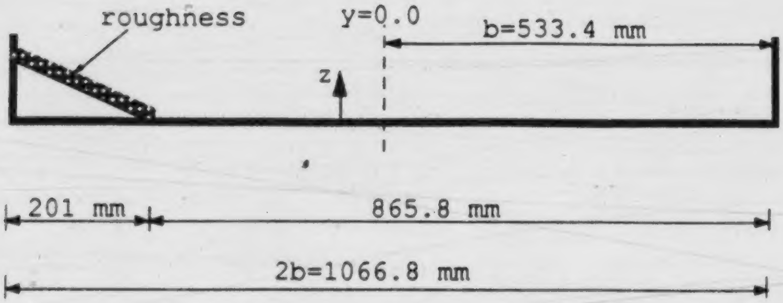
roughness
y=0.0
b=533.4 mm
z
201 mm
865.8 mm
2b=1066.8 mm

Figure 4.1 Dimensions of the channel section

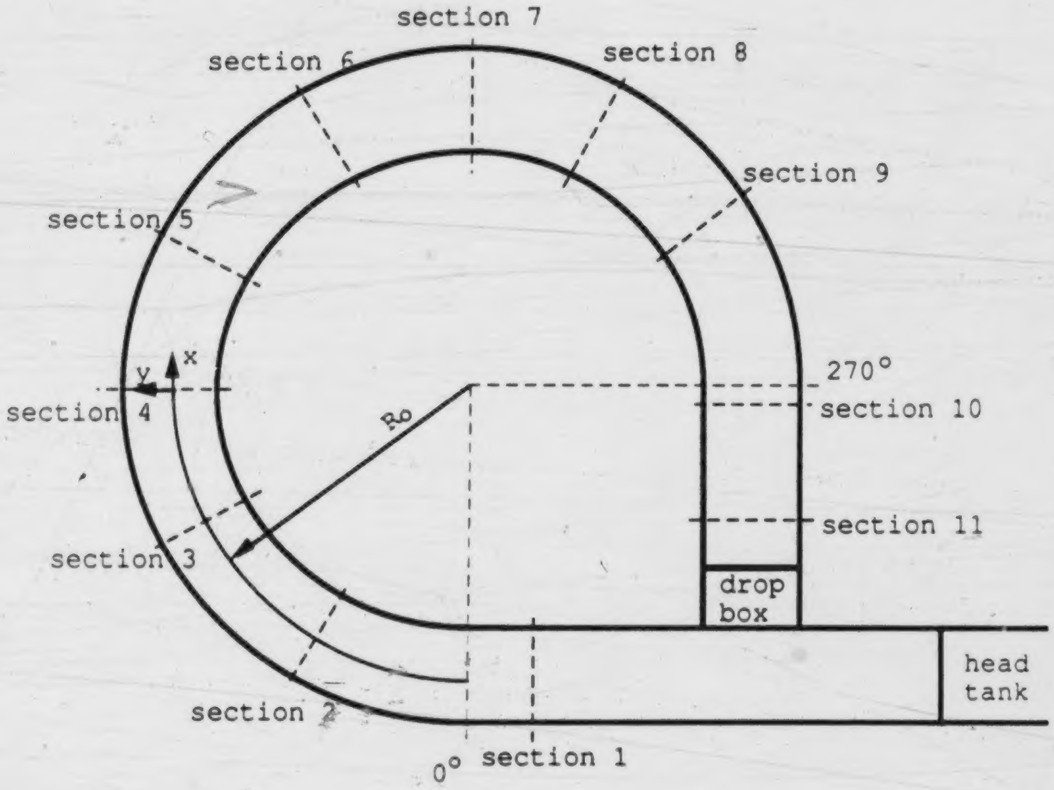
section 7
section 6
section 8
section 9
section 5
y
x
270°
section 4
section 10
Ro
section 11
section 3
drop box
head tank
section 2
0°
section 1

Figure 4.2 Flume and locations of the measurement stations

2

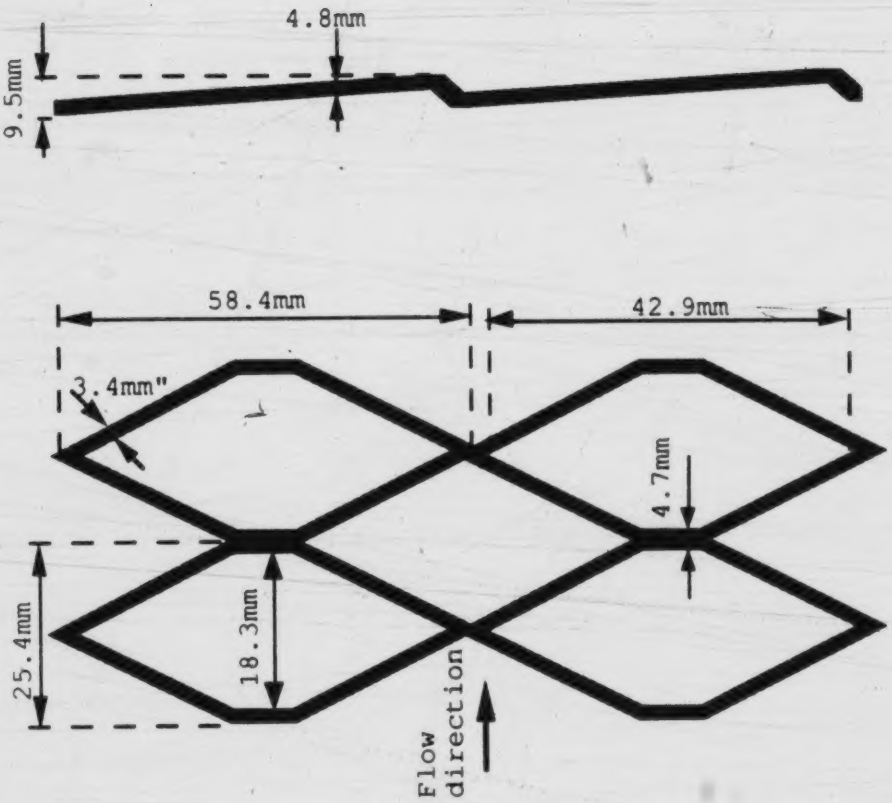
4.8mm
9.5mm
58.4mm
42.9mm
3.4mm"
4.7mm
25.4mm
18.3mm
Flow direction

Figure 4.3 Details of Roughness #2

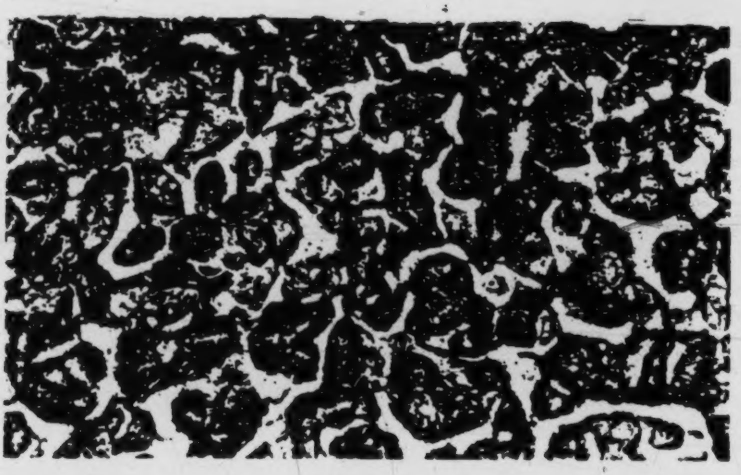

Plan View

Scale in millimeters

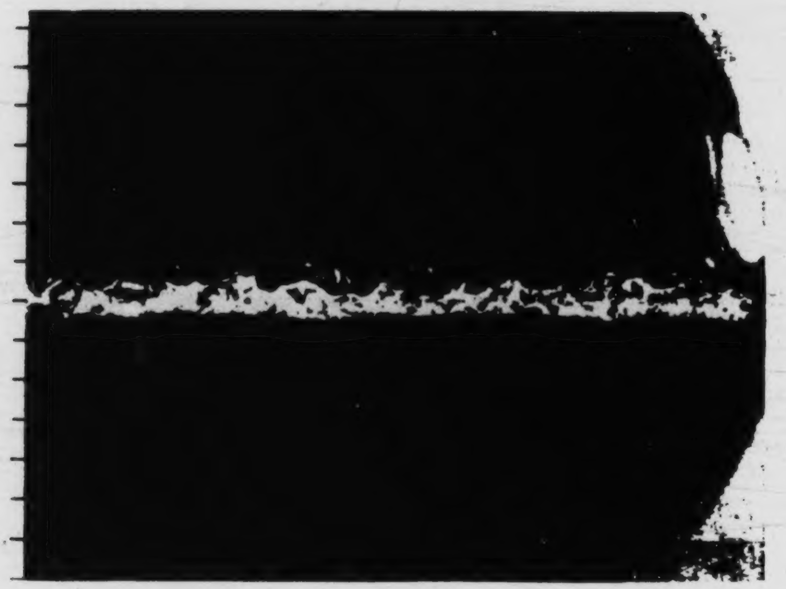

Section

Scale in millimeters

Figure 4.4 Details of Roughness #1 (Hollingshead, 1972)

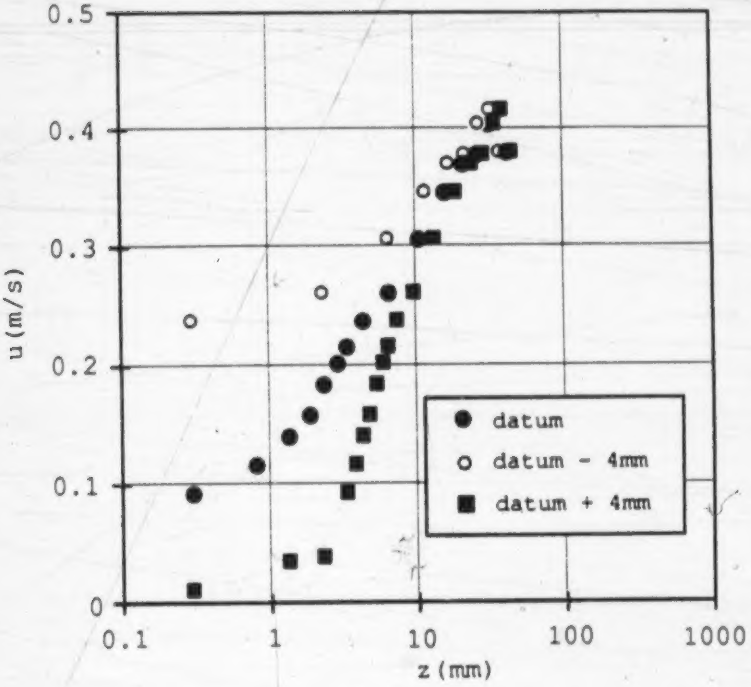

Figure 4.5 Determination of roughness datum

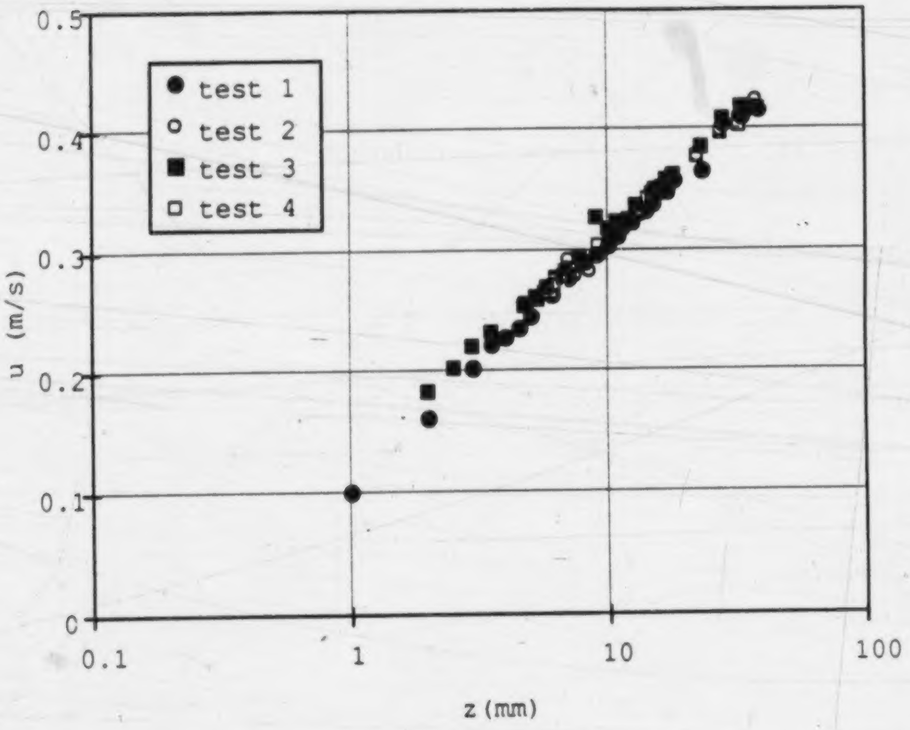

Figure 4.6 Velocity profile normal to the boundary

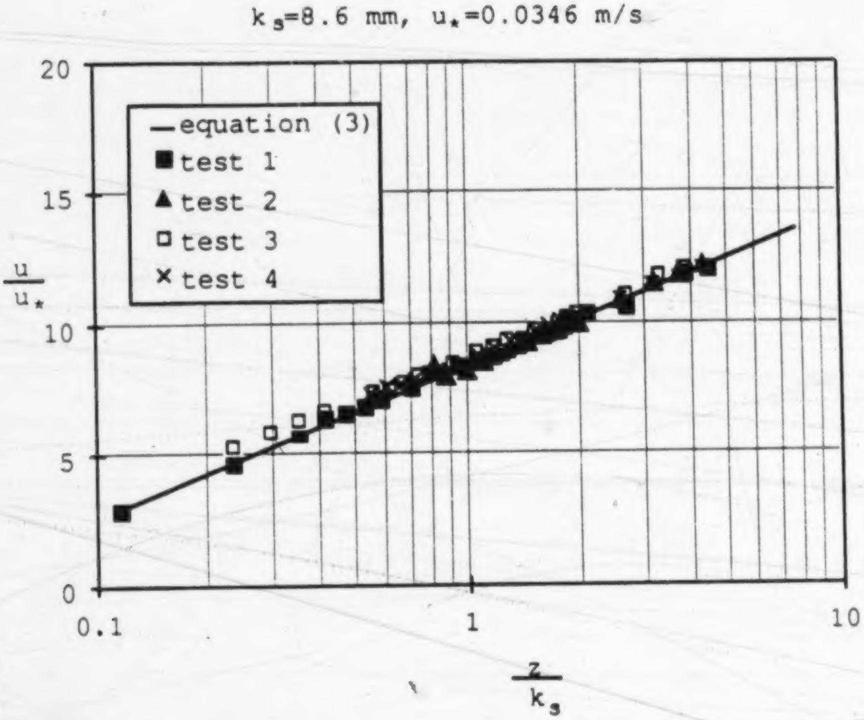

Figure 4.7 Dimensionless velocity profile

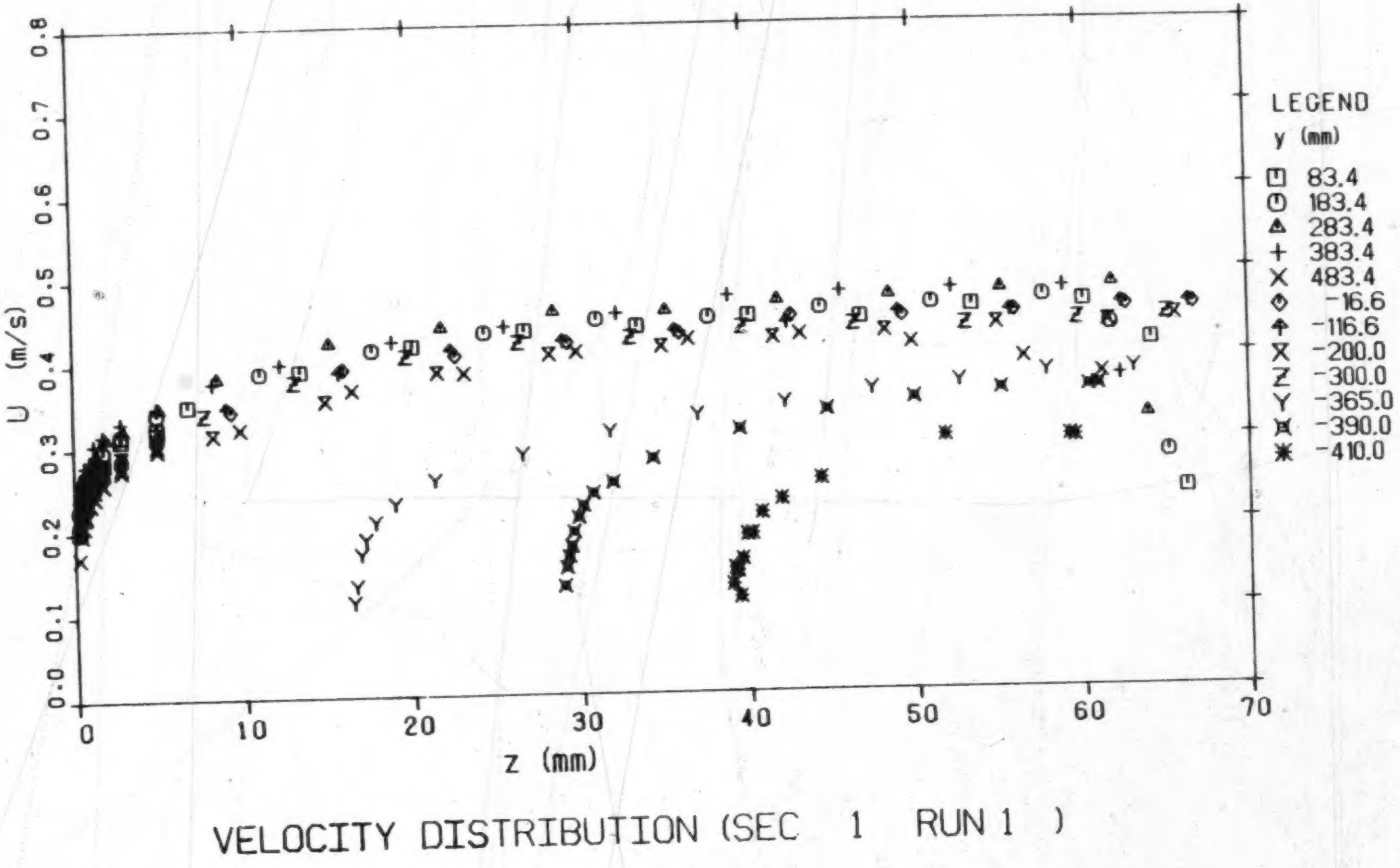

Figure 4.8 u velocity distribution (run 1, section 1)

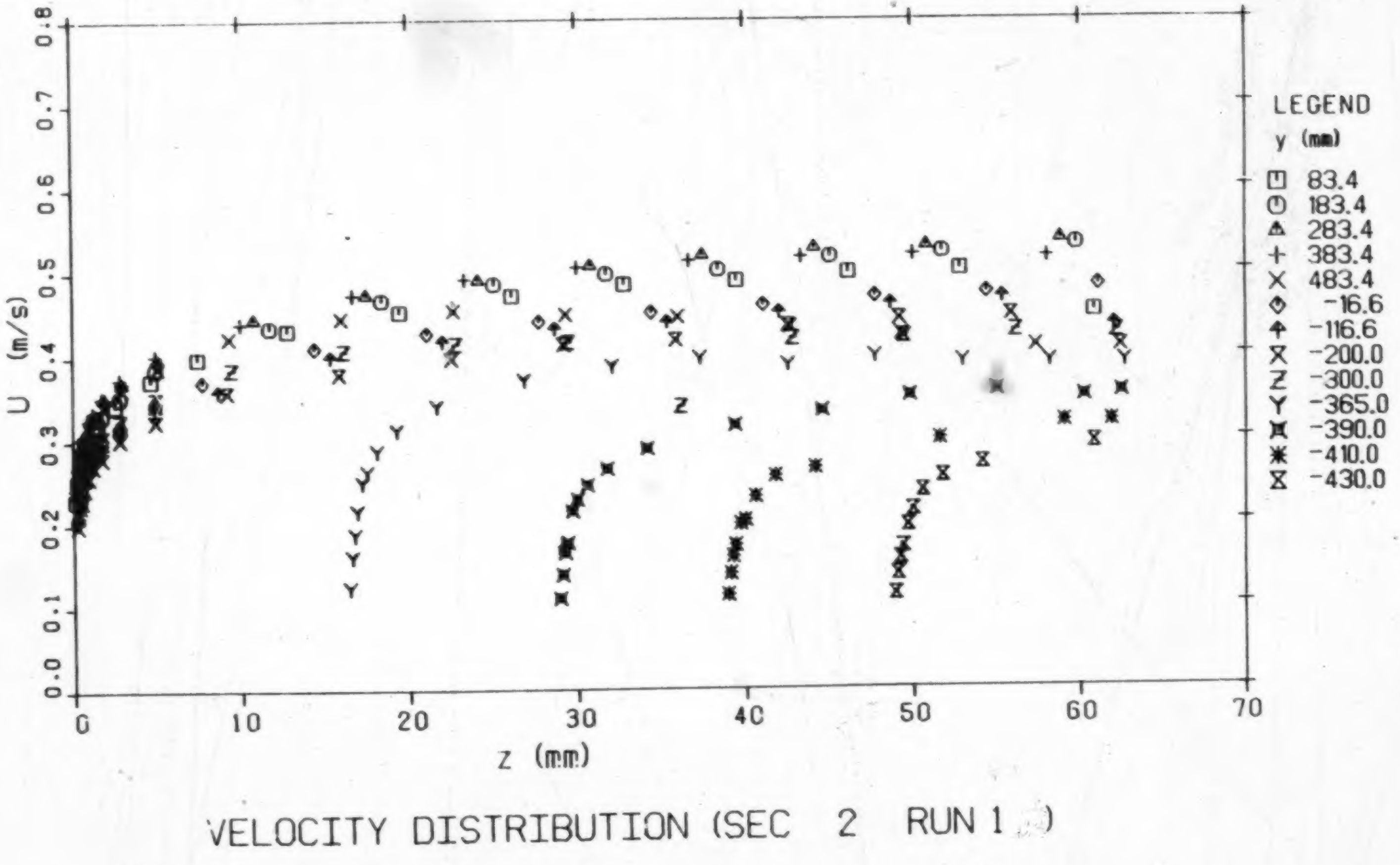

Figure 4.9 u velocity distribution (run 1, section 2)

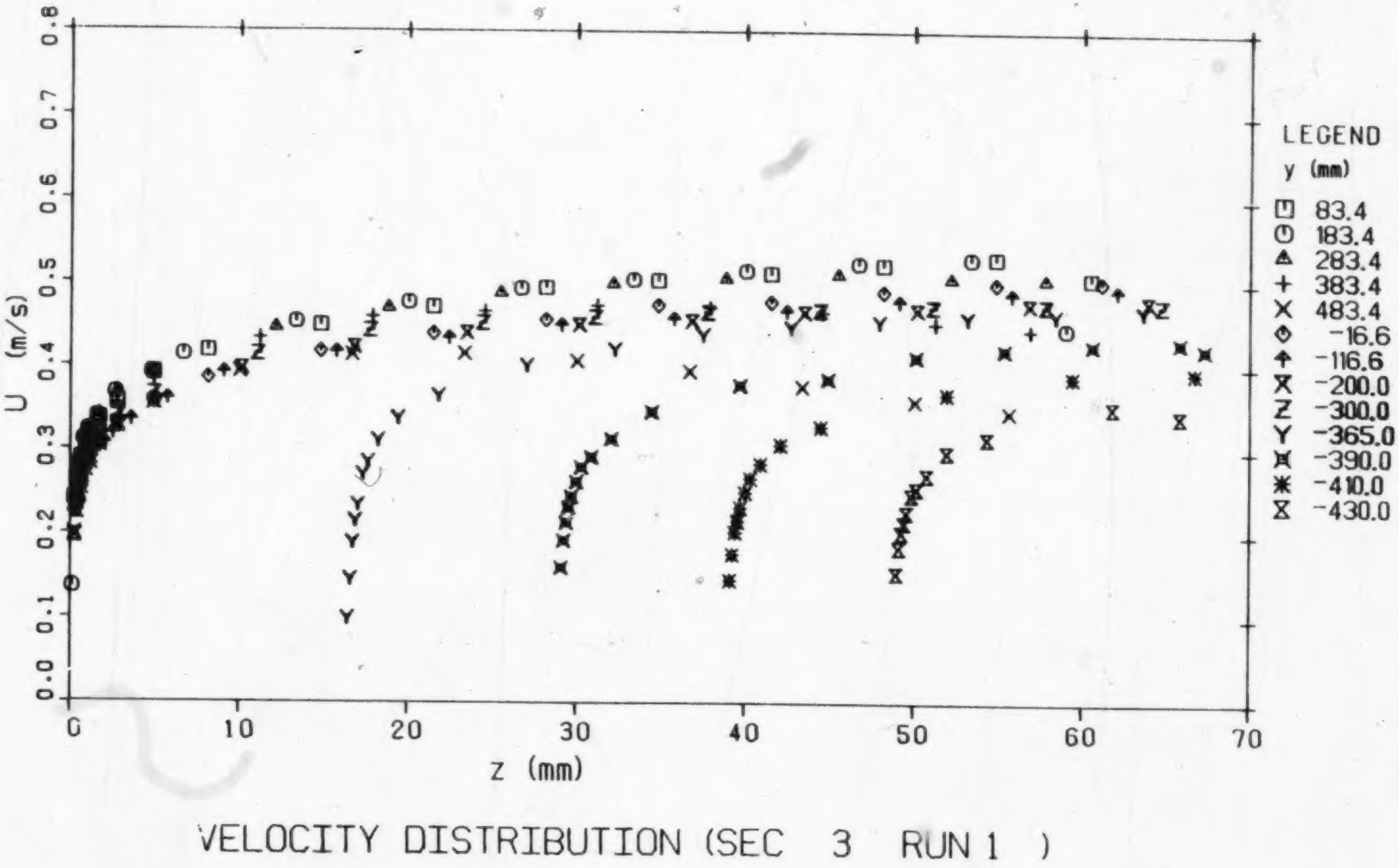

Figure 4.10 u velocity distribution (run.1, section 3)

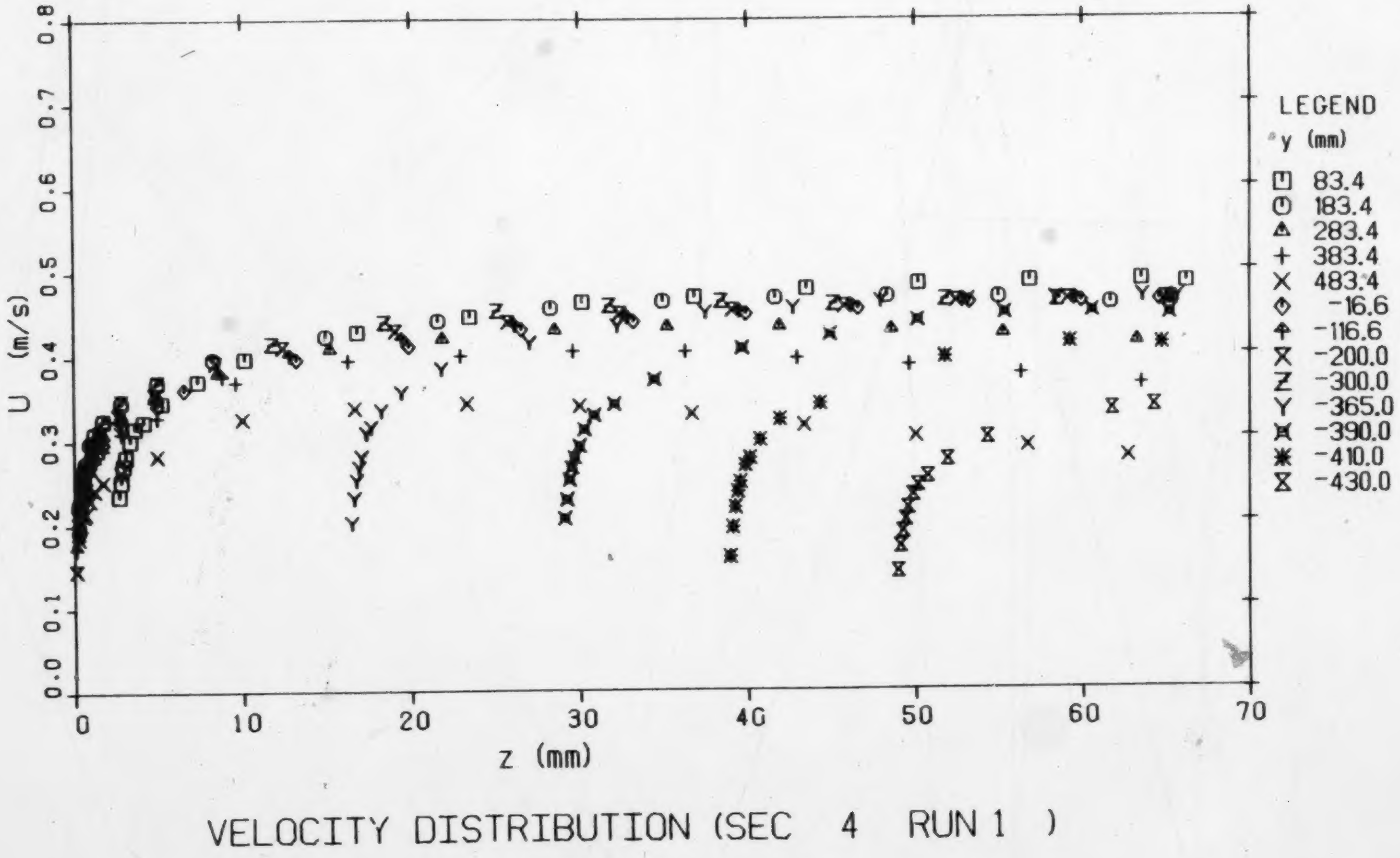

Figure 4.11 u velocity distribution (run 1, section 4)

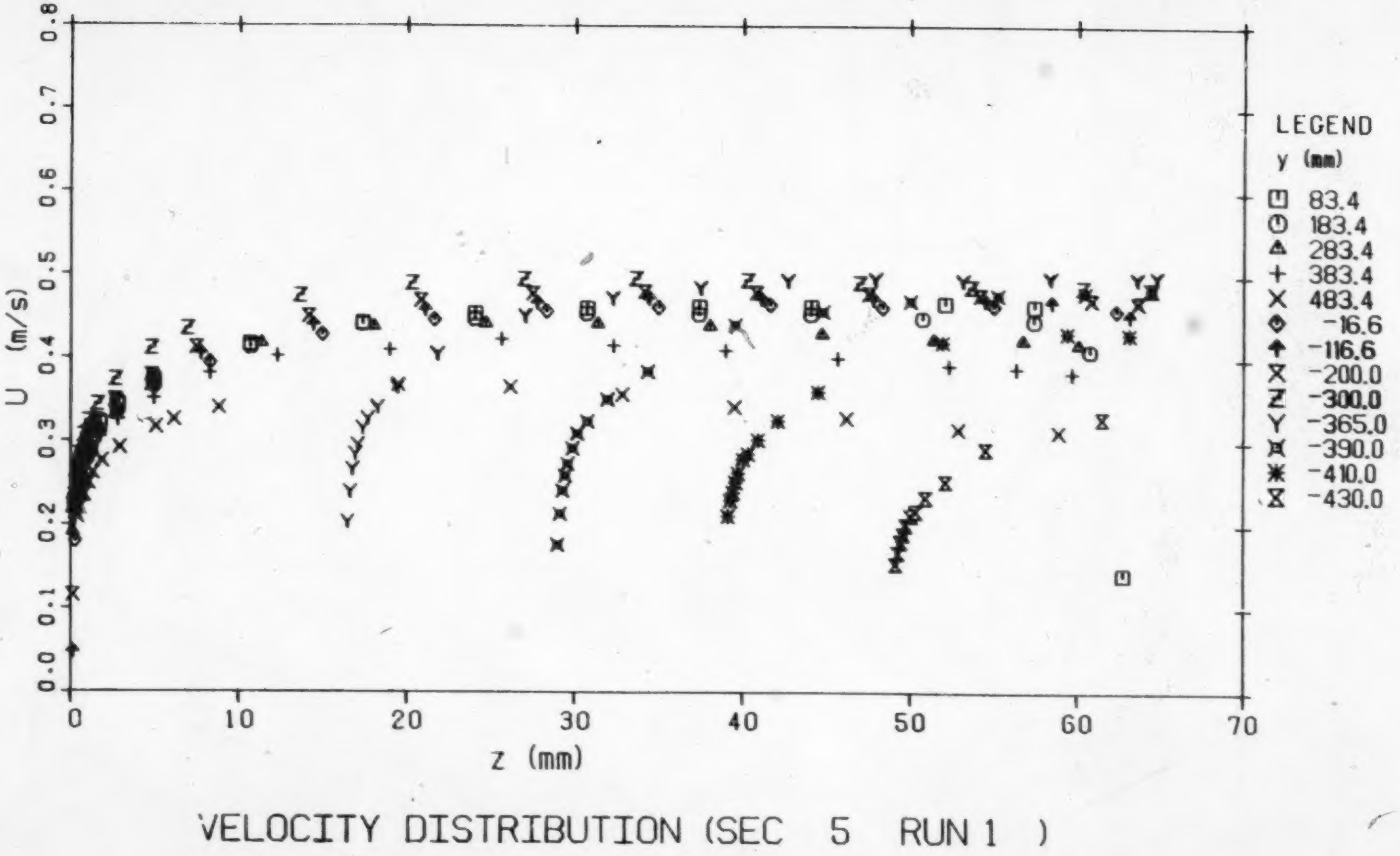

VELOCITY DISTRIBUTION (SEC 5 RUN 1)

Figure 4.12 u velocity distribution (run 1, section 5)

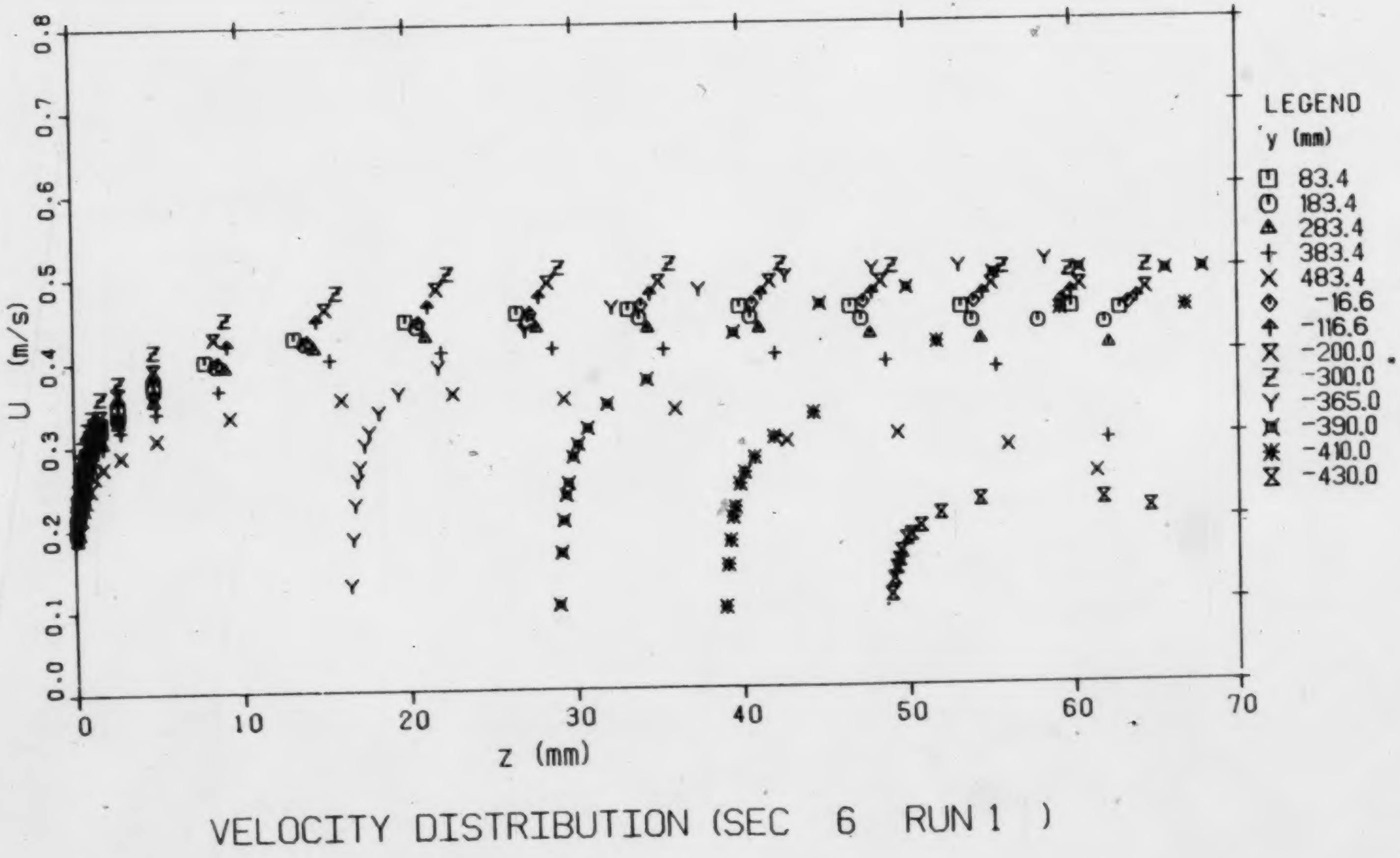

Figure 4.13 u velocity distribution (run 1, section 6)

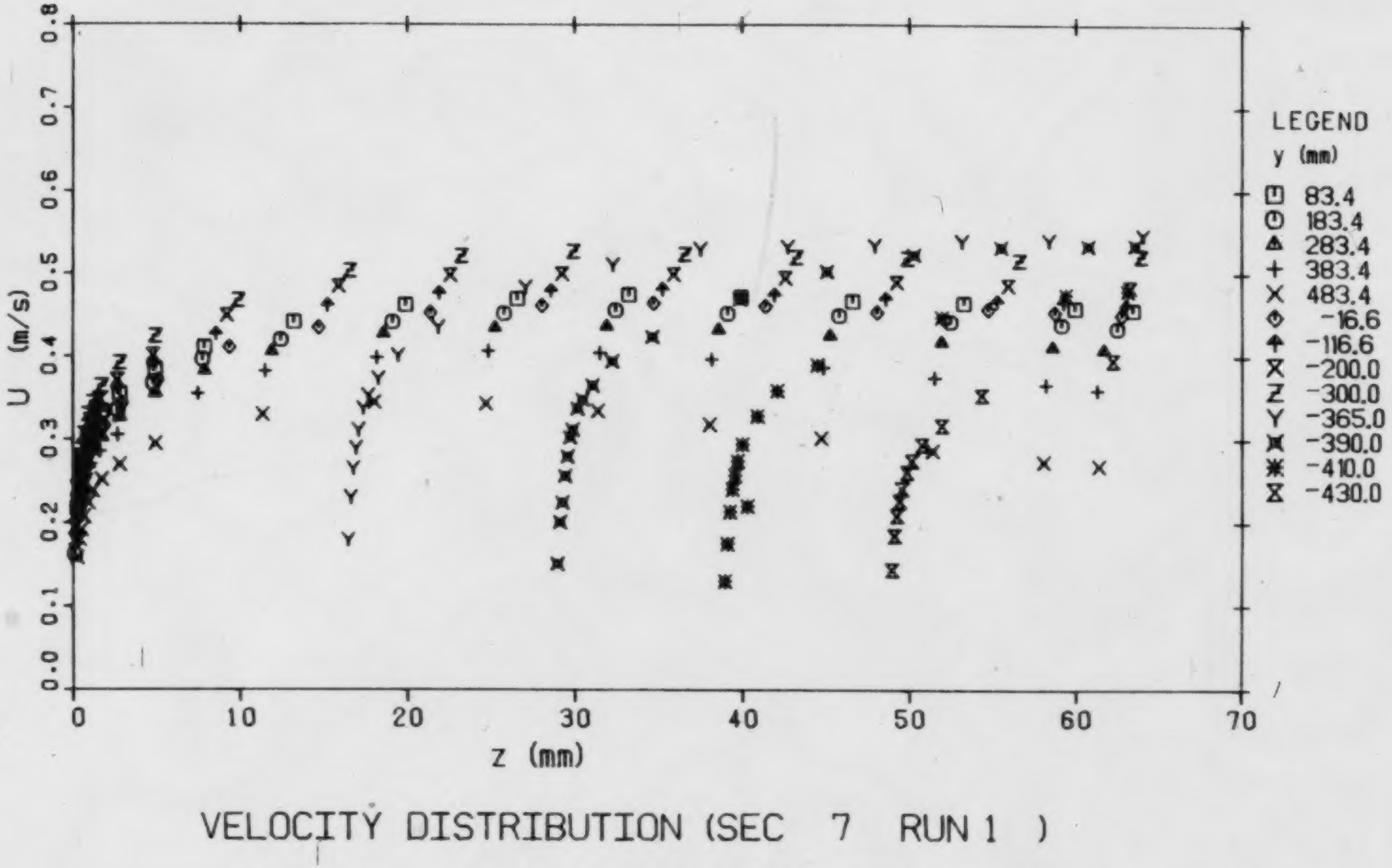

Figure 4.14 u velocity distribution (run 1, section 7)

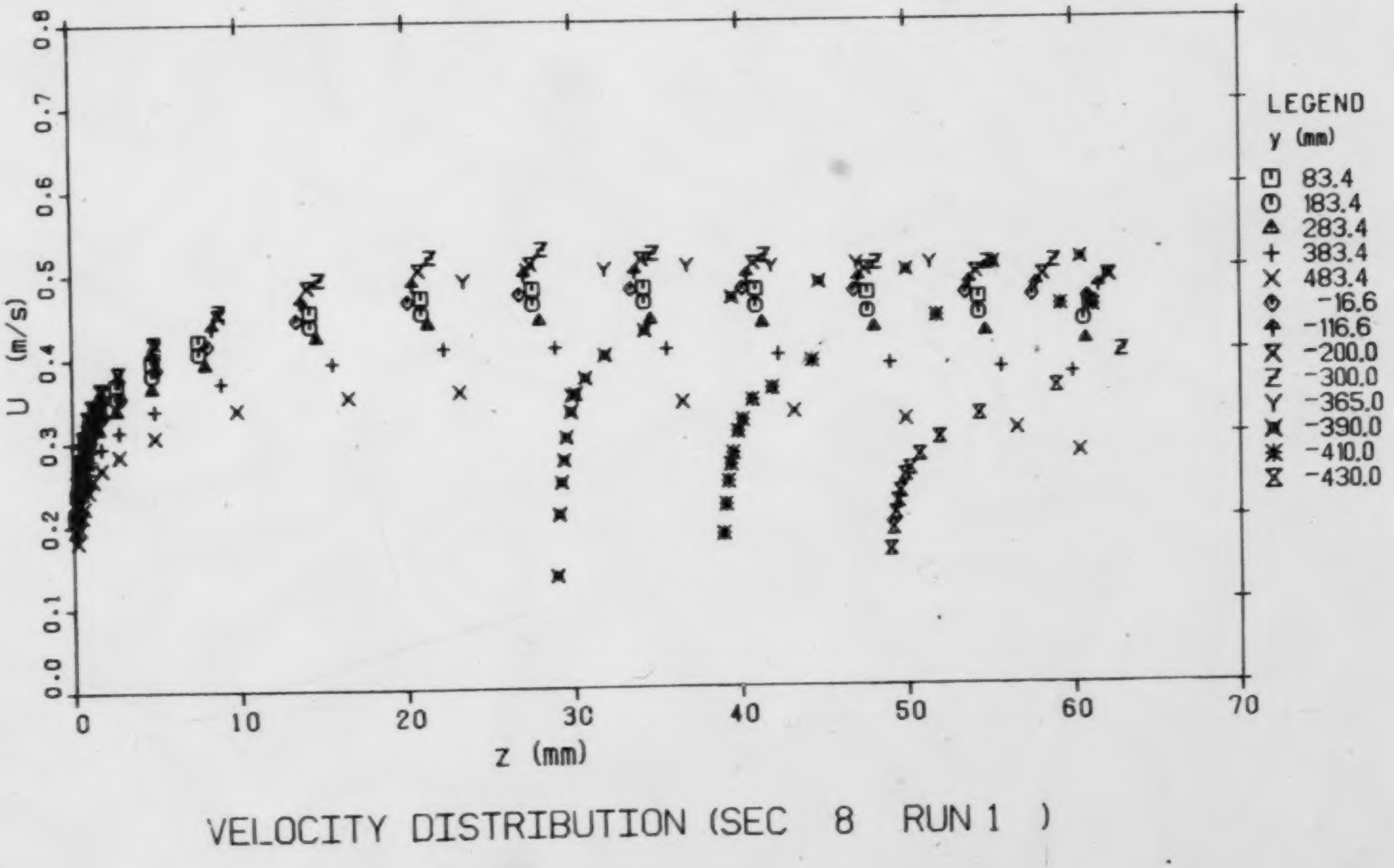

Figure 4.15 u velocity distribution (run 1, section 8)

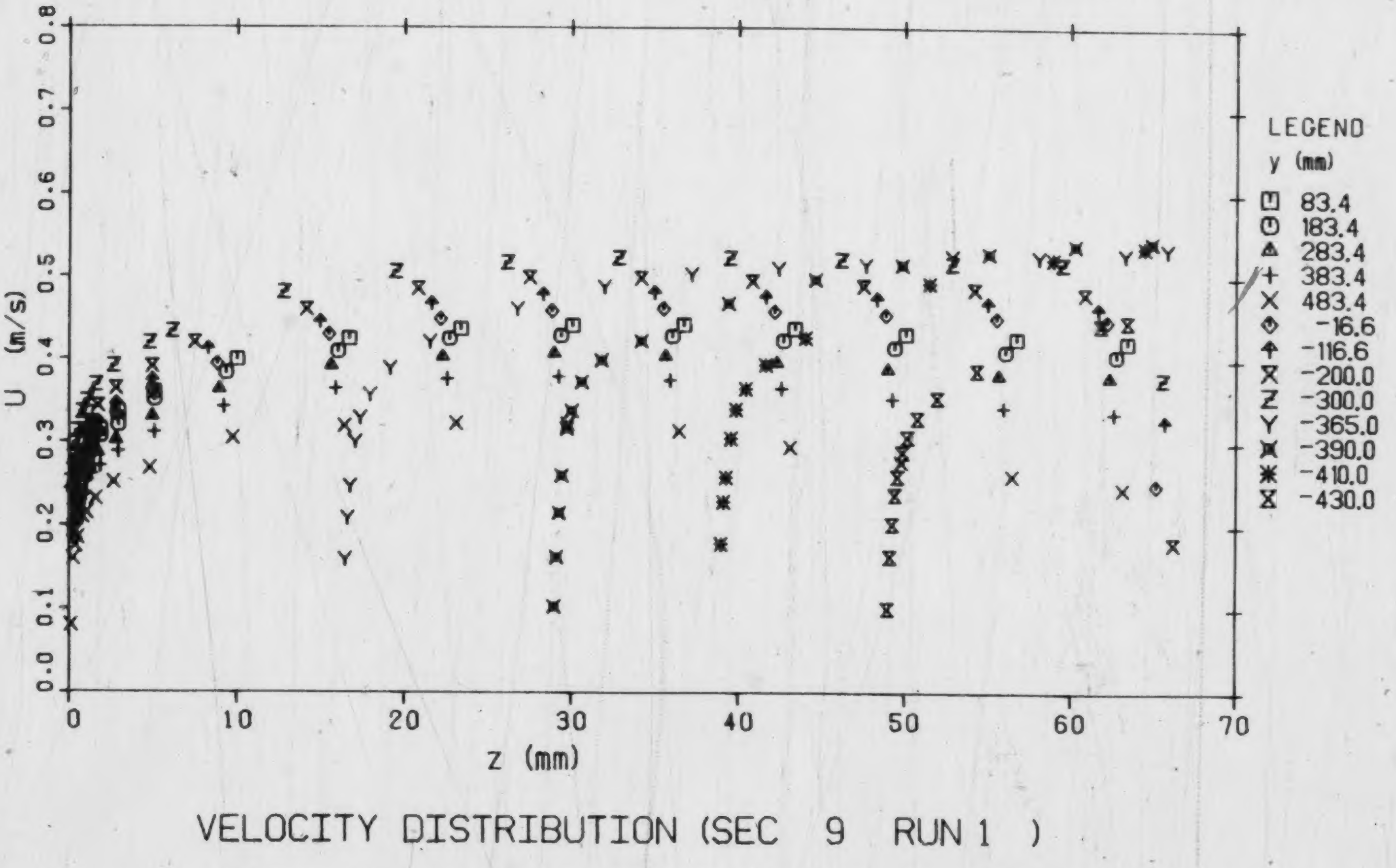

Figure 4.16 u velocity distribution (run 1, section 9)

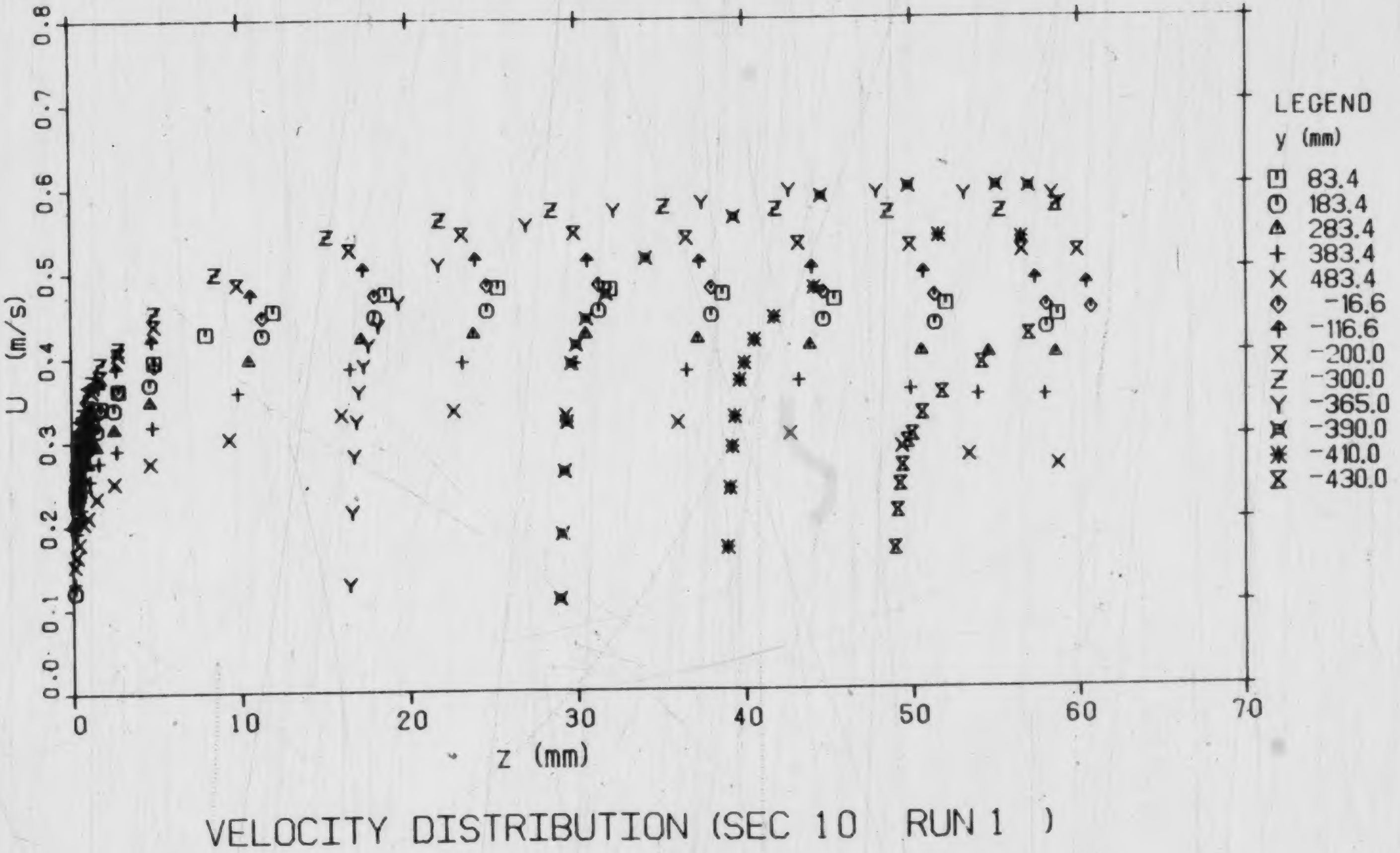

Figure 4.17 u velocity distribution (run 1, section 10)

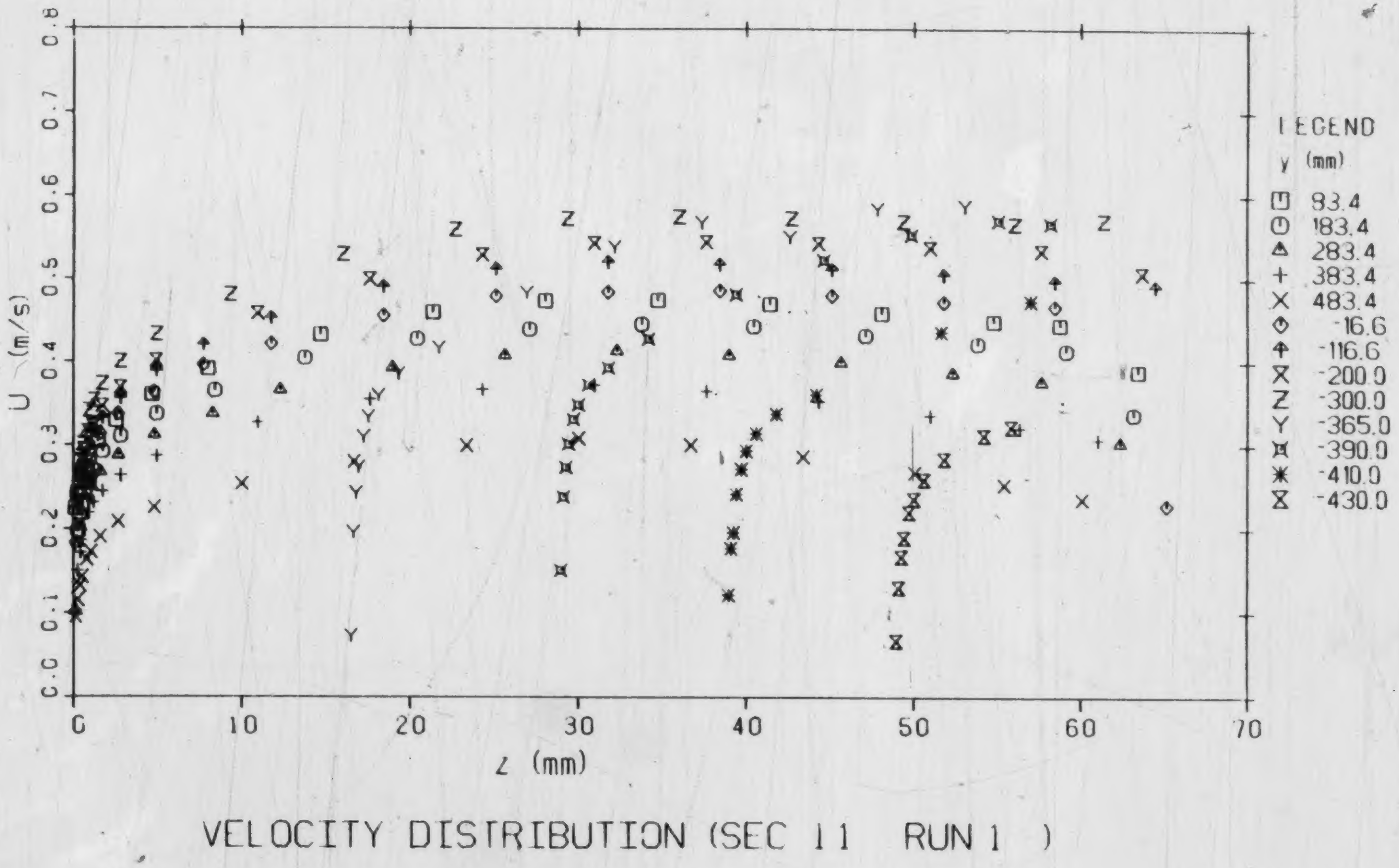

Figure 4.18 u velocity distribution (run 1, section 11)

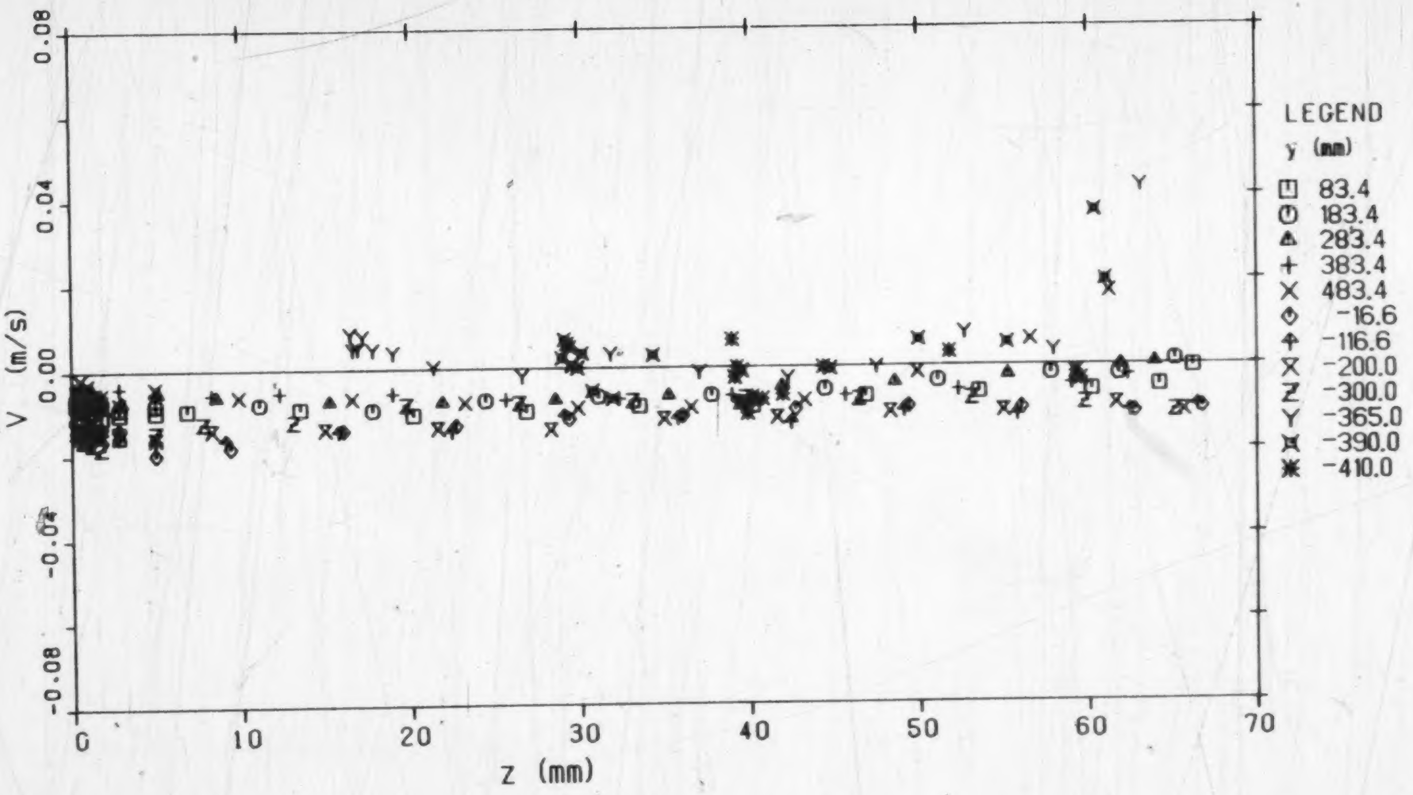

VELOCITY DISTRIBUTION (SEC 1 RUN 1)

Figure 4.19 v velocity distribution (run 1, section 1)

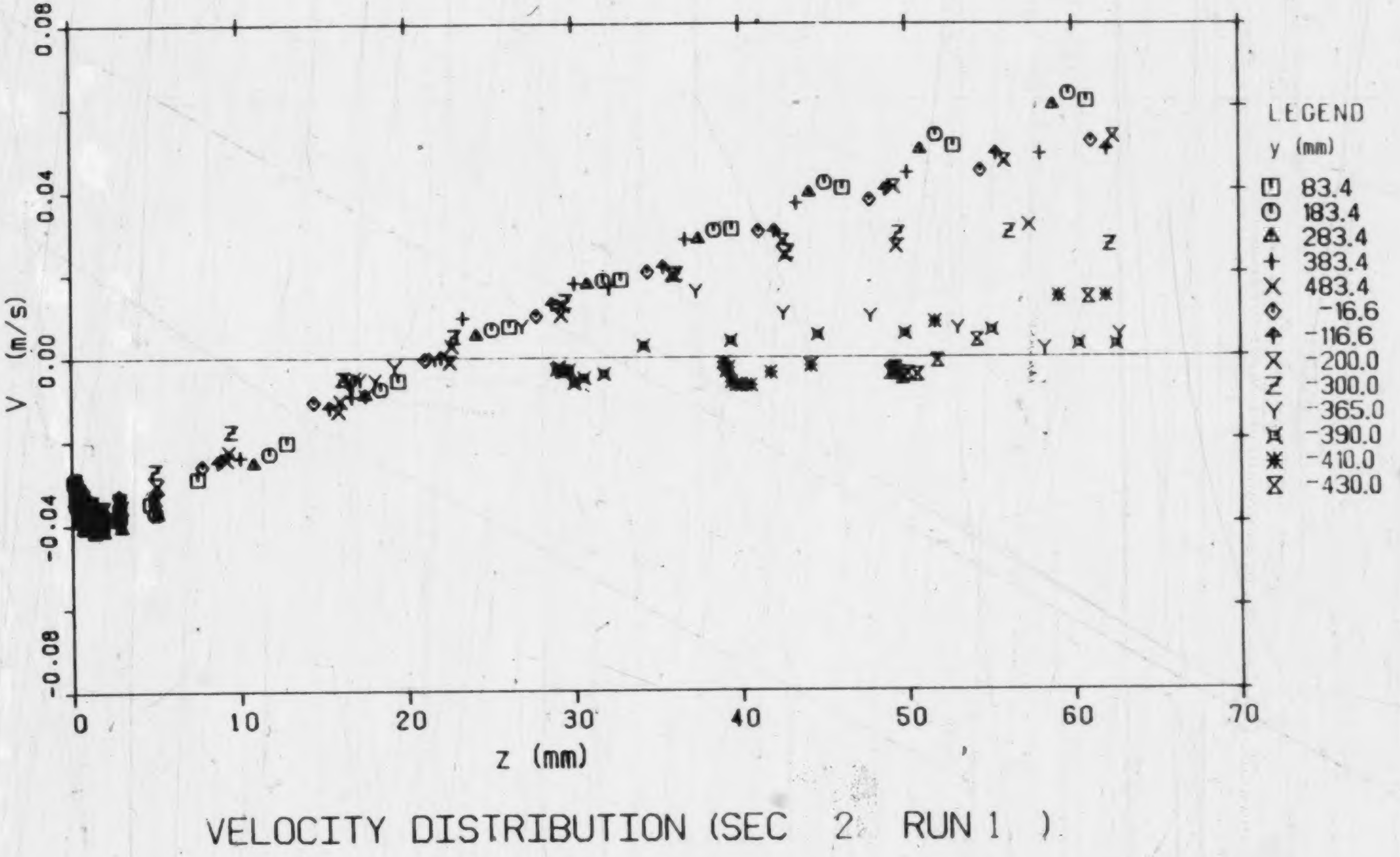

Figure 4.20 v velocity distribution (run 1, section 2)

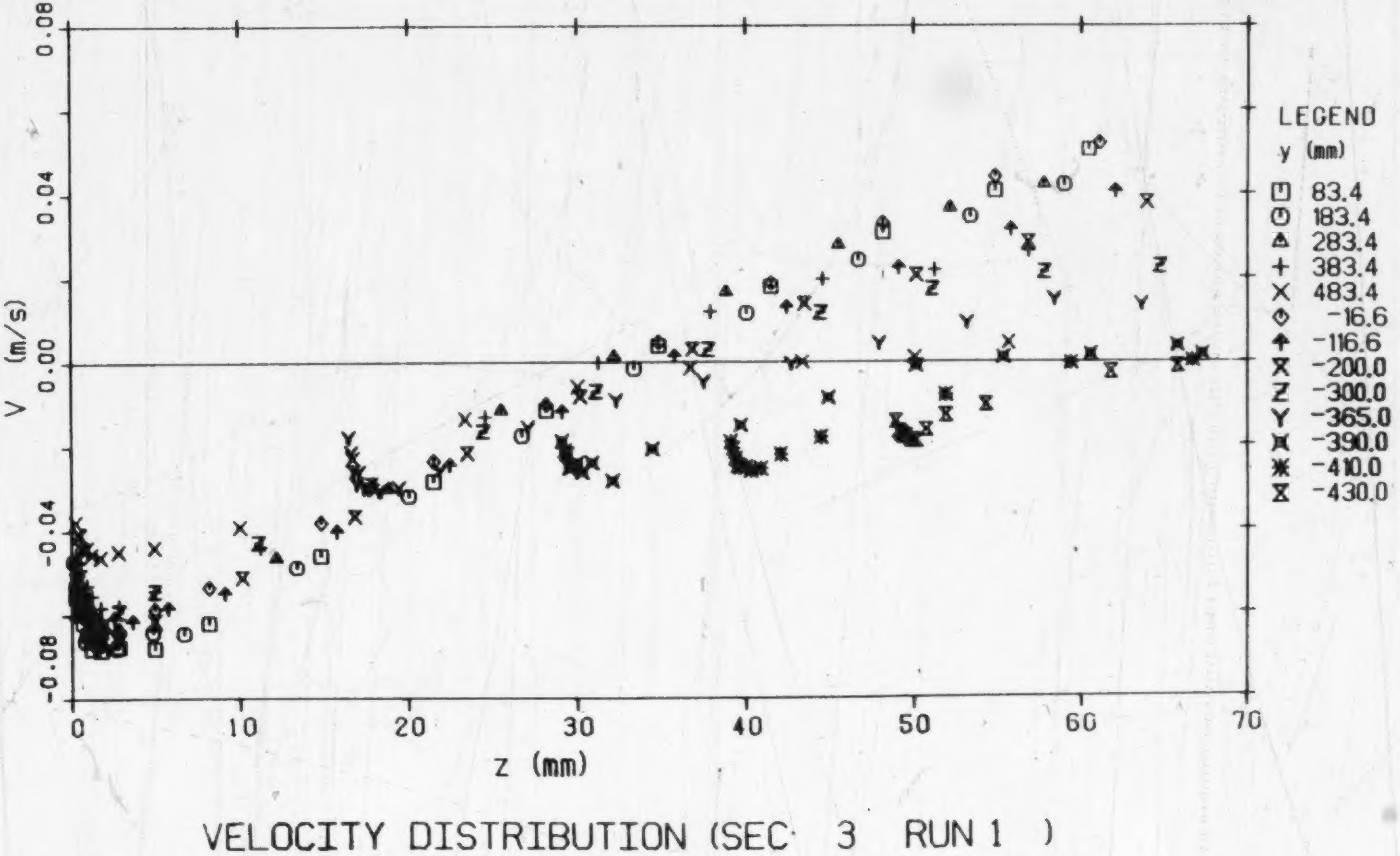

Figure 4.21 v velocity distribution (run 1, section 3)

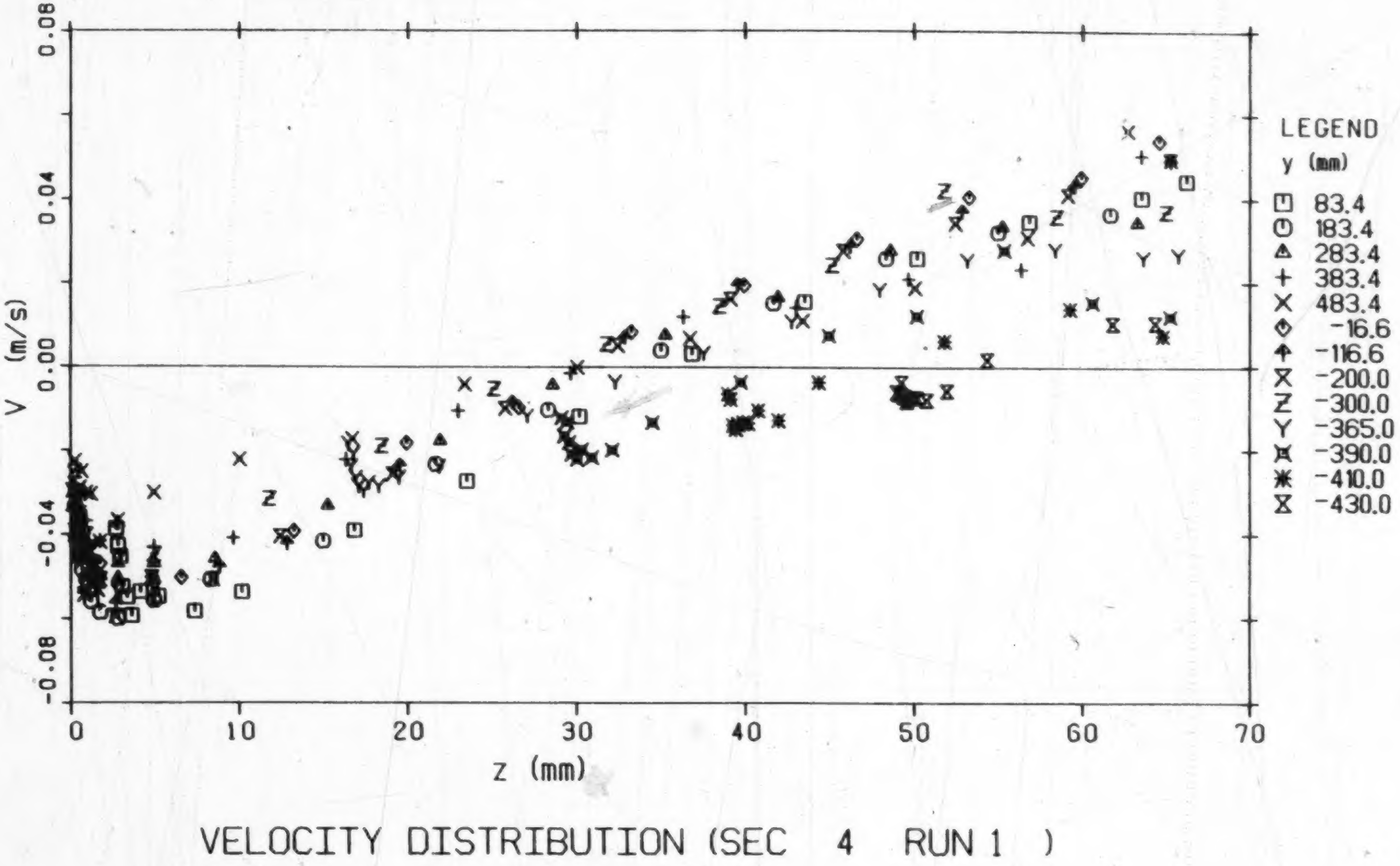

Figure 4.22 v velocity distribution (run 1, section 4)

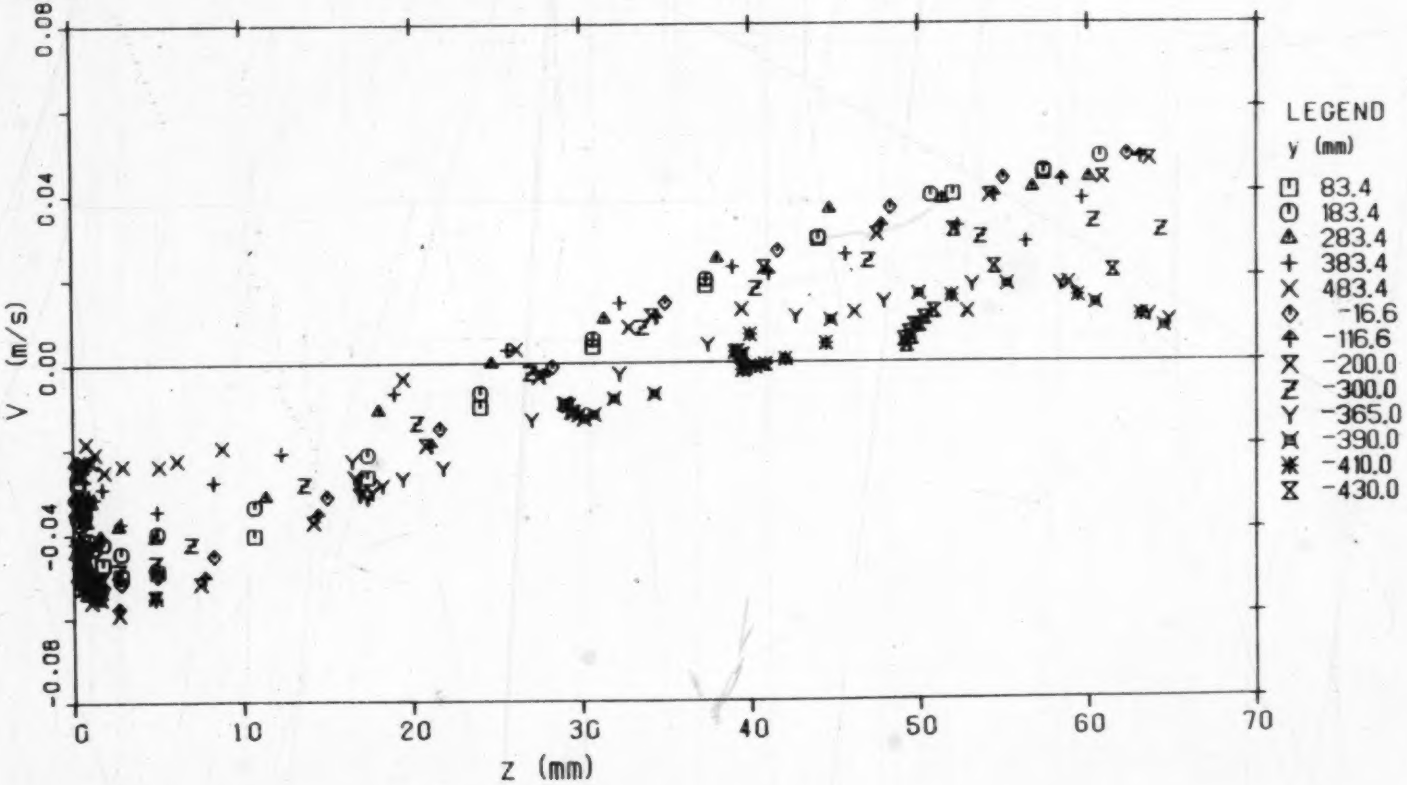

VELOCITY DISTRIBUTION (SEC 5 RUN 1)

Figure 4.23 v velocity distribution (run 1, section 5)

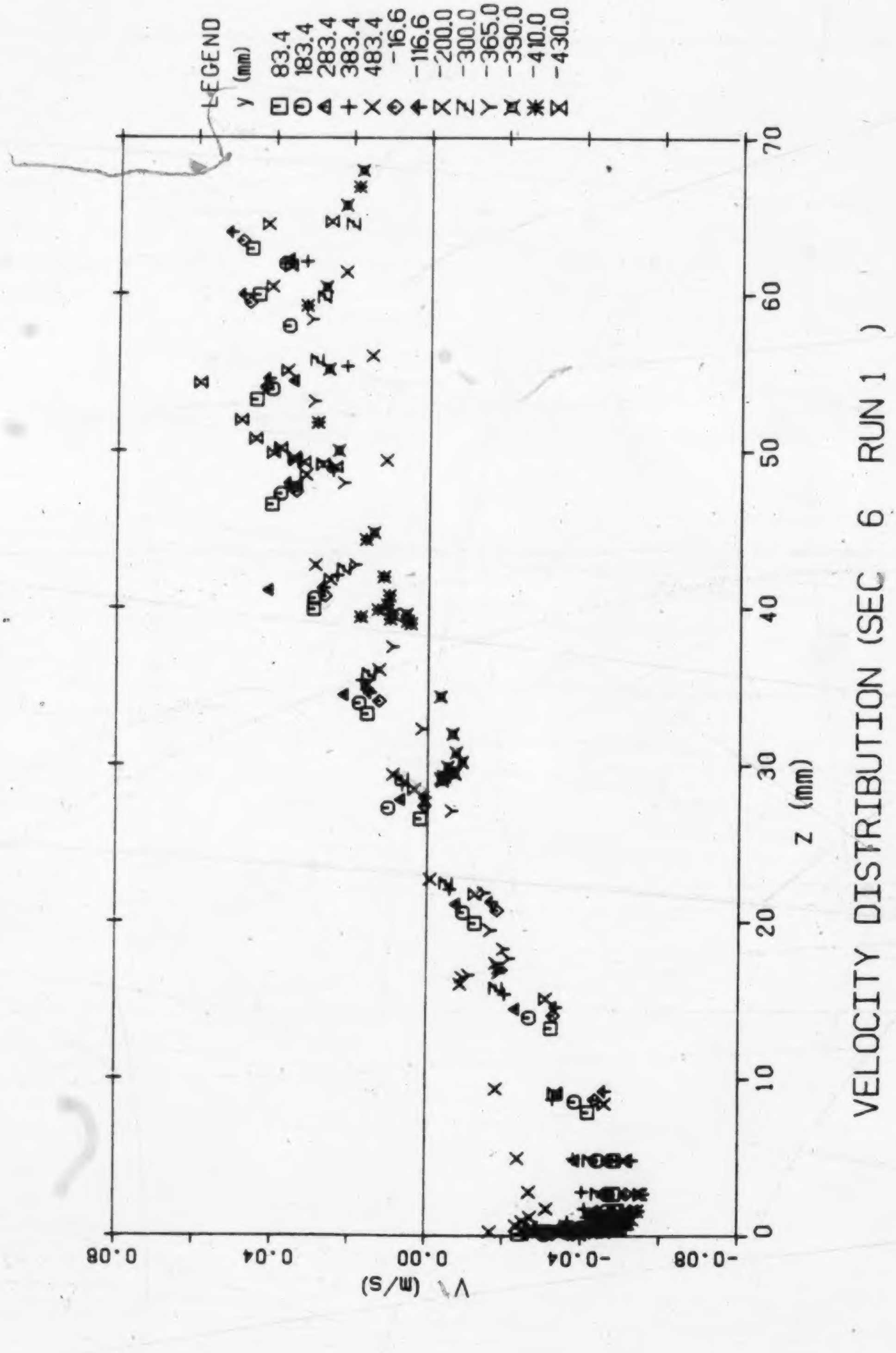

Figure 4.24 v velocity distribution (run 1, section 6)

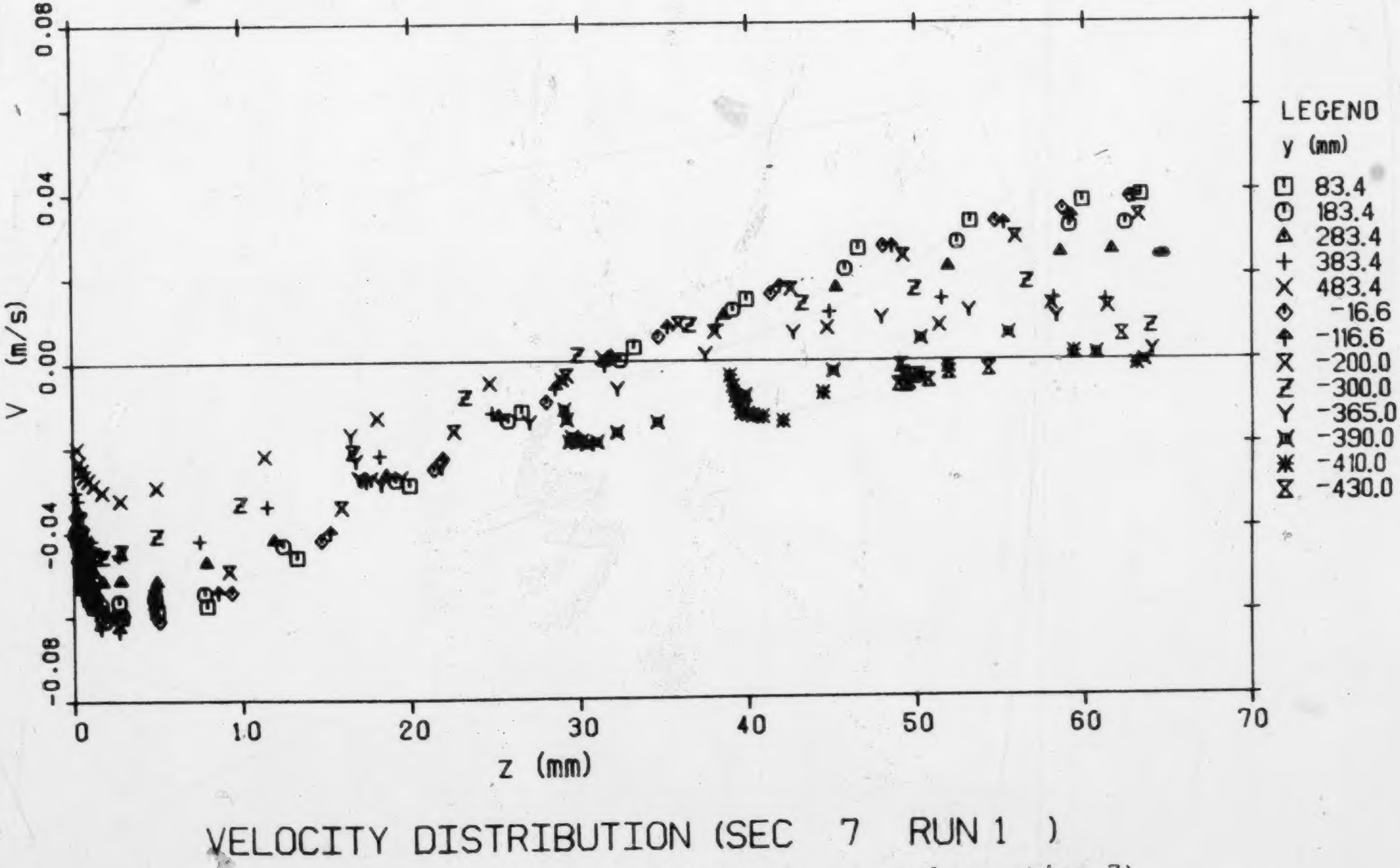

Figure 4.25 v velocity distribution (run 1, section 7)

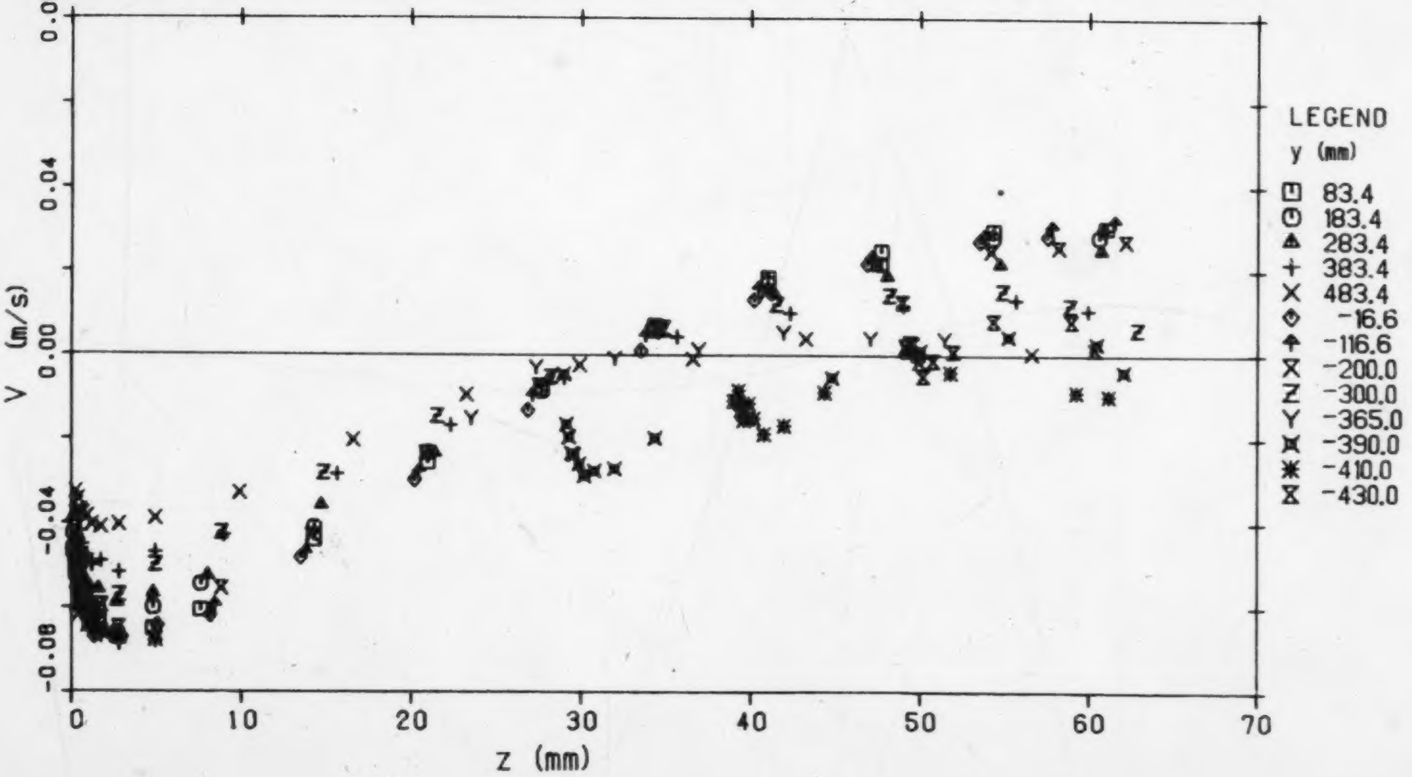

VELOCITY DISTRIBUTION (SEC 8 RUN 1)

Figure 4.26 v velocity distribution (run 1, section 8)

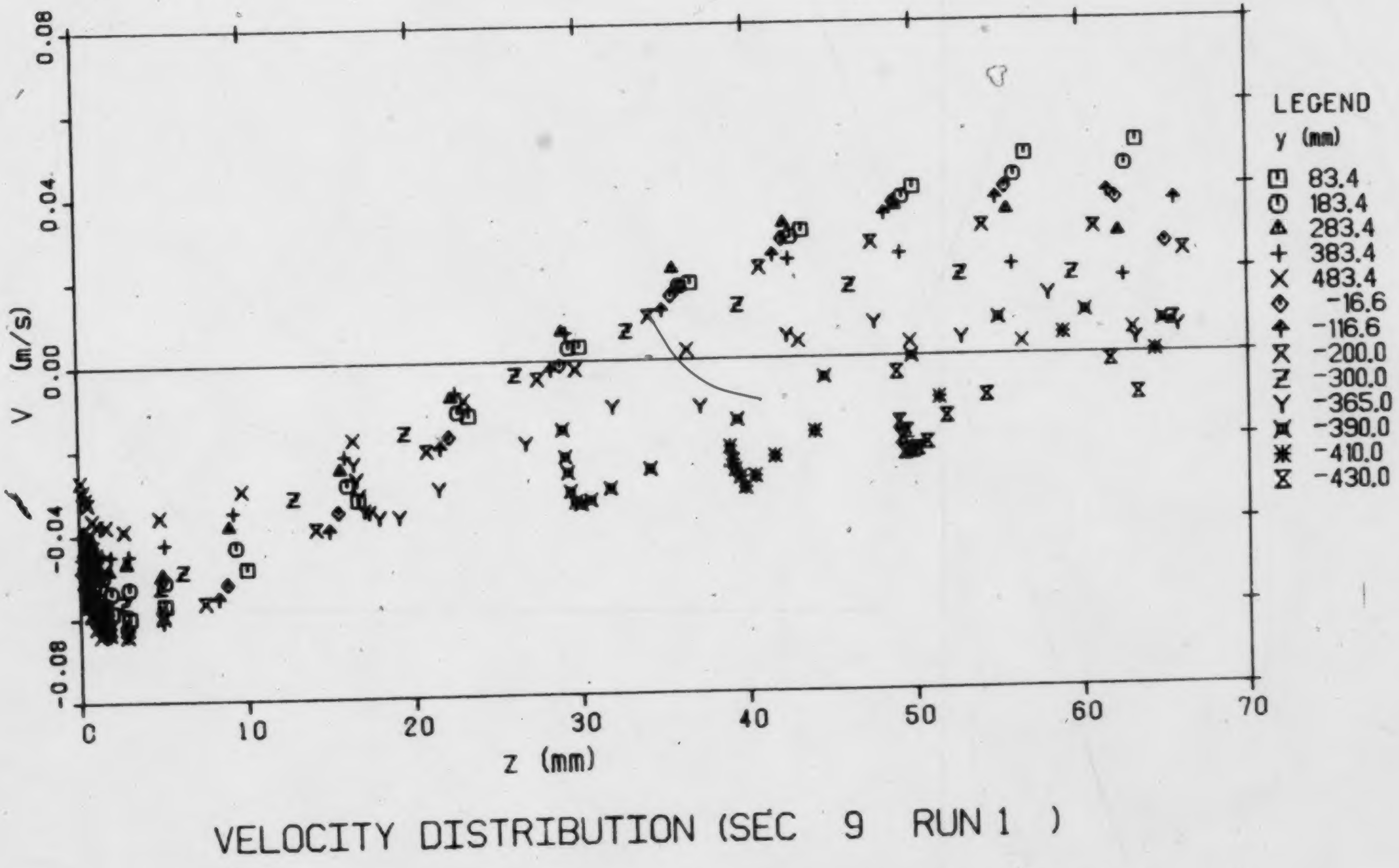

Figure 4.27 v velocity distribution (run 1, section 9)

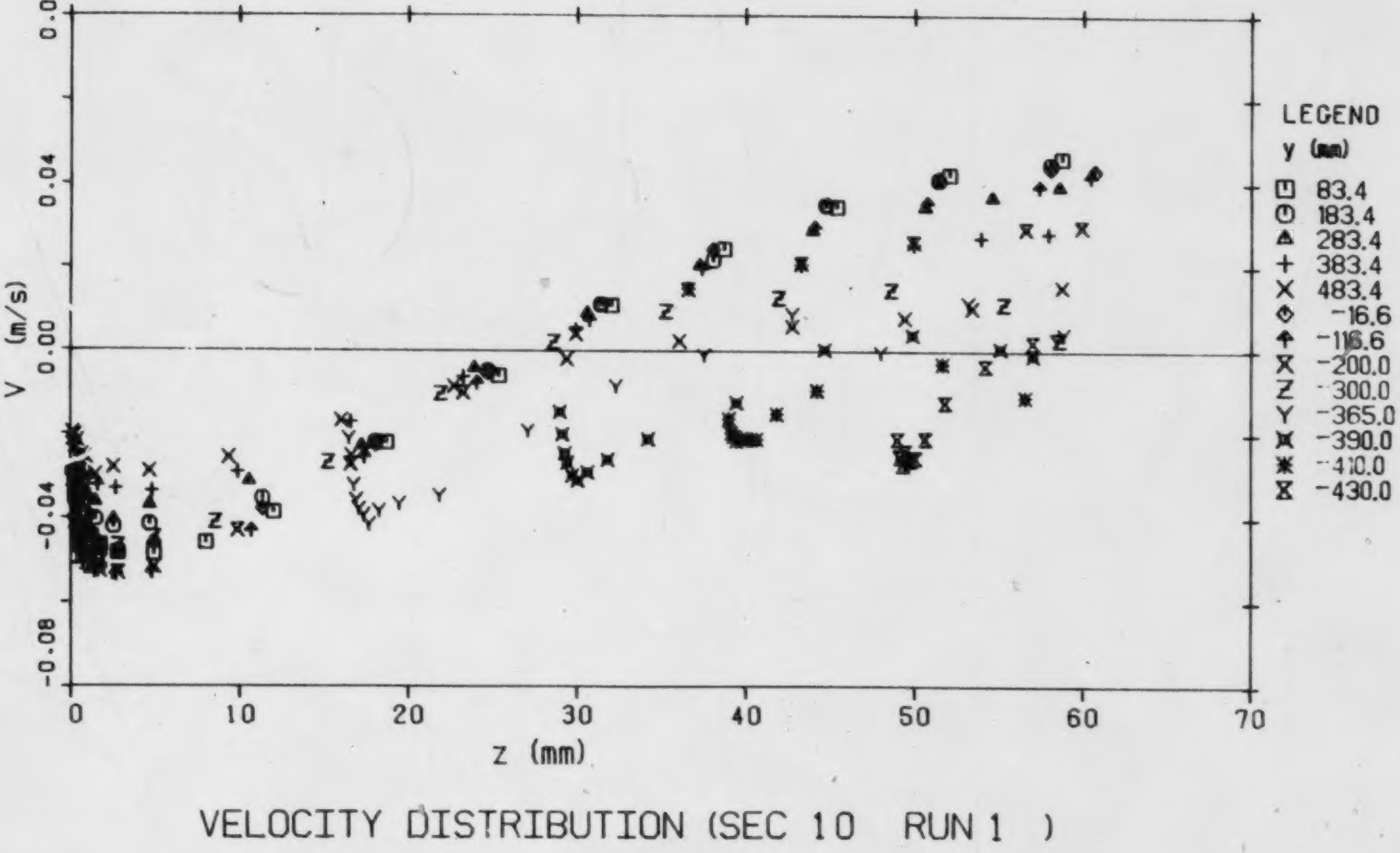

Figure 4.28 v velocity distribution (run 1, section 10)

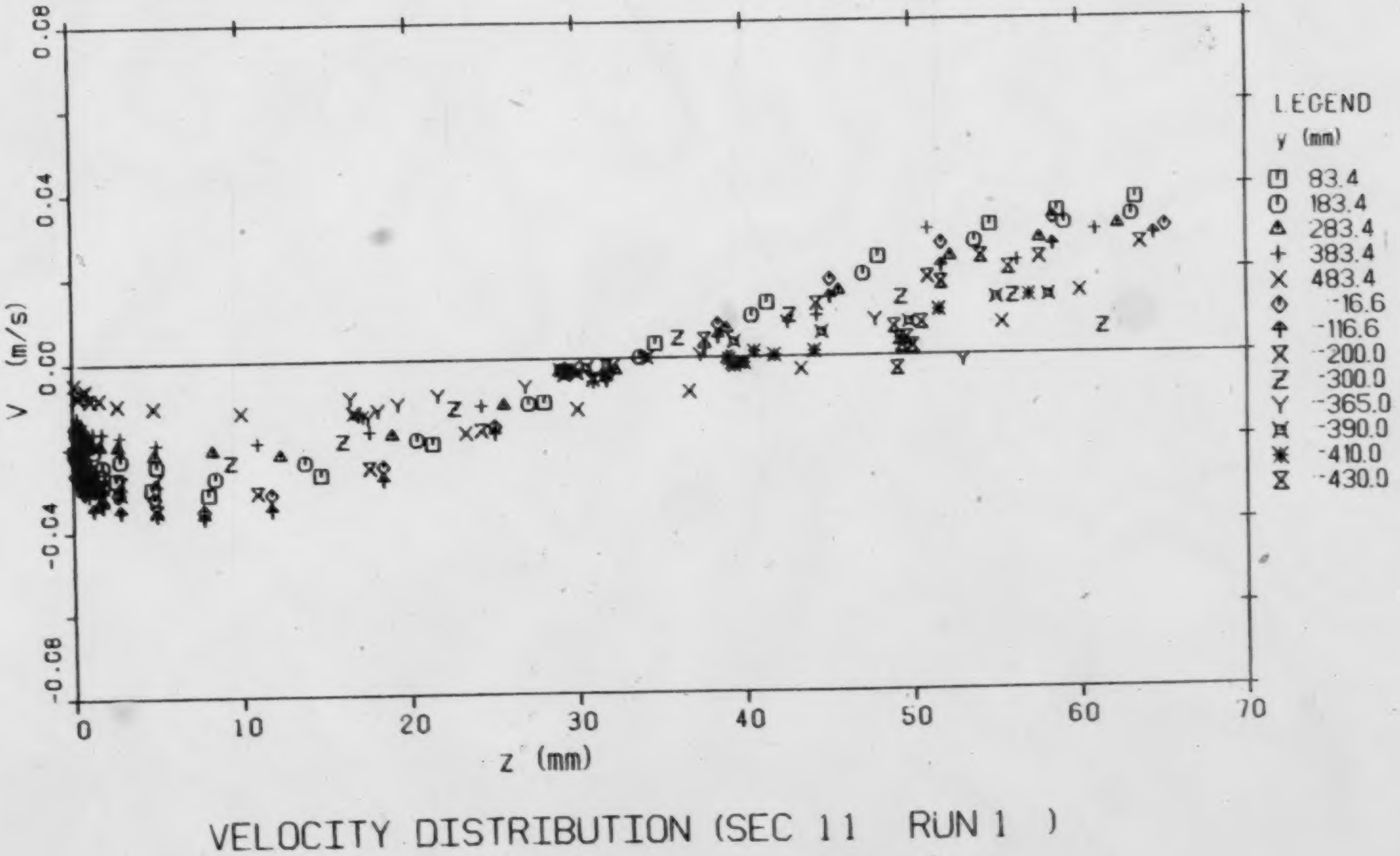

Figure 4.29 v velocity distribution (run 1, section 11)

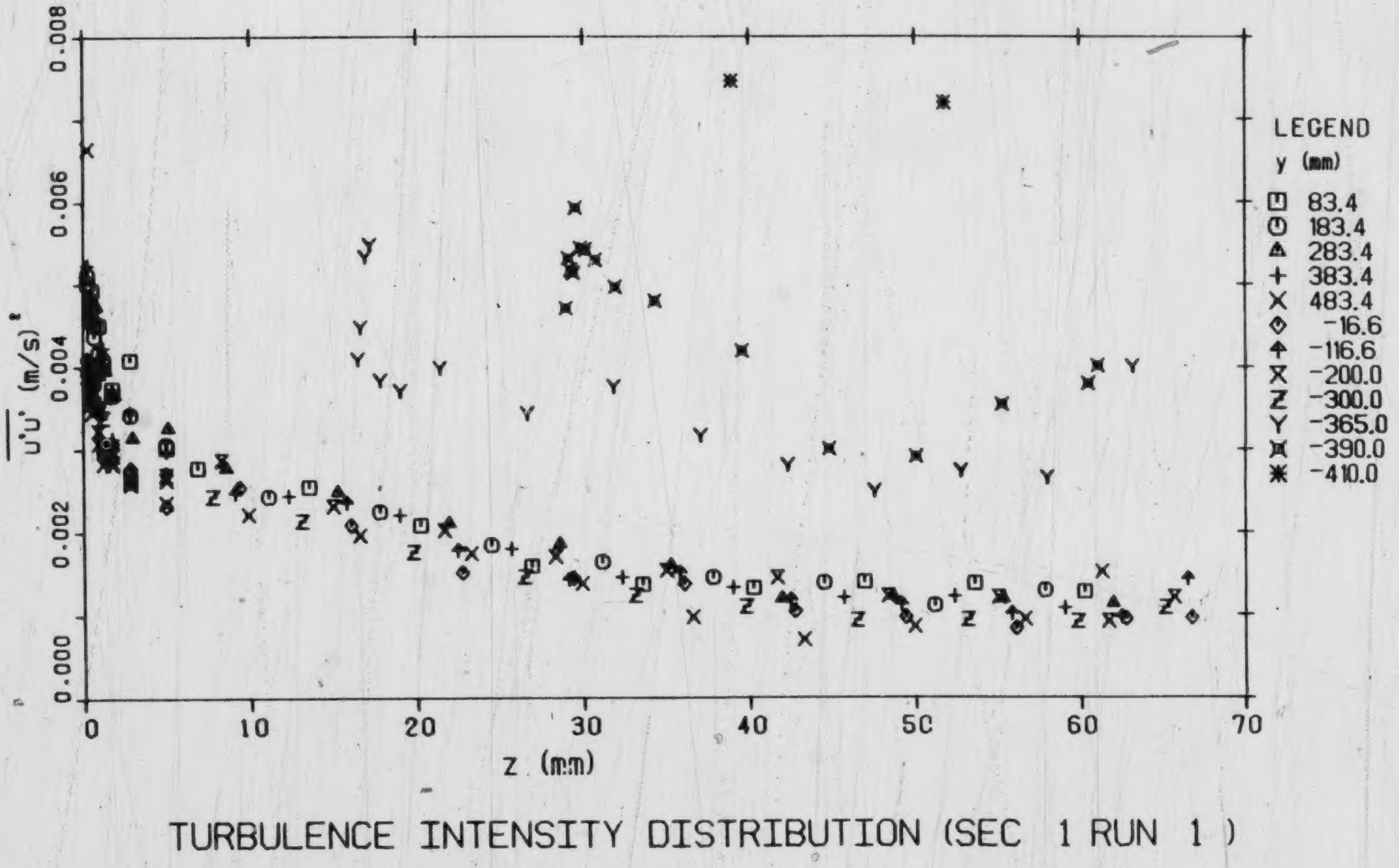

Figure 4.30 $\overline{u'u'}$ turbulence intensity distribution (run 1, section 1)

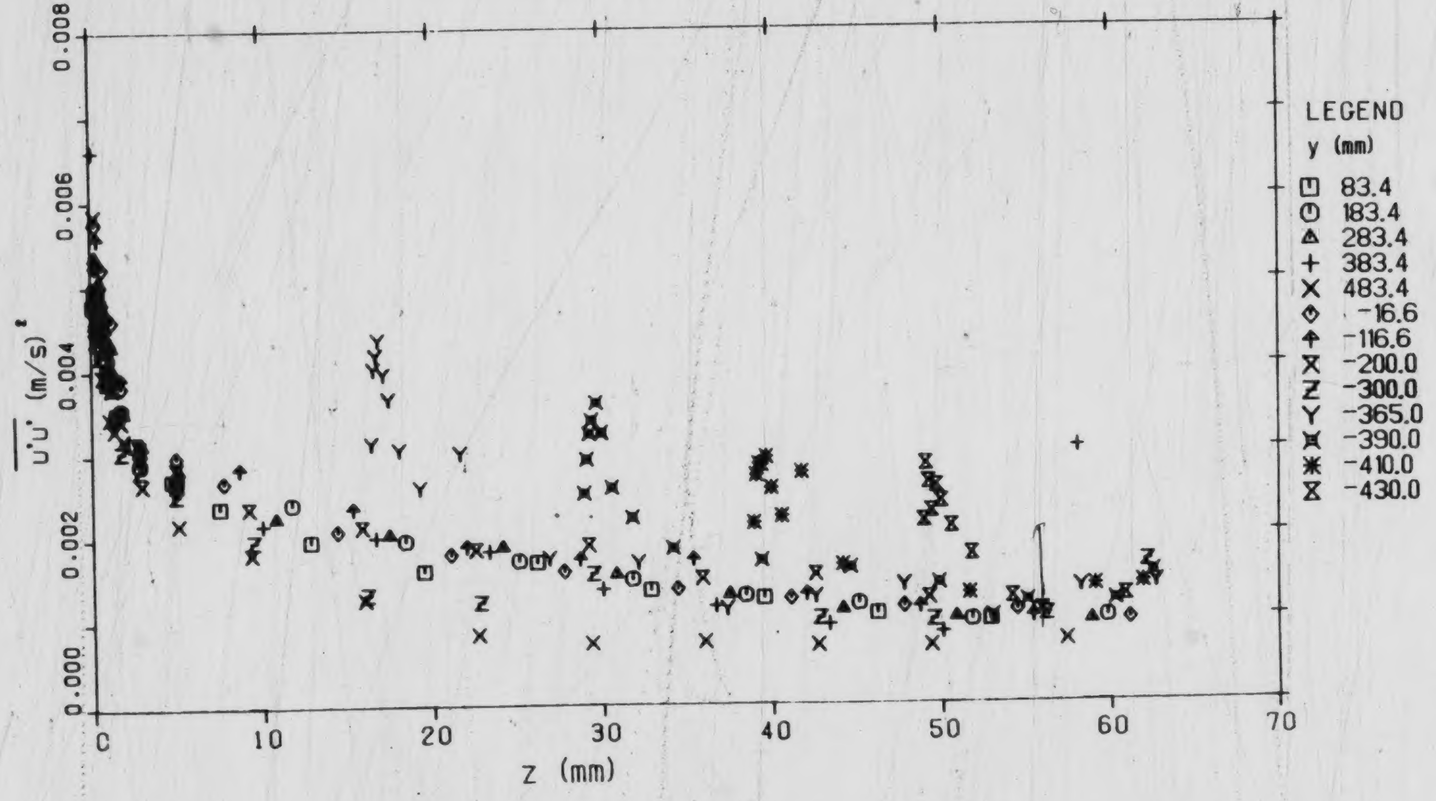

TURBULENCE INTENSITY DISTRIBUTION (SEC 2 RUN 1)

Figure 4.31 $\overline{u'u'}$ turbulence intensity distribution (run 1, section 2)

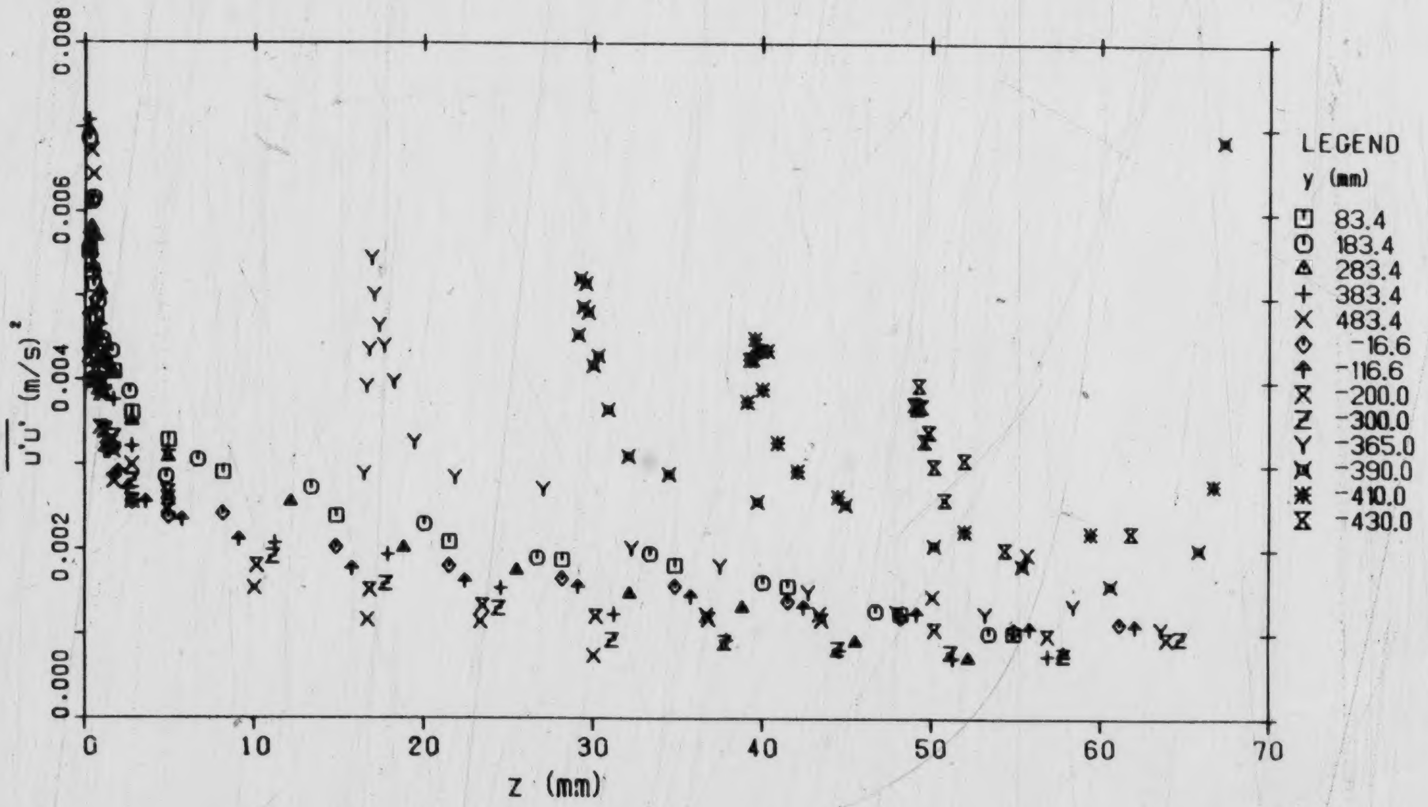

TURBULENCE INTENSITY DISTRIBUTION (SEC 3 RUN 1)

Figure 4.32 $\overline{u'u'}$ turbulence intensity distribution (run 1, section 3)

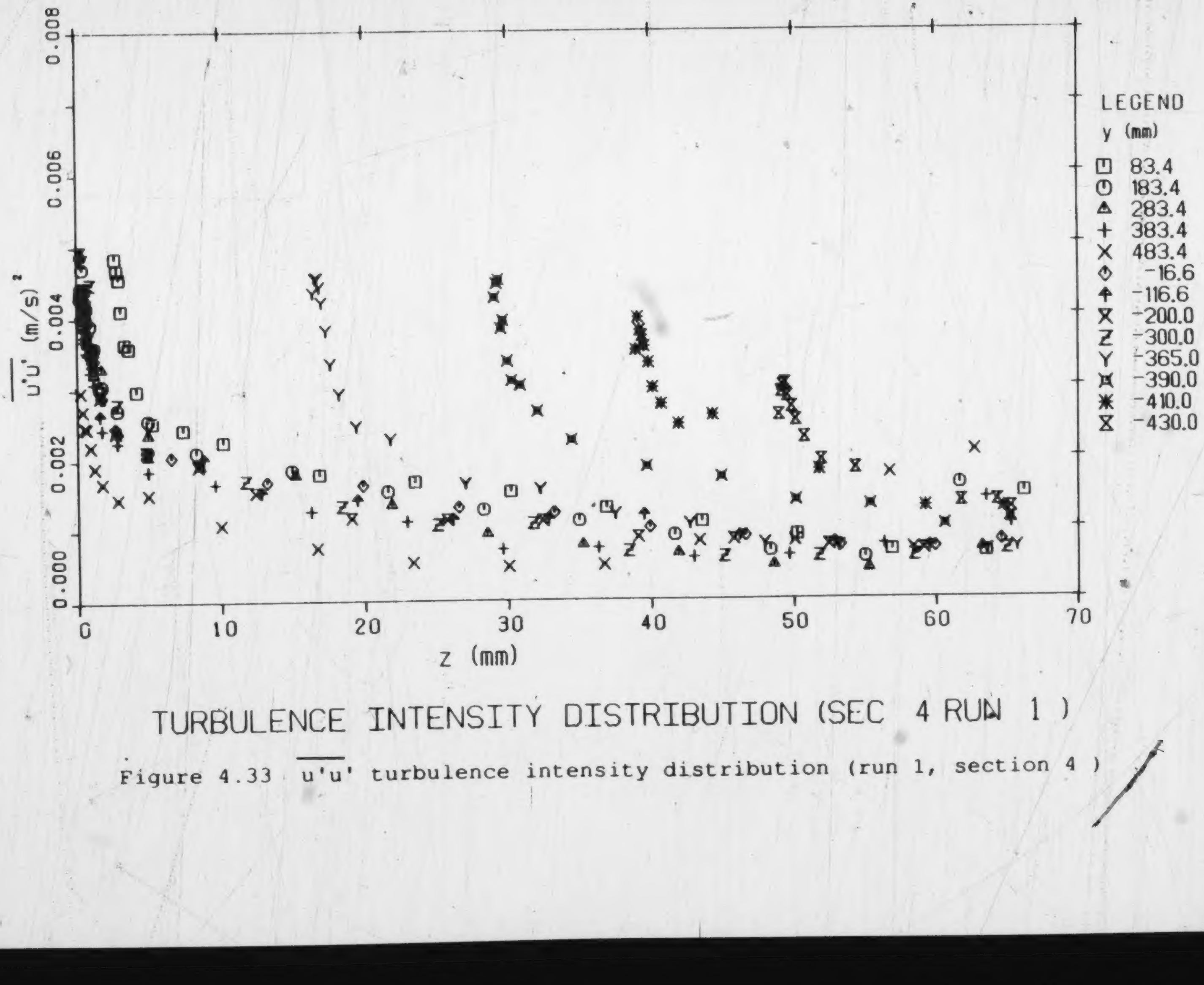

Figure 4.33 $\overline{u'u'}$ turbulence intensity distribution (run 1, section 4)

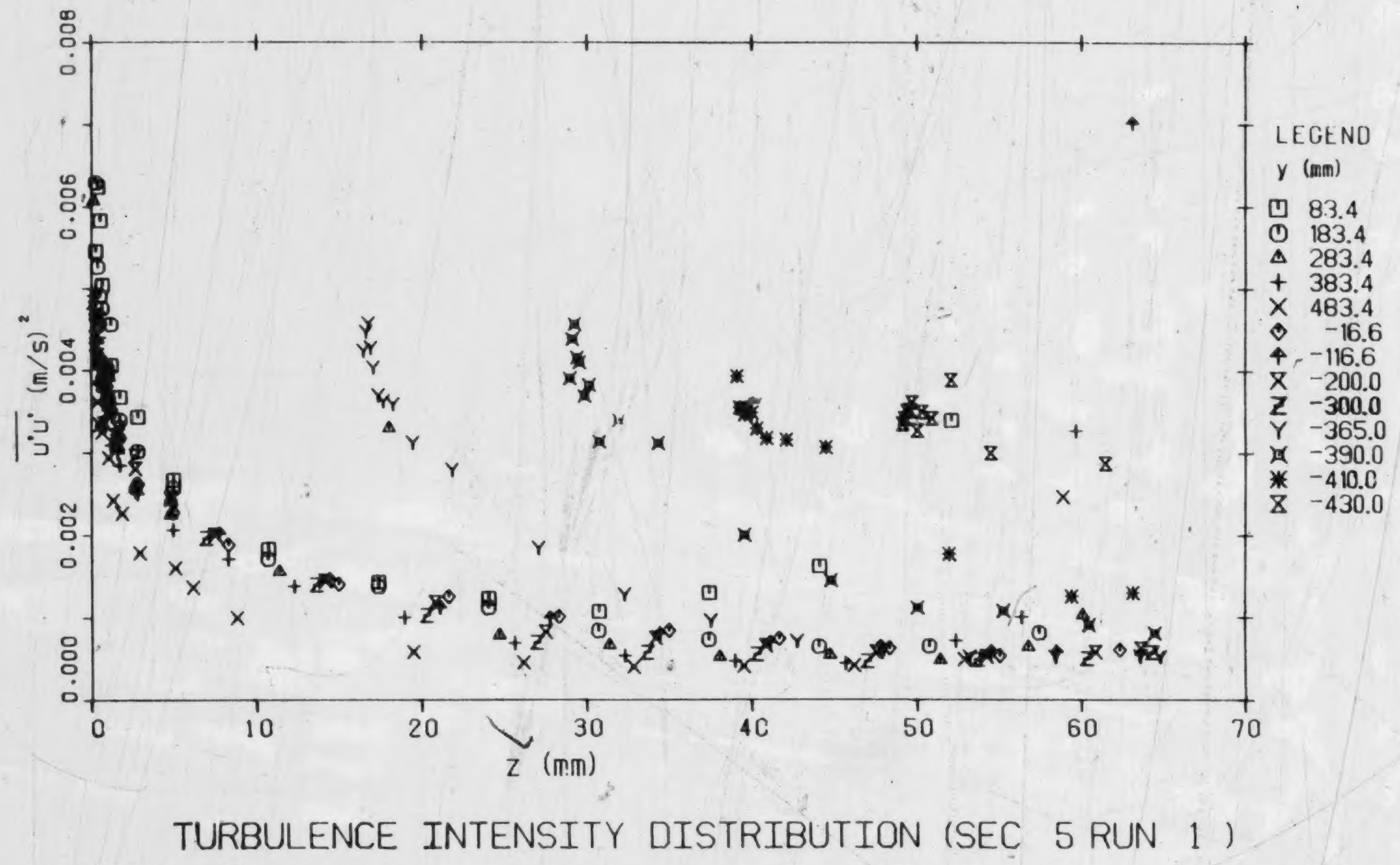

Figure 4.34 $\overline{u'u'}$ turbulence intensity distribution (run 1, section 5)

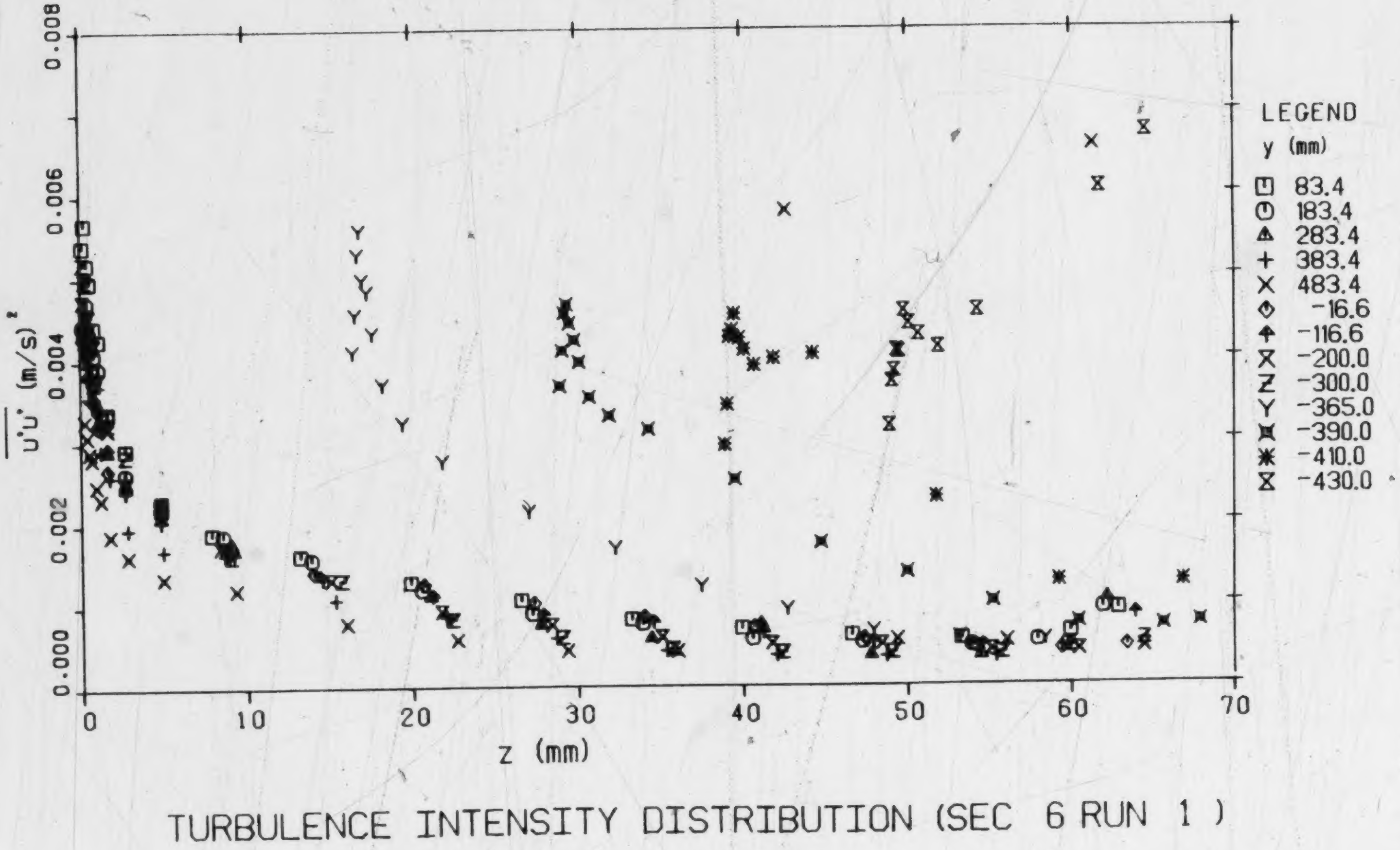

Figure 4.35 $\overline{u'u'}$ turbulence intensity distribution (run 1, section 6)

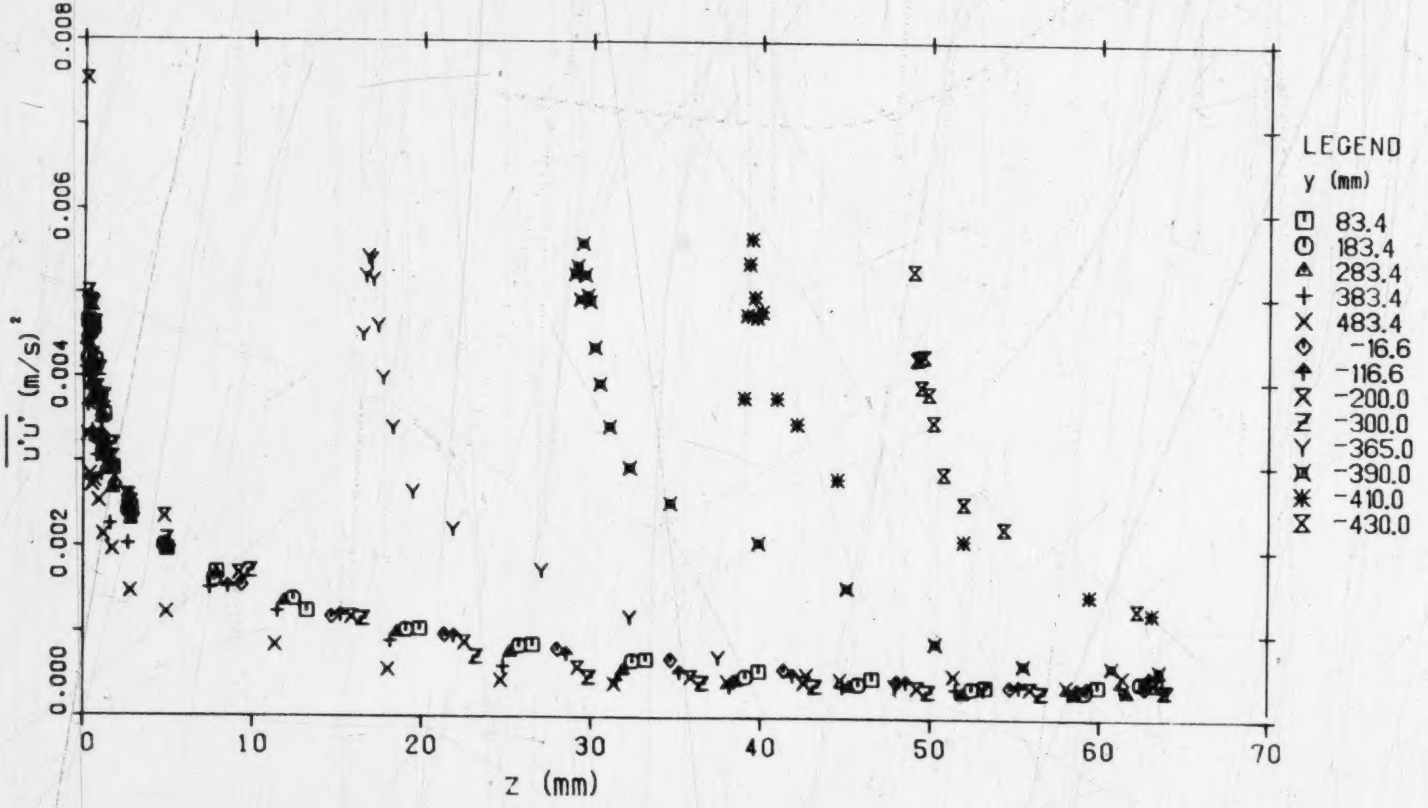

TURBULENCE INTENSITY DISTRIBUTION (SEC 7 RUN 1)

Figure 4.36 $\overline{u'u'}$ turbulence intensity distribution (run 1, section 7)

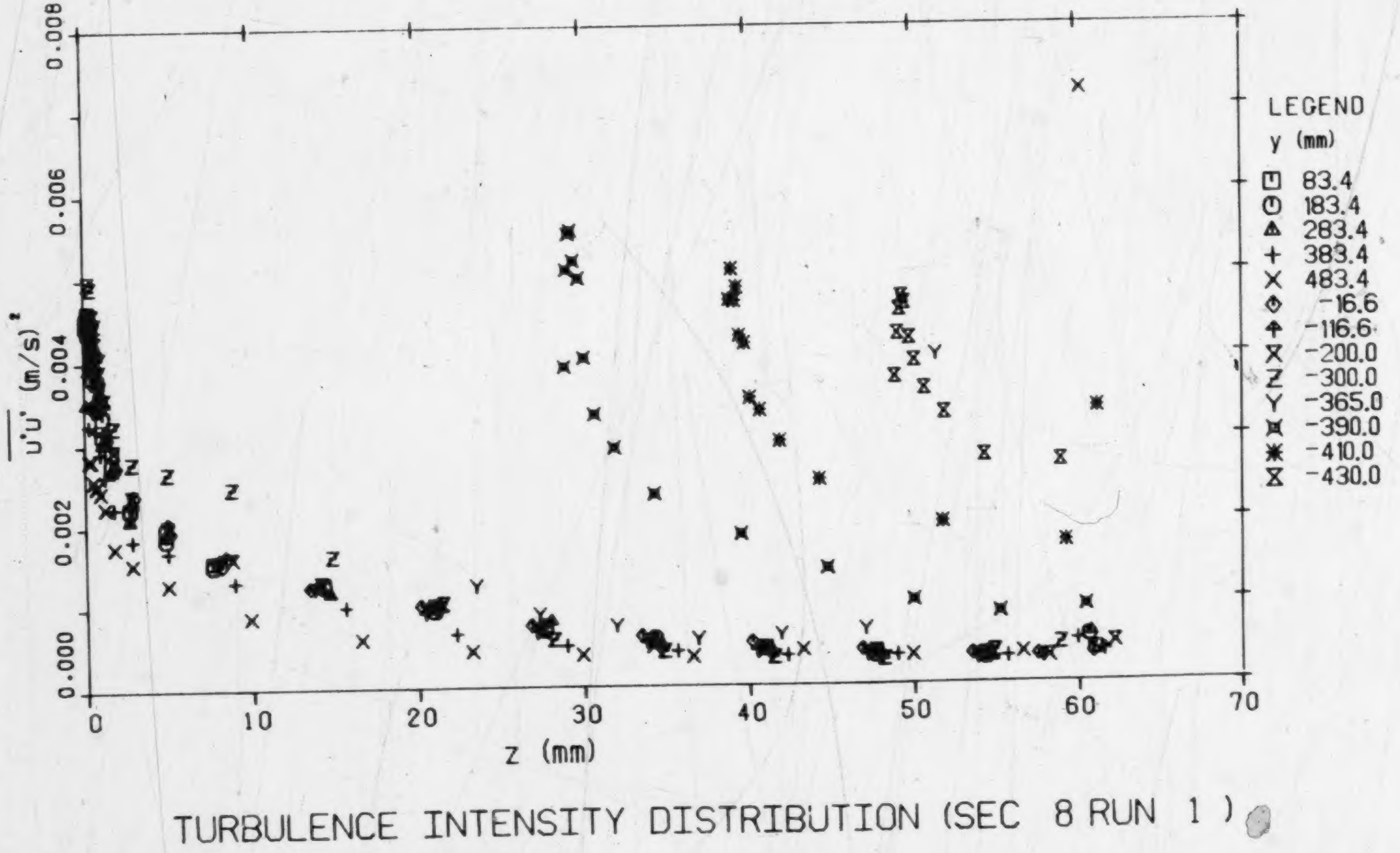

Figure 4.37 $\overline{u'u'}$ turbulence intensity distribution (run 1, section 8)

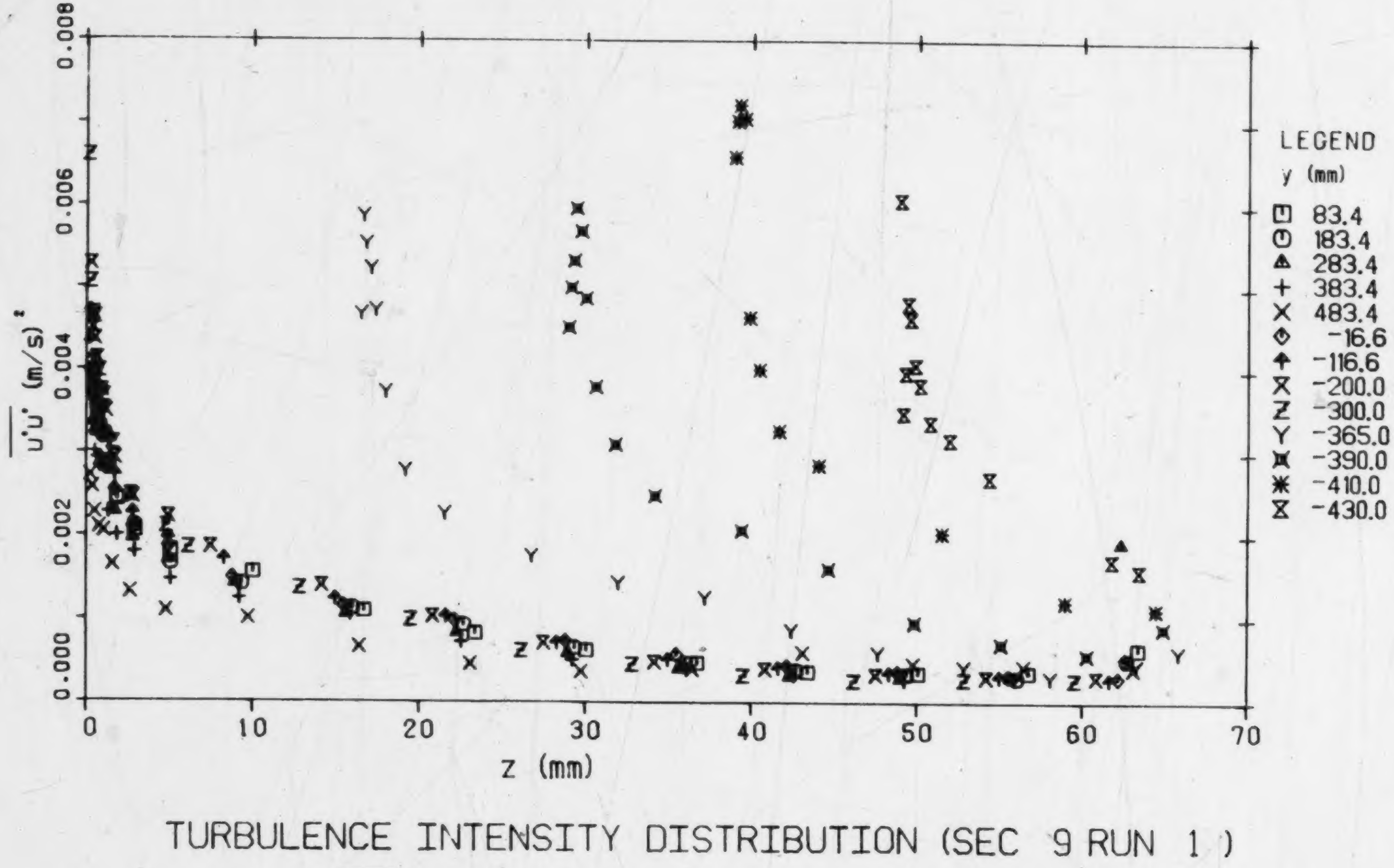

Figure 4.38 $\overline{u'u'}$ turbulence intensity distribution (run 1, section 9)

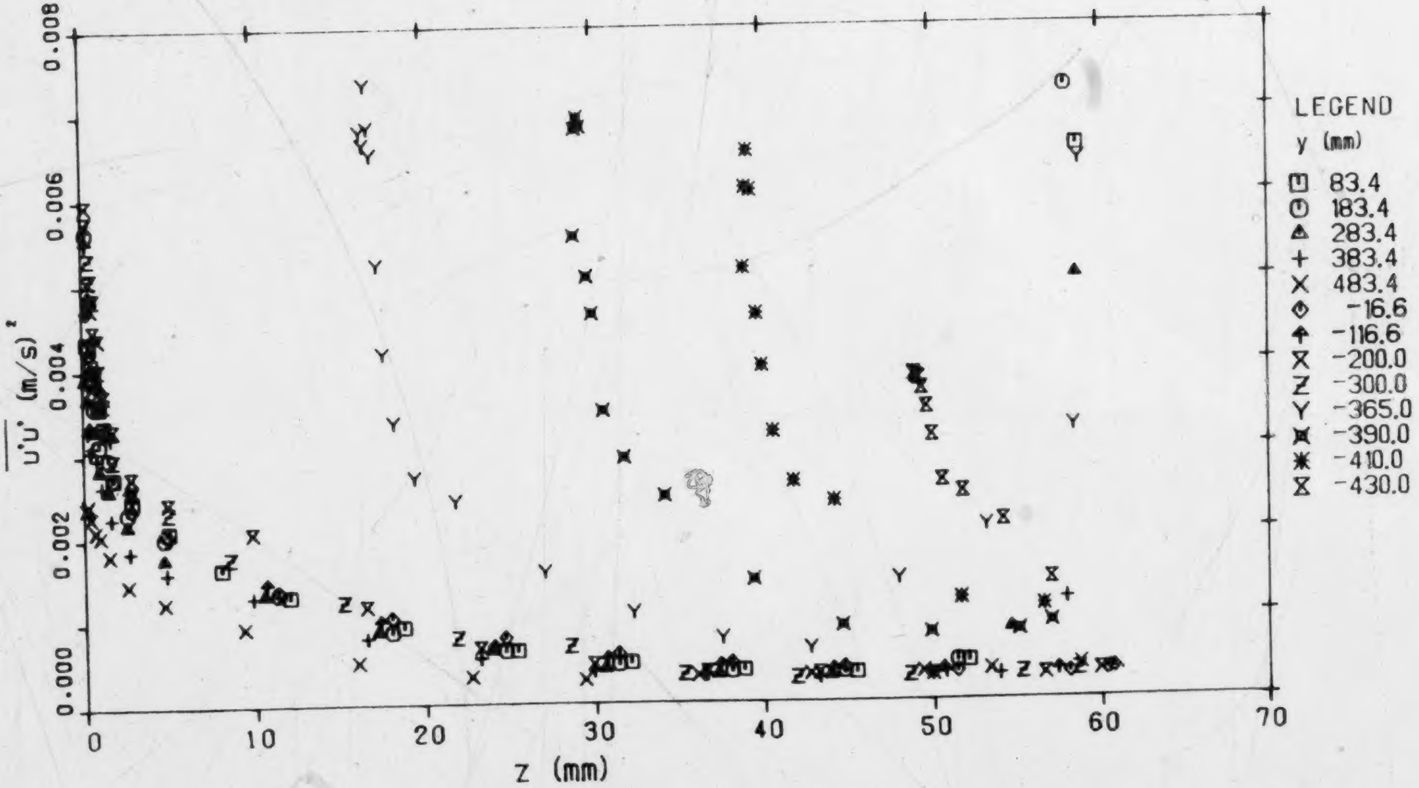

TURBULENCE INTENSITY DISTRIBUTION (SEC 10 RUN 1)

Figure 4.39 $\overline{u'u'}$ turbulence intensity distribution (run 1, section 10)

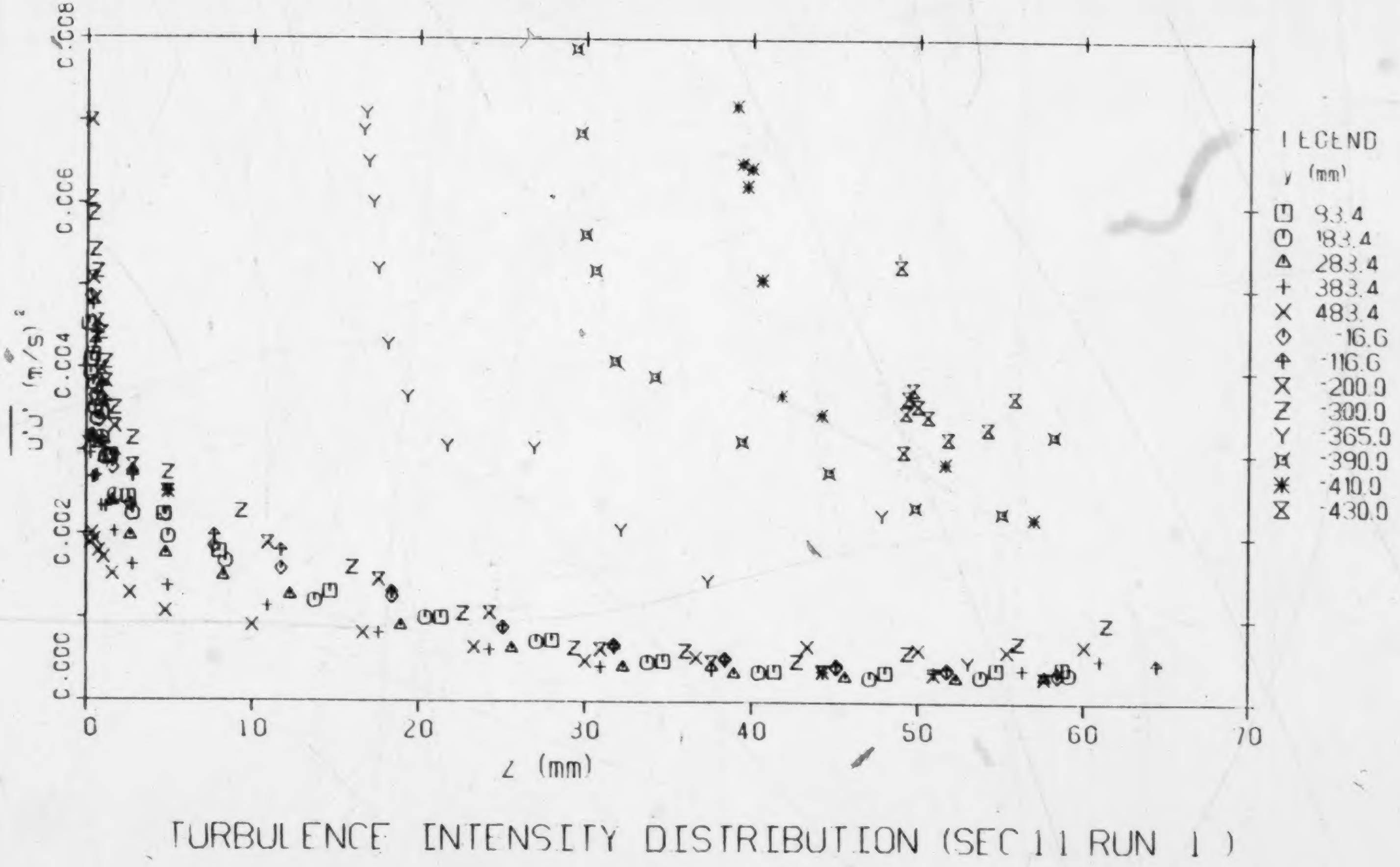

Figure 4.40 $\overline{u'u'}$ turbulence intensity distribution (run 1, section 11)

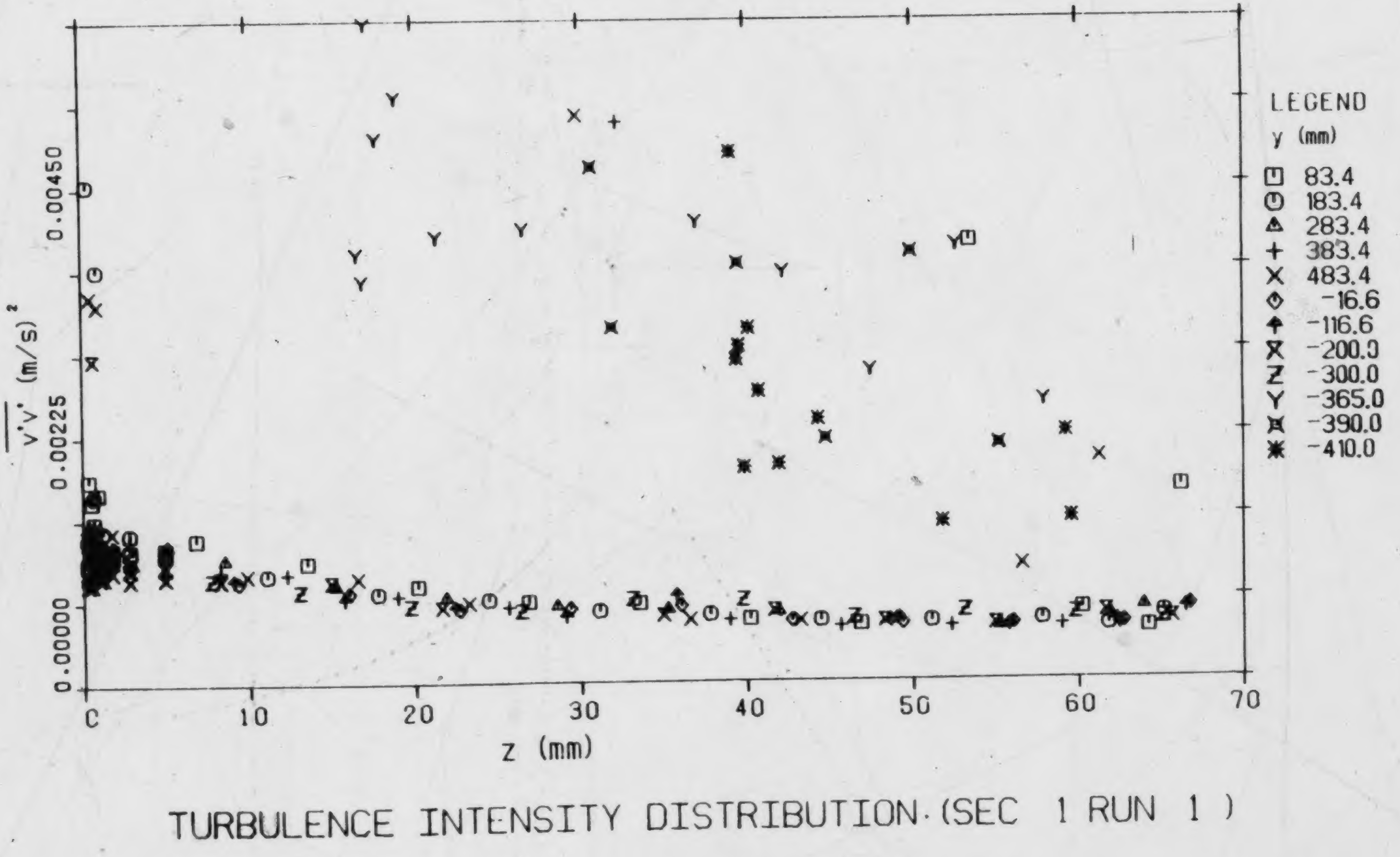

Figure 4.41 $\overline{v'v'}$ turbulence intensity distribution (run 1, section 1)

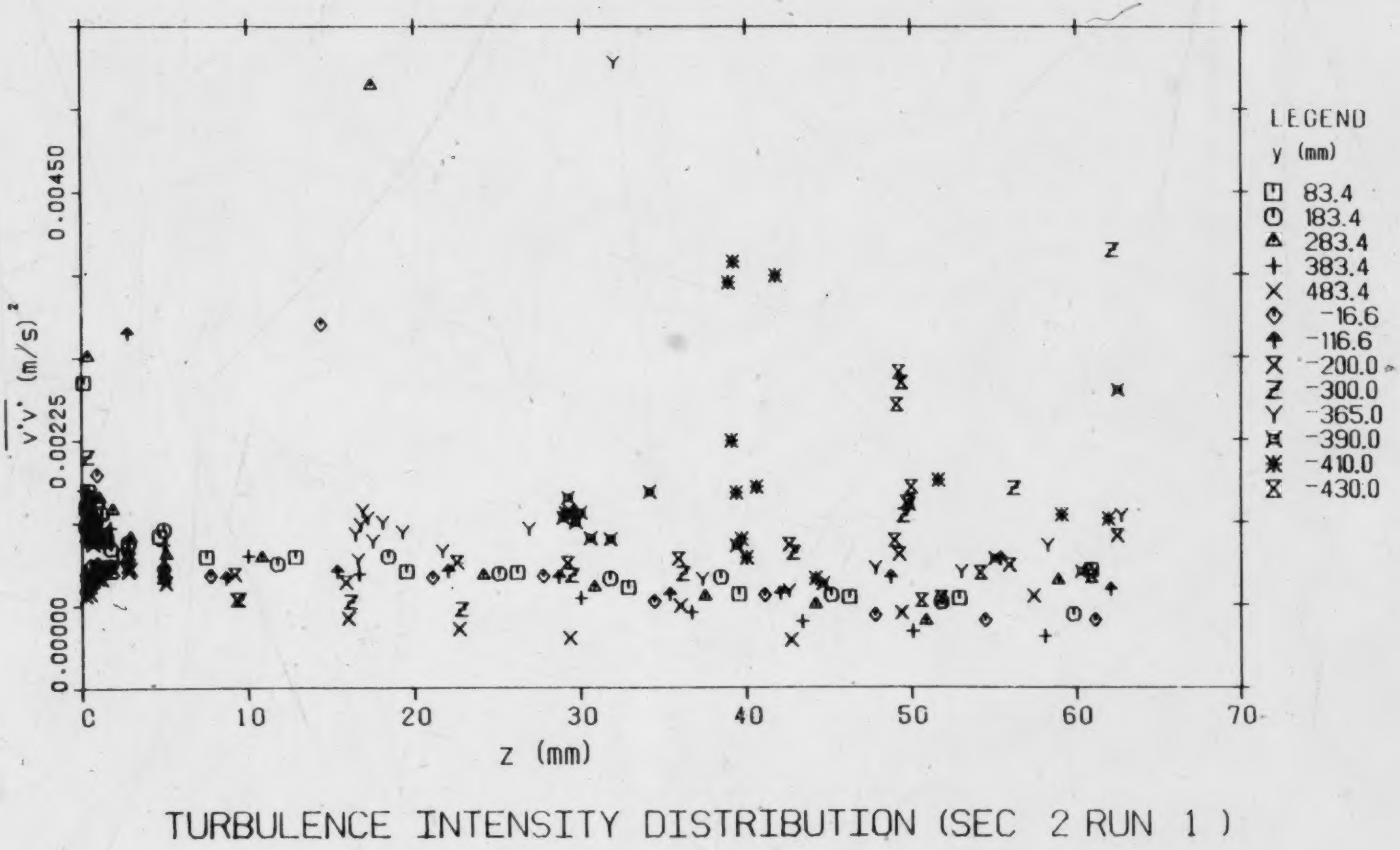

Figure 4.42 $\overline{v'v'}$ turbulence intensity distribution (run 1, section 2)

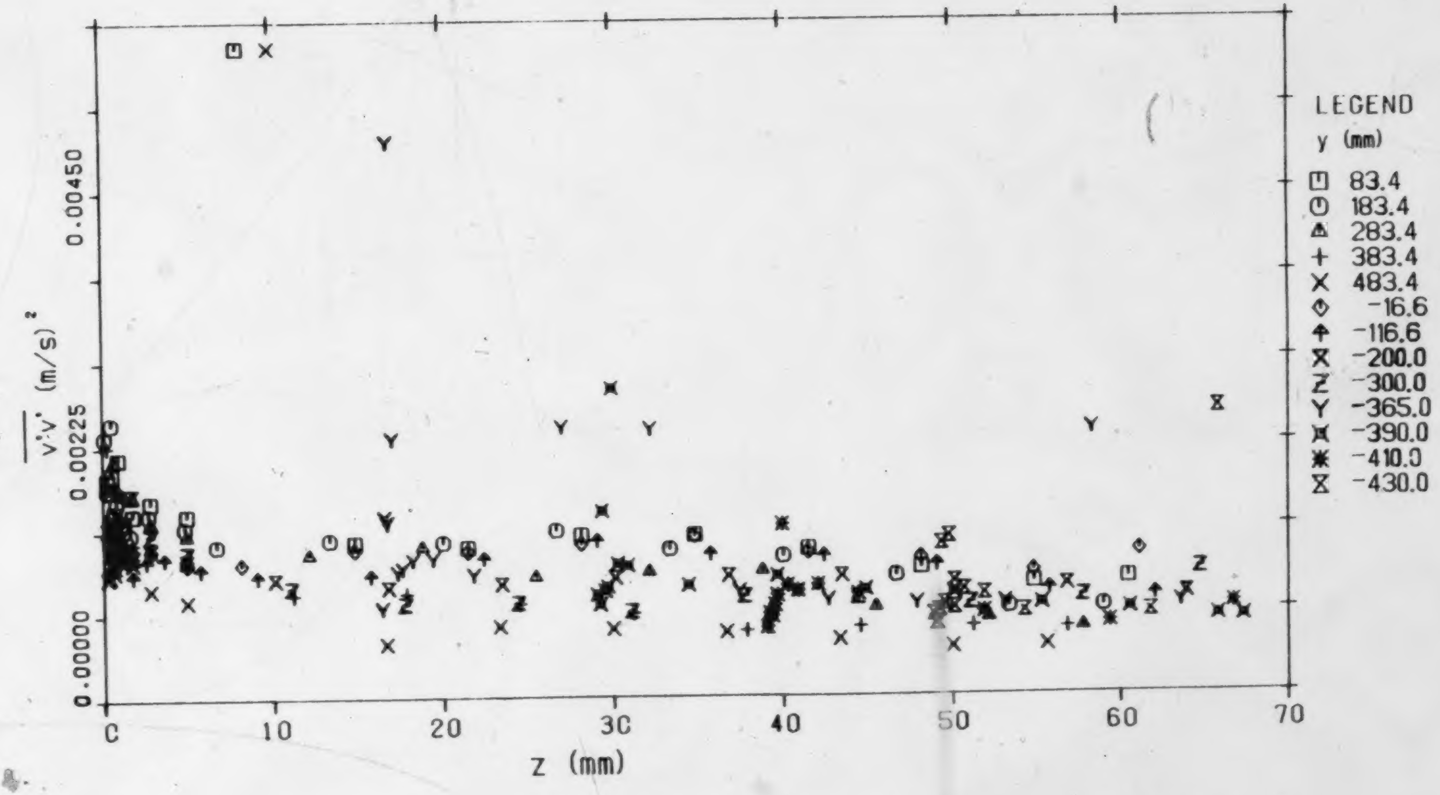

TURBULENCE INTENSITY DISTRIBUTION (SEC 3 RUN 1)

Figure 4.43 $\overline{v'v'}$ turbulence intensity distribution (run 1, section 3)

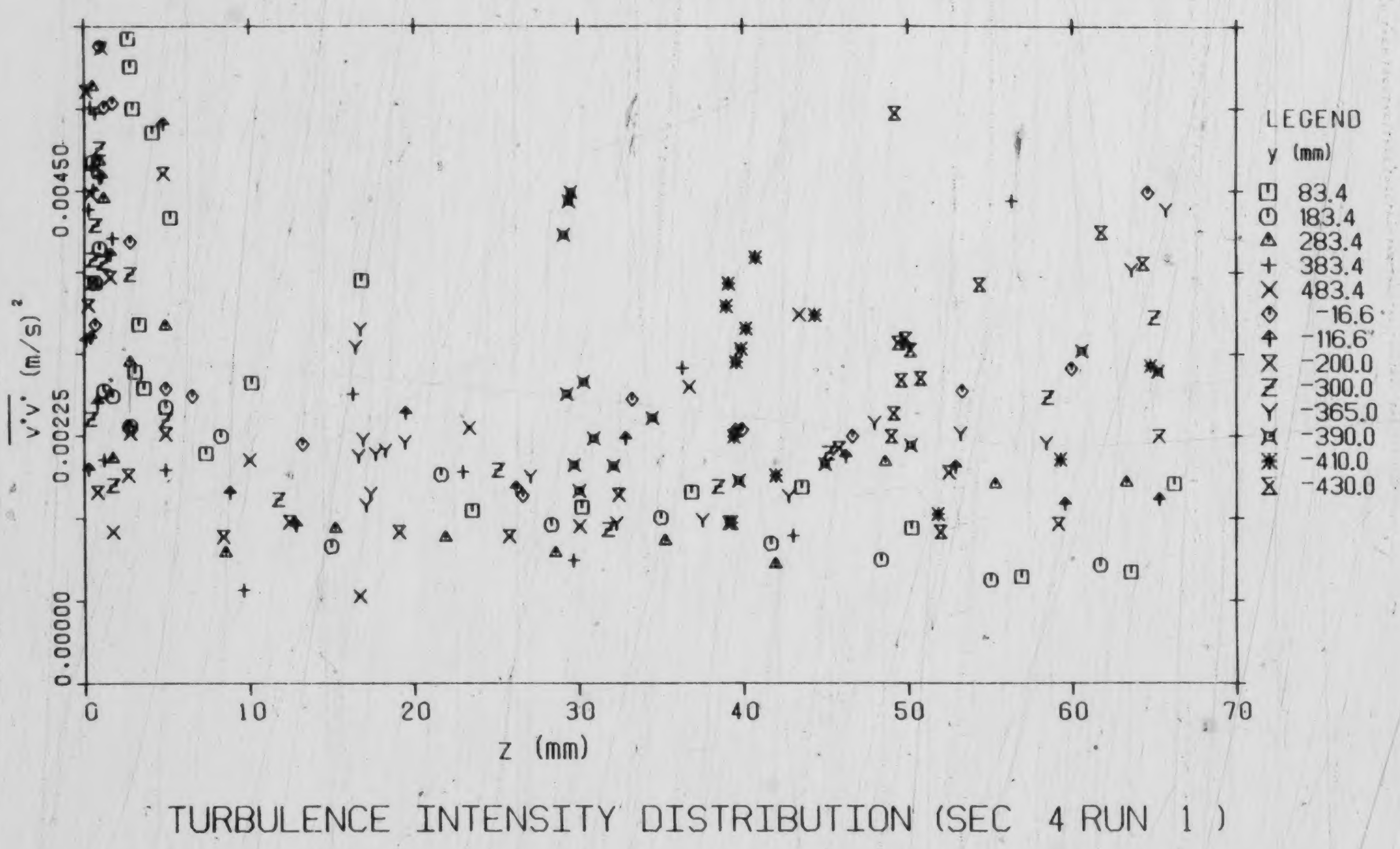

Figure A.44 $\overline{v'v'}$ turbulence intensity distribution (run 1, section 4)

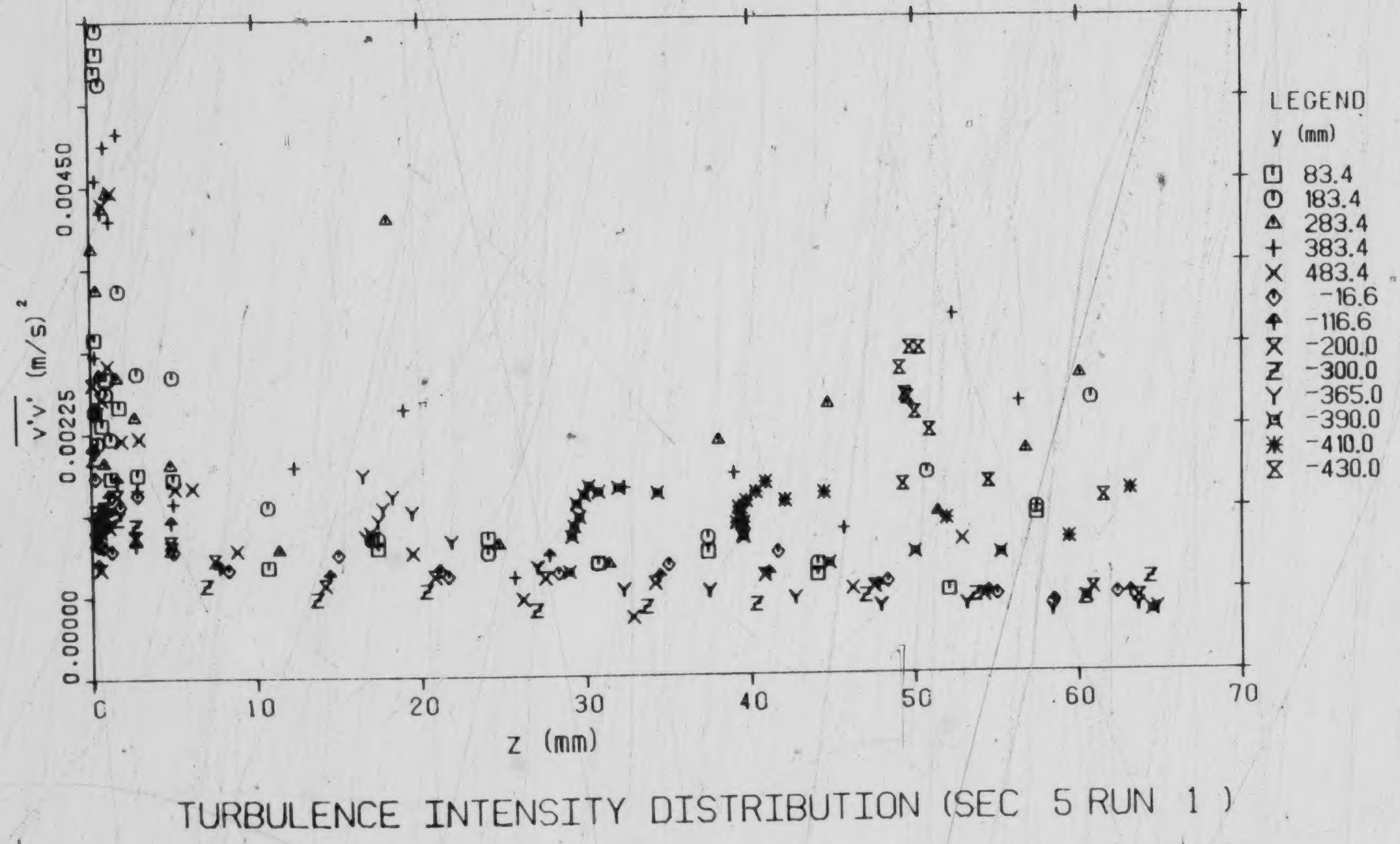

Figure 4.45 $\overline{v'v'}$ turbulence intensity distribution (run 1, section 5)

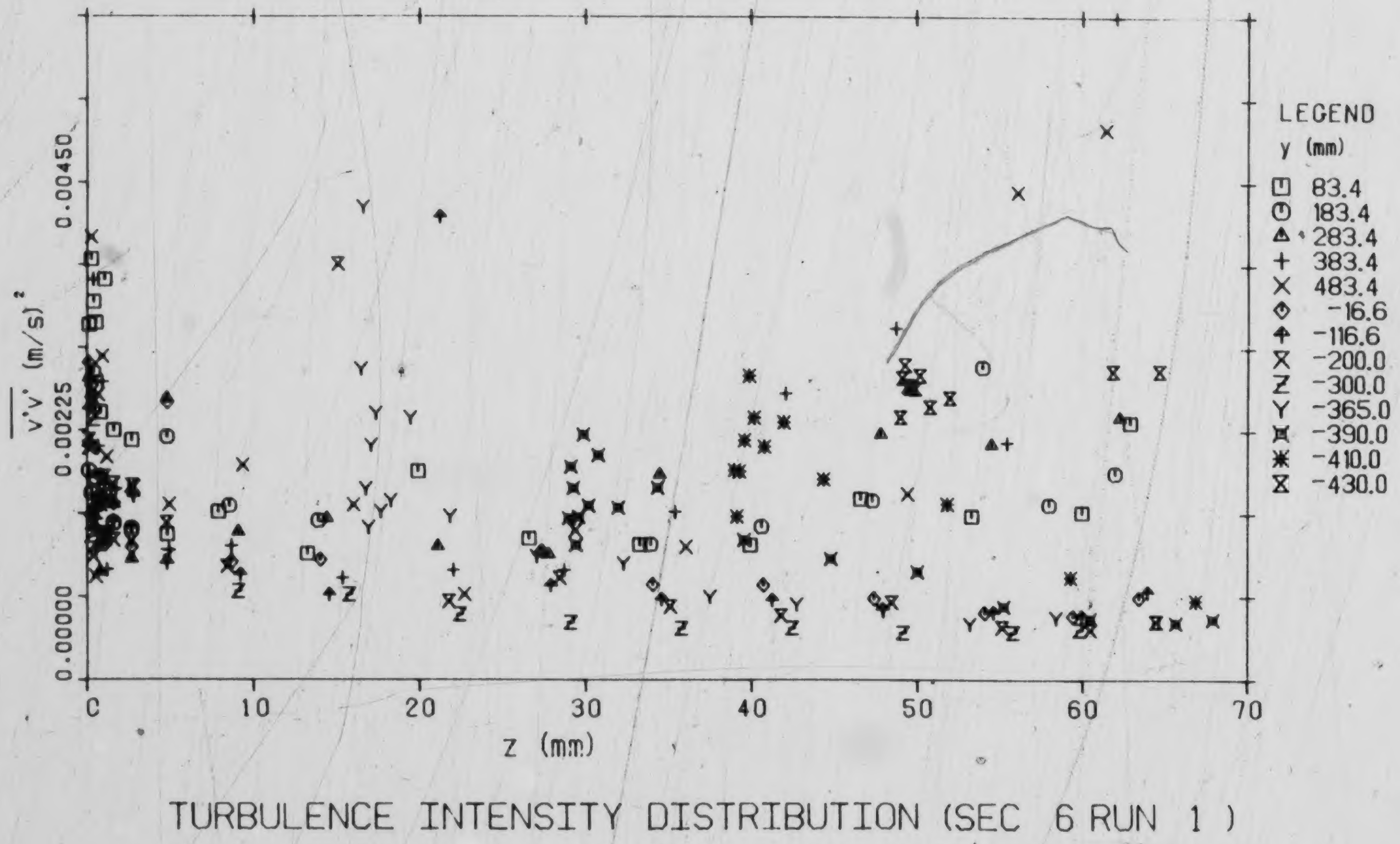

Figure 4.46 $\overline{v'v'}$ turbulence intensity distribution (run 1, section 6)

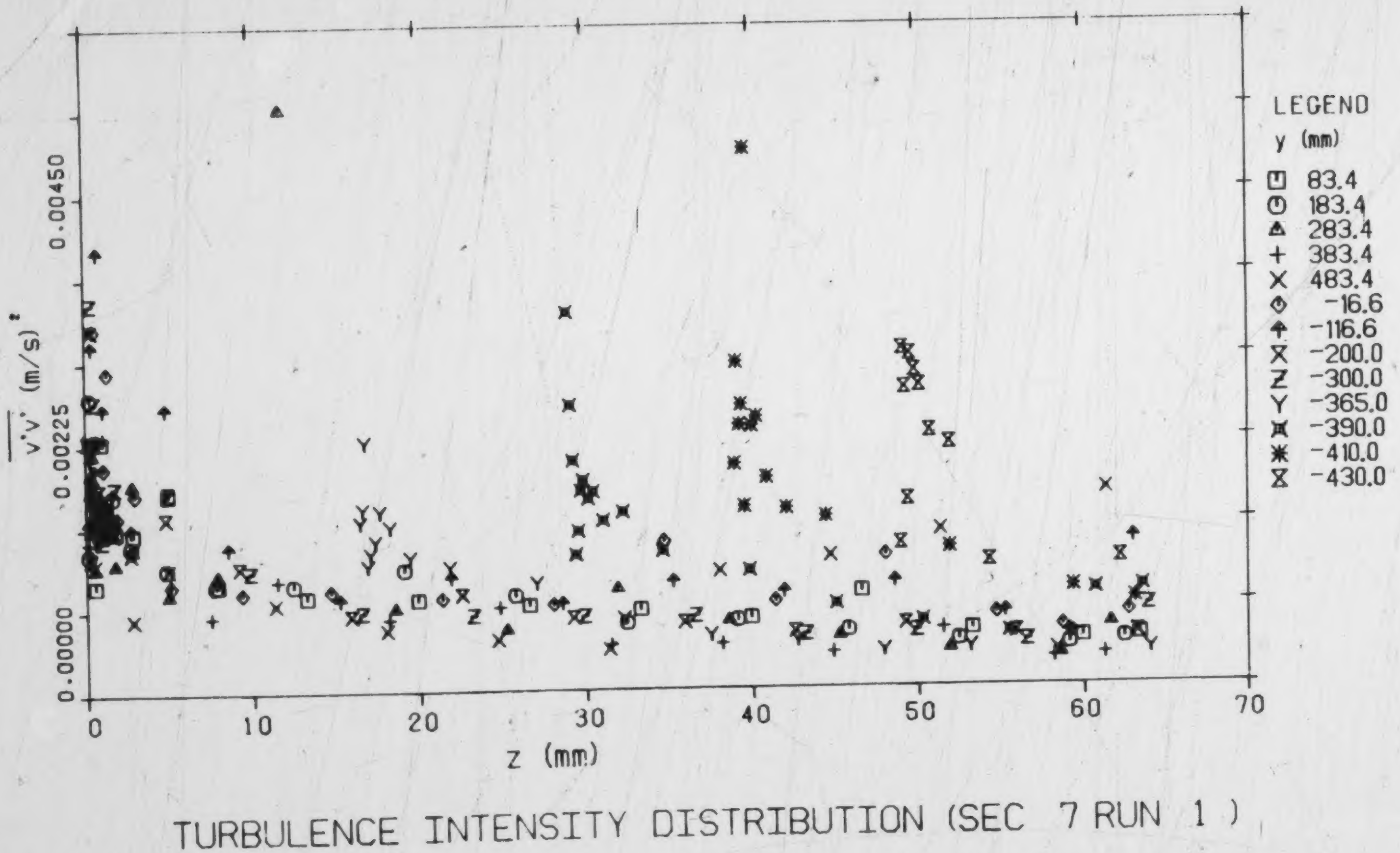

Figure 4.47 $\overline{v'v'}$ turbulence intensity distribution (run 1, section 7)

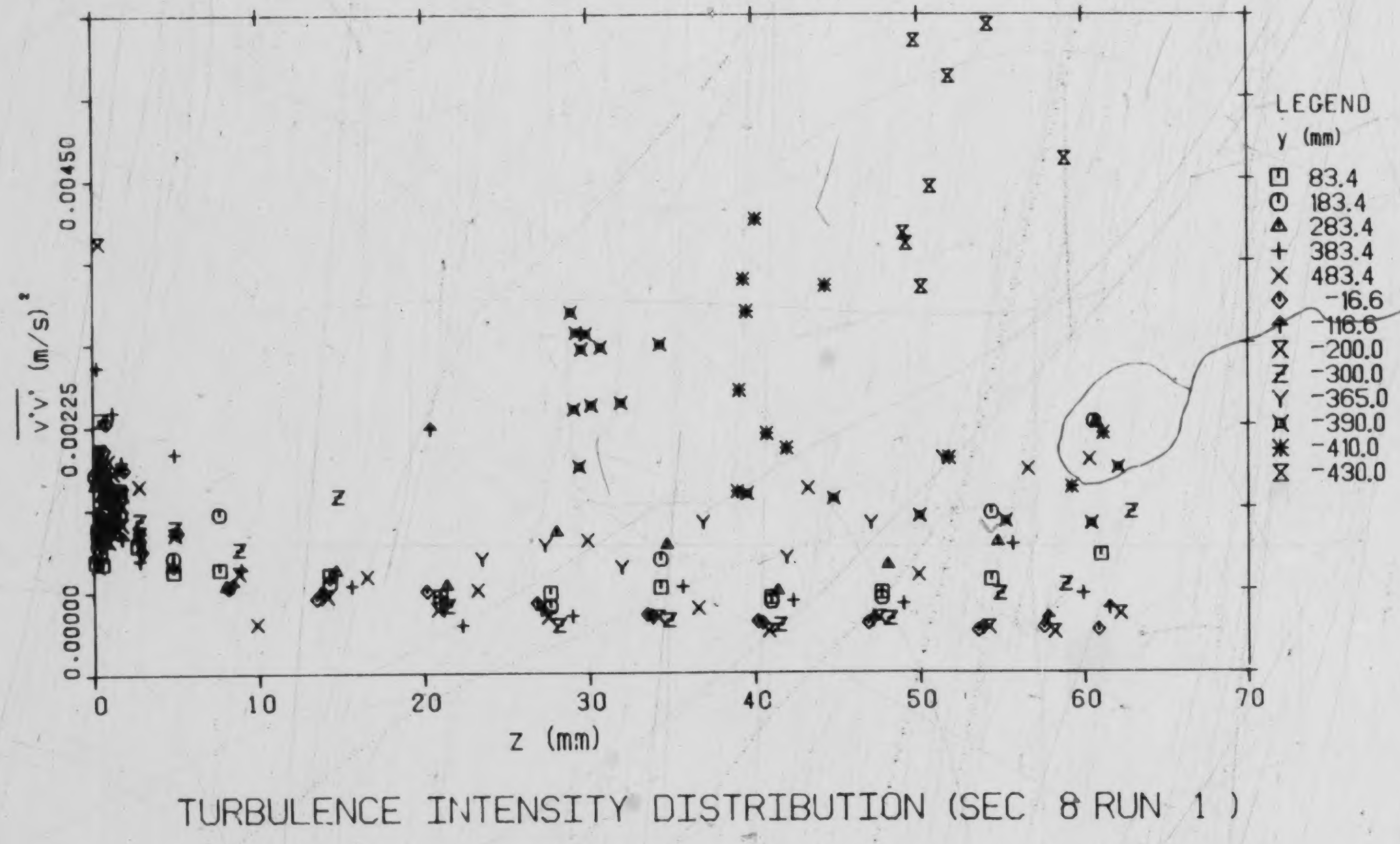

Figure 4.48 $\overline{v'v'}$ turbulence intensity distribution (run 1, section 8)

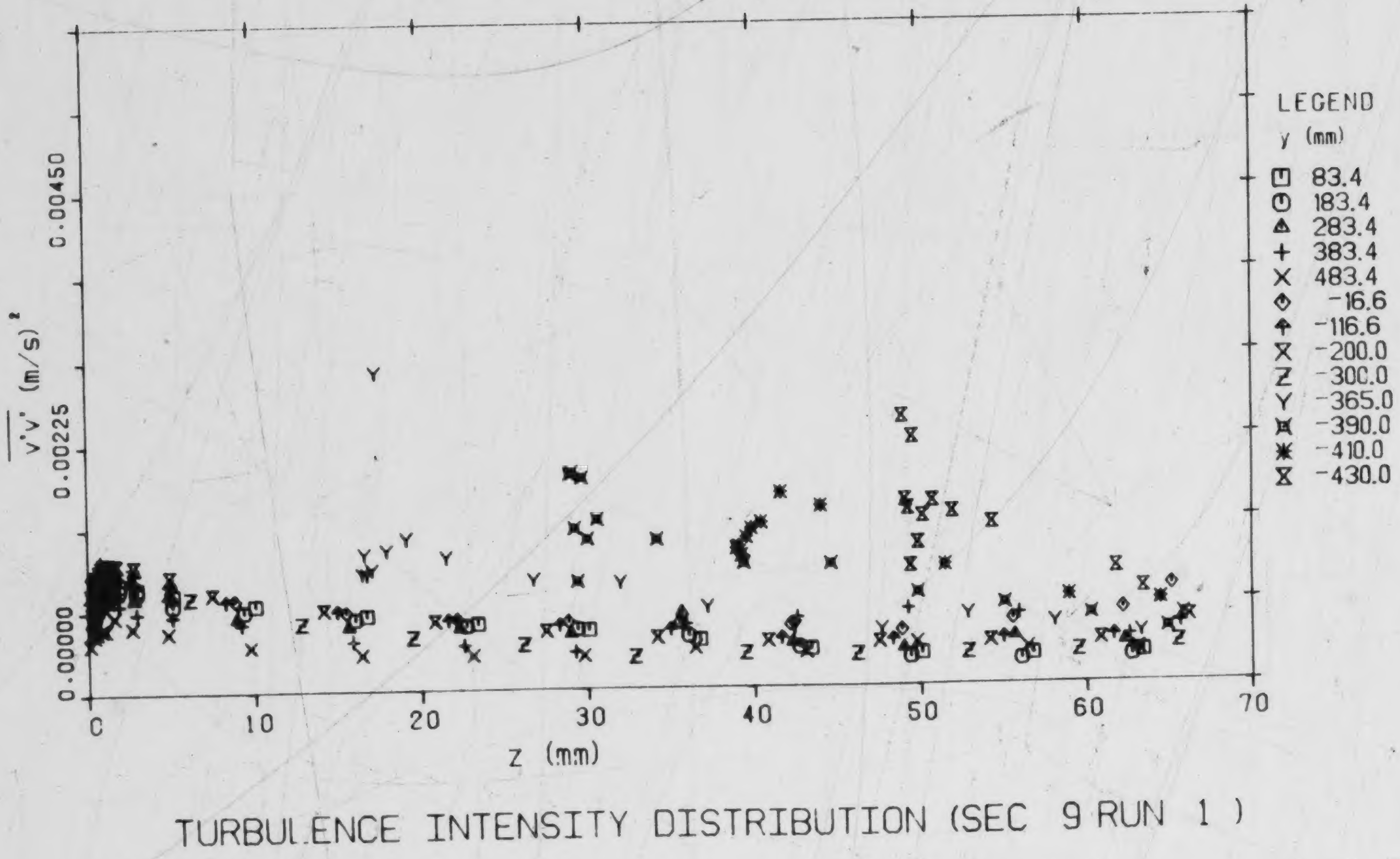

Figure 4.49 $\overline{v'v'}$ turbulence intensity distribution (run 1, section 9)

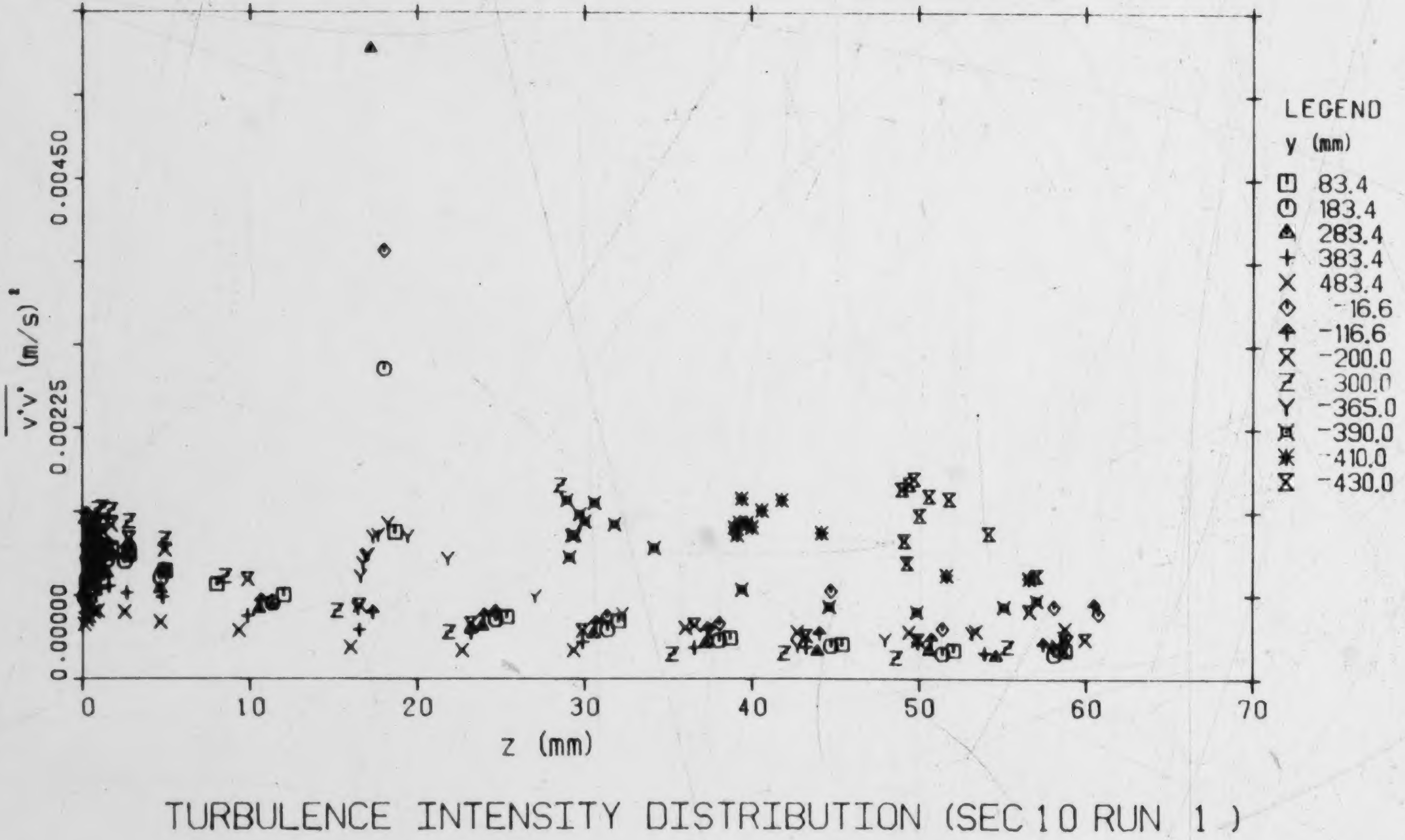

Figure 4.50 $\overline{v'v'}$ turbulence intensity distribution (run 1, section 10)

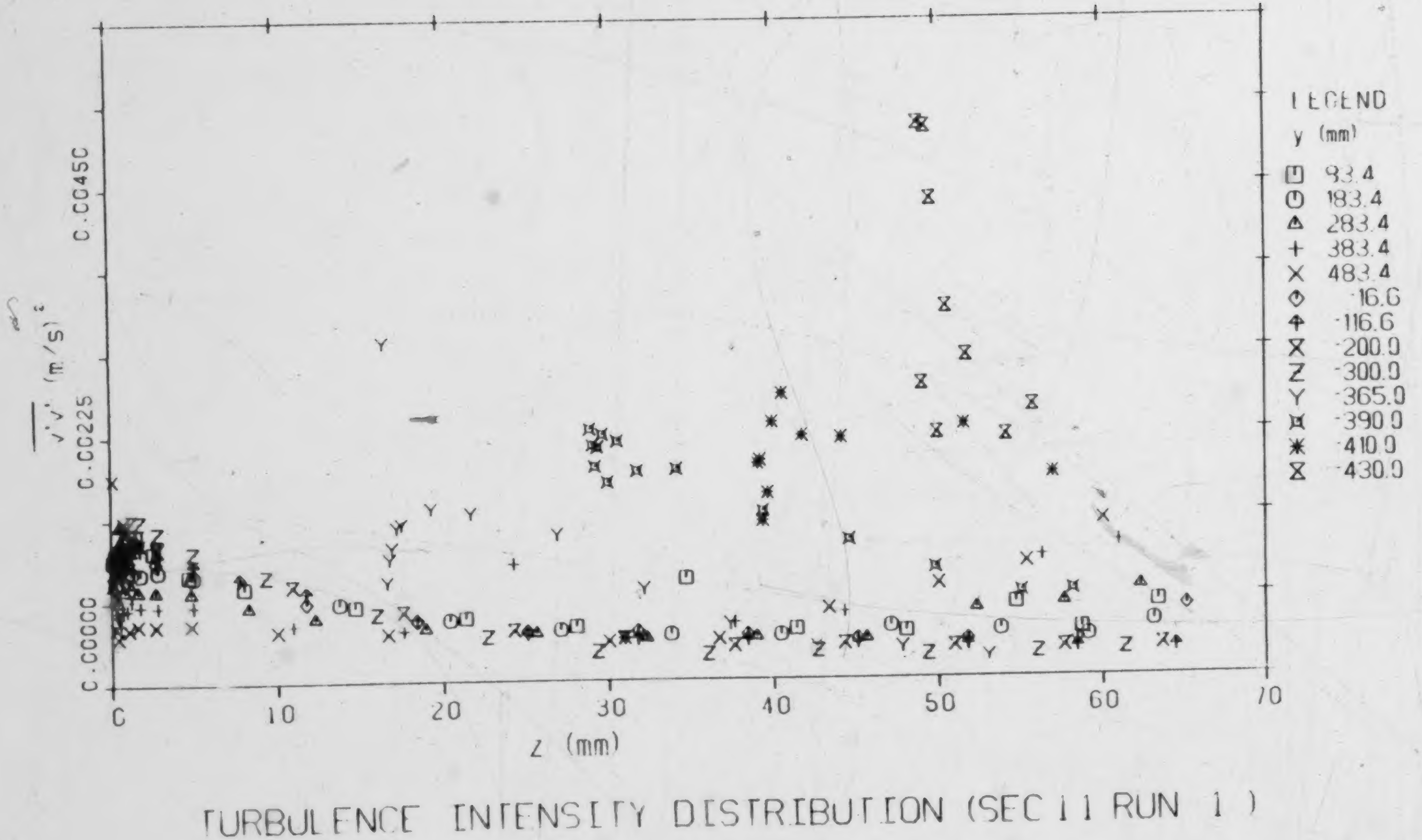

Figure 4.51 $\overline{v'v'}$ turbulence intensity distribution (run 1, section 11)

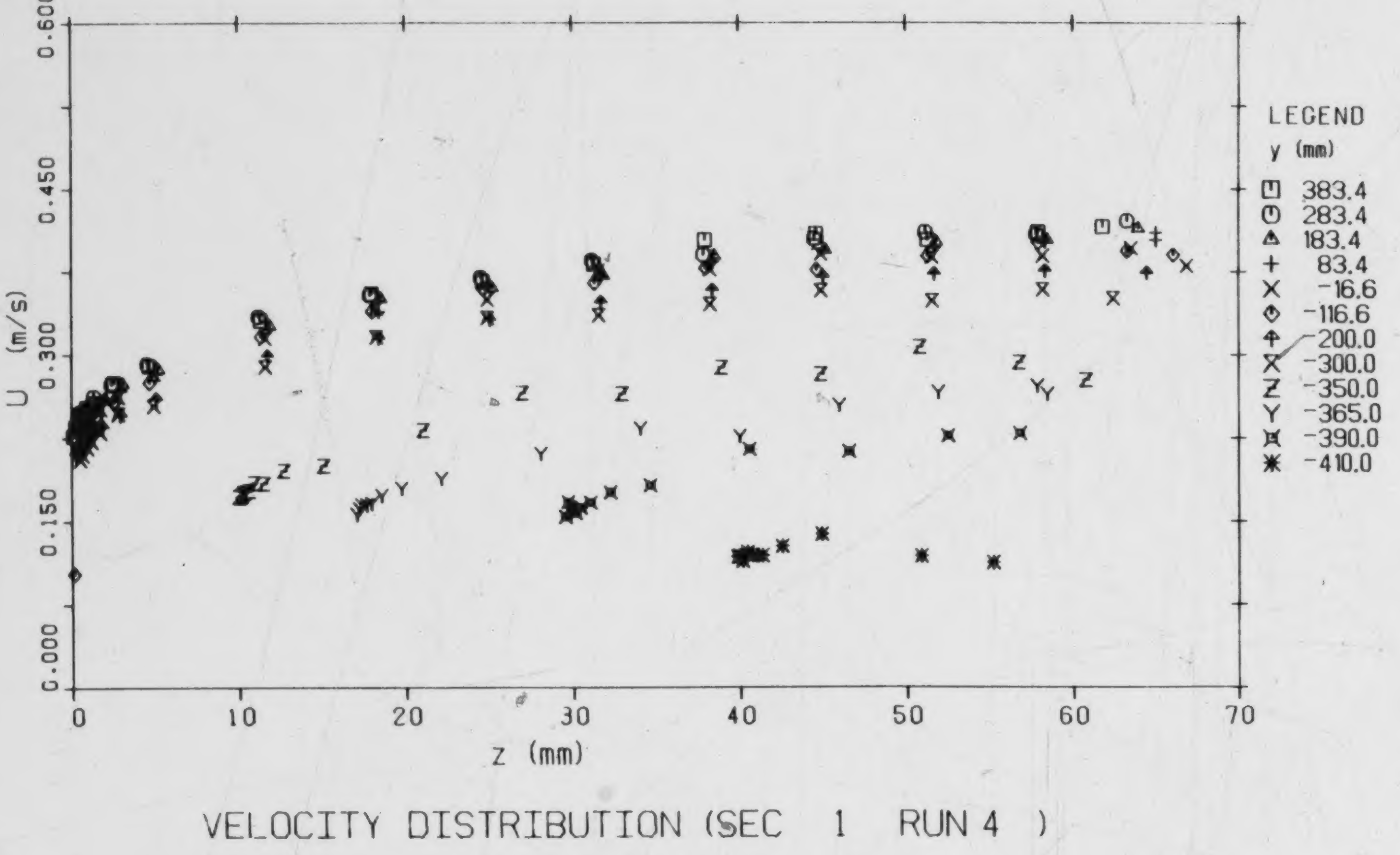

Figure 4.52 u velocity distribution (run 4, section 1)

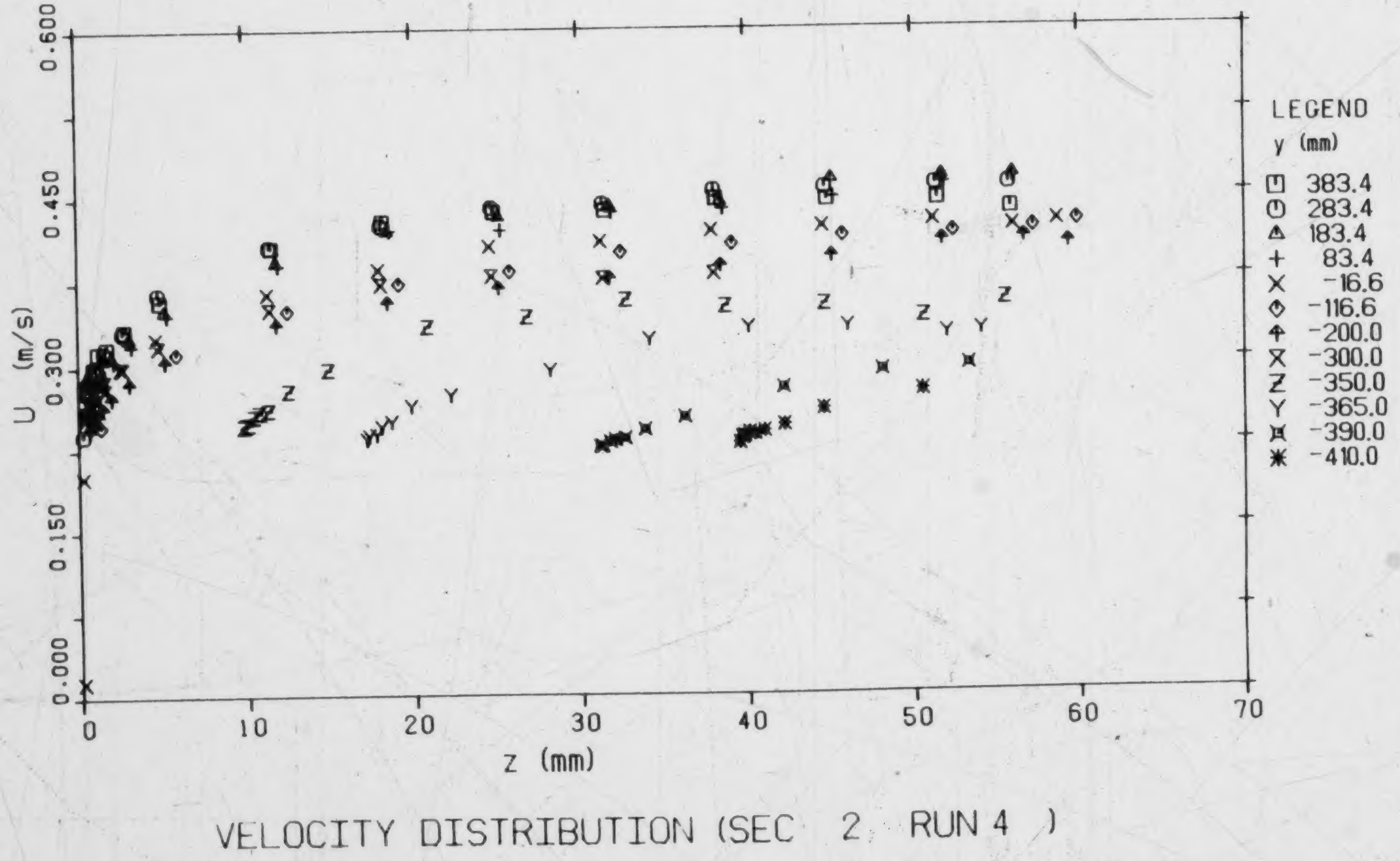

Figure 4.53 u velocity distribution (run 4, section 2)

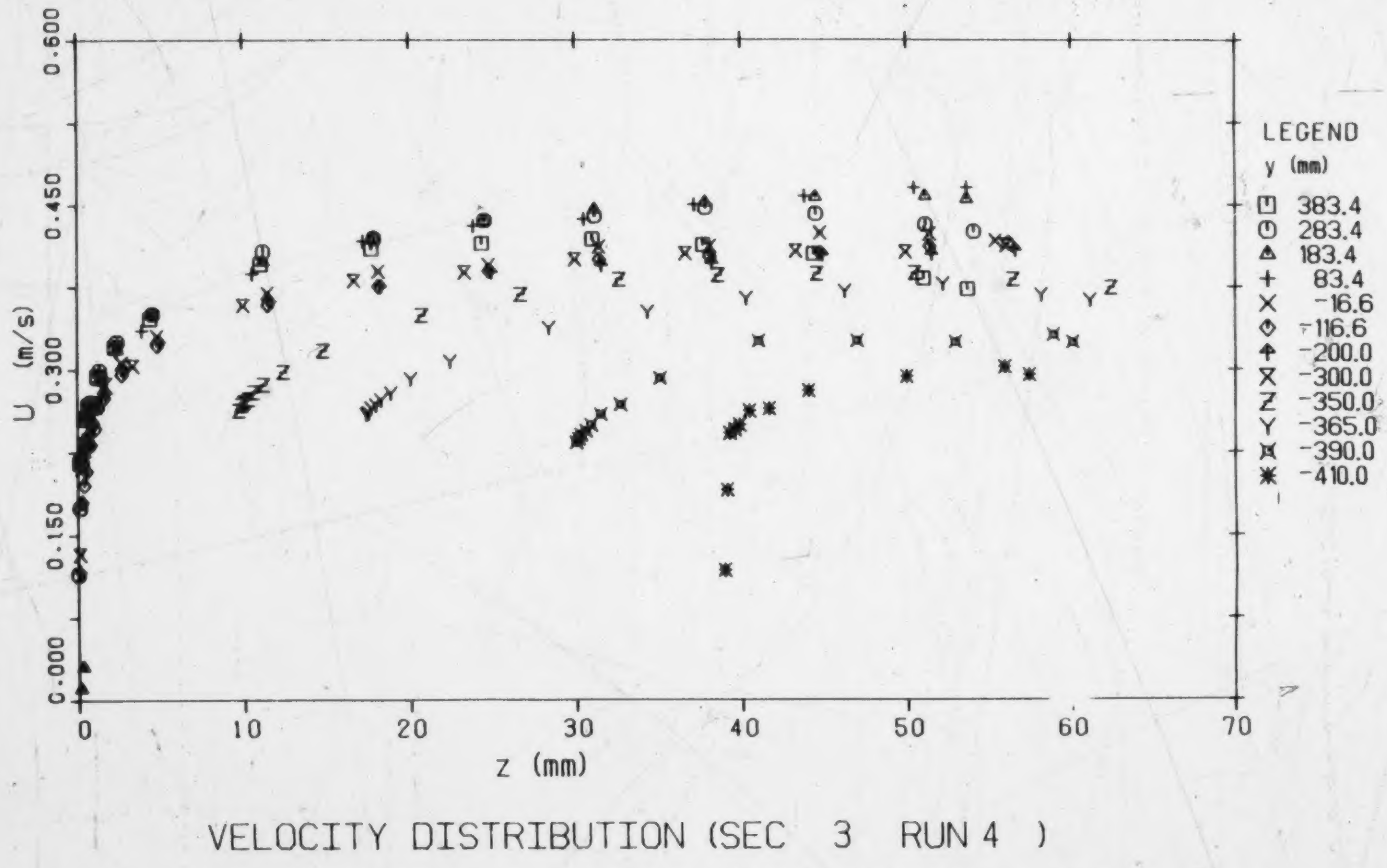

Figure 4.54 u velocity distribution (run 4, section 3)

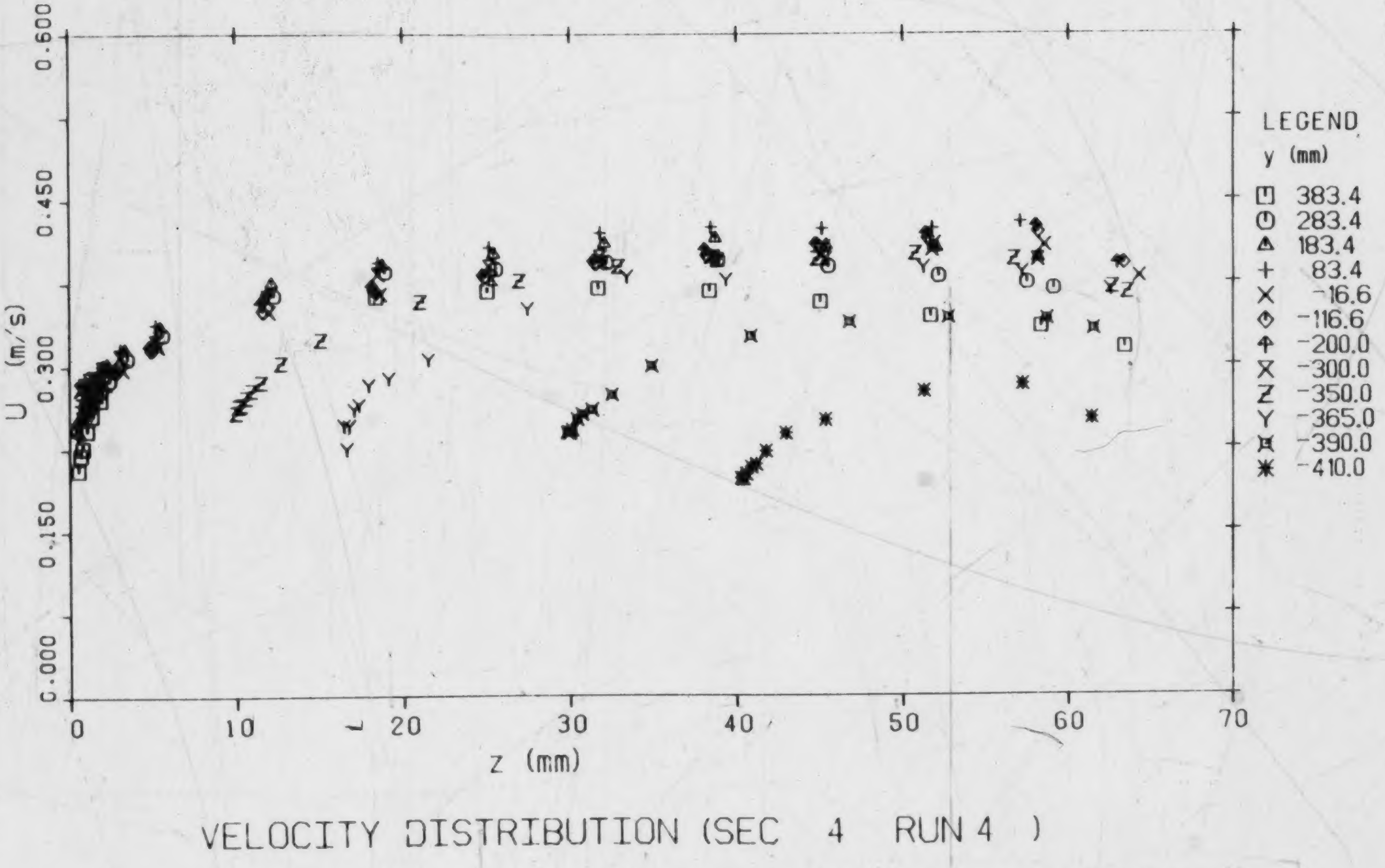

Figure 4.55 u velocity distribution (run 4, section 4)

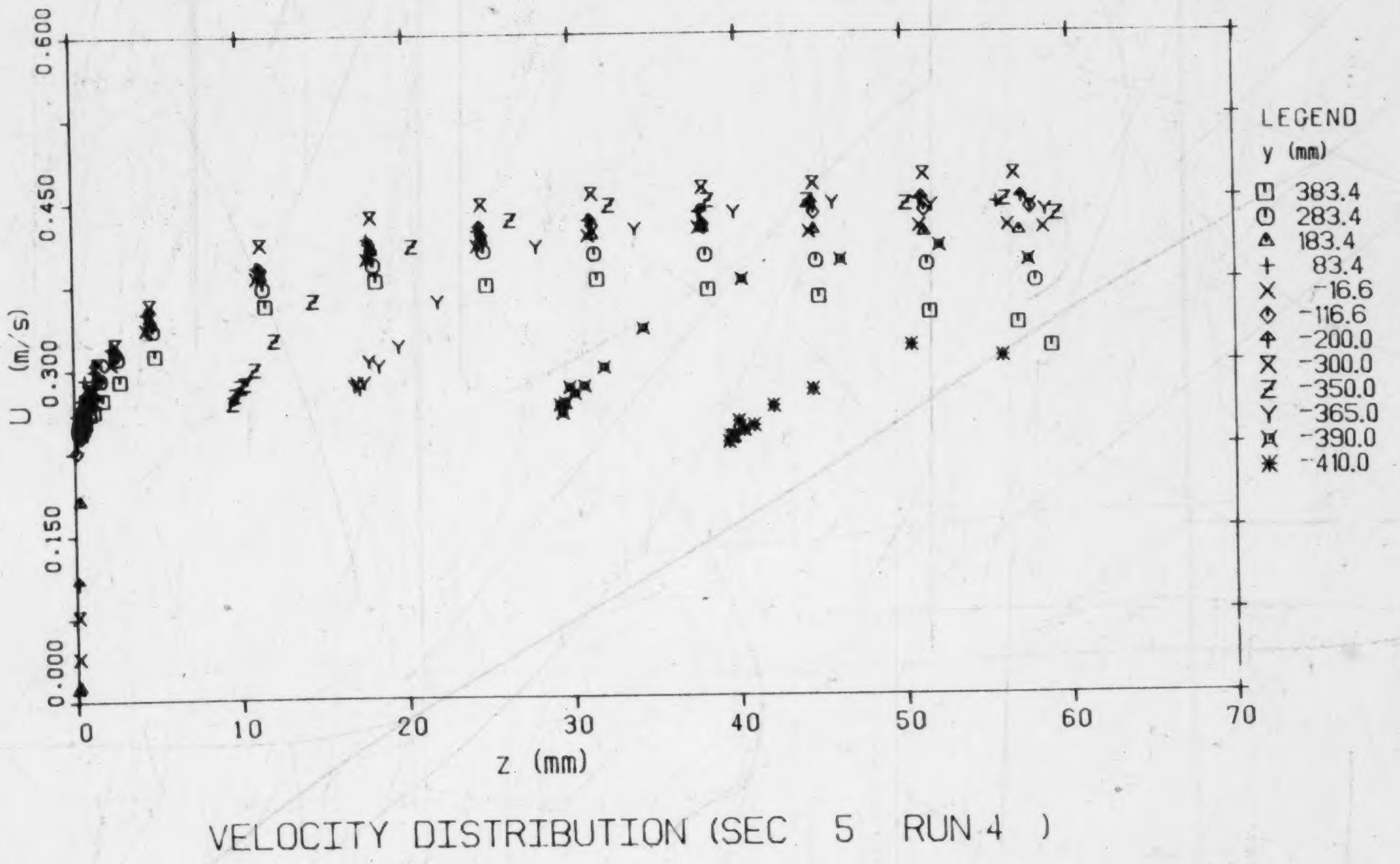

Figure 4.56 u velocity distribution (run 4, section 5)

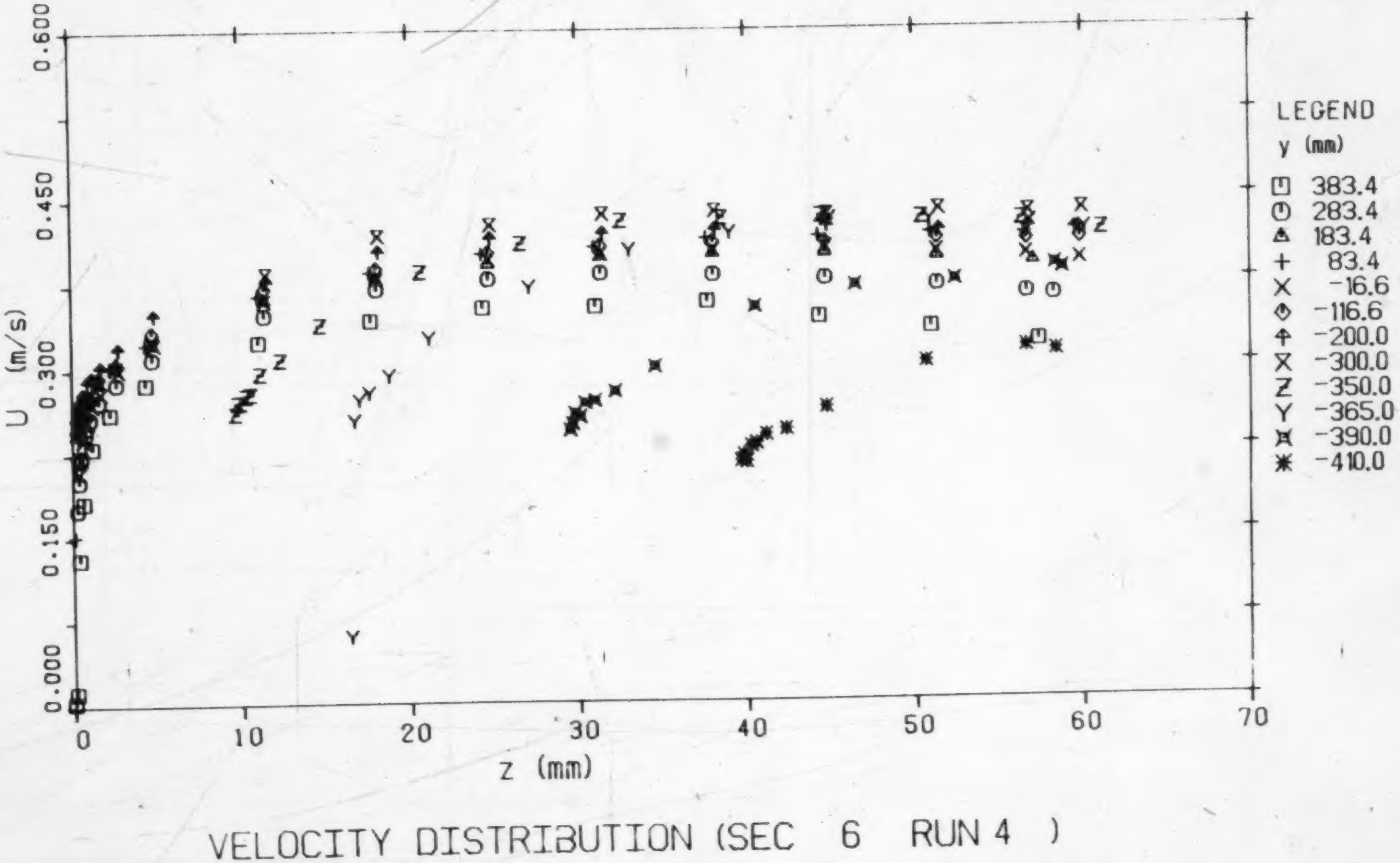

Figure 4.57 u velocity distribution (run 4, section 6)

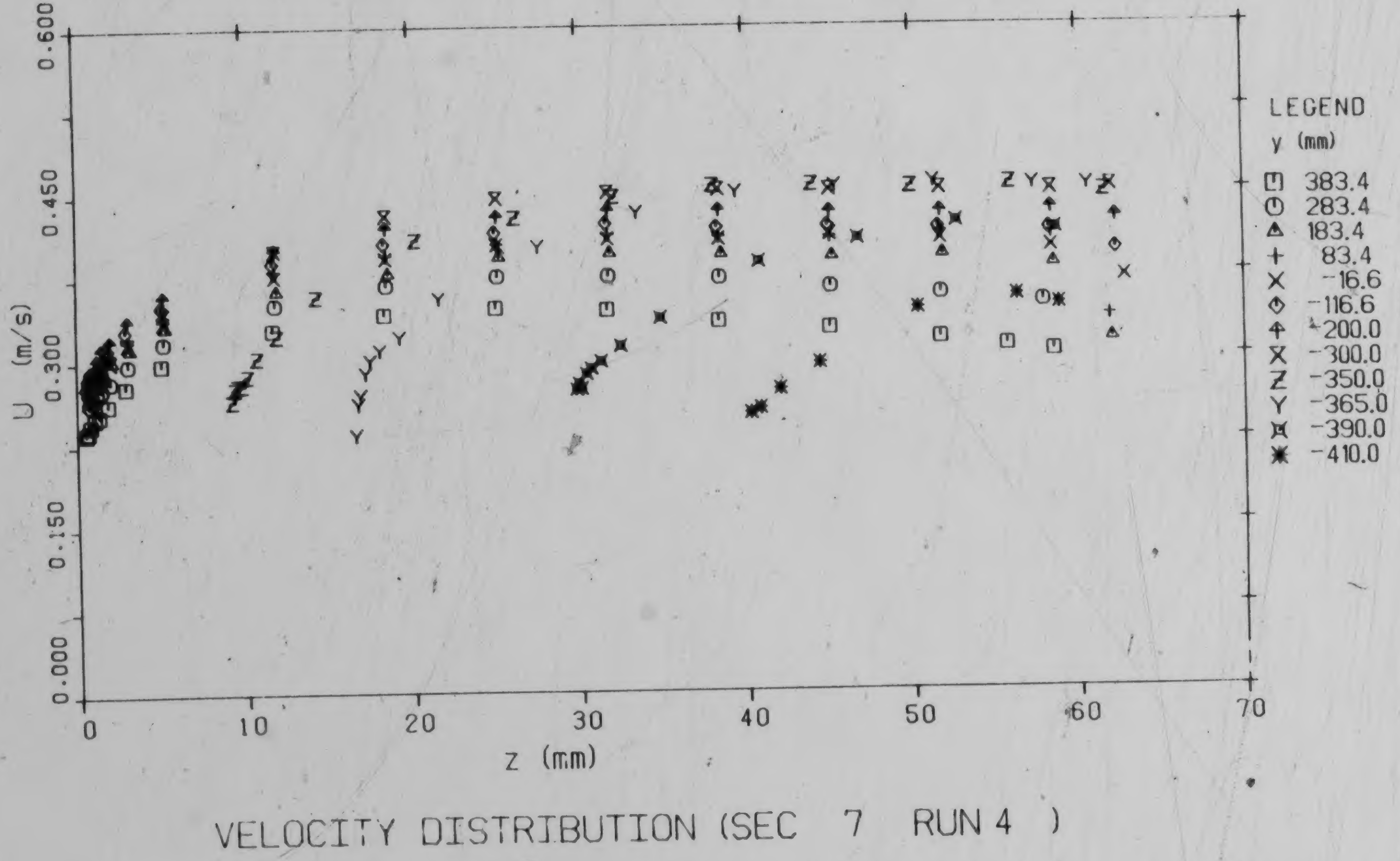

Figure 4.58 u velocity distribution (run 4, section 7)

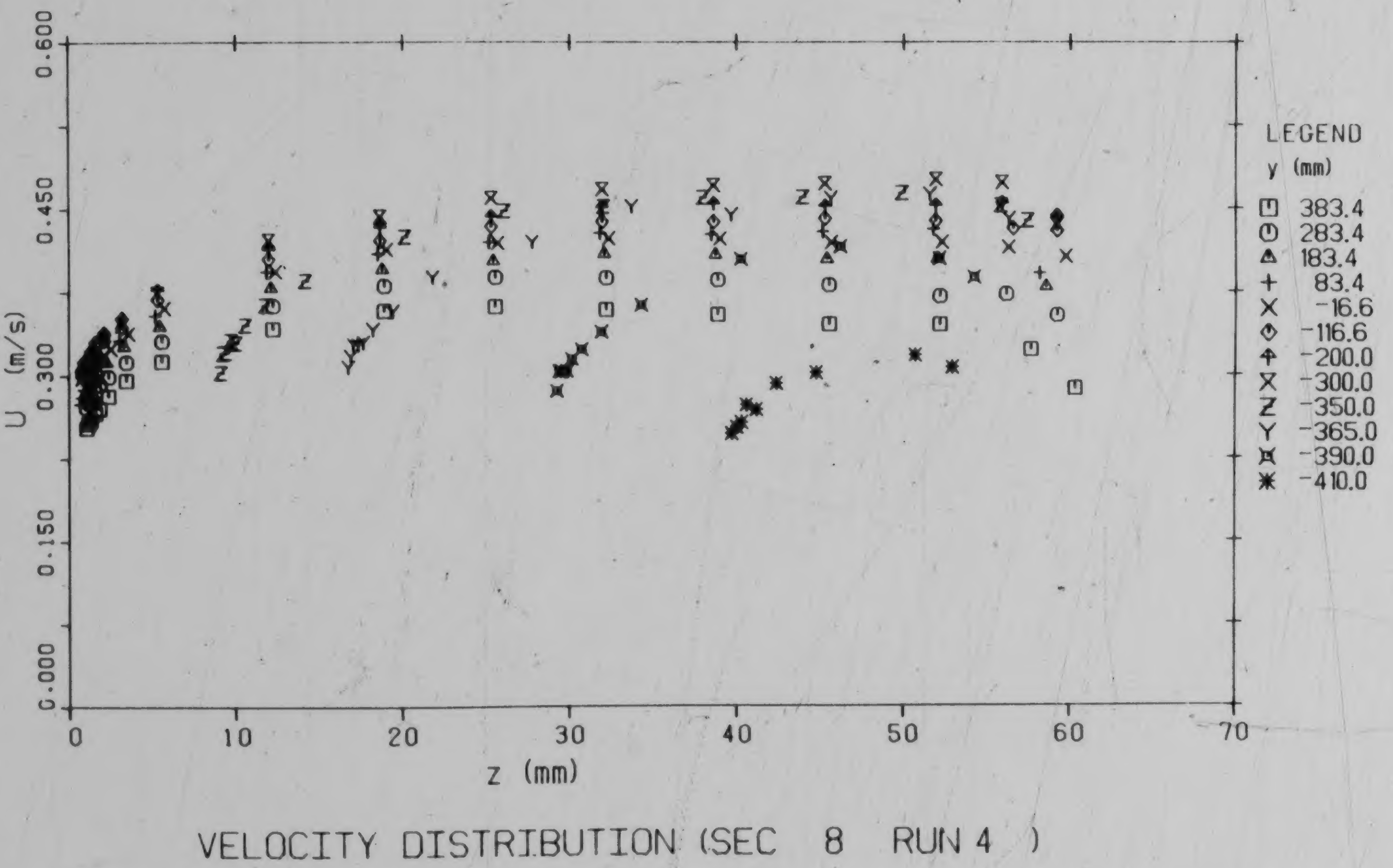

Figure 4.59 u velocity distribution (run 4, section 8)

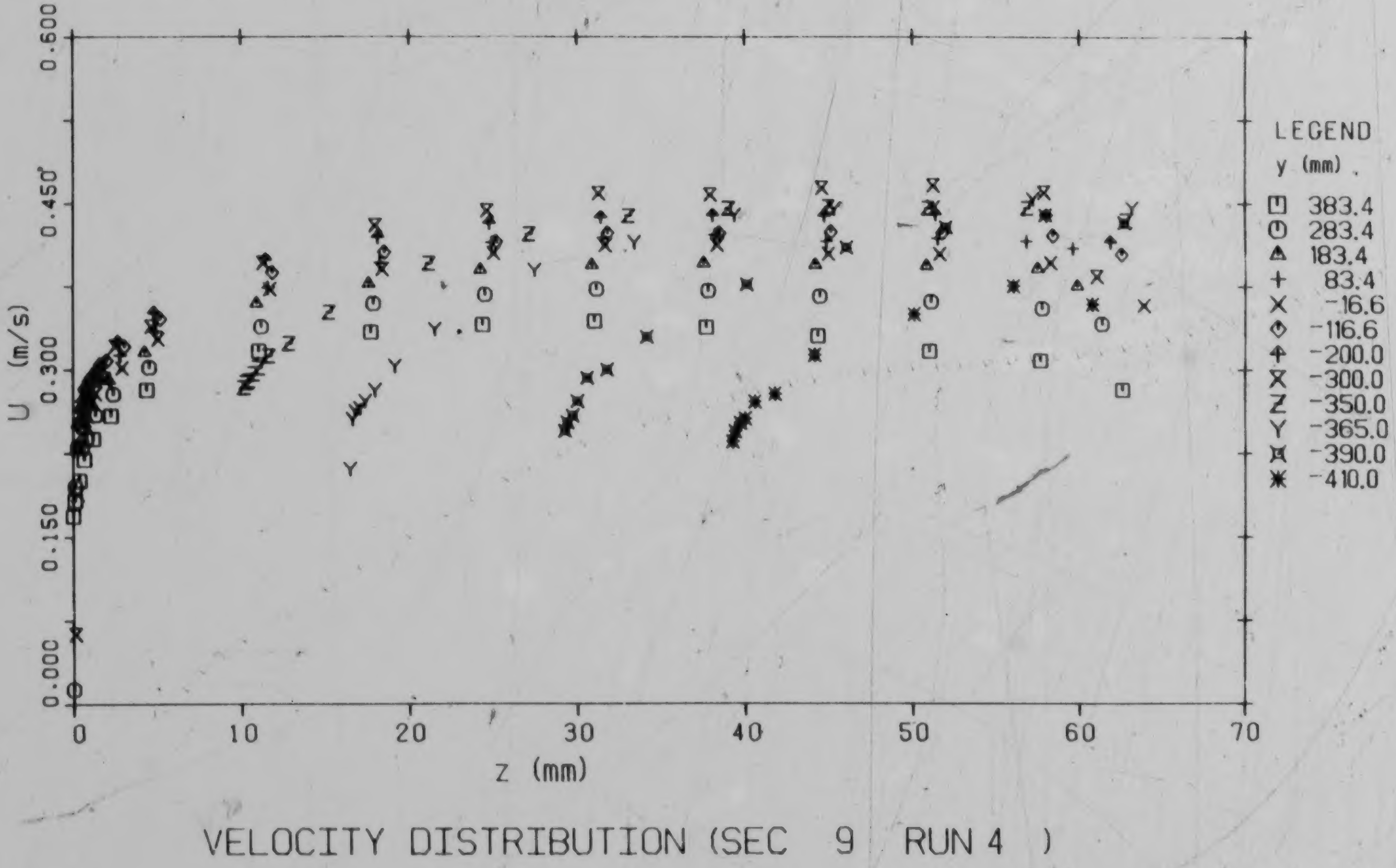

Figure 4.60 u velocity distribution (run 4, section 9)

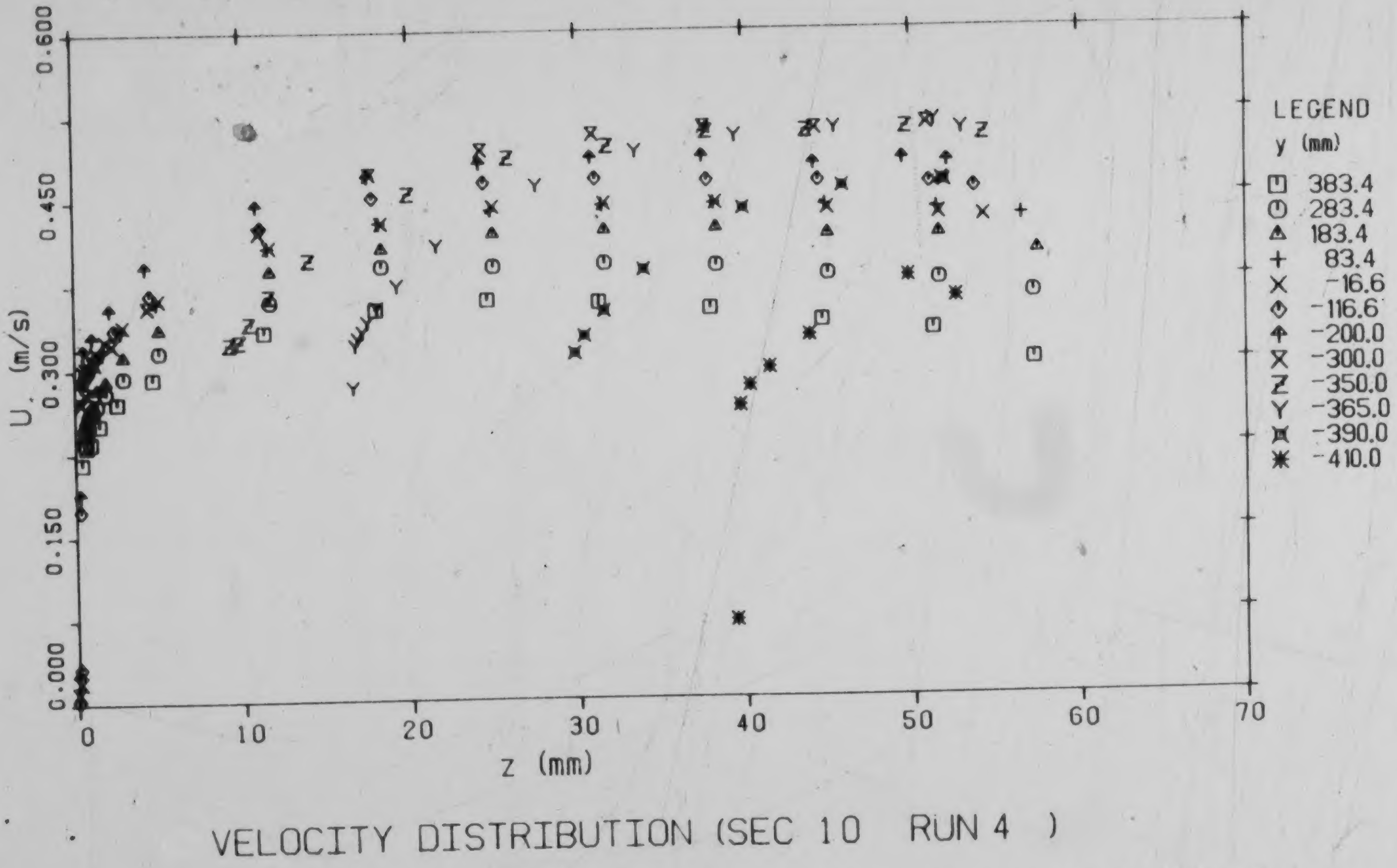

Figure 4.61 u velocity distribution (run 4, section 10)

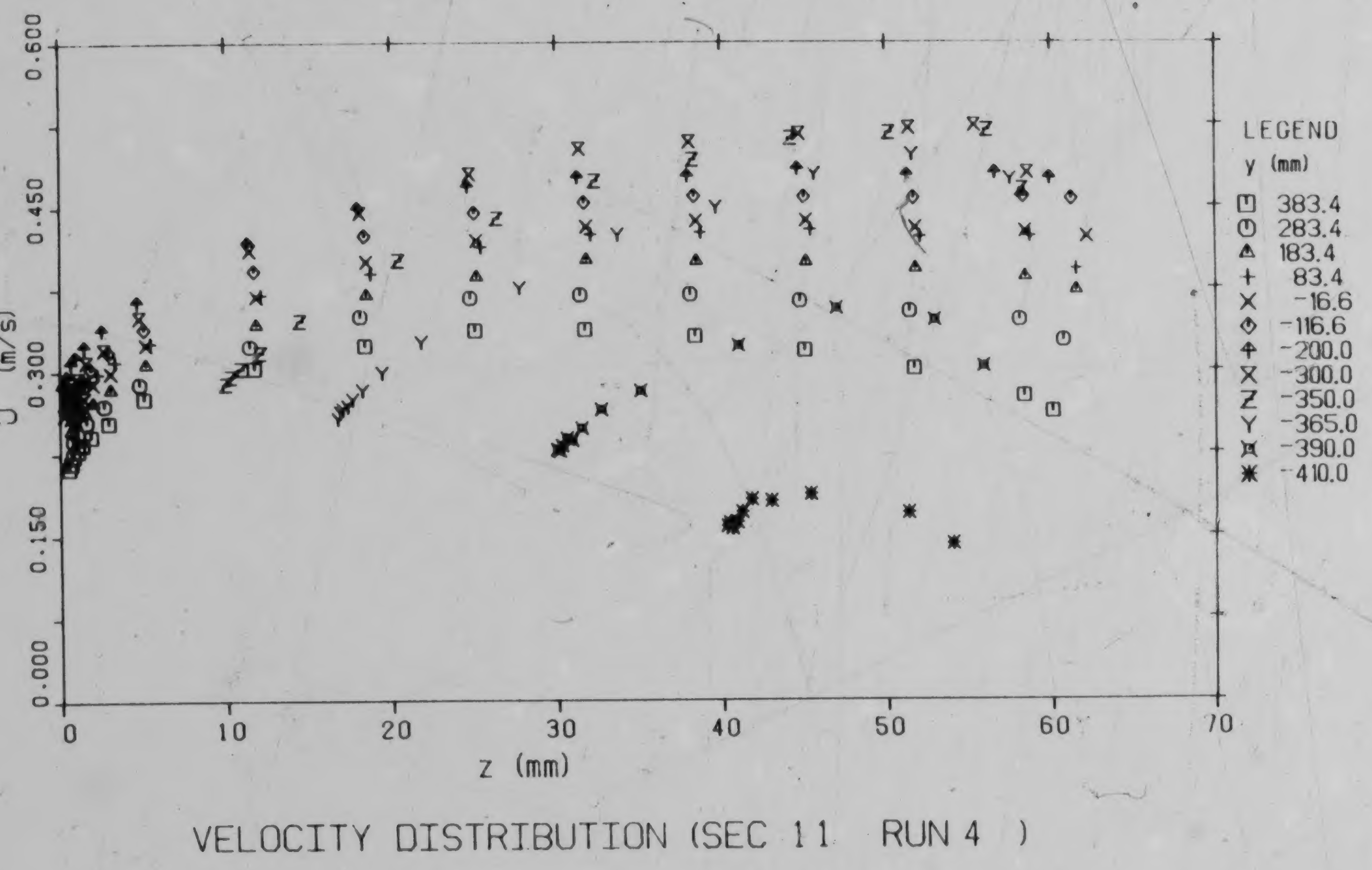

Figure 4.62 u velocity distribution (run 4, section 11)

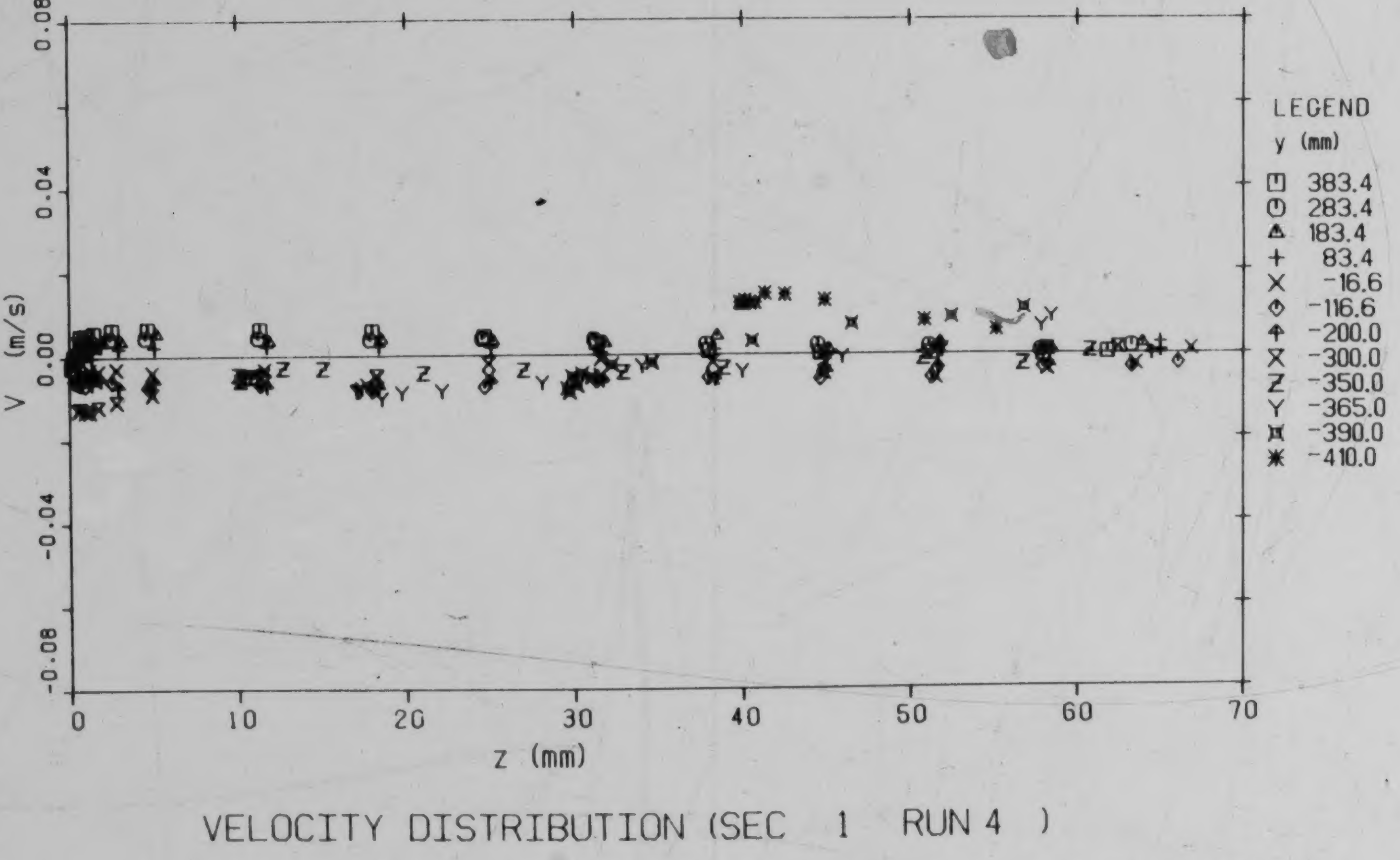

Figure 4.63 v velocity distribution (run 4, section 1)

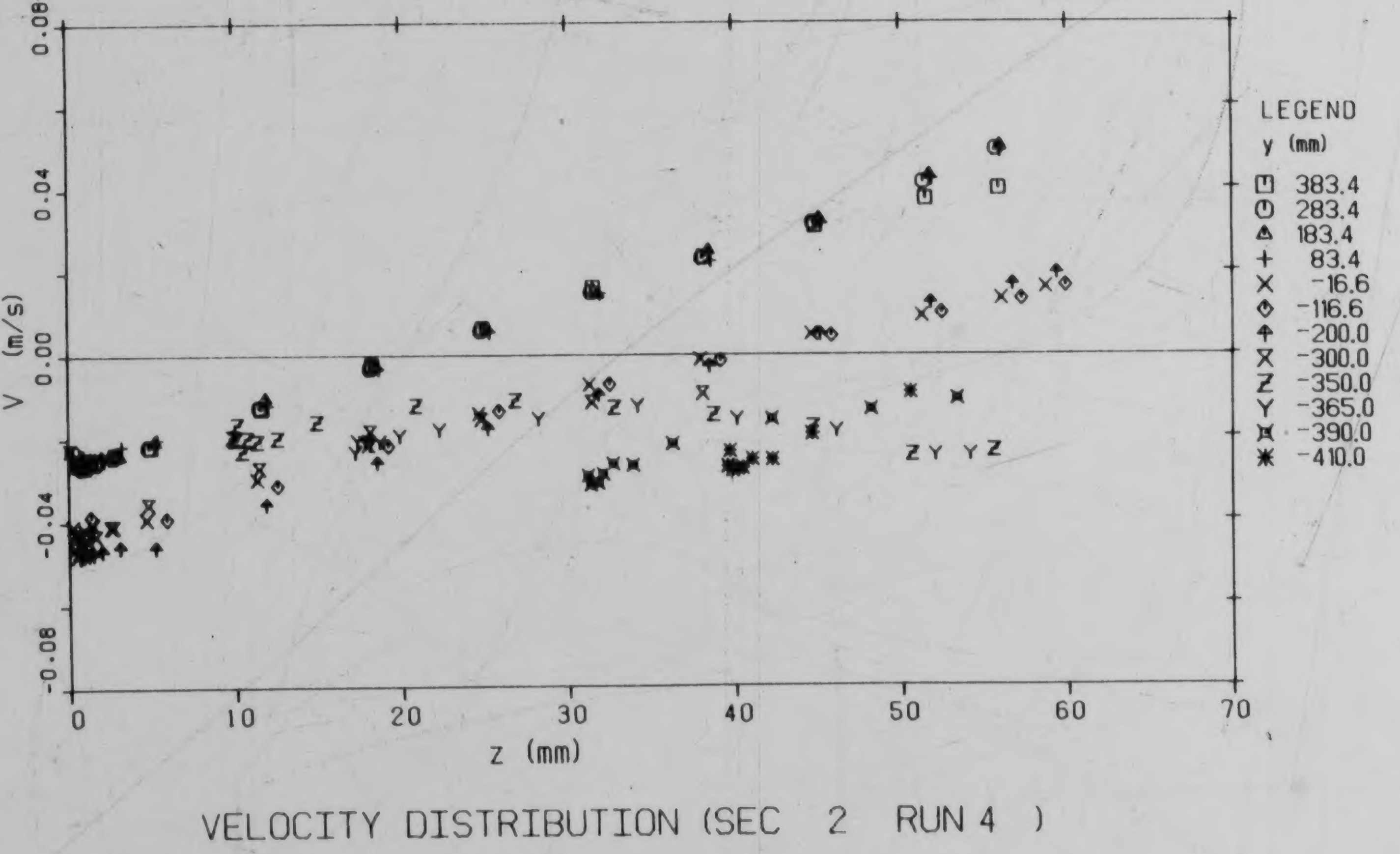

Figure 4.64 v velocity distribution (run 4, section 2)

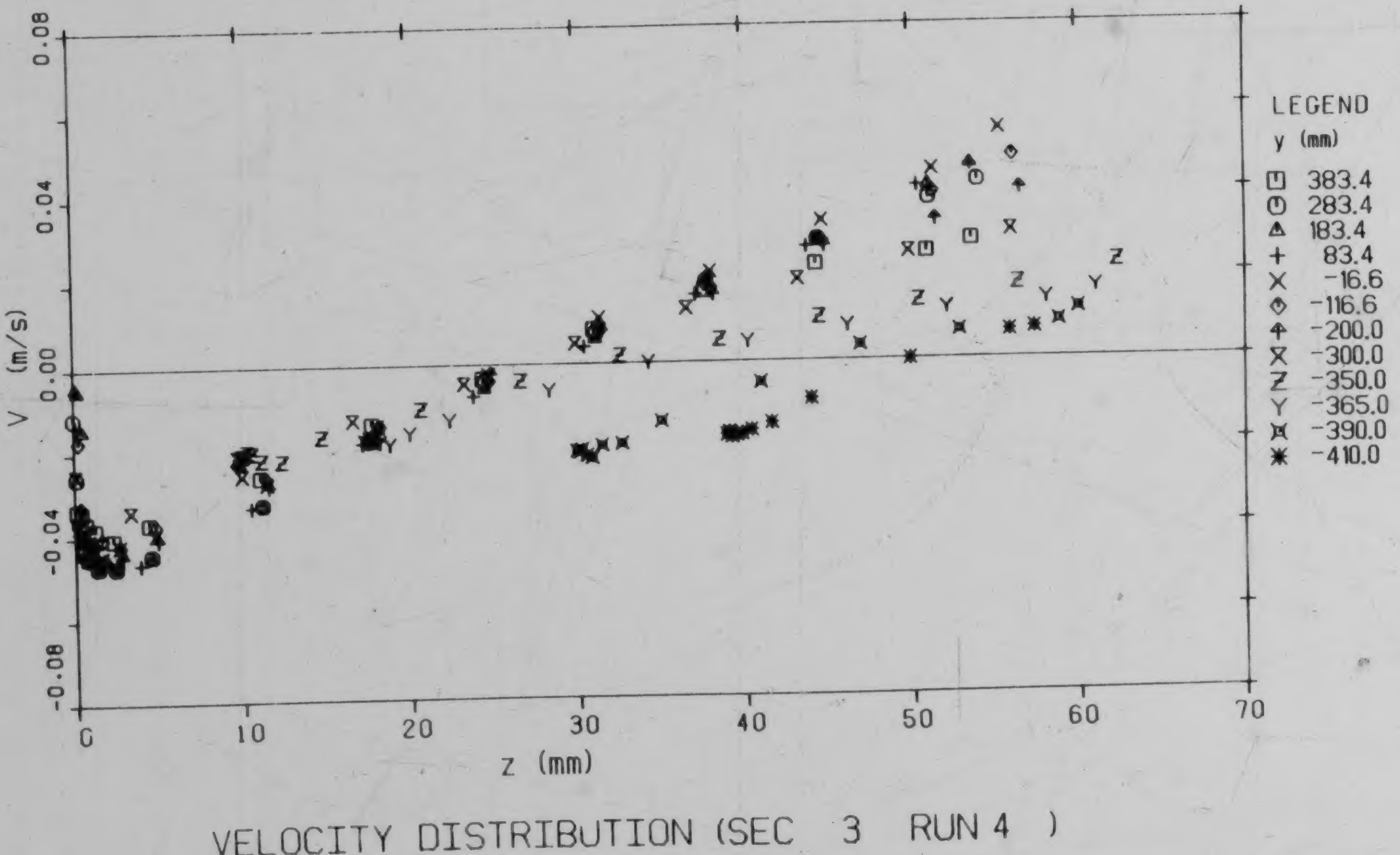

Figure 4.65 v velocity distribution (run 4, section 3)

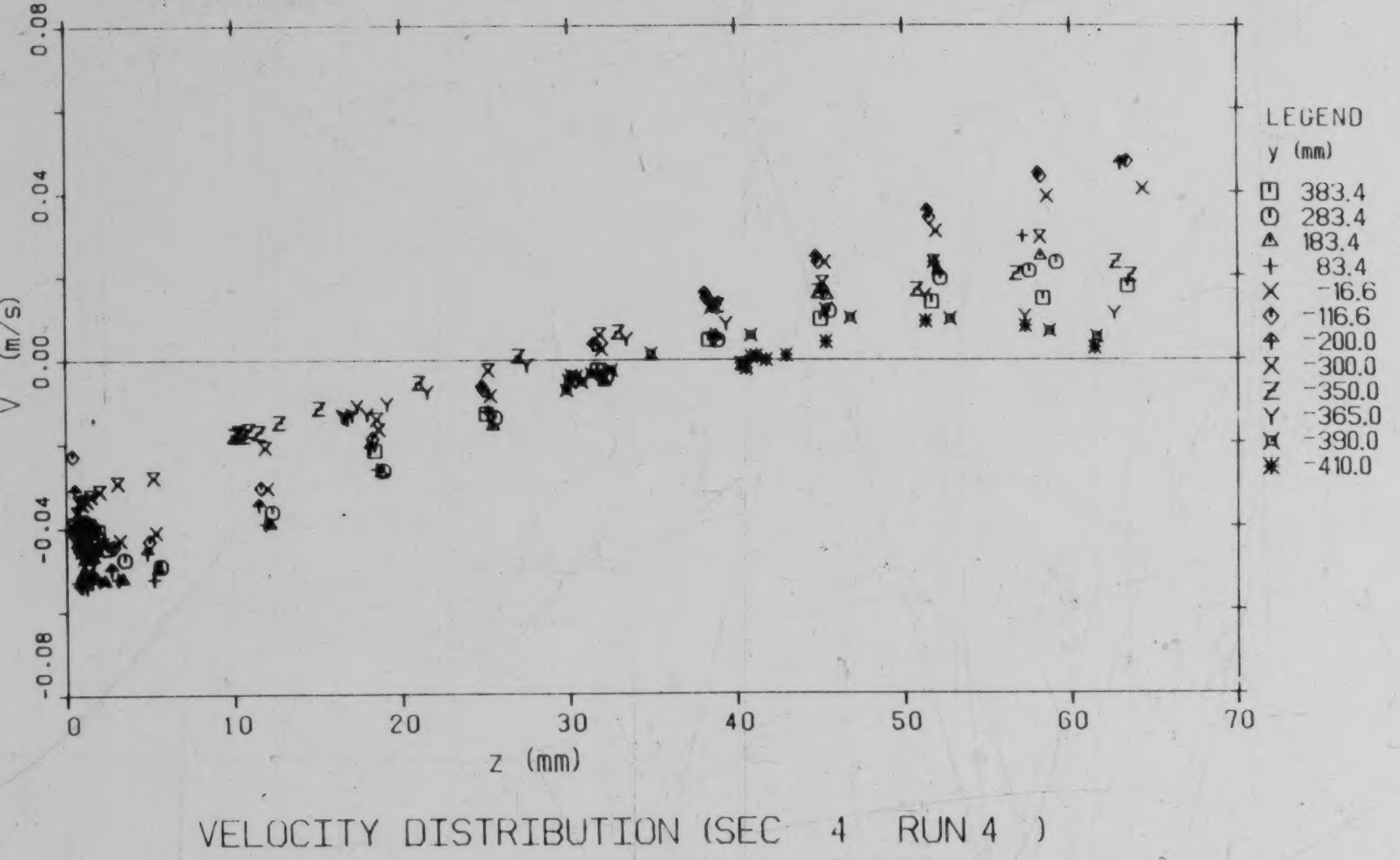

Figure 4.66 v velocity distribution (run 4, section 4)

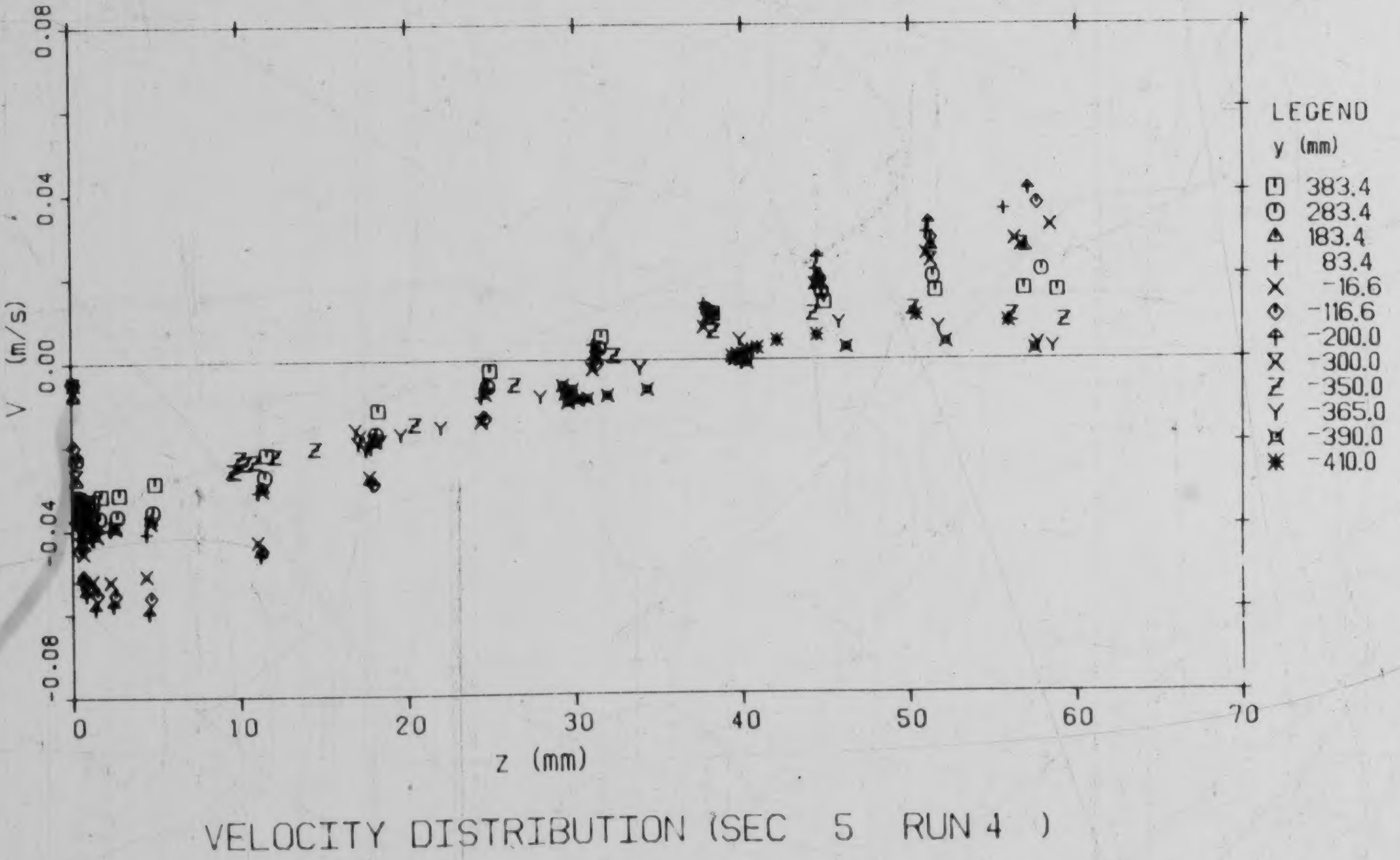

Figure 4.67 v velocity distribution (run 4, section 5)

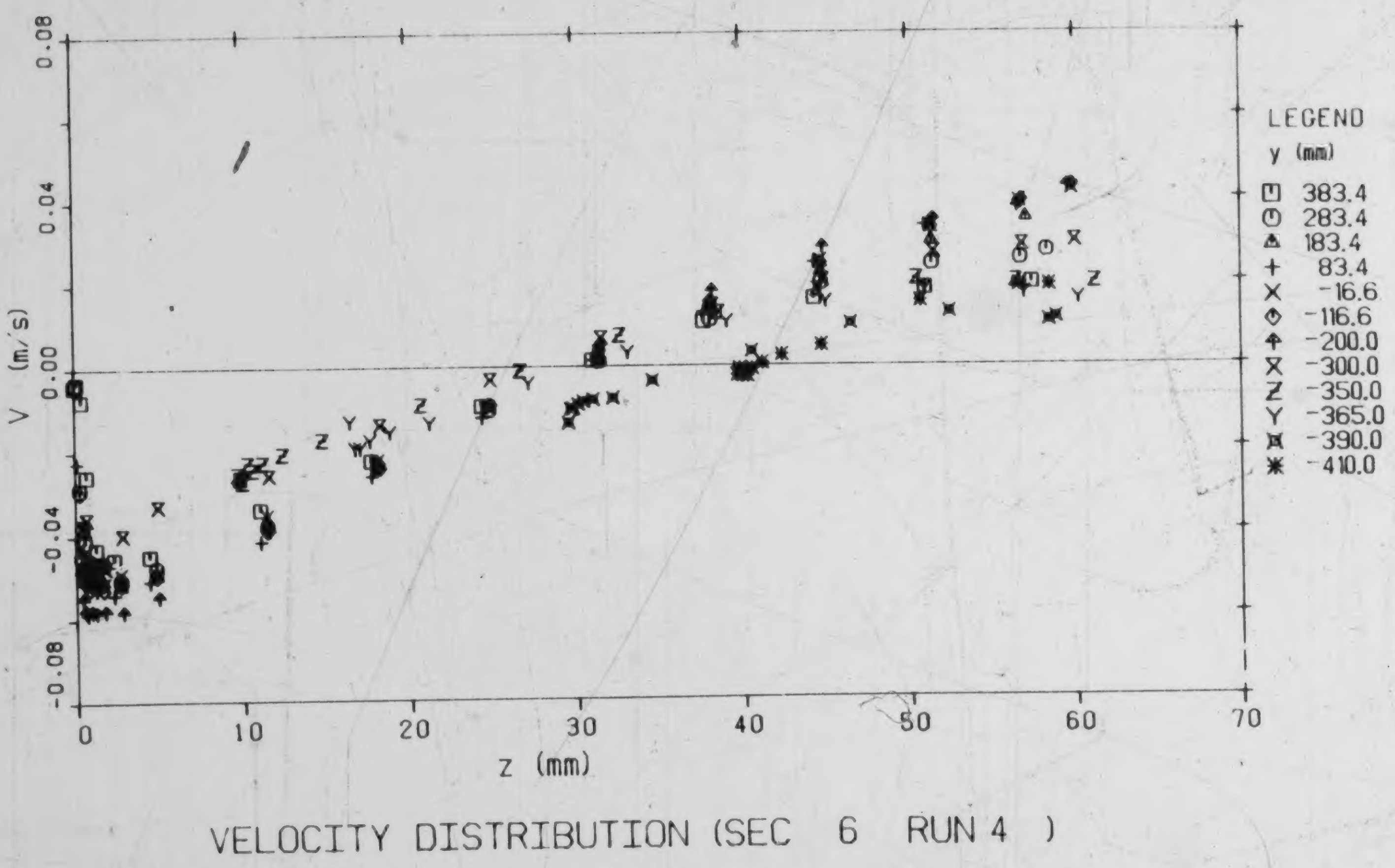

Figure 4.68 v velocity distribution (run 4, section 6)

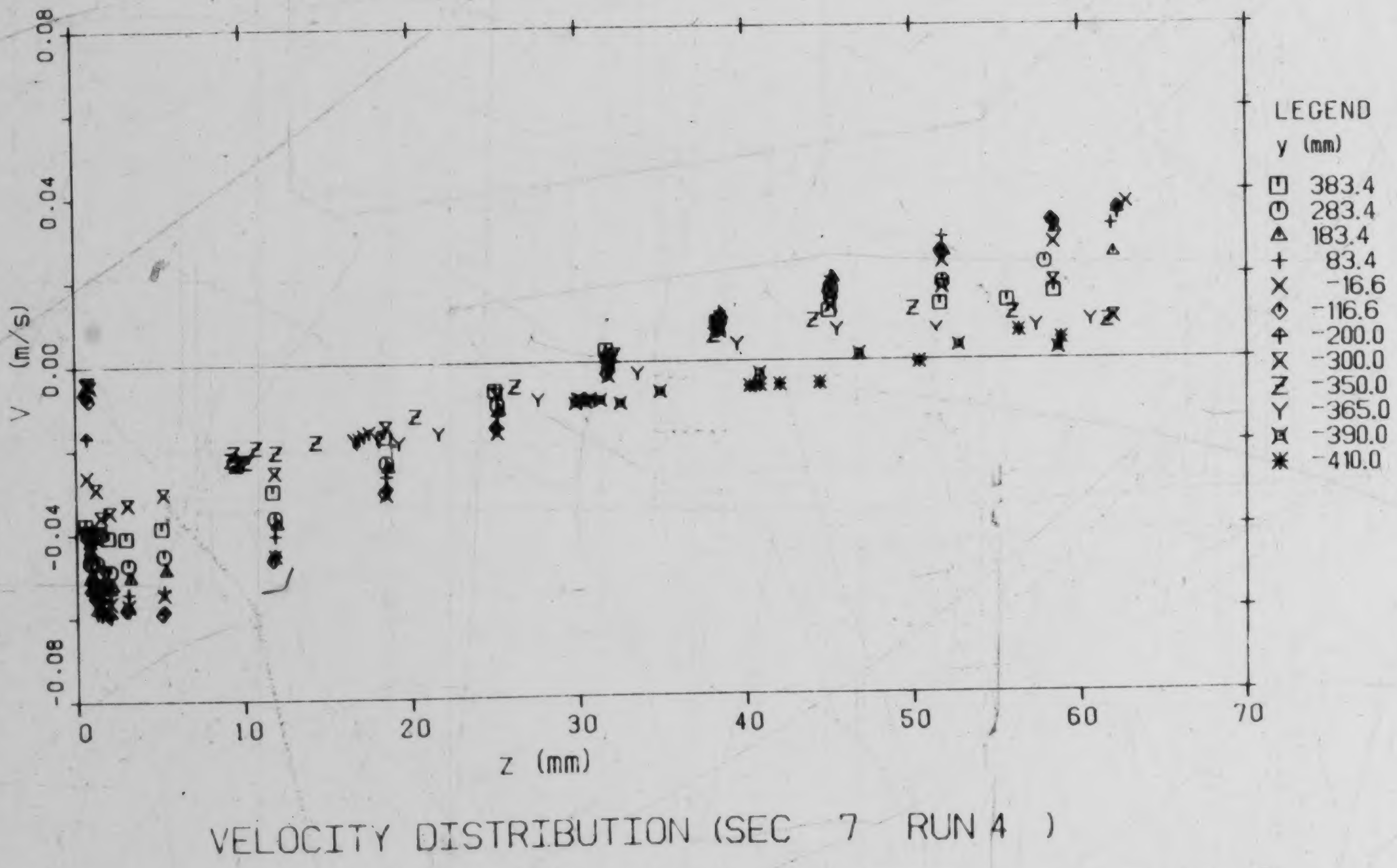

Figure 4.69 v velocity distribution (run 4, section 7)

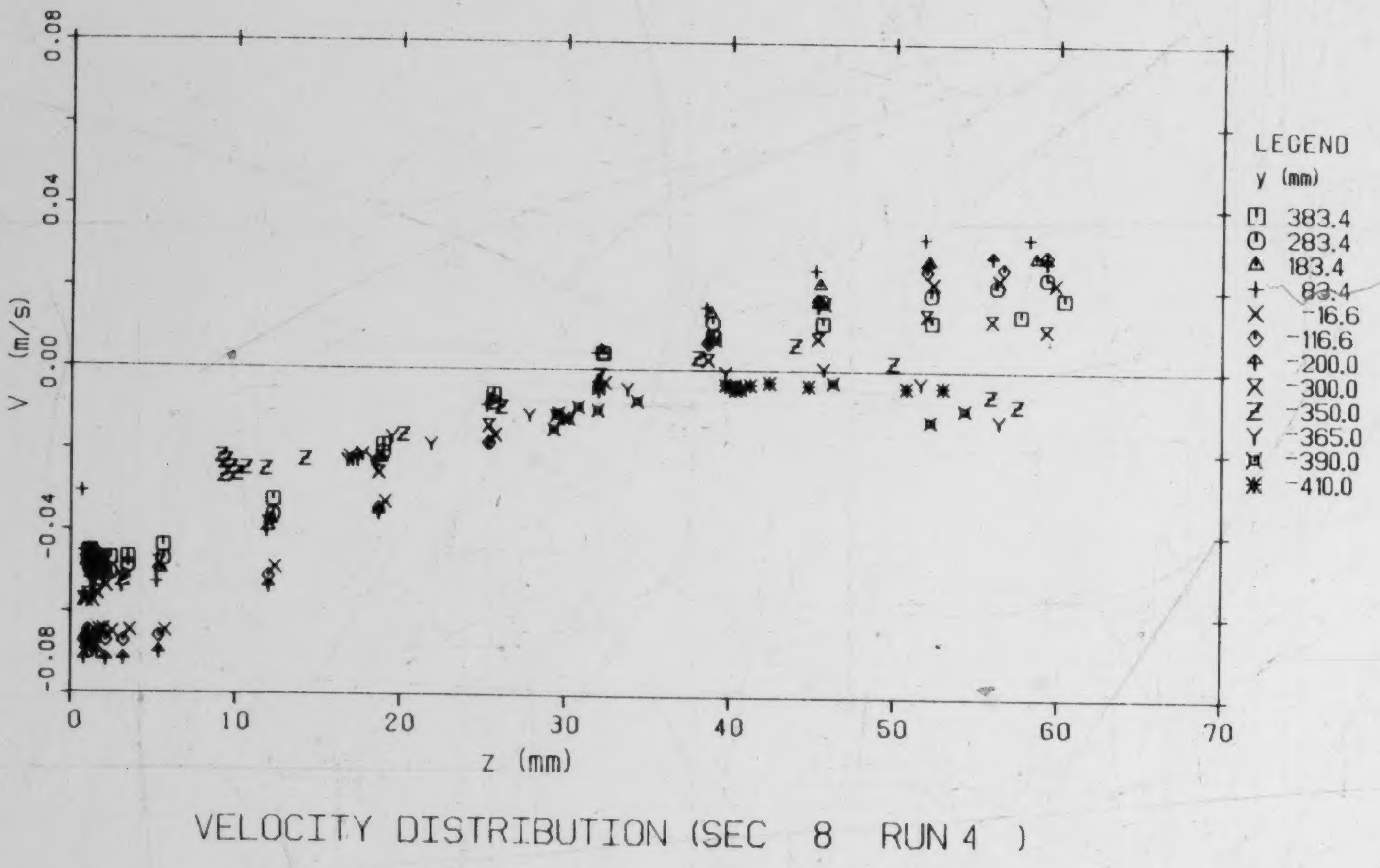

Figure 4.70 v velocity distribution (run 4, section 8)

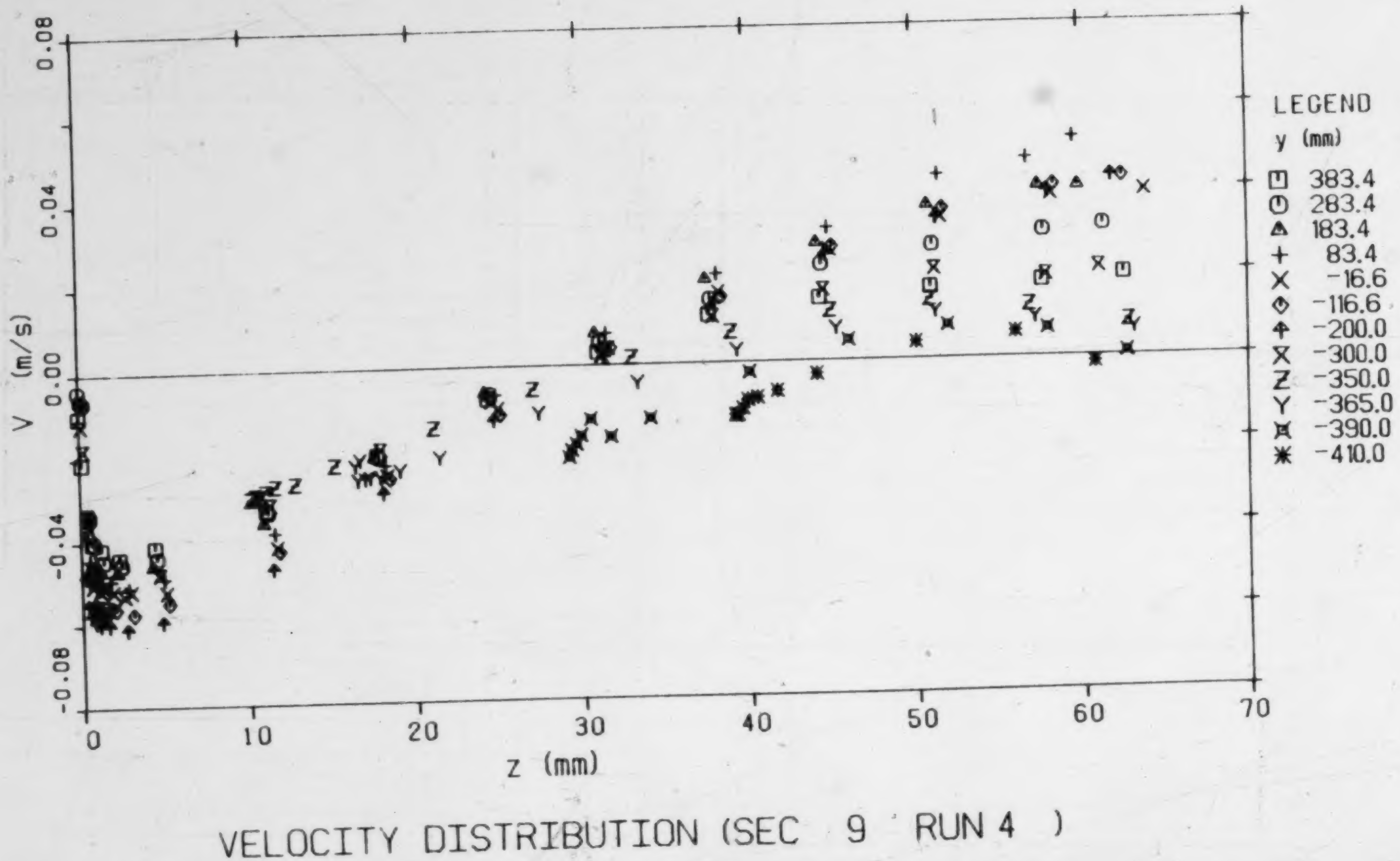

Figure 4.71 v velocity distribution (run 4, section 9)

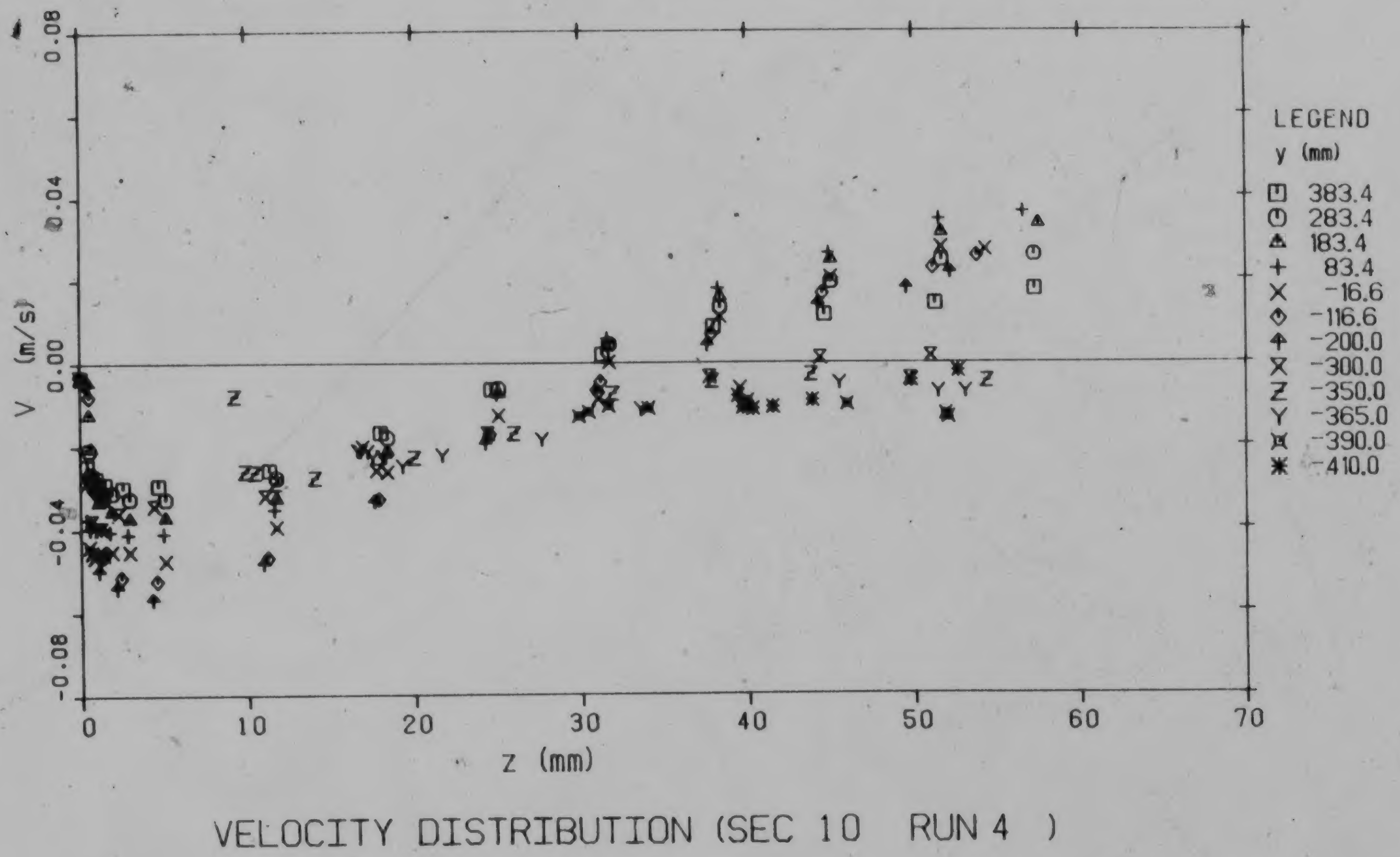

Figure 4.72 v velocity distribution (run 4, section 10)

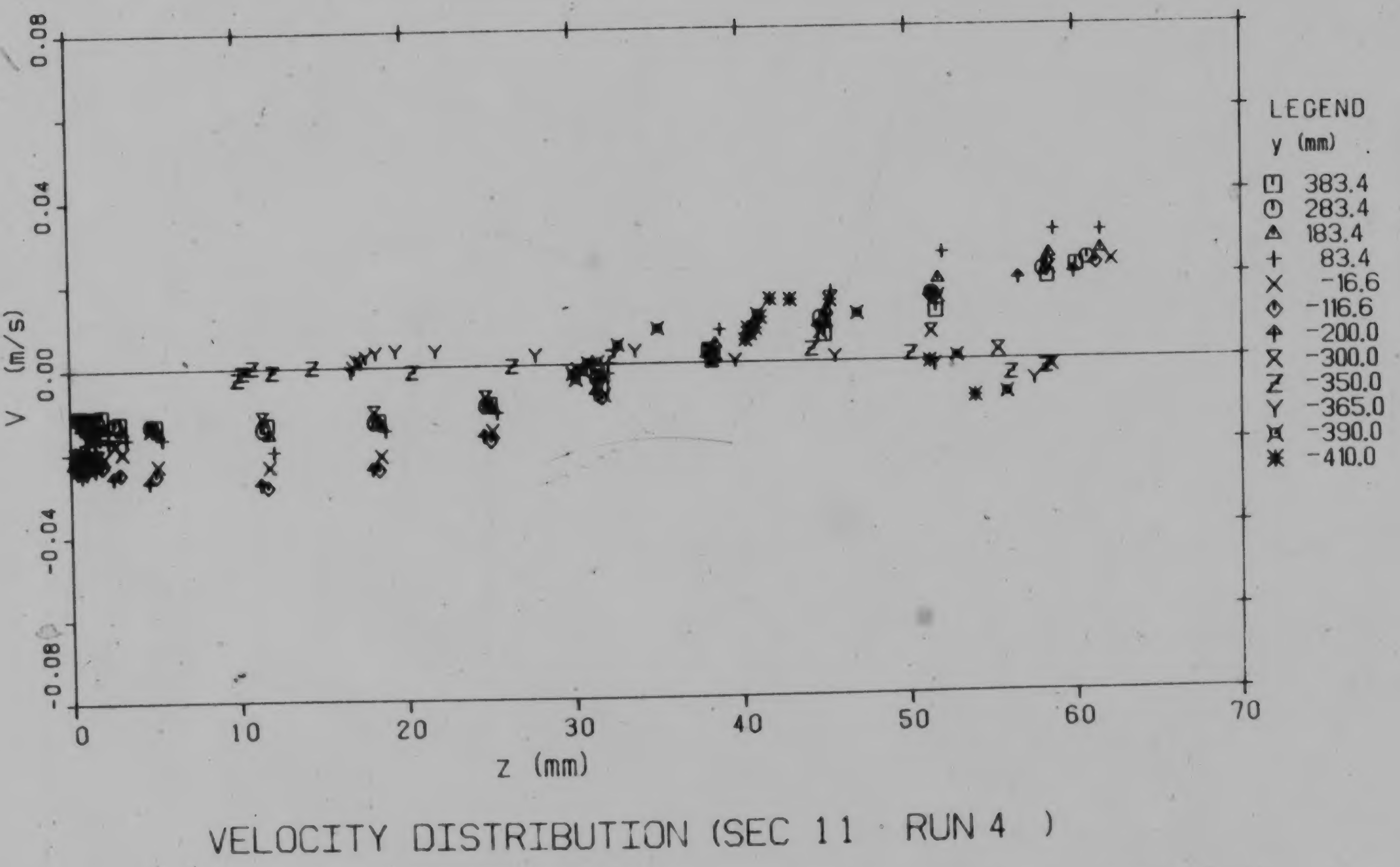

Figure 4.73 v velocity distribution (run 4, section 11)

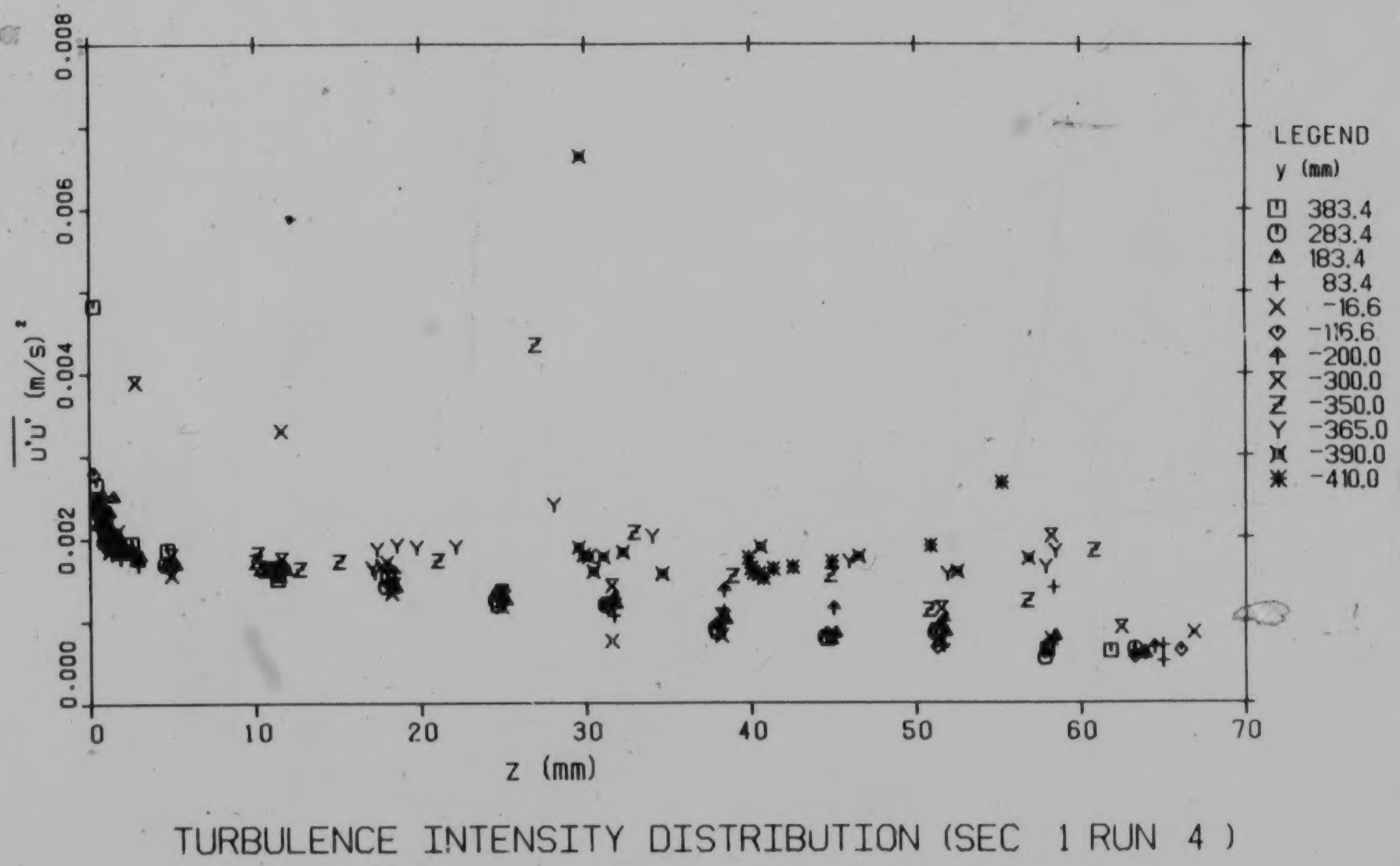

Figure 4.74 $\overline{u'u'}$ turbulence intensity distribution (run 4, section 1)

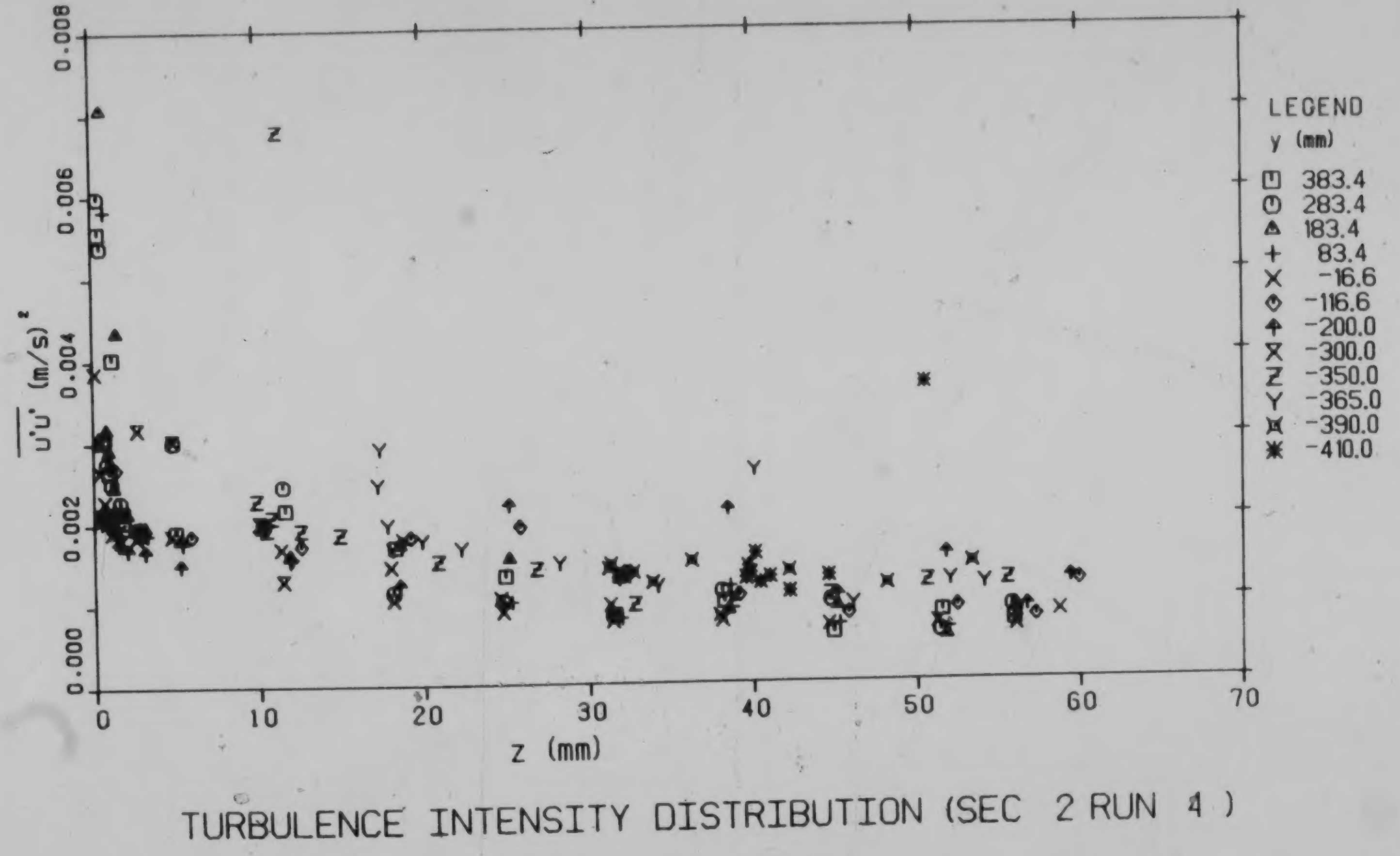

Figure 4.75 $\overline{u'u'}$ turbulence intensity distribution (run 4, section 2)

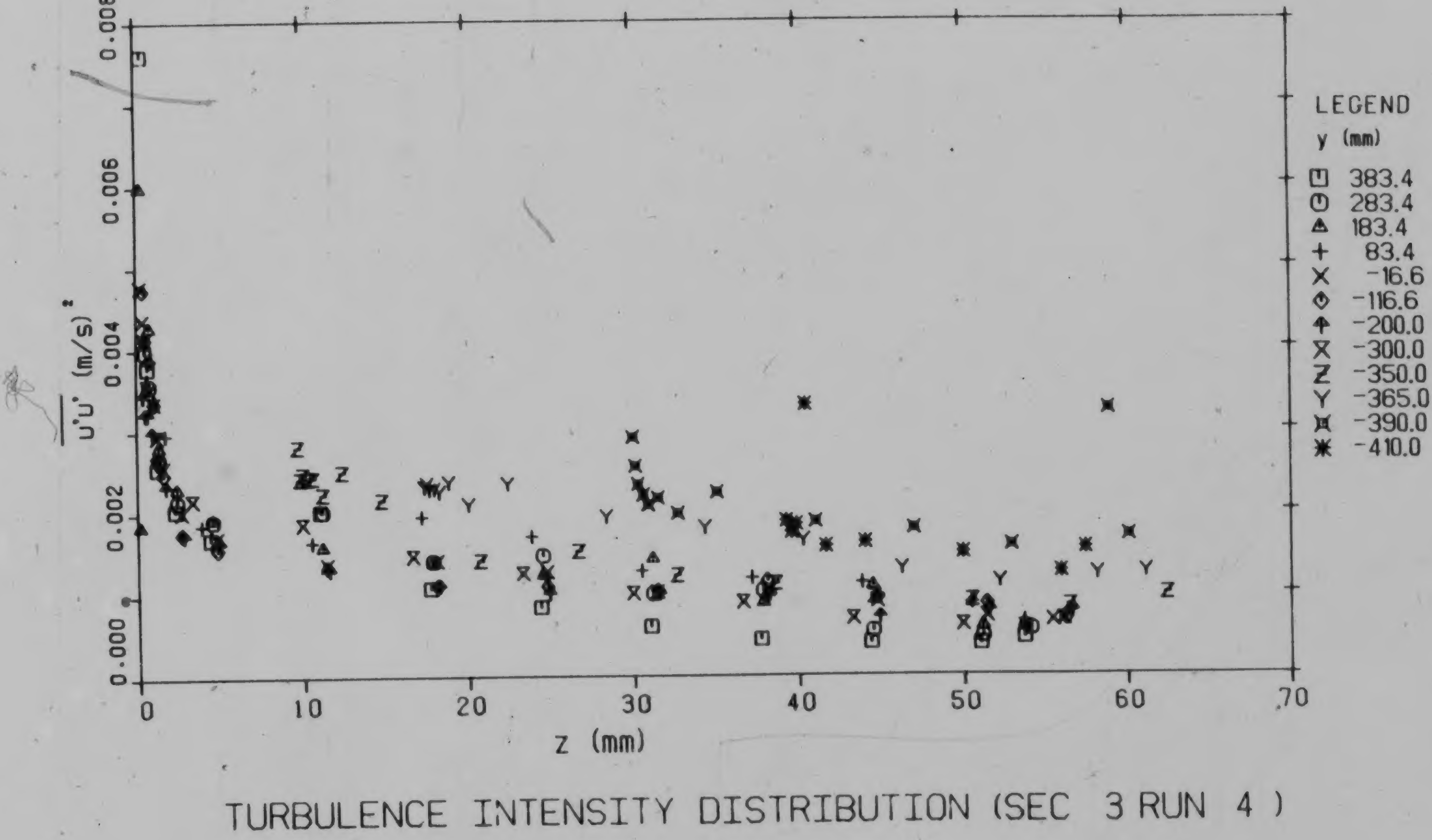

Figure 4.76 $\overline{u'u'}$ turbulence intensity distribution (run 4, section 3)

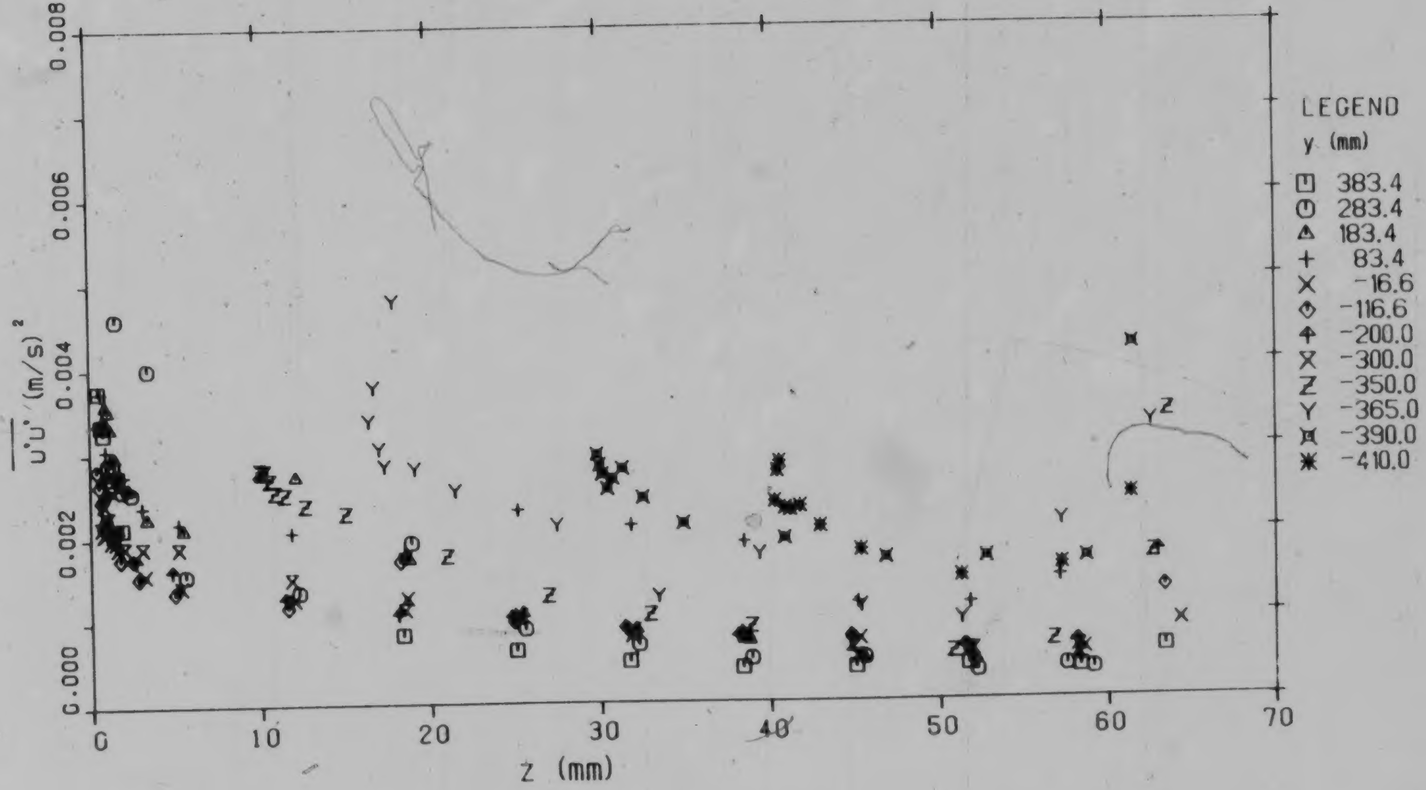

TURBULENCE INTENSITY DISTRIBUTION (SEC 4 RUN 4)

Figure 4.77 $\overline{u'u'}$ turbulence intensity distribution (run 4, section 4)

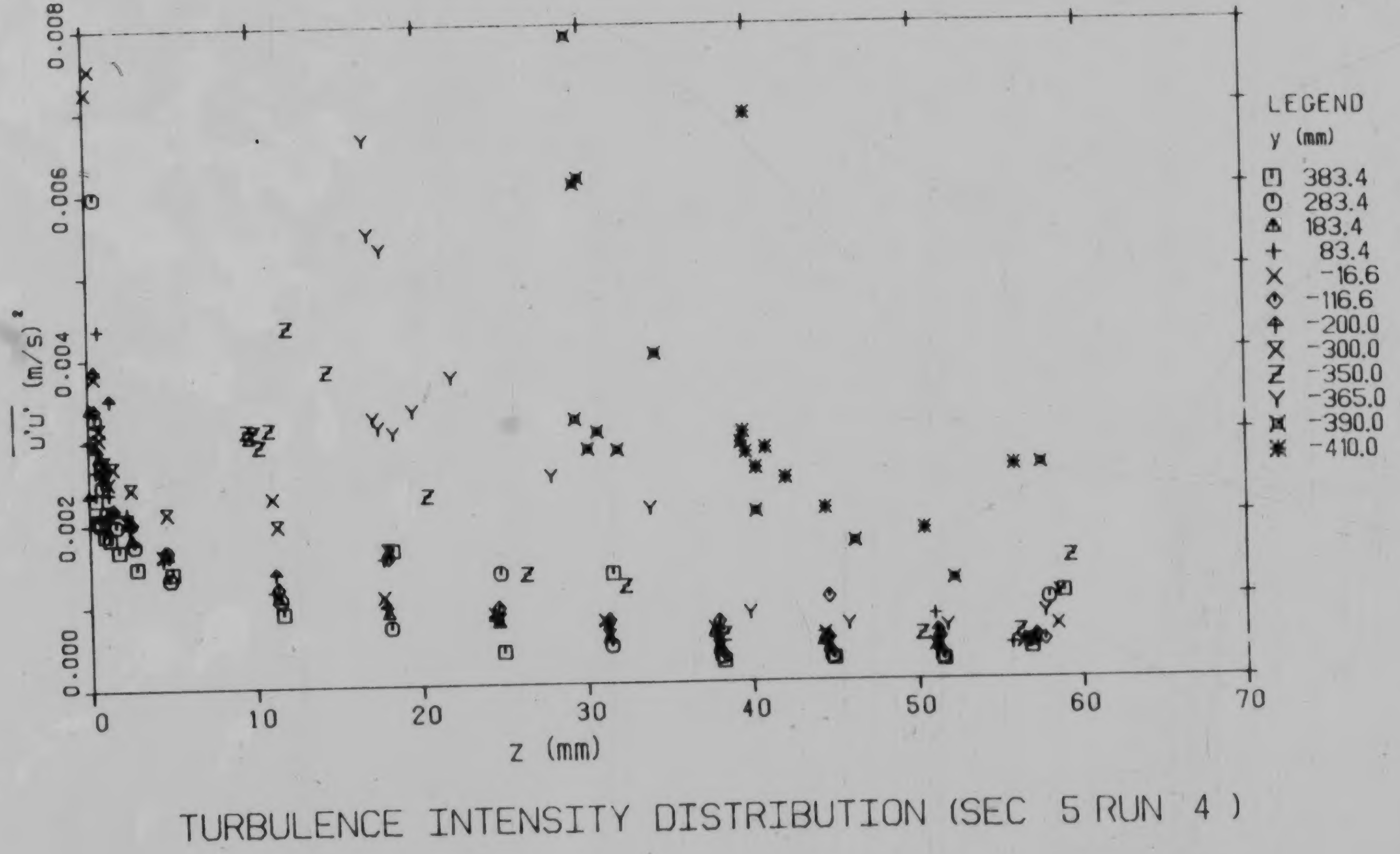

Figure 4.78 $\overline{u'u'}$ turbulence intensity distribution (run 4, section 5)

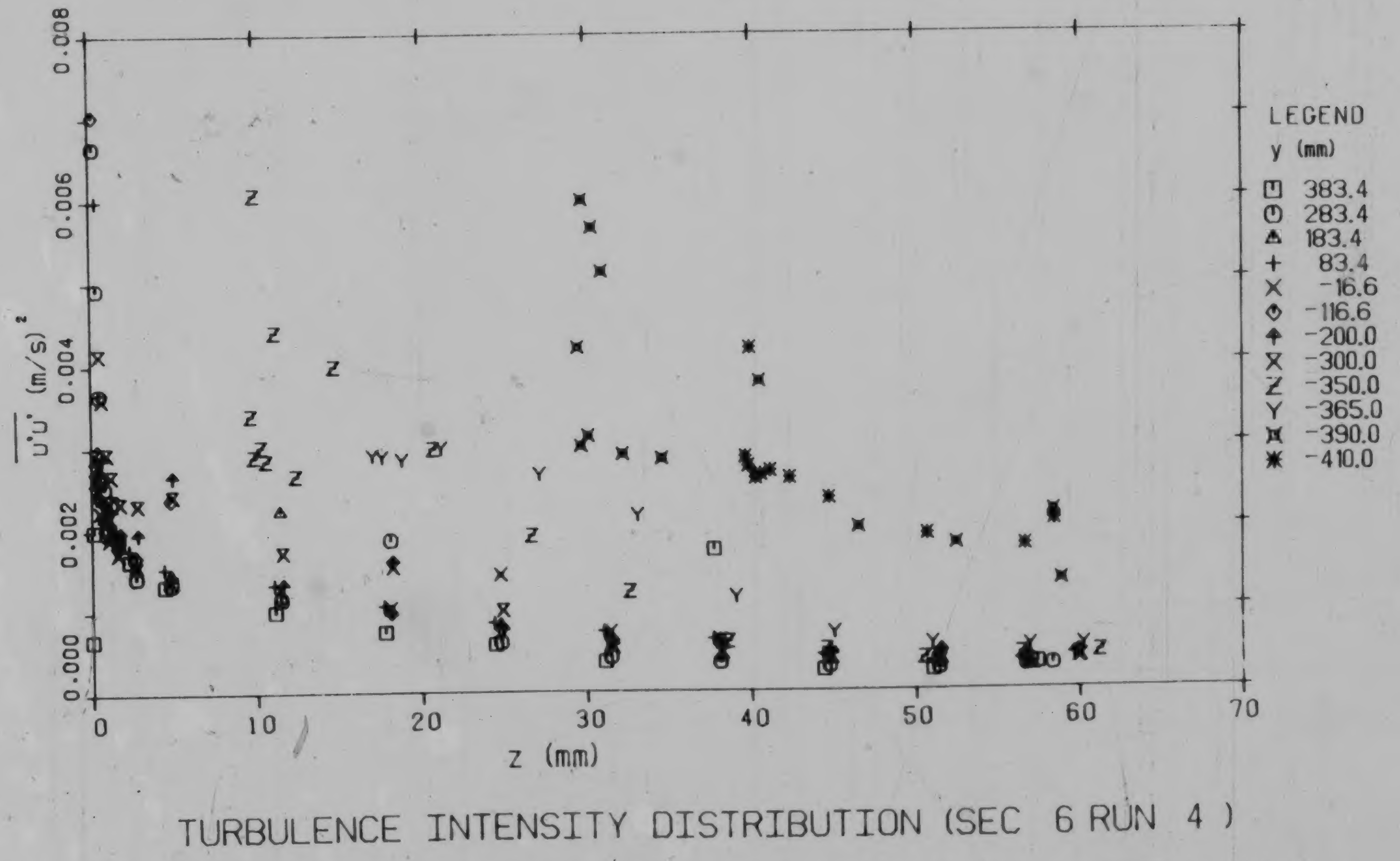

Figure 4.79 $\overline{u'u'}$ turbulence intensity distribution (run 4, section 6)

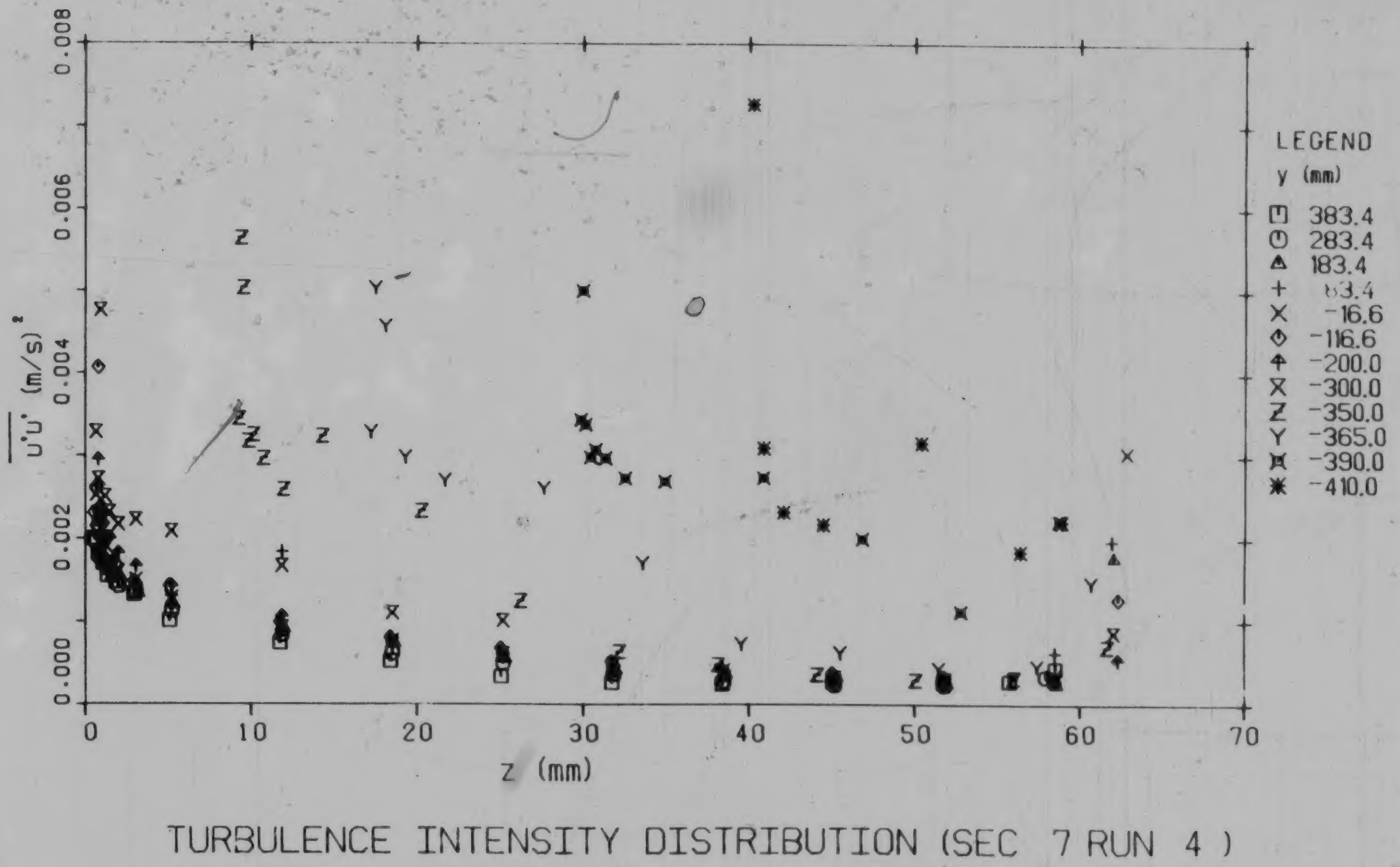

Figure 4.80 $\overline{u'u'}$ turbulence intensity distribution (run 4, section 7)

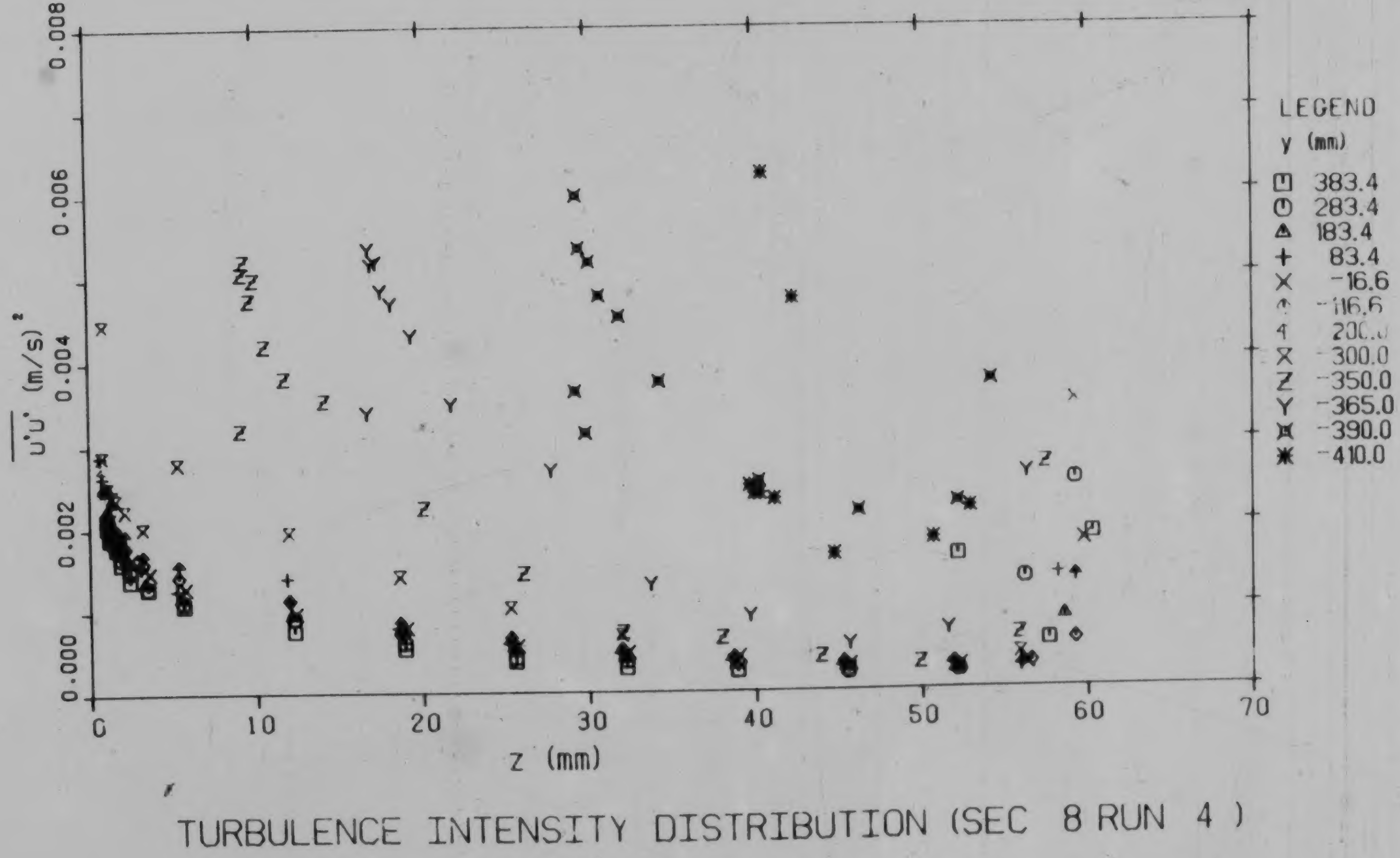

Figure 4.81 $\overline{u'u'}$ turbulence intensity distribution (run 4, section 8)

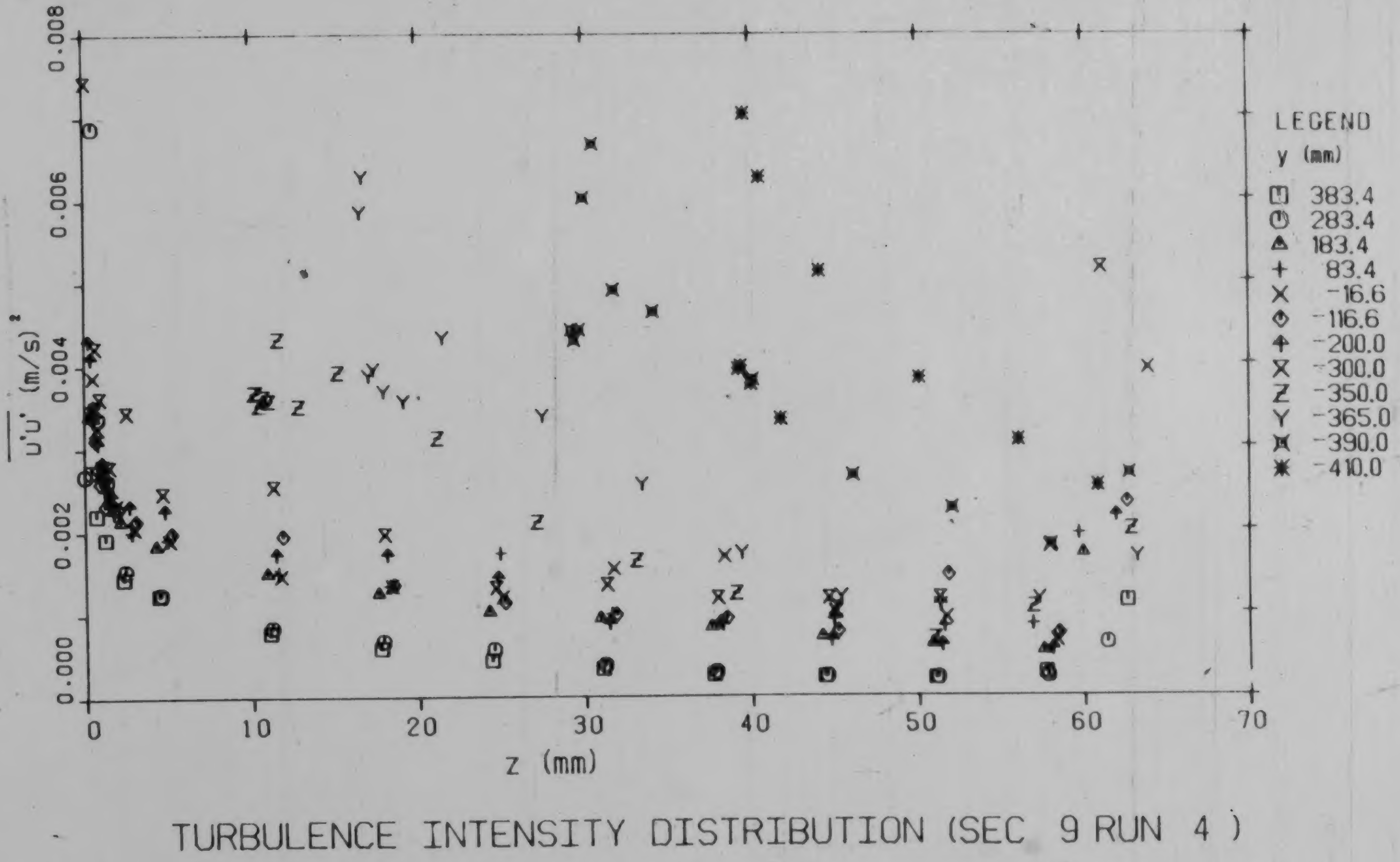

Figure 4.82 $\overline{u'u'}$ turbulence intensity distribution (run 4, section 9)

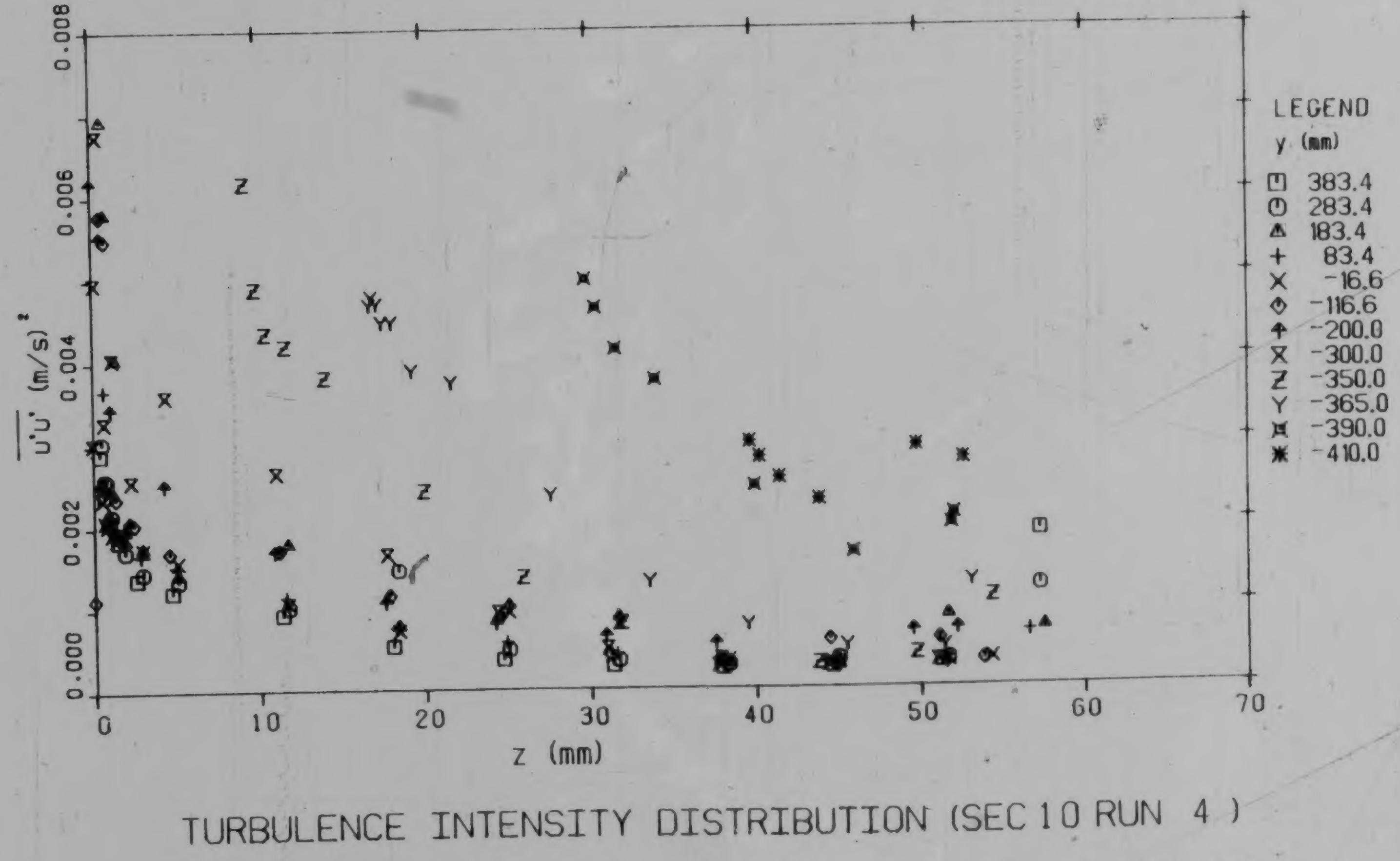

TURBULENCE INTENSITY DISTRIBUTION (SEC 10 RUN 4)

Figure 4.83 $\overline{u'u'}$ turbulence intensity distribution (run 4, section 10)

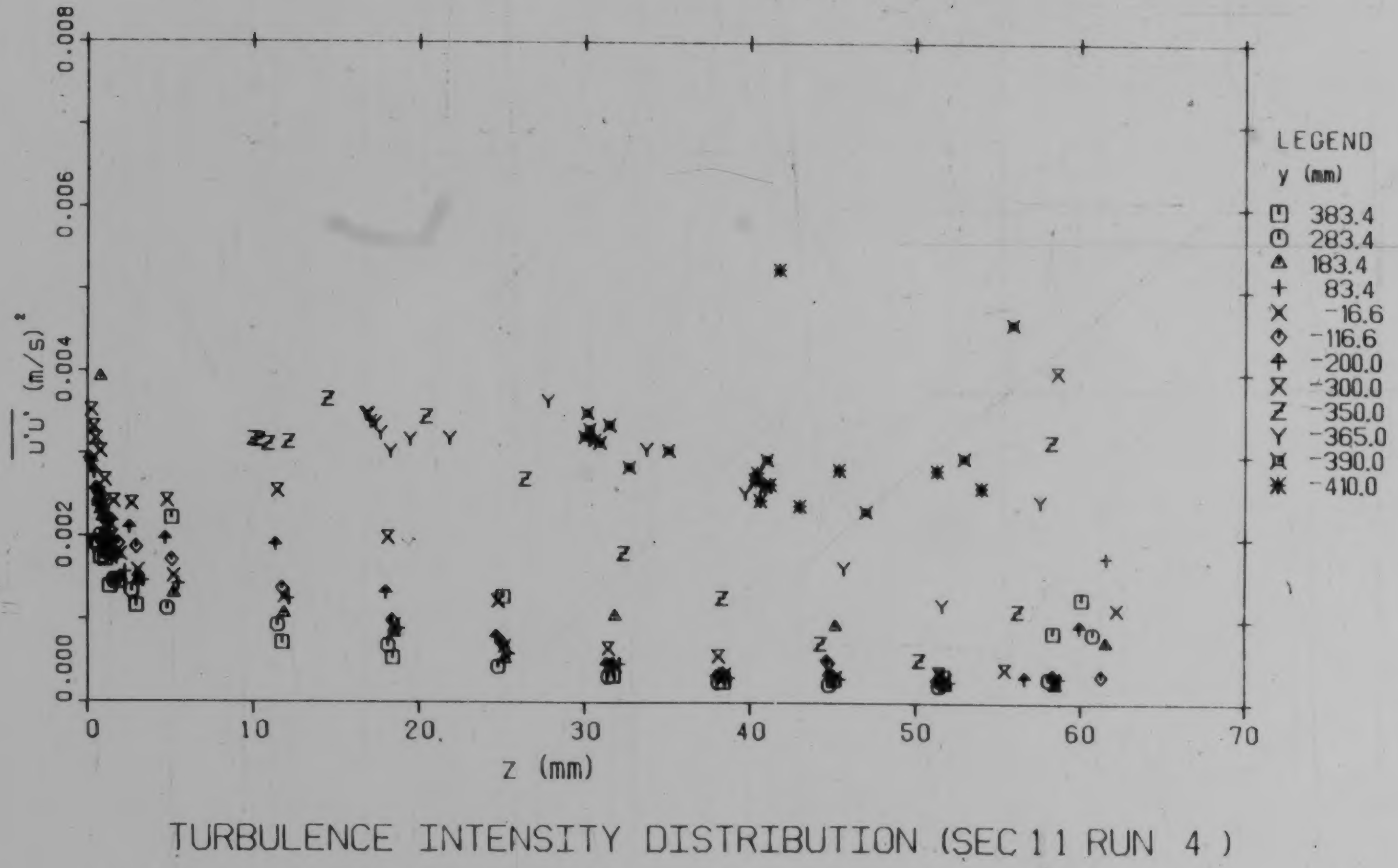
TURBULENCE INTENSITY DISTRIBUTION (SEC 11 RUN 4)

Figure 4.84 $\overline{u'u'}$ turbulence intensity distribution (run 4, section 11)

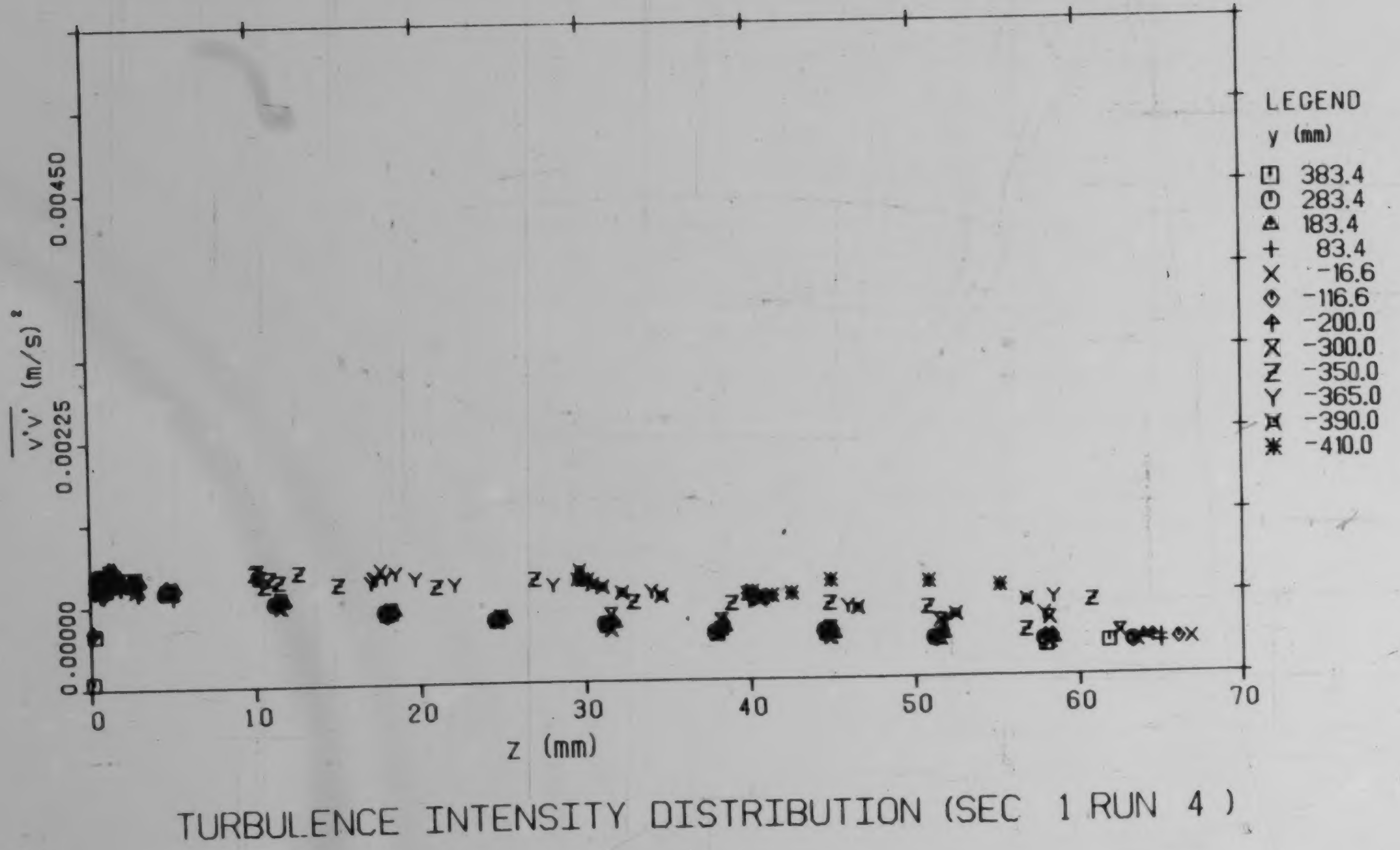

Figure 4.85 $\overline{v'v'}$ turbulence intensity distribution (run 4, section 1)

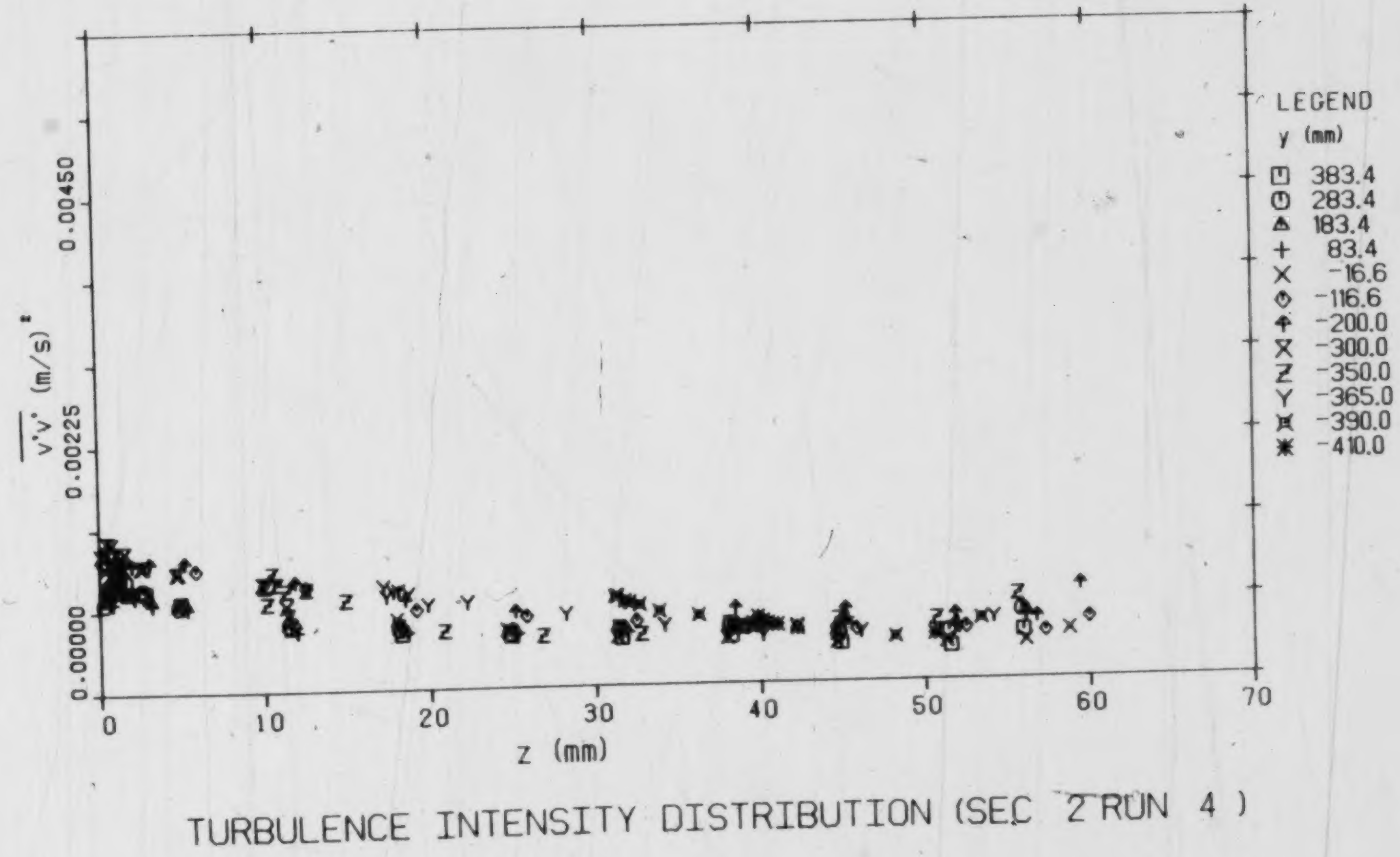

Figure 4.86 $\overline{v'v'}$ turbulence intensity distribution (run 4, section 2)

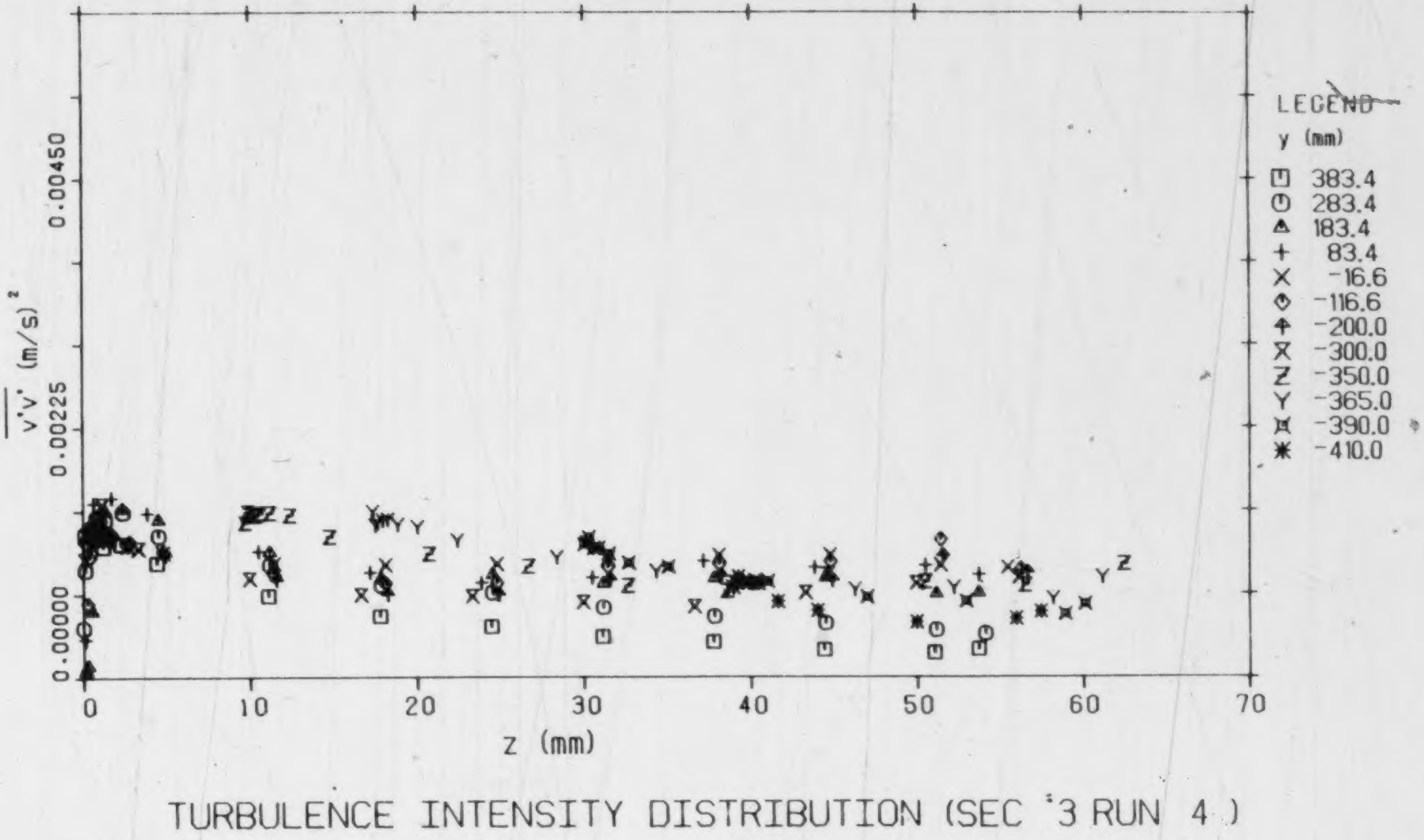

Figure 4.87 $\overline{v'v'}$ turbulence intensity distribution (run 4, section 3)

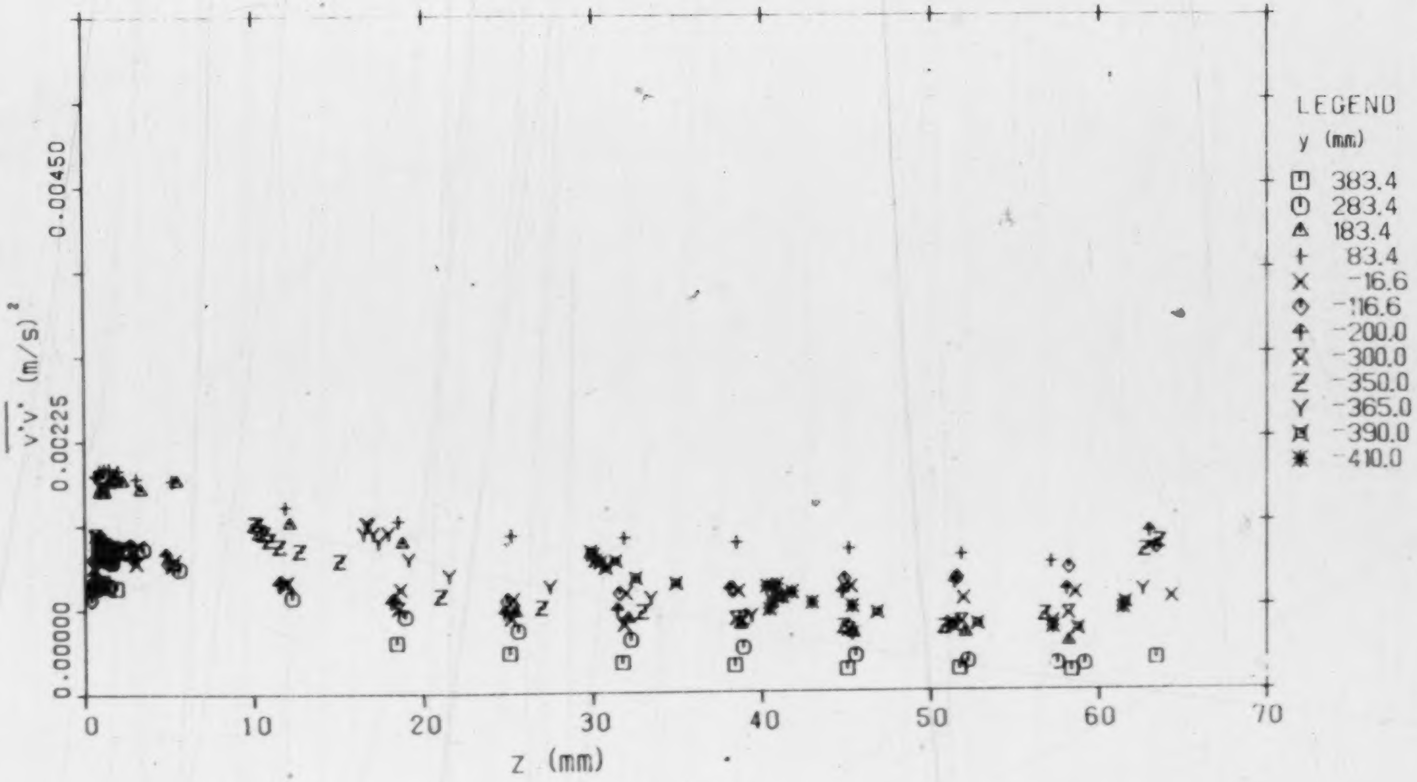

TURBULENCE INTENSITY DISTRIBUTION (SEC 4 RUN 4)

Figure 4.88 $\overline{v'v'}$ turbulence intensity distribution (run 4, section 4)

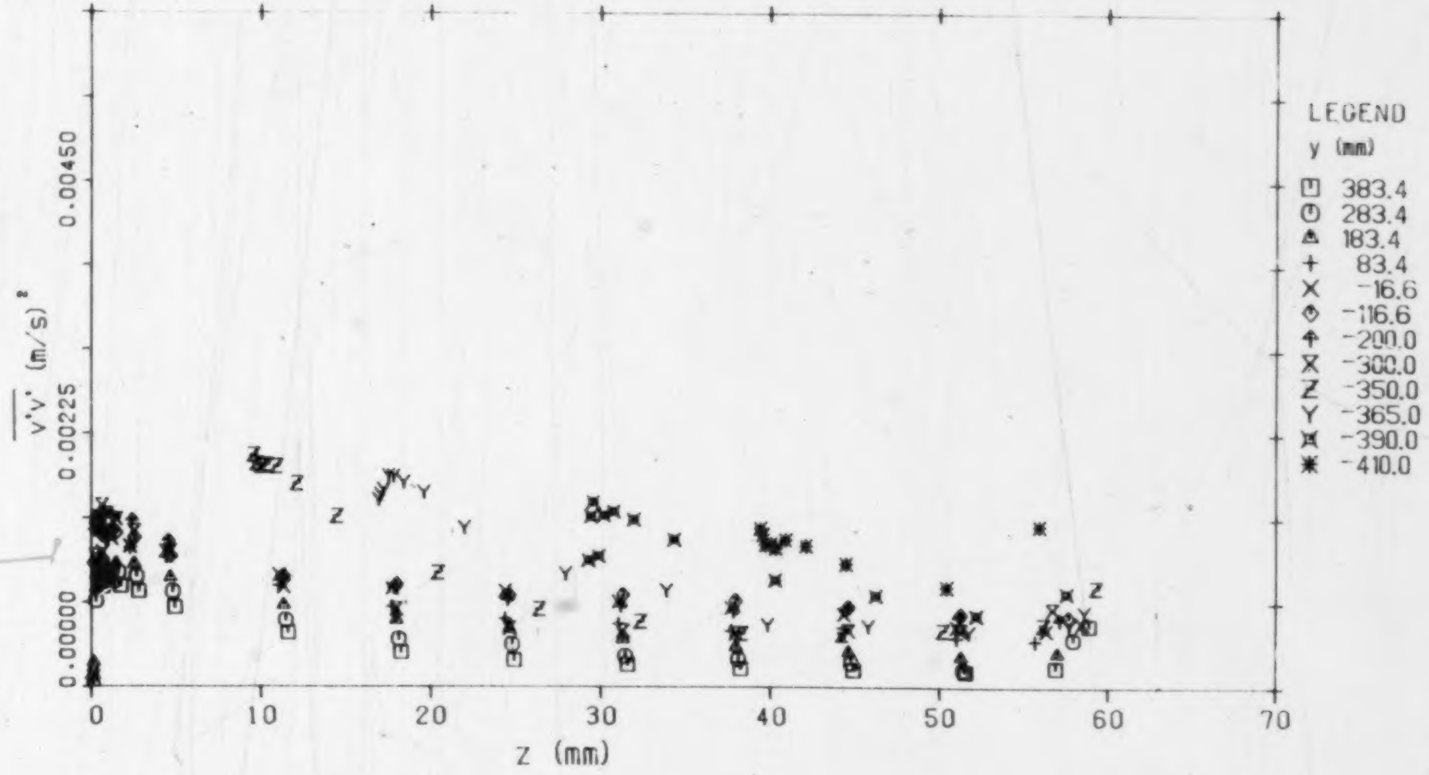

TURBULENCE INTENSITY DISTRIBUTION (SEC 5 RUN 4)

Figure 4.89 $\overline{v'v'}$ turbulence intensity distribution (run 4, section 5)

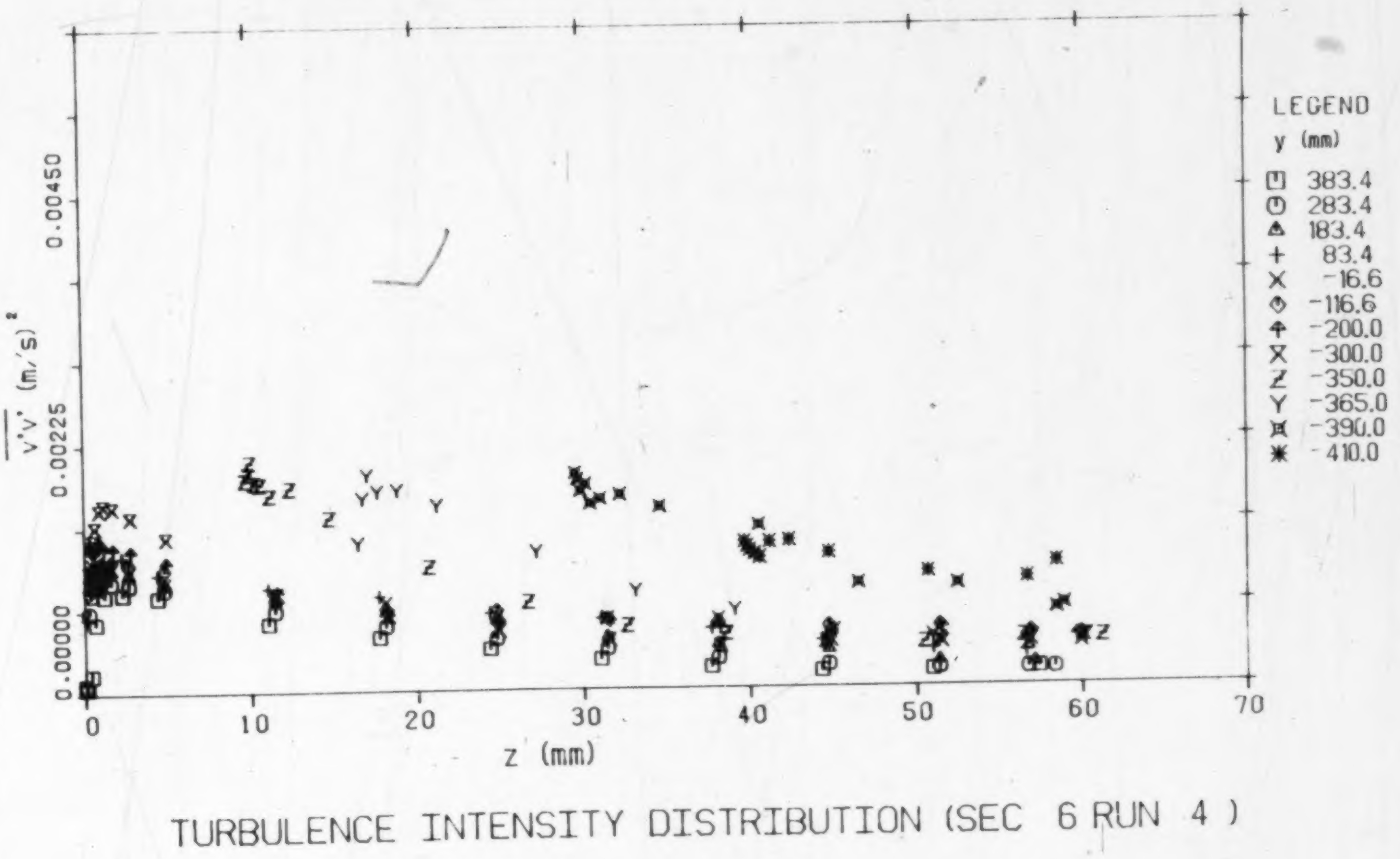

Figure 4.90 $\overline{v'v'}$ turbulence intensity distribution (run 4, section 6)

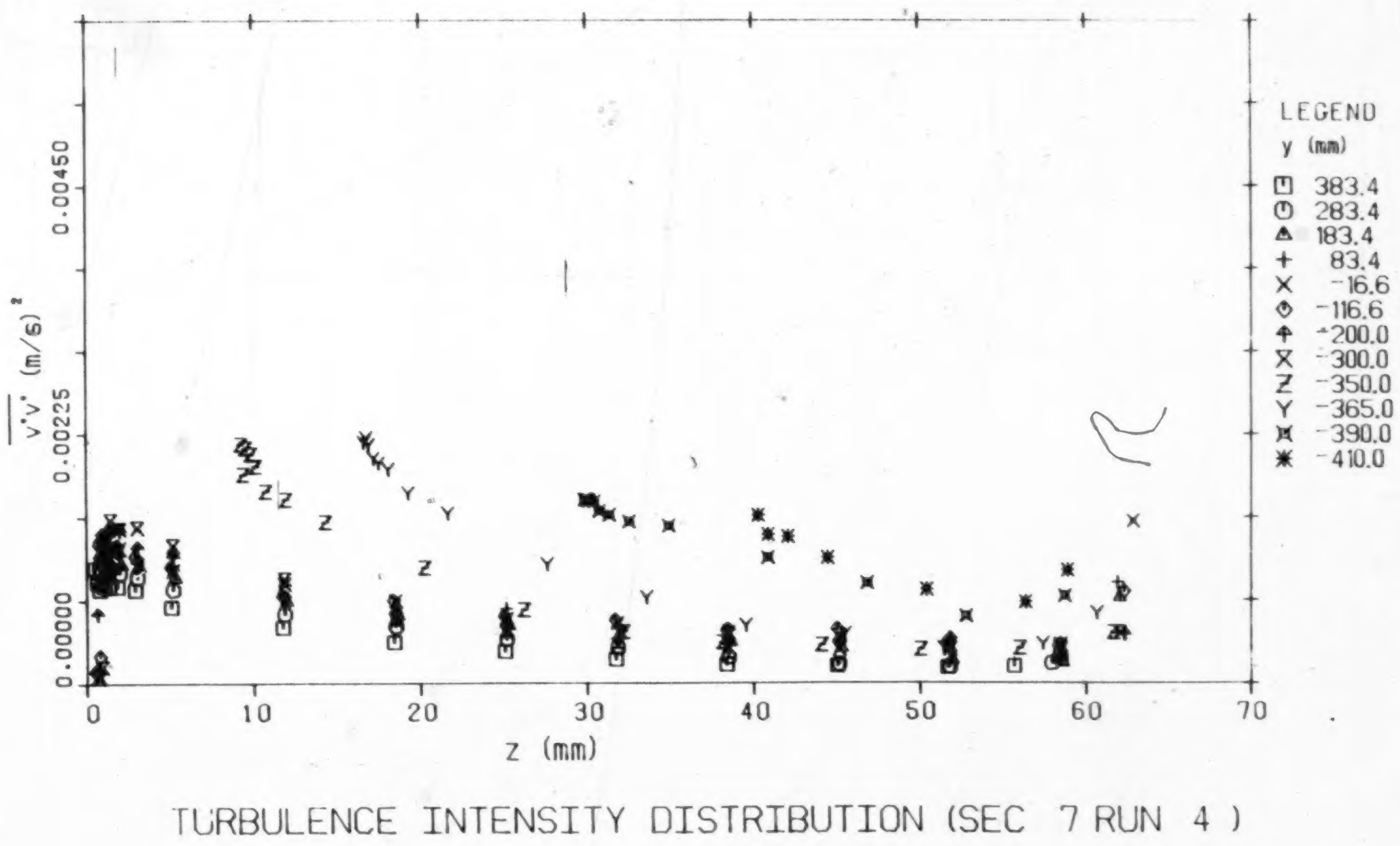

Figure 4.91 $\overline{v'v'}$ turbulence intensity distribution (run 4, section 7)

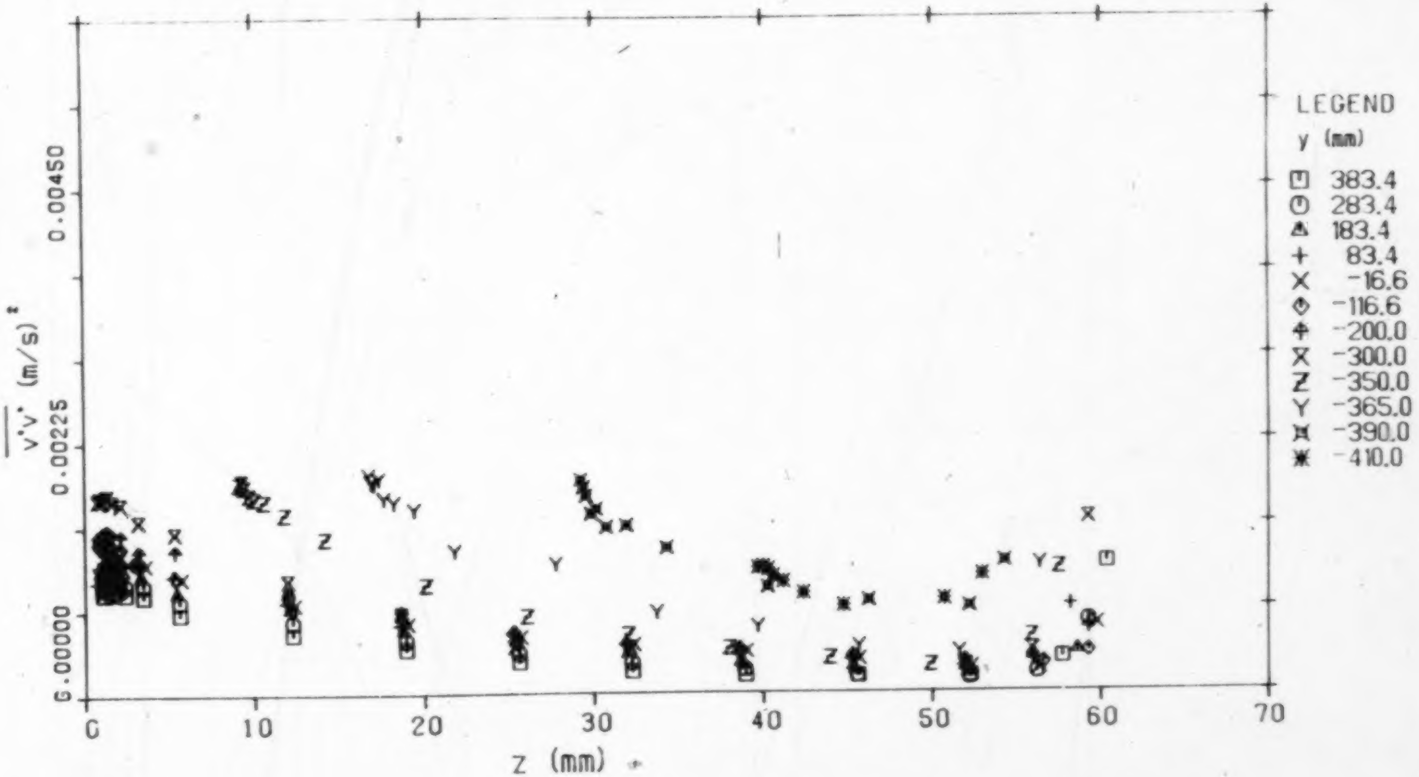

TURBULENCE INTENSITY DISTRIBUTION (SEC 8 RUN 4)

Figure 4.92 $\overline{v'v'}$ turbulence intensity distribution (run 4, section 8)

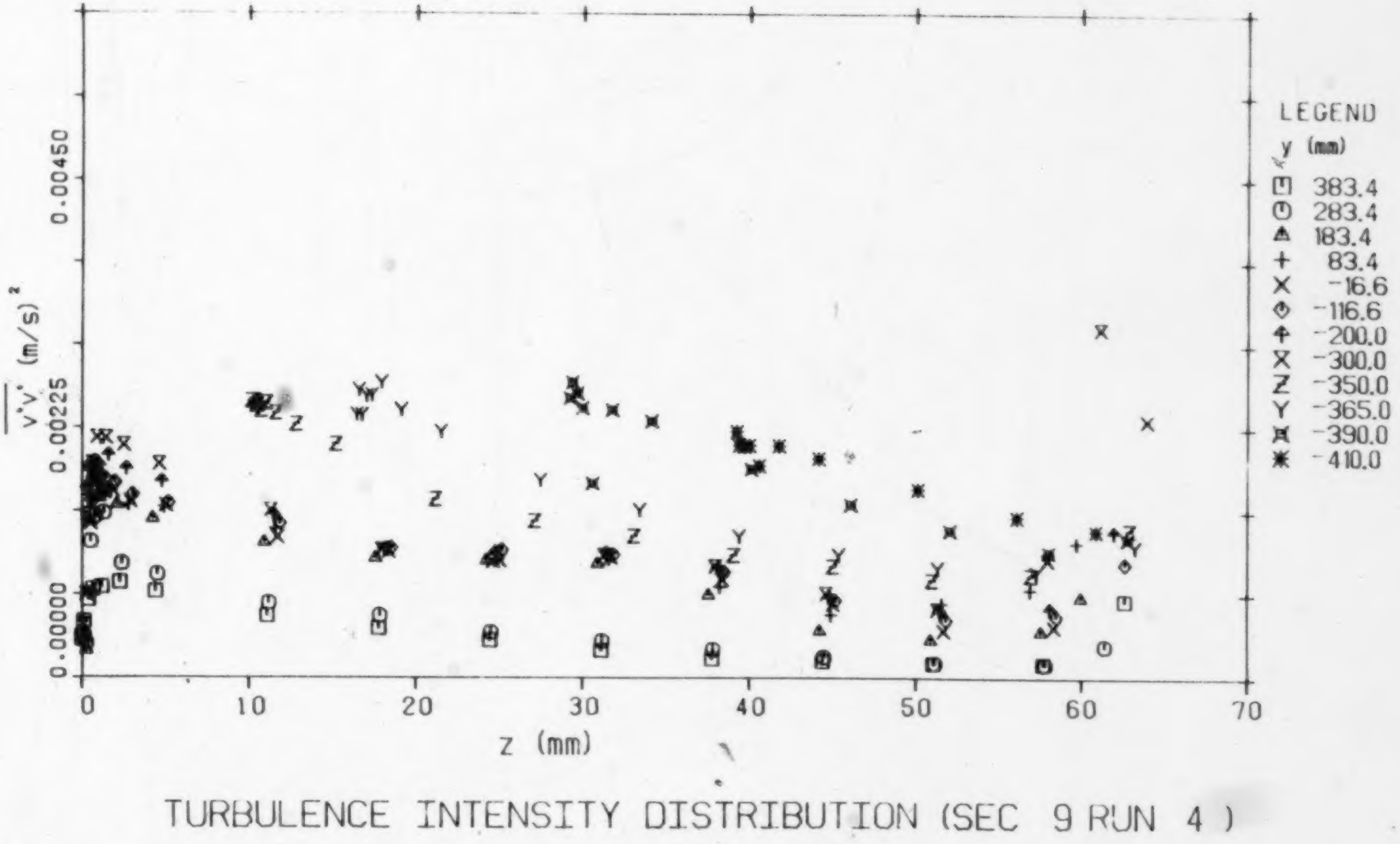

Figure 4.93 $\overline{v'v'}$ turbulence intensity distribution (run 4, section 9)

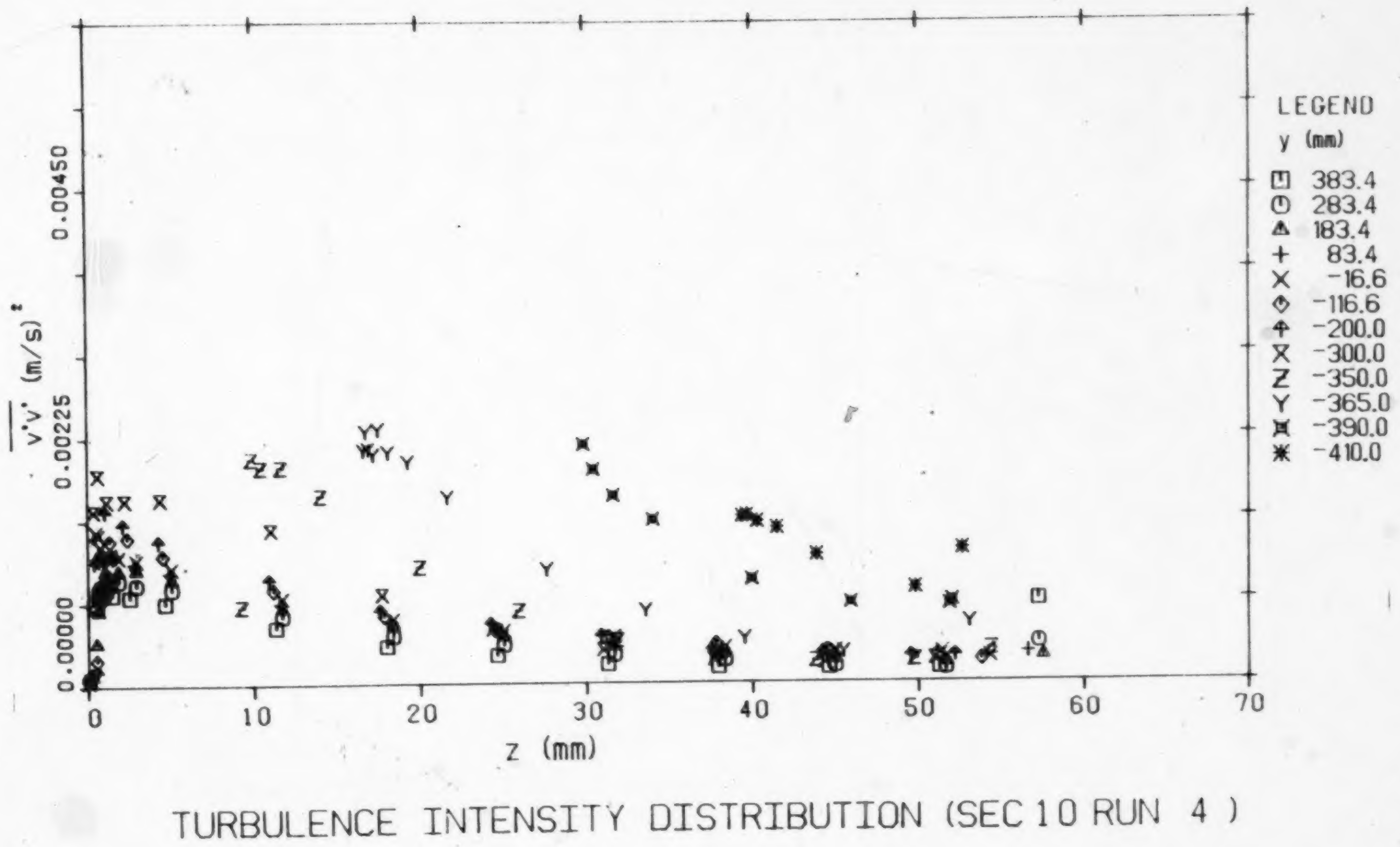

Figure 4.94 $\overline{v'v'}$ turbulence intensity distribution (run 4, section 10)

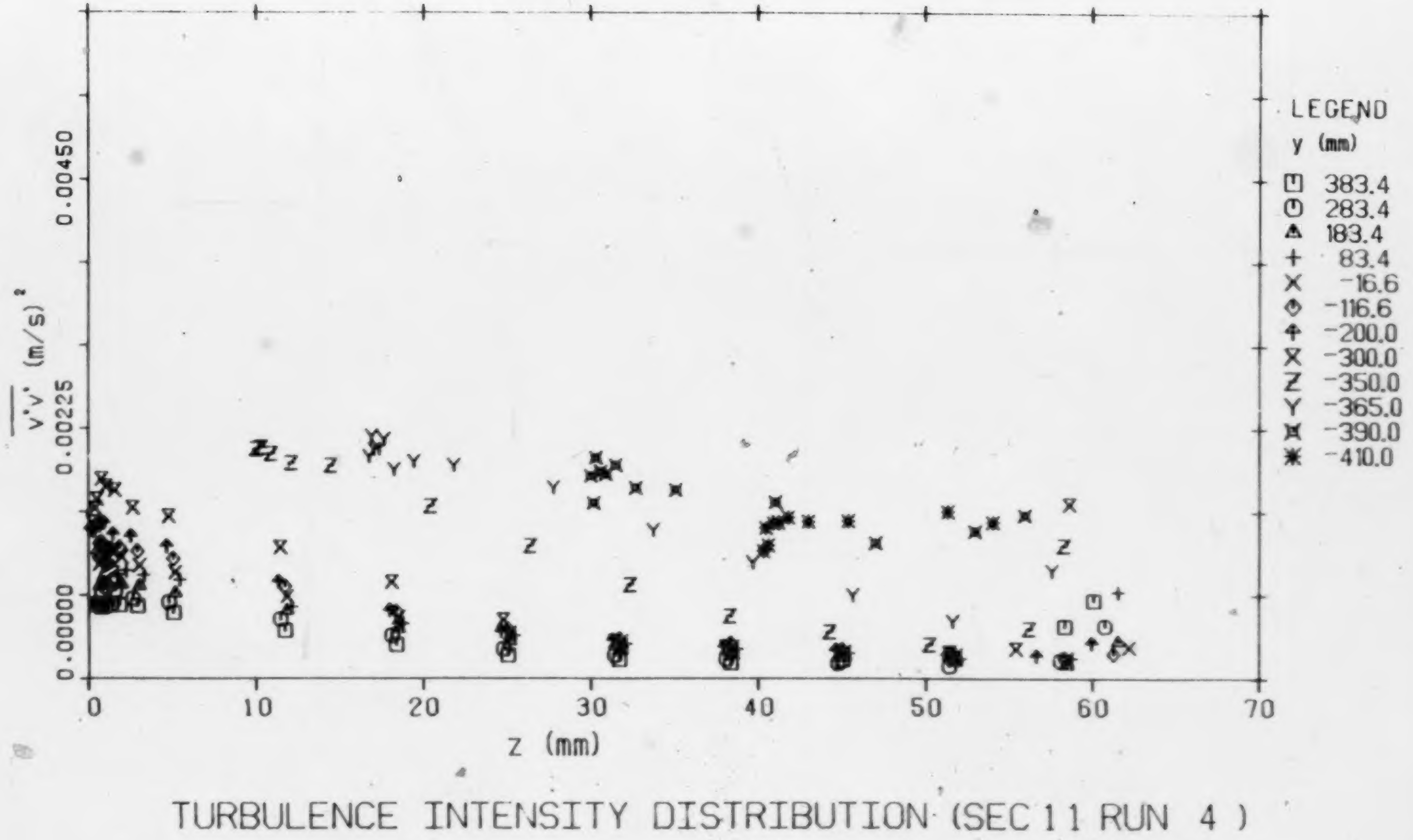

Figure 4.95 $\overline{v'v'}$ turbulence intensity distribution (run 4, section 11)

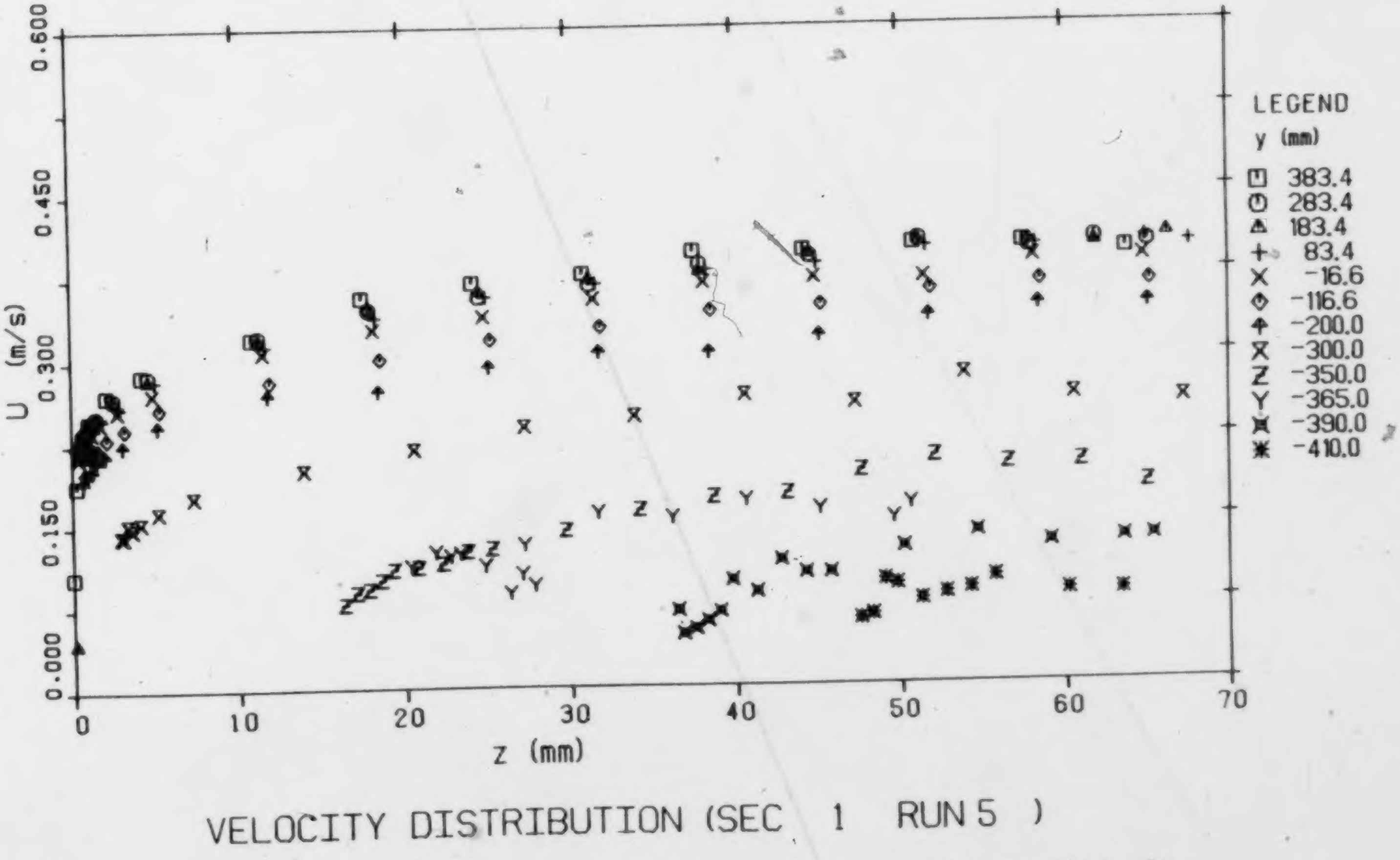

Figure 4.96 u velocity distribution (run 5, section 1)

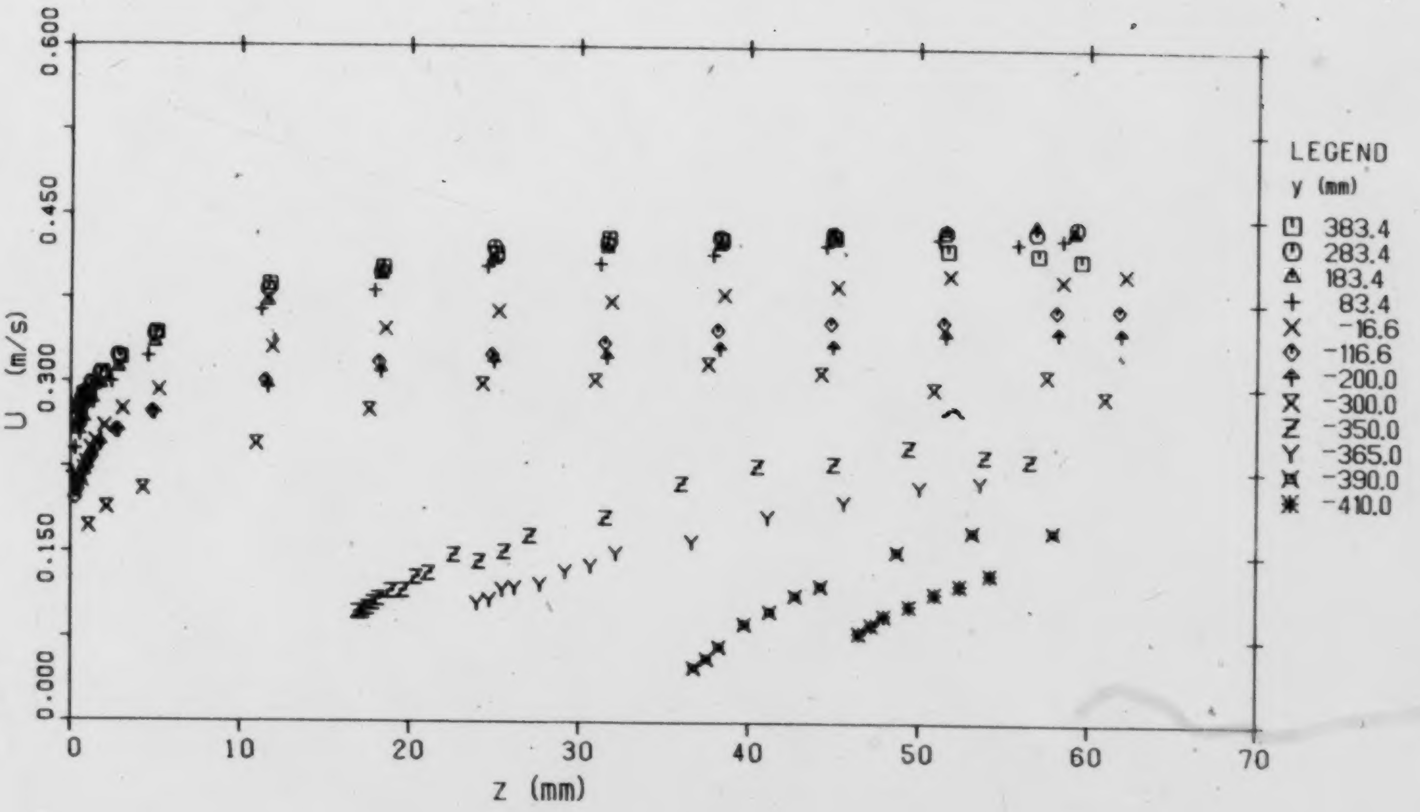

VELOCITY DISTRIBUTION (SEC 2 RUN 5)

Figure 4.97 u velocity distribution (run 5, section 2)

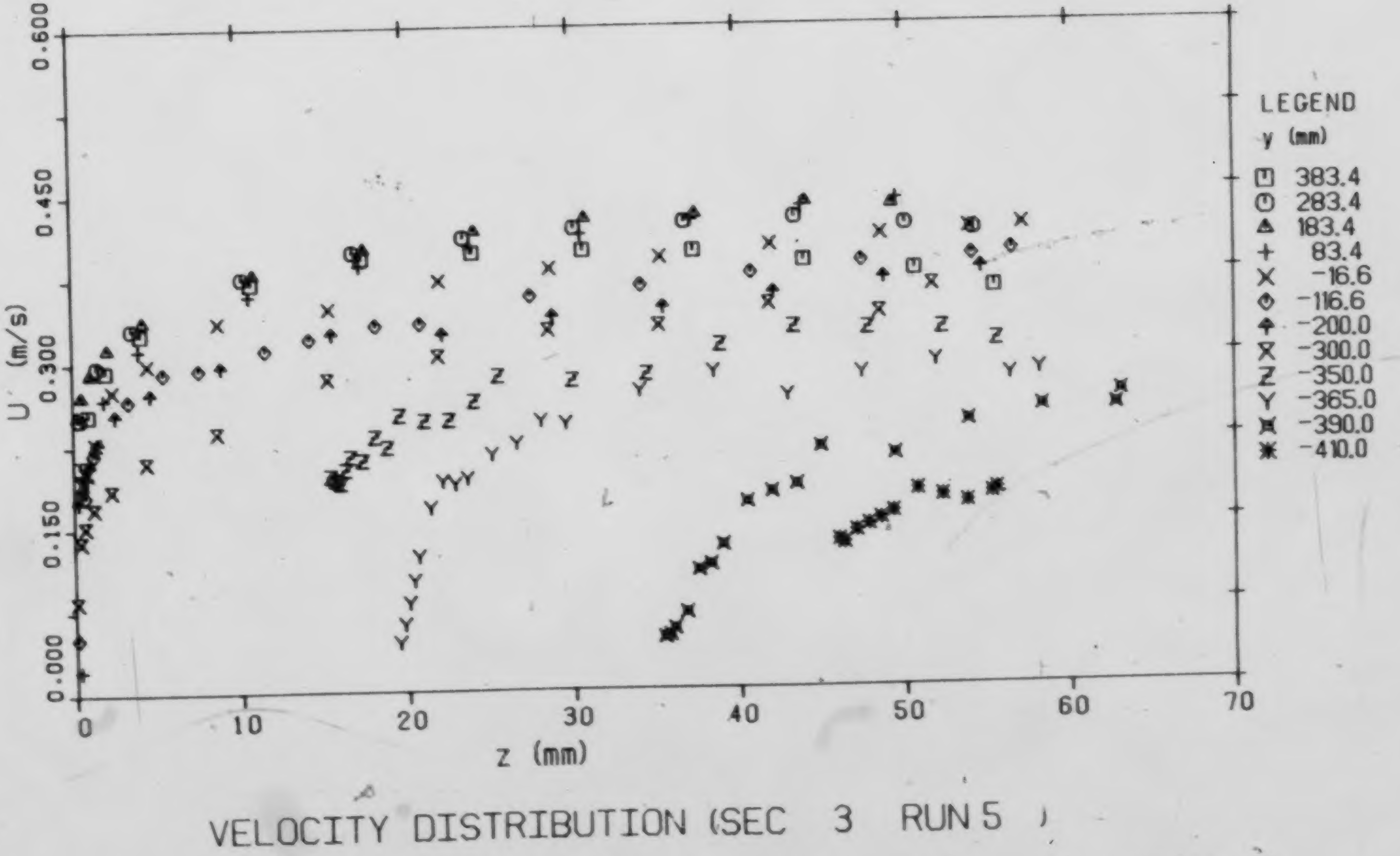

Figure 4.98 u velocity distribution (run 5, section 3)

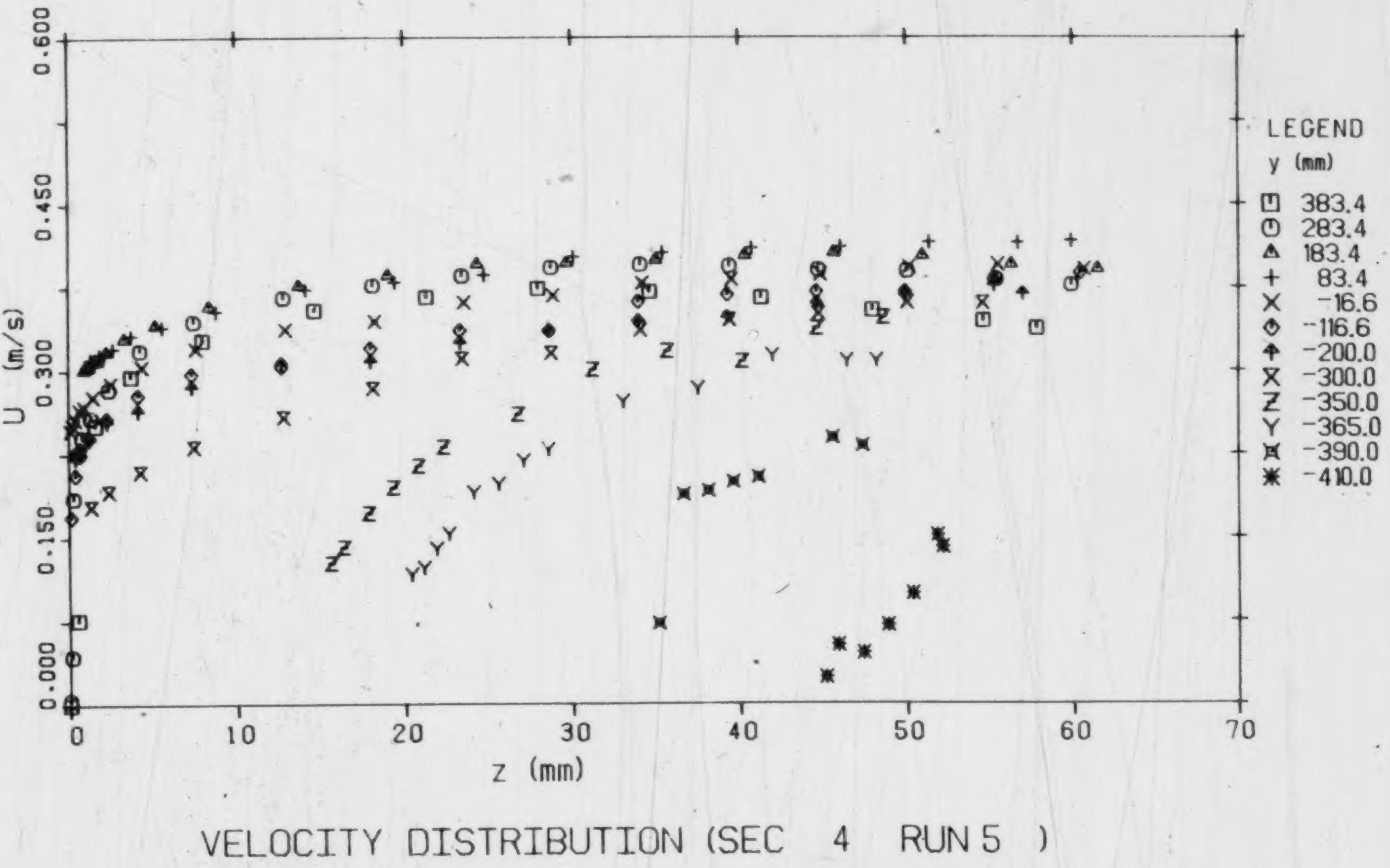

Figure 4.99 u velocity distribution (run 5, section 4)

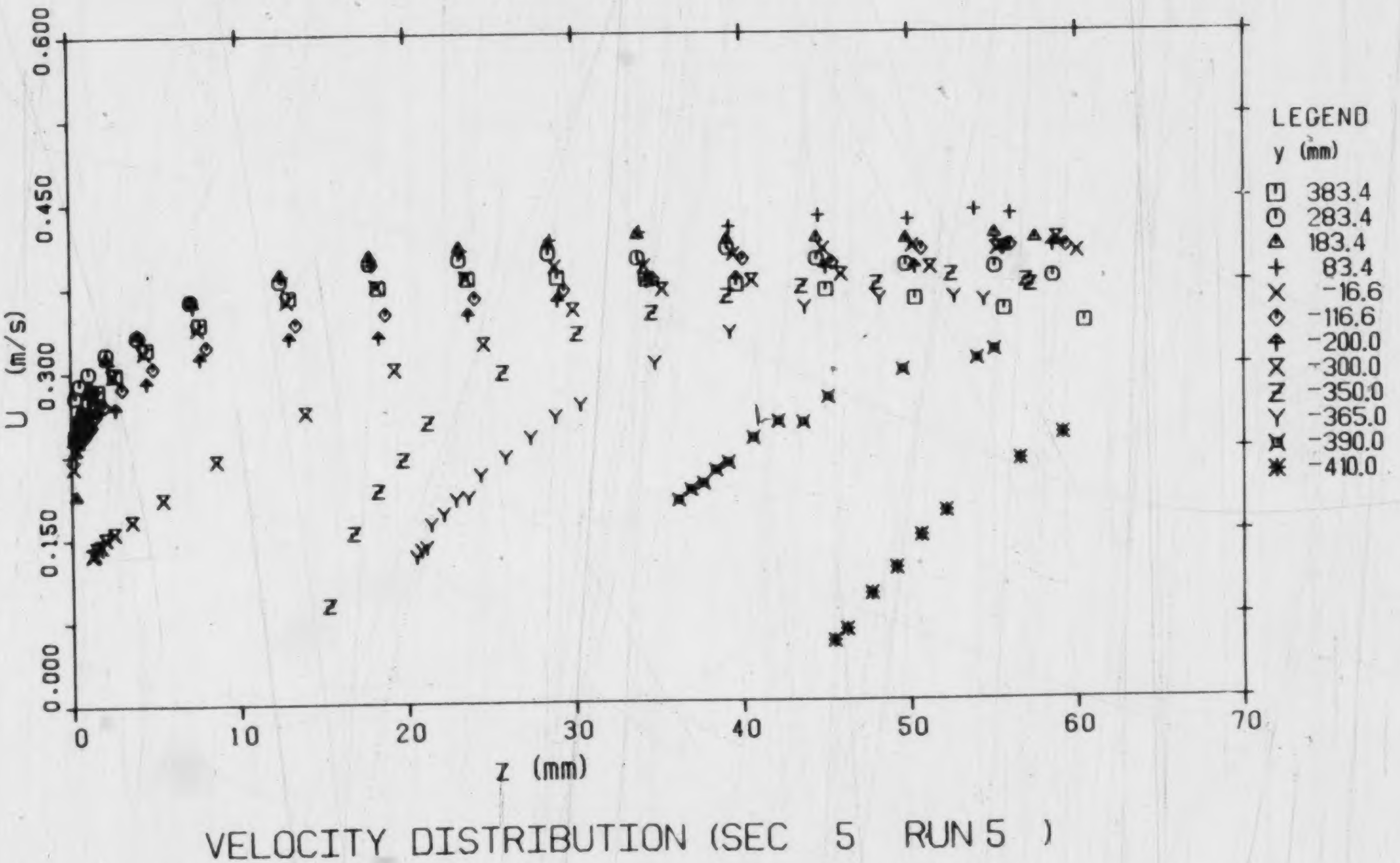

Figure 4.100 u velocity distribution (run 5, section 5)

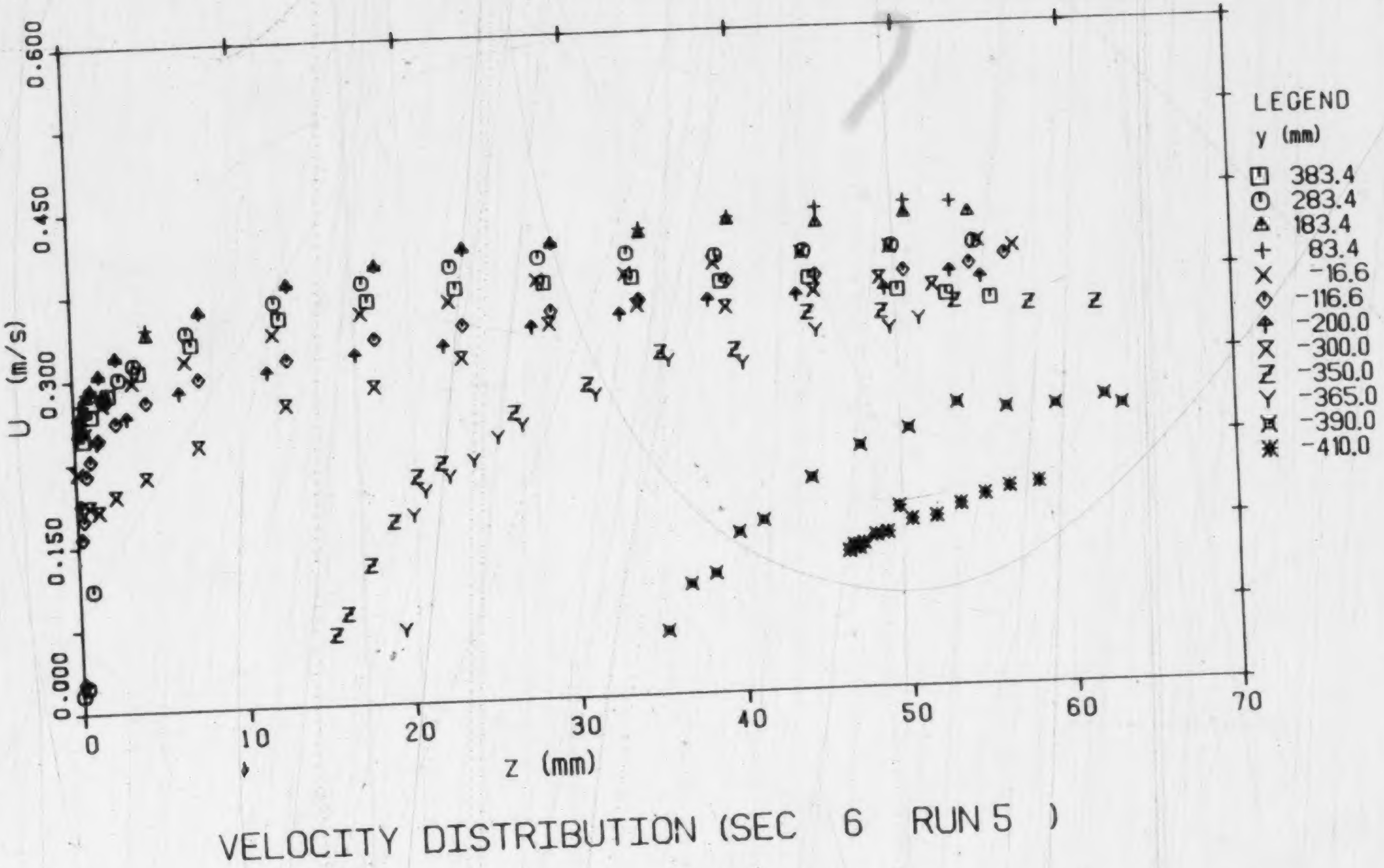

Figure 4.101 u velocity distribution (run 5, section 6)

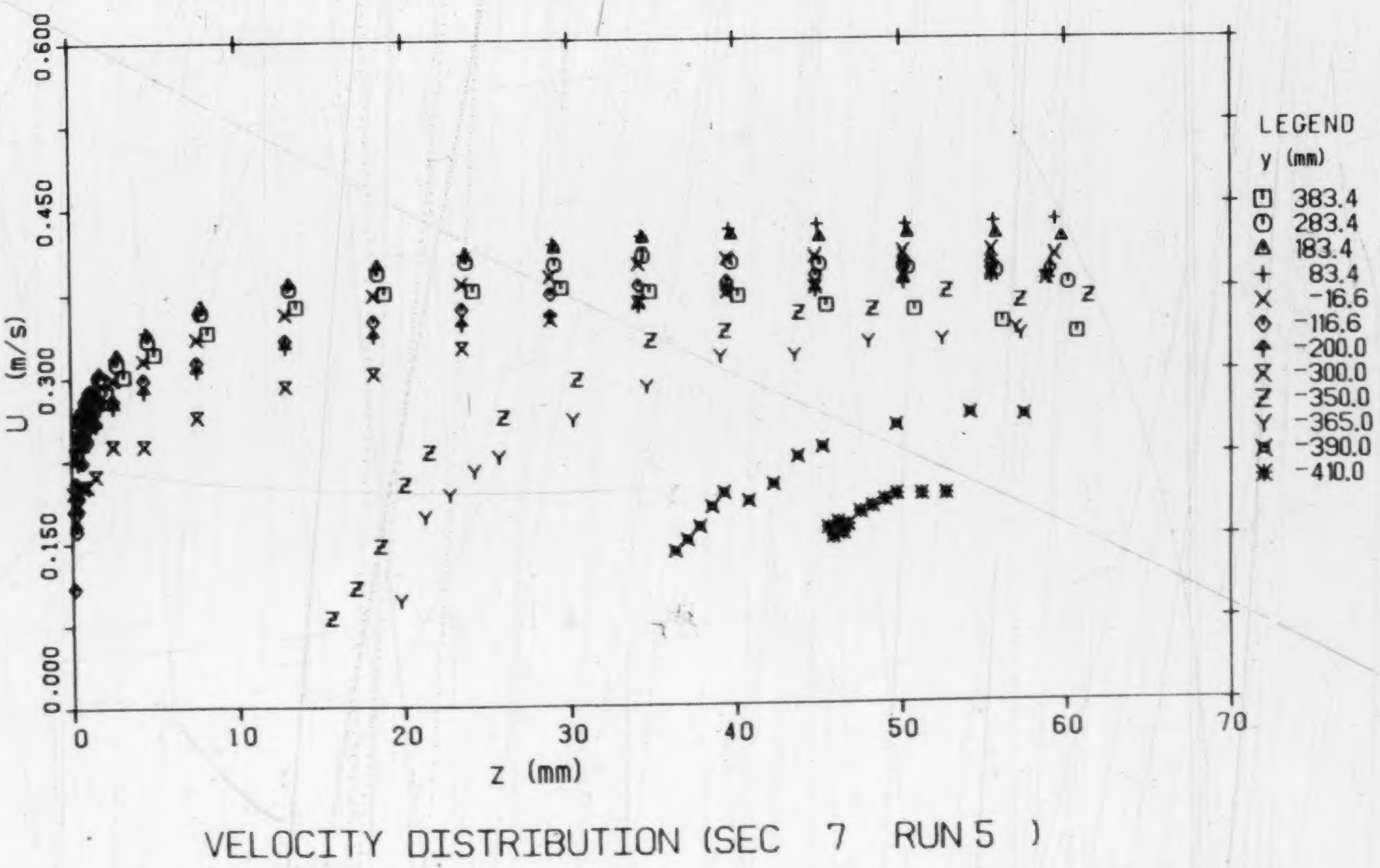

Figure 4.102 u velocity distribution (run 5, section 7)

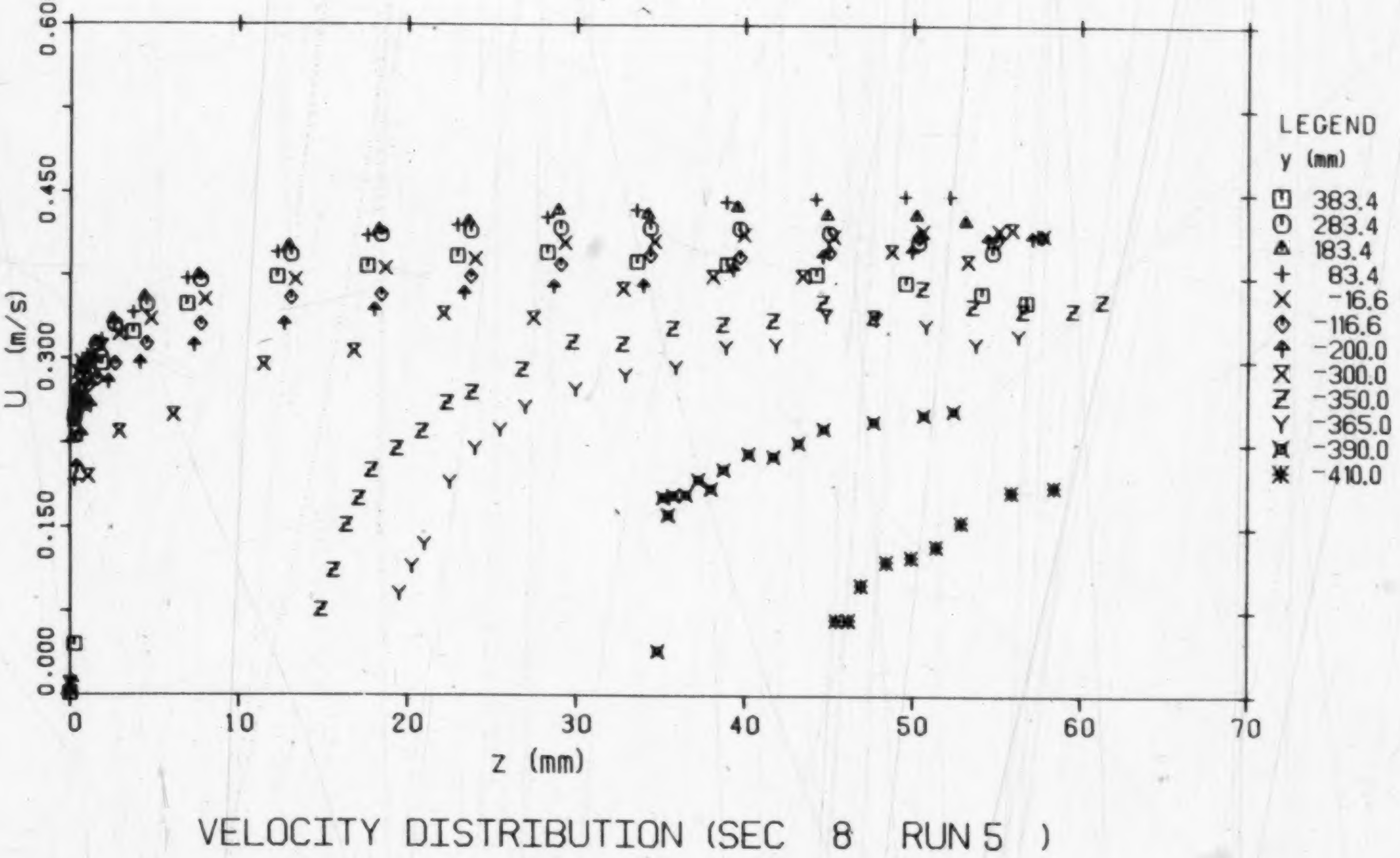

Figure 4.103 u velocity distribution (run 5, section 8)

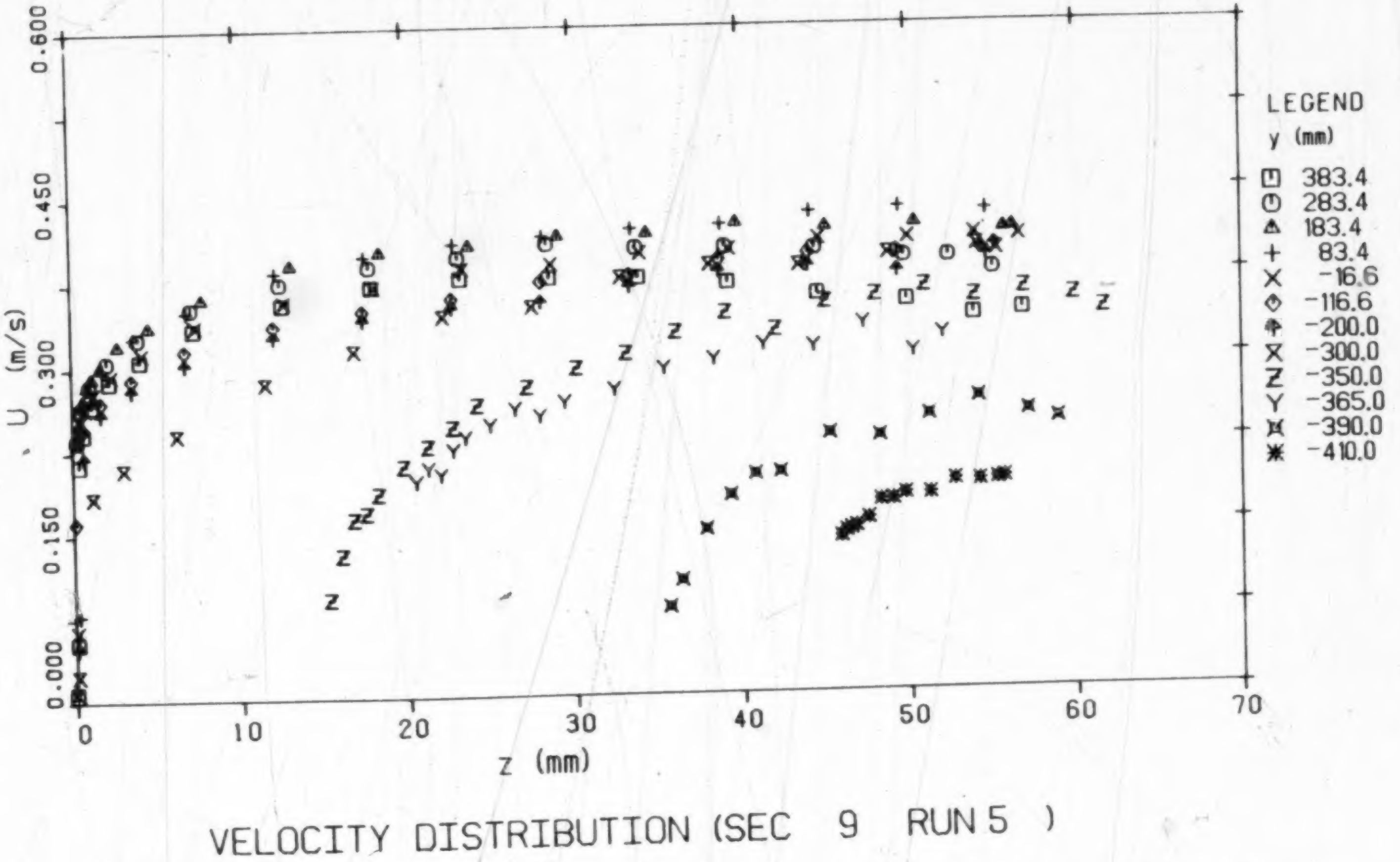

Figure 4.104 u velocity distribution (run 5, section 9)

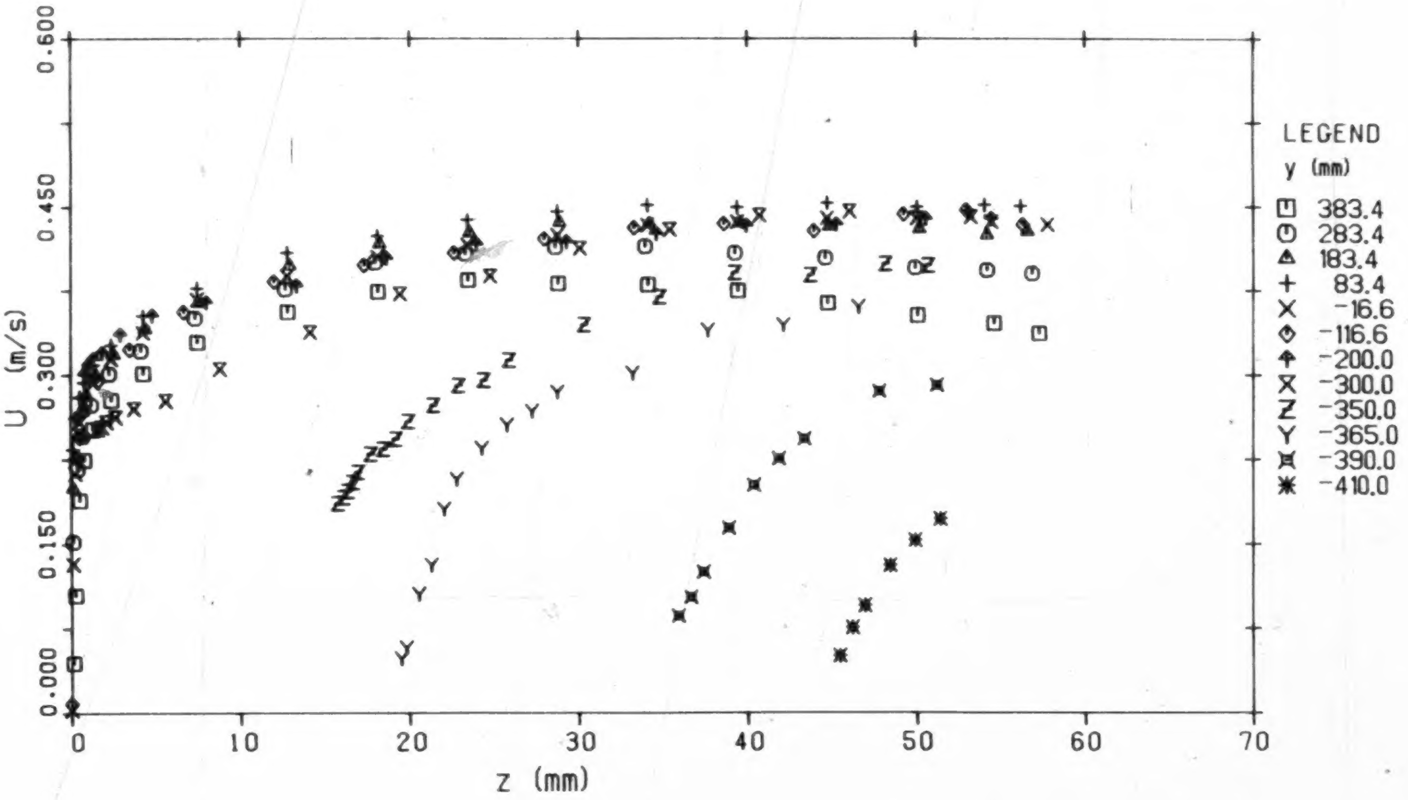

VELOCITY DISTRIBUTION (SEC 10 RUN 5)

Figure 4.105 u velocity distribution (run 5, section 10)

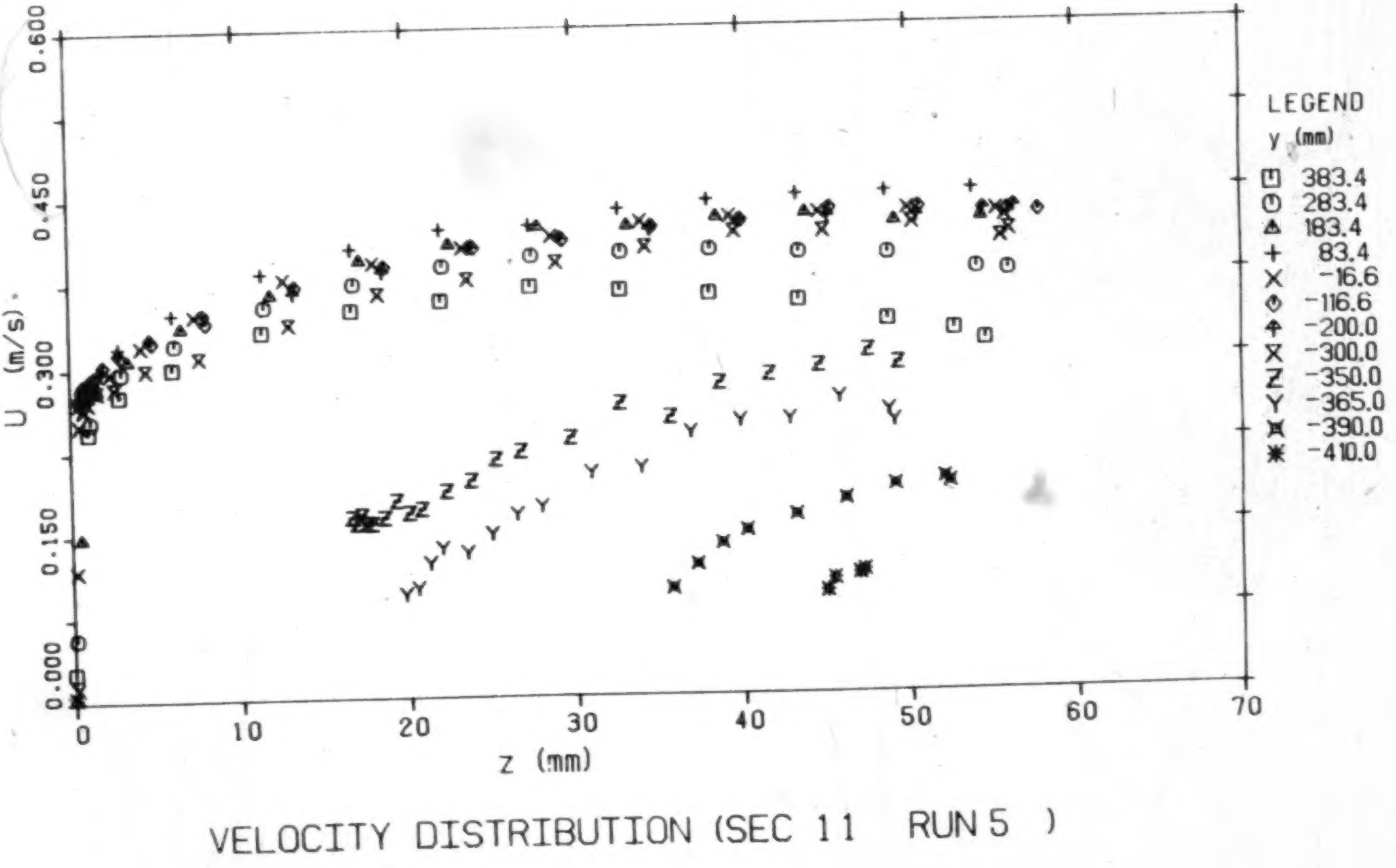

Figure 4.106 u velocity distribution (run 5, section 11)

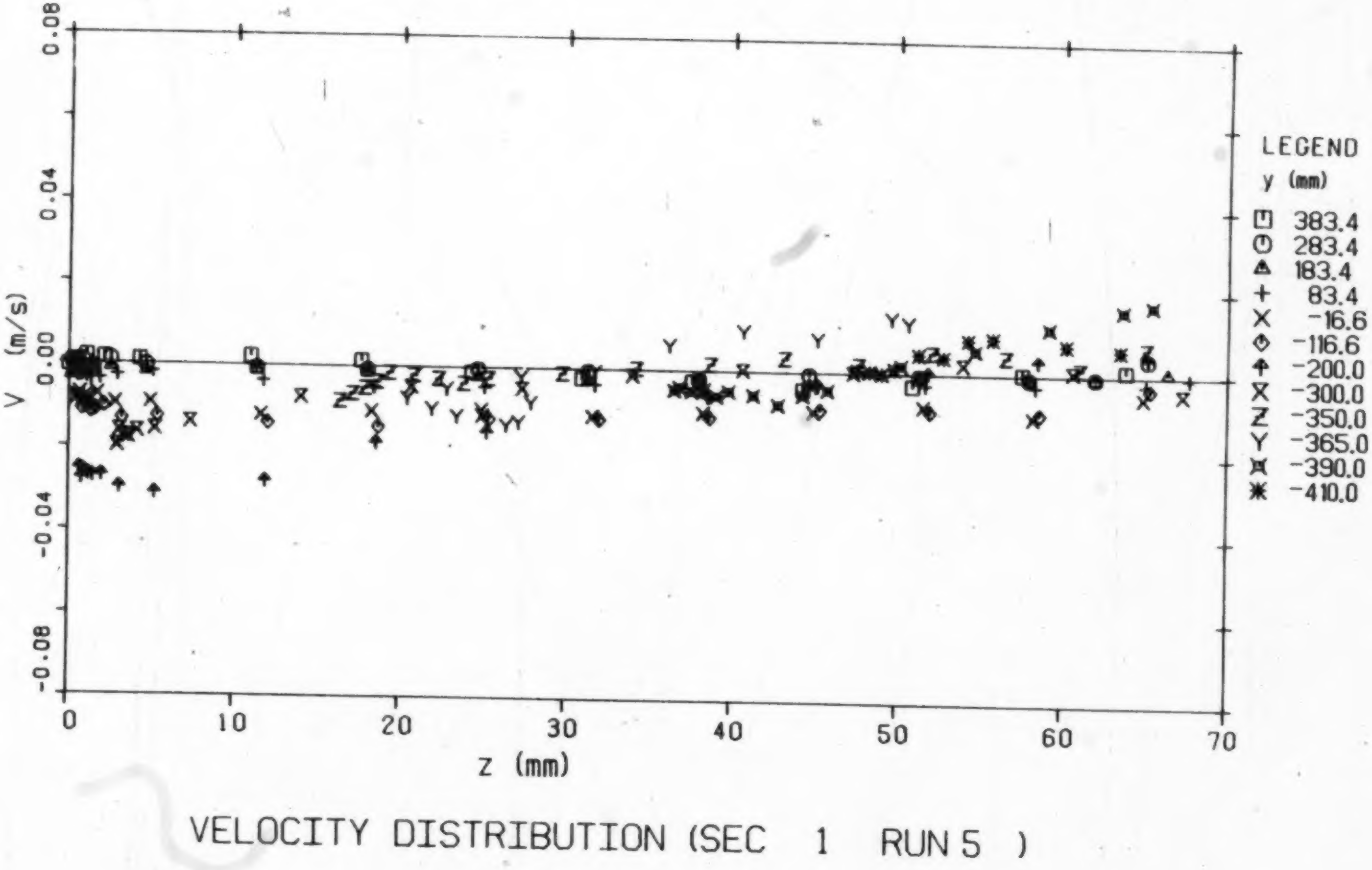

Figure 4.107 v velocity distribution (run 5, section 1)

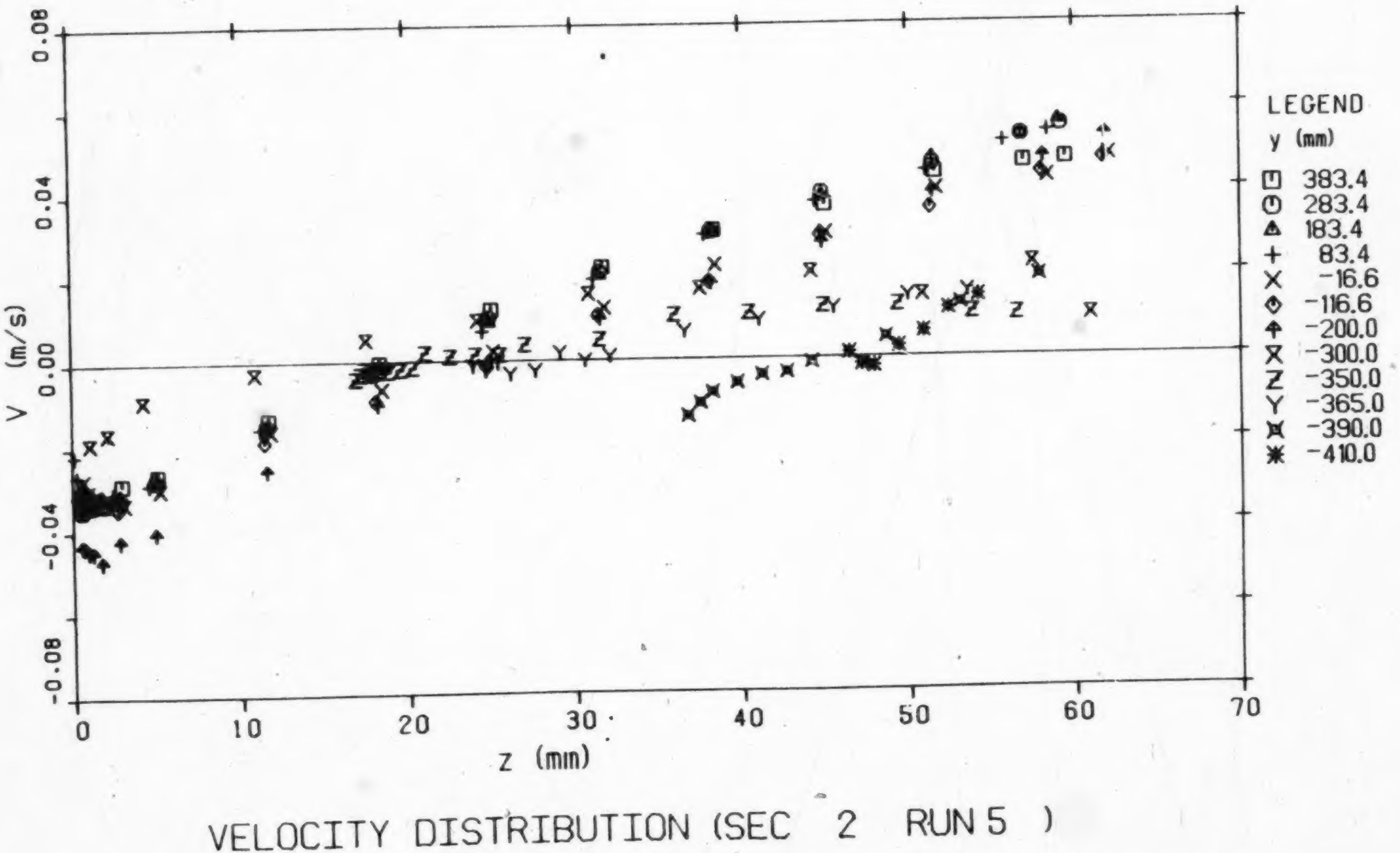

Figure 4.108 v velocity distribution (run 5, section 2)

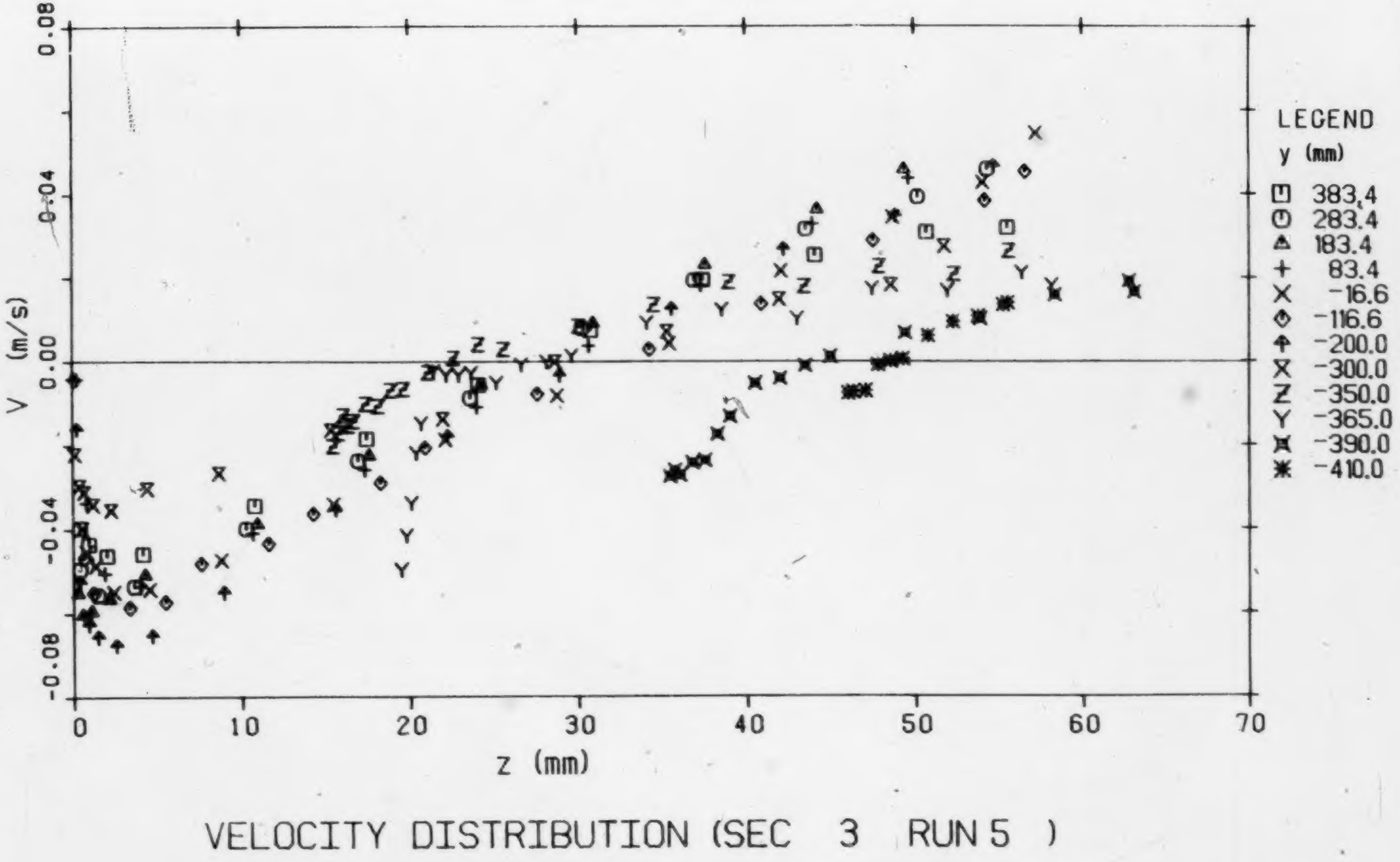

Figure 4.109 v velocity distribution (run 5, section 3)

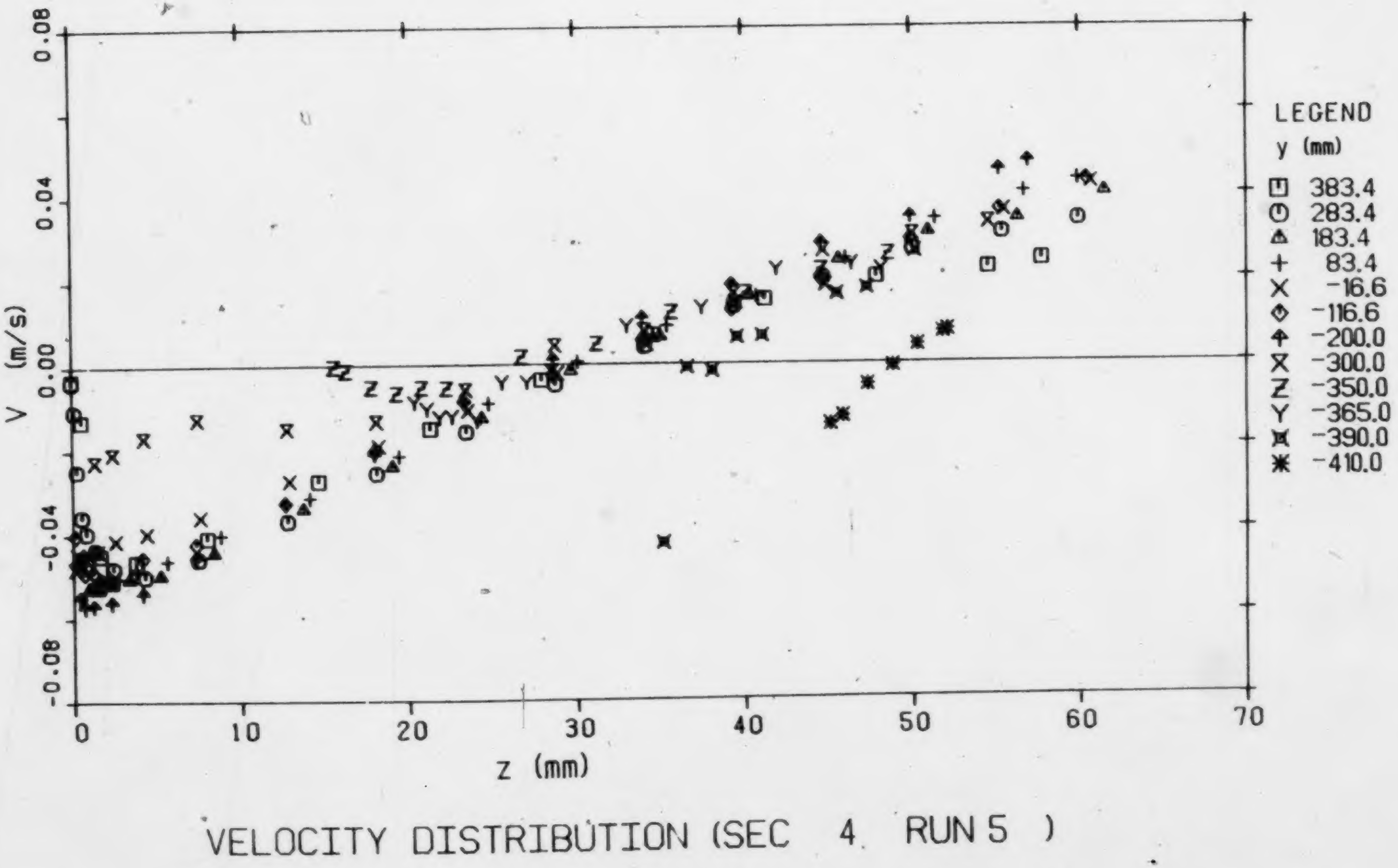

Figure 4.110 v velocity distribution (run 5, section 4)

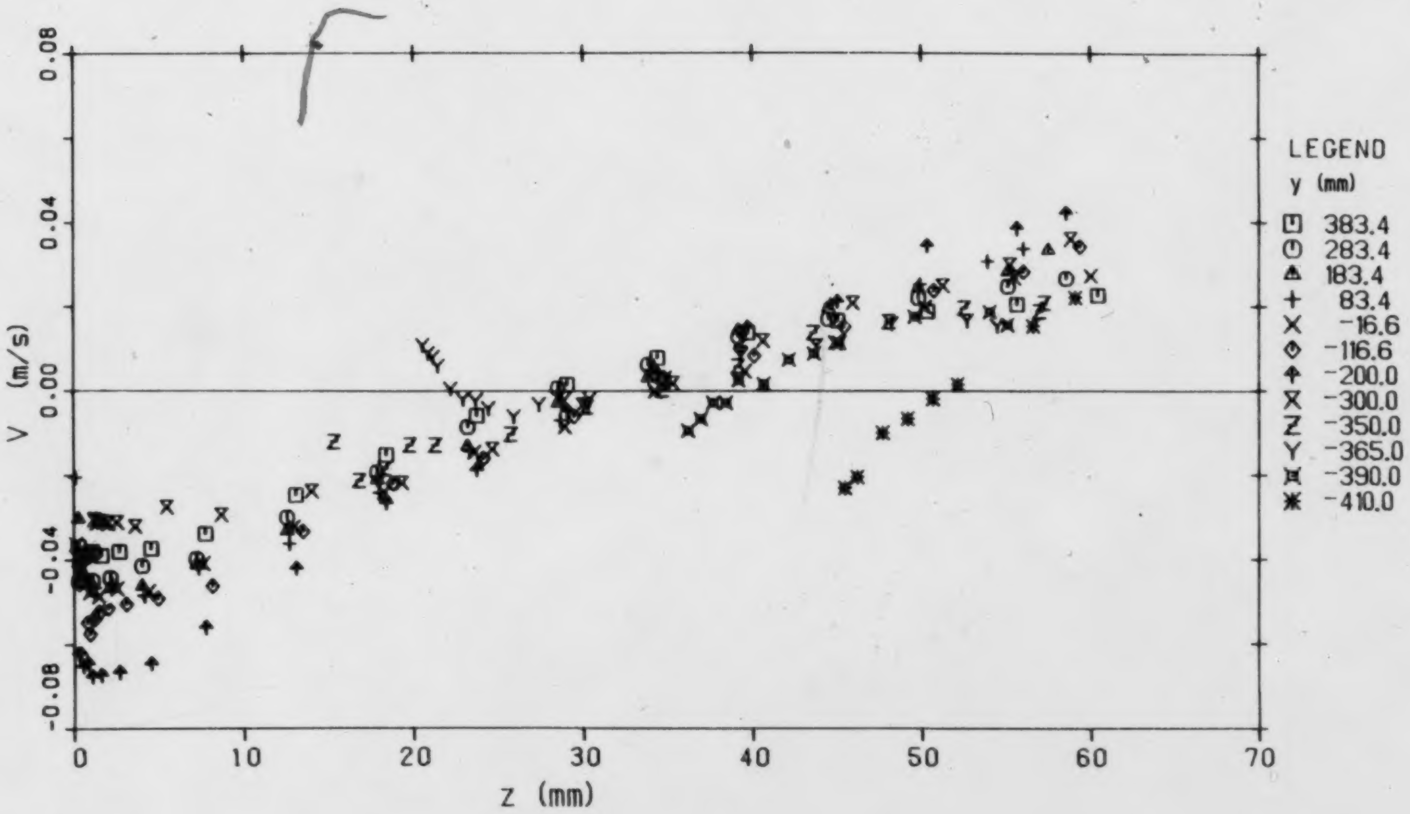

VELOCITY DISTRIBUTION (SEC 5 RUN 5)

Figure 4.111 v velocity distribution (run 5, section 5)

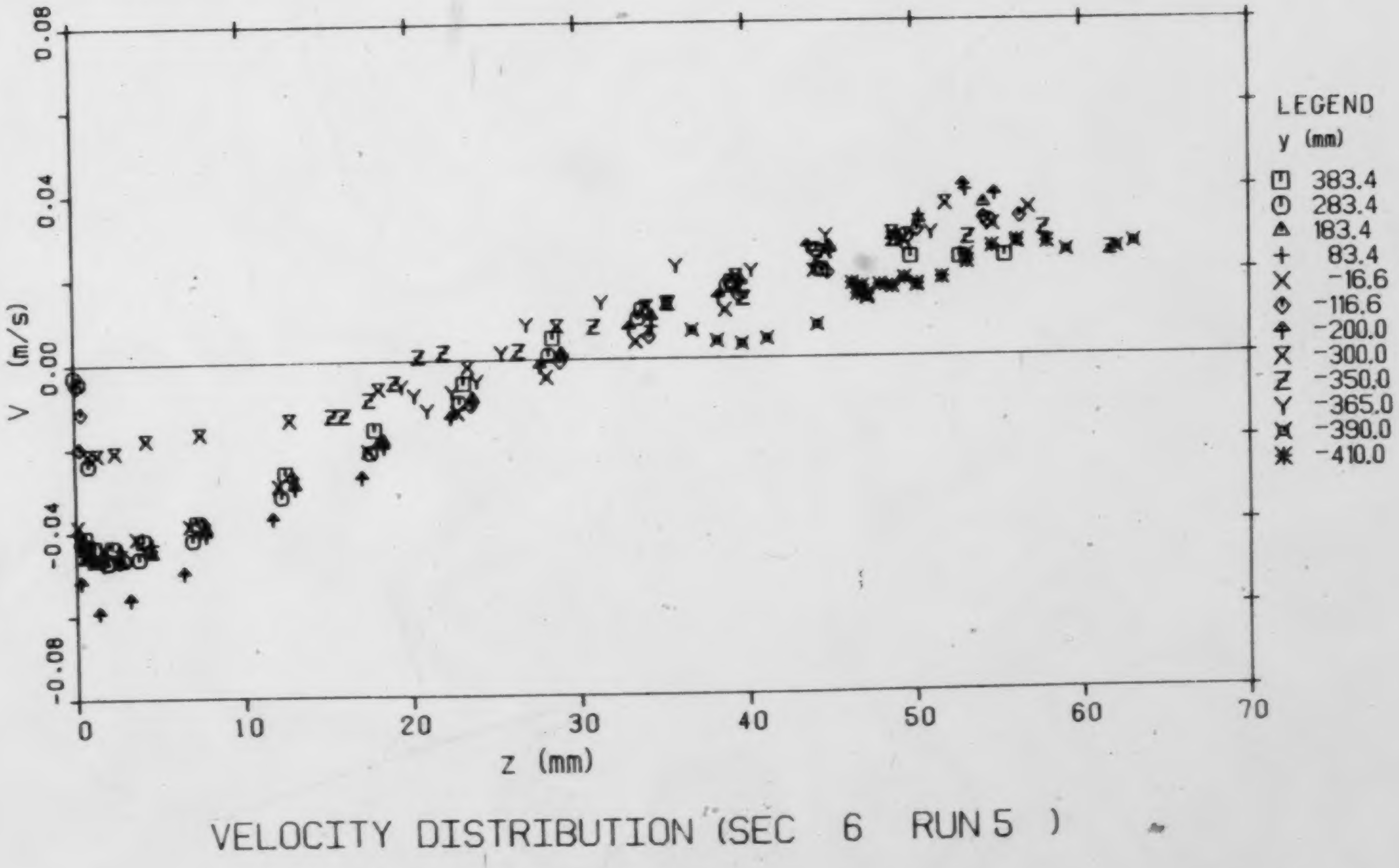

Figure 4.112 v velocity distribution (run 5, section 6)

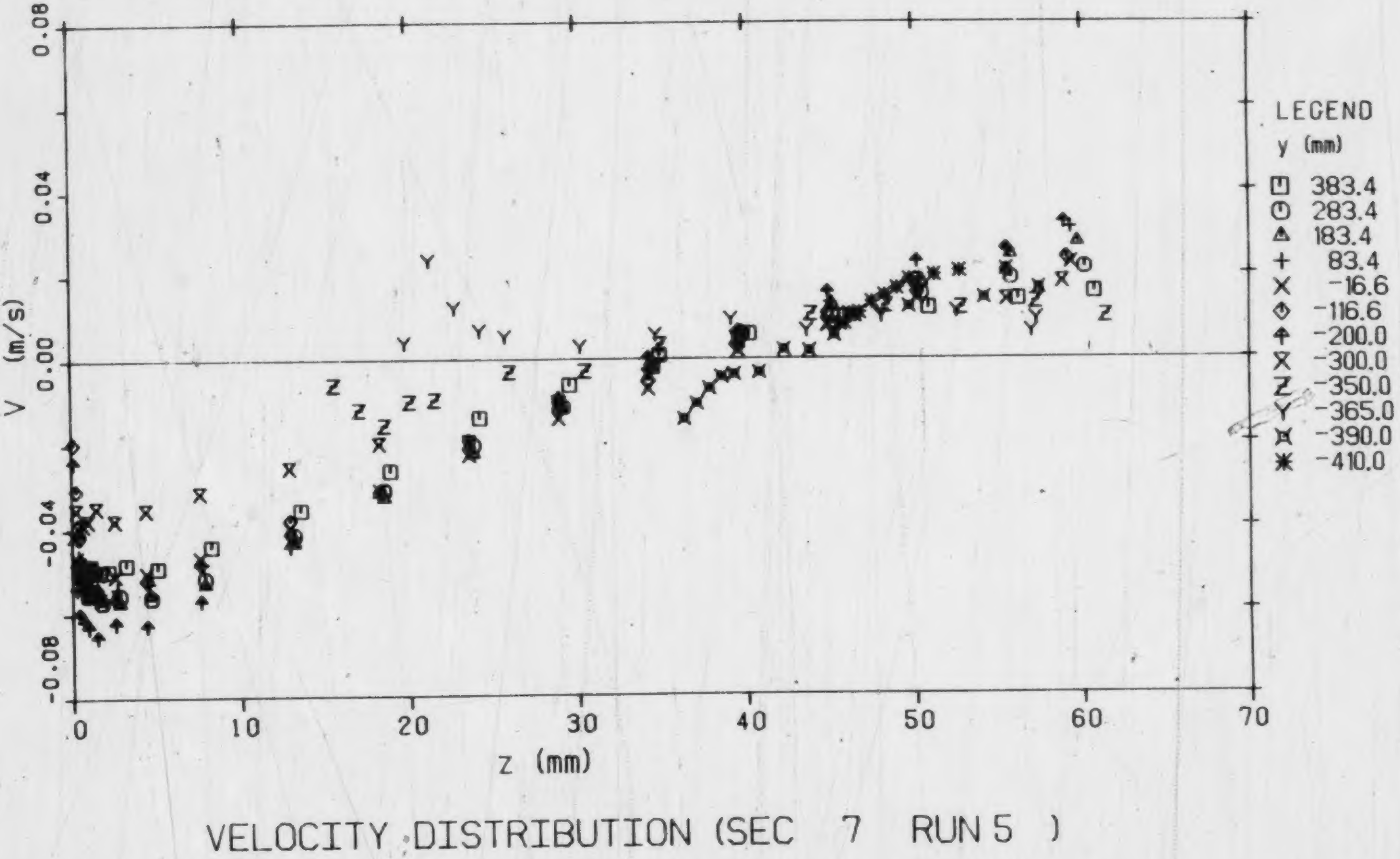

Figure 4.113 v velocity distribution (run 5, section 7)

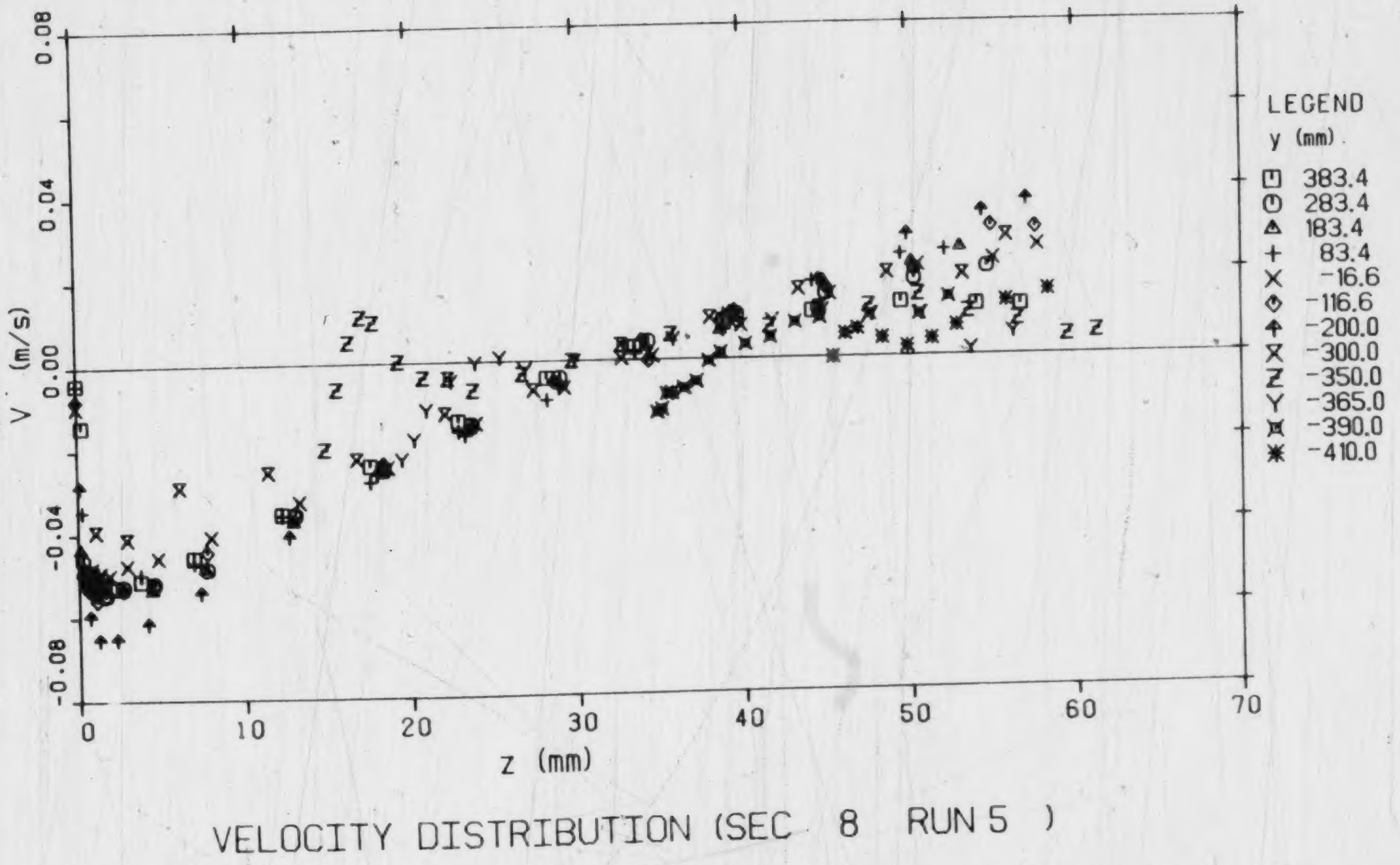

Figure 4.114 v velocity distribution (run 5, section 8)

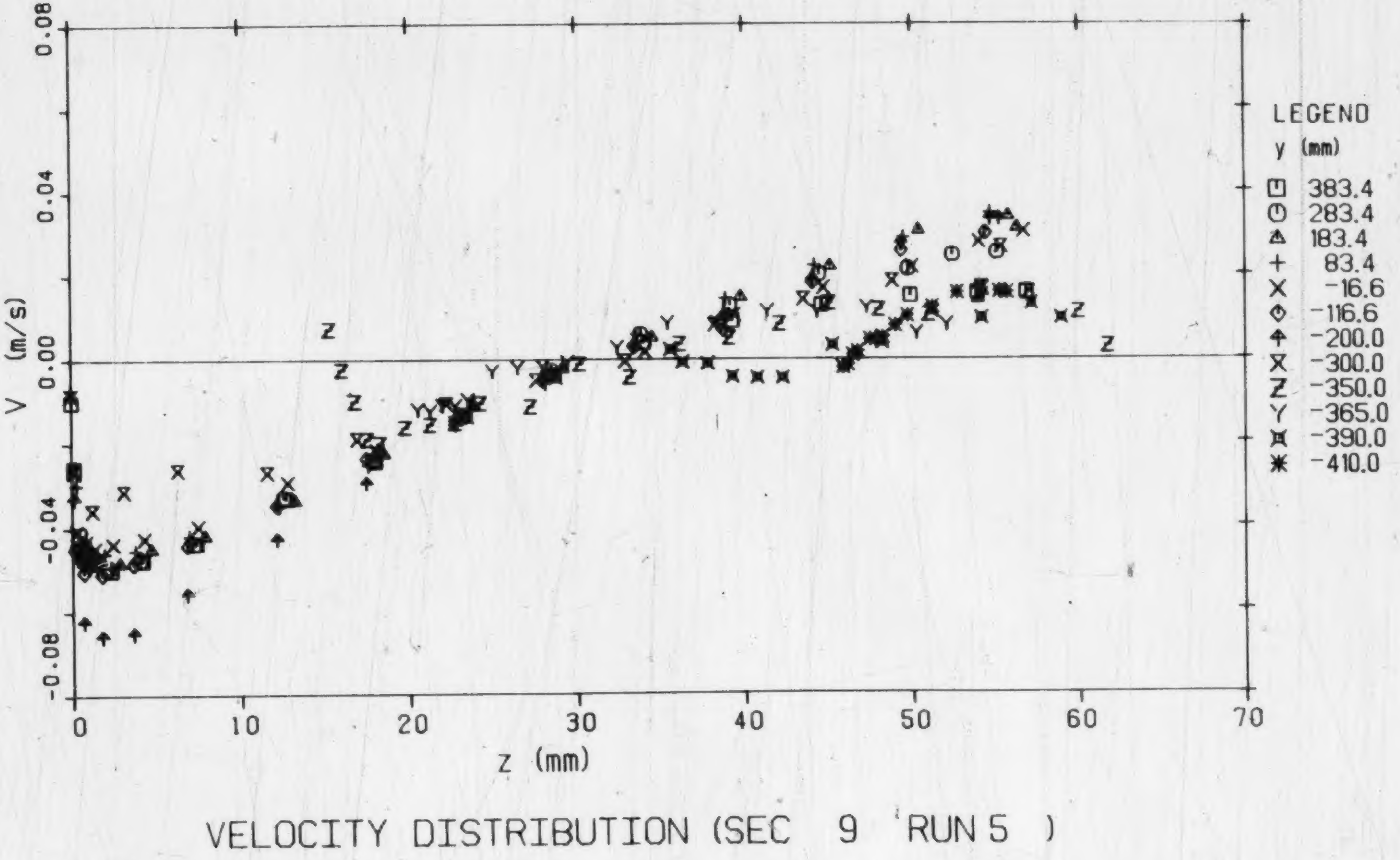

Figure 4.115 v velocity distribution (run 5, section 9)

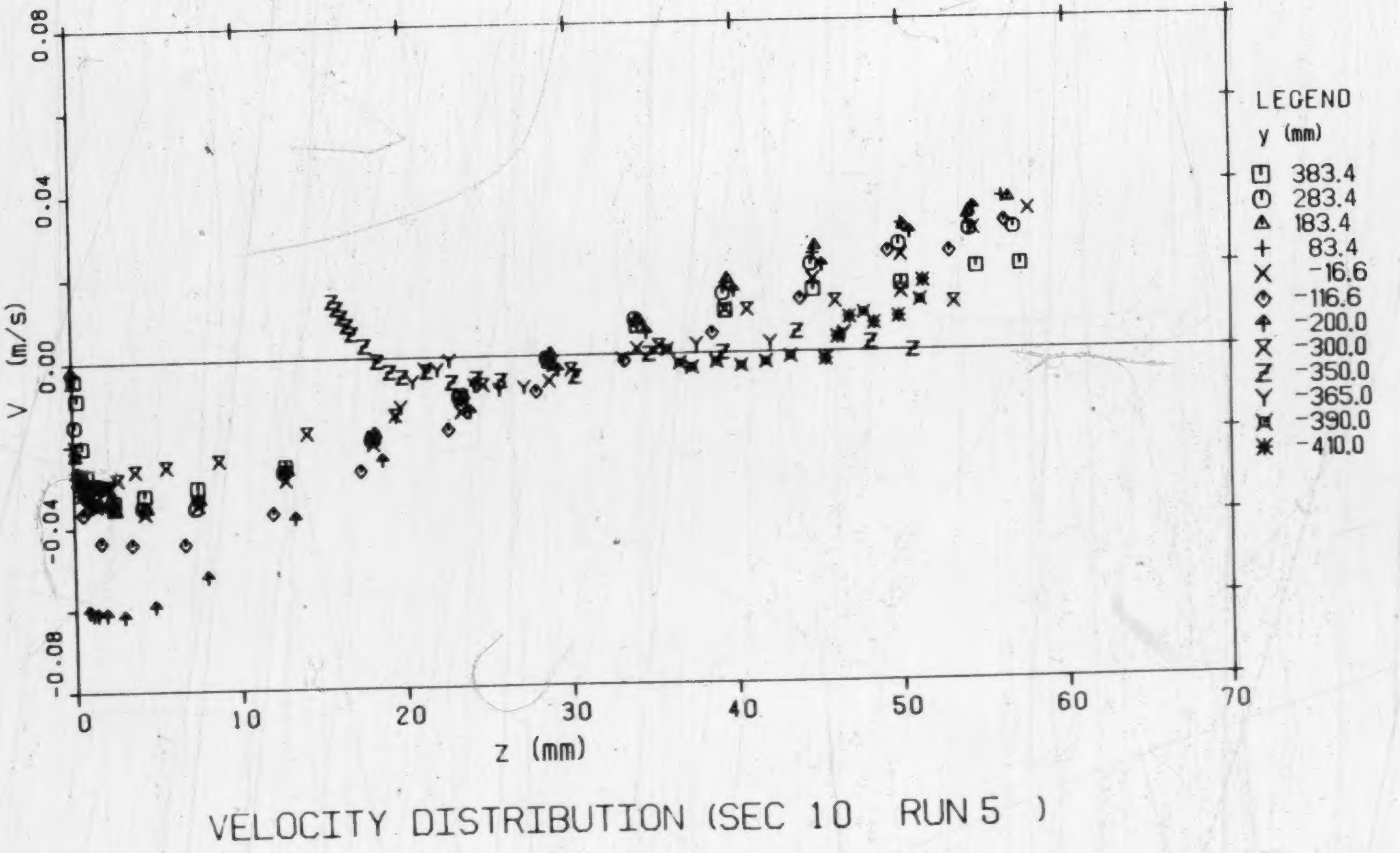

Figure 4.116 v velocity distribution (run 5, section 10)

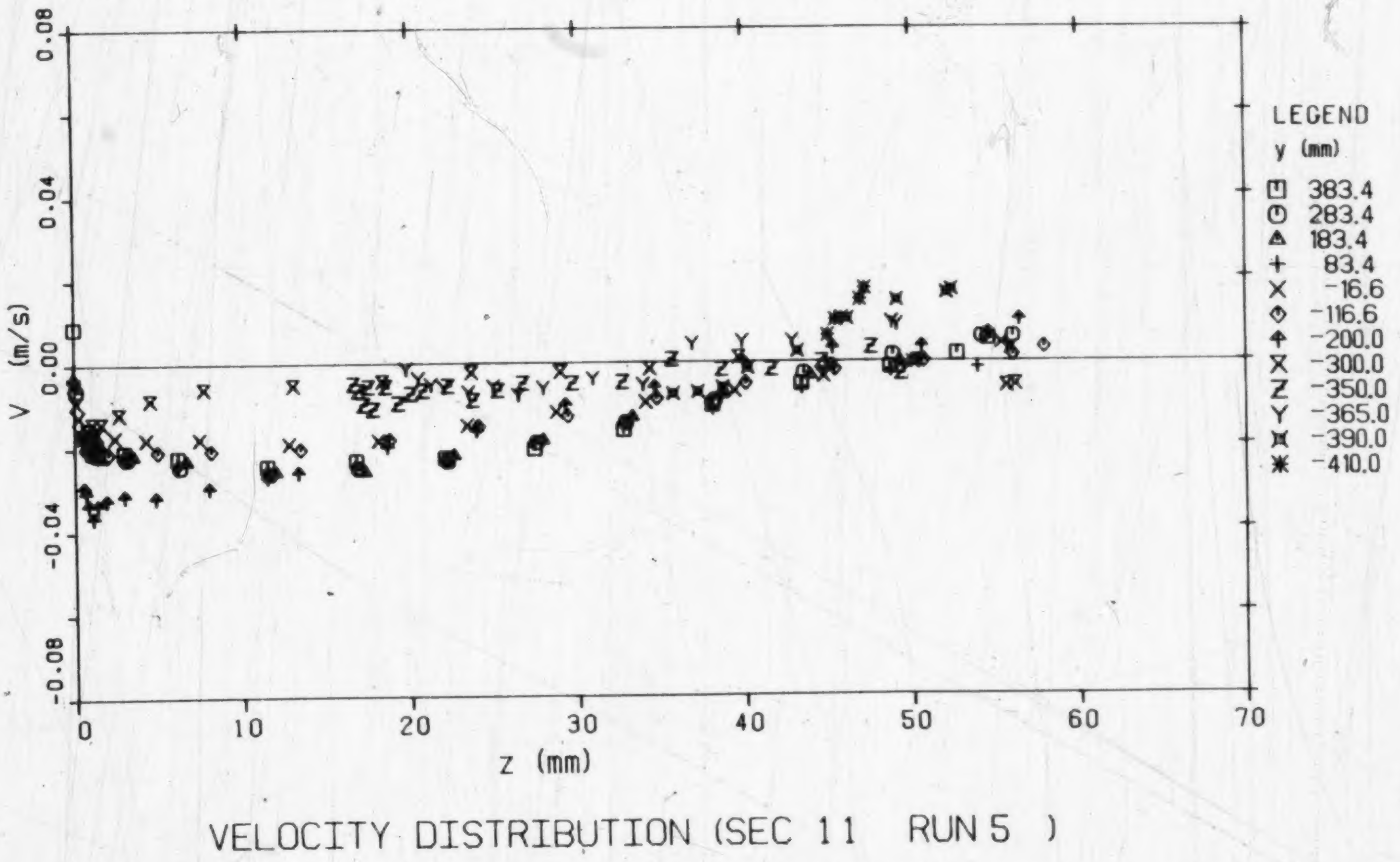

Figure 4.117 v velocity distribution (run 5, section 11)

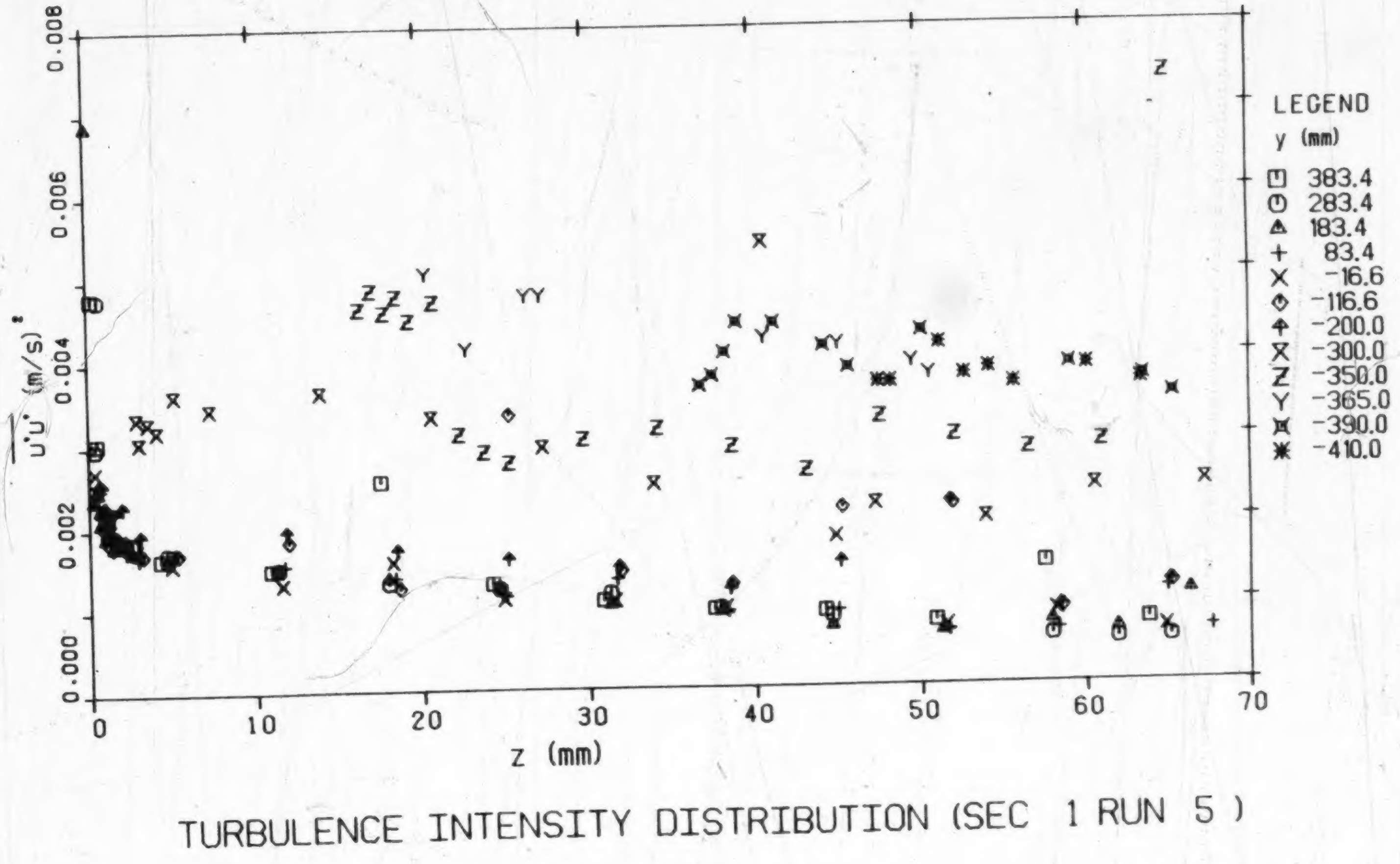

Figure 4.118 $\overline{u'u'}$ turbulence intensity distribution (run 5, section 1)

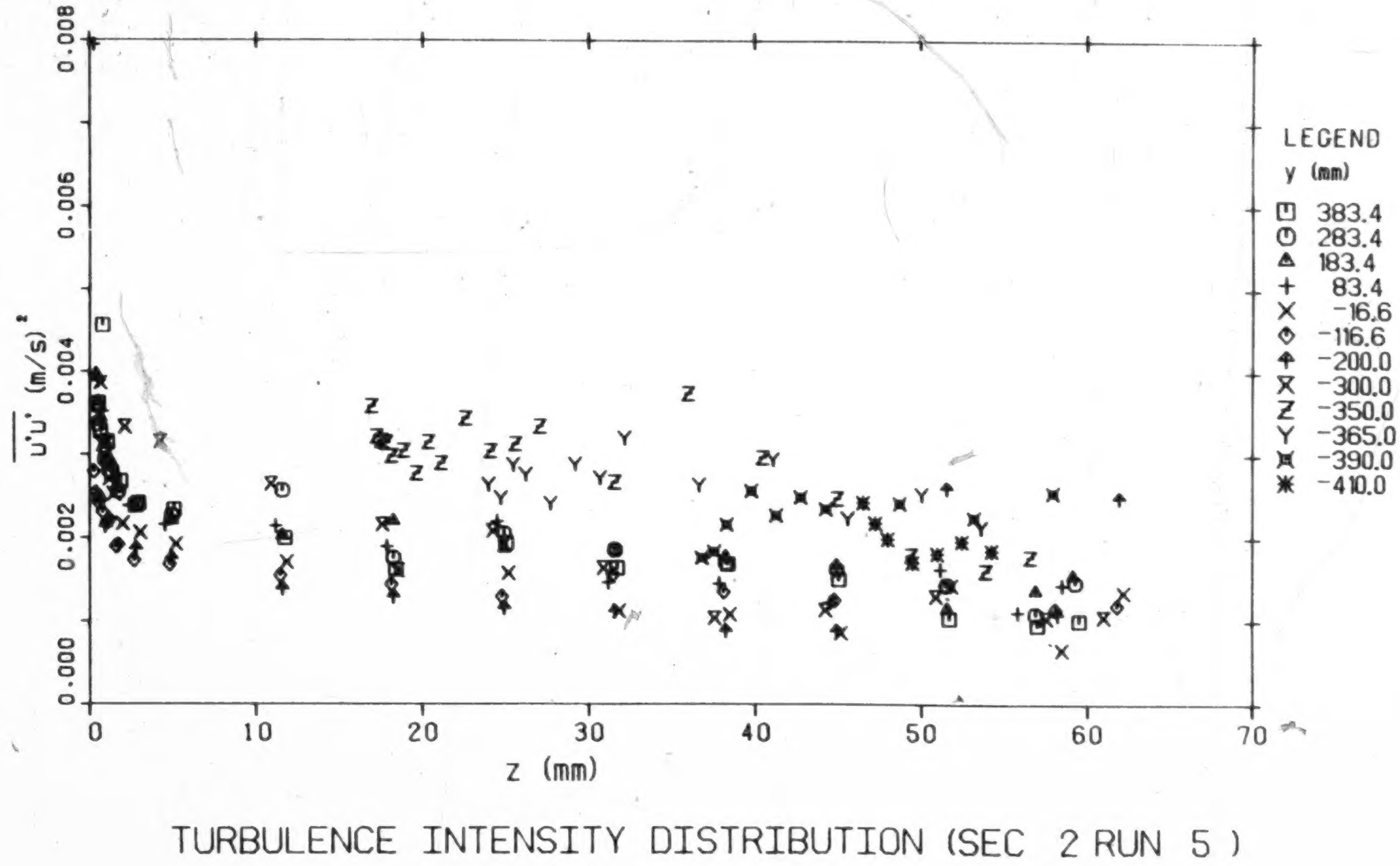

Figure 4.119 $\overline{u'u'}$ turbulence intensity distribution (run 5, section 2)

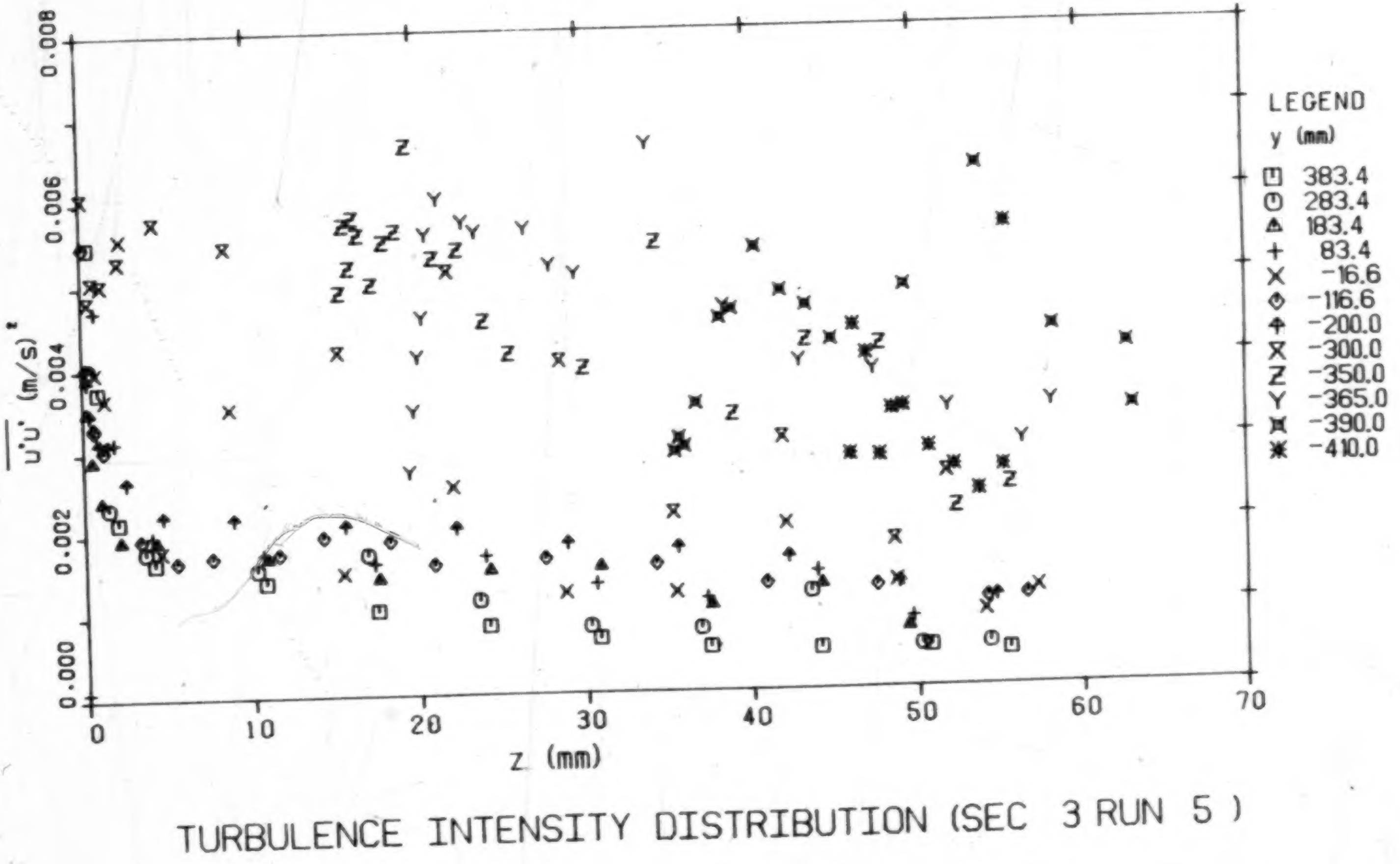

Figure 4.120 $\overline{u'u'}$ turbulence intensity distribution (run 5, section 3)

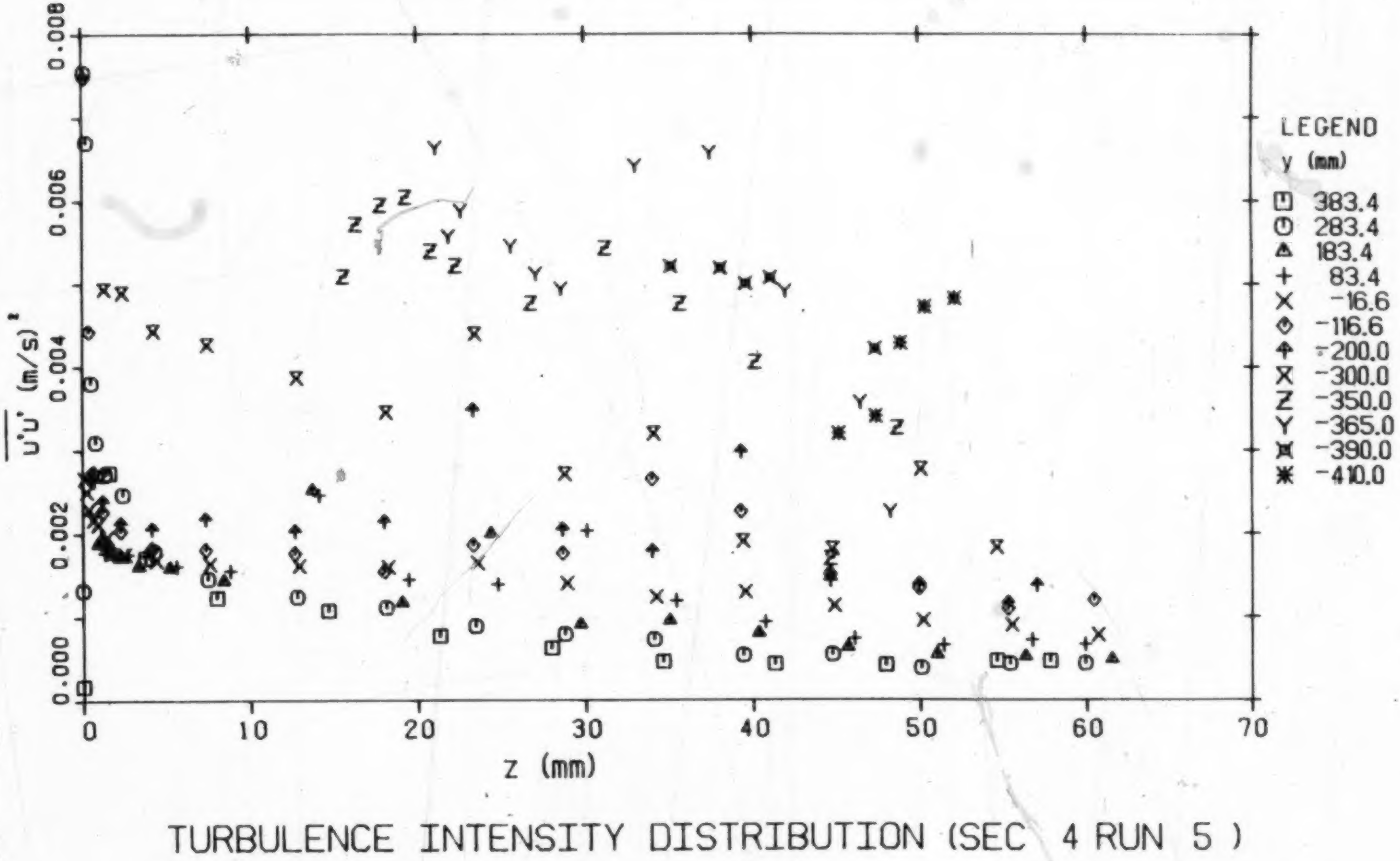

Figure 4.121 $\overline{u'u'}$ turbulence intensity distribution (run 5, section 4)

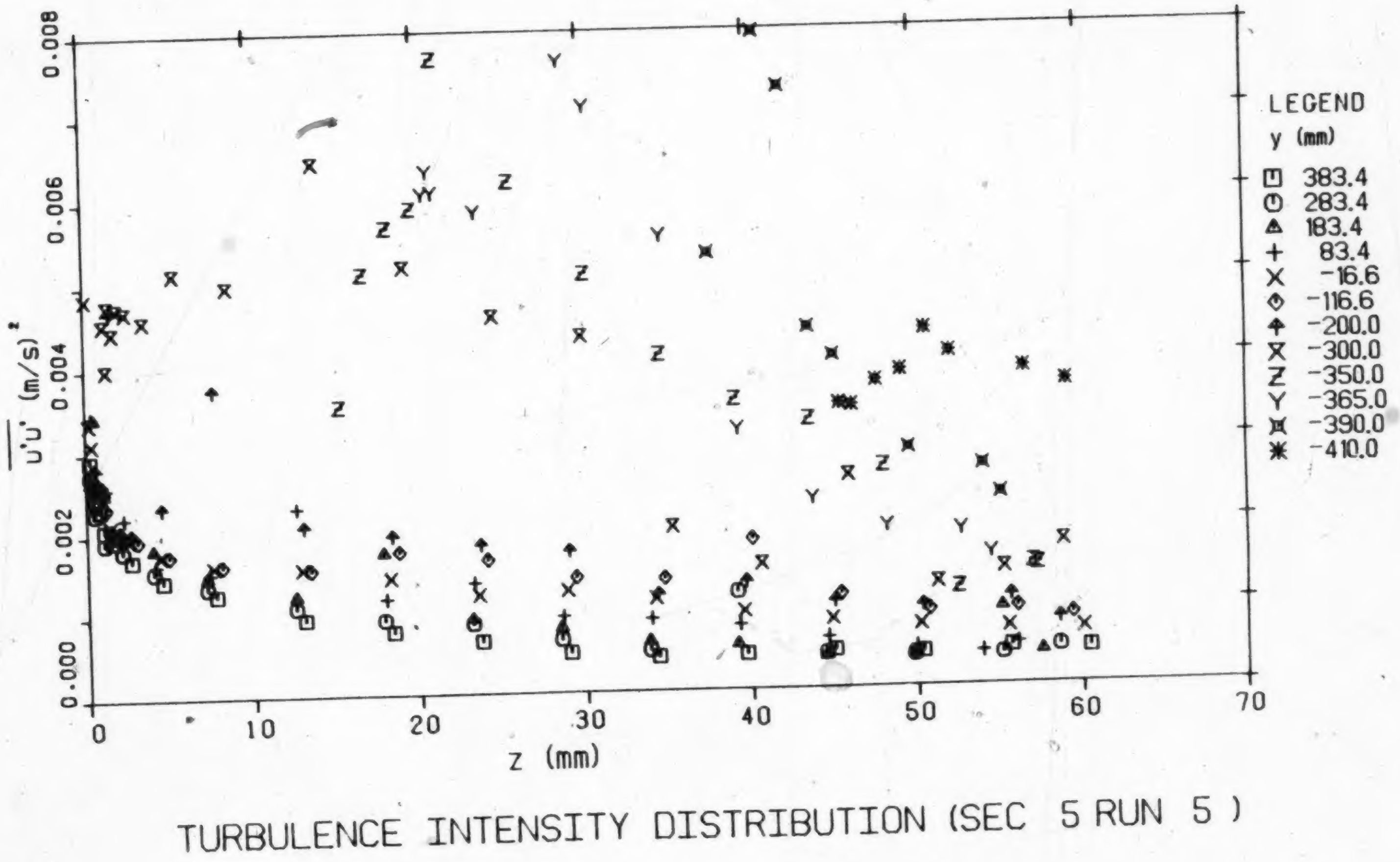

Figure 4.122 $\overline{u'u'}$ turbulence intensity distribution (run 5, section 5)

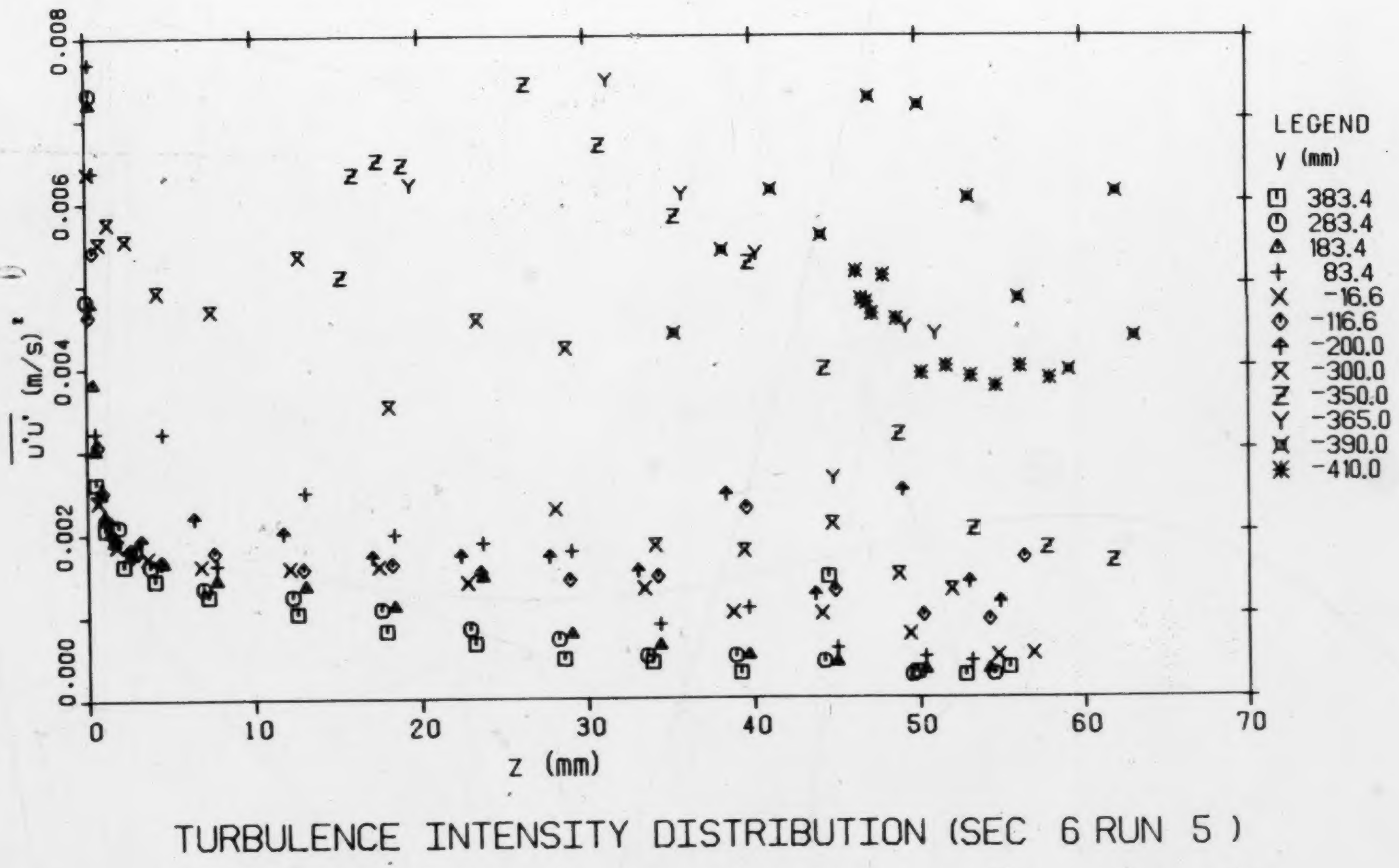

Figure 4.123 $\overline{u'u'}$ turbulence intensity distribution (run 5, section 6)

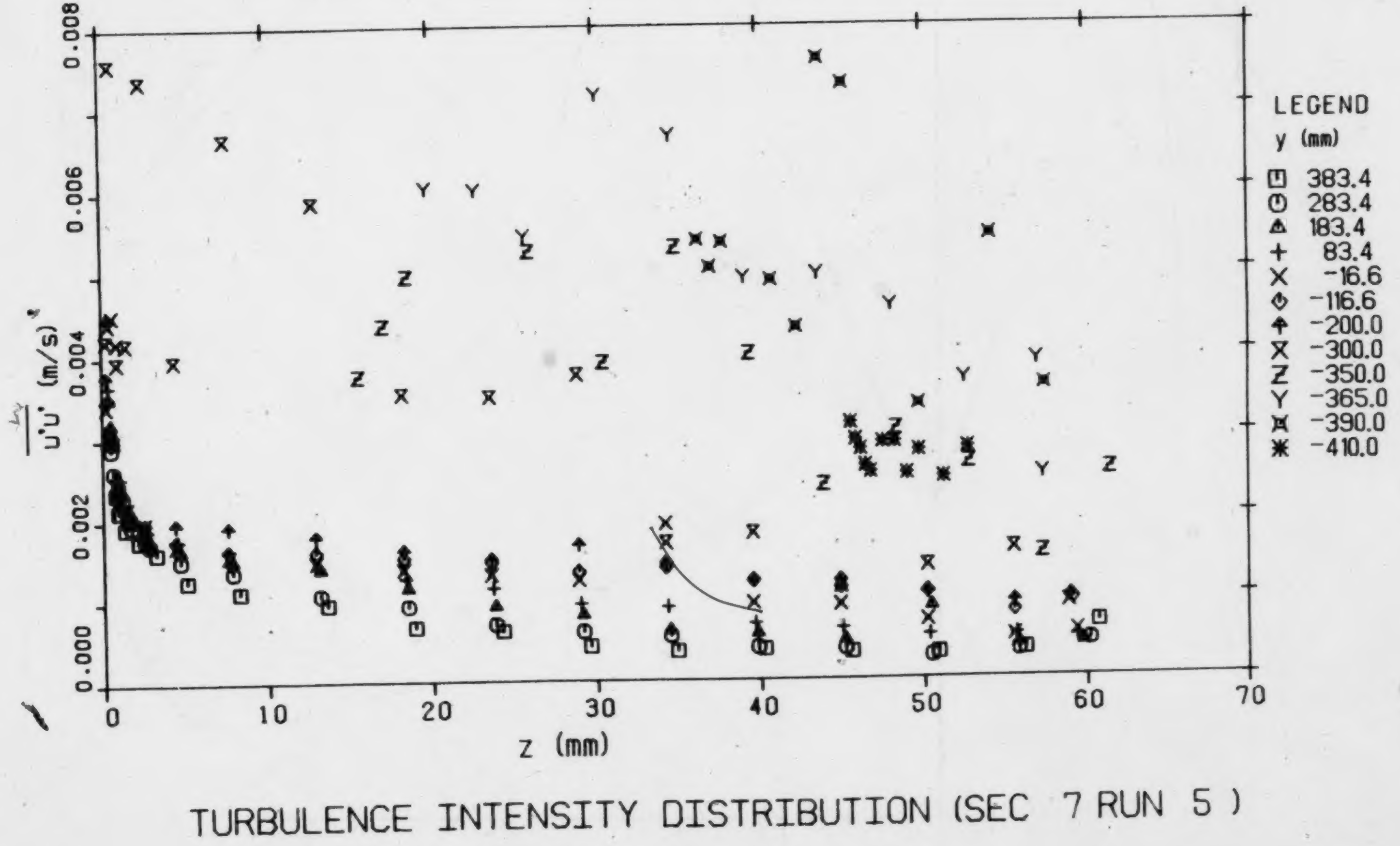

Figure 4.124 $\overline{u'u'}$ turbulence intensity distribution (run 5, section 7)

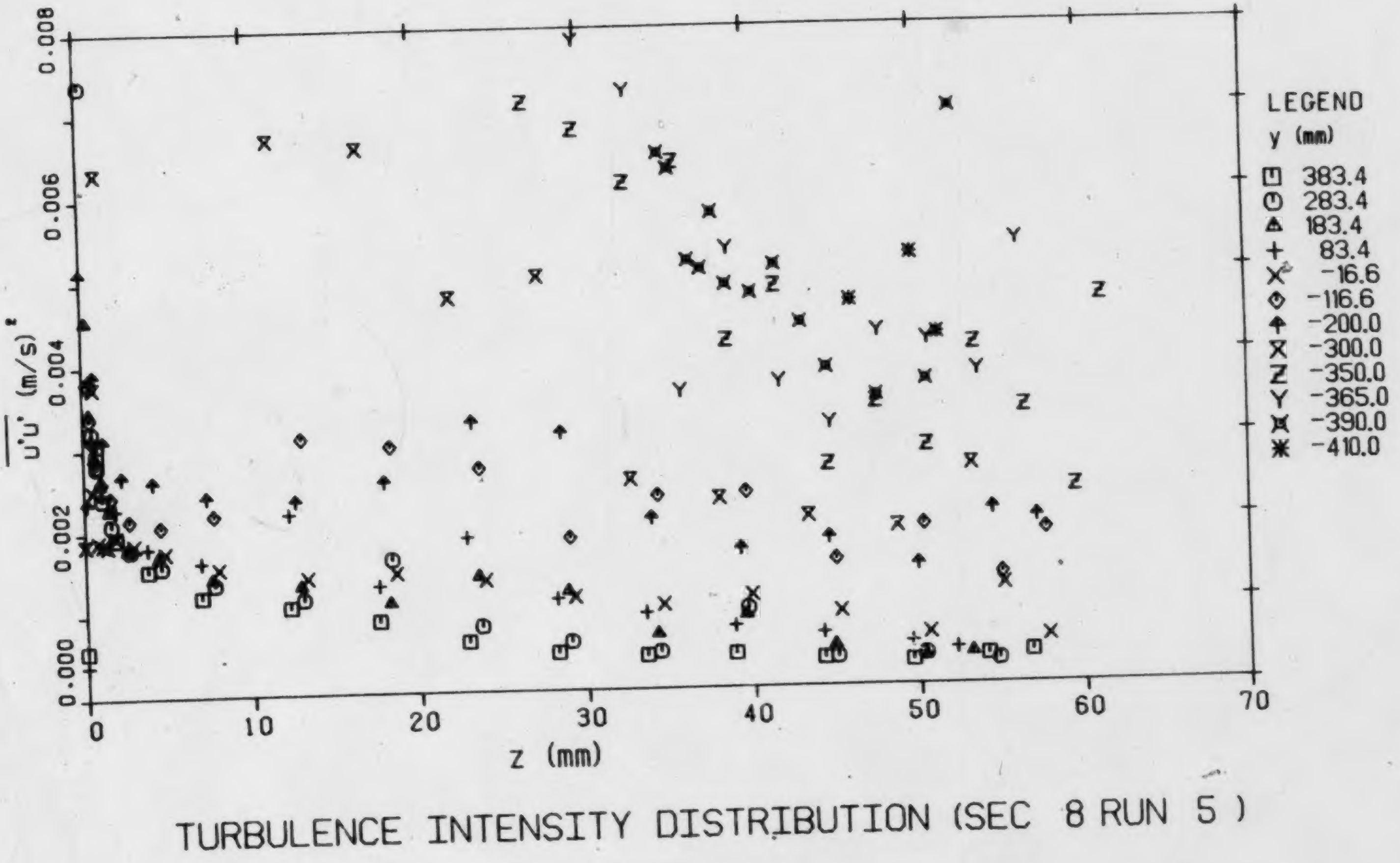

Figure 4.125 $\overline{u'u'}$ turbulence intensity distribution (run 5, section 8)

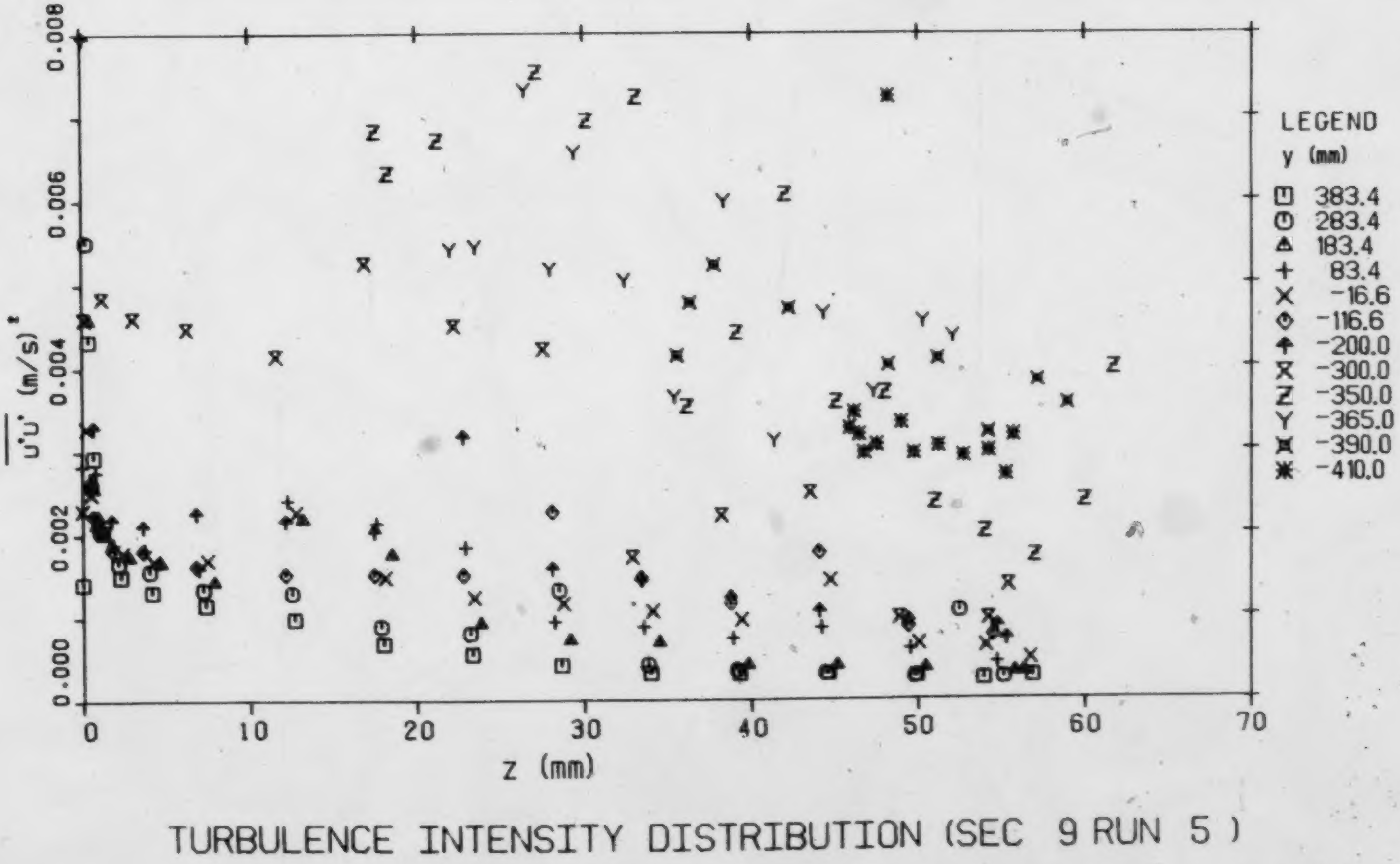

Figure 4.126 $\overline{u'u'}$ turbulence intensity distribution (run 5, section 9)

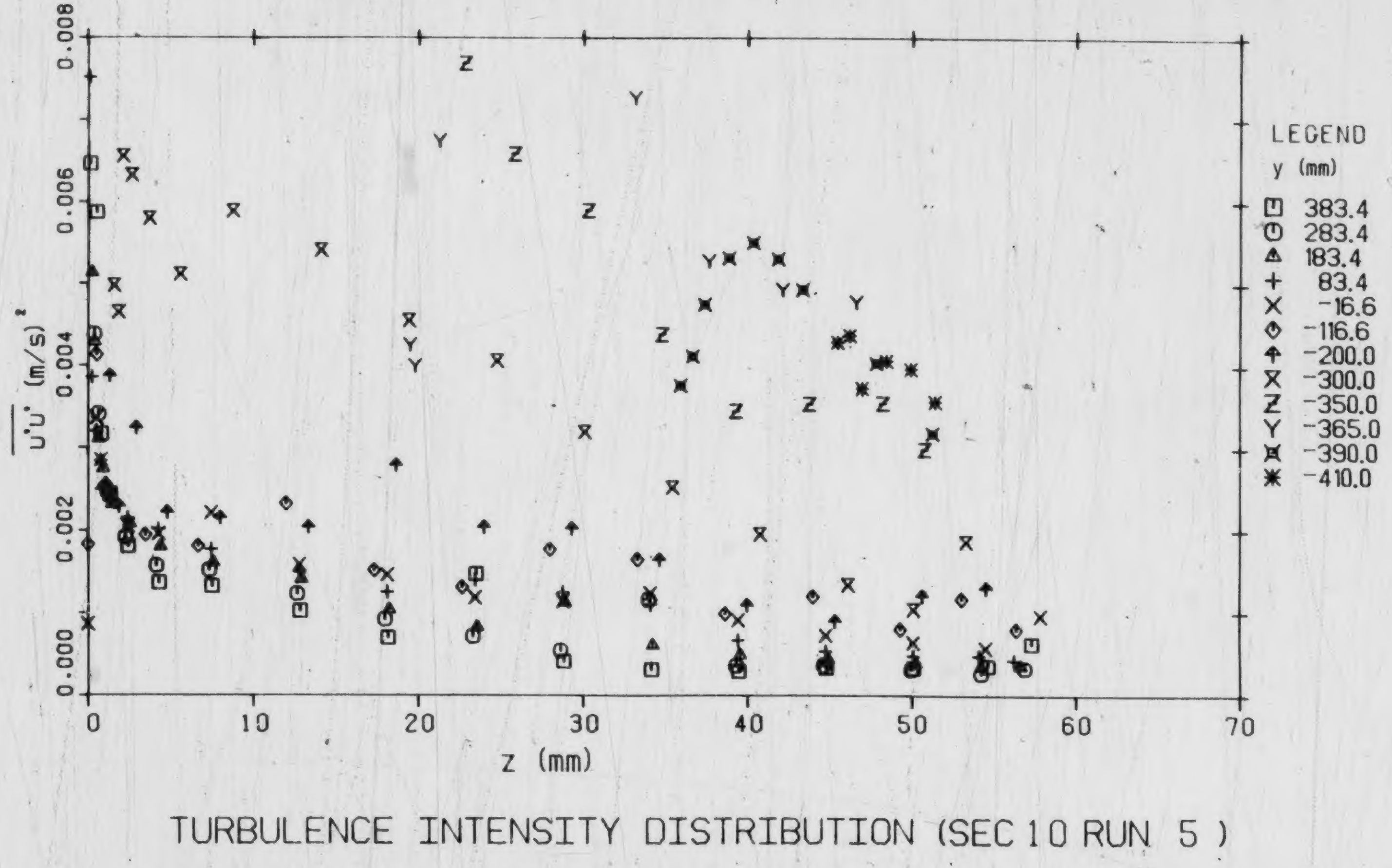

Figure 4.127 $\overline{u'u'}$ turbulence intensity distribution (run 5, section 10)

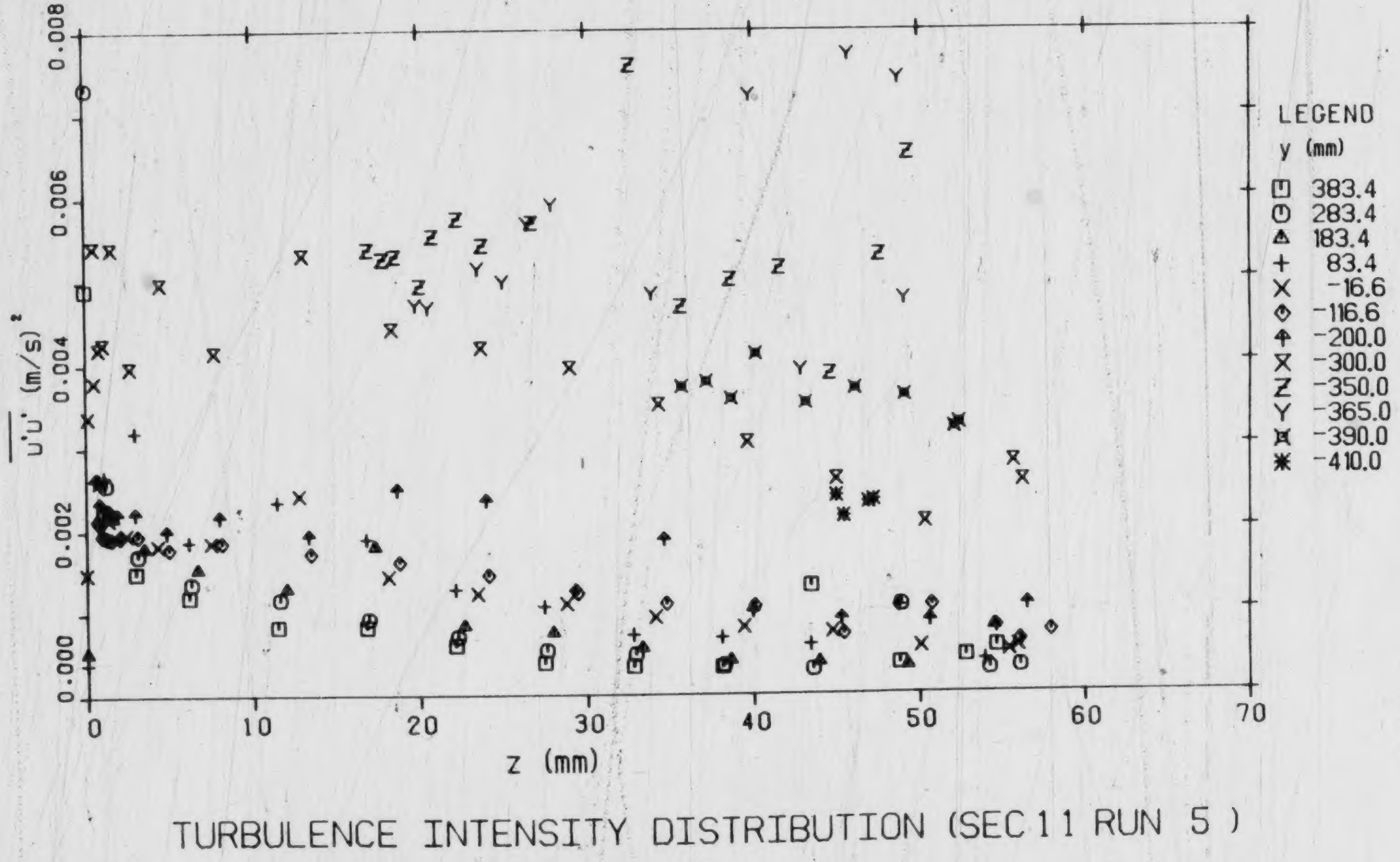

Figure 4.128 $\overline{u'u'}$ turbulence intensity distribution (run 5, section 11)

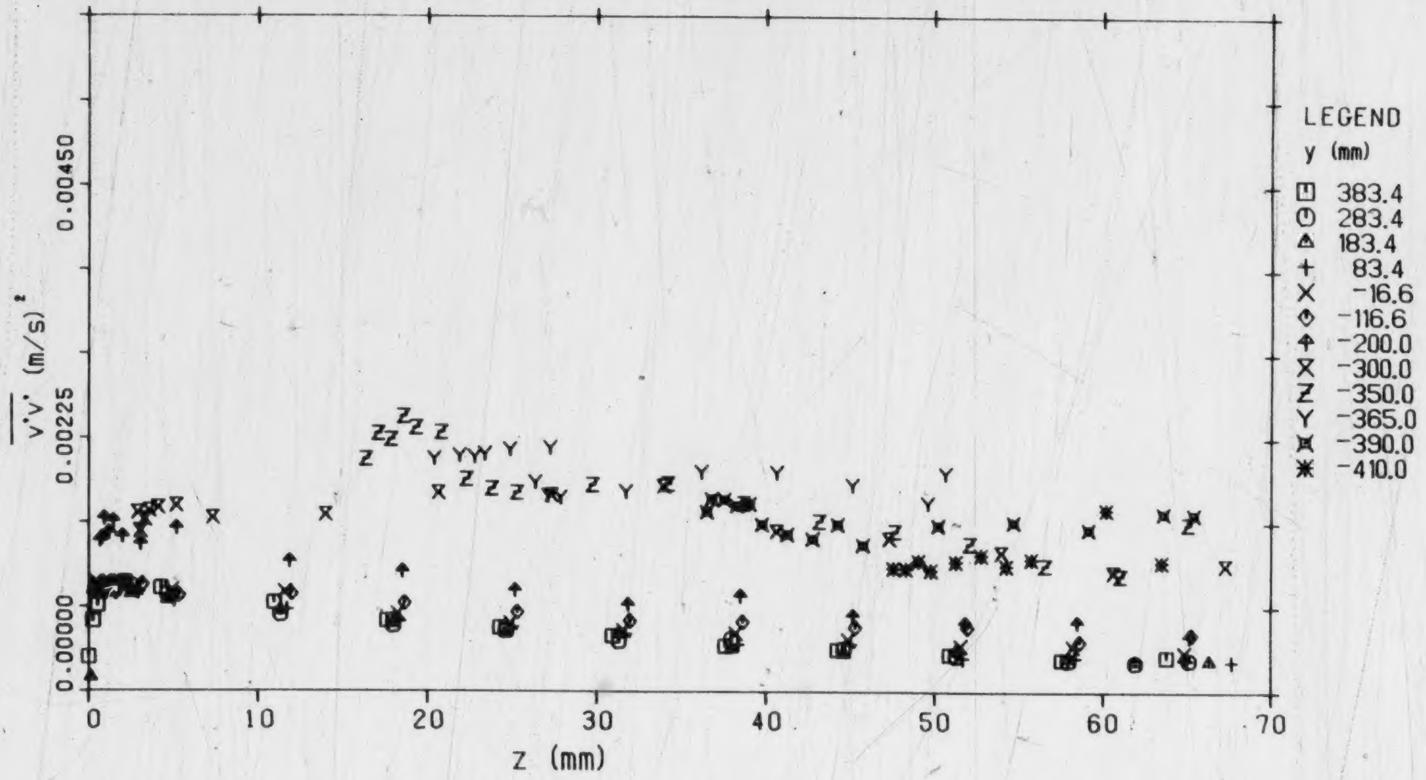

TURBULENCE INTENSITY DISTRIBUTION (SEC 1 RUN 5)

Figure 4.129 $\overline{v'v'}$ turbulence intensity distribution (run 5, section 1)

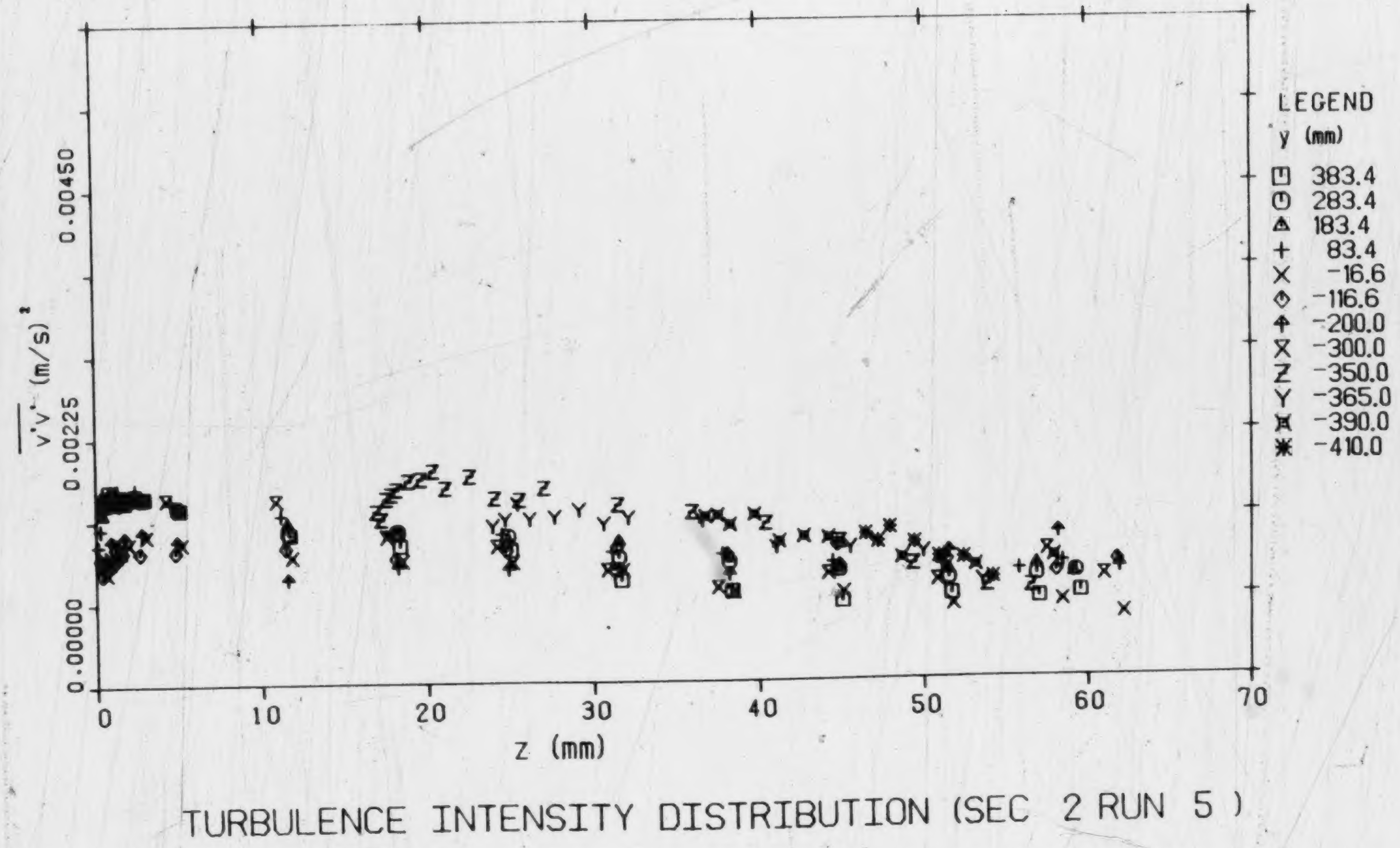

Figure 4.130 $\overline{v'v'}$ turbulence intensity distribution (run 5, section 2)

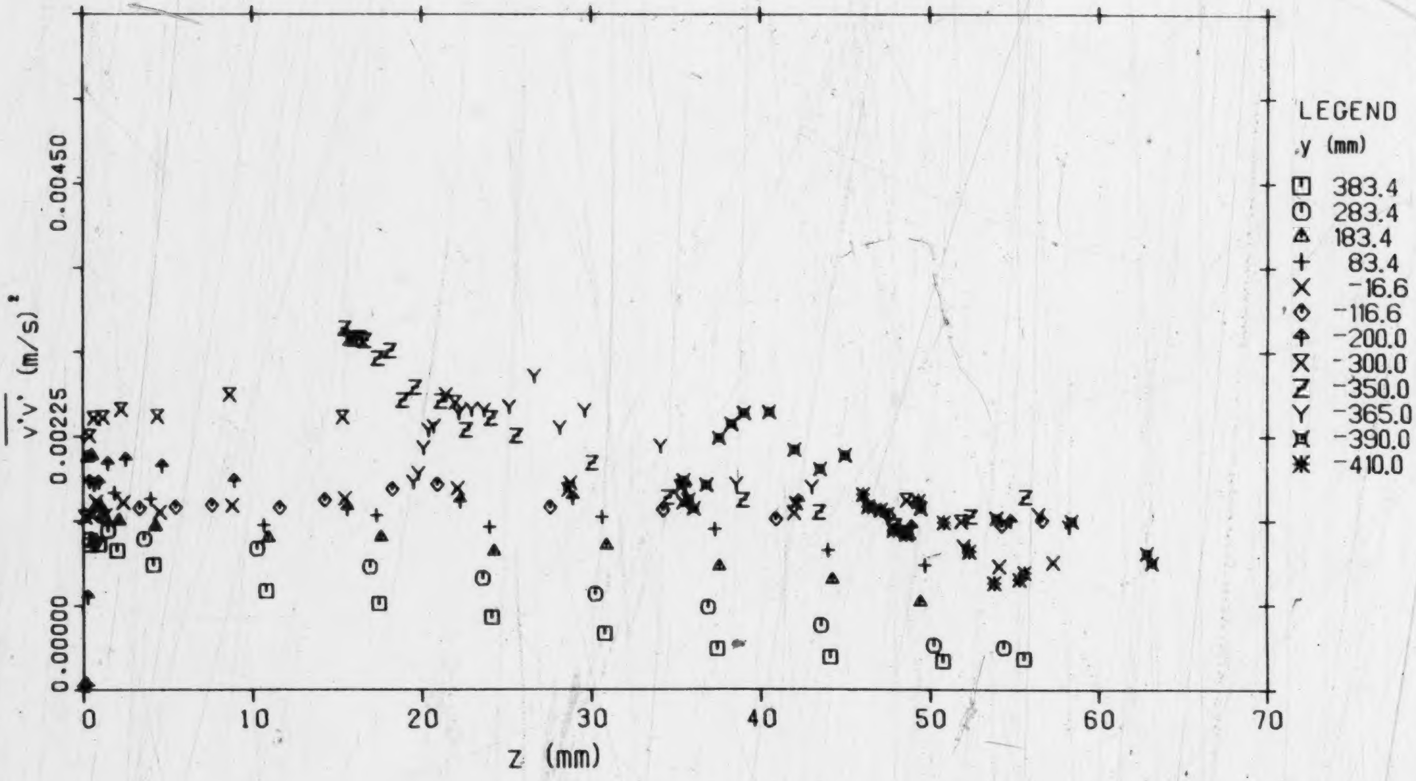

TURBULENCE INTENSITY DISTRIBUTION (SEC 3 RUN 5)

Figure 4.131 $\overline{v'v'}$ turbulence intensity distribution (run 5, section 3)

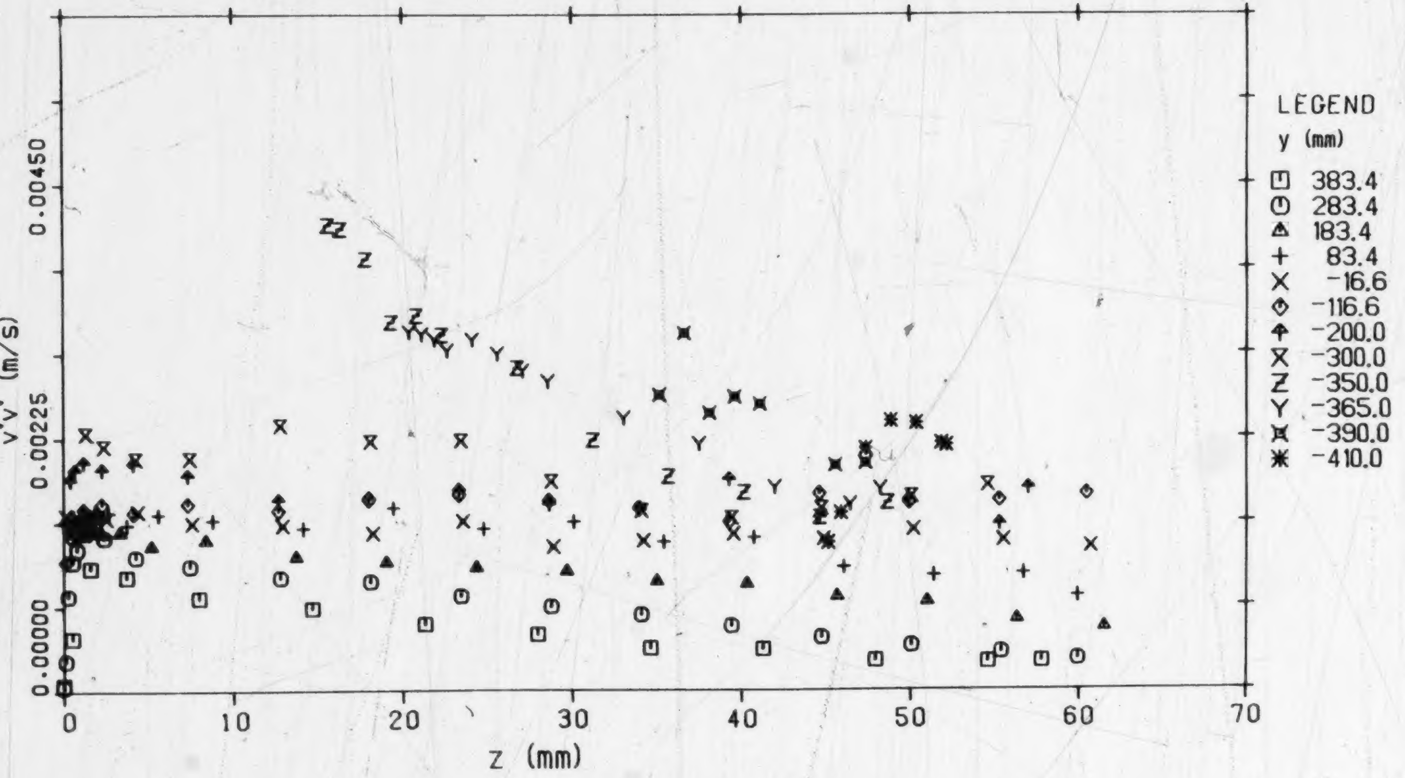

Figure 4.132 $\overline{v'v'}$ turbulence intensity distribution (run 5, section 4)

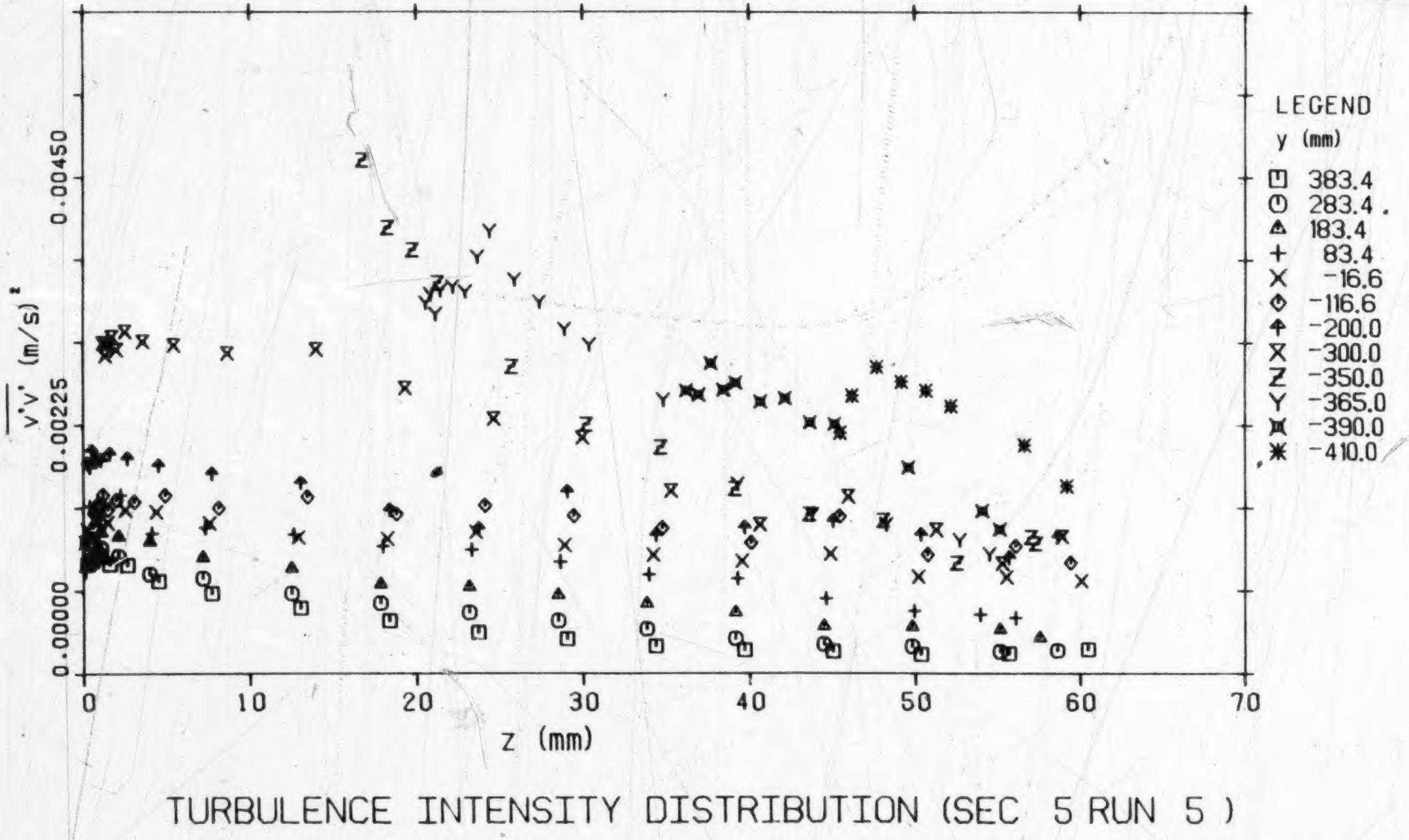

Figure 4.133 $\overline{v'v'}$ turbulence intensity distribution (run 5, section 5)

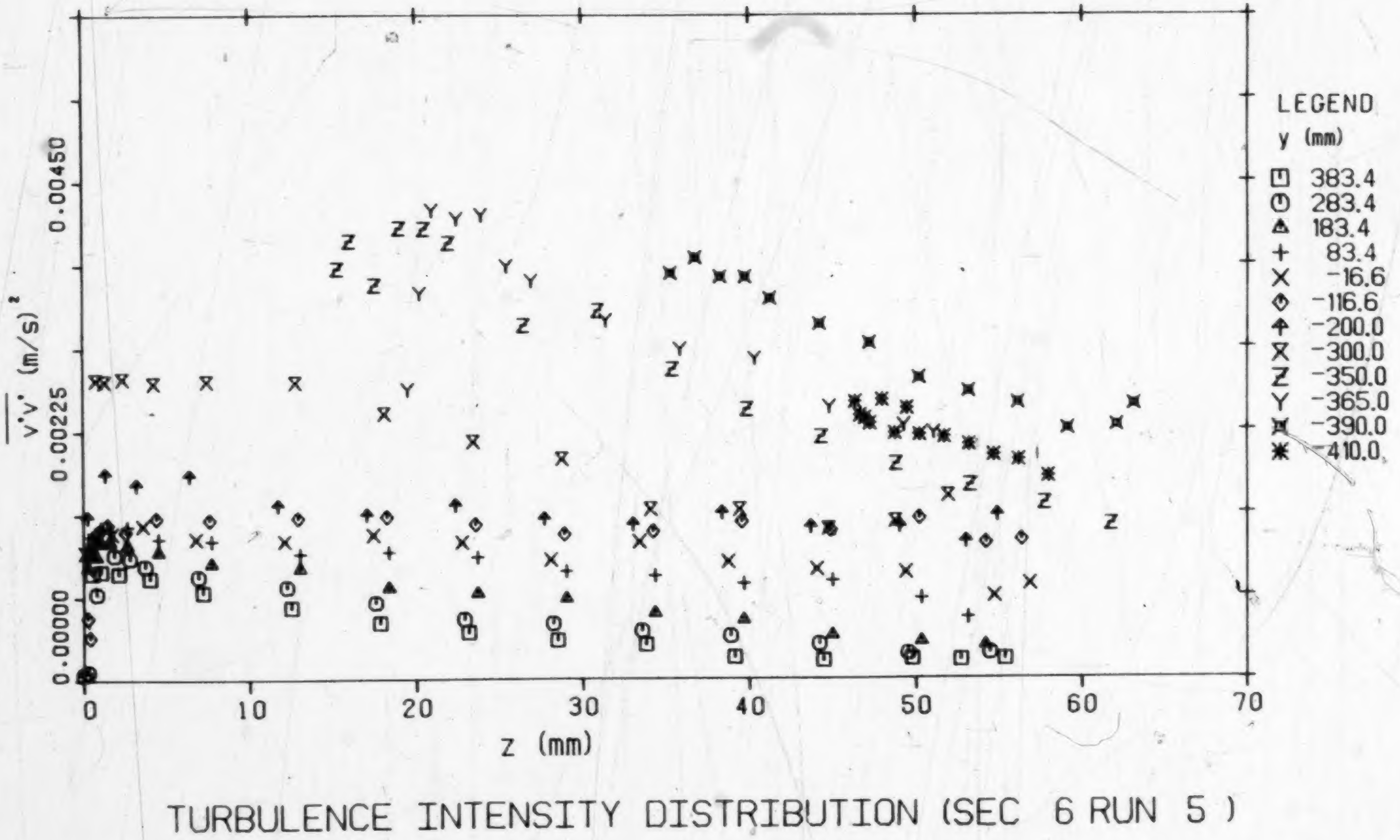

Figure 4.134 $\overline{v'v'}$ turbulence intensity distribution (run 5, section 6)

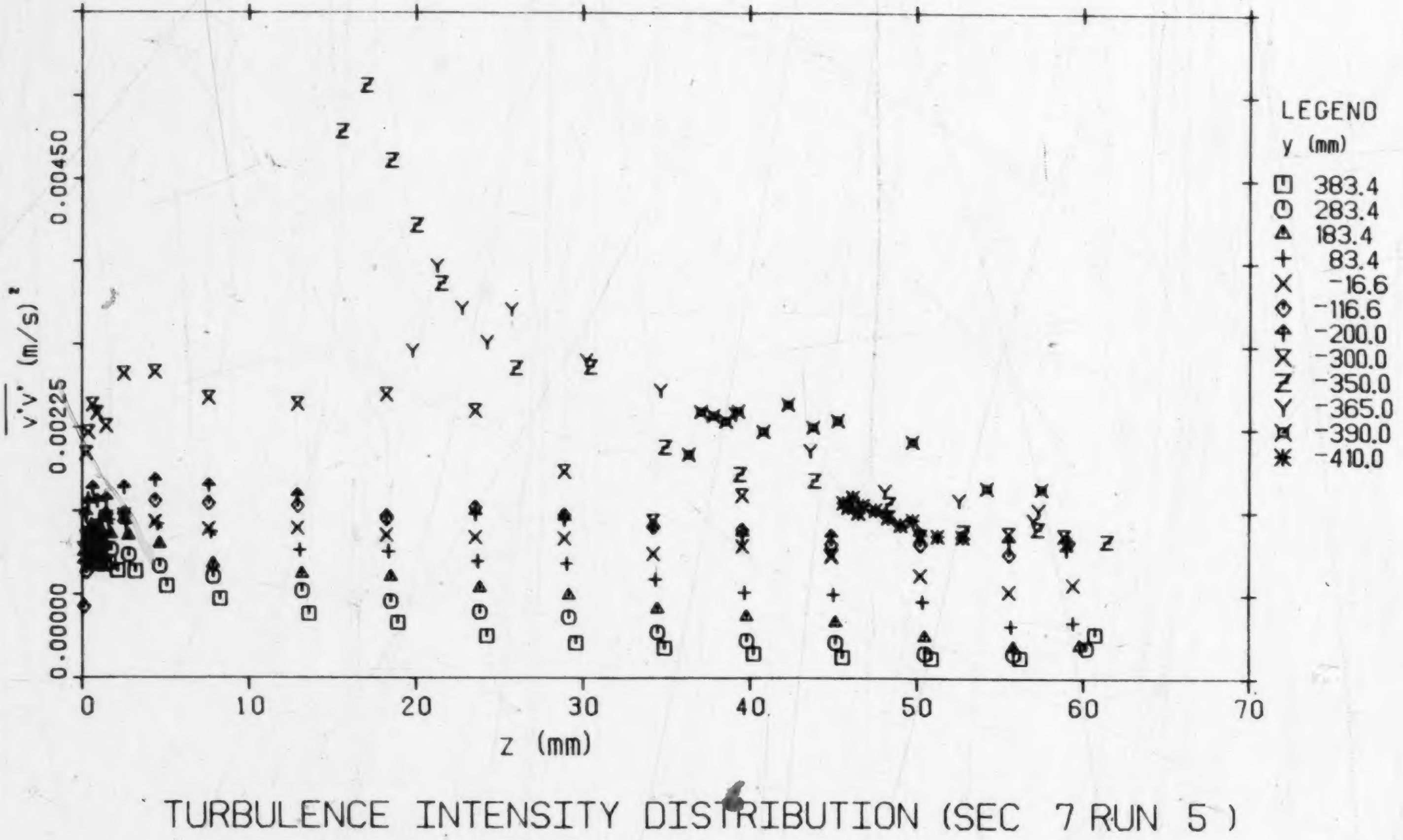

Figure 4.135 $\overline{v'v'}$ turbulence intensity distribution (run 5, section 7)

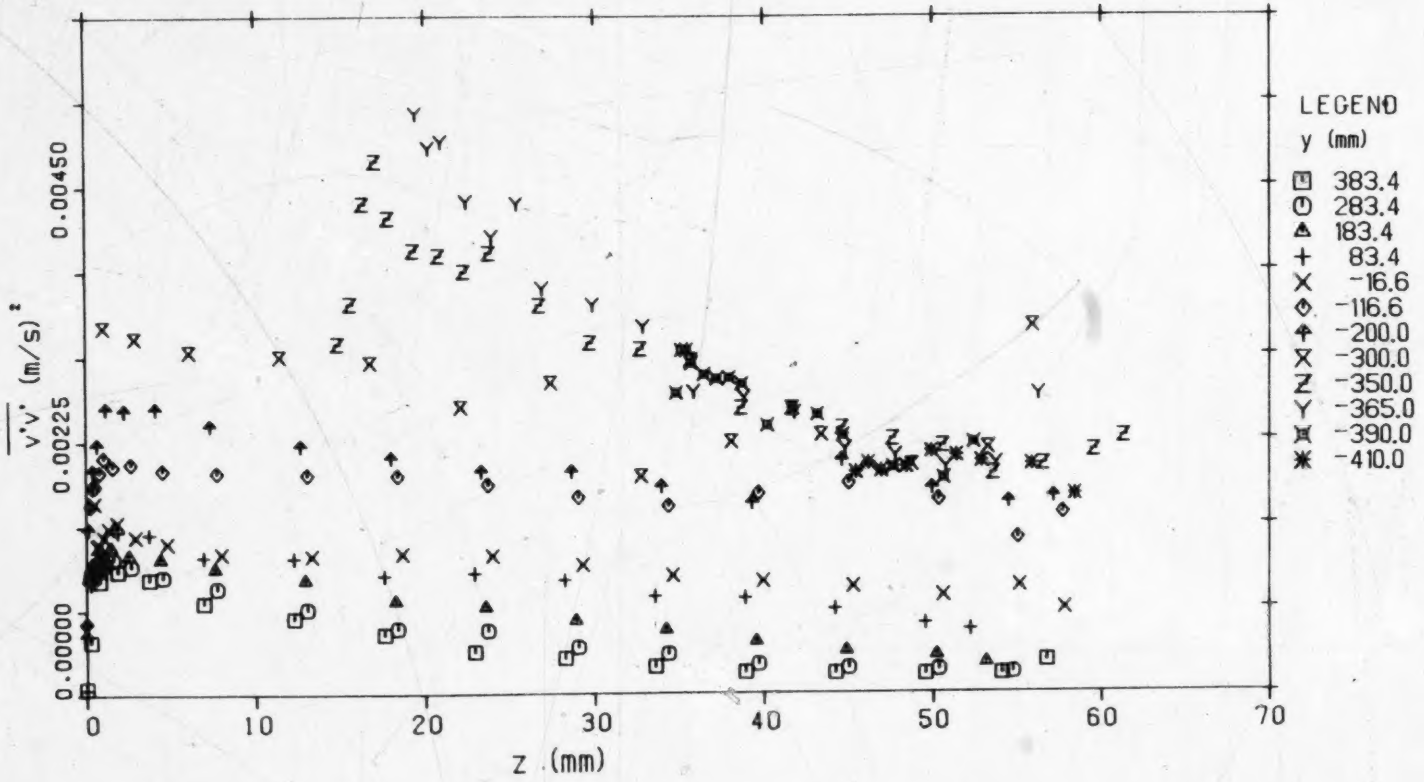

TURBULENCE INTENSITY DISTRIBUTION (SEC 8 RUN 5)

Figure 4.136 $\overline{v'v'}$ turbulence intensity distribution (run 5, section 8)

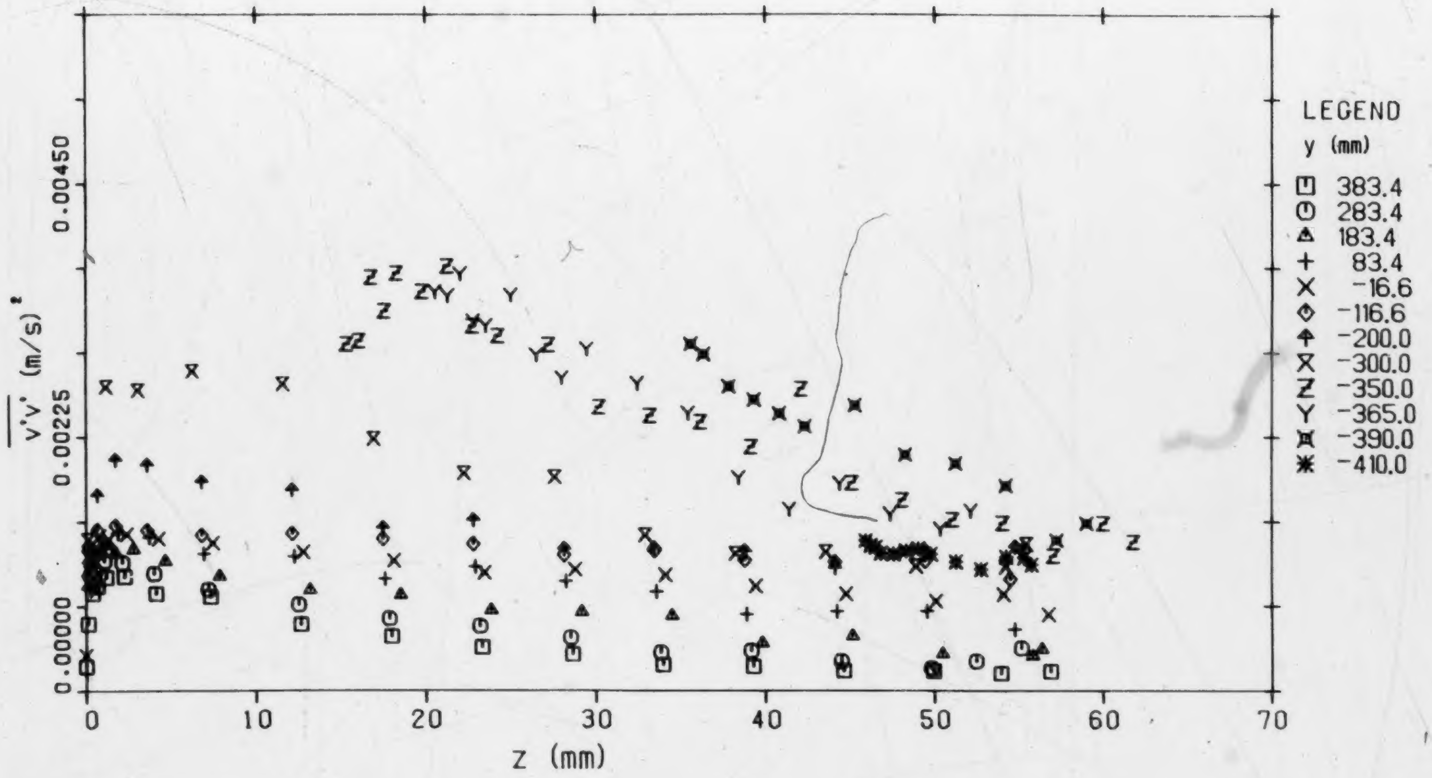

TURBULENCE INTENSITY DISTRIBUTION (SEC 9 RUN 5)

Figure 4.137 $\overline{v'v'}$ turbulence intensity distribution (run 5, section 9)

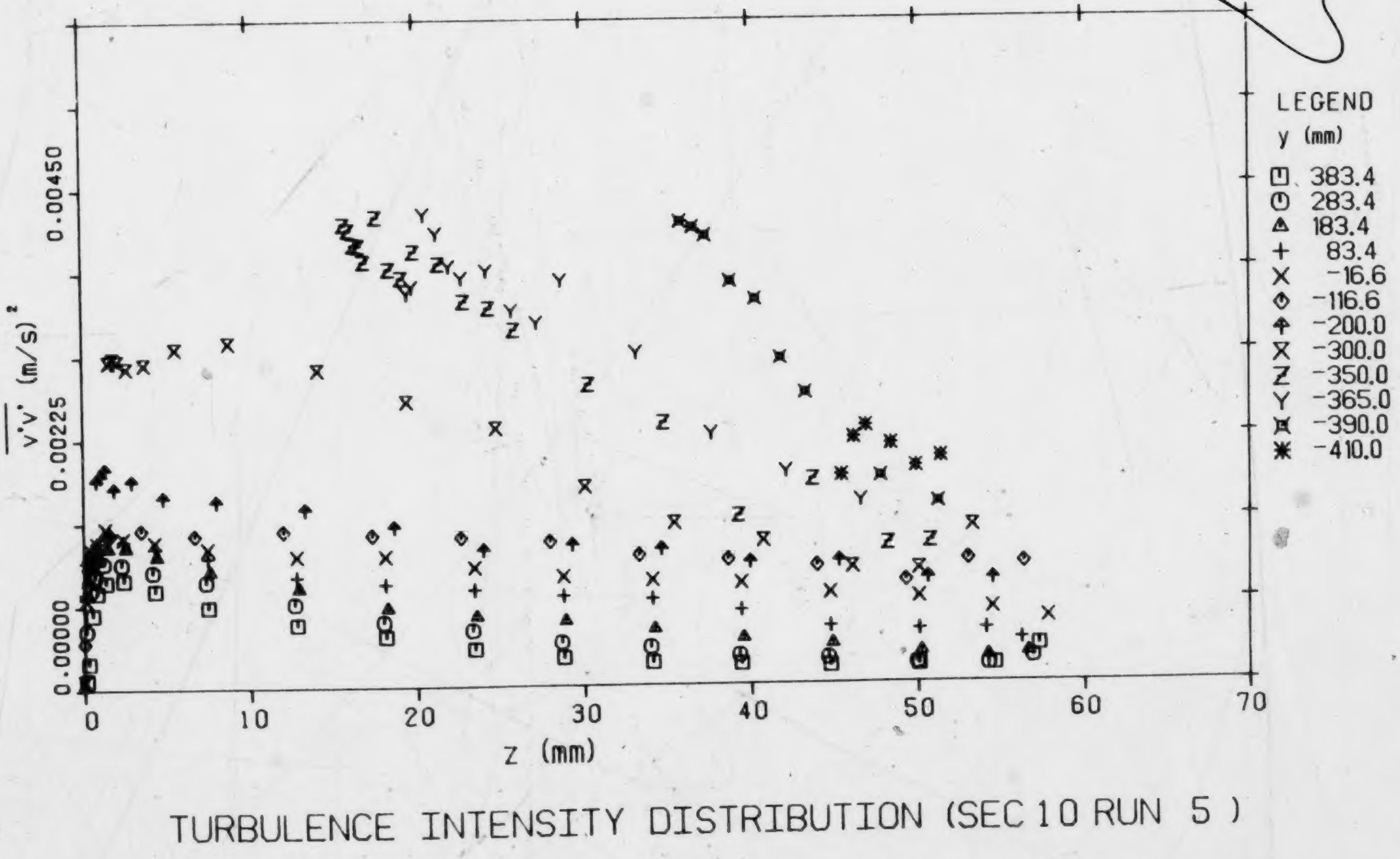

Figure 4.138 $\overline{v'v'}$ turbulence intensity distribution (run 5, section 10)

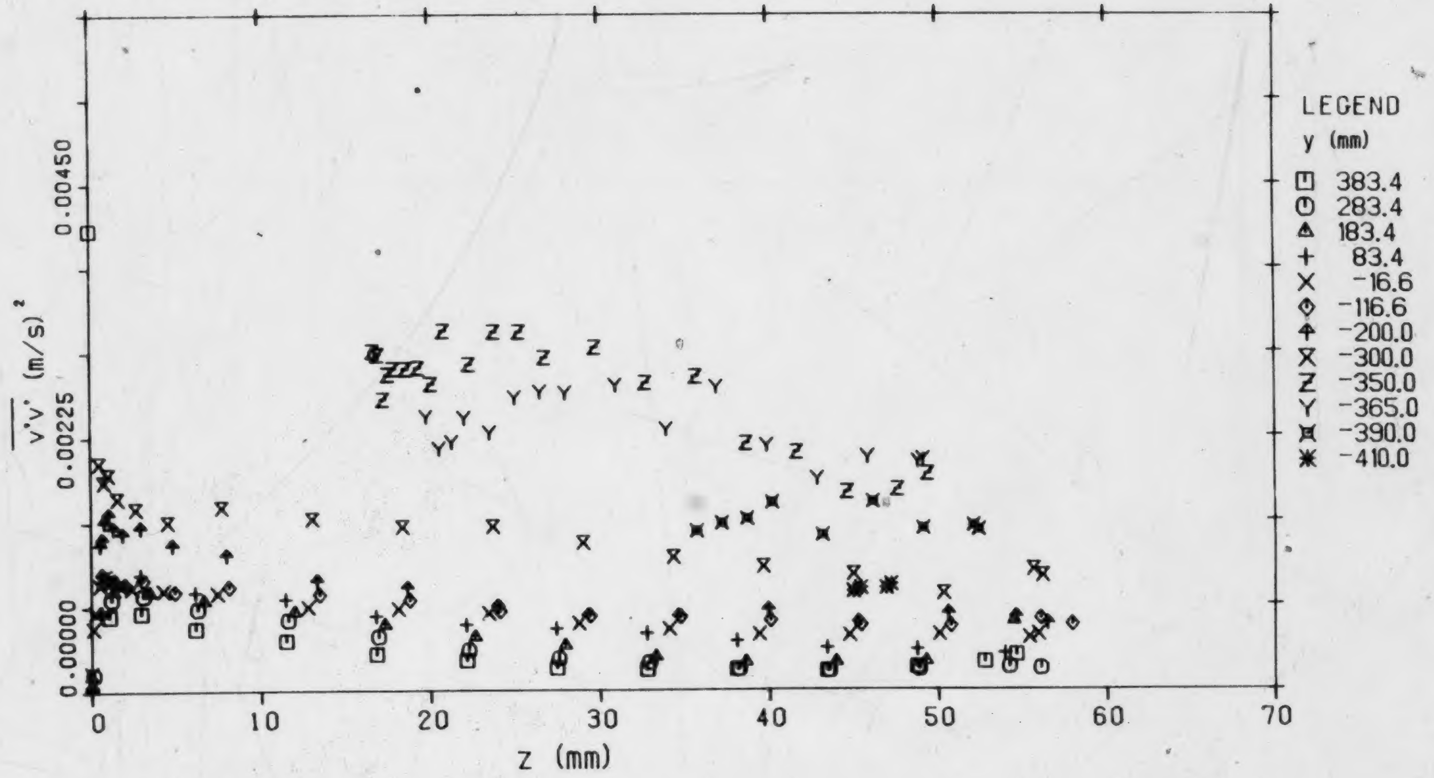

TURBULENCE INTENSITY DISTRIBUTION (SEC 11 RUN 5)

Figure 4.139 $\overline{v'v'}$ turbulence intensity distribution (run 5, section 11)

5 DISCUSSION OF THE EXPERIMENTAL RESULTS

5.1 Introduction

The data presented in chapter 4, while revealing intricate flow details, is too voluminous and detailed for use in engineering design. Depth-averaged velocities and bed shear stresses for each profile were computed to put this data into a more manageable form and to clarify the essential features of the flow. The depth-averaged velocities in both directions were calculated by numerical integration of the measured velocity profiles using a simple trapezoidal rule. The bed shear stresses were evaluated by fitting the measured profiles to an appropriate universal logarithmic law. A discussion of the applicability and implementation of this approach is presented. The results of this analysis are also discussed.

5.2 Discussion

5.2.1 Longitudinal Velocity

Comparison of the depth-averaged longitudinal velocity at the various sections is shown in figure 5.1 for run 1. The velocity and the cross channel distance y have been non-dimensionalized by the channel average velocity U_0 and the channel half width b respectively. It also should be noted that the velocity profiles are taken at the following locations across the channel: 483.4mm, 383.4mm, 283.4mm, 183.4mm, 83.4mm, -16.6mm, -116.6mm, -200mm, -300mm, -365mm, -390mm, -410mm and -430mm. For run 3, one extra profile was taken at y=-450mm. For the rough runs, there is no measurements on y=-483.4mm, y=-430mm and y=-450mm, however y=-350mm was added to investigate the velocity changes close to the toe of the sloped bank.

The velocity redistribution can be clearly observed. Figure 5.1 also shows that as the flow progressed through the bend the maximum velocity shifted to the toe of the slope. Figure 5.2 shows the longitudinal variation of the depth-averaged longitudinal velocity $\bar{u}$ for each section of run 1. It appears as if the flow is fully developed after $\theta=90^\circ$ since $\bar{u}$ is close to a constant.

Figures 5.3 and 5.4 show the tranverse and longitudinal variations of depth-averaged velocity in the longitudinal direction for run 2. Since the difference in parameters for run 2 (see table 1) is not large enough to have a significant effect, these results were similar to run 1.

The transverse and the longitudinal variation of the depth-averaged velocity for run 3 are shown in figures 5.5 and 5.6. The u/U_o ratio was smaller than in run 2. Figures 5.1 to 5.6 show that the flow is similar in smooth channel with different flow depths, therefore one depth was chosen for the rough channel runs.

Figure 5.7 shows the variation of the depth-averaged longitudinal velocity for run 4. The velocities on the roughened slope were smaller than those found in run 1 which had a similar flow condition. The longitudinal variation of the depth-averaged longitudinal velocities are shown in figure 5.8. Comparing figure 5.2 (run 1) and figure 5.8 (run 4) shows the similarity in flow pattern between run 1 and 4.

Figure 5.9 shows the transverse variation of the depth-averaged longitudinal velocity in run 5 while figure 5.10 shows the longitudinal variation. The velocities on the side slope in section 1 have been decreased by the existence of the roughness. As usual the velocity along the inside bank increased as flow entered the bend. However, the velocities along the outside bank seemed to reach a constant value at section 3 (θ=60°) which indicates that the flow had developed more quickly. The tenth section, just past 270°, shows an increase in the velocity along the outside bank and the velocity at section eleven shows an even larger variation. Comparison of figure 5.2 (run 1), figure 5.8 (run 4) and figure 5.10 (run 5) show that the roughness decreased the averaged velocity and increased the flow depth.

5.2.2 Longitudinal Shear Velocity

Figure 5.11 shows the distribution of the longitudinal shear velocity at all sections in the transverse direction while figure 5.12 shows the variation of the longitudinal shear velocity in the streamwise direction for run 1. The figures show that the shear stress follows the same tendencies as the velocity. At section 1, the shear velocity increased slightly toward the outside bank. It seemed that the shear stresses decreased up the slope and near the vertical wall. As the flow entered the bend, the shear velocity was maximum at the inside bank and minimum at the outside. With increased bend angle θ, x/b=12 or $\theta=60^\circ$, the maximum shear velocity shifted to the outside bank and reached a maximum value at the exit of the bend.

The variation of shear velocity in both tranverse and longitudinal directions for run 2 are shown in figures 5.13 and 5.14. These results are similar to run 1 with the exception that the non-dimensionalized shear velocity u_*/U on the slope in run 2 is larger at the same location due to the deeper flow depth. Figure 5.15 shows the variations of the depth-averaged longitudinal velocity in streamwise direction while figure 5.16 shows the variations in lateral direction.

Figure 5.17 shows the shear stress profile in run 4. It is interesting that the shear stress was much larger on the rough slope. The longitudinal variation of the shear velocities are shown in figure 5.18. Comparing figure 5.12 (run 1) with figure 5.18 (run 4), shows that the shear stress on the roughened slope was higher than that for the smooth slope, but that the rest of the channel was relatively unaffected.

The profiles of the longitudinal shear velocity at each section for run 5 are shown in figure 4.19. A sudden increase in the shear stress occurred where the secondary velocity began developing beyond θ=30°. Again, the higher bed shear stress was expected as the roughness was greater. It was also found that the peak of the shear stress was at the toe of the side slope. Turbulent intensity, shown in figures 4.84 to 4.117, also indicated that higher turbulence was located on the side slope. As the flow passed the end of the bend it tended to be uniform again. Figure 5.20 shows the longitudinal variation of the shear velocity for run 5.

As observed by Hicks (1985) the shear distribution on the smooth slope is uniform. For the rough banks, however, the shear decreases significantly up the slope. The shear near the top of the slope appears to reduce to approximately equal the main channel value.

5.2.3 Correlation of Depth Averaged Velocity and Shear Stress

The non-dimensional Chezy coefficient C_* is defined as

$$C_* \equiv \frac{u}{u_*} \tag{5.1}$$

From the logrithmic law for uniform flow in wide open channel, C_* may be evaluated from a form of the Colebrook equation (Gerard et. al., 1988)

$$C_* = 5.75 \log\left(\frac{h}{k_e}\right) + 6.2 \qquad (5.2)$$

where k_e is the effective roughness defined as

$$k_e = k_s + \frac{3.3\nu}{u_*} \qquad (5.3)$$

For a wide open channel, Manning's n is related to C_* by

$$n = \frac{h^{1/6}}{C_* \sqrt{g}} \qquad (5.4)$$

Figures 5.21 to 5.25 show C_* for each profile for runs 1 to 5 respectively. For the smooth channel runs 1 to 3 it may be observed that C_* decreased up the slope from its main channel value of about 20. For run 4 C_* on the slope was approximatly constant at about 15 to 16 while the main channel remained at about 20. For the last run the expanded metal appeared to have C_* of 6 to 8 while the main channel remained unaffected. These C_* values correspond to Manning's n values of 0.010, 0.013, 0.029 for the smooth, sandpaper and metal roughness respectively. The relative consistency of these values is notable considering the highly non-uniform nature of curved channel flow. Indeed, most of the observed variation may be explained by reference to equation (5.2) or (5.4) which indicated that C_* should decrease with flow depth for constant k_s or n. Compared to C_* in the second section and the first section (in the straight channel), the change in C_* is very abrupt. This is likely due to momentum transfer by the secondary flow near the bank.

5.2.4 Momentum Transport

For practical bank protection design purposes, the critcal parameter is the bank shear distribution. To be able to generalize the results of a small scale model to prototype situations, it is necessary to investigate the relationship between bank shear and depth averaged velocity. In the complicated three-dimensional flow field in the vicinity of the bank, other momentum transfer effects may also be important and significantly alter the resulting distributions. The depth-averaged momentum equation in the longitudinal direction is used as a guide in the subsequent analysis. Insofar as the experimental data can be used to evaluate modelling assumptions and formulations in this equation, the present results may be of more general applicability. Integrating the three dimensional momentum equations over the flow depth, and assuming a hydrostatic pressure distribution and negelecting viscous terms, leads to the depth-averaged equations (Rodi, 1981)

$$\frac{\partial h\overline{u}^2}{\partial x} + \frac{\partial h\overline{u}\ \overline{v}}{\partial y} + gh\frac{\partial(h+z_b)}{\partial x} - \frac{1}{\rho}\frac{\partial T_{xx}}{\partial x} - \frac{1}{\rho}\frac{\partial T_{xy}}{\partial y} - \frac{\tau_{bx}}{\rho} = 0 \qquad (5.5)$$

$$\frac{\partial h\bar{u}\,\bar{v}}{\partial x} + \frac{\partial h\overline{v^2}}{\partial y} + gh\frac{\partial (h+z_b)}{\partial y} - \frac{1}{\rho}\frac{\partial T_{xy}}{\partial x} - \frac{1}{\rho}\frac{\partial T_{yy}}{\partial y} - \frac{\tau_{by}}{\rho} = 0 \qquad (5.6)$$

where T_{xx}, T_{xy} and T_{yy} are effective shear stresses defined as

$$T_{ij} = \frac{1}{h}\int_{z_b}^{z_b+h} (-\rho u_i' u_j' - \rho U_i U_j)\, dz \qquad (5.7)$$

where (u_i', u_j') are the temporal fluctuations and (U_i, U_j) are the velocity deviations of the local time averaged velocity from the depth averaged velocity. The effective stress consists of the depth averaged turbulent Reynold's stress and stress due to the depth averaging process. Among these stresses T_{xy} is the major stress to be considered in curved channel problems (Flokstra, 1977). The term T_{xy} can be rewritten as

$$T_{xy} = \frac{1}{h}\int_{z_b}^{z_b+h} (-\rho u'v' - \rho UV)\, dz = h\overline{\tau_{xy}} + \rho h\overline{UV} \qquad (5.8)$$

The experimental data can be used to estimate the magnitude of these stresses. Figures 5.26 and 5.27 show the longitudinal variation of $\overline{UV}$ (depth averaged UV) and $\overline{\tau_{xy}}/\rho$ evaluated by numerically integrating the measured velocity profiles and turbulent intensity at sections y=-16.6mm and y=-300mm, the locations of which correspond to the channel centreline and close to the toe of the slope, for runs 1 and 5. As can be seen, $\overline{UV}$ is at least five times larger than $\overline{\tau_{xy}}$ in both runs through the bend. This shows that the $\overline{UV}$ terms should be included during the calculation by the depth averaged equations for curved channel flows. The depth-radius ratio, h/R, for run 1 was 0.017. If $\overline{\tau_{xy}}$ is a function h/R, one fifth of h/R ratio may make $\overline{UV}$ to be as small as $\overline{\tau_{xy}}$. In other words for $h/R<0.003$ the $\overline{UV}$ may be negelected. For $h/R<0.003$ the curvature is small enough to assume that the channel is straight where the effective shear stress is negligible. The $\overline{UV}$ varies significantly along the channel as the secondary flow develops.

Figure 5.28 shows the transverse variation of $\overline{UV}$ and $\overline{\tau_{xy}}$ at section 2 ($\theta=30^\circ$), section 4 ($\theta=90^\circ$), section 7 ($\theta=180^\circ$) and section 10 ($\theta=210^\circ$) for runs 1 and 5. It also shows the difference between these two types of stress. The $\overline{UV}$ variation in the lateral direction is similar to the longitudinal velocity variation, i.e. the velocity re-distribution. The gradient of $\overline{UV}$ represents the net longitudinal momentum transport across the channel. The momentum was transported to the inner bank first as shown at $\theta=30^\circ$, then back to the outside bank ($\theta=90^\circ, 180^\circ$ and 270°). The secondary flow and $\overline{UV}$ were almost fully developed after 30° as shown in figures 5.28 and the figures showing the secondary velocity profiles in the previous chapter. The $\overline{UV}$ of the fully developed flow increased from the inner bank toward the outer bank and started to decrease at the toe of the slope. This was not because of the small secondary flows but due to the longitudinal "skew back" velocity profile shapes. The $\overline{UV}$ and $\overline{\tau_{xy}}$ at sections near the inner wall may have the same order of magnitude as shown in the figure. However, the gradient of these two stresses shows $\partial\overline{UV}/\partial y$ is larger and more important in the depth averaged equations. The gradient of $\overline{UV}$ in the radial direction in the inner two thirds of the channel is positive indicating that $u\partial u/\partial x$ will tend, in the absences of other effects, to be negative so that the flow is decelerating while the flow in the outer part of the channel is accelerating. It therefore appears that the combination of secondary flow and longitudinal velocity profile distortion leads to a significant net momentum transfer toward the outer bank.

5.2.5 Transverse Velocity

Figures 5.29 to 5.33 show the longitudinal variation of the depth-averaged transverse velocity. These velocities are small compared with the longitudinal velocity. At the entrance of the bend, there is a relatively large outward flow for all runs. Comparing figure 5.29 (run 1) and figure 5.33 (run 5), at the mid-point of the slope (y=-390mm), the flow is inward for the smooth boundary and outward for the rough boundary. When the transverse velocity close to channel bed is larger than the transverse surface velocity, the depth-averaged transverse velocity has the same direction as the 'bed velocity' which means that the fluid flows inward. It also indicates that the bank erosion may happen on the side slope for the channel with a smooth boundary.

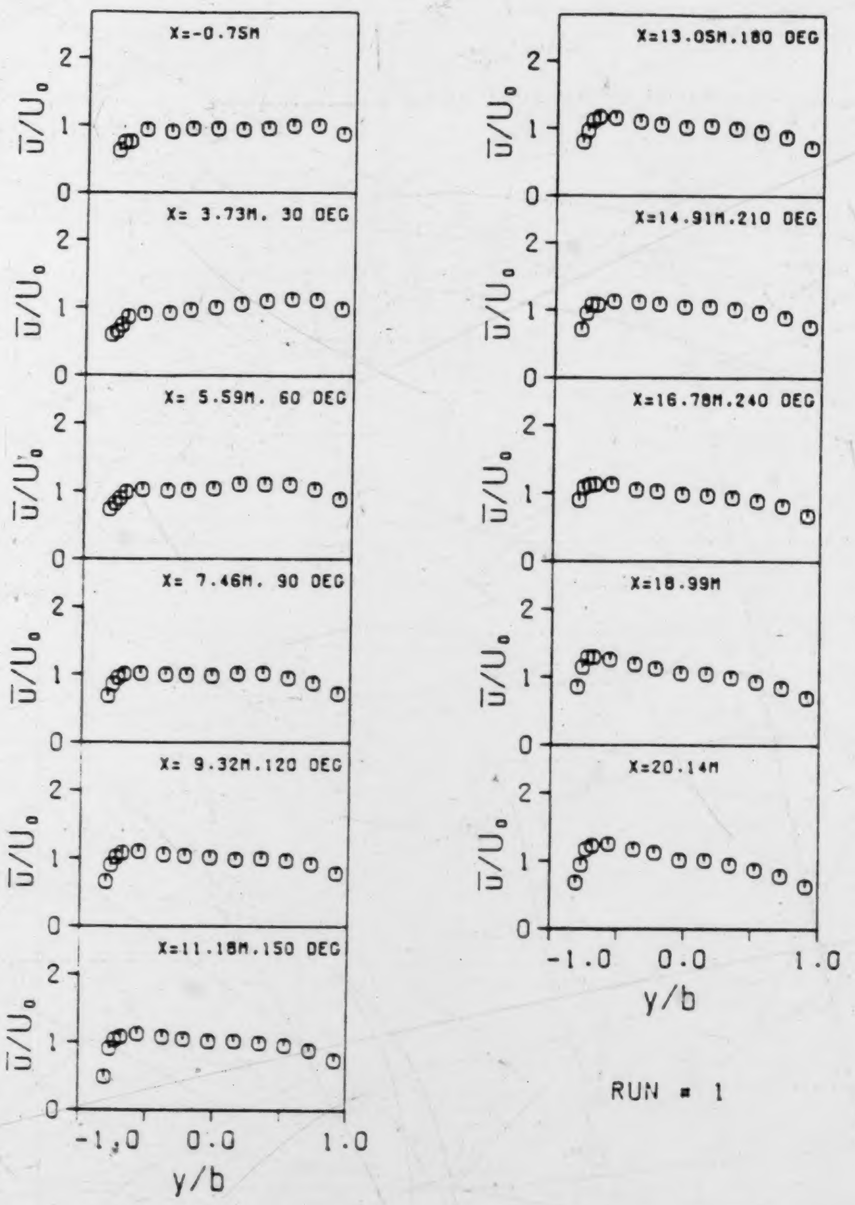

Figure 5.1 Profiles of depth-averaged longitudinal velocity(run 1)

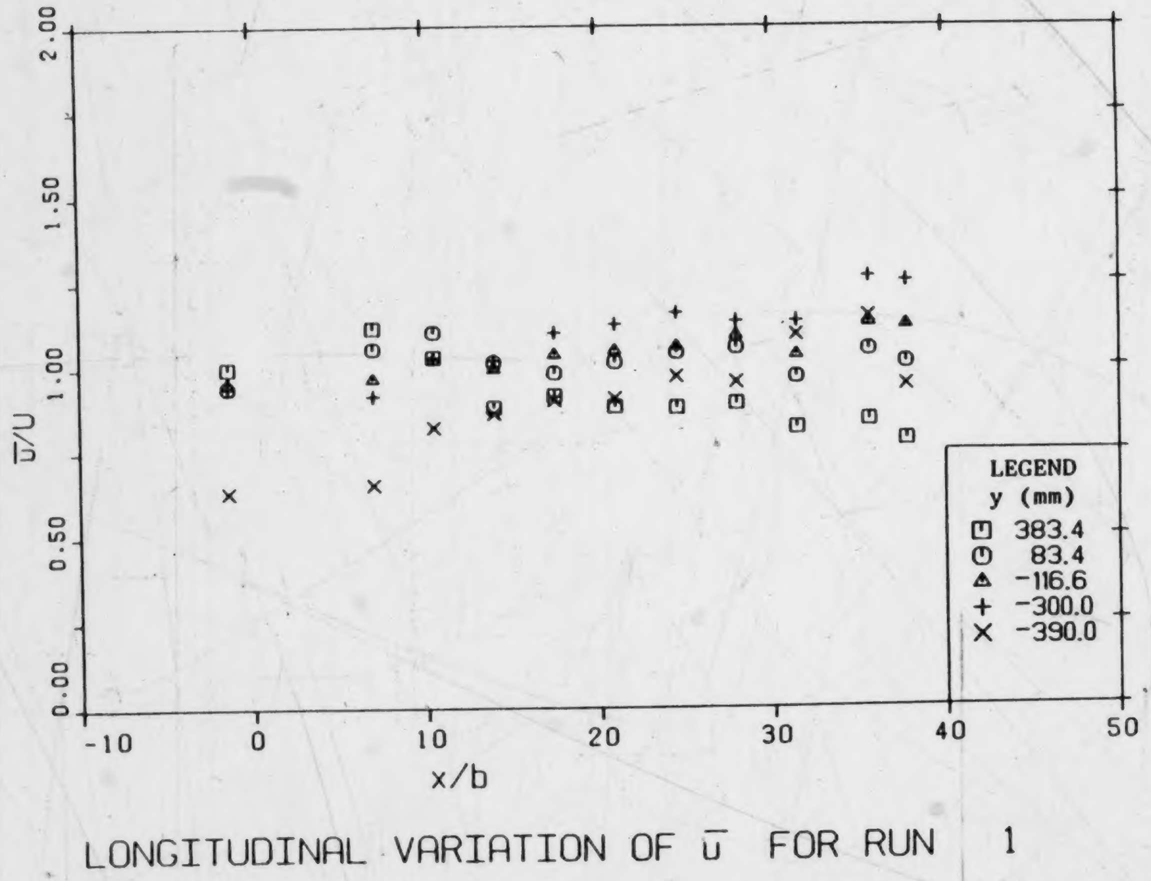

Figure 5.2 Longitudinal variations of longitudinal depth-averaged velocity (Run 1)

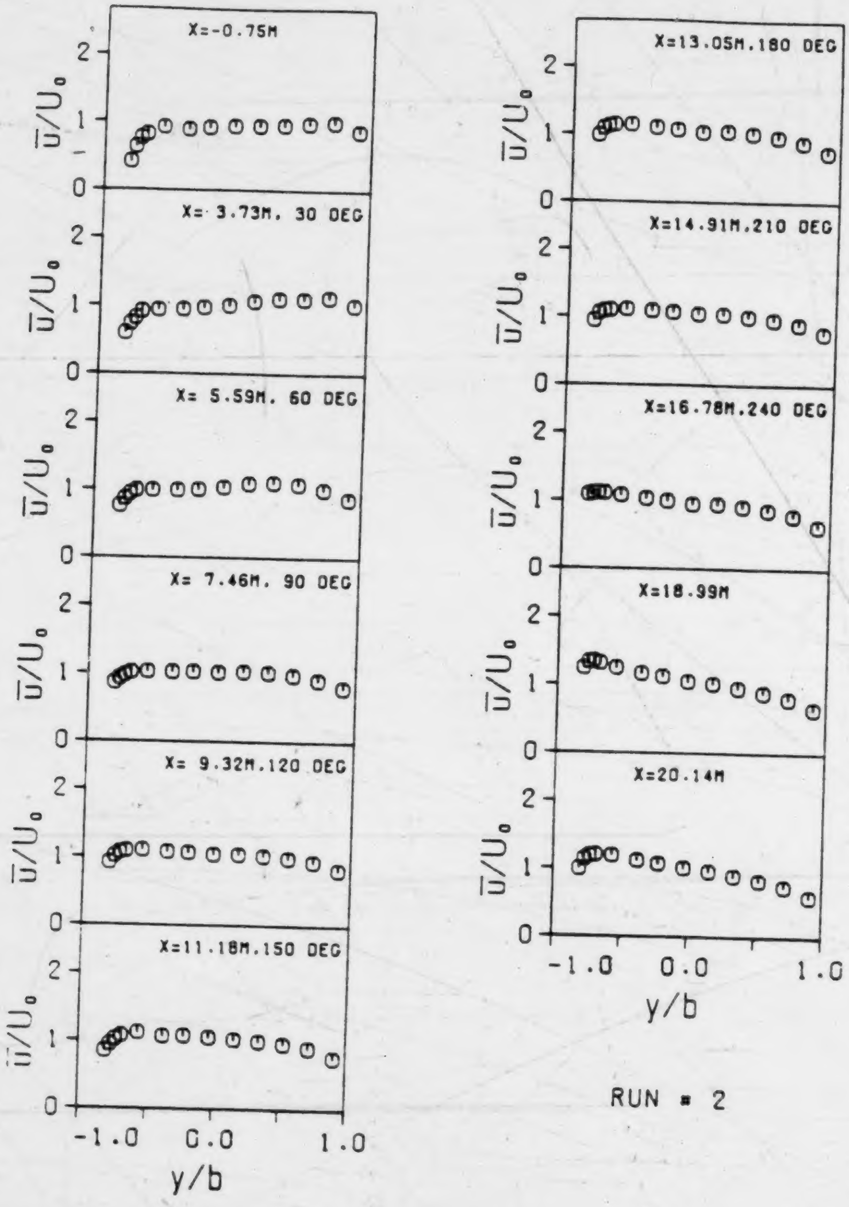

Figure 5.3 Profiles of depth-averaged longitudinal velocity (run 2)

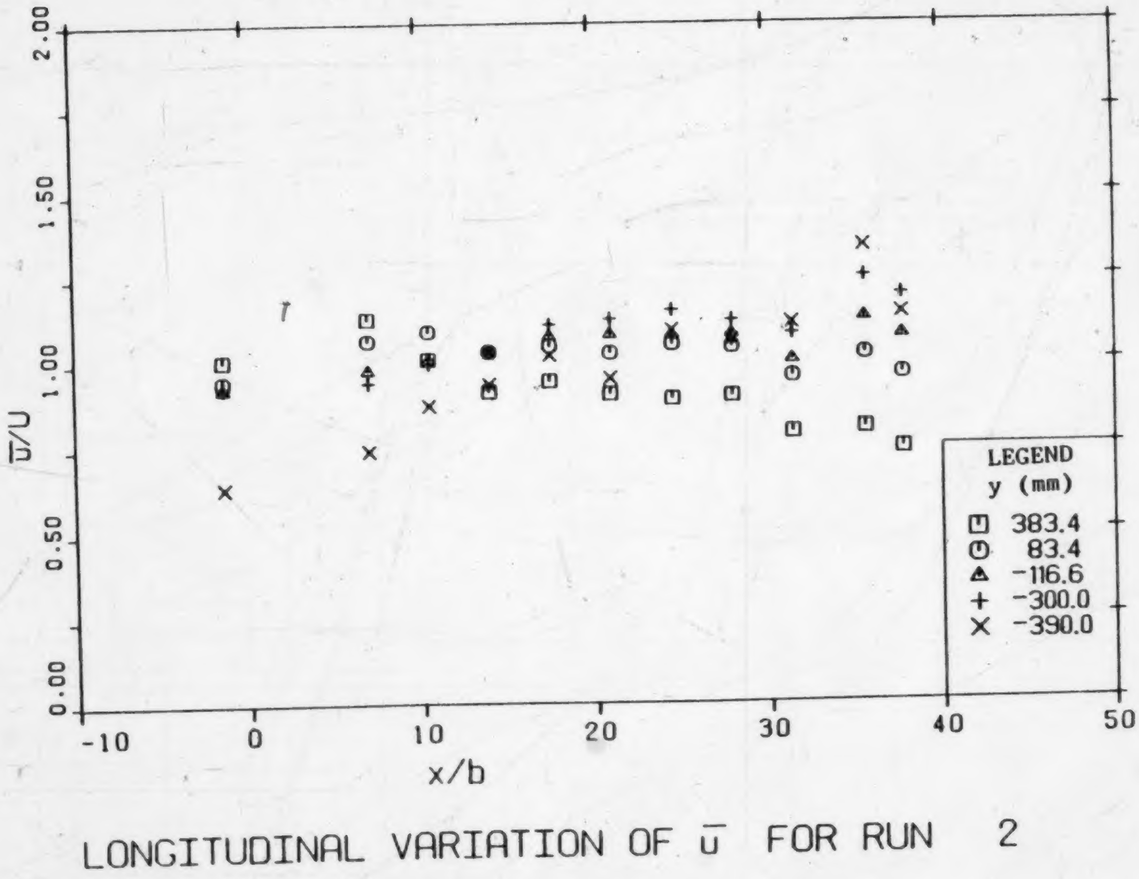

Figure 5.4 Longitudinal variations of longitudinal depth-averaged velocity (Run 2)

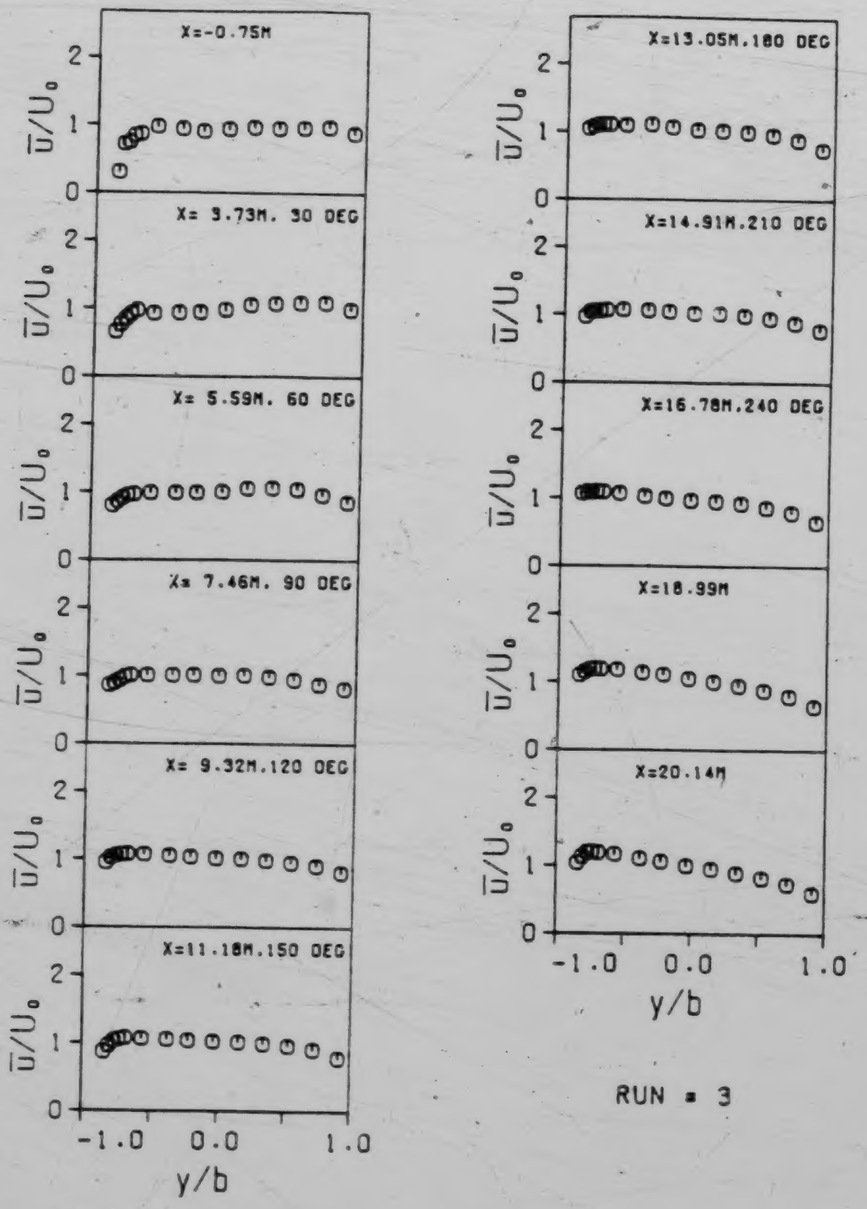

Figure 5.5 Profiles of depth-averaged longitudinal velocity (run 3)

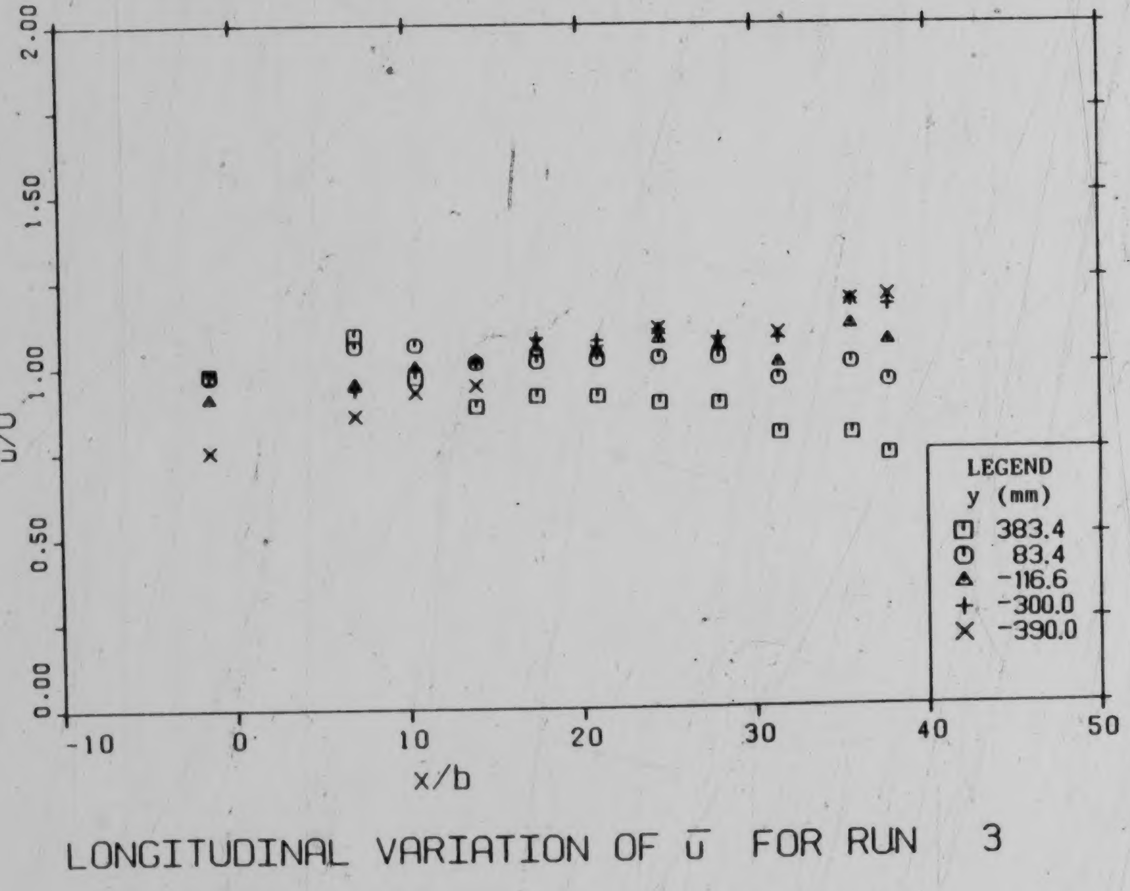

Figure 5.6 Longitudinal variations of longitudinal depth-averaged velocity (Run 3)

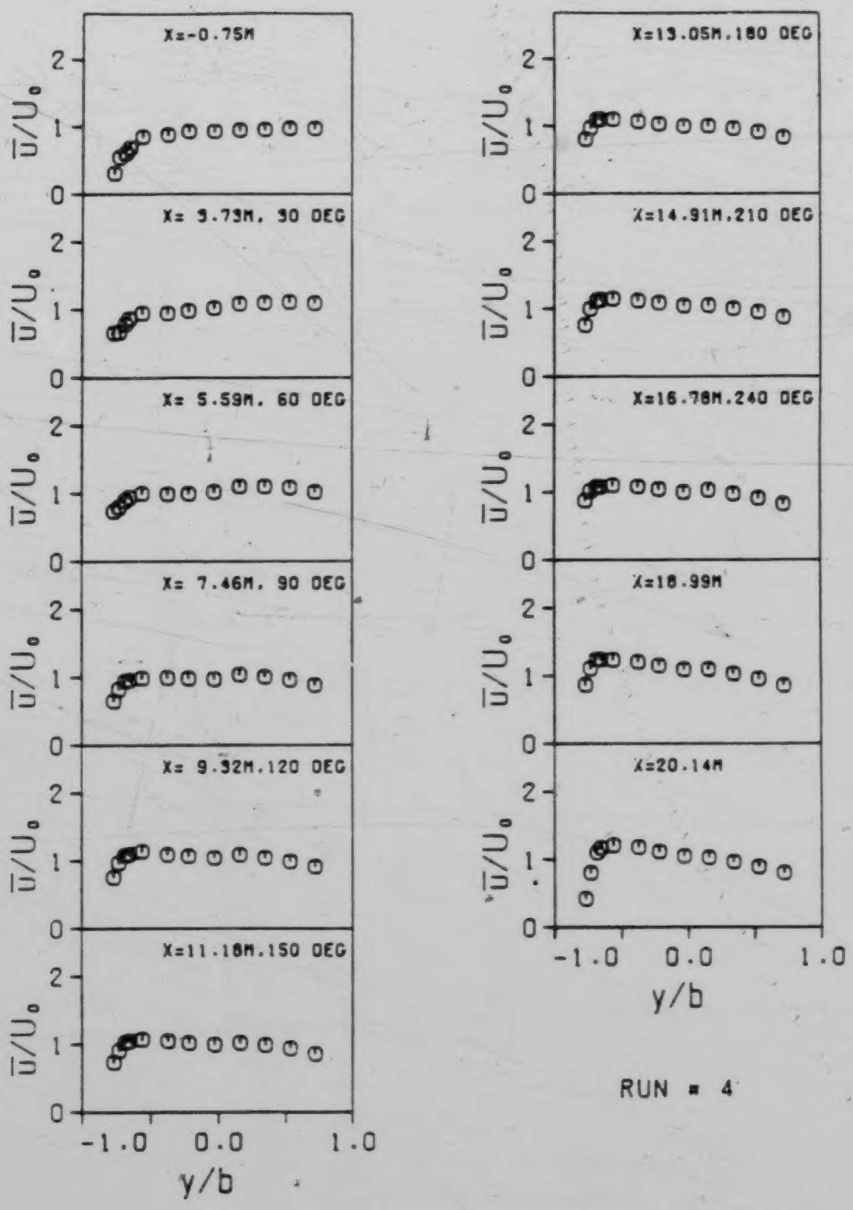

Figure 5.7 Profiles of depth-averaged longitudinal velocity (run 4)

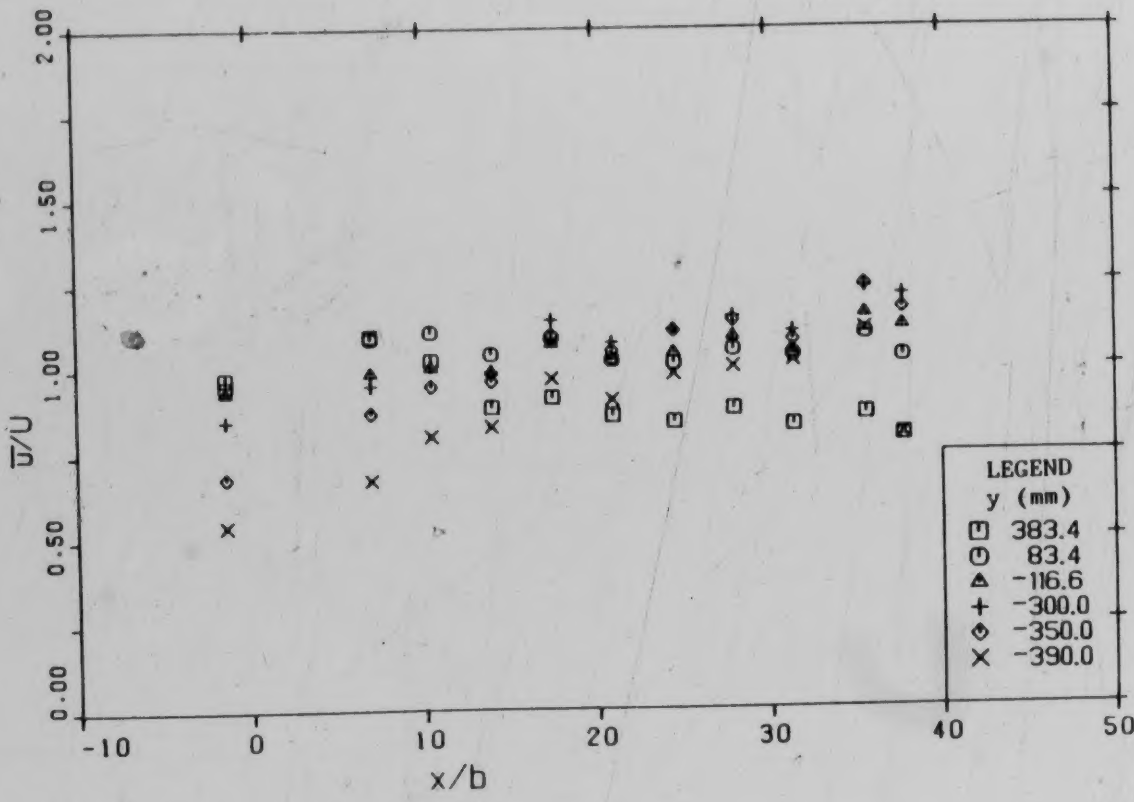

Figure 5.8 Longitudinal variations of longitudinal depth-averaged velocity (Run 4)

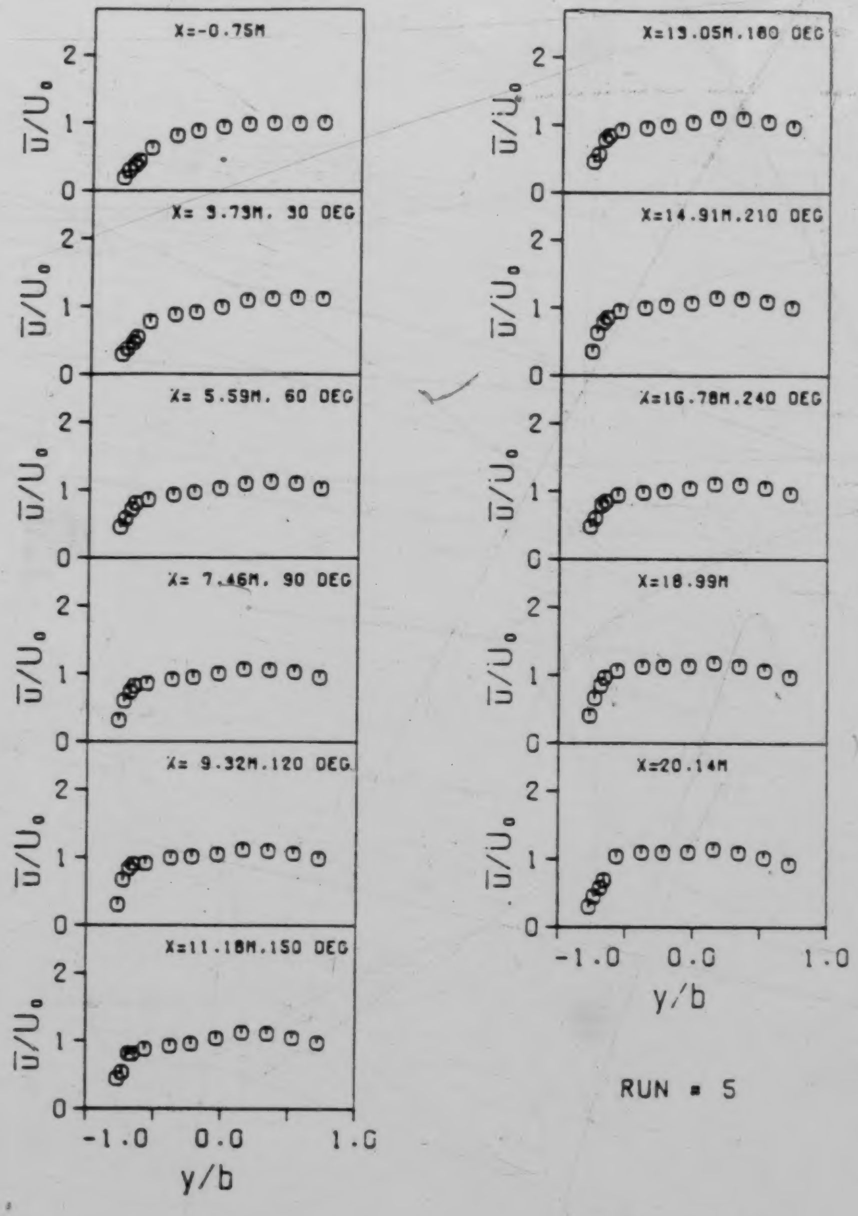

Figure 5.9 Profiles of depth-averaged longitudinal velocity (run 5)

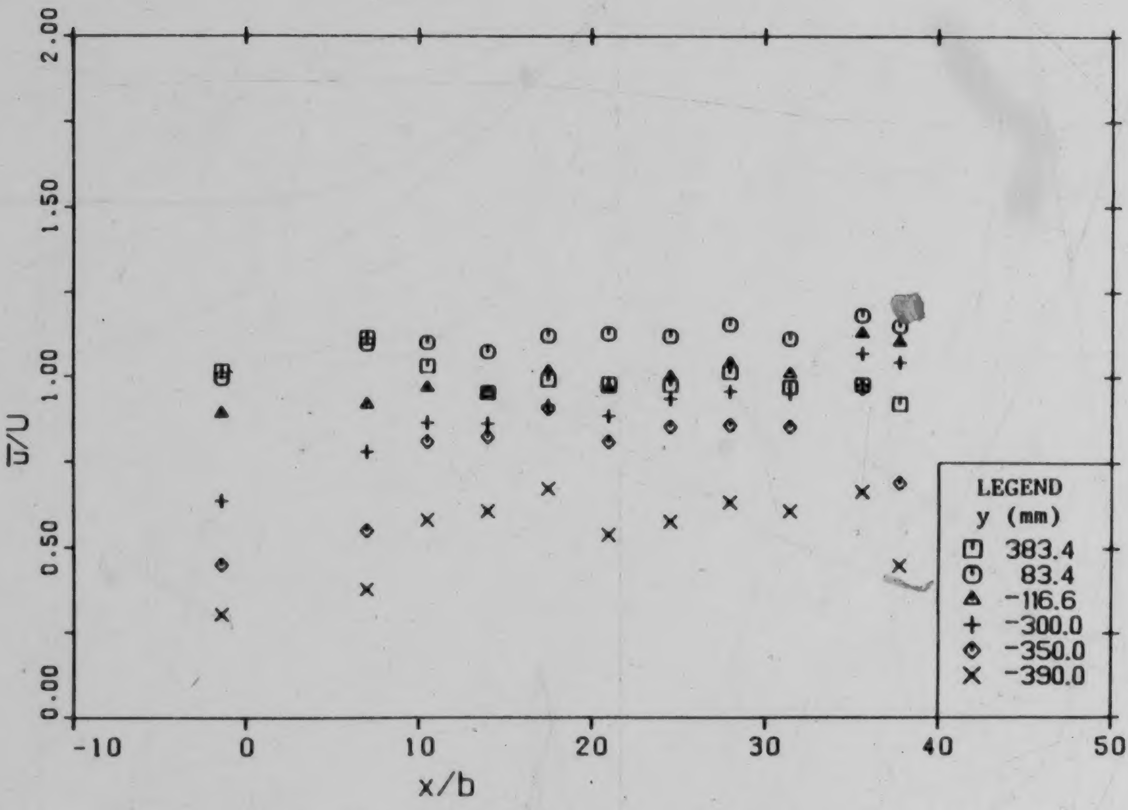

LONGITUDINAL VARIATION OF $\overline{u}$ FOR RUN 5

Figure 5.10 Longitudinal variations of longitudinal depth-averaged velocity (run 5)

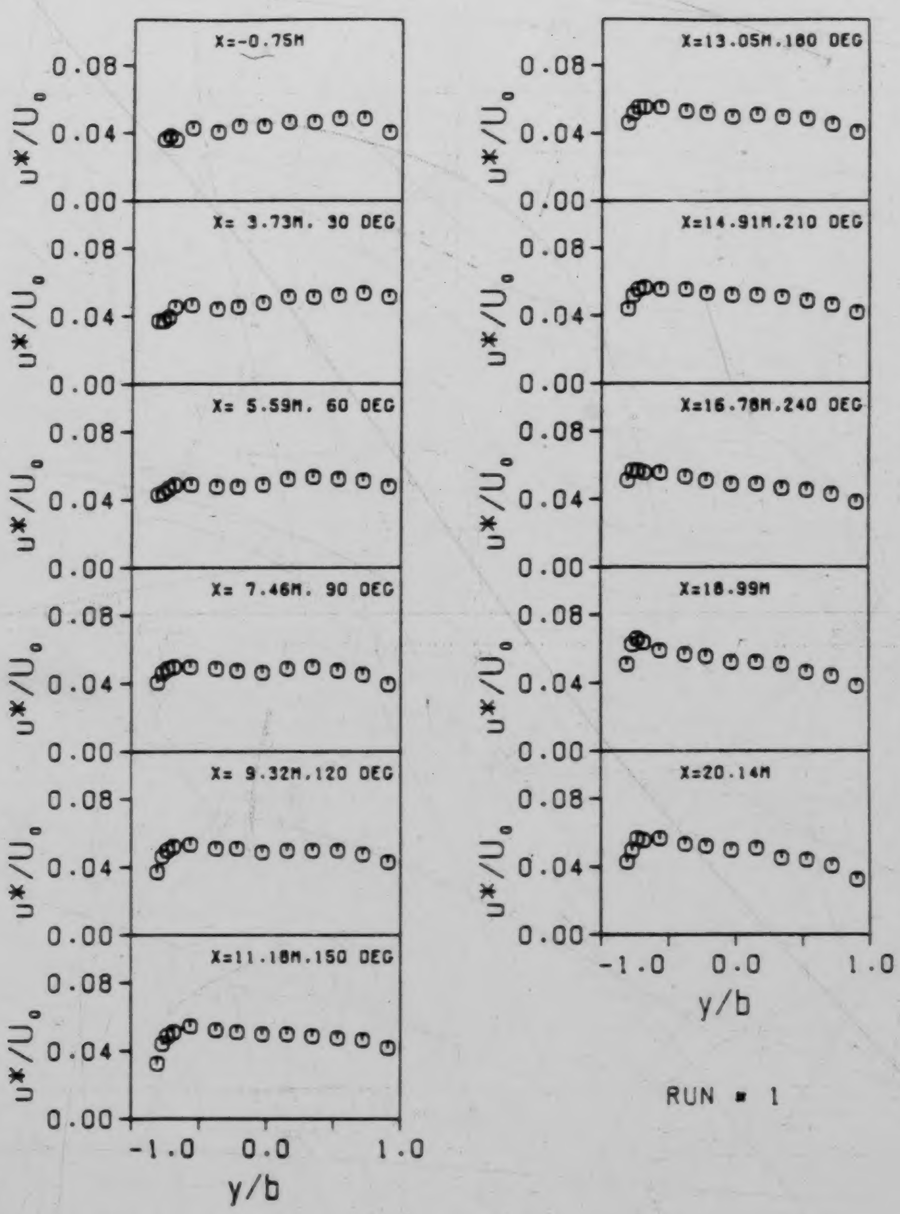

Figure 5.11 Profiles of longitudinal shear velocity (run 1)

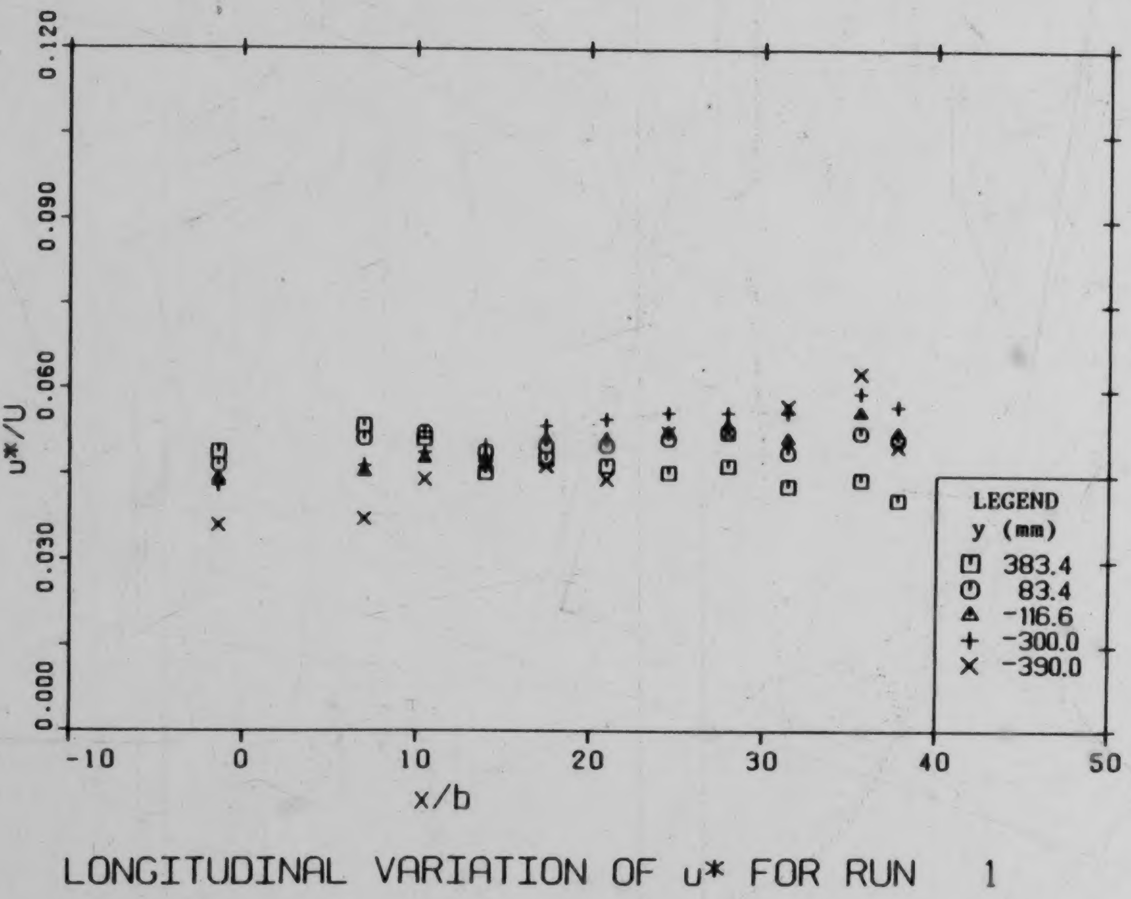

Figure 5.12 Longitudinal variations of shear velocity (run 1)

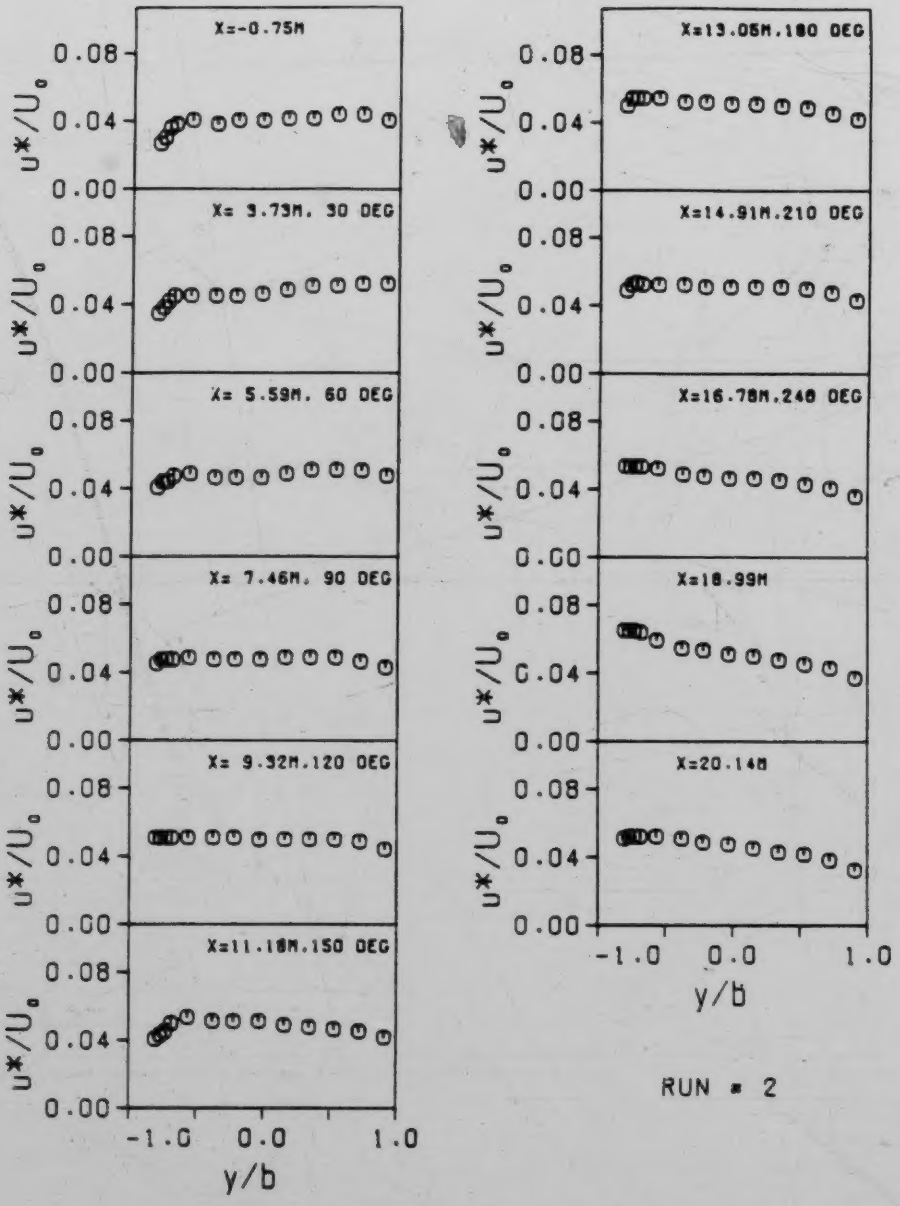

Figure 5.13 Profiles of longitudinal shear velocity (run 2)

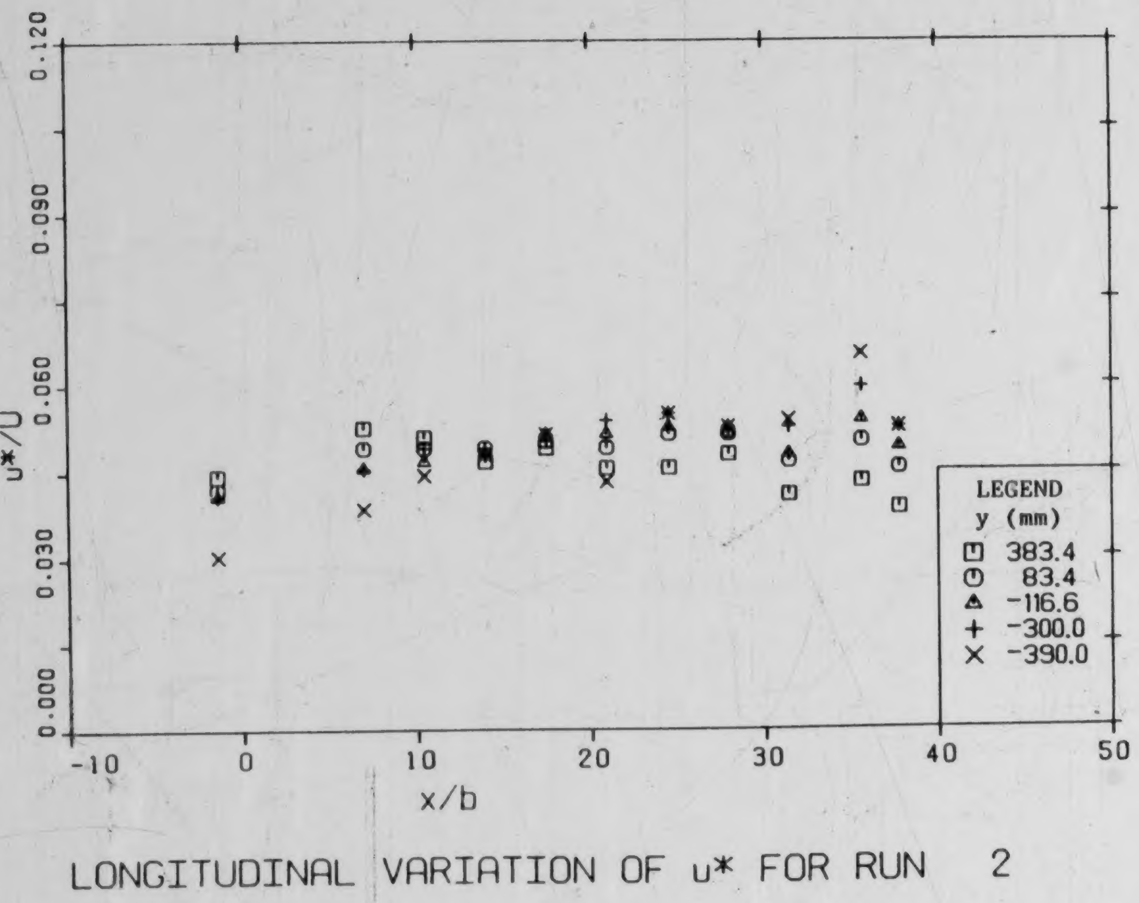

Figure 5.14 Longitudinal variations of shear velocity (run 2)

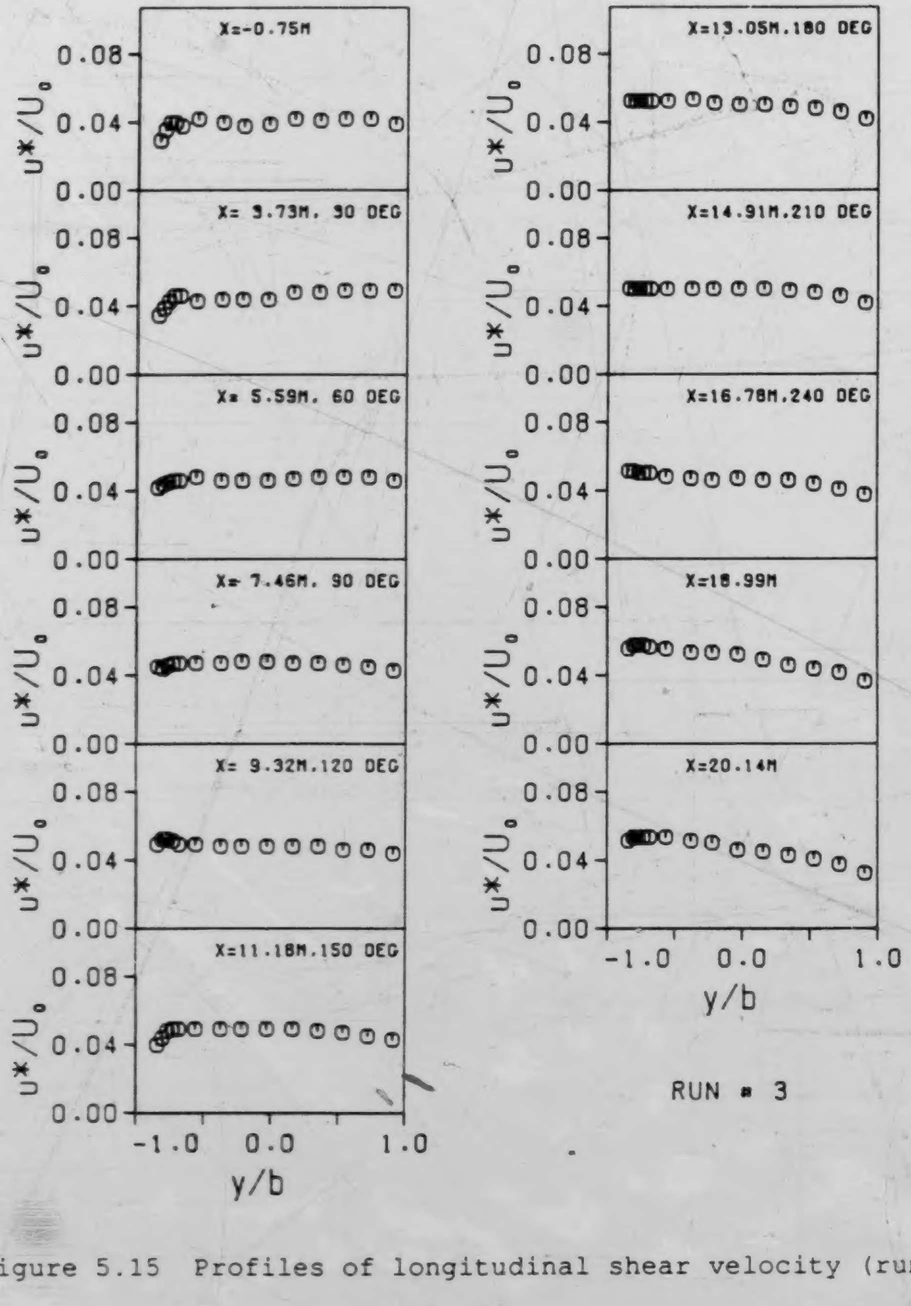

Figure 5.15 Profiles of longitudinal shear velocity (run 3)

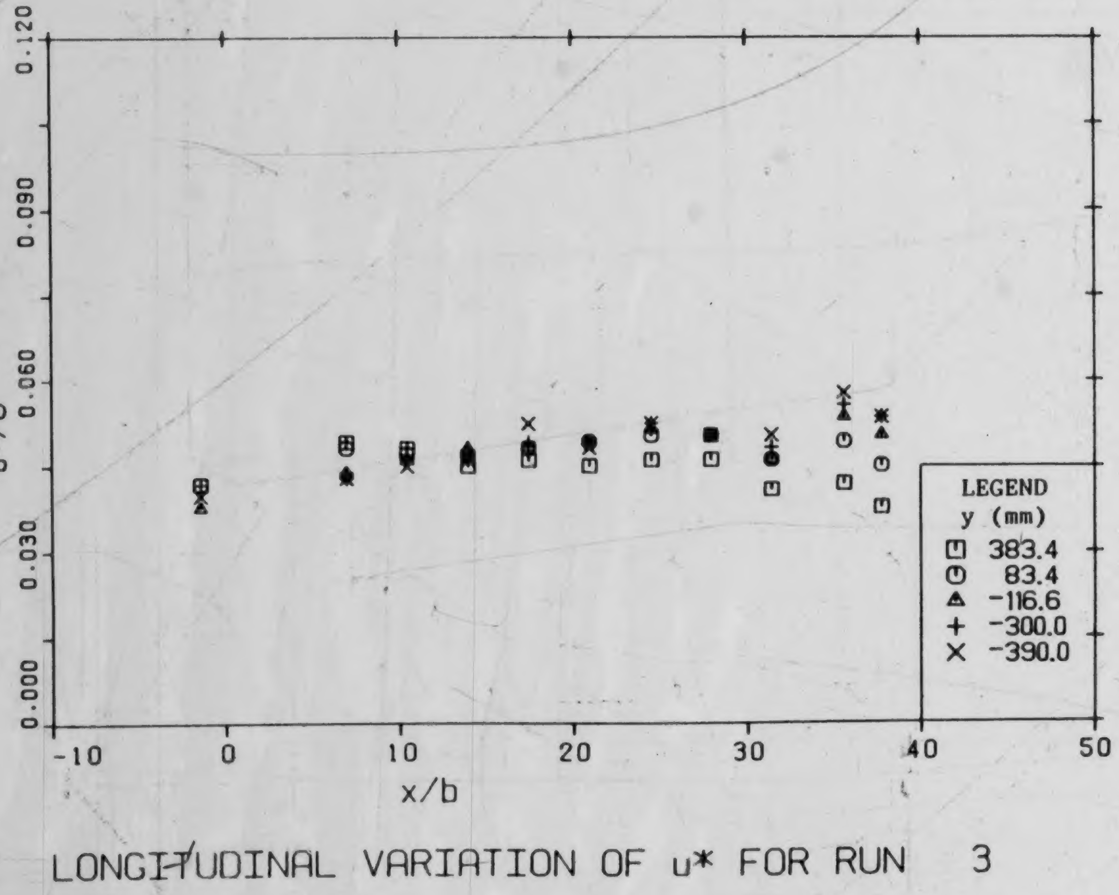

Figure 5.16 Longitudinal variations of shear velocity (run 3)

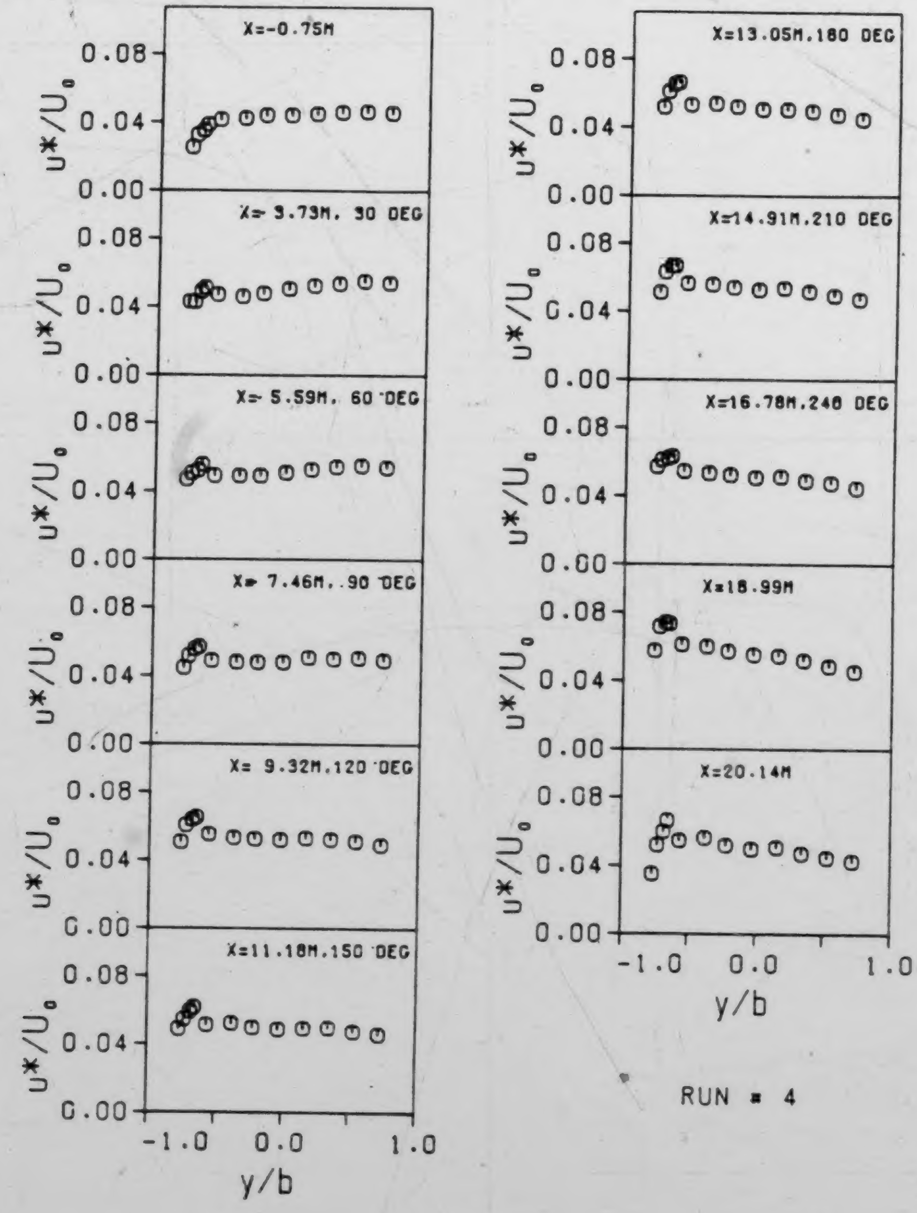

Figure 5.17 Profiles of longitudinal shear velocity (run 4)

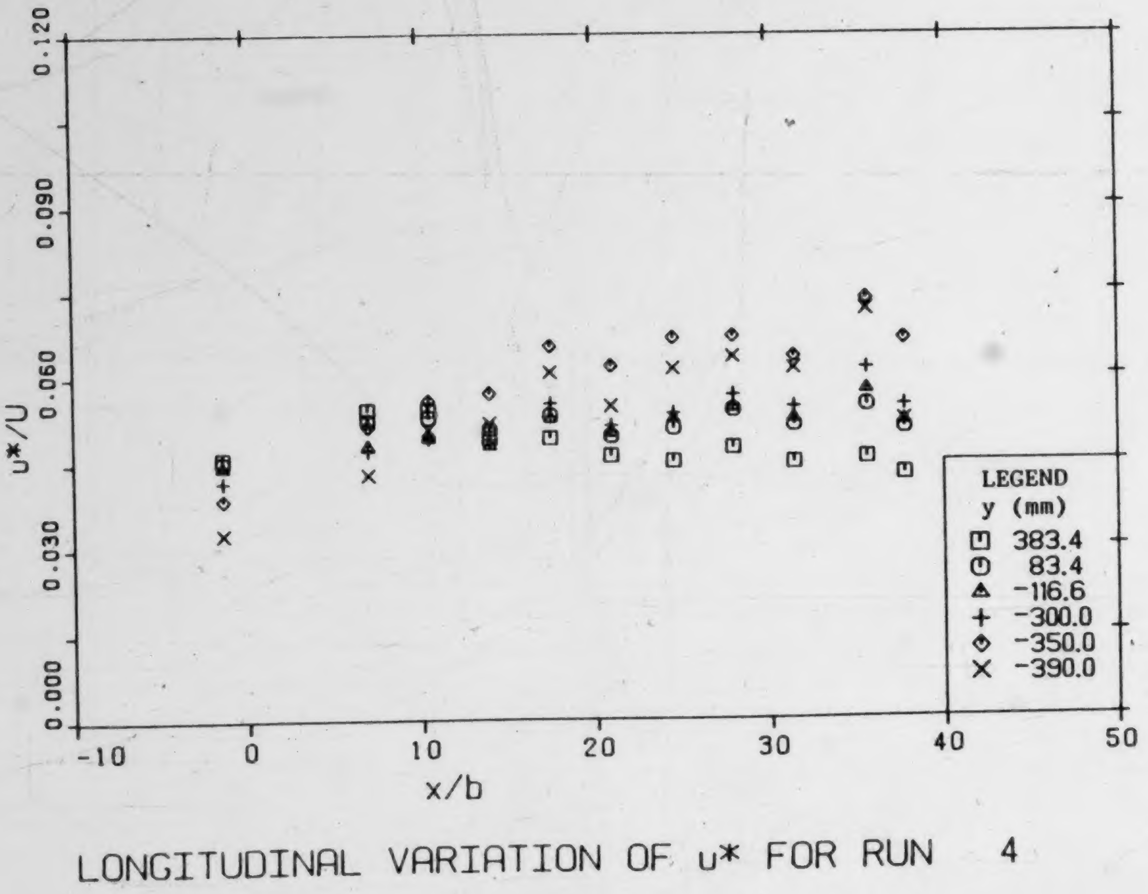

Figure 5.18 Longitudinal variations of shear velocity (run 4)

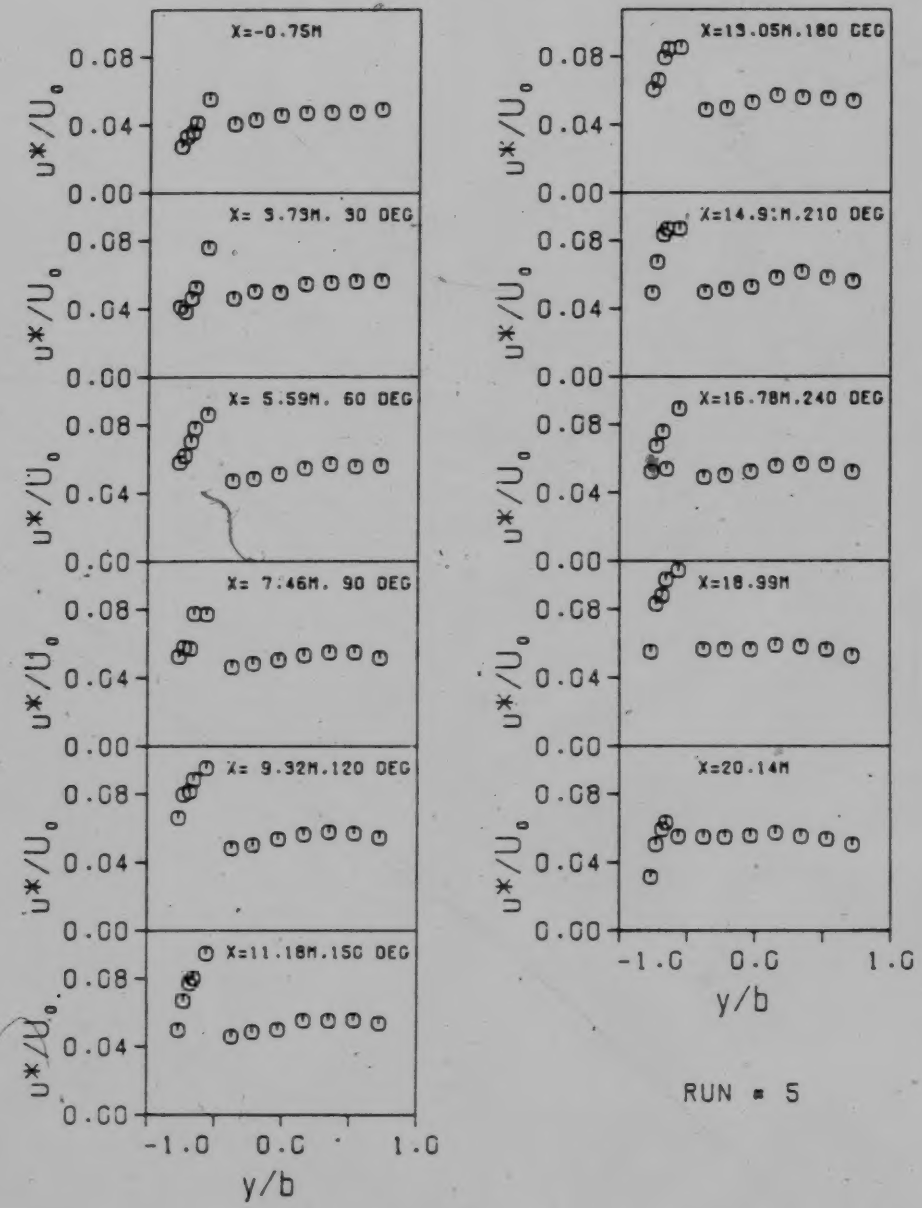

Figure 5.19 Profiles of longitudinal shear velocity (run 5)

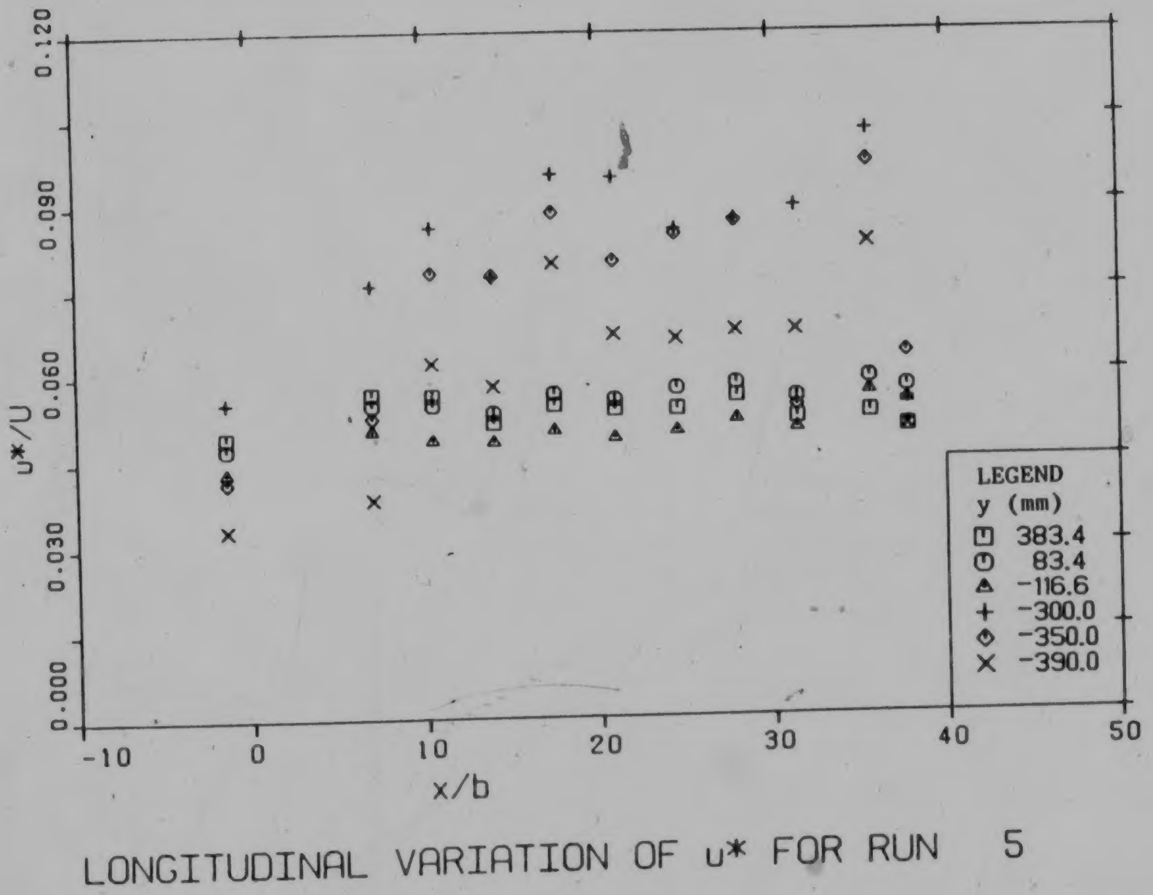

Figure 5.20 Longitudinal variations of shear velocity (run 5)

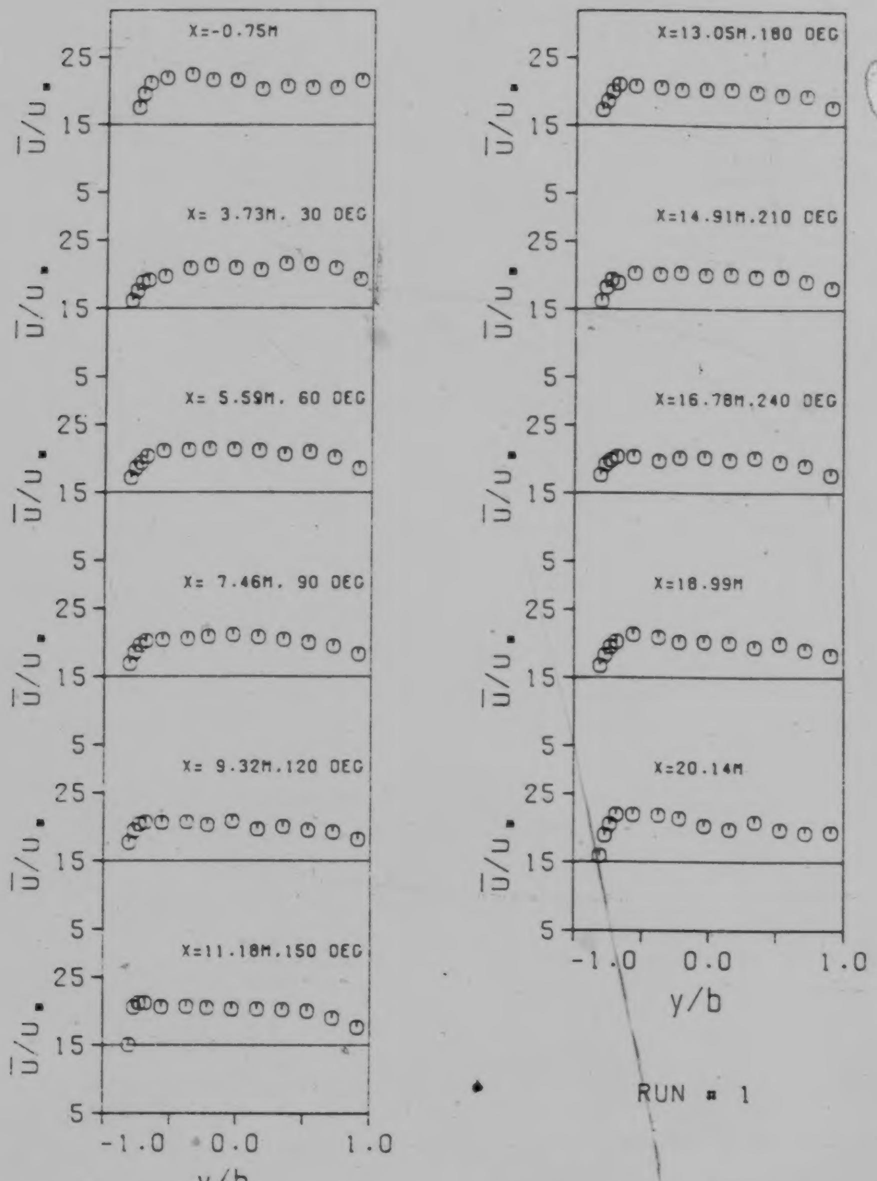

Figure 5.21 Distribution of longitudinal C_* (run 1)

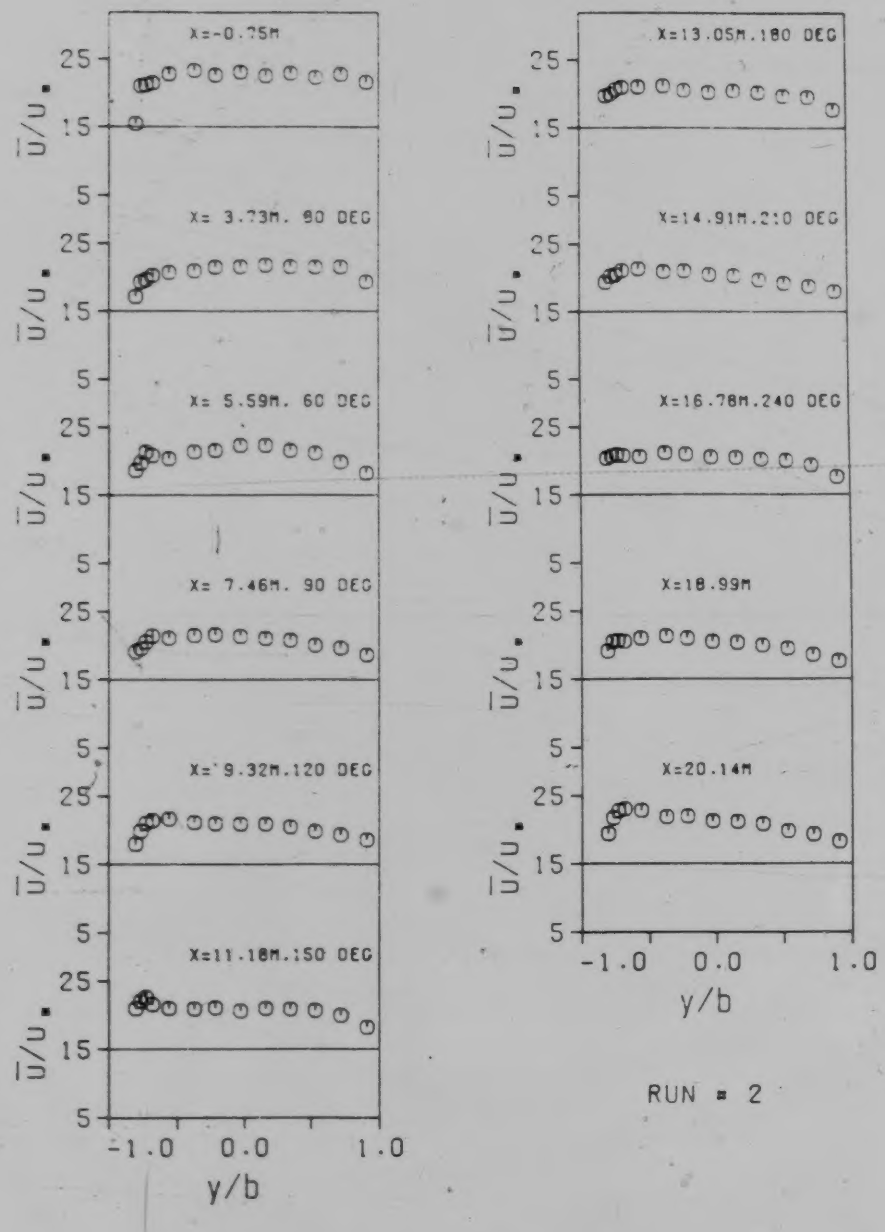

Figure 5.22 Distribution of longitudinal C_* (run 2)

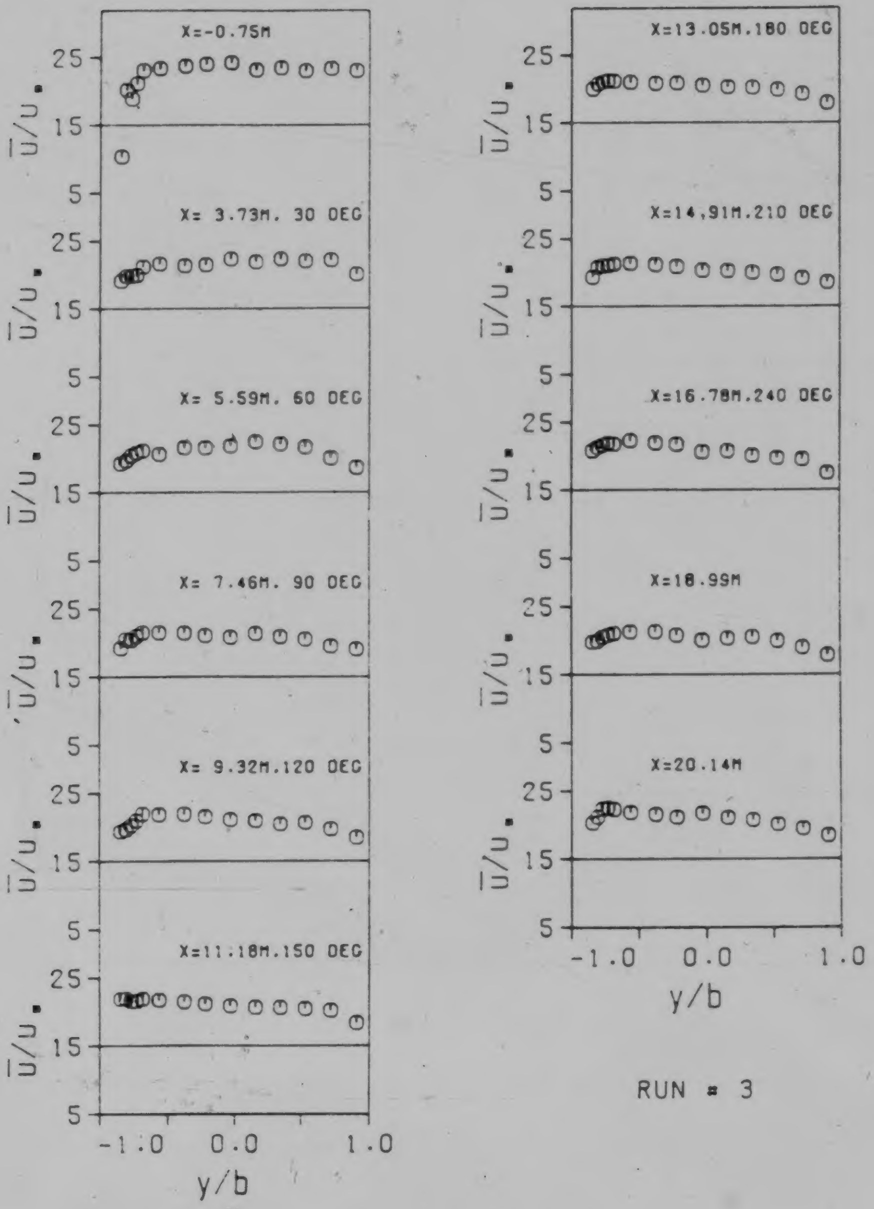

Figure 5.23 Distribution of longitudinal C_* (run 3)

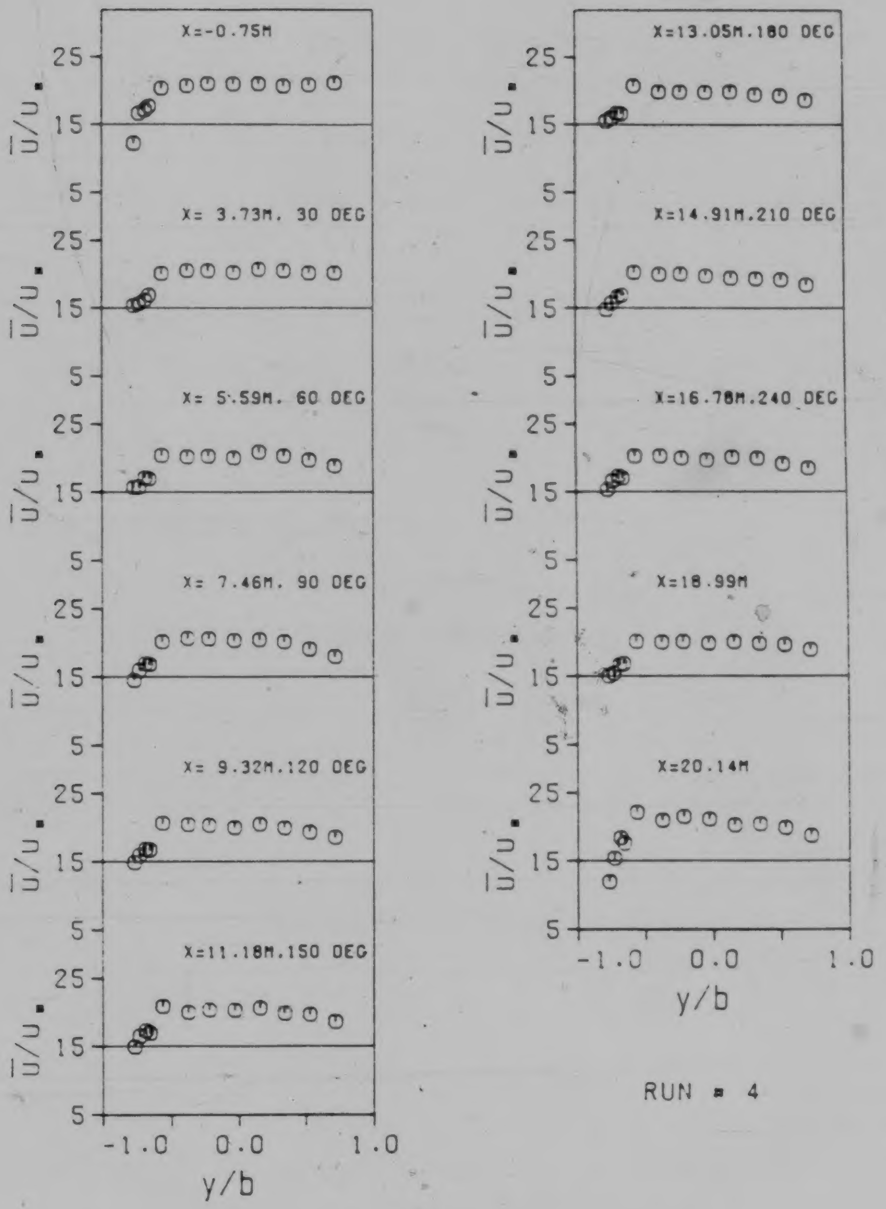

Figure 5.24 Distribution of longitudinal C* (run 4)

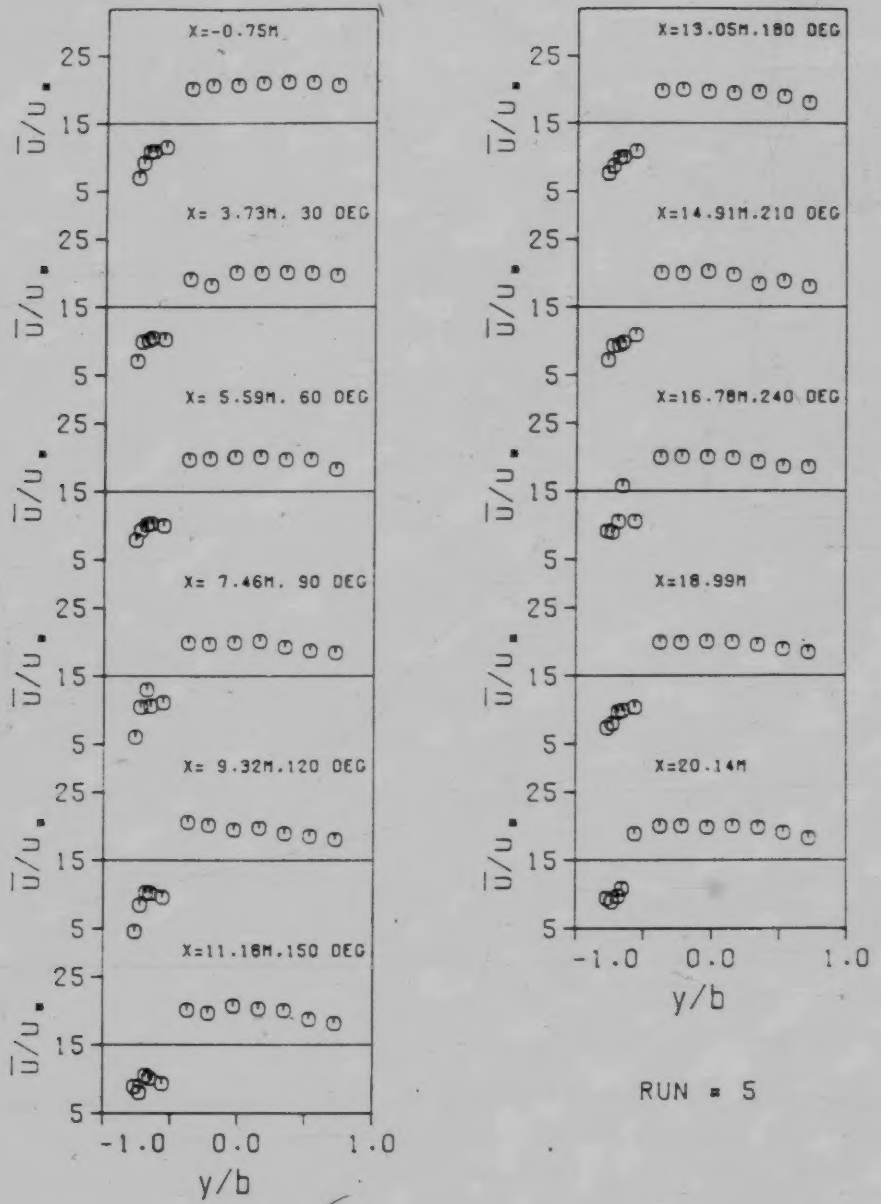

Figure 5.25 Distribution of longitudinal C_* (run 5)

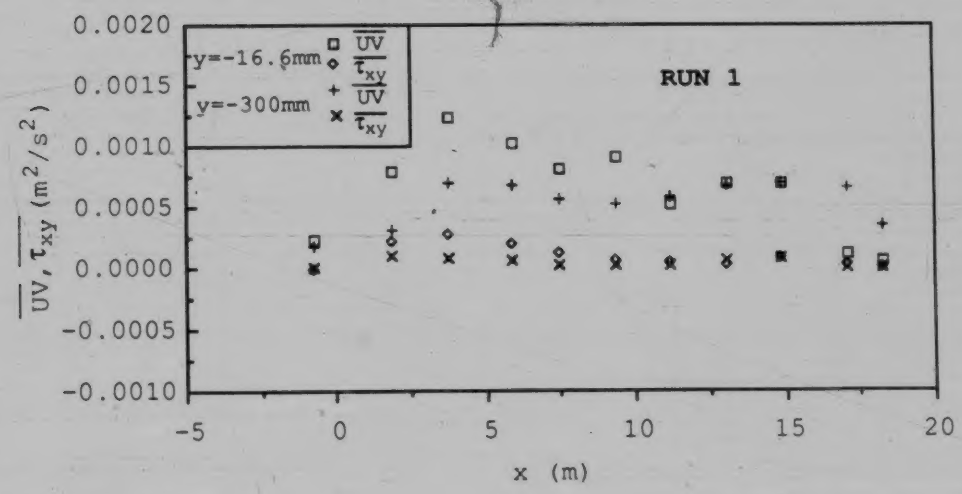

Figure 5.26 Longitudinal variation of $\overline{UV}$ and $\overline{\tau_{xy}}$ for run 1

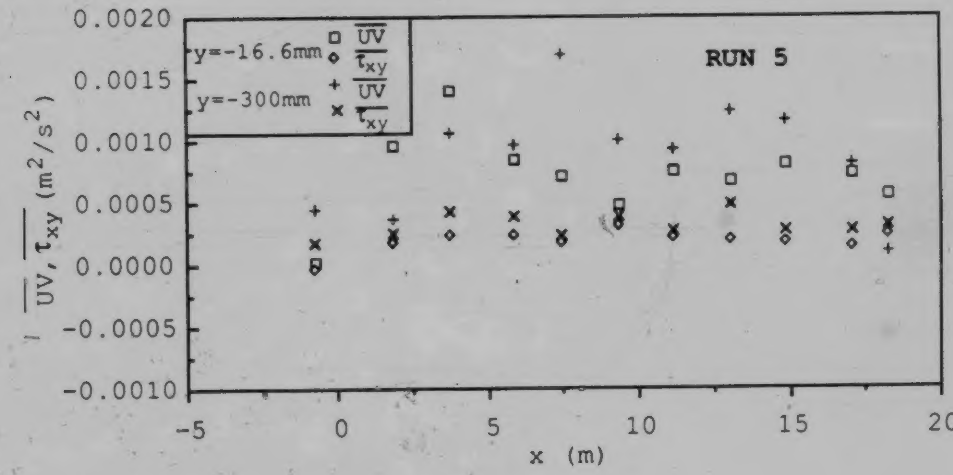

Figure 5.27 Longitudinal variation of $\overline{UV}$ and $\overline{\tau_{xy}}$ for run 5

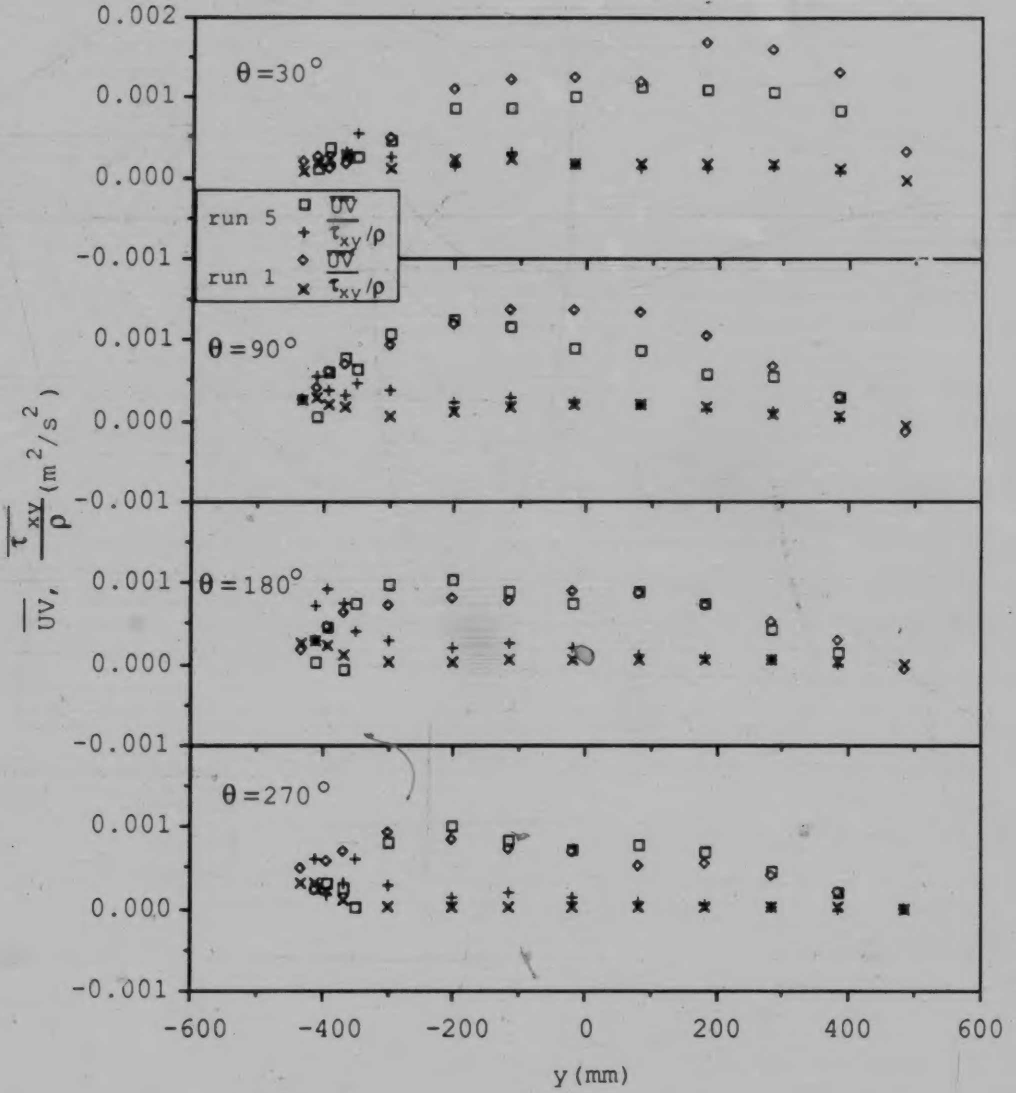

Figure 5.28 Transverse variation of $\overline{UV}$ and $\overline{\tau_{xy}}$ for runs 1 and 5

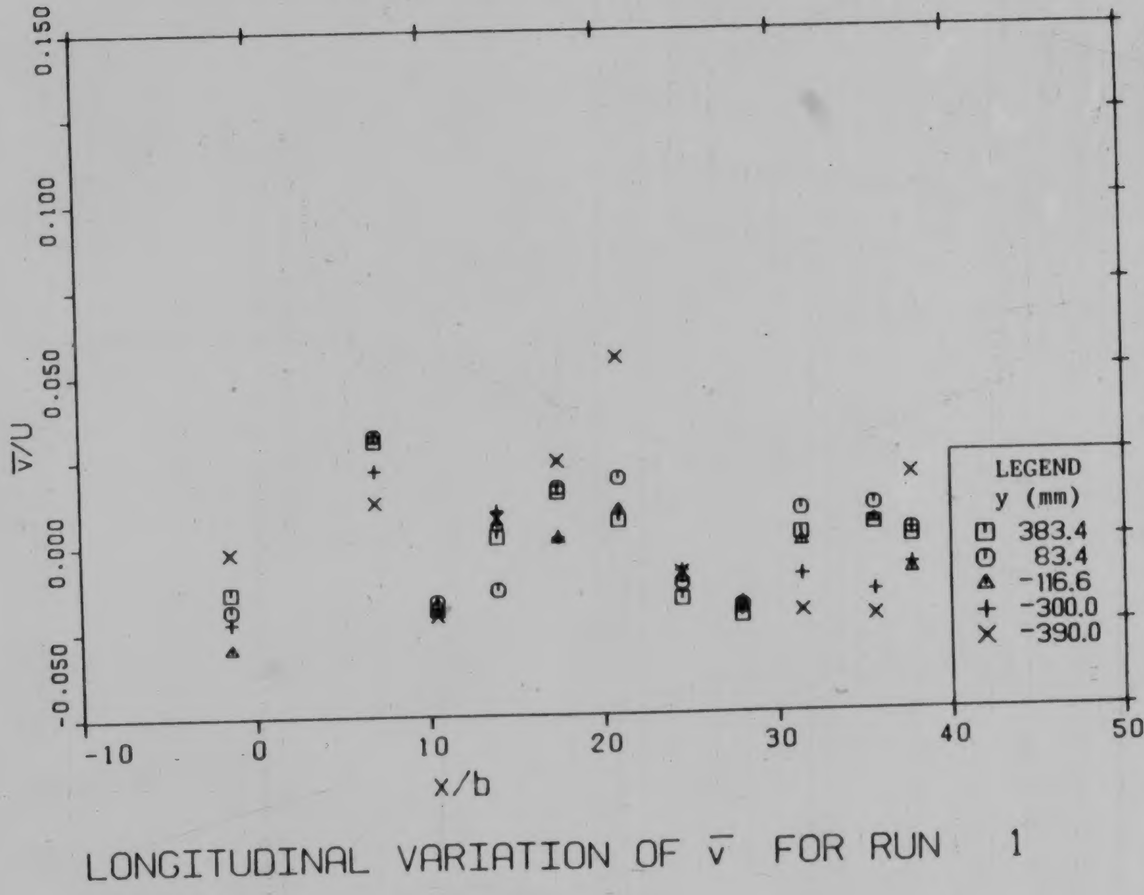

Figure 5.29 Longitudinal variations of depth-averaged tranverse velocity (run 1)

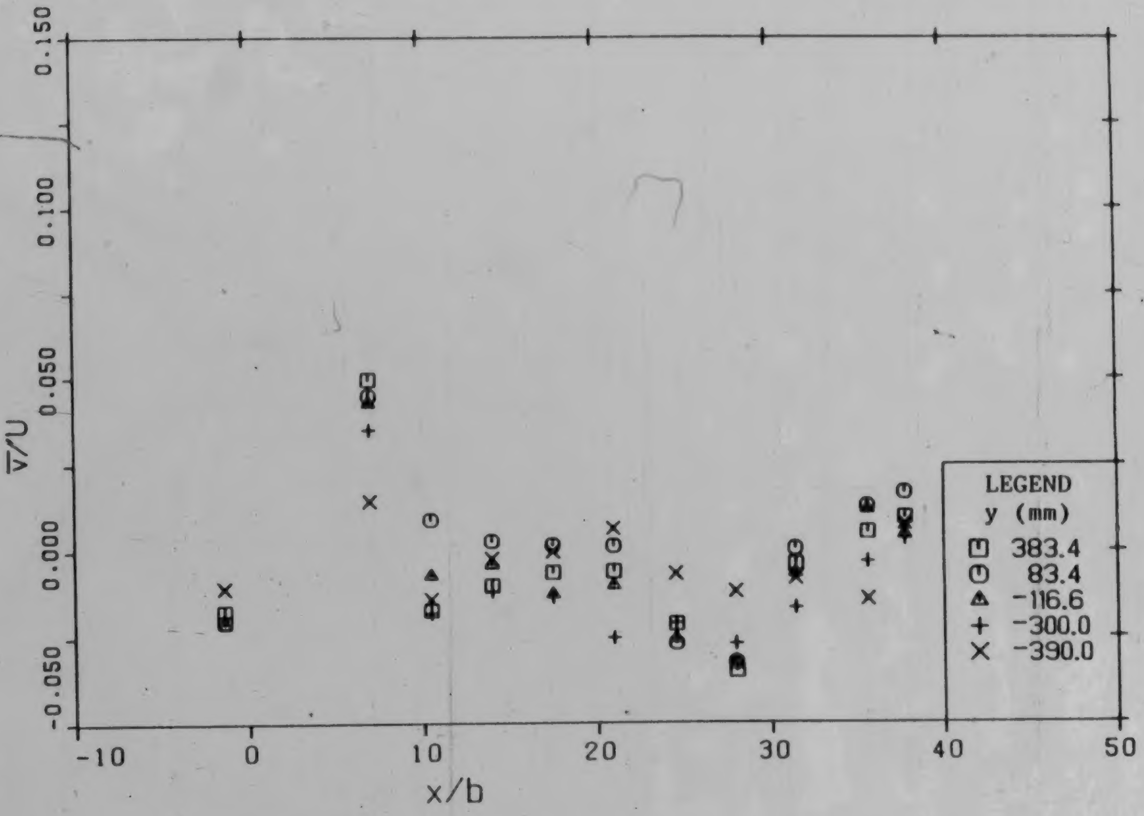

LONGITUDINAL VARIATION OF $\overline{v}$ FOR RUN 2

Figure 5.30 Longitudinal variations of depth-averaged tranverse velocity (run 2)

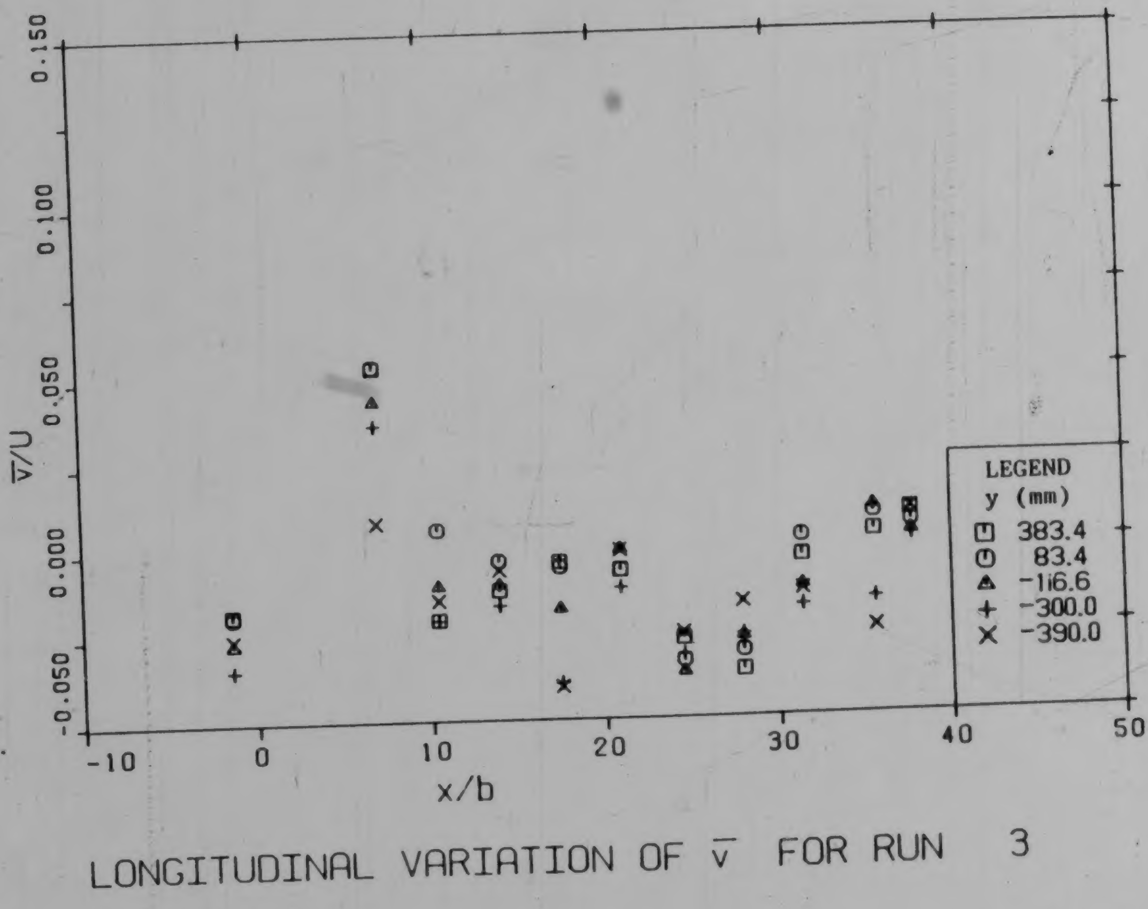

Figure 5.31 Longitudinal variations of depth-averaged tranverse velocity (run 3)

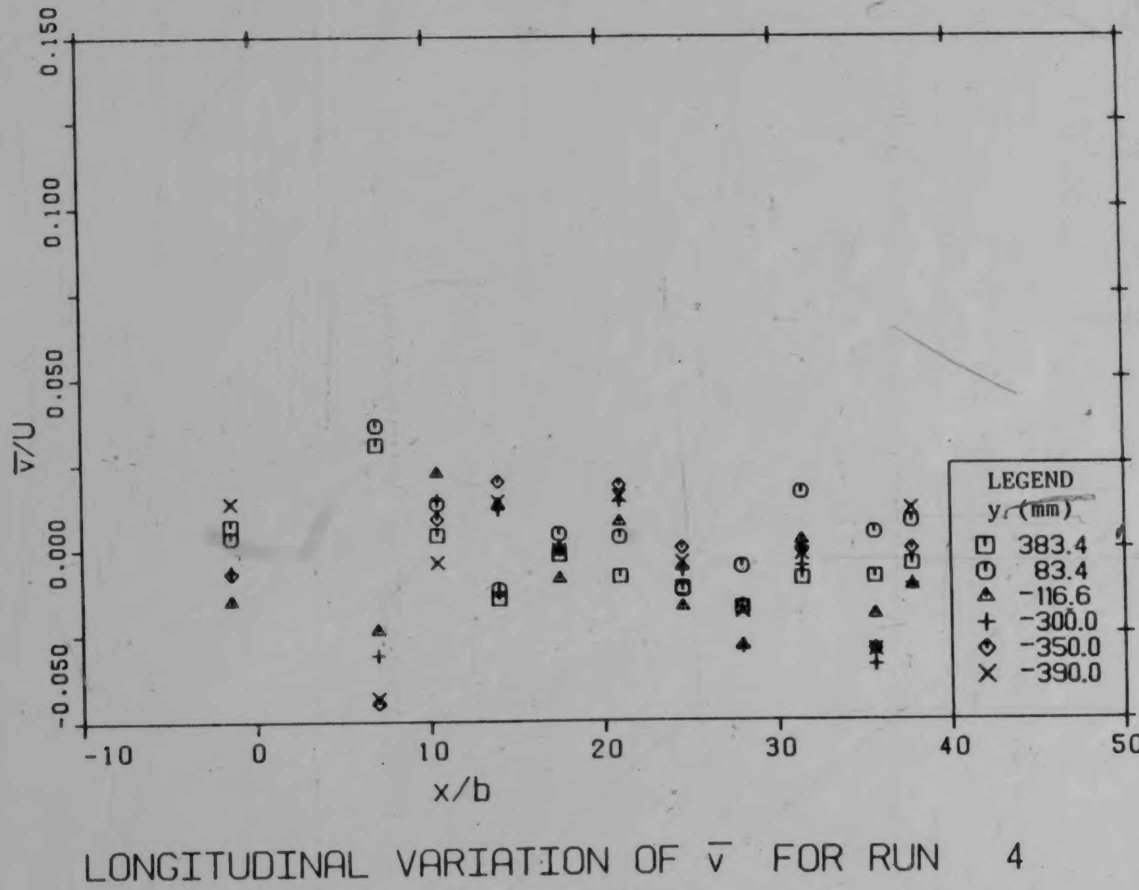

Figure 5.32 Longitudinal variations of depth-averaged tranverse velocity (run 4)

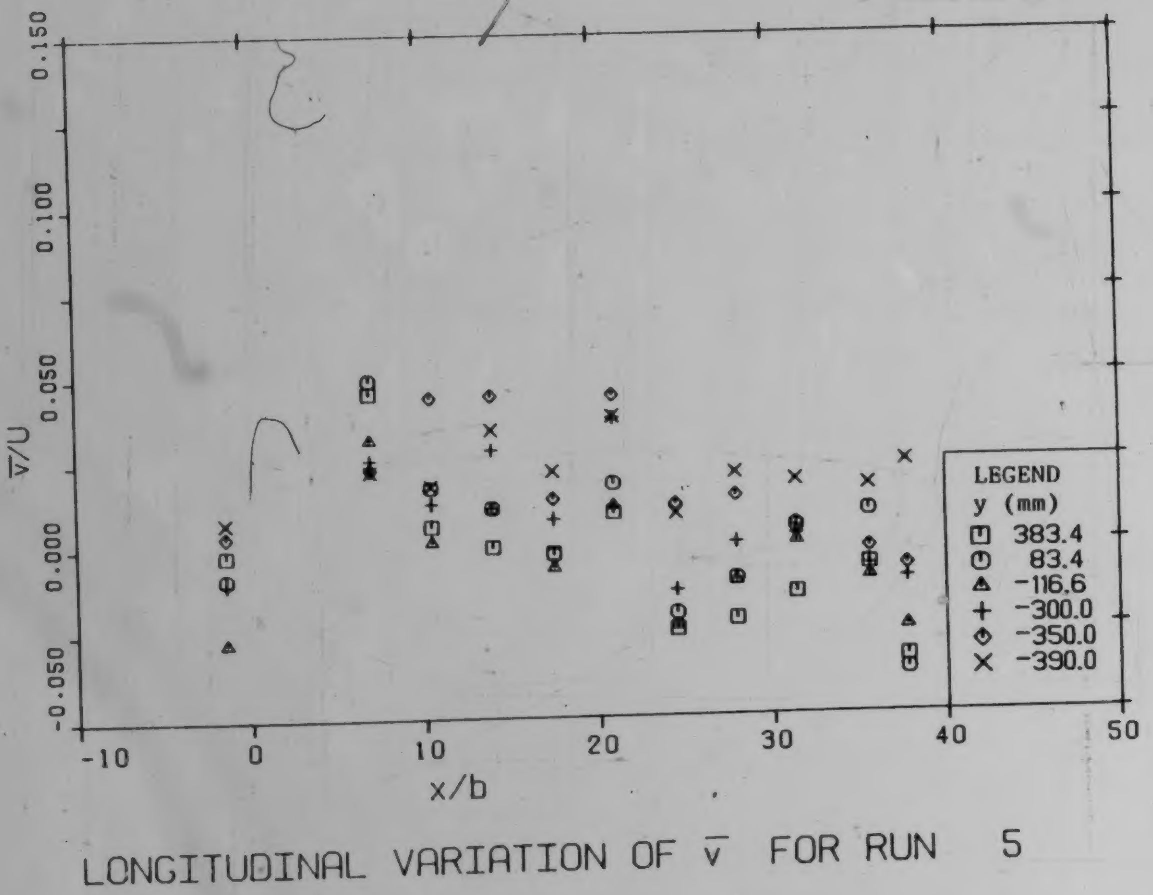

Figure 5.33 Longitudinal variations of depth-averaged tranverse velocity (run 5)

6 COMPARISON AND DISCUSSION

There is a large amount of experimental data on curved open channel flow suitable for comparison with the results of numerical calculation. However, detailed and reliable data are scarce and hard to obtain. The experimental results obtained by Steffler (1984) and De Vriend (1976,77) were used first to assess the reliability of the numerical prediction. The experimental data of run 1 from the previous chapter is also compared and discussed.

6.1 Steffler's Experiments

The experimental set up was introduced in section 2.2.2.1. Figure 6.1 shows the finite elements mesh with 504 nodes and 451 elements used in the calculation. The flow was assumed to be uniform at the beginning and the end sections.

Equation 2.80 is used to obtain $k_*=-2$ for the computation. Figure 6.2 shows the longitudinal velocity distribution found by solving the depth-averaged continuity and two momentum equations, neglecting the depth-averaged fluctuating velocities U and V. The figure shows that as the flow enters the bend, the velocity decreases on the outside bank and increases on the inside bank. The longitudinal velocity profiles remain unchanged throughout the bend. At the exit of the bend, the velocity at the outside starts to decrease and velocity becomes uniform very quickly. This phenomenon is different from the velocity redistribution of weakly curved bends illustrated by Rozovskii (1957). Therefore, it might be necessary to model the curved open channel problem with the complete set of equations presented earlier. The following analysis is to show the use of the complete set of equations is adequate.

Figure 6.3 shows the solution given by the present model. The velocity redistribution illustrated by previous investigators (Ippen et. al., 1962 and Yen, 1965) is clearly preserved. The maximum velocity first occurred at the inner bank of the entrance to the bend, then the velocity distribution tends to be uniform. At about 60° in the flow the maximum velocity starts to shift to the outer bank. At the exit of the bend the velocity at outer bank reaches a maximum. The comparison of Figures 6.2 and 6.3 shows that the present model can predict the longitudinal velocity redistribution well.

In a curved channel the streamline does not necessarily have to follow the channel geometry. However, this has been implied in other two dimensional analysis using cylindrical coordinate system modelling the flow in bend. The velocity vectors shown in figure 6.3 do not coincide with the channel, and may befit the real flow situation more.

The comparison for the longitudinal depth-averaged velocity between the numerical prediction and the experimental results is shown in figure 6.4. For ten cross sections (0° to 270°) the numerical calculation provides a good estimation except near the inner bank of the channel where the wall effect is not well described in the analysis.

Figure 6.5 compares results for the surface velocity in the transverse direction. As can be seen, the agreement is only fair. However, the characteristic features of the secondary flow such as the outward flow at the entrance and the tendency of the velocity profile have been preserved. It also should be noted that the surface velocity used is a "scale" of secondary flow in the calculation and relies on the linear profile assumption (equation 2.65). Therefore a good fit for the secondary velocity through most of the depth need not imply a good prediction of the surface velocity if the velocity distribution is significantly non-linear.

In figure 6.6, the predicted and experimental depths are compared for the 10 cross sections. The downstream depth has been set as a fixed boundary condition in the numerical calculation, but in the experiment the downstream depth is fixed by a tailgate. The difference between the two can be attributed to backwater effects. The discrepancy found at the upstream may also be explained by the fixed depth downstream boundary condition used.

In figure 6.7, predicted and experimental vertical distributions of longitudinal velocity at cross sections θ=0°, 90°, 180° and 270° are compared. The agreement is very satisfactory for velocity profiles at $y/b=-0.4$, 0 and 0.4.

The surface velocities closed to the wall are overestimated by 10 to 20 percent.

Figure 6.8 shows predicted and measured vertical distributions of the transverse velocity at the same sections as in figures 6.7. The agreement is fair in general. The model gave good predictions for the profiles away from the side walls. Since the depth-averaged model is limited to wide open channels, the discrepancy in the profiles near the wall are to be expected. This can also be explained as a consequence of the linear function used in modelling the secondary flow motion. Despite the above discrepancy, the model still satisfactorily predicts the surface velocity at the inside bank and the velocity close to the bed at the outside bank. It should be noted here that the secondary flow is a perturbation on the main flow. This implies that a relatively large error in secondary flow prediction corresponds to small error in the overall flow. Therefore, the discrepancy found in the secondary flow prediction while the good fit for the main flow calculation is resonable.

The comparison of velocities for run 2 is plotted in figures 6.9 and 6.10. Here again satisfactory agreement is achieved between the experimental and numerical results. The wall effect in the second run is more obvious than the first run. The comparison of the predicted and measured vertical distributions of the longitudinal velocity and transverse velocity at cross sections $\theta=0^\circ$, 90°, 180° and 270° are plotted in figures 6.11 and 6.12 respectively. The agreement is fair in general. As shown in figures 6.5 and 6.10 the experimental data of the secondary surface velocity near the outer wall tends to flow inward. The reverse flow can not be predicted by the linear function used. However, as can be seen in figures 6.8 and 6.12, the surface velocity in the inner bend and velocity close to bed in the outer bend are predicted well.

6.2 LFM Experiments

De Vriend (1976) conducted a series of experiments in a 180° curved flume at the laboratory of fluid mechanics of the Department of Civil Engineering, Delft University of Technology. One of these experiments was selected to assess the present model. The flume was rectangular in shape, 1.7m wide with a centreline radius of 4.25m. The discharge was 0.19 m^3/s, the Froude number $V^2/gd=0.215$ and a Chezy C=57 $m^{1/2}/s$ was used. The downstream water surface was constant and kept at 0.18m by a tailgate.

Figure 6.13 shows the longitudinal depth-averaged velocity distribution for the experimental data and the numerical prediction. As can be seen, the velocity distribution is represented very well.

6.3 De Vriend's Experiments

The experiment conducted by De Vriend (1977) for the flow of water in a curved channel with a fixed uneven bed was employed. Two runs were conducted in this experiment, only the one with a discharged of $0.463 m^3/s$ is compared. The channel used is similar to the one mentioned in section 2.2.2.2. Since a different Chezy C was used in De Vriend's original experimental report, the following logarithmic relation for Chezy C and local depth h is also used to estimate local C for each section

$$C = C_o + 18 \log\left(\frac{h}{h_o} \right) \tag{6.1}$$

in which C_o denotes the value of Chezy C at a uniform depth of h_o.

Figure 6.14 shows the comparison of the depth-averaged longitudinal velocities. The velocity scale is given for section A_1 and the subsequent sections have been raised by 0.4m/s each. The numerical prediction compares reasonably well with the experimental result. To keep the element aspect ratio smaller than 1 to 10 and minimized the number of nodes used in the finite element mesh, a coarse mesh was created in the calculation. There is a significant difference for the velocity close to the side wall as might be expected. The comparison of the transverse surface velocity is shown in figure 6.15 with velocity scale equal to 0.04m/s. Despite the approximate longitudinal bed slope of 0.0003 (the actual channel slope is non-uniform) and constant

k_* used in the calculation, this mathematical equation models the secondary flow fairly reasonably.

6.4 Comparison of the Experimental Data

Since all of those simulations in the previous sections indicated that the wall effect and the use of a linear distribution caused the model not to predict the secondary flow near the bank well, the secondary flow near the sloped bank in the experiment will not be predicted as expected. Therefore, only the first run among those five runs conducted was employed in the comparison. The roughened cases, which are of considerable interest, are not compared..

The simulation used a coarse mesh with 504 nodes and 451 elements. The grid is similar to the one used in section 6.1 except that the mesh was finer on the side slope. Since the code needs an initial guess to solve momentum equations, the uniform velocities and constant depth are used.

Figure 6.16 shows the numerical prediction of the longitudinal velocity distribution for run 1. The phenomena of the longitudinal velocity redistribution is well preserved.

Figures 6.17(a), (b) and (c) show the comparison of the longitudinal velocity profiles for each measurement section. With the uniform flow conditions provided in the approach, the numerical calculation shows that the flow is still uniform at the entrance of the curve. At section 2, $\theta=30°$, the model predicts a smaller depth averaged velocity close to the inner wall but agrees quite well in the outer section. The prediction is lower at the outer section at section 4 and following sections, indicating that the secondary flow predicted is less than the actual flow. The lateral distribution of the secondary flow surface velocity is compared in figures 6.18(a), (b) and (c). The secondary flow is under-estimated. The discrepancy may be due to the constant Chezy C used, the improper k_* derived, the linear function used for the secondary flow or the extrapolated experimental surface velocity.

Figure 6.19 shows the comparison of the momentum transport at section 2 (θ=30°), section 4 (θ=90°), section 7 (θ=180°) and section 10 (θ=210°). The calculated $\overline{UV}$ agrees well with the experimental data except at section 10. However, comparing with figure 5.28 in section 5.2.4 shows that the numerical prediction of the $\overline{UV}$ profile for section 10 is similar to experimental data of run 5. The calculated section is exactly at the exit of the curve and the experimental measurement station is at 0.15m downstream of the exit. This may explain the discrepancy shown in the comparison of section 10.

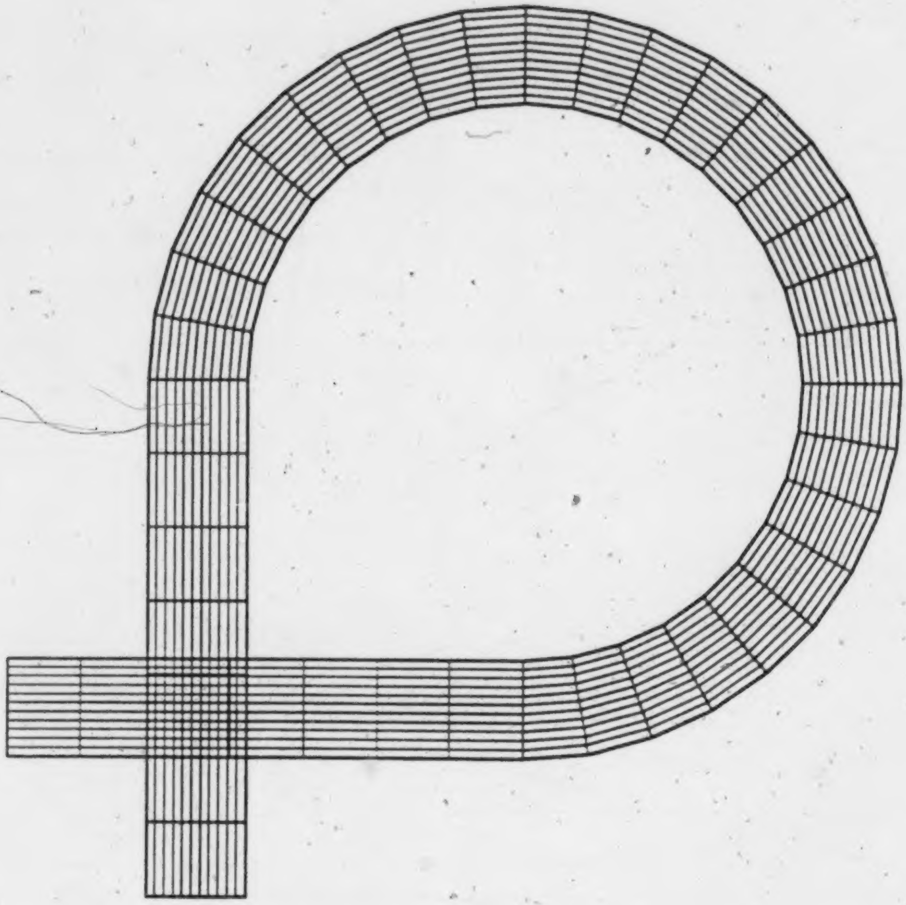

Figure 6.1 Finite element mesh for Steffler's experiment

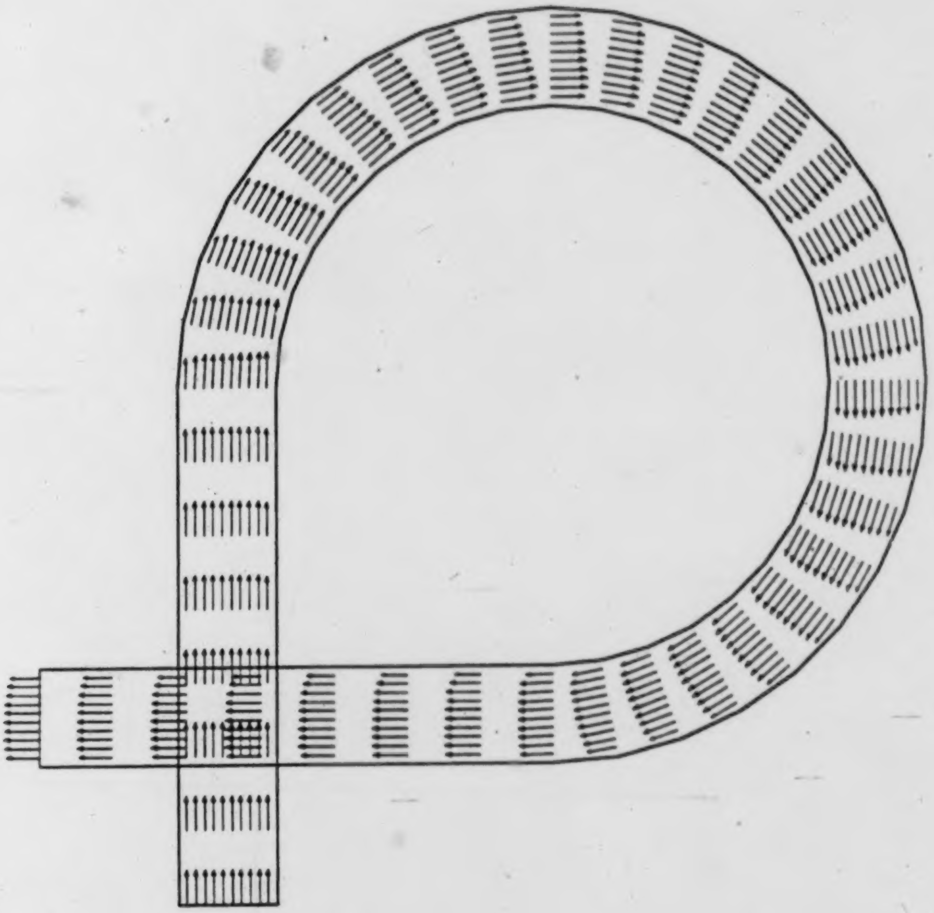

Figure 6.2 Numerical prediction of Steffler's run 1(solved with continuity and momentum equations)

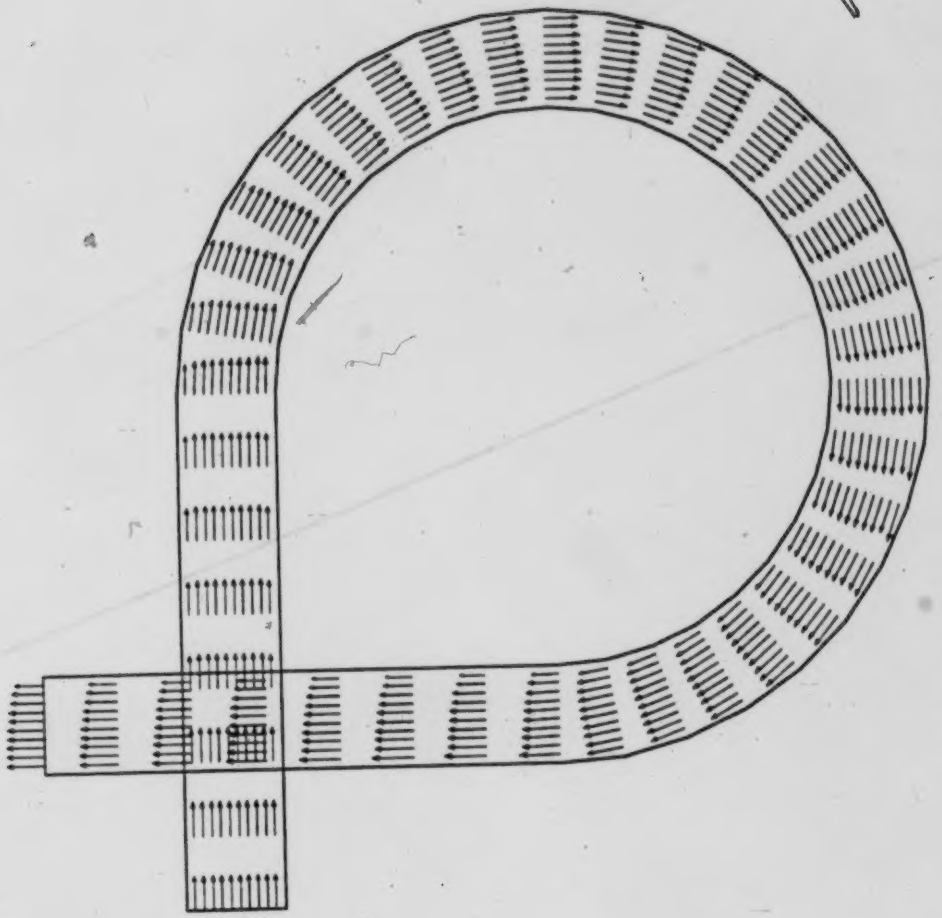

Figure 6.3 Numerical prediction of Steffler's run 1 (solved with continuity, momentum and momemt of momentum equations)

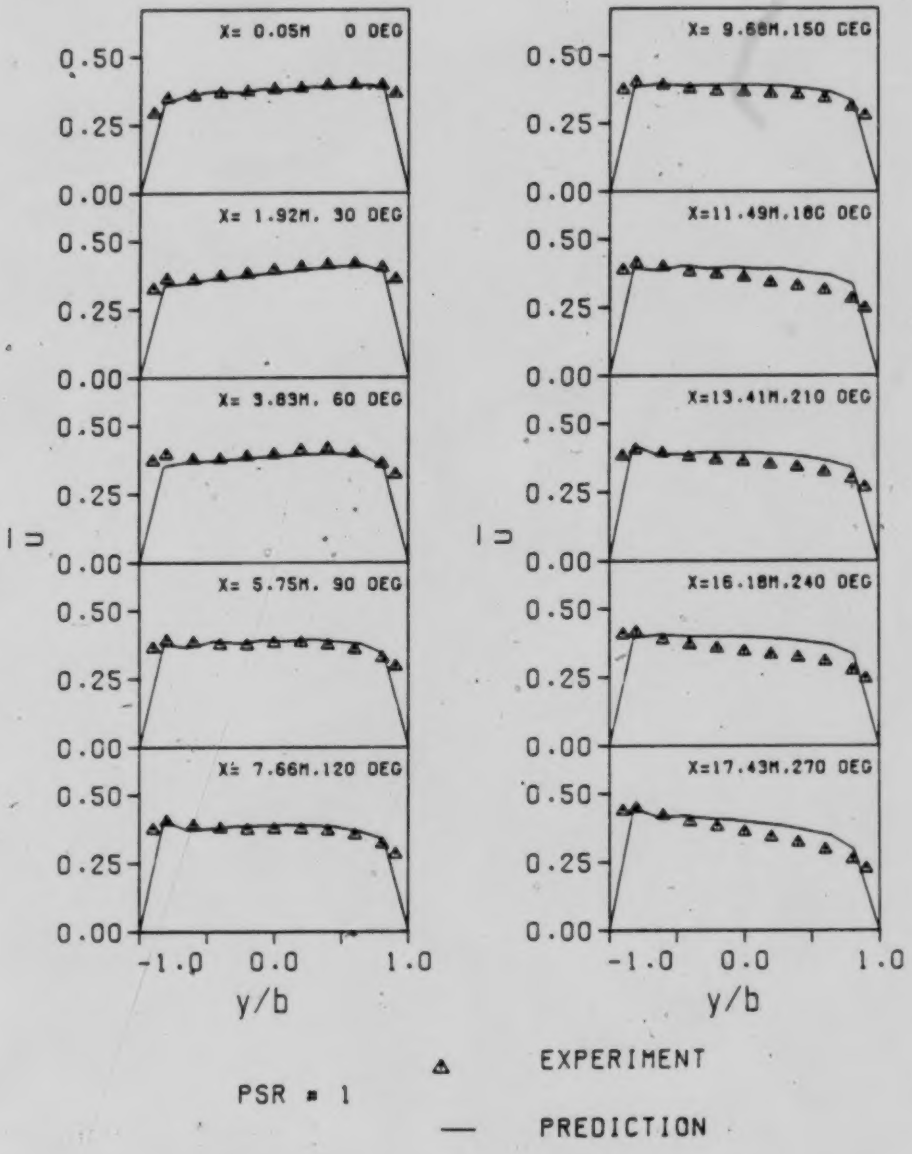

Figure 6.4 The comparison of depth-averaged longitudinal velocity distribution for Steffler's run 1

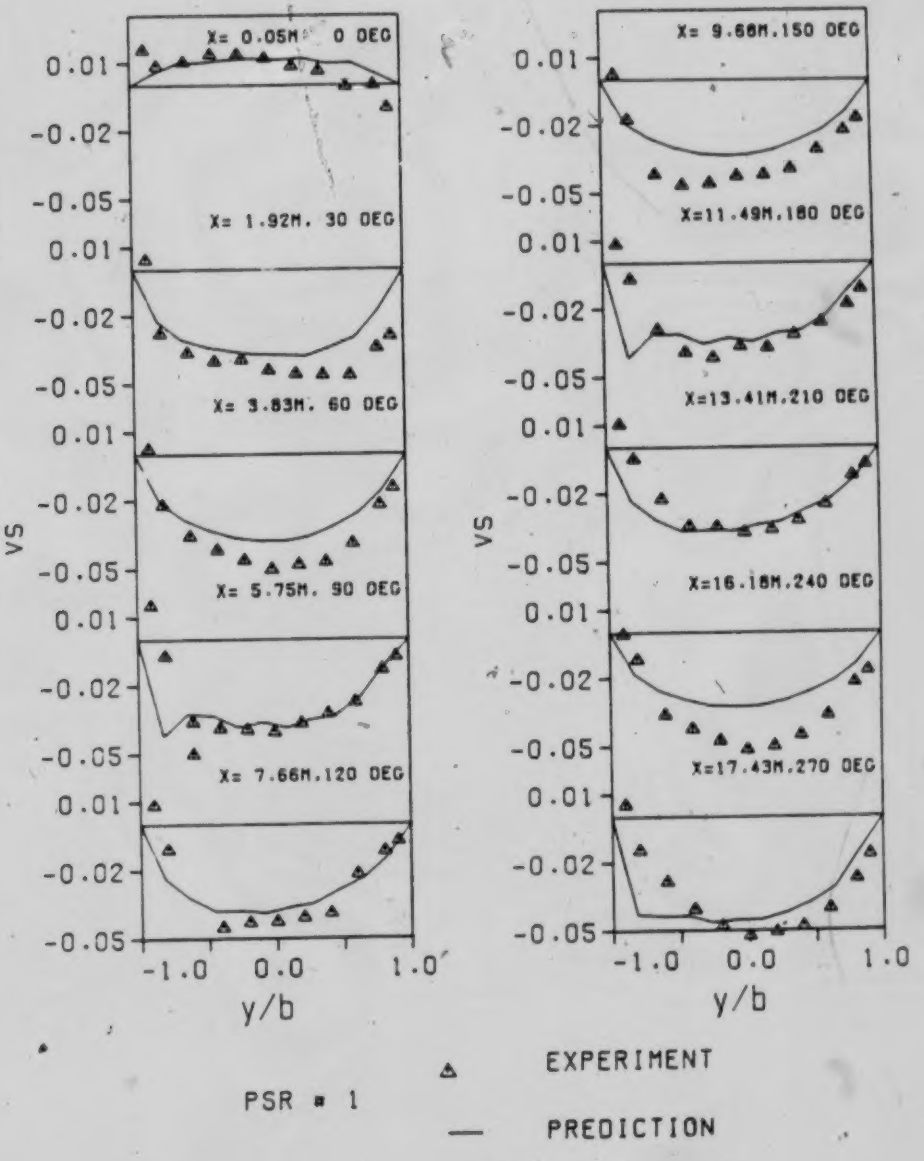

Figure 6.5 The comparison of transverse surface velocity distribution for Steffler's run 1

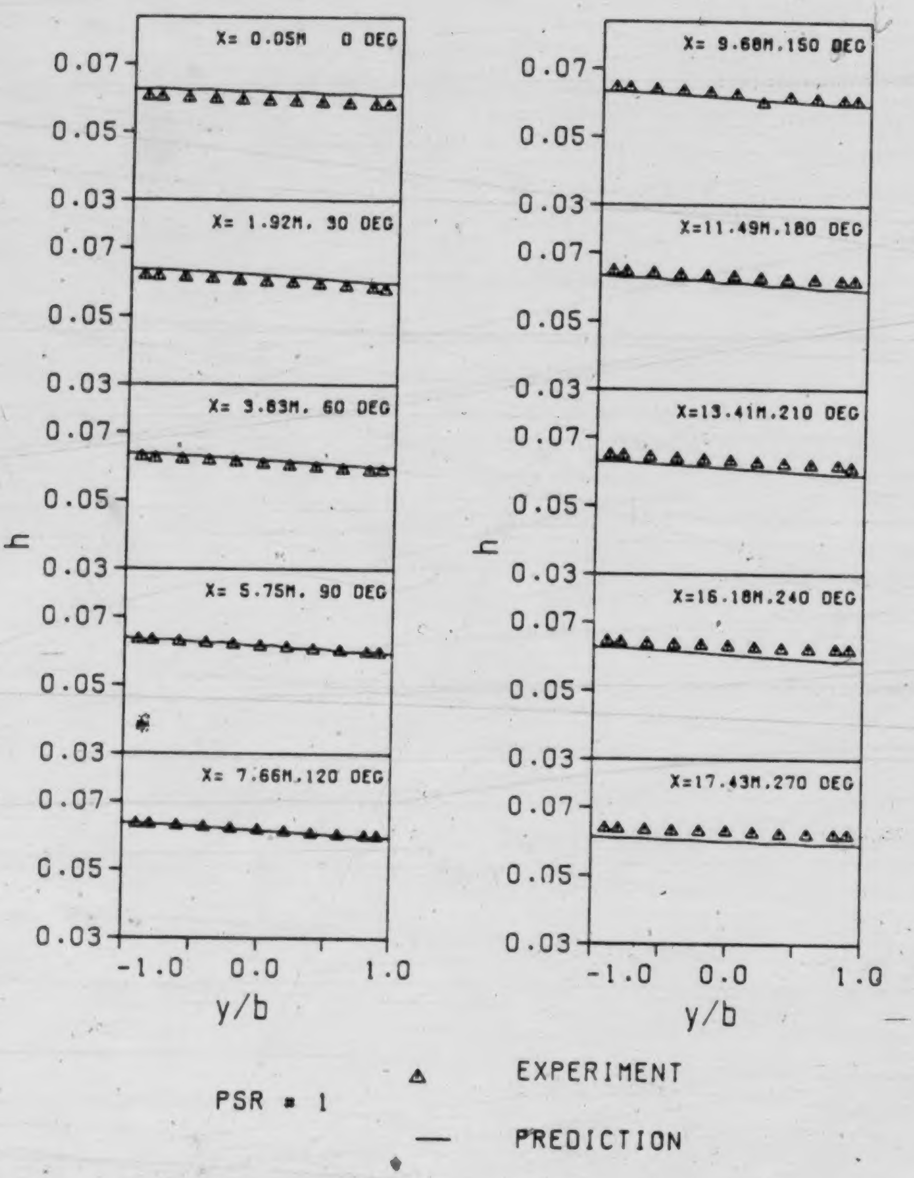

Figure 6.6 The comparison of surface elevation for Steffler's run 1

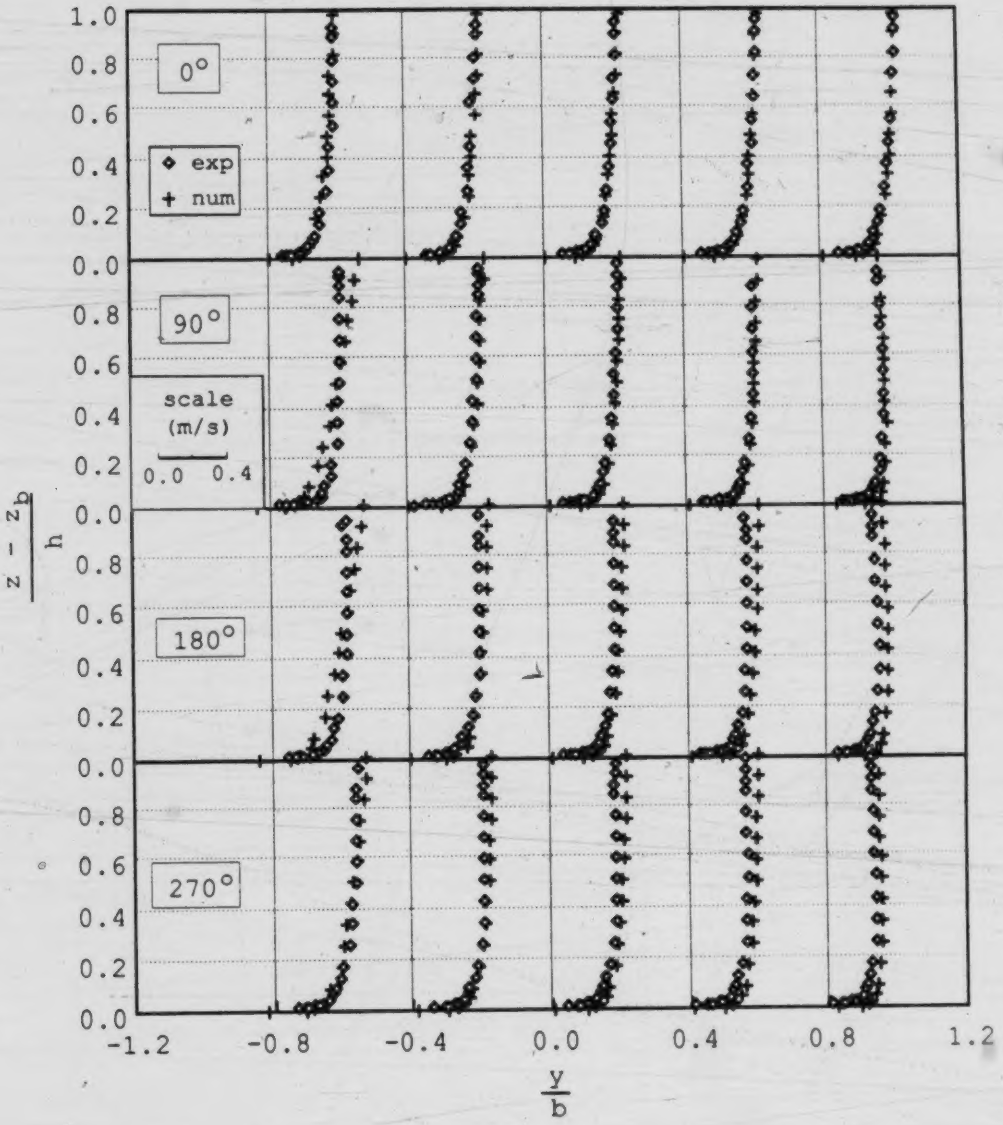

Figure 6.7 The comparison of longitudinal velocity profiles for Steffler's run 1

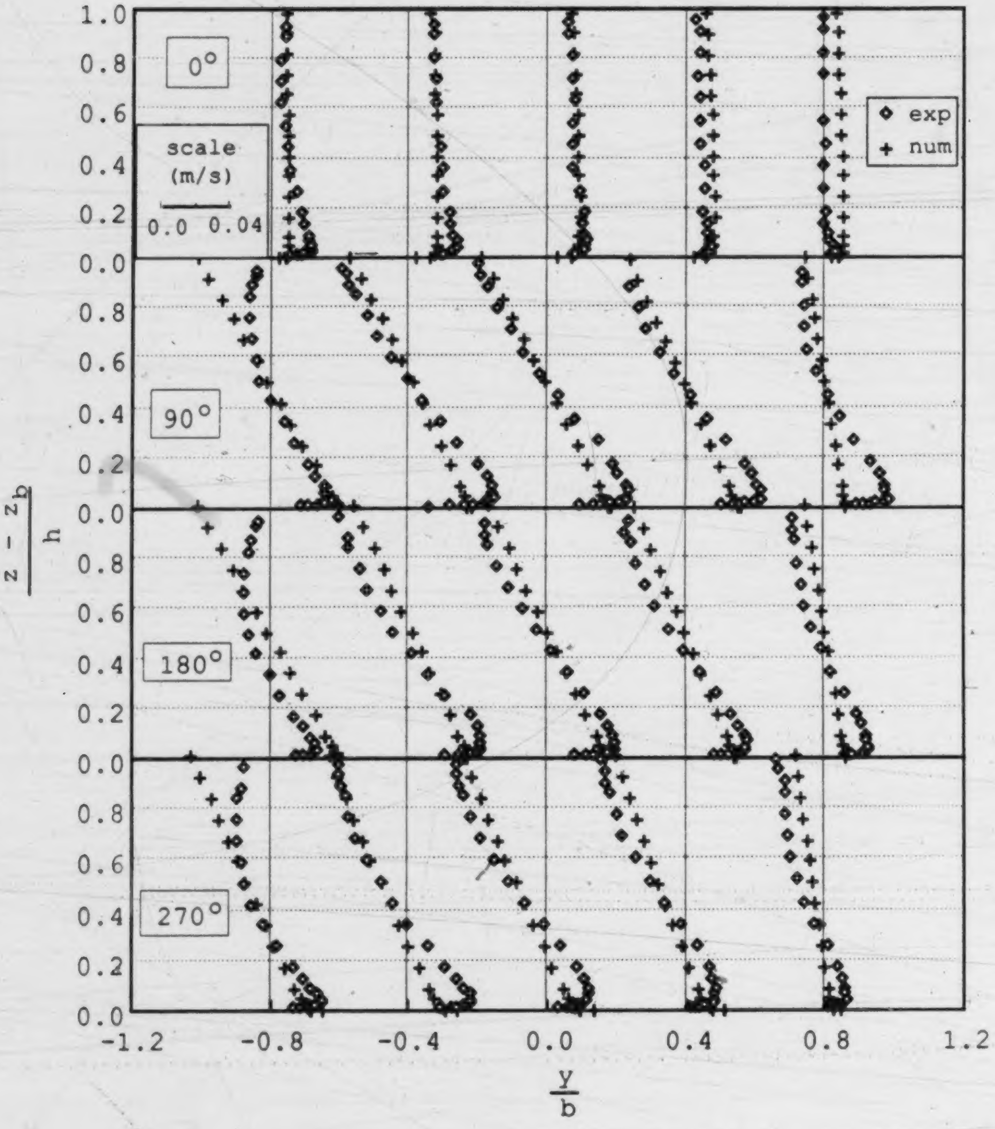

Figure 6.8 The comparison of transverse velocity profiles for Steffler's run 1

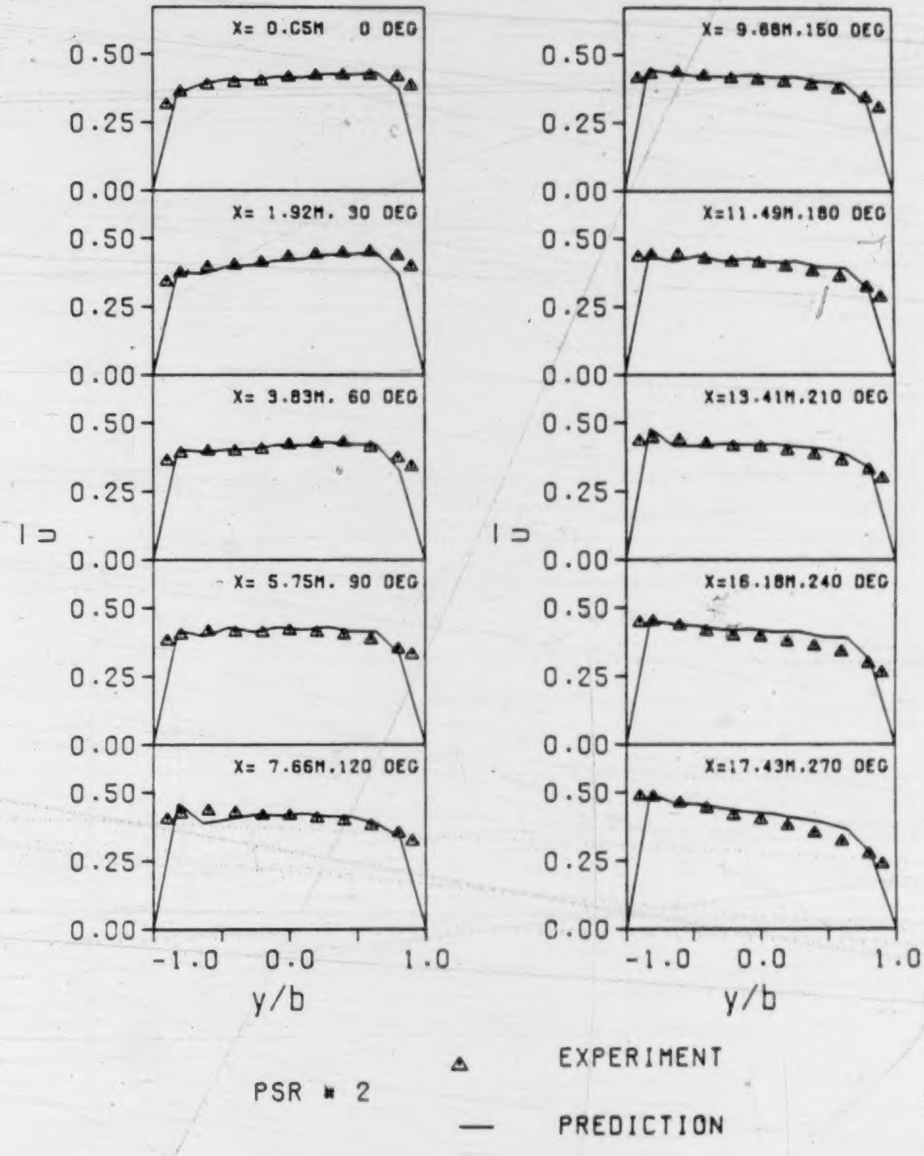

Figure 6.9 The comparison of depth-averaged longitudinal velocity distribution for Steffler's run 2

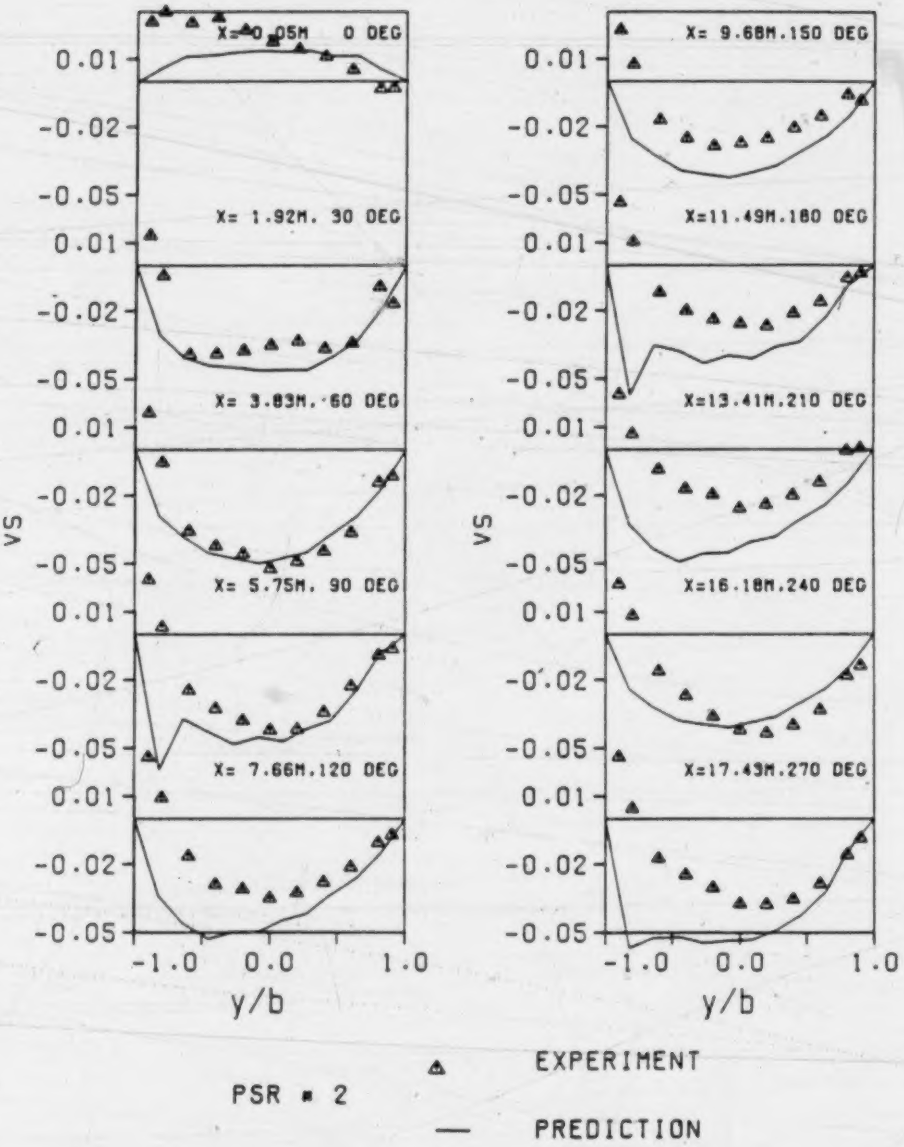

Figure 6.10 The comparison of transverse surface velocity distribution for Steffler's run 2

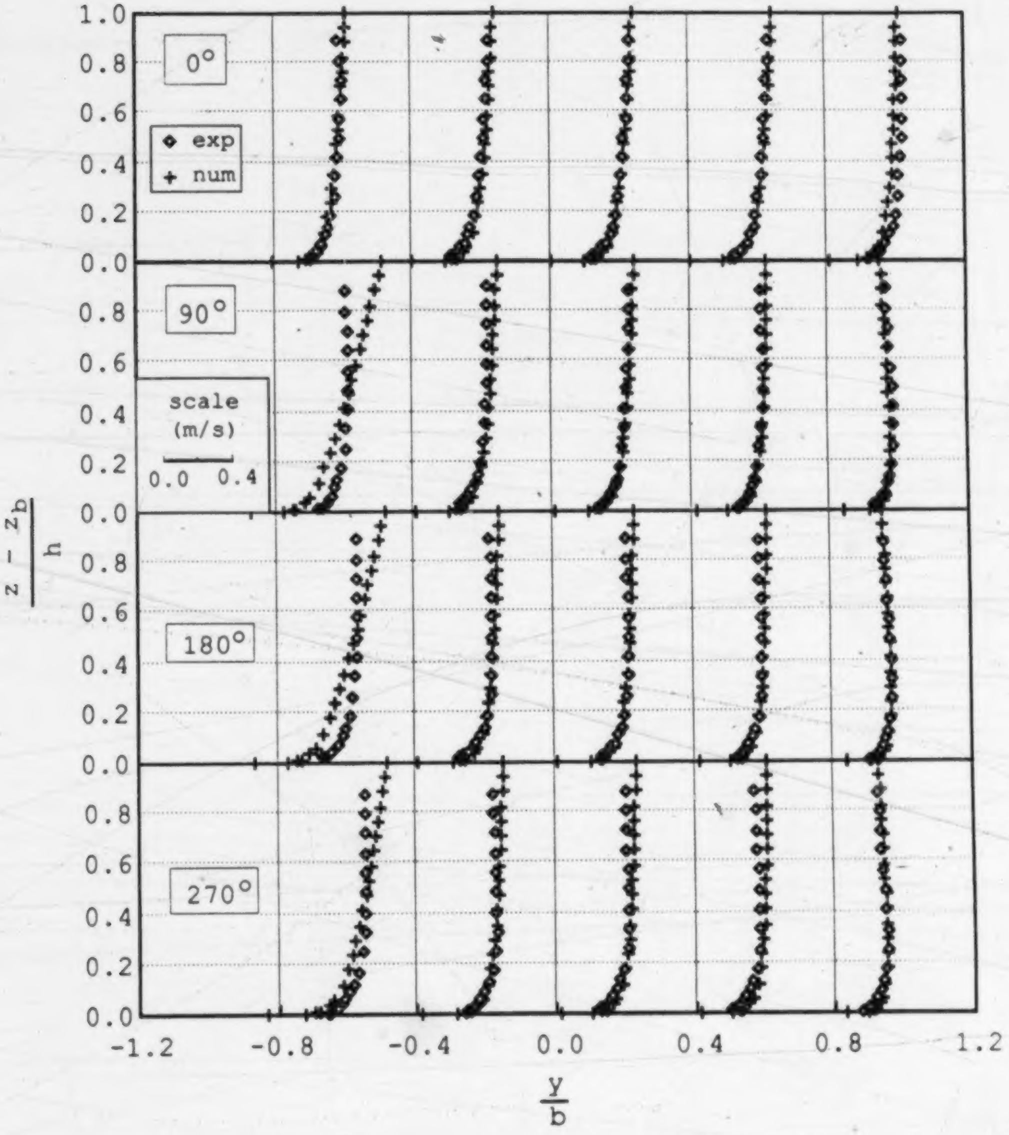

Figure 6.11 The comparison of longitudinal velocity profiles for Steffler's run 2

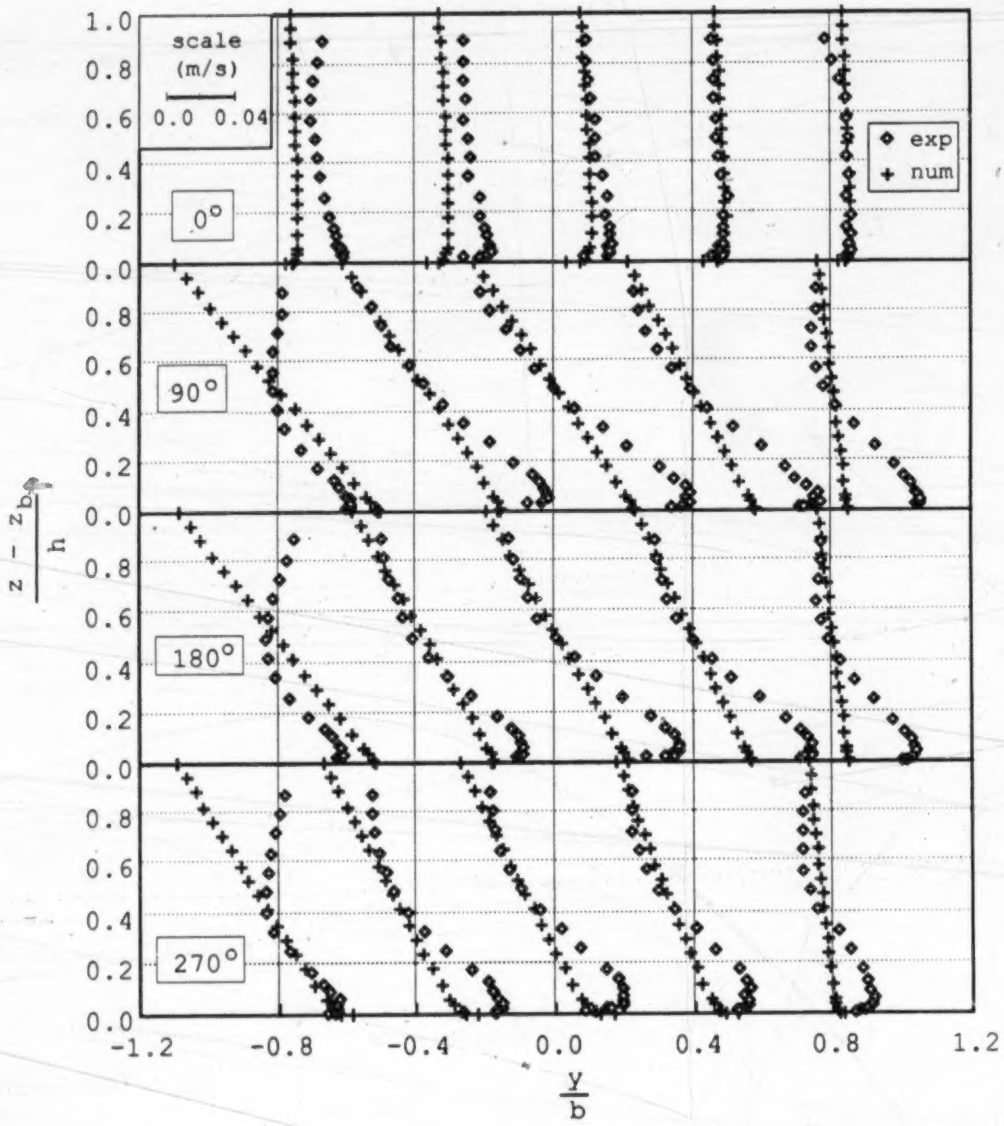

Figure 6.12 The comparison of transverse velocity profiles for Steffler's run 2

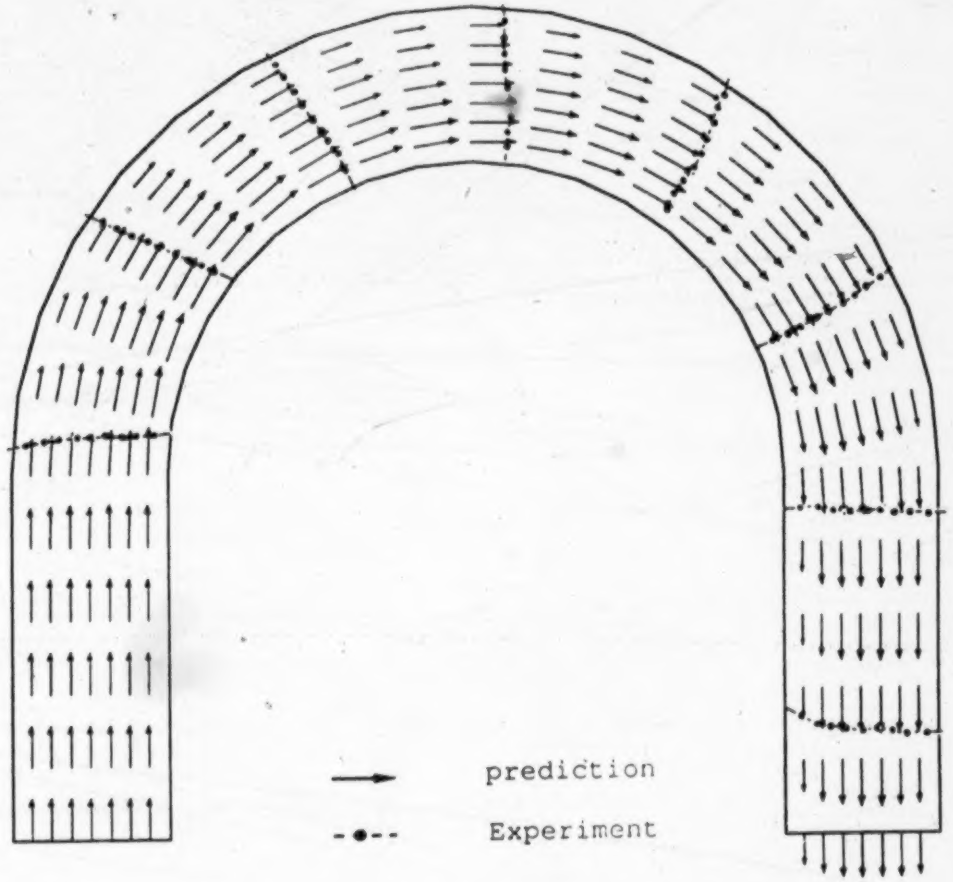

Figure 6.13 The comparison of depth-averaged longitudinal velocity distribution for LFM experiment

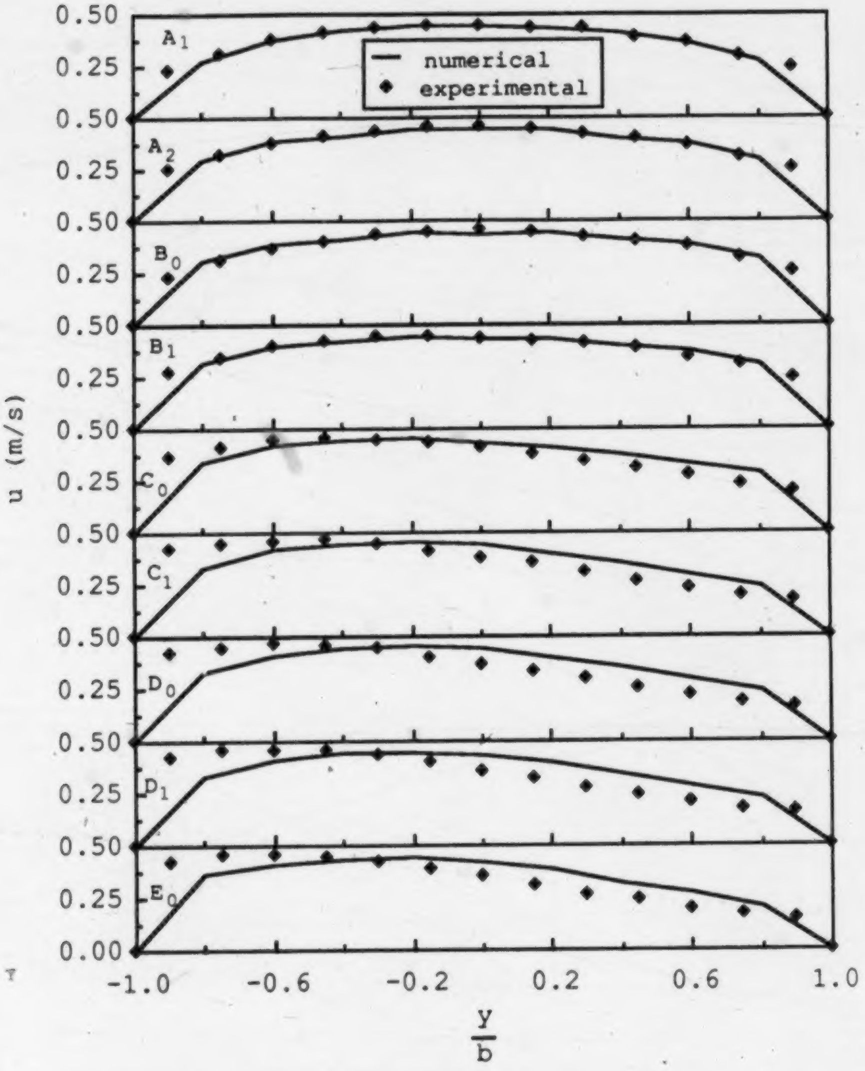

Figure 6.14 Comparison of the depth averaged longitudinal velocity for De Vriend's experiment

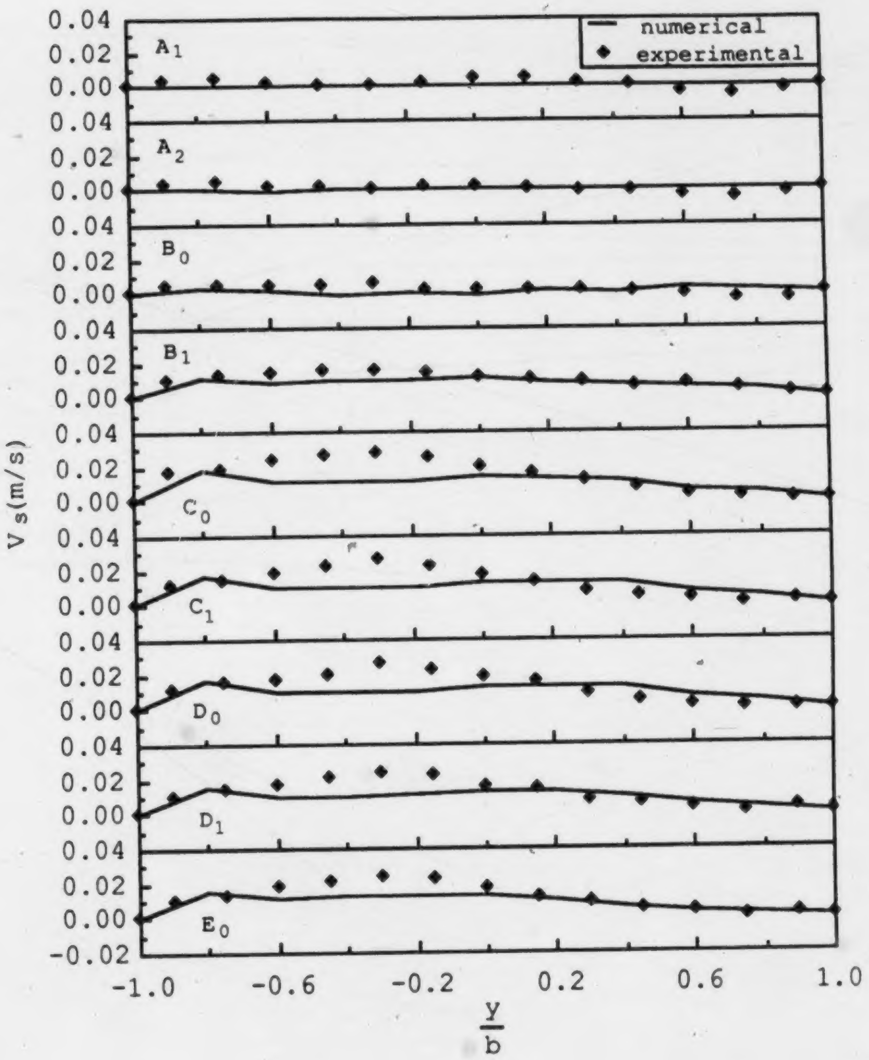

Figure 6.15 Comparison of transverse surface velocity for De Vriend's experiment

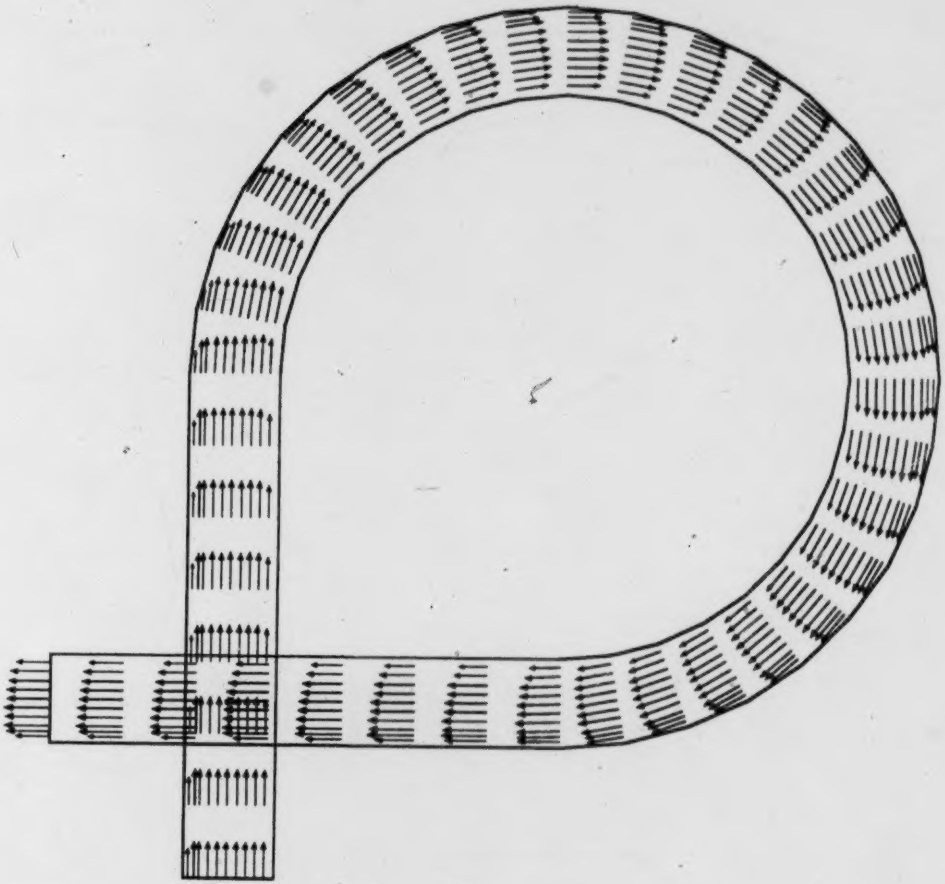

Figure 6.16 Numerical prediction of run 1

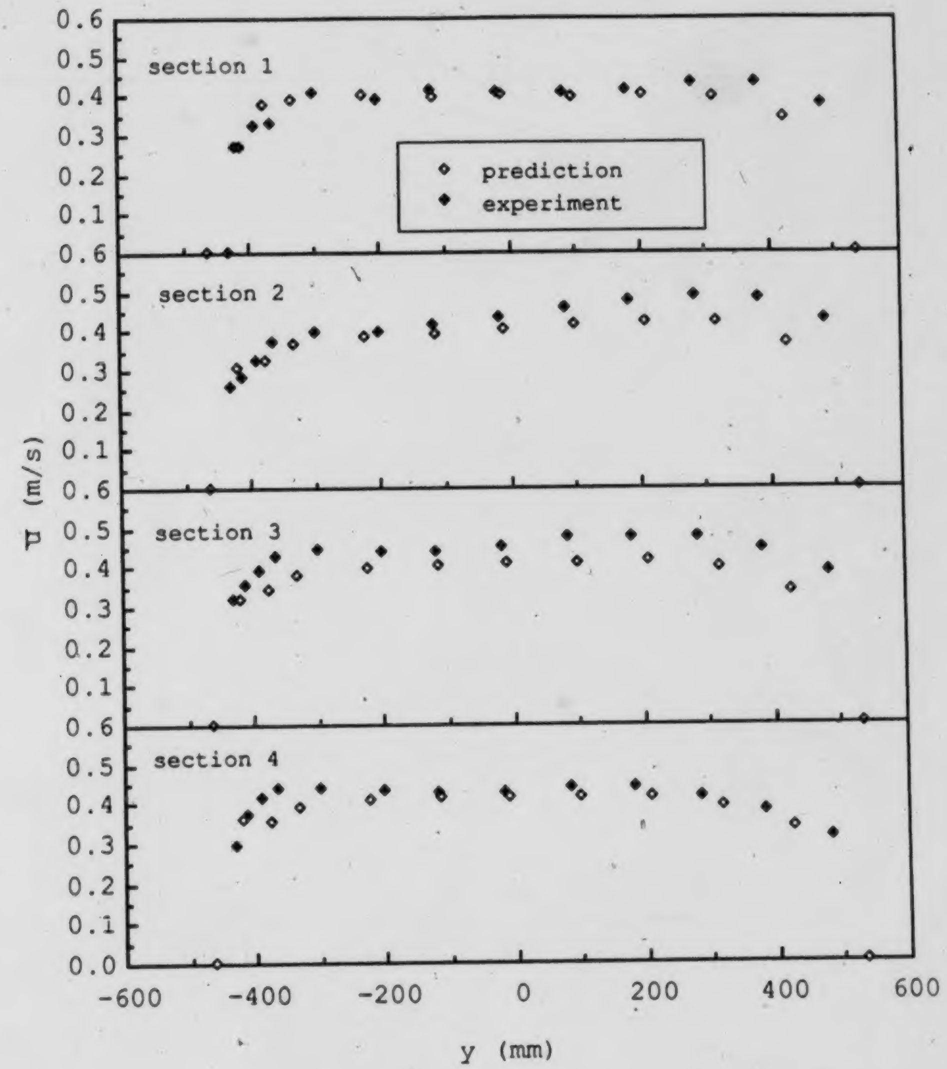

Figure 6.17(a) The comparison of depth averaged longitudinal velocity profile between the prediction and experimental data for run 1

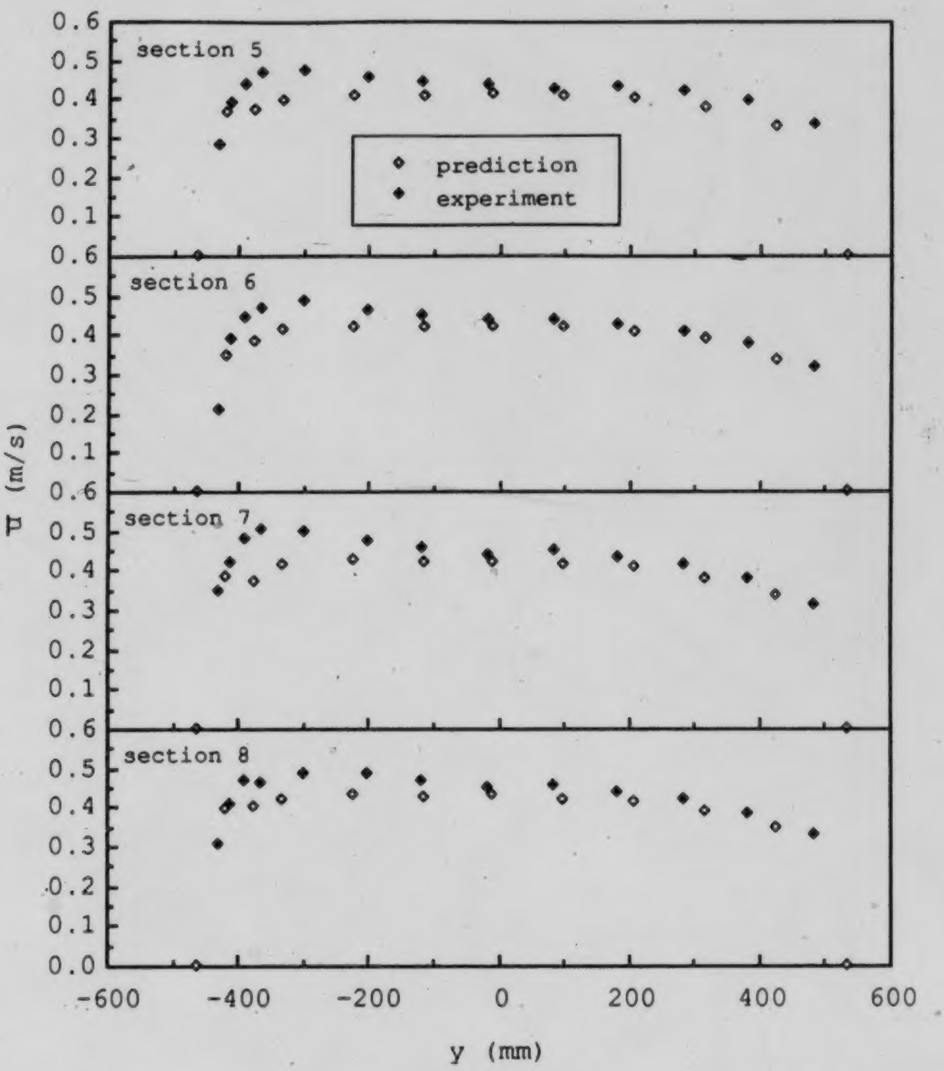

Figure 6.17(b) The comparison of depth averaged longitudinal velocity profile between the prediction and experimental data for run 1

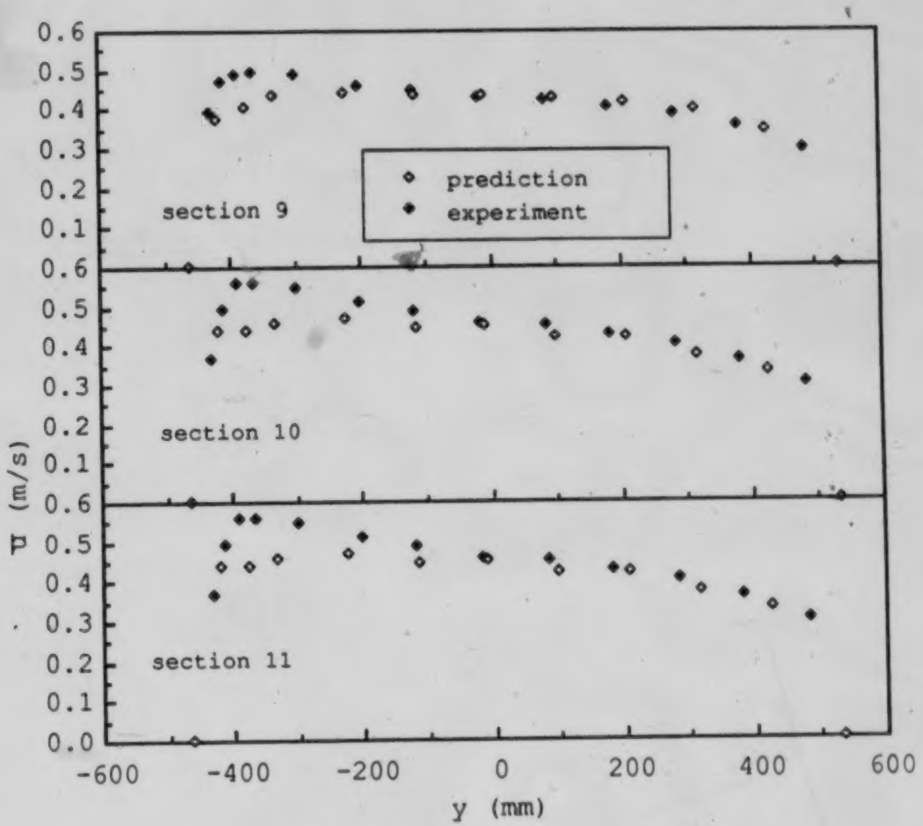

Figure 6.17(c) The comparison of depth averaged longitudinal velocity profile between the prediction and experimental data for run 1

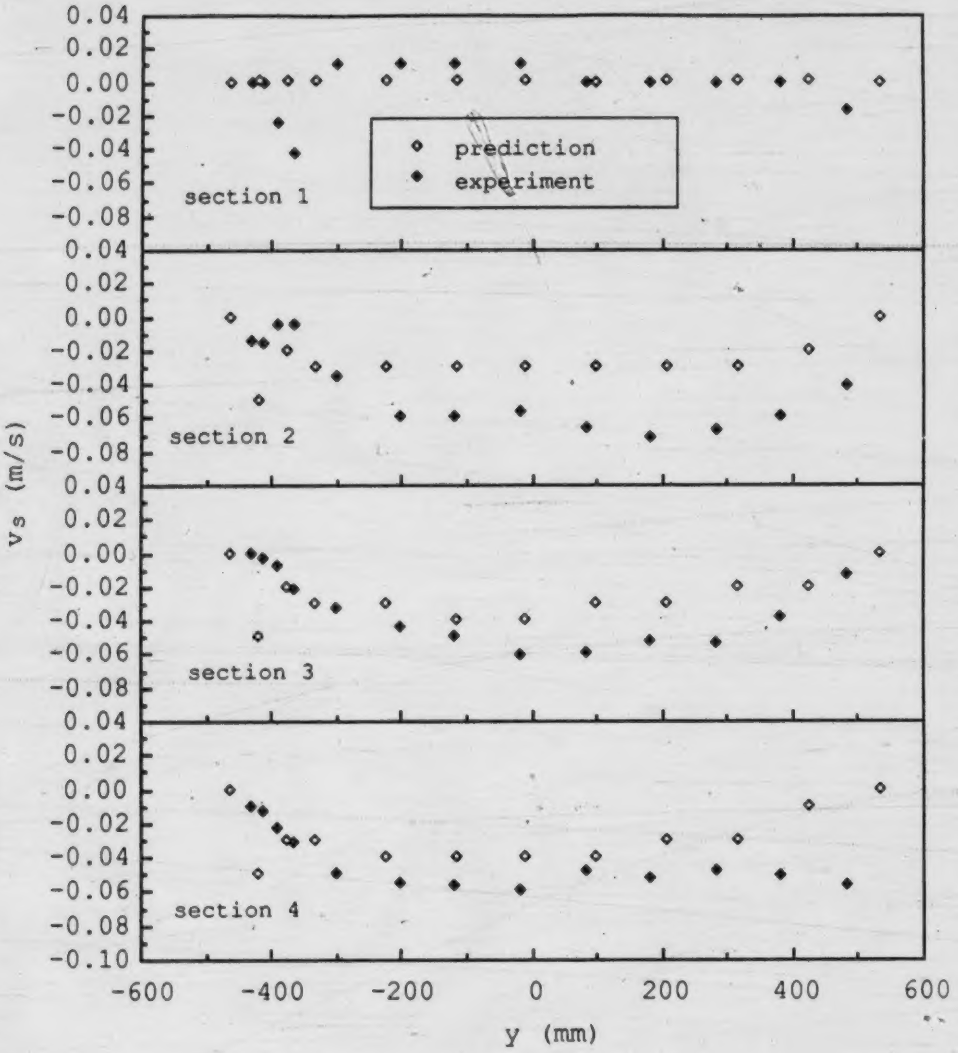

Figure 6.18(a) The comparison of secondary flow surface velocity between the prediction and experimental data for run 1

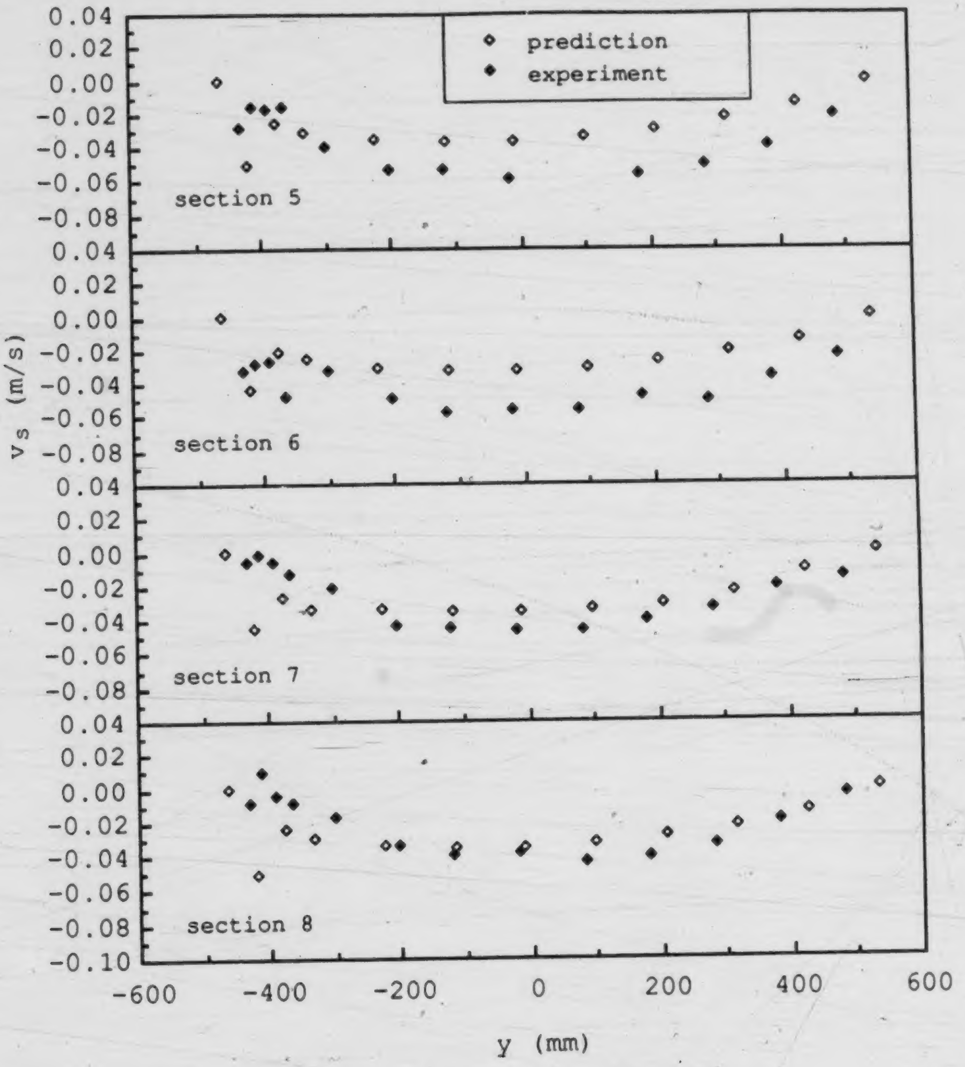

Figure 6.18(b) The comparison of secondary flow surface velocity between the prediction and experimental data for run 1

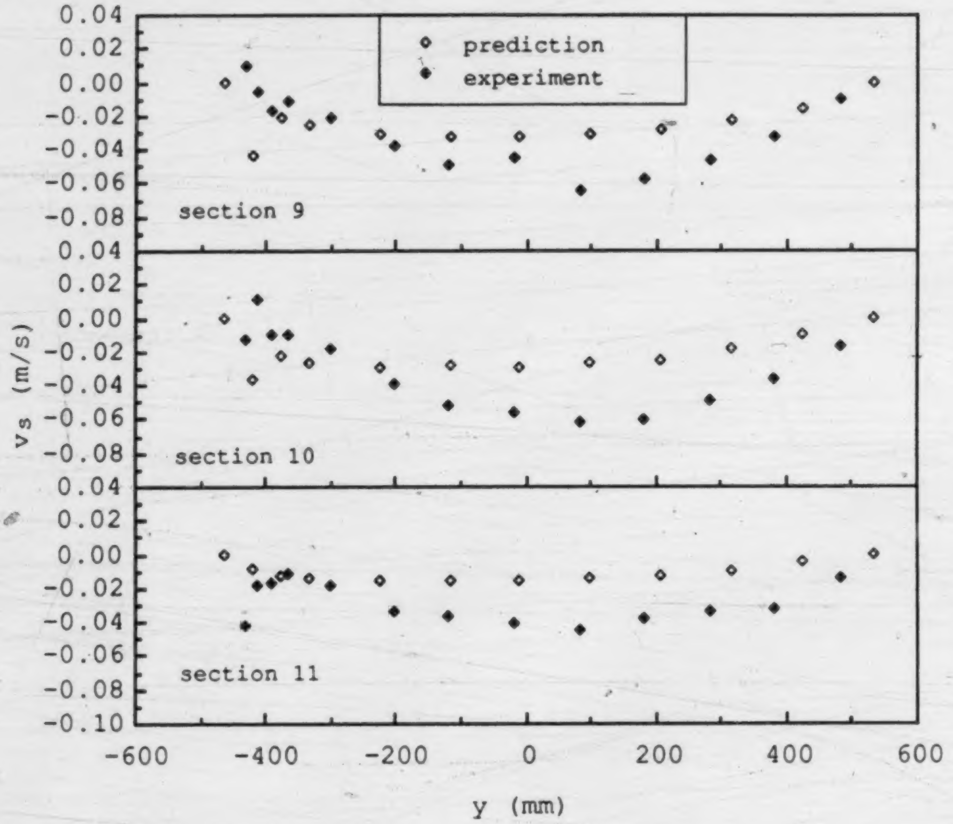

Figure 6.18(c) The comparison of secondary flow surface velocity between the prediction and experimental data for run 1

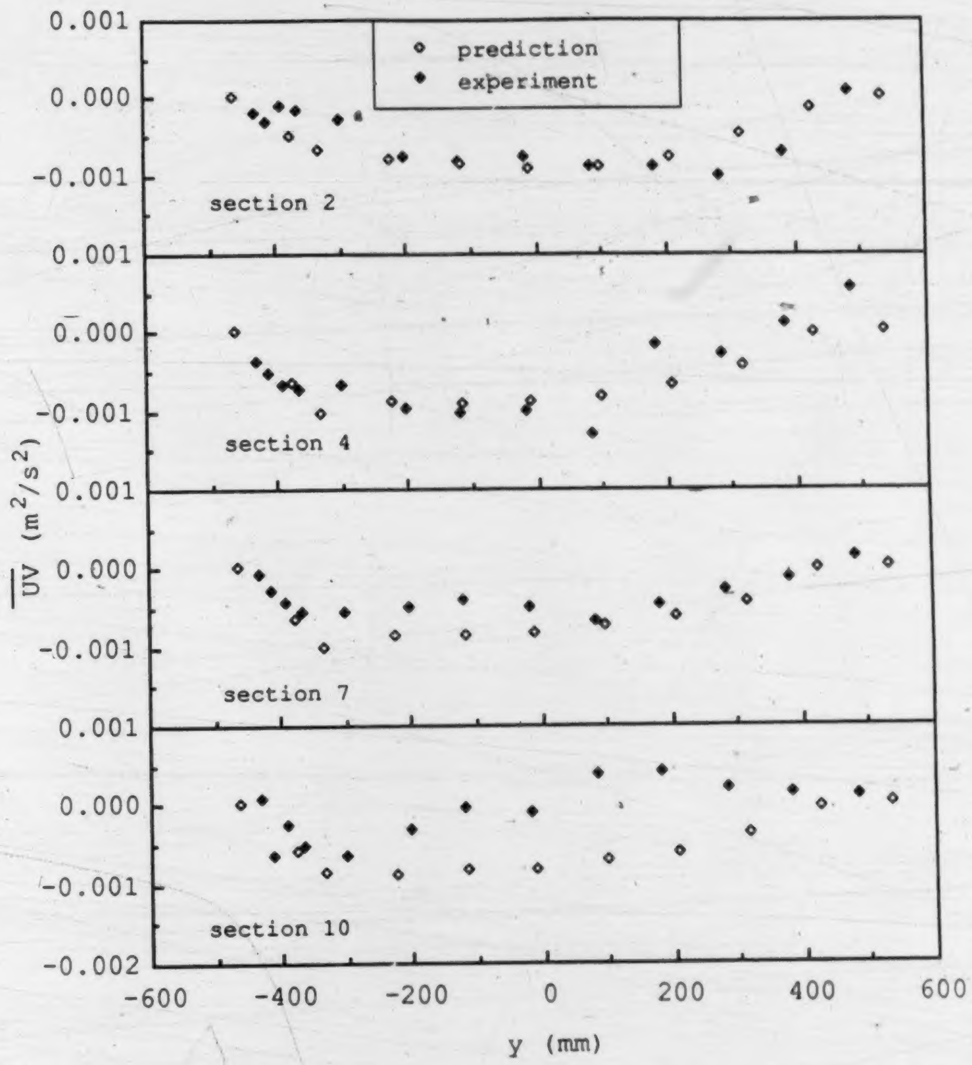

Figure 6.19 The comparison of the numerical calculation and experimental data of $\overline{UV}$ for run 1

7 CONCLUSIONS

The mathematical model developed herein for the flow in wide curved open channels can be summarized as follow:

1. Since the flow in a natural curved channel is non-axisymmetric and it is difficult to find the uniform curvature of the bend, a Cartesian coordinate system is used to replace the commonly used cylindrical or curvilinear coordinate system.

2. With the assumption of hydrostatic pressure distribution and the water surface boundary condition, the three-dimensional Reynolds equations can be simplified into a two dimensional version by integrating over the water depth. These depth-averaged continuity and momentum equations contain five unknowns: depth, two velocity components and components of two velocity variations.

3. Two extra equations were created by taking the moment of the two appropriate momentum equations and integrating over the depth. For the sake of simplicity, the power law and linear function were used for the main flow and secondary flow velocity profile and being substituted into the moment-of-momentum equations.

4. The effect of the secondary flow on the bed shear stress was evaluated from channel roughness, the variable k_* which was used to estimate the bed shear stress contributed by the secondary flow, depth-averaged velocity components and

surface velocity of the secondary flow. The variable k_* can be estimated by the channel roughness and secondary velocity.

Because of the irregular channel geometry in field situations and the irregular grid system required, the finite element method was used in the numerical simulation. Three experimental data sets from the literature and one set of data from this study were selected to evaluate the present model.

Generally, a satisfactory agreement was obtained between the numerical calculation and the experimental data. The characteristic features of the curved channel such as the longitudinal velocity redistribution, superelevation and secondary flow have been predicted well.

As has been demonstrated by means of the comparison of numerical and experimental result, the longitudinal velocity profile shows that the power law used to described the main velocity is adequate. The model employed to predict the secondary velocity profile is good, except for those profiles close to the side wall. These indicate that the depth-averaged model is limited to wide open channels because the hydrostatic pressure was assumed, which is not valid on the boundary. A higher order function for the secondary velocity profile may decrease the minor discrepancy found in the centre region of the channel. The effect of the secondary flow on bed shear stress was evaluated well by introducing a variable factor k_* into the model.

The shear and velocity distribution along a sloped bank in a curved channel with both smooth and rough boundaries has been examined also in this study. A detailed experimental investigation was conducted including the measurement of the longitudinal and lateral velocity and the measurement of the turbulent intensity in both directions. The longitudinal shear velocity has been determined by applying the logarithmatic velocity equation. Rough bank protection will decrease the longitudinal velocity, but increase the shear stress, in the vicinity of the bank. In particular, the roughness change combined with secondary flow leads to large bed stress magnifications in the vicinity of the toe of the slope which indicates that extra protection is needed at the bottom of the slope.

Shear stress on the roughened banks diminished considerably up the bank while remaining relatively constant for a smooth bank. Lateral momentum transfer both by the secondary flow and by turbulent shear were found to be significant in the bank region. The present numerical model including these terms were proved to be adequate.

The velocities and shear stresses on an unprotected bank vary from section to section especially for those sections close to the entrance and exit. Therefore, zoning rock sizes around the bend would be quite feasible. For the protected bank, the flow seems to become uniform along the channel more rapidly. However, the shear stress and the velocity vary significantly across the slope indicating that zoning the rock up the slope may be possible and practical. It would be desirable to test such a configuration to determine its feasibility.

BIBLIOGRAPHY

ASCE Task Committee on Turbulence Models in Hydraulic Computations, (1988). "Turbulence Modeling of Surface Water Flow and Transport: Part I." J. Hydraul. Engrg., ASCE, 114(9), 970-991.

Brooks, A. N. and Hughes, T. J. R. (1982), "Streamline Upwind/Petrov-Galerkin Formulations for Convection Dominated Flows with Particular Emphesis on the Incompressible Navier-Stokes Equations." Computer Methods in Applied Mechanics and Enginering, 32(1982), 199-259.

Dandekar, M. M. and Rodi, P. N. (1982), Discussion of "Resistance Equation for Large Scale Roughness."by Bathurst, C. J. and Li, R.,J. Hydraul. Div., ASCE, 107(HY 12), 1593-1613.

De Vriend, H.J. (1976). "A Mathematical Model of Steady Flow in Curved Shallow Channels." Communications on Hydraulics, Department of Civil Engineering, Delft University of Technology. Report No. 76-1, 116pp.

De Vriend, H. J.and Koch, F. G. (1978). "Flow of Water in a Curved Open Channel with a Fixed Uneven Bed." Delft Univ. of Technology, R657-VI, M1415 Part II.

De Vriend, H.J. (1981). "Steady Flow in Shallow Channel Bends. Part I" Communications on Hydraulics, Department of Civil Engineering, Delft University of Technology. Report No. 81-3, 260pp.

Engelund, F. (1974). "Flow and Bed Topography in Channel Bends." J. Hydraul. Div., ASCE, Vol 100(HY 11), 1631-1648.

Falcon Ascanio, M.A. (1979) ."Analysis of Flow in Alluvial Channel Bends." Ph.D. Thesis, University of Iowa, Iowa City.

Flokstra, C. (1977)."The Closure Problem for Depth-Averaged 2-D Flow." Proc. 18th Congress of IAHR, paper A106.

French, R. H. (1985)."Open-channel Hydraulics." McGraw-Hill Book Co., New York.

Gerard, R., Bouthillier P. and Besmehn J. (1988). "Field Measurements of the Hydraulic Resistance of Sanitary Sewers." 1988 Annual Conference of CSCE, Calgary, Alberta, Canada.

Ghosh, S. N. (1972). "Boundary Shear Distribution in Channels with varying wall roughness." Proc. of the Institution of Civil Engineers, Vol 53, Part 2, Proc. paper 7572, 471-430.

Ghosh, S. N. and Roy, N.(1970). "Boundary Shear Distribution in Open Channel Flow." J. Hydraul. Div., ASCE, Vol 96(HY 4), 967-994.

Kalkwijk, J.P.Th. and De Vriend, H.J. (1980)."Computation of the Flow in Shallow River Bends." J. of Hydraul. Res. 18(4), 327-341.

Harrington, R.A., Kouwen, N. and Farquhar, G.J.(1978). "Behavior of a Hydrodynamic Finite Element Model."Finite Elements in Water Resources, Proceedings of the second International Conference on Finite Element in Water resources.

Hicks, F.E. (1985). "Shear and Velocity near a Sloped Bank in a Curved Channel." M. Sc. Thesis, University of Alberta.

Hicks, F.E., Jin, Y.C. and Steffler, P.M. (1990). "Flow Near Sloped Bank in Curved Channel."J. Hydraul. Engrg., ASCE, 116(1), 55-70.

Hollingshead, A. B. (1972). "Boundary Shear Stress Distribution in Open Channel Flow." Ph.D. Thesis, University of Alberta.

Ippen A. T. and Drinker, P. A. (1962). "Boundary Shear Stress in Curved Trapezoidal Channel."J. Hydraul. Div., ASCE, 88(HY 5), 143-179.

Jin, Y.C., et al. (1988). "Flow and Shear Stress in Curved Channels-Phase IV - Velocity and Shear Streses near Smooth and Roughed Outside Bank Slopes." Water Resour. Engrg. Rept., Dept. of Civil Engrg., Univ. of Alberta, Edmontom, Alberta, Canada..

Jasek, M.J. (1989). "Boundary Layer Growth in Open Channels." M. Sc. Thesis, University of Alberta(in publishing).

Leschziner, M.A., and Rodi,W. (1979). "Calculation of Strongly Curved Open Channel Flow."J. Hydraul. Div., ASCE, 105(HY10), 1297-1314.

Naot, D. (1983)."Response of Channel Flow to Roughness Heterogeneity."J. of Hydraul. Engrg., ASCE, 110(11), 1568-1587

Nezu, I. and Rodi, W. (1986)."Open-channel Flow Measurements with a Laser Doppler Anemometer."J. of Hydraul. Engrg., ASCE, 112(5), 335-355.

Odgaard, A.J. (1986). "Meander Flow Model. I: Development."J. Hydraul. Engrg., ASCE, 112(12), 1117-1136.

Pe, J. A. (1975)."Implicit Erosion in High Gradient Open Channel Flow with Artificial Roughness Elements."Proc. 16th Congress of IAHR, Vol 2, 173-180.

Pinder, G.F. and Gray, W.G. (1977). "Finite Element Simulation in Surface and Subsurface Hydrology." Academic Press.

Rajaratnam, N. and Muralidhar, D. (1968)."Characteristics of the Rectangular Free Overfall." J. of Hydraul. Res. 6(3), 233-258.

Rodi, W. (1980). "Turbulence Model and Their Application in Hydraulics." IAHR, Delft, The Netherland.

Rozovskii I. L. (1957). "Flow of Water in Bends of Open Channels." Israel Program for Scientific Translations.

Solanki, S. (1988). "Turbulent Flow in a Curved Rectangular Channel." Master Thesis, University of Alberta.

Steffler, P.M. (1984). "Turbulent Flow in a Curved Rectangular Channel." Ph.D. Thesis, University of Alberta.

Steffler, P.M., Rajaratnam N. and Peterson A.W. (1983). "Flow in Curved Channels: A Review of the Present Knowledge." Prep. for the Research Management Division, Alberta Environment by the Department of Civil Engineering, University of Alberta. RMD Report L-82.

Taylor, C., and Hughes, T.G. (1981). "Finite Element Programming of the Navier-Stokes Equations." Prineridge Press Ltd.

Yen, B. C. (1965). "Characteristics of Subcritical Flow in a Meandering Channel." Institute of Hydraulic Research, The University of Iowa.

Yuan S.W. (1967). "Foundations of Fluid Mechanics" Prentice-Hall Inc. New Jersey.

Zimmermann, C. (1977)."Roughness Effects on the Flow Direction near Curved Stream Bends." J. of Hydraul. Res. 15(1), 73-85.

Zimmermann, C. and Kennedy, J. F. (1978). "Transverse Slopes in Curved Alluvial Streams." J. Hydraul. Divi., ASCE, 104(HY1), 33-48.

APPENDIX COMPUTER PROGRAM

```
C$$$$$$$$$$$$$$$$$$$$$$$$$$$$$$$$$$$$$$$$$$$$$$$$$$$$$$$$$$$$$$$$$
C                                                                $
C          ASSIGN DIMENSIONS                                     $
C    MELEM  :  NUMBER OF ELEMENTS                                $
C    MPOIN  :  NUMBER OF NODAL POINTS                            $
C    MFRON  :  FRONTAL WIDTH                                     $
C    MTOTV  :  3*MPOIN                                           $
C    MVARB  :  5*MPOIN                                           $
C                                                                $
C$$$$$$$$$$$$$$$$$$$$$$$$$$$$$$$$$$$$$$$$$$$$$$$$$$$$$$$$$$$$$$$$$
      PARAMETER(MELEM=460,MPOIN=510,MTOTV=1530,MFRON=80,MVARB=2550)
CCCCCCCCCCCCCCCCCCCCCCCCCCCCCCCCCCCCCCCCCCCCCCCCCCCCCCCCCCCCCCCCCC
C                                                                C
C         adapted from Taylor and Hughes(1981)                   C
C                 BY YEE CHUNG JIN                               C
C           verson 8.1(MacII v1.0)                               C
C                                                                C
CCCCCCCCCCCCCCCCCCCCCCCCCCCCCCCCCCCCCCCCCCCCCCCCCCCCCCCCCCCCCCCCCC
C
C
C****** MASTER PROGRAM
C
C
C-----------------------------------------
C     EXTERNAL SUBROUTINE                -
C     DINPUT                             -
C     DRIVES                             -
C     ITERUV                             -
C     RESULT                             -
C-----------------------------------------
```

```
      IMPLICIT REAL*8 (A-H,P-Z)
      DIMENSION BOUDV(MTOTV),COORD(MPOIN,3),GFLUM(MFRON,MFRON),
     -          GRADB(MPOIN,8),LHEDV(MFRON),LBOUD(MTOTV),LNODS(MELEM,4),
     -         LGRAD(MPOIN),PNORM(MFRON),POSGP(3),WEIGP(3),EQRHS(MTOTV),
     -          VARB1(MVARB),VARB2(MVARB),BOUVS(MTOTV),LBUVS(MTOTV)
      COMMON ESPON,DENSY,GRVTY,RELAX,STARC,TOLER,OXMIN,OXDEL,
     -       OYMIN,OYDEL
      COMMON NEVAB,NBCNF,NBCNS,NELEM,NGARD,NGAUS,NITER,NNODP,
     -       NPOIN,NTOTV,NUNKN,NBCN1,NBCN2
      CHARACTER*12 FILE5,FILE6
C
C***  ASSIGN FILENAMES FOR ALL I/O UNITS
C
      PRINT *,' Input file name for unit 5 '
      READ(*,'(A)')FILE5
      PRINT *,' Output file name '
      READ(*,'(A)')FILE6
      OPEN(UNIT=5,FILE=FILE5,STATUS='OLD')
      OPEN(UNIT=12,FILE=FILE6,STATUS='UNKNOWN')
      OPEN(UNIT=10,FILE='TEMP.PPP',STATUS='UNKNOWN'
     -          ,FORM='UNFORMATTED')
      OPEN(UNIT=4,FILE='TEMP.PP',STATUS='UNKNOWN'
     -          ,BLOCK=-1,FORM='UNFORMATTED')
C
      CALL TIME(ISEC0)
      CALL DINPUT(BOUDV,COORD,GRADB,LBOUD,LNODS,LGRAD,MELEM,
     -            MFRON,MPOIN,MTOTV,MVARB,VARB1,VARB2,BOUVS,
     -            LBUVS)
      CALL DRIVES(COORD,LNODS,MELEM,MPOIN,POSGP,WEIGP)
      CALL ITERUV(BOUDV,COORD,EQRHS,GFLUM,GRADB,LBOUD,LGRAD,
     -            LHEDV,LNODS,MFRON,MELEM,MPOIN,MTOTV,MVARB,
     -            PNORM,POSGP,VARB1,VARB2,WEIGP,BOUVS,LBUVS)
      CALL RESULT(COORD,LNODS,MELEM,MPOIN,MVARB,VARB2)
      CALL TIME(ISEC1)
      ISEC=ISEC1-ISEC0
      WRITE(12,'(16H  TOTAL TIME USE,I10,4H SEC)')ISEC
      STOP
      END
C$$$$$$$$$$$$$$$$$$$$$$$$$$$$$$$$$$$$$$$$$$$$$$$$$$$$$$$$$$$$$$$$$$$$
C                                                                    $
C     INPUT SUBROUTINE                                               $
C                                                                    $
C$$$$$$$$$$$$$$$$$$$$$$$$$$$$$$$$$$$$$$$$$$$$$$$$$$$$$$$$$$$$$$$$$$$$
      SUBROUTINE DINPUT(BOUDV, COORD, GRADB,LBOUD, LNODS, LGRAD, MELEM,
     -                  MFRON,MPOIN,MTOTV,MVARB,VARB1,VARB2,BOUVS,
     -                  LBUVS)
      IMPLICIT REAL*8 (A-H,P-Z)
      DIMENSION BOUDV(MTOTV),COORD(MPOIN,3),GRADB(MPOIN,8),
     -          LBOUD(MTOTV),LGRAD(MPOIN),LNODS(MELEM,4),
     -          OTITL(12),VARB1(MVARB),VARB2(MVARB),BOUVS(MTOTV),
     -          LBUVS(MTOTV)
      COMMON ESPON,DENSY,GRVTY,RELAX,STARC,TOLER,OXMIN,OXDEL,
     -       OYMIN,OYDEL
      COMMON NEVAB,NBCNF,NBCNS,NELEM,NGARD,NGAUS,NITER,NNODP,
     -       NPOIN,NTOTV,NUNKN,NBCN1,NBCN2
C
C***  NUNKN : NUMBER OF UNKNOWNS (CAN NOT BE CHANGED)
C***  NGAUS : 2 POINTS OR 3 POINTS GAUSS INTEGRATION
C
      NUNKN=3
C
C***  READ IN EACH CARD AND ECHO IMMEDIATELY
C
      READ(5,1000)OTITL
      WRITE(12,2000)OTITL
      READ(5,1010) NNODP,NGAUS,NELEM,NITER,NPOIN,NRPON
      WRITE(12,2010)NNODP,NGAUS,NELEM,NPOIN,NITER,NRPON
      READ(5,1010) NICON,NBCNS,NBCNF,NGRAD
      WRITE(12,2020)NICON,NBCNS,NBCNF,NGRAD
      NEVAB=NUNKN*NNODP
C
C***  CHECK INITIAL DATA
```

```
C
C     CALL DIAGN1(NBCON,NGRAD,NELEM,NICON,NPOIN,NRPON)
C
C***  READ FLOW PARAMETERS ETC.
C
      READ(5,1020) DENSY,RELAX,TOLER,STARC,GRVTY,ESPON
      WRITE(12,2030)DENSY,RELAX,TOLER,STARC,GRVTY,ESPON
C
C***  ZERO ALL COORDINATE ARREY
C
      DO 10 IPOIN=1,MPOIN
      DO 10 IDIME=1,3
      COORD(IPOIN,IDIME)=0.
   10 CONTINUE
C
C***  READ IN NODAL COORDINATE (X THEN Y)
C
      NTOTV=3*NPOIN
      DO 20 IPOIN=1,NRPON
      READ(5,1030)JPOIN,(COORD(JPOIN,IDIME),IDIME=1,3)
   20 CONTINUE
C
C***  READ IN NODAL CONNECTION AND ECHO IMMEDINATELY
C
      WRITE(12,2040)
      DO 30 IELEM=1,NELEM
      READ(5,1010) JELEM,(LNODS(JELEM,INODP),INODP=1,NNODP)
      WRITE(12,2050)JELEM,(LNODS(JELEM,INODP),INODP=1,NNODP)
   30 CONTINUE
C
C***  INITIATE THE REMAINING ARRAYS
C
      NNTOT=5*NPOIN
      DO 90 ITOTV=1,MVARB
      VARB2(ITOTV)=0.1
   90 CONTINUE
```

```
      DO 92 IBNDY=1,MTOTV
      LBOUD(IBNDY)=0
      BOUDV(IBNDY)=0.
      LBUVS(IBNDY)=0
      BOUVS(IBNDY)=0.
   92 CONTINUE
      DO 94 ITOTV=1,MPOIN
      LGRAD(ITOTV)=0
      DO 94 JTOTV=1,8
      GRADB(ITOTV,JTOTV)=1.0E-20
   94 CONTINUE
C
C***  READ INITIAL CONDITION IF ANY
C
      DO 100 IICON=1,NICON
      READ(5,1040)IPOIN,TEMP1,TEMP2,TEMP3,TEMP4,TEMP5
      IICN1=(IPOIN-1)*3
      IICN2=NPOIN*3+(IPOIN-1)*2
      VARB2(IICN1+1)=TEMP1
      VARB2(IICN1+2)=TEMP2
      VARB2(IICN1+3)=TEMP3
      VARB2(IICN2+1)=TEMP4
      VARB2(IICN2+2)=TEMP5
  100 CONTINUE
  110 CONTINUE
C
C***  READ IN BOUNDARY CONDITIONS, ONLY THE NON-ZERO BNDY
C
      NBCNN=NBCNF+NBCNS
      DO 170 IBCNF=1,NBCNN
      READ(5,1040)IPOIN,TEMP1,TEMP2,TEMP3,TEMP4,TEMP5
      IICN1=(IPOIN-I)*3
      IICN2=NPOIN*3+(IPOIN-1)*2
      IICN3=(IPOIN-1)*2
      IF(TEMP1.GE.50.)GO TO 171
      LBOUD(IICN1+1)=1
      BOUDV(IICN1+1)=TEMP1
      VARB2(IICN1+1)=TEMP1
  171 IF(TEMP2.GE.50.)GO TO 172
      LBOUD(IICN1+2)=1
      BOUDV(IICN1+2)=TEMP2
      VARB2(IICN1+2)=TEMP2
  172 IF(TEMP3.GE.50.)GO TO 173
      LBOUD(IICN1+3)=1
      BOUDV(IICN1+3)=TEMP3
      VARB2(IICN1+3)=TEMP3
  173 IF(TEMP4.GE.50.)GO TO 174
      LBUVS(IICN3+1)=1
      BOUVS(IICN3+1)=TEMP4
      VARB2(IICN2+1)=TEMP4
  174 IF(TEMP5.GE.50.)GO TO 170
      LBUVS(IICN3+2)=1
      BOUVS(IICN3+2)=TEMP5
      VARB2(IICN2+2)=TEMP5
  170 CONTINUE
      NBCN1=0
      DO 135 INBCN=1,NTOTV
      IF(LBOUD(INBCN).NE.1)GO TO 135
      NBCN1=NBCN1+1
  135 CONTINUE
      NBCN2=0
      DO 137 INBCN=1,NTOTV
      IF(LBOUD(INBCN).NE.1)GO TO 137
      NBCN2=NBCN2+1
  137 CONTINUE
C
C***  WRITE OUT COORDINATE AND INITIAL CONDITIONS
C
      WRITE(12,2060)
      DO 130 IPOIN=1,NPOIN
      IICN1=(IPOIN-1)*3
      IICN2=NPOIN*3+(IPOIN-1)*2
      WRITE(12,2080)IPOIN,(COORD(IPOIN,IDIME),IDIME=1,3),
     -VARB2(IICN1+1),VARB2(IICN1+2),VARB2(IICN1+3),
     -VARB2(IICN2+1),VARB2(IICN2+2)
  130 CONTINUE
      DO 140 I140=1,MVARB
      VARB1(I140)=VARB2(I140)
  140 CONTINUE
C
C***  PLOT THE MESH
C
C
C***  READ IN ELEMENTS AND SIDES WITH GRADIENT BOUNDARY CONDITIONS
C
      IF(NGRAD.EQ.0)RETURN
      WRITE(12,2100)
      DO 180 IEBCN=1,NGRAD
      READ(5,1030) LGRAD(IEBCN),(GRADB(IEBCN,JEBCN),JEBCN=1,4)
      WRITE(12,2070)LGRAD(IEBCN),(GRADB(IEBCN,JEBCN),JEBCN=1,4)
  180 CONTINUE
  200 CONTINUE
      RETURN
  250 WRITE(12,2290)
      RETURN
 1000 FORMAT(12A4)
 1010 FORMAT(10I5)
 1020 FORMAT(5F10.5,E10.2)
 1030 FORMAT(1I5,10F10.6)
 1040 FORMAT(I5,10F10.6)
 2000 FORMAT(1H1,//1X,12A4)
 2010 FORMAT(//13H CONTROL DATA,/13H ************,//
     -' ELEMENT TYPE    =',I4,4X,'# OF GAUSS RULE   =',I4,4X/
     -' # OF ELEMENTS   =',I4,4X,'TOTAL NODAL POINTS=',I4,4X/
     -' # OF ITERATIONS =',I4,4X,'INPUT NODAL POINTS=',I4)
 2020 FORMAT(' # INITIAL POINTS=',I4,4X,'# BNDY PTS AT WALL=',I4,4X/
     -' # BNDY FREE SUF =',I4,4X,'# GRADIENT BNDY PT=',I4)
 2030 FORMAT(//20H PHYSICAL PROPERTIES,/20H *******************,//
     -' DENSITY     =',F10.5,4X,'RELAXATION =',F10.5/
     -' TOLERANCE =',F10.5,4X,'Chezy''s C  =',F10.5/
     -' GRAVITY     =',F10.5,4X,'PENALTY e  =',E10.2)
 2040 FORMAT(//17H ELEMENT TOPOLOGY,/17H ****************,//
     -8H ELEMENT,6X,12HNODE NUMBERS)
 2050 FORMAT(1X,I5,8X,8I5)
 2060 FORMAT(//' NODE POINT DATA AND INITIAL CONDITIONS',/38('*')//
     -' NODE  X-COORD  Y-COORD       Z-COORD       U-VEL',
     -' V-VEL       H   Us    Vs')
 2080 FORMAT(I4,3F9.3,5(2X,F5.2))
 2070 FORMAT(I4,1X,10(F9.4,1X))
 2090 FORMAT(//20H BOUNDARY CONDITIONS,/20H *******************,//
     -' NODE          U-VEL  V-VEL        H    Us    Vs')
 2100 FORMAT(//18H GRADIENT BOUNDARY,/20H *******************,//,
     -1X,'NODE',3X,' DU/DX ',3X,' DU/DY ',3X,' DV/DX ',3X,' DV/DX '
     -,' DV/DY ',3X,'DUs/DX ',3X,'DUs/DY ','DVs/DX ',3X,'dVs/dY ')
 2200 FORMAT(I5,5(3X,F5.2))
 2220 FORMAT(I5,10X,F5.2)
 2240 FORMAT(I5,17X,F5.2)
 2260 FORMAT(I5,24X,F5.2)
 2280 FORMAT(I5,31X,F5.2)
 2290 FORMAT(' INITIALIZE ALL UNKNOWN POINTS !!!')
      END
C$$$$$$$$$$$$$$$$$$$$$$$$$$$$$$$$$$$$$$$$$$$$$$$$$$$$$$$$$$$$
C                                                           $
C   SUBROUTINE TO CALCULATE                                 $
C                                                           $
C$$$$$$$$$$$$$$$$$$$$$$$$$$$$$$$$$$$$$$$$$$$$$$$$$$$$$$$$$$$$
      SUBROUTINE DRIVES(COORD,LNODS,MELEM,MPOIN,POSGP,WEIGP)
C - -- - - - - - - - - - - -
C -                        -
C -   EXTERNAL SUBROUTINES -
C -   SHAPE8 OR SHAPE4     -
C -   DJACOB               -
C - - - - - - - - - - - - - -
      IMPLICIT REAL*8 (A-H,P-Z)
      DIMENSION AREAW(9),CARPG(2,72),CARTP(2,8),COORD(MPOIN,3),
     -          DERIV(2,8),DJACI(2,2),DJACK(2,2),LNODS(MELEM,4),
     -          POSGP(3),SHAPE(8),SHAPG(72),WEIGP(3)
      COMMON ESPON,DENSY,GRVTY,RELAX,STARC,TOLER,OXMIN,OXDEL,
     -       OYMIN,OYDEL
      COMMON NEVAB,NBCNF,NBCNS,NELEM,NGARD,NGAUS,NITER,NNODP,
     -       NPOIN,NTOTV,NUNKN,NBCN1,NBCN2
C
C***  REWIND
C
      REWIND 10
C
C***  SET UP POSITIONS AND WEIGHTS FOR 3POINT GAUSS RULE
C
      IF(NGAUS.EQ.2)GO TO 90
      POSGP(1)=0.774596692
      POSGP(2)=0.0
      POSGP(3)=-POSGP(1)
      WEIGP(1)=0.555555556
      WEIGP(2)=0.888888889
      WEIGP(3)=WEIGP(1)
      GO TO 100
   90 POSGP(1)=1./SQRT(3.)
      POSGP(2)=-POSGP(1)
      WEIGP(1)=1.0
      WEIGP(2)=1.0
C
C***  CALCULATE SHAPE FUNCTIONS AND DERIVATIES FOR ELEMENTS
C
  100 DO 60 IELEM=1, NELEM
      LGAUS=0
      DO 50 IGAUS=1,NGAUS
      DO 50 JGAUS=1,NGAUS
      LGAUS=LGAUS+1
      XEQIV=POSGP(IGAUS)
      YEQIV=POSGP(JGAUS)
```

```
C
C***  USE GAUSS POSITIONS TO CALCULATE LOCAL VALUES
C
      IF(NNODP.EQ.8)GO TO 30
      CALL SHAPE4(DERIV,SHAPE,XEQIV,YEQIV)
      GO TO 40
30    CONTINUE
C30    CALL SHAPE8(DERIV,SHAPE,XEQIV,YEQIV)
40    CONTINUE
C
C***  SET UP JACOBIAN MATRIX AND INVERSE
C
      CALL DJACOB(COORD,DERIV,DETJB,DJACI,DJACK,IELEM,LNODS,
     -            MELEM,MPOIN,NNODP)
C
C**   CALCULATE GLOBAL DERIVATIVES AND AREA*GAUSS WEIGHTS
C
      DO 10 IDIME=1,2
      DO 10 INODP=1,NNODP
      CARTP(IDIME,INODP)=0.0
      DO 10 JDIME=1,2
      CARTP(IDIME,INODP)=CARTP(IDIME,INODP)+
     -DJACI(IDIME,JDIME)*DERIV(JDIME,INODP)
   10 CONTINUE
      AREAW(LGAUS)=DETJB*WEIGP(IGAUS)*WEIGP(JGAUS)
C
C***  PUT SHAPE FUNCTIONS AND DERIVATIVES IN ELEMENT MATRIX
C
      DO 20 INODP=1,NNODP
      KGAPA=(LGAUS-1)*NNODP+INODP
      SHAPG(KGAPA)=SHAPE(INODP)
      DO 20 IDIME=1,2
      CARPG(IDIME,KGAPA)=CARTP(IDIME,INODP)
   20 CONTINUE
   50 CONTINUE
C
```

```
C***  NOW WRITE ALL THE ELEMENT SHAPE FUNCTIONS ON TAPE
C
      NGAPA=LGAUS*NNODP
      WRITE(10) IELEM,LGAUS,NGAPA,
     -((CARPG(IDIME,IGAPA),IDIME=1,2),SHAPG(IGAPA),IGAPA=1,NGAPA),
     -(AREAW(IGAUS),IGAUS=1,LGAUS)
   60 CONTINUE
      RETURN
      END
C$$$$$$$$$$$$$$$$$$$$$$$$$$$$$$$$$$$$$$$$$$$$$$$$$$$$$$$$$$
C                                                         $
C   4 NODE SHAPE FUNCTION                                 $
C                                                         $
C$$$$$$$$$$$$$$$$$$$$$$$$$$$$$$$$$$$$$$$$$$$$$$$$$$$$$$$$$$
      SUBROUTINE SHAPE4(DERIV,SHAPE,XEQIV,YEQIV)
      IMPLICIT REAL*8 (A-H,P-Z)
      DIMENSION DERIV(2,8),SHAPE(8)
C
C***  1INEAR ELEMENT ANTI-CLOCKWISE NODE NUMBERING
C
      X=XEQIV
      Y=YEQIV
      XY=X*Y
      SHAPE(1) =(1.-X-Y+XY)*.25
      SHAPE(2) =(1.+X-Y-XY)*.25
      SHAPE(3)  =(1.+X+Y+XY)*.25
      SHAPE(4)  =(1.-X+Y-XY)*.25
      DERIV(1,1) =(-1.+Y)*.25
      DERIV(1,2) =( 1.-Y)*.25
      DERIV(1,3) =( 1.+Y)*.25
      DERIV(1,4) =(-1.-Y)*.25
      DERIV(2,1) =(-1.+X)*.25
      DERIV(2,2) =(-1.-X)*.25
      DERIV(2,3) =( 1.+X)*.25
      DERIV(2,4) =( 1.-X)*.25
      RETURN
      END
C$$$$$$$$$$$$$$$$$$$$$$$$$$$$$$$$$$$$$$$$$$$$$$$$$$$$$$$$
C                                                       $
C   SUBROUTINE TO CALCULATE THE JACOBIAN MATRIX         $
C                                                       $
C$$$$$$$$$$$$$$$$$$$$$$$$$$$$$$$$$$$$$$$$$$$$$$$$$$$$$$$$
      SUBROUTINE DJACOB(COORD,DERIV,DETJB,DJACI,DJACK,IELEM,LNODS,
     -                  MELEM,MPOIN,NNODP)
      IMPLICIT REAL*8 (A-H,P-Z)
      DIMENSION COORD(MPOIN,3),DERIV(2,8),DJACI(2,2),DJACK(2,2),
     -          LNODS(MELEM,4)
C
C***  SET UP TEMPORARY MATRIX TO ALLOW THE JACOBIAN TO BE FORMED
C
      DO 20 IDIME=1,2
      DO 20 JDIME=1,2
      TEMPY=0.0
      DO 10 INODP=1,NNODP
      KPOIN=IABS(LNODS(IELEM,INODP))
      TEMPY=TEMPY+DERIV(IDIME,INODP)*COORD(KPOIN,JDIME)
   10 CONTINUE
      DJACK(IDIME,JDIME)=TEMPY
   20 CONTINUE
      DETJB=DJACK(1,1)*DJACK(2,2)-DJACK(2,1)*DJACK(1,2)
C
C***  CHECK FOR ZERO OR NEGATIVE DETERMINANT
C
      IF(DETJB)30,30,40
   30 CONTINUE
      WRITE(12,2000)IELEM
      STOP
   40 CONTINUE
C
C***  INVERT TEMPORARY MATRIX TO FORM JACOBIAN
C
      DJACI(1,1)=DJACK(2,2)/DETJB
      DJACI(2,2)=DJACK(1,1)/DETJB
      DJACI(1,2)=-DJACK(1,2)/DETJB
      DJACI(2,1)=-DJACK(2,1)/DETJB
2000  FORMAT(//37H NON POSITIVE DETERMINANT FOR ELEMENT,I4)
      RETURN
      END
C$$$$$$$$$$$$$$$$$$$$$$$$$$$$$$$$$$$$$$$$$$$$$$$$$$$$$$$$$$$$$$$$$$$$$$$$
C                                                                       $
C SUBROUTINE FRONT1                                                     $
C         ASSEMBLY MATRIX TO SOLVE  u,v AND h                           $
C                                                                       $
C$$$$$$$$$$$$$$$$$$$$$$$$$$$$$$$$$$$$$$$$$$$$$$$$$$$$$$$$$$$$$$$$$$$$$$$$
      SUBROUTINE FRONT1(BOUDV,COORD,EQRHS,GFLUM,LBOUD,LHEDV,LNODS,
     -                  MELEM,MFRON,MPOIN,MTOTV,MVARB,PNORM,VARB1,
     -                  VARB2,IITER,IMASS,IUSVS,LBUVS,BOUVS,FUNCN)
C-------------------------------
C                              -
C     EXTERNAL SUBROUTINES     -
C     MATRIX                   -
C                              -
C-------------------------------
      IMPLICIT REAL*8 (A-H,P-Z)
      DIMENSION COORD(MPOIN,3),BOUDV(MTOTV),EQRHS(MTOTV),
     -          FLUMX(12,12),GFLUM(MFRON,MFRON),LBOUD(MTOTV),
     -          LHEDV(MFRON),LNODS(MELEM,4),LOCEL(12),NDEST(12),
     -          PNORM(MFRON),VARB1(MVARB),VARB2(MVARB),
     -          BOUVS(MTOTV),LBUVS(MTOTV),FUNCN(7)
      COMMON ESPON,DENSY,GRVTY,RELAX,STARC,TOLER,OXMIN,OXDEL,
     -       OYMIN,OYDEL
      COMMON NEVAB,NBCNF,NBCNS,NELEM,NGARD,NGAUS,NITER,NNODP,
     -       NPOIN,NTOTV,NUNKN,NBCN1,NBCN2
C
C***  REWIND BEFORE SOLUTION PROCEDURE
C
      NUNKN=3
      NBCNS=NBCN1
      IF(IUSVS.EQ.0)GO TO 1
      NUNKN=2
      NBCNS=NBCN2
      DO 3 ITOTV=1,NPOIN
      IS=(ITOTV-1)*2+1
      IV=(ITOTV-1)*3+1
      VARB1(IS)=VARB2(IV)*VARB2(IV+2)*VARB2(IV+2)*FUNCN(4)+
     -        VARB2(NPOIN*3+IS)*VARB2(IV+2)*VARB2(IV+2)*FUNCN(5)
      VARB1(IS+1)=VARB2(IV+1)*VARB2(IV+2)*VARB2(IV+2)*FUNCN(4)+
     -        VARB2(NPOIN*3+IS+1)*VARB2(IV+2)*VARB2(IV+2)*FUNCN(5)
    3 CONTINUE
    1 NEVAB=NNODP*NUNKN
      NTOTV=NPOIN*NUNKN
      DO 2 I1=1,12
      LOCEL(I1)=0
2     CONTINUE
      IF(IMASS.GT.1)GO TO 40
C
C***  ON FIRST ITERATION ONLY FIND LAST APPERENCE OF EACH NODE
C
      DO 30 IPOIN=1,NPOIN
      LASTE=0
      DO 20 IELEM=1,NELEM
      DO 10 INODP=1,NNODP
      IF(LNODS(IELEM,INODP).NE.IPOIN) GO TO 10
      LASTE=IELEM
      LASTN=INODP
      GO TO 20
   10 CONTINUE
   20 CONTINUE
      LNODS(LASTE,LASTN)=-IPOIN
   30 CONTINUE
   40 CONTINUE
C
C***  INITIALIZE HEADING AND GRAND FLUID MATRIX
C
```

```
      REWIND 4
      REWIND 10
      NCRIT=MFRON-NEVAB
      NFRON=0
      DO 50 IFRON=1,MFRON
      DO 50 JFRON=1,MFRON
      GFLUM(IFRON,JFRON)=0.0
   50 CONTINUE
      KELEM=0
C
C***  START ASSEMBLY BY FORMING ELEMENT MATRIX
C
   60 CONTINUE
      KELEM=KELEM+1
      IF(IUSVS.EQ.1)GO TO 65
      CALL MATRIX(COORD,EQRHS,FLUMX,KELEM,LNODS,MFRON,MELEM,
     -            MPOIN,MTOTV,MVARB,VARB2,FUNCN,LBOUD)
      GO TO 66
 65   CALL SURFAS(COORD,EQRHS,FLUMX,FUNCN,IELEM,LNODS,MBNDY,
     -            MELEM,MPOIN,MTOTV,MVARB,VARB2)
66    KEVAB=0
C
C***  CREATE GLOBAL DOF ARRAY FOR EACH LOCAL ELEMENT DOF
C
      DO 70 INODP=1,NNODP
      KPOIN=LNODS(KELEM,INODP)
      LODFM=NUNKN
      IADFM=NUNKN*(IABS(KPOIN)-1)+1
      DO 70 IODFM=1,LODFM
      KEVAB=KEVAB+1
      LOCEL(KEVAB)=IADFM+IODFM-1
      IF(KPOIN.LT.0)LOCEL(KEVAB)=-LOCEL(KEVAB)
   70 CONTINUE
C     DO 1980 KK=1,NEVAB
C
C***  FIT EACH DOF INTO THE FRONT WIDTH EXTENDING IF NECESSARY
```

```
C
      DO 120 IEVAB=1,NEVAB
      KTOTV=LOCEL(IEVAB)
      IF(NFRON.EQ.0)GO TO 90
      DO 80 IFRON=1,NFRON
      KFRON=IFRON
      IF(IABS(KTOTV).EQ.IABS(LHEDV(KFRON)))GO TO 110
   80 CONTINUE
   90 CONTINUE
      NFRON=NFRON+1
      IF(NFRON.LE.MFRON)GO TO 100
      WRITE(12,2000)
      STOP
  100 CONTINUE
      NDEST(IEVAB)=NFRON
      LHEDV(NFRON)=KTOTV
      GO TO 120
  110 CONTINUE
      NDEST(IEVAB)=KFRON
      LHEDV(KFRON)=KTOTV
  120 CONTINUE
C
C***  ASSEMBLE NEW ELEMENT INTO GRAND FLUID MATRIX
C
      DO 130 IEVAB=1,NEVAB
      IFRON=NDEST(IEVAB)
      DO 130 JEVAB=1,NEVAB
      JFRON=NDEST(JEVAB)
      GFLUM(JFRON,IFRON)=GFLUM(JFRON,IFRON)+FLUMX(JEVAB,IEVAB)
  130 CONTINUE
      IF(NFRON.LT.NCRIT.AND.KELEM.LT.NELEM)GO TO 60
  140 CONTINUE
      NFSUM=0
      PIVOT=0.0
C
C***  CHECK LAST APPEARENCE OF EACH DOF PROCESS BOUNDARY CONDITIONS
```

```
C
      DO 170 IFRON=1,NFRON
      IF(LHEDV(IFRON).GE.0)GO TO 170
      NFSUM=1
      IF(IUSVS.EQ.1)GO TO 171
      IF(LBOUD(IABS(LHEDV(IFRON))).NE.1)GO TO 160
      GO TO 172
  171 IF(LBUVS(IABS(LHEDV(IFRON))).NE.1)GO TO 160
  172 CONTINUE
      KTOTV=IABS(LHEDV(IFRON))
      IF(IUSVS.EQ.1)GO TO 175
      LBOUD(KTOTV)=-1
      EQRHS(KTOTV)=BOUDV(KTOTV)
      GO TO 176
  175 LBUVS(KTOTV)=-1
      EQRHS(KTOTV)=BOUVS(KTOTV)
  176 CONTINUE
      DO 150 LFRON=1,NFRON
      GFLUM(IFRON,LFRON)=0.0
  150 CONTINUE
      GFLUM(IFRON,IFRON)=1.0
  160 CONTINUE
C
C***  SEARCH FOR LARGEST PIVOTAL VALUE
C
      PIVOG=GFLUM(IFRON,IFRON)
      IF(DABS(PIVOG).LT.DABS(PIVOT))GO TO 170
      PIVOT=PIVOG
      LPIVT=IFRON
  170 CONTINUE
C       PRINT9991,NFSUM
C9991 FORMAT('TO DO IF, NFSUM= ',I4)
      IF(NFSUM.EQ.0)GO TO 60
      KTOTV=IABS(LHEDV(LPIVT))
      IF(DABS(PIVOT).GT.1E-08) GO TO 180
      WRITE(12,2010)KTOTV,PIVOT
      STOP
  180 CONTINUE
C
C***  NORMALIZE PIVOTAL EQUATIONS
C
      DO 190 IFRON=1,NFRON
      PNORM(IFRON)=GFLUM(LPIVT,IFRON)/PIVOT
  190 CONTINUE
      RHSID=EQRHS(KTOTV)/PIVOT
      EQRHS(KTOTV)=RHSID
C
C***  ELIMINATION OF PIVOTAL EQUATIONS REDUCING FRONT WIDTH
C
      IF(LPIVT.EQ.1)GO TO 250
      LPIVT1=LPIVT-1
      DO 240 IFRON=1,LPIVT1
      FACOR=GFLUM(IFRON,LPIVT)
      IF(FACOR.EQ.0)GO TO 210
      DO 200 JFRON=1,LPIVT1
      GFLUM(IFRON,JFRON)=GFLUM(IFRON,JFRON)-FACOR*PNORM(JFRON)
  200 CONTINUE
  210 CONTINUE
      IF(LPIVT.EQ.NFRON)GO TO 230
      LPIVT2=LPIVT+1
      DO 220 JFRON=LPIVT2,NFRON
      GFLUM(IFRON,JFRON-1)=GFLUM(IFRON,JFRON)-FACOR*PNORM(JFRON)
  220 CONTINUE
  230 CONTINUE
      ITOTV=IABS(LHEDV(IFRON))
      EQRHS(ITOTV)=EQRHS(ITOTV)-FACOR*RHSID
  240 CONTINUE
  250 CONTINUE
      IF(LPIVT.EQ.NFRON)GO TO 300
      LPIVT2=LPIVT+1
      DO 290 IFRON=LPIVT2,NFRON
      FACOR=GFLUM(IFRON,LPIVT)
      IF(LPIVT.EQ.1)GO TO 270
      LPIVT1=LPIVT-1
      DO 260 JFRON=1,LPIVT1
      GFLUM(IFRON-1,JFRON)=GFLUM(IFRON,JFRON)-FACOR*PNORM(JFRON)
  260 CONTINUE
  270 CONTINUE
      DO 280 JFRON=LPIVT2,NFRON
      GFLUM(IFRON-1,JFRON-1)=GFLUM(IFRON,JFRON)-FACOR*PNORM(JFRON)
  280 CONTINUE
      ITOTV=IABS(LHEDV(IFRON))
      EQRHS(ITOTV)=EQRHS(ITOTV)-FACOR*RHSID
  290 CONTINUE
  300 CONTINUE
C
C***  WRITE OUT NON-FIXED PIVOTAL EQUATIONS ON TAPE
C
      IF(IUSVS.EQ.1)GO TO 305
      IF(LBOUD(KTOTV).NE.0)GO TO 310
      GO TO 306
  305 IF(LBUVS(KTOTV).NE.0)GO TO 310
  306 CONTINUE
      WRITE(4)NFRON,LPIVT,(LHEDV(IFRON),PNORM(IFRON),IFRON=1,NFRON)
  310 CONTINUE
      DO 320 IFRON=1,NFRON
      GFLUM(IFRON,NFRON)=0.0
      GFLUM(NFRON,IFRON)=0.0
  320 CONTINUE
      IF(LPIVT.EQ.NFRON)GO TO 340
      NFRON1=NFRON-1
      DO 330 IFRON=LPIVT,NFRON1
      LHEDV(IFRON)=LHEDV(IFRON+1)
  330 CONTINUE
  340 CONTINUE
      NFRON=NFRON-1
C
C***  ASSEMBLE ELIMINATE OR BACK SUBSITUTE
```

```
C
      IF(NFRON.GT.NCRIT)GO TO 140
      IF(KELEM.LT.NELEM)GO TO 60
      IF(NFRON.GT.0)GO TO 140
C
C***  BACK SUBSITUTION
C
      IF(IUSVS.EQ.1)GO TO 345
      DO 350 ITOTV=1,NTOTV
      VARB1(ITOTV)=BOUDV(ITOTV)
      LBOUD(ITOTV)=-LBOUD(ITOTV)
  350 CONTINUE
      GO TO 346
  345 DO 355 ITOTV=1,NTOTV
      VARB1(ITOTV)=BOUVS(ITOTV)
      LBUVS(ITOTV)=-LBUVS(ITOTV)
  355 CONTINUE
  346 CONTINUE
      NTON=NTOTV-NBCNS
      DO 370 ITOTV=1,NTON
      BACKSPACE 4
      READ(4)NFRON,LPIVT,(LHEDV(IFRON),PNORM(IFRON),IFRON=1,NFRON)
      KTOTV=IABS(LHEDV(LPIVT))
      TEMPR=0.0
      PNORM(LPIVT)=0.0
      DO 360 IFRON=1,NFRON
      TEMPR=TEMPR-PNORM(IFRON)*VARB1(IABS(LHEDV(IFRON)))
  360 CONTINUE
      VARB1(KTOTV)=EQRHS(KTOTV)+TEMPR
      BACKSPACE 4
  370 CONTINUE
      RETURN
 2000 FORMAT(//39H PROGRAM HALTED FRONTWIDTH IS TOO SMALL)
 2010 FORMAT(//32H PROGRAM HALTED ILL-CONDITIONING,//
     -17H D.O.FREEDOM     ,I4,/13H PIVOT VALUE ,E9.2)
      END
```

```
C$$$$$$$$$$$$$$$$$$$$$$$$$$$$$$$$$$$$$$$$$$$$$$$$$$$$$$$$$$$$$$$$
C                                                              $
C SUBROUTINE MATRIX                                            $
C           FORM THE ELEMENT MATRIX FOR u,v AND h              $
C                                                              $
C$$$$$$$$$$$$$$$$$$$$$$$$$$$$$$$$$$$$$$$$$$$$$$$$$$$$$$$$$$$$$$$$
      SUBROUTINE MATRIX(COORD,EQRHS,FLUMX,IELEM,LNODS,MFRON,MELEM,
     -                  MPOIN,MTOTV,MVARB,VARB2,FUNCN,LBOUD)
      IMPLICIT REAL*8 (A-H,P-Z)
      DIMENSION AREAW(9),CARPG(2,72),CARTP(2,8),COORD(MPOIN,3),
     -          EQRHS(MTOTV),ERHSU(4),ERHSV(4),LBOUD(MTOTV),
     -          FLUMX(12,12),FUNCN(7),LNODS(MELEM,4),SHAPG(72),
     -          SHAPP(8),VARB2(MVARB)
      COMMON ESPON,DENSY,GRVTY,RELAX,STARC,TOLER,OXMIN,OXDEL,
     -       OYMIN,OYDEL
      COMMON NEVAB,NBCNF,NBCNS,NELEM,NGARD,NGAUS,NITER,NNODP,
     -       NPOIN,NTOTV,NUNKN,NBCN1,NBCN2
C
C
C***  INITIALIZE ARRAYS
C
      DO 10 INODP=1,NNODP
      ERHSU(INODP)=0.0
      ERHSV(INODP)=0.0
   10 CONTINUE
      NEVAB=NNODP*NUNKN
      DO 20 IEVAB=1,NEVAB
      DO 20 JEVAB=1,NEVAB
      FLUMX(IEVAB,JEVAB)=0.0
   20 CONTINUE
C
C***  READ IN SHAPE FUNCTION VALUES AND DERIVATIVES
C
      READ(10) IELEM,LGAUS,NGAPA,
     -((CARPG(IDIME,IGAPA),IDIME=1,2),SHAPG(IGAPA),IGAPA=1,NGAPA),
     -(AREAW(IGAUS),IGAUS=1,LGAUS)
```

```
C     CALL SLOPE(COORD,IELEM,LNODS,MELEM,MPOIN,SLOPX,SLOPY)
C
C***  LOOP TO CARRY OUT GAUSS INTERGRATION
C
      DO 100 IGAUS=1,LGAUS
      DAREA=AREAW(IGAUS)
C     PRINT THE MATRIX
C     WRITE(12,2900)IGAUS,IELEM,(LNODS(IELEM,INODE),INODE=1,NNODP)
C2900  FORMAT('IGAUS=',I2,'    ELEMENT #',I3,'     NODE',8I5)
      DO 30 INODP=1,NNODP
      SHAPP(INODP)=SHAPG(NNODP*(IGAUS-1)+INODP)
      DO 30 IDIME=1,2
      CARTP(IDIME,INODP)=CARPG(IDIME,NNODP*(IGAUS-1)+INODP)
   30 CONTINUE
C     PRINT
C     WRITE(12,2910)(SHAPP(III),III=1,NNODP)
C     WRITE(12,2910)(CARTP(1,III),III=1,NNODP)
C     WRITE(12,2910)(CARTP(2,III),III=1,NNODP)
C     WRITE(12,2910)DAREA
2910  FORMAT(20F6.2)
      ZFX=0.
      ZFY=0.
      UY=0.0
      VY=0.0
      HY=0.0
      PY=0.0
      QY=0.0
      PFX=0.
      PFY=0.
      QFX=0.
      QFY=0.
      HFX=0.
      HFY=0.
      UFX=0.
      UFY=0.
      VFX=0.
      VFY=0.
      CC=STARC/DSQRT(GRVTY)
C
C***  EVALUATE PREVIOUS VELOCITIES AT GAUSS POINTS
C
      DO 40 INODP=1,NNODP
      KPOIN=IABS(LNODS(IELEM,INODP))
      SHAPE=SHAPP(INODP)
      DFIDX=CARTP(1,INODP)
      DFIDY=CARTP(2,INODP)
      ITOTV=(KPOIN-1)*NUNKN
C     WRITE(6,1234)ITOTV
      UY=UY+VARB2(ITOTV+1)*SHAPE
C     WRITE(6,1234)ITOTV
      VY=VY+VARB2(ITOTV+2)*SHAPE
C     WRITE(6,1234)ITOTV
 1234 FORMAT('ITOTV',I4)
      HY=HY+VARB2(ITOTV+3)*SHAPE
      HFX=HFX+VARB2(ITOTV+3)*DFIDX
      HFY=HFY+VARB2(ITOTV+3)*DFIDY
      UFX=UFX+VARB2(ITOTV+1)*DFIDX
      UFY=UFY+VARB2(ITOTV+1)*DFIDY
      VFX=VFX+VARB2(ITOTV+2)*DFIDX
      VFY=VFY+VARB2(ITOTV+2)*DFIDY
      PY=PY+VARB2(NPOIN*3+(KPOIN-1)*2+1)*SHAPE
      QY=QY+VARB2(NPOIN*3+KPOIN*2)*SHAPE
      PFX=PFX+VARB2(NPOIN*3+KPOIN*2-1)*DFIDX
      PFY=PFY+VARB2(NPOIN*3+KPOIN*2-1)*DFIDY
      QFX=QFX+VARB2(NPOIN*3+KPOIN*2)*DFIDX
      QFY=QFY+VARB2(NPOIN*3+KPOIN*2)*DFIDY
      ZFX=ZFX+COORD(KPOIN,3)*DFIDX
      ZFY=ZFY+COORD(KPOIN,3)*DFIDY
   40 CONTINUE
C
C***  CALL SUROUTINE TO FORM THE INTEGRAL OF F,G TERMS
C
```

```
      CALL VINTGL(EDDY,FH,FUNCN,GH,MTOTV,MVARB,STARK,VARB2)
C
C***  FORM THE LOCAL RHS TERMS
C
      DO 60 INODP=1,NNODP
      ERHSU(INODP)=ERHSU(INODP)+SHAPP(INODP)*DAREA*(
     --DSQRT(UY*UY+VY*VY)*(UY+STARK*PY)/(CC*CC)-
     -GRVTY*HY*ZFX-
     -(2.*UY*HY*FUNCN(3)+2.*PY*HY*FUNCN(2))*PFX-
     -(QY*HY*FUNCN(2)+VY*HY*FUNCN(3))*PFY-
     -(PY*HY*FUNCN(2)+UY*HY*FUNCN(3))*QFY)
      ERHSV(INODP)=ERHSV(INODP)+SHAPP(INODP)*DAREA*(
     --DSQRT(UY*UY+VY*VY)*(VY+STARK*QY)/(CC*CC)-
     -GRVTY*HY*ZFY-
     -(2.*VY*HY*FUNCN(3)+2.*QY*HY*FUNCN(2))*QFY-
     -(PY*HY*FUNCN(2)+UY*HY*FUNCN(3))*QFX-
     -(QY*HY*FUNCN(2)+VY*HY*FUNCN(3))*PFX)
   60 CONTINUE
      DO 90 I=1,NNODP
      IROWU=(I-1)*NUNKN+1
      IROWV=IROWU+1
      IROWH=IROWV+1
      SHAPI=SHAPP(I)
      CARXI=CARTP(1,I)
      CARYI=CARTP(2,I)
      DO 90 K=1,NNODP
      KPOIN=IABS(LNODS(IELEM,K))
      ITOTV=(KPOIN-1)*NUNKN
      KCOLU=(K-1)*NUNKN+1
      KCOLV=KCOLU+1
      KCOLH=KCOLV+1
      SHAPK=SHAPP(K)
      CARXK=CARTP(1,K)
      CARYK=CARTP(2,K)
C
C***  FORM THE COMMON USED TERMS IN EQUATIONS
```

```
C
      WF=SHAPI*SHAPK
      WFX=SHAPI*CARXK
      WFY=SHAPI*CARYK
      WXFX=CARXI*CARXK
      WYFY=CARYI*CARYK
      WYFX=CARYI*CARXK
      WXFY=CARXI*CARYK
C
C***  U MOMENTUM EQUATION
C
      AK1=0.001
      AK4=0.001
C
C***  THE BOUNDARY POINTS (NOTE:USE DIFFERENT EDDY)
C
       ACEDY=0.21
      KCHKP=(KPOIN-1)*3+1
      IF(LBOUD(KCHKP).NE.0)ACEDY=0.15
 46   CONTINUE
      EDDY=ACEDY*HY*DSQRT(UY*UY+VY*VY)/CC
      FLUMX(IROWU,KCOLU)=FLUMX(IROWU,KCOLU)+(UY*HY*WFX+
     -VY*HY*WFY+EDDY*HY*WXFX+EDDY*HY*WYFY-
     &HFX*EDDY*WFX-HFY*EDDY*WFY+
     -(2.*UY*HY*FUNCN(1)+2.*PY*HY*FUNCN(3))*WFX+
     -(VY*FUNCN(1)+QY*FUNCN(3))*WFY*HY+HY*DSQRT(DAREA)*
     &(WYFY*DABS(VY*AK1+AK4*VFY*DSQRT(DAREA))
     &+WXFX*DABS(UY*AK1+AK4*UFX*DSQRT(DAREA))))*DAREA
       FLUMX(IROWU,KCOLV)=FLUMX(IROWU,KCOLV)+(
     -UY*FUNCN(1)*WFY+PY*FUNCN(3)*WFY)*HY*DAREA
       FLUMX(IROWU,KCOLH)=FLUMX(IROWU,KCOLH)+(
     -GRVTY*HY*WFX+EDDY*UY*WXFX+EDDY*UY*WYFY+WFX*
     -(UY*UY*FUNCN(1)+2.*PY*UY*FUNCN(3)+PY*PY*FUNCN(2))+
     -(UY*VY*FUNCN(1)+PY*QY*FUNCN(2)+PY*VY*FUNCN(3)+
     -QY*UY*FUNCN(3))*WFY)*DAREA
C
```

```
C***  V MOMENYUM
C
      FLUMX(IROWV,KCOLV)=FLUMX(IROWV,KCOLV)+(VY*HY*WFY+
     -UY*HY*WFX+EDDY*HY*WXFX+EDDY*HY*WYFY-
     &HFX*EDDY*WFX-HFY*EDDY*WFY+
     -(2.*VY*FUNCN(1)+2.*QY*FUNCN(3))*HY*WFY+
     -(UY*FUNCN(1)+PY*FUNCN(3))*HY*WFX+HY*DSQRT(DAREA)*
     &(WYFY*DABS(VY*AK1+AK4*VFY*DSQRT(DAREA))
     &+WXFX*DABS(UY*AK1+AK4*UFX*DSQRT(DAREA))))*DAREA
      FLUMX(IROWV,KCOLU)=FLUMX(IROWV,KCOLU)+(
     -VY*FUNCN(1)*WFX+QY*FUNCN(3)*WFX)*HY*DAREA
      FLUMX(IROWV,KCOLH)=FLUMX(IROWV,KCOLH)+(
     -GRVTY*HY*WFY+EDDY*VY*WYFY+EDDY*VY*WXFX+WFY*
     -(VY*VY*FUNCN(1)+2.*QY*VY*FUNCN(3)+QY*QY*FUNCN(2))+
     -(UY*VY*FUNCN(1)+PY*QY*FUNCN(2)+QY*UY*FUNCN(3)+
     -PY*VY*FUNCN(3))*WFX)*DAREA
C
C***  CONTINUITY
C
      AK3=0.01
      VART=DSQRT(UY*UY+VY*VY)
      FLUMX(IROWH,KCOLU)=FLUMX(IROWH,KCOLU)+HY*WFX*DAREA
      FLUMX(IROWH,KCOLV)=FLUMX(IROWH,KCOLV)+HY*WFY*DAREA
      FLUMX(IROWH,KCOLH)=FLUMX(IROWH,KCOLH)+(
     -UY*WFX+VY*WFY+AK3*
     &(WYFY*DABS(VY)+WXFX*DABS(UY))*DSQRT(DAREA))*DAREA
   80 CONTINUE
   90 CONTINUE
  100 CONTINUE
C
C***  ADD LOCAL RHS VECTOR TO GLOBAL ARRAY
C
      DO 110 INODP=1,NNODP
      KPOIN=IABS(LNODS(IELEM,INODP))
      ITOTU=(KPOIN-1)*3+1
      ITOTV=ITOTU+1
      EQRHS(ITOTU)=EQRHS(ITOTU)+ERHSU(INODP)
      EQRHS(ITOTV)=EQRHS(ITOTV)+ERHSV(INODP)
  110 CONTINUE
C     WRITE(12,2500)IELEM,(LNODS(IELEM,I),I=1,NNODP)
C     DO 2510 I=1,NEVAB
 2510 CONTINUE
 2500 FORMAT('      ELEMENT #',I3,'    NODE',8I5)
 2540 CONTINUE
 2560 FORMAT(' ITOTV=',I5,'   EQRHS=',E12.4)
      RETURN
      END
C$$$$$$$$$$$$$$$$$$$$$$$$$$$$$$$$$$$$$$$$$$$$$$$$$$$$$$$$$$
C                                                         $
C   SUBROUTINE TO GET ALL INTERGATION TO BE USED          $
C                                                         $
C$$$$$$$$$$$$$$$$$$$$$$$$$$$$$$$$$$$$$$$$$$$$$$$$$$$$$$$$$$
      SUBROUTINE VINTGL(EDDY,FH,FUNCN,GH,MTOTV,MVARB,STARK,VARB2)
C
C***  SUBROUTINE TO EVALUATE INTEGRATIONS IN U,V,P,Q
C     3 PTS GAUSIAN INTEGRATION
C
      IMPLICIT REAL*8 (A-H,P-Z)
      DIMENSION POS(3),WEI(3),FUNCN(7),VARB2(MVARB)
      COMMON ESPON,DENSY,GRVTY,RELAX,STARC,TOLER,OXMIN,OXDEL,
     -       OYMIN,OYDEL
      COMMON NEVAB,NBCNF,NBCNS,NELEM,NGARD,NGAUS,NITER,NNODP,
     -       NPOIN,NTOTV,NUNKN,NBCN1,NBCN2
C     m=ku/u*=k*SQRT(f/8)=kC/SQRT(g)
C     CM=0.4*STATC/DSQRT(GRVTY)=7.28 for 180 bend
      F(Z) = (0.4*STARC/DSQRT(GRVTY)+1)/(0.4*STARC/DSQRT(GRVTY))
     -*Z**(1./(0.4*STARC/DSQRT(GRVTY)))
C     F(Z) = (3.69+1.)/3.69*(Z/HEIGH)**(1/3.69)
      G(Z) = 2.*Z-1.
      F1(Z)= (F(Z)-1.)*(F(Z)-1.)
      F2(Z)= G(Z)*G(Z)
      F3(Z)= (F(Z)-1.)*G(Z)
      F4(Z)= (F(Z)-1.)*Z
      F5(Z)= G(Z)*Z
      F6(Z)= F(Z)-1
      F7(Z)= G(Z)
      STARK=-1.5
      EDDY=0.0
      POS(1)=0.7745966692
      POS(2)=0.0
      POS(3)=-POS(1)
      WEI(1)=0.5555555556
      WEI(2)=0.8888888889
      WEI(3)=WEI(1)
      DO 2 I2=1,7
      FUNCN(I2)=0.0
    2 CONTINUE
      DO 1 I1=1,3
      XTMPY=(POS(I1)+1.)/2.
      FUNCN(1)=FUNCN(1)+0.5*WEI(I1)*F1(XTMPY)
      FUNCN(2)=FUNCN(2)+0.5*WEI(I1)*F2(XTMPY)
      FUNCN(3)=FUNCN(3)+0.5*WEI(I1)*F3(XTMPY)
      FUNCN(4)=FUNCN(4)+0.5*WEI(I1)*F4(XTMPY)
      FUNCN(5)=FUNCN(5)+0.5*WEI(I1)*F5(XTMPY)
      FUNCN(6)=FUNCN(6)+0.5*WEI(I1)*F6(XTMPY)
      FUNCN(7)=FUNCN(7)+0.5*WEI(I1)*F7(XTMPY)
    1 CONTINUE
C
C
C
      CM=0.4*STARC/DSQRT(GRVTY)
      FUNCN(1)= 1./(CM*(CM+2.))
      FUNCN(2)=1./3.
      FUNCN(3)=1./(2.*CM+1)
      FUNCN(4)=.5/(2.*CM+1)
      FUNCN(5)=1./6.
C
C***  USE SIMPLE RELATIONSHIP
```

```
C
    3 CONTINUE
      SUMUV=0.
      SUMHH=0.
      DO 4 I4=1,NPOIN
C
C***  IF U-VELOCITY IS TOO SMALL, SQRT WON'T WORK
C
      TEST1=VARB2((I4-1)*3+1)
      TEST2=VARB2((I4-1)*3+2)
      TEMPS=DMAX1(TEST1,TEST2)
      IF(TEST1.LE.0.000001.OR.TEST2.LE.0.000001)GO TO 41
      TEMPS=DSQRT(VARB2((I4-1)*3+1)**2.+VARB2((I4-1)*3+2)**2.)
   41 SUMUV=SUMUV+TEMPS
      SUMHH=SUMHH+VARB2(I4*3)
    4 CONTINUE
      EDDY=10.*SUMUV/NPOIN*SUMHH/NPOIN/(STARC*STARC)
C       EDDY=0.0016
      FH=F(1.0D0)
      GH=G(1.0D0)
      RETURN
      END
C$$$$$$$$$$$$$$$$$$$$$$$$$$$$$$$$$$$$$$$$$$$$$$$$$$$$$$$$$
C                                                        $
C   ITERATION TO SOLVE U,V,H                             $
C                                                        $
C$$$$$$$$$$$$$$$$$$$$$$$$$$$$$$$$$$$$$$$$$$$$$$$$$$$$$$$$$
      SUBROUTINE ITERUV(BOUDV,COORD,EQRHS,GFLUM,GRADB,LBOUD,LGRAD,
     -                  LHEDV,LNODS,MFRON,MELEM,MPOIN,MTOTV,MVARB,
     -                  PNORM,POSGP,VARB1,VARB2,WEIGP,BOUVS,LBUVS)
C-----------------------------------
C                                  -
C   EXTERNAL SUBROUTINE            -
C   PRESCR                         -
C   FRONT1                         -
C-----------------------------------
```

```
      IMPLICIT REAL*8 (A-H,P-Z)
      DIMENSION COORD(MPOIN,3),BOUDV(MTOTV),EQRHS(MTOTV),
     -          FLUMX(12,12),GFLUM(MFRON,MFRON),GRADB(MFRON,8),
     -          LBOUD(MTOTV),LGRAD(MPOIN),LHEDV(MFRON),
     -          LNODS(MELEM,4),POSGP(3),PNORM(MFRON),WEIGP(3),
     -          VARB1(MVARB),VARB2(MVARB),
     -          BOUVS(MTOTV),LBUVS(MTOTV),FUNCN(7)
      COMMON ESPON,DENSY,GRVTY,RELAX,STARC,TOLER,OXMIN,OXDEL,
     -       OYMIN,OYDEL
      COMMON NEVAB,NBCNF,NBCNS,NELEM,NGARD,NGAUS,NITER,NNODP,
     -       NPOIN,NTOTV,NUNKN,NBCN1,NBCN2
      CALL VINTGL(EDDY,FH,FUNCN,GH,MTOTV,MVARB,STARK,VARB2)
      DO 3 ITOTV=1,NPOIN
      IS=(ITOTV-1)*2+1
      IV=(ITOTV-1)*3+1
      BOUVS(IS)=VARB2(IV)*VARB2(IV+2)*VARB2(IV+2)*FUNCN(4)+
     -          BOUVS(IS)*VARB2(IV+2)*VARB2(IV+2)*FUNCN(5)
      BOUVS(IS+1)=VARB2(IV+1)*VARB2(IV+2)*VARB2(IV+2)*FUNCN(4)+
     -            BOUVS(IS+1)*VARB2(IV+2)*VARB2(IV+2)*FUNCN(5)
    3 CONTINUE
C
C***  SET UP ITERATION COUNTER AND LOOP ADRESS
C
       IMASS=0
       ITOTS=0
    1 CONTINUE
      IITER=0
       ITOTS=ITOTS+1
   10 CONTINUE
       IMASS=IMASS+1
      IUSVS=0
      IITER=IITER+1
      DO 20 ITOTV=1,NTOTV
      EQRHS(ITOTV)=0.0
   20 CONTINUE
      WRITE(12,2800)IITER
      PRINT2800,IITER
 2800 FORMAT(' FOR U,V,H ITERATION #',I4)
C
C***  CALL PRESCR FOR ELEMENT NON-ZERO BOUNDARY GRADIENTS
C
C     DO 30 IELEM=1,NELEM
C     IF(LGRAD(IELEM).EQ.0)GO TO 30
C     CALL PRESCR ----------------- INCOMPLETE
C  30 CONTINUE
C
C***  CALL FRONTS TO SET UP AND SOLVE GOVERNING EQUATIONS
C
      CALL FRONT1(BOUDV,COORD,EQRHS,GFLUM,LBOUD,LHEDV,LNODS,
     -            MELEM,MFRON,MPOIN,MTOTV,MVARB,PNORM,VARB1,
     -            VARB2,IITER,IMASS,IUSVS,LBUVS,BOUVS,FUNCN)
C
C***  PRINT RESULTS OF EACH ITERATION
C
      WRITE(12,2810)
 2810    FORMAT('  the result is ')
        DO 2720 I272=1,NPOIN
        IX=(I272-1)*3
2720     WRITE(12,2710)I272,VARB1(IX+1),VARB1(IX+2),VARB1(IX+3)
2710     FORMAT(I5,3(3X,G15.5))
C
C***  CALL TOLREL TO CHECK CONVERGENCE AND RELAX VALUES IF NOT
C
      NTOCK=3*NPOIN
      CALL TOLREL(IUSVS,MVARB,NCONV,NTOCK,VARB1,VARB2)
C
C***  RETURN TO MASTER NUMBER IF ITERATIONS EXCEEDS MAXIMUM
C
      IF(NCONV.EQ.1)GO TO 100
      IF(IITER.LT.NITER)GO TO 10
      WRITE(12,2000)
 2000 FORMAT(//32H SOLUTION HAS FAILED TO CONVERGE)
```

```
C
C***
C
  100 CONTINUE
      IUSVS=1
      DO 220 ITOTV=1,NTOTV
      EQRHS(ITOTV)=0.0
  220 CONTINUE
      CALL FRONT1(BOUDV,COORD,EQRHS,GFLUM,LBOUD,LHEDV,LNODS,
     -            MELEM,MFRON,MPOIN,MTOTV,MVARB,PNORM,VARB1,
     -            VARB2,IITER,IMASS,IUSVS,LBUVS,BOUVS,FUNCN)
      NTOCK=2*NPOIN
      WRITE(12,2820)
 2820 FORMAT('  the result is ')
      DO 2721 I272=1,NPOIN
      IX=(I272-1)*2
2721  WRITE(12,2711)I272,VARB1(IX+1),VARB1(IX+2)
2711  FORMAT(I5,2(3X,G15.5))

      DO 260 I60=1,NPOIN
      IS=(I60-1)*2+1
      IV=(I60-1)*3+1
      IF(LBUVS(IS).EQ.0.AND.VARB2(IV+2).GT.0.0005)GO TO 261
      VARB1(IS)=0.0
      GO TO 262
 261  VARB1(IS)=(VARB1(IS)-VARB2(IV)*VARB2(IV+2)*VARB2(IV+2)
     &*FUNCN(4))/(VARB2(IV+2)*VARB2(IV+2)*FUNCN(5))
 262  IF(LBUVS(IS+1).EQ.0.AND.VARB2(IV+2).GT.0.0005)GO TO 263
      VARB1(IS+1)=0.0
      GO TO 260
 263  VARB1(IS+1)=(VARB1(IS+1)-VARB2(IV+1)*VARB2(IV+2)*VARB2(IV+2)
     &*FUNCN(4))/(VARB2(IV+2)*VARB2(IV+2)*FUNCN(5))
 260  CONTINUE
       DO 2722 I272=1,NPOIN
       IX=(I272-1)*2
2722   WRITE(12,2712)I272,VARB1(IX+1),VARB1(IX+2)
```

```
 2712  FORMAT(I5,2(3X,G15.5))
       CALL TOLREL(IUSVS,MVARB,NCNDS,NTOCK,VARB1,VARB2)
       DO 230 ITOTV=1,NPOIN
       I230=(ITOTV-1)*2+1
       VARB2(NPOIN*3+I230)=VARB1(I230)
       VARB2(NPOIN*3+I230+1)=VARB1(I230+1)
   230 CONTINUE
       IF(NCNDS.EQ.1)RETURN
       IF(ITOTS.LT.5)GO TO 1
       RETURN
       END
C$$$$$$$$$$$$$$$$$$$$$$$$$$$$$$$$$$$$$$$$$$$$$$$$$$$$$$$$$$$$$$$$$$$$$
C                                                                    $
C   CHECK THE VARIABLE IS WITHIN IN TOLERANCE                        $
C                                                                    $
C$$$$$$$$$$$$$$$$$$$$$$$$$$$$$$$$$$$$$$$$$$$$$$$$$$$$$$$$$$$$$$$$$$$$$
       SUBROUTINE TOLREL(IUSVS,MVARB,NCONV,NTOCK,VARB1,VARB2)
       IMPLICIT REAL*8 (A-H,P-Z)
       DIMENSION VARB1(MVARB),VARB2(MVARB)
       COMMON ESPON,DENSY,GRVTY,RELAX,STARC,TOLER,OXMIN,OXDEL,
     -        OYMIN,OYDEL
       COMMON NEVAB,NBCNF,NBCNS,NELEM,NGARD,NGAUS,NITER,NNODP,
     -        NPOIN,NTOTV,NUNKN,NBCN1,NBCN2
C
C***  CHECK FOR CONVERGENCE TO REQUIRED TOLERANCE
C
       CANLA=0.0
       NCONV=1
       IF(IUSVS.EQ.1)GO TO 100
       DO 10 ITOTV=1,NTOCK
       IF(DABS(VARB1(ITOTV)).LT.0.005)GO TO 10
       CANGE=DABS((VARB1(ITOTV)-VARB2(ITOTV))/VARB1(ITOTV))
       IF(CANGE.GT.TOLER)NCONV=0
       IF(CANLA.GT.CANGE) GO TO 10
       CANLA=CANGE
       LTOLA=ITOTV
   10 CONTINUE
      WRITE(12,2000)LTOLA,CANLA
      IF(NCONV.EQ.0)GO TO 20
      WRITE(12,2010)
      RETURN
   20 CONTINUE
      IF(IITER.EQ.1)GO TO 40
C
C***  RELAX VARIABLES FOR NEXT ITERATION
C
      DO 30 ITOTV=1,NTOCK
      VARB2(ITOTV)=VARB2(ITOTV)+RELAX*(VARB1(ITOTV)-VARB2(ITOTV))
   30 CONTINUE
      RETURN
   40 CONTINUE
      DO 50 ITOTV=1,NTOCK
      VARB2(ITOTV)=VARB1(ITOTV)
   50 CONTINUE
      RETURN
  100 CONTINUE
      DO 110 ITOTV=1,NTOCK
      IF(DABS(VARB1(ITOTV)).LT.0.005)GO TO 110
      CANGE=DABS((VARB1(ITOTV)-VARB2(NPOIN*3+ITOTV))/VARB1(ITOTV))
      IF(CANGE.GT.TOLER)NCONV=0
      IF(CANLA.GT.CANGE) GO TO 110
      CANLA=CANGE
      LTOLA=ITOTV
  110 CONTINUE
 2000 FORMAT(/37H LARGEST CHANGE OCCURS AT DOF NUMBER ,
     -I5, 10H CHANGE = ,F10.4)
 2010 FORMAT(//45H SOLUTION HAS CONVERGED TO REQUIRED TOLERANCE)
      RETURN
      END

C$$$$$$$$$$$$$$$$$$$$$$$$$$$$$$$$$$$$$$$$$$$$$$$$$$$$$$$$$$$$$$$$$$$$$$$$
C                                                                       $
```

```
C   SUBROUTINE TO PRINT RESULT                        $
C                                                     $
C$$$$$$$$$$$$$$$$$$$$$$$$$$$$$$$$$$$$$$$$$$$$$$$$$$$$$
      SUBROUTINE RESULT(COORD,LNODS,MELEM,MPOIN,MVARB,VARB2)
      IMPLICIT REAL*8 (A-H,P-Z)
      DIMENSION COORD(MPOIN,3),LNODS(MELEM,4),VARB2(MVARB)
      COMMON ESPON,DENSY,GRVTY,RELAX,STARC,TOLER,OXMIN,OXDEL,
     -       OYMIN,OYDEL
      COMMON NEVAB,NBCNF,NBCNS,NELEM,NGARD,NGAUS,NITER,NNODP,
     -       NPOIN,NTOTV,NUNKN,NBCN1,NBCN2
C
C***  PRINT THE RESULT
C
      WRITE(12,2000)
 2000 FORMAT(//' FINAL SOLUTIONS ARE :'//' NODE',7X,'Uave',
     -9X,'Vave',10X,'H',11X,'Usur',9X,'Vsur')
      DO 10 IPOIN=1,NPOIN
      JPOIN=3*(IPOIN-1)
      KPOIN=3*NPOIN+(IPOIN-1)*2
      WRITE(12,2010)IPOIN,VARB2(JPOIN+1),VARB2(JPOIN+2),
     -VARB2(JPOIN+3),VARB2(KPOIN+1),VARB2(KPOIN+2)
 2010 FORMAT(I3,5(3X,F10.5))
   10 CONTINUE
      RETURN
      END
C$$$$$$$$$$$$$$$$$$$$$$$$$$$$$$$$$$$$$$$$$$$$$$$$$$$$$$$$$$$$$$
C                                                             $
C SUBROUTINE SURFAS                                           $
C       FORM THE ELEMENT MATRIX FOR Us AND Vs                 $
C                                                             $
C$$$$$$$$$$$$$$$$$$$$$$$$$$$$$$$$$$$$$$$$$$$$$$$$$$$$$$$$$$$$$$
      SUBROUTINE SURFAS(COORD,EQRHS,FLUMX,FUNCN,IELEM,LNODS,MBNDY,
     -                  MELEM,MPOIN,MTOTV,MVARB,VARB2)
      IMPLICIT REAL*8 (A-H,P-Z)
      DIMENSION AREAW(9),CARPG(2,72),CARTP(2,8),COORD(MPOIN,3),
     -          EQRHS(MTOTV),ERHSU(4),ERHSV(4),
     -          FLUMX(12,12),FUNCN(7),LNODS(MELEM,4),SHAPG(72),
     -          SHAPP(8),VARB2(MVARB)
      COMMON ESPON,DENSY,GRVTY,RELAX,STARC,TOLER,OXMIN,OXDEL,
     -       OYMIN,OYDEL
      COMMON NEVAB,NBCNF,NBCNS,NELEM,NGARD,NGAUS,NITER,NNODP,
     -       NPOIN,NTOTV,NUNKN,NBCN1,NBCN2
C
C
C***  INITIALIZE ARRAYS
C
      DO 10 INODP=1,NNODP
      ERHSU(INODP)=0.0
      ERHSV(INODP)=0.0
   10 CONTINUE
      DO 20 IEVAB=1,NEVAB
      DO 20 JEVAB=1,NEVAB
      FLUMX(IEVAB,JEVAB)=0.0
   20 CONTINUE
C
C***  READ IN SHAPE FUNCTION VALUES AND DERIVATIVES
C
      READ(10) IELEM,LGAUS,NGAPA,
     -((CARPG(IDIME,IGAPA),IDIME=1,2),SHAPG(IGAPA),IGAPA=1,NGAPA),
     -(AREAW(IGAUS),IGAUS=1,LGAUS)
C
C***  LOOP TO CARRY OUT GAUSS INTERGRATION
C
      DO 100 IGAUS=1,LGAUS
      DAREA=AREAW(IGAUS)
      DO 30 INODP=1,NNODP
      SHAPP(INODP)=SHAPG(NNODP*(IGAUS-1)+INODP)
      DO 30 IDIME=1,2
      CARTP(IDIME,INODP)=CARPG(IDIME,NNODP*(IGAUS-1)+INODP)
   30 CONTINUE
      UY=0.0
      VY=0.0
      HY=0.0
      ZY=0.0
      UFX=0.
      UFY=0.
      VFX=0.
      VFY=0.
      HFX=0.
      HFY=0.
      ZFX=0.
      ZFY=0.
      CC=STARC/DSQRT(GRVTY)
C
C***  EVALUATE PREVIOUS VELOCITIES AT GAUSS POINTS
C
      DO 40 INODP=1,NNODP
      KPOIN=IABS(LNODS(IELEM,INODP))
      SHAPE=SHAPP(INODP)
      DFIDX=CARTP(1,INODP)
      DFIDY=CARTP(2,INODP)
      ITOTV=(KPOIN-1)*3
      UY=UY+VARB2(ITOTV+1)*SHAPE
      VY=VY+VARB2(ITOTV+2)*SHAPE
      HY=HY+VARB2(ITOTV+3)*SHAPE
      ZY=ZY+COORD(KPOIN,3)*SHAPE
      UFX=UFX+VARB2(ITOTV+1)*DFIDX
      UFY=UFY+VARB2(ITOTV+1)*DFIDY
      VFX=VFX+VARB2(ITOTV+2)*DFIDX
      VFY=VFY+VARB2(ITOTV+2)*DFIDY
      HFX=HFX+VARB2(ITOTV+3)*DFIDX
      HFY=HFY+VARB2(ITOTV+3)*DFIDY
      ZFX=ZFX+COORD(KPOIN,3)*DFIDX
      ZFY=ZFY+COORD(KPOIN,3)*DFIDY
   40 CONTINUE
C
C***  CALL SUROUTINE TO FORM THE INTEGRAL OF F,G TERMS
C
```

```
      CALL VINTGL(EDDY,FSUF,FUNCN,GSUF,MTOTV,MVARB,STARK,VARB2)
C
C***  FORM THE LOCAL RHS TERMS
C
C
C     TEST THE COEFFICIENT
      CM=0.4*STARC/DSQRT(GRVTY)
      CEDDY=0.077
      EDDY=CEDDY*HY*DSQRT(UY*UY+VY*VY)/CC
       EDDY1=0.21*HY*DSQRT(UY*UY+VY*VY)/CC
      CTLT=2.0
      CNST=-STARK/2./CC+CTLT*CEDDY
C    EDDY=0.0
C     CNST=1.0
      DO 60 INODP=1,NNODP
      WX=CARTP(1,INODP)
      WY=CARTP(2,INODP)
      UVQRT=DSQRT(UY*UY+VY*VY)/(CC*CC)
      ERHSU(INODP)=ERHSU(INODP)+SHAPP(INODP)*DAREA*(
     &EDDY1*(HY*UFX*(ZFX+0.5*HFX)+UFY*HY*(ZFY+0.5*HFY))+CNST*
     &HY*UY*FUNCN(4)/FUNCN(5)*UVQRT*CC)
      ERHSV(INODP)=ERHSV(INODP)+SHAPP(INODP)*DAREA*(
     &EDDY1*(HY*VFY*(ZFY+0.5*HFY)+VFX*HY*(ZFX+0.5*HFX))+CNST*
     &HY*VY*FUNCN(4)/FUNCN(5)*UVQRT*CC)
   60 CONTINUE
      DO 90 I=1,NNODP
      IROWP=(I-1)*2+1
      IROWQ=IROWP+1
      SHAPI=SHAPP(I)
      CARXI=CARTP(1,I)
      CARYI=CARTP(2,I)
      DO 90 K=1,NNODP
      KPOIN=IABS(LNODS(IELEM,K))
      KCOLP=(K-1)*2+1
      KCOLQ=KCOLP+1
      SHAPK=SHAPP(K)
      CARXK=CARTP(1,K)
      CARYK=CARTP(2,K)
C
C***  FORM THE COMMON USED TERMS IN EQUATIONS
C
      WF=SHAPI*SHAPK
      WFX=SHAPI*CARXK
      WFY=SHAPI*CARYK
      WXF=SHAPK*CARXI
      WYF=SHAPK*CARYI
      WXFX=CARXI*CARXK
      WYFY=CARYI*CARYK
      WYFX=CARYI*CARXK
      WXFY=CARXI*CARYK
      UVQRT=DSQRT(UY*UY+VY*VY)/(CC*CC)
C
C***  ZU-MOMENTUM EQUATION
C
      AK2=0.25
      FLUMX(IROWP,KCOLP)=FLUMX(IROWP,KCOLP)+DAREA*(
     &UY*WFX+2.*UFX*WF+VY*WFY+VFY*WF+
     &CNST*CC*UVQRT/FUNCN(5)/HY*WF
     &+(WYFY*DABS(VY)+WXFX*DABS(UY))*DSQRT(DAREA)*AK2)
      FLUMX(IROWP,KCOLQ)=FLUMX(IROWP,KCOLQ)+DAREA*(
     &UFY*WF)
C
C***  ZV MOMENTUM EQUATION
C
      FLUMX(IROWQ,KCOLQ)=FLUMX(IROWQ,KCOLQ)+DAREA*(
     &VY*WFY+2.*VFY*WF+UY*WFX+UFX*WF+
     &CNST*CC*UVQRT/FUNCN(5)/HY*WF
     &+(WYFY*DABS(VY)+WXFX*DABS(UY))*DSQRT(DAREA)*AK2)
      FLUMX(IROWQ,KCOLP)=FLUMX(IROWQ,KCOLP)+DAREA*(
     &VFX*WF)
   80 CONTINUE
   90 CONTINUE
```

```
  100 CONTINUE
C
C***  ADD LOCAL RHS VECTOR TO GLOBAL ARRAY
C
      DO 110 INODP=1,NNODP
      KPOIN=IABS(LNODS(IELEM,INODP))
      ITOTP=(KPOIN-1)*2+1
      ITOTQ=ITOTP+1
      EQRHS(ITOTP)=EQRHS(ITOTP)+ERHSU(INODP)
      EQRHS(ITOTQ)=EQRHS(ITOTQ)+ERHSV(INODP)
  110 CONTINUE
C     WRITE(12,2500)IELEM,(LNODS(IELEM,I),I=1,NNODP)
C     DO 2510 I=1,8
C     WRITE(12,2910)(FLUMX(I,J),J=1,8)
2510  CONTINUE
2500  FORMAT('       ELEMENT #',I3,'     NODE',8I5)
C      DO 2540 I=1,N
C      WRITE(12,2560)I,EQRHS(I)
2540  CONTINUE
2560  FORMAT(' ITOTV=',I5,'   EQRHS=',E12.4)
      RETURN
      END
```